Chiral metallosupramolecular species with amino acid functionalised ligands

Stephanie Alison Boer

B. Sc. (Hons.)

A thesis submitted for the degree of Doctor of Philosophy at
Monash University in 2017

School of Chemistry

To fall in love with God is the greatest romance;

to seek him the greatest adventure;

to find him, the greatest human achievement.

- *St. Augustine*

Copyright notice

© Stephanie Alison Boer (2017).

I certify that I have made all reasonable efforts to secure copyright permissions for third-party content included in this thesis and have not knowingly added copyright content to my work without the owner's permission.

Abstract

This thesis describes the synthesis of a library of amino acid substituted diimide ligands and their use in the formation of discrete and polymeric coordination complexes, and the properties of selected chiral coordination compounds. The synthesis of chiral coordination compounds are of such interest because they have been shown to have applications in enantioselective catalysis, separation and sensing. Although achiral ligands have been shown to form chiral coordination compounds, the most reliable method is the use of enantiopure ligands which are guaranteed to form homochiral coordination compounds. Of particular interest in the synthesis of enantiopure ligands is the chiral pool method, in which naturally occurring chiral molecules such as amino acids are incorporated into ligands. Therefore this research used diimide ligands, which are synthetically accessible and versatile, substituted with amino acids, in order to form enantiopure chiral ligands for the synthesis of chiral coordination compounds. The diimide ligands were separated into two main categories, those with a linear core and those with a bent core.

The linear diimide ligands were investigated for the formation of chiral coordination polymers with transition metals. A secondary dipyridyl ligand, was also often included in these coordination polymers, as they presented the opportunity to add dimensionality or new modes of interpenetration in the coordination polymers. The steric bulk and functionality of the amino ac side chain was shown to have an influence on the structure and interpenetration of the coordination polymers obtained.

The naphthalene diimide (NDI) ligands have interesting fluorescent properties, which were analysed in the form of the NDI carboxylic acid and upon incorporation into a discrete NDI macrocycle and catenane.

The ligands with a bent core formed a series of quadruple stranded helicate or mesocate complexes with paddlewheel nodes. The use of a chiral ligand formed chiral helicate cages, while the use of

an achiral ligand formed mesocate cages. A quadruple stranded helicate is a robust supramolecular motif for this series of ligands, as it formed with two different ligands with a bent core and two different paddlewheel nodes. It is also demonstrated that only one chiral ligand is required per complex in order to induce the helicity of the cages.

The combination of linear diimide ligands and copper paddlewheel nodes formed discrete coordination compounds, in which the influence of the size, shape, bend and flexibility of all four ligands was shown by the structures of the discrete coordination complexes formed with each class of ligands and paddlewheel nodes.

The research reported herein demonstrates that amino acid substituted diimides are a reliable class of ligands for the synthesis of chiral metallosupramolecular assemblies which have fascinating structures, topologies and properties.

Declaration

This thesis contains no material which has been accepted for the award of any other degree or diploma at any university or equivalent institution and that, to the best of my knowledge and belief, this thesis contains no material previously published or written by another person, except where due reference is made in the text of the thesis.

Signature: …[redacted]…

Print Name: …Stephanie Boer….

Date: …4th November 2017….

Acknowledgements

First of all I would like to thank my main supervisor Dr David Turner, whom it has been a wonderful experience working with for the last few years. I couldn't have known when we first met that our association would last so long or would yield so many good discussions about science and about life, but I am so glad that I ended up in your group. Thank you also to my other supervisor, Prof. Stuart Batten, for adding a third opinion when needed. Thank you to the two group Post Docs whom I shared time with during my PhD, Dr Chris Hawes and Dr Jamie Hicks. Both of you were very different people, and I appreciated my time with both of you and learnt many valuable lessons about science, and about the correct volume of the word "buddy".

My PhD took some interesting turns which led me into areas of chemistry which I had not previously had experience. I therefore need to thank the many people who shared their expertise, time and equipment with me in order to better understand my results. I would like to thank Phillip Holt at Monash University for helping me in many ways, including with circular dichroism and chiral HPLC. I would also like to thank Dr Yada Nolvachai in the Marriott group at Monash University, for always being willing to have a go at analysing various products which I made. Many of my compounds were analysed by mass spectrometry by Sally Duck and Dr Boujemaa Moubaraki at Monash University and by Dr W. Alex Donald and Huixin Wang at the University of New South Wales. Thanks also go to Dr Keith White at the University of Melbourne and Adrian Emerson at Monash University for running the gas sorption measurements of some of my compounds. I would also like to thank Ben Slater, part of the Hill group at Monash University, for exploring chiral separation properties of some of my compounds. I never thought I would do any physical chemistry, but somehow it happened, and so I would like to thank Dr Toby Bell, Dr Rosalind Cox and Lukas Willig for helping me to get my head around this new area and teaching me many new techniques. Finally all of the crystallographic data presented herein would not have been possible without the Australian Synchrotron and all the helpful staff on the MX1 and MX2 beamlines, and Dr Craig Forsyth at Monash University.

During the writing of my thesis I have had good friends help proof read and edit my thesis, so I would like to thank Drs Jas Ward, Lauren Macreadie and Nick White for constantly being willing to read my chapters. There have been many iterations of the Turner group during my time as part of it. I would like to thank Lauren, Greg, Melina, Bianca, Adrian, Nick, Ali, Michael and Sam. I would especially like to thank my coffee buddy, Sam, for becoming a great friend in the last few months. I'm sorry I left you just as we became friends.

A very special thanks goes to my new supervisor, Dr Nick White at Australian National University, for deciding to hire me before I had even finished my PhD. I am very excited to learn about new areas of supramolecular chemistry while in your group. And thank you also to the members of my new group, Rosie, Tom and Chriso, for being patient and understanding with me while I lived the double life of finishing my thesis while also trying to be a helpful Post Doc. Thanks to my new housemates to Canberra, Suz and Tara, for being patient with me as I have been less than social while finishing off my thesis in the last few weeks. There have also been innumerable people who have supported me outside of while I have been working on my PhD. Thank you to my many Christian Union and church friends, and of course my housemates, for supporting me throughout my PhD and especially towards the end. Thank you to my lovely friend Kirsty, for all the Sassafras trips to buy tea and drink massive coffees. I definitely would not have made it through my PhD, and especially not my writing without your support and all that tea. Thank you to my wonderful sisterly Susannah for all the phone conversations all the way from Darwin, and for being a wonderful role model of a successful woman in STEM. I don't know if I would be in this position without your influence and support. Thank you also to my wonderful brother, for looking out for me throughout my PhD, and my life in general, and thanks so much for all your help moving me to Canberra. Thank you to my absolutely wonderful housemate/bestie Mel, for constantly listening to the updates about life in the lab and the status of my research. It was amazing having a friend outside of uni who understood what I was talking about! But mostly thanks for being a wonderful friend to me over the last few years. I am so glad you moved into our house all those years ago, you bring constant joy to my life. Of course I wouldn't be here without the

support of my wonderful parents. I love that you didn't even question my somewhat surprising life decision to do a PhD, and thank you for constantly trying to understand when I explained my research and results. Above all I thank my Lord and Saviour Jesus Christ. There is no greater achievement or higher ambition than to live a life serving and glorifying you.

Table of Contents

Abstract iv

Acknowledgements vii

Abbreviations xv

Chapter 1: Introduction 1

1.1 Introduction and scope 1

1.2 Supramolecular chemistry 1

1.2.1 Host-guest chemistry 1
1.2.2 Crystal engineering 5
1.2.3 Chiral supramolecular chemistry 5

1.3 Coordination polymers 8

1.3.1 Metal-organic frameworks 9
1.3.2 Applications of MOFs and coordination polymers 13
1.3.3 Chiral coordination polymers 14
1.3.4 Applications of chiral coordination polymers 17

1.4 Discrete coordination complexes 26

1.4.1 Coordination cage complexes 27
1.4.3 Applications of coordination cage complexes 30
1.4.2 Chiral coordination cage complexes 32
1.4.3 Applications of chiral coordination cage complexes 35

1.5 Ligands utilised in this study 38

1.5.1 Ditopic ligands 38
1.5.2 Mixed ligand coordination networks 38
1.5.3 Diimide ligands 40
1.5.4 Amino acid based ligands 41

1.6 Project aims 42

Chapter 2: Coordination polymers with naphthalene diimide ligands 44

2.1 Introduction 44

2.1.1 Naphthalene diimides 44

2.1.2 Previous work with naphthalene diimide ligands 45

2.2 Ligands utilised in this study 47

2.2.1 Synthesis of naphthalene diimide ligands 47

2.3 Coordination polymers with the non-bulky AlaNDI ligand 50

2.4 Coordination polymers using the bulky LeuNDI ligand 67

2.5 Coordination polymers utilising the PheNDI ligand with a bulky aromatic side chain 79

2.6 Conclusions 93

Chapter 3: Coordination compounds with biphenyl diimide ligands 96

3.1 Introduction 96

3.1.1 Biphenyl diimide ligands 96

3.1.2 Isophthalic acid substituted diimide ligands 98

3.2 Ligands utilised in this study 99

3.3 Discrete macrocycles containing BDI ligands 101

3.4 Coordination complexes containing BDI and dipyridyl ligands 107

3.5 Discrete Cu^{II} square complexes incorporating BDI ligands 111

3.6 Infinite networks with IsoBDI ligand 115

3.7 Conclusion 122

Chapter 4: Fluorescent properties of naphthalene diimides 125

4.1 Introduction 125

4.1.1 Fluorescence 125

4.1.2 Physical properties of naphthalene diimides 127

4.2 Fluorescence of the leucine substituted NDI 129

4.2.1 Fluorescence of H_2LeuNDI in non-aromatic solvents 130
4.2.2 Fluorescence of H_2LeuNDI in aromatic solvents 132
4.2.3 Fluorescence titration of H_2LeuNDI in chloroform and aromatic solvents 134
4.2.4 ^{1}H-NMR studies of H_2LeuNDI exciplex formation 136
4.2.5 Time resolved fluorescence studies of H_2LeuNDI 138

4.3 Discrete LeuNDI coordination complexes 140

4.3.1 Discrete metallomacrocycle with LeuNDI 141
4.3.2 Discrete [2]-catenane with LeuNDI 142
4.3.3 Fluorescence properties of LeuNDI macrocycle (4.1) and catenane (4.2) 145

4.4 Conclusion 156

Chapter 5: Helicate and mesocate cage complexes 158

5.1 Introduction 158

5.1.1 Helicates in metallosupramolecular chemistry 158
5.1.2 Helicate cage complexes 158
5.1.3 Chiral paddlewheel motifs 160
5.1.4 Transition-metal-catalysed cyclopropanation reactions 161
5.1.5 Bent diimide ligands 163

5.2 Synthesis of biphenyl sulfone diimides 164

5.3 Quadruple stranded helicate and mesocate cages 165

5.2.1 Homochiral quadruple stranded helicate cages 165
5.2.2 Self-selection of homochiral quadruple stranded helicate cages 171
5.2.3 Mesocate cage complexes 172
5.2.4 Retention of helicity upon incorporation of achiral ligand 175

5.4 A larger helicate complex utilising a larger ligand 185

5.4.1 Synthesis of larger diimide ligand 185
5.4.2 Quadruple stranded helicate with EADI ligand 187

5.5 Helicate cages with rhodium metal centres 189

5.5.1 Homochiral helicate cage with Rhodium paddlewheels 190
5.5.2 Enantioselective catalysis with rhodium(II) helicate cages 192

5.6 Conclusion 197

Chapter 6: A chiral octahedral cage complex 199

6.1 Introduction 199

6.1.1 Chiral higher order polyhedral cages 199

6.1.2 Chiral octahedral cages 200

6.2 Chiral octahedral complex 202

6.3 Achiral copper coordination polymer with GlyNDI ligands 206

6.3.1 Synthesis of H_2GlyNDI 206

6.3.2 Synthesis of an achiral coordination polymer with GlyNDI 207

6.4 Porosity of chiral octahedron 209

6.5 Fluorescent properties of chiral octahedron 220

6.6 Chiral separation properties of chiral octahedron 224

6.7 Conclusion 227

Chapter 7: Conclusions 229

Chapter 8: Experimental 233

8.1 Materials and methods 233

8.2 Synthesis of diimide compounds 239

8.2.1 Synthesis of naphthalene diimide compounds 239

8.2.2 Synthesis of biphenyl diimide compounds 240

8.2.3 Synthesis of biphenyl sulfone diimide compounds 244

8.2.4 Synthesis of ethanoanthracene diimide molecule 248

8.3 Synthesis of coordination complexes 249

8.4 Enantioselective catalysis experiments 272

8.5 Mixed ligand BPSD cage experiments 273

8.6 Fluorescence experiments 274

8.7 Chiral separation tests of compound 6.1 275

8.8 X-ray crystallography details 276

8.8.1 X-ray crystallographic information 278

8.8.2 X-ray crystallographic refinement details 288

References 301

Appendix – Publications from this work

Boer, S. A.; Turner, D. R., Self-selecting homochiral quadruple-stranded helicates and control of supramolecular chirality. *Chem. Commun.* **2015,** 51, (98), 17375-17378.

Boer, S. A.; Turner, D. R., Interpenetration in π-Rich Mixed-Ligand Coordination Polymers. *Cryst. Growth Des.* **2016,** 16, (11), 6294-6303.

Boer, S. A.; Turner, D. R., A robust metallomacrocyclic motif for the formation interpenetrated coordination polymers. *CrystEngComm* **2017,** 19, 2402-2412.

Abbreviations

°: Degree

Å: Angstrom

ATR: Attenuated Total Reflectance

ASU: Asymmetric Unit

a.u.: arbitrary units

°C: Degrees Celsius

cm^{-1}: units of wavenumber

nm: nanometers

ppm: parts per million

J: coupling constant (NMR)

K: Kelvin

s: seconds

mbar: millibar

MPa: Megapascals

λ: wavelength

RBF: round bottom flask

NMR: Nuclear Magnetic Resonance

TGA: Thermo-gravimetric Analysis

PXRD: Powder X-ray Diffraction

GC: Gas Chromatography

CD: Circular Dichroism

LC: liquid chromatography

HPLC: High performance liquid chromatography

IR: Infrared Spectroscopy

UV/Vis: Ultraviolet/Visible

FID: Flame Ionisation Detector

M.p.: Melting Point

NDI: 1,4,5,8-naphthalene tetracarboxylic diimide

BPSD: 3,3′,4,4′-biphenyl sulfone tetracarboxylic diimide

BDI: 3,3′,4,4′-biphenyl tetracarboxylic diimide

EADI: 9,10-dimethyl-9,10-dihydro-2,3,6,7-diimido-9,10-ethanoanthracene

PI: Phthalimide

EDA: Ethyl diazoacetate

Gly: Glycine

Ala: Alanine

Leu: Leucine

Phe: Phenylalanine

DCM: dichloromethane

MeCN: Acetonitrile

MeOH: Methanol

DMSO: Dimethylsulfoxide

DMF: *N*,*N*-dimethylformamide

DMA: *N*,*N*-dimethylacetamide

OAc: acetate (CH_3COO^-)

4,4′-bipy: 4,4′-bipyridine

2,2′-bipy: 2,2′-bipyridine

4PyNDI: *N*,*N*′-bis(4-pyridyl)-1,4,5,8-naphthalene tetracarboxylic diimide

bpb: 1,4-bis-(4-pyridyl)benzene

dpe: 1,2-di(4-pyridyl)ethylene

dabco: diazabicyclo[2.2.2]octane

MOF: Metal-Organic framework

SCSC: single crystal to singe crystal

Boc: *tert*-butyloxycarbonyl protecting group

BINOL: 1,1′-bi-2-naphthol

CDs: Cyclodextrins

Chapter 1: Introduction

1.1 Introduction and scope

The research in this thesis investigates the coordination chemistry of amino acid functionalised diimide ligands with specific focus on the synthesis of coordination polymers and coordination cage complexes. The aim of the use of these ligands is to increase the understanding of the influence of the side chain and core group of the ligand on their coordination chemistry with transition metals. The physical properties of some of the coordination complexes obtained have also been examined.

As this research involves both infinite and discrete coordination chemistry, both within the context of chirality, these areas will be introduced separately before the subset of chirality in each of them is also presented. The field of supramolecular coordination chemistry is much too broad to describe herein, therefore only a brief summary of the motivations, design strategy and potential applications of selected supramolecular materials will be discussed below. More specific descriptions of the field will be provided in individual chapters as necessary.

1.2 Supramolecular chemistry

Supramolecular chemistry can be defined in a variety of ways, the most widely circulated definition however was given by Jean-Marie Lehn, a Nobel Prize winner in the field, who described supramolecular chemistry as *"chemistry beyond the molecule"*.[1] As opposed to the strong covalent bonds of molecular chemistry, supramolecular chemistry deals with many non-covalent interactions of varying strength.

1.2.1 Host-guest chemistry

Early supramolecular chemistry was focused on the design of host-guest systems and the interactions between the host and guest. Donald Cram, one of the other winners of the Nobel Prize alongside Lehn, describes an ideal host-guest system as *"a host-guest relationship involv(ing) a complementary stereoelectronic arrangement of binding sites in host and guest"*.[2] A stable host-guest compound should

involve a host molecule with as many as possible potential interactions which cooperate to be convergent to the guest, and a guest of a suitable size and shape to have interactions which are divergent to the host. If a host and guest fulfil this criteria they are called complementary.[3] The aim of the design of complementary hosts is to achieve selectivity, in which a host can differentiate between guests in a mixture and bind only to the desired guest. The design of selective host molecules must take into consideration a variety of supramolecular interactions which vary in strength, including ion-ion, ion-dipole, dipole-dipole, hydrogen bonding, π-interactions and van der Waals interactions, Table 1.1.[4]

Table 1.1 Summary of supramolecular interactions.

Interaction	**Strength (kJ mol^{-1})**
Ion-ion	200-300
Ion-dipole	50-200
Dipole-dipole	5-50
Hydrogen bonding	4-120
Cation-π	5-80
π-π	0-50
Van der Waals	< 5 variable on surface area

Although supramolecular chemistry began with the design and study of host-guest systems, a topic which still garners much interest, the field also includes metallosupramolecular chemistry, which is supramolecular chemistry involving metal-ligand coordination bonds.[5] In a similar manner to the design of host molecules in host-guest systems, organic ligands can be designed to be complementary to the coordination number and geometry of the metal ions employed. In general, ligands will be designed to have convergent coordinating groups to form discrete coordination compounds, or divergent coordinating groups in order to form polymeric coordination compounds.

Metallosupramolecular compounds are formed by self-assembly, which is *"the spontaneous and reversible association of molecules or ions to form larger, more complex supramolecular entities according to the*

intrinsic information contained in molecules themselves".[6] Self-assembly is influenced by the components in the system, the interactions between components, reversibility of bonds formed and the environment in which the reaction takes place.[7] The reversibility of coordination bonds, in contrast to covalent bonds, allows supramolecular systems to have inbuilt 'error-checking' in their synthesis, which leads to the thermodynamic product. The metal ions must be chosen carefully, as stronger coordination bonds will form more stable compounds, but are less reversible than weaker coordination bonds. Transition metals in the 2+ oxidation state have a balance of good coordination bond strength and predictable coordination geometries, so are most often used for synthesis of metallosupramolecular compounds.[8]

In the field of supramolecular chemistry, building blocks that offer strong, directional interactions are labelled tectons,[9] and the predictable interactions between tectons in a supramolecular system are termed synthons.[10] Therefore by taking into account the supramolecular tectons of the ligands and metals, and considering the synthons which are applicable to the system, for example coordination bonds, hydrogen bonds, π-interactions and other weak intermolecular interactions, metallosupramolecular systems can be designed and synthesised.

Just as the design of host-guest systems must take into account a variety of intermolecular interactions to design a host with the desired selectivity, these interactions must also be taken into account when designing metallosupramolecular systems which will form by self-assembly. The primary structure of a coordination compound will be defined by the metal-ligand bonds, but the secondary structure will involve a variety of weaker intermolecular interactions. The presence of hydrogen bonding donor or acceptor groups within a ligand will influence how the coordination compounds pack in the solid state, Figure1.1.[11] Most ligands in coordination chemistry have some aromatic functionality, leading to the prevalence of π-interactions in the secondary structure of coordination compounds. A number of different motifs of π-interactions are possible, including offset face-to-face π-stacking and perpendicular edge-to-face C-H···π interactions, Figure 1.1.[12] Through the judicious design and synthesis of ligands, metallosupramolecular systems may be prepared for a variety of applications.

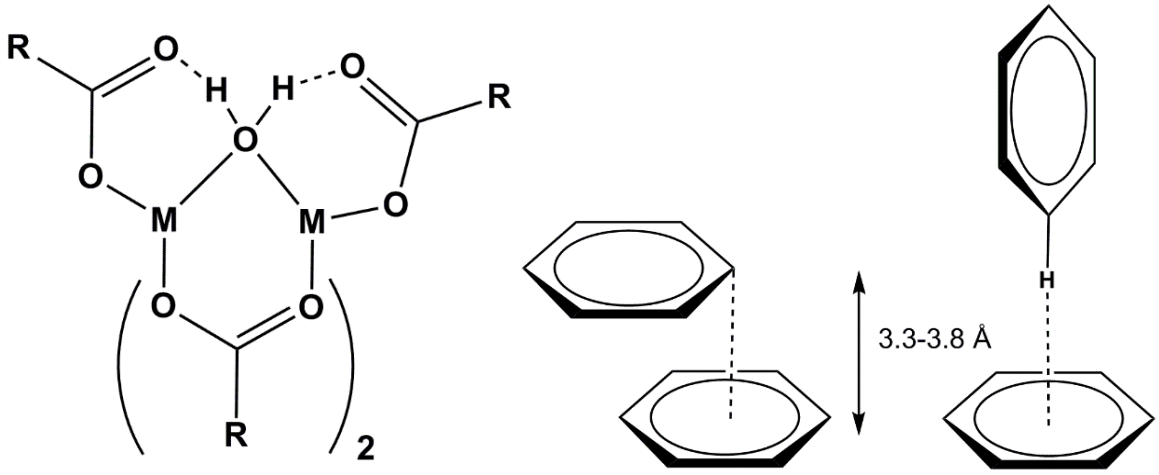

Figure 1.1. An example of a supramolecular complex involving coordination bonds and hydrogen bonding (shown as dashed lines) (left)[13] and schematic of π-interactions, such as offset π-π stacking and C-H···π-interactions (right).

Supramolecular chemistry is also focused on the design, synthesis and properties of a number of discrete assemblies such as catenanes and rotaxanes.[14] A catenane is a set of two or more mechanically interlocking rings, such that the rings are not connected by covalent or coordination bonds but may not be separated without the breaking on covalent or coordination bonds, Figure 1.2.[15-17] A rotaxane is a linear molecule which is thread through a macrocycle and held in place with bulky capping ligands, Figure 1.2.[18-20]

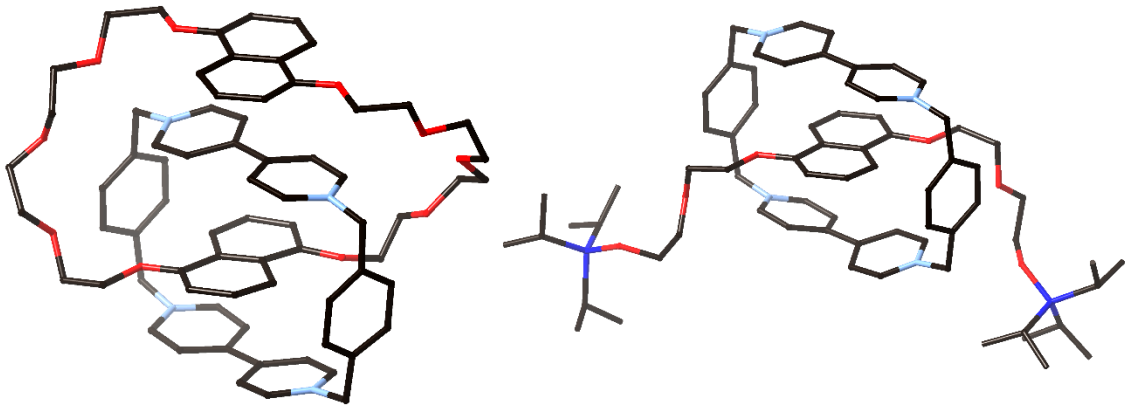

Figure 1.2. Examples of a [2]-catenane (left) and a [2]-rotaxane (right), reported by Stoddart et al.[15, 18]

1.2.2 Crystal engineering

The design and synthesis of new supramolecular coordination compounds for solid state applications requires a good understanding and utilisation of crystal engineering. The introduction of supramolecular chemistry represented a paradigm shift in chemistry, as it moved from the focus on atoms and their bonds to that of molecules and their intermolecular bonding, and focused attention on the collective properties of a chemical system.[21] This paradigm shift leads the field of supramolecular chemistry directly into that of crystal engineering, as both are concerned with the design and function of chemical systems formed by non-covalent bonds.[22] The term crystal engineering was first used by Pepinsky, who stated that crystal structures *"are to a good extent controllable: hence crystals with advantageous properties can be engineered"*.[21]

1.2.3 Chiral supramolecular chemistry

As early supramolecular chemistry was centred on the design of host-guest systems, it is only a small leap to begin consideration of chiral host-guest systems, and the recognition of a chiral guest in a supramolecular host. Due to the inherent chirality in nature, most research into the synthesis of biologically active molecules will require stereoselective reactions or chiral separation. Chiral supramolecular chemistry has therefore been an important area of research for applications in chiral separation, sensing and catalysis.[23, 24] The interaction of an enantiopure chiral host with racemic guests will lead to the formation of diastereomeric host-guest complexes, which will differ in thermodynamic stability.[25] Chiral interactions in supramolecular chemistry relies on a minimum of three simultaneous interactions between host and guest, and at least one of these interactions must be enantioselective, in order to form diastereomeric complexes which may be separated; this is called the three-point rule.[26] The same non-covalent interactions that are important in supramolecular chemistry are also important for understanding biomolecular interactions in biological processes, and therefore must be considered when designing chiral supramolecular host-guest systems.

In general there are four different ways in which a supramolecular assembly may be chiral. The first is if the components of the assembly are inherently chiral, including molecules with stereocenters or axial chirality. The second is if the components are achiral but form as a chiral complex, termed spontaneous

resolution. In the context of crystalline samples, spontaneous resolution may form a racemic compound if both handednesses are present in the unit cell, or a conglomerate if the system forms a mixture of enantiopure crystals.[27] The third option is the use of a chiral component in the reaction to form a chiral supramolecular assembly in which the final product does not include the chiral component, but the system preserves its chirality, termed the "memory of chirality effect".[28] Finally a complex can be formed around a chiral guest, inducing chirality of the complex.[29, 30]

Chiral hosts may also act as chiral catalysts, with the goal of achieving high enantiomeric excesses and yields of products.[31] Enantioselective recognition of chiral biological molecules, such as amino acids and peptides, is fundamental for developing procedures of synthesis, purification and separation of these molecules. Organic chiral hosts include cyclodextrins, chiral calixarenes, cyclophanes, and functionalised cucurbiturils and chiral crown ethers. For the sake of brevity only cyclodextrins and calixarenes will be discussed herein.

A cyclodextrin is a torus which is made of six, seven or eight α-1,4-D-glucopyranose units, forming a hydrophobic cavity and a hydrophilic exterior, Figure 1.3.[32] Cyclodextrins (CDs) have been shown to have applications in pharmacy, medicine, organometallic chemistry, foods, cosmetics, catalysis, biotechnology and textiles.[33-35] The majority of biological and chemical applications of cyclodextrins centre on the ability of CDs to form chiral inclusion compounds.[36] Complexation of guest molecules usually involves inclusion of hydrophobic molecules or fragments inside the cavity of the CD. Unmodified CDs are relatively ineffective at chiral discrimination, as there is limited interaction of chiral molecules with the chiral groups of the CD. However, modification around the upper or lower rim can improve chiral discrimination properties.[37-40]

Calixarenes are another major class of macrocyclic organic host complexes which may be modified to be chiral and therefore have applications in chiral supramolecular chemistry, Figure 1.3.[41] Chirality can be added to calixarenes by appending chiral groups to the lower or upper ring, or by making the calixarenes inherently chiral by asymmetric addition of groups into the calixarenes skeleton. Original research into chiral calixarenes was inhibitory, as the chiral calixarenes were formed as racemates and separation was

required by HPLC, recrystallisation with a chiral auxiliary as diastereomers, or kinetic resolution after synthesis. However new types of optical resolution have been developed which can produce enantiopure calixarenes on gram scales.[42] Calixarenes are of interest due to their 3D surface and conformationally rigid structure and can be utilised in separations, and as sensors and catalysts due to their cavity and preorganised binding sites and ability to reversibly complex neutral and charged compounds.[43-48]

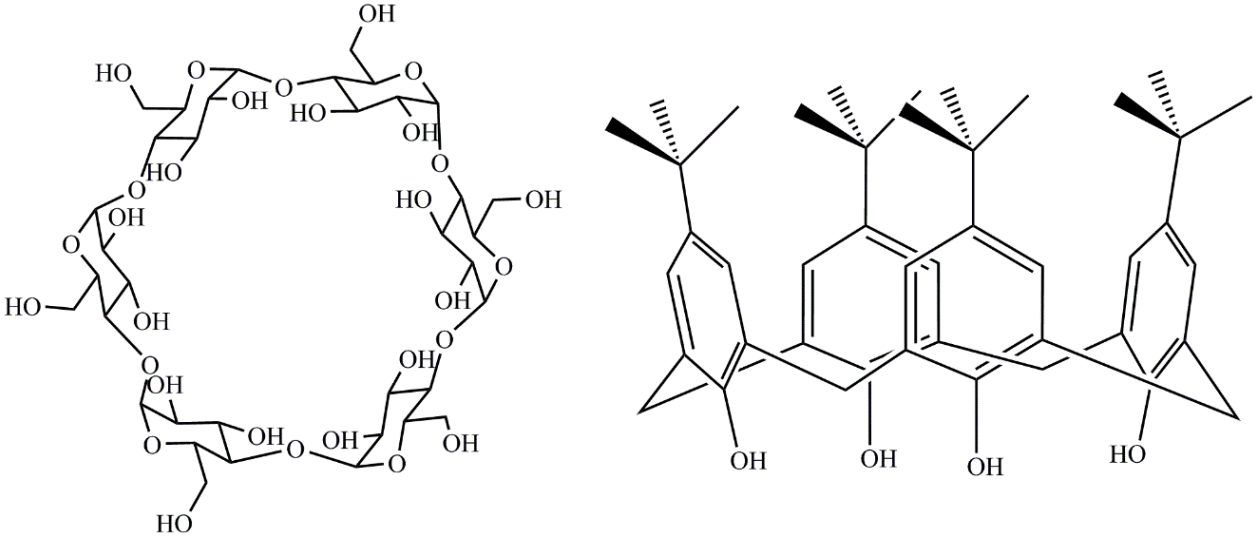

Figure 1.3. The unmodified α-cyclodextrin (left) and an unmodified calix[4]arene with para-tert-butyl substituents (right).

Just as supramolecular chemistry evolved to include metallosupramolecular chemistry, so also chiral supramolecular chemistry has developed to include chiral systems incorporating metal-ligand coordination bonds. Similar to chiral supramolecular systems, metallosupramolecular chiral systems may gain their chirality from chiral components, spontaneous resolution, the "memory of chirality effect" or forming around a chiral guest. An additional source of chirality applicable to metallosupramolecular complexes is chirality due to the arrangement of coordinating groups around a metal, for example three bidentate ligands coordinated to an octahedral metal will exist in a Λ or Δ configuration, Figure 1.4. Chiral metallosupramolecular chemistry includes both discrete and infinite coordination complexes, which will be discussed further in sections 1.3 and 1.4

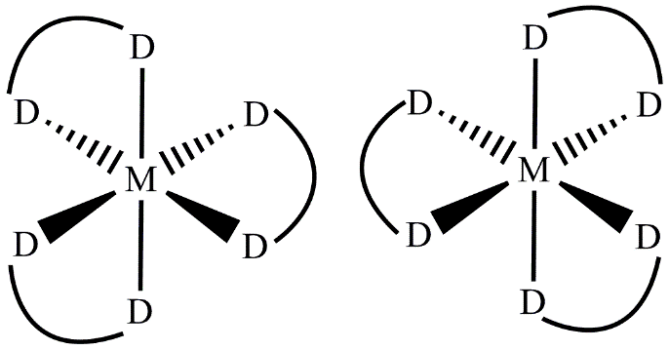

Figure 1.4. Enantiomeric forms of an octahedral metal with bidentate ligands.

1.3 Coordination polymers

In the late 1980s Robson and Hoskins proposed a new class of polymeric metallosupramolecular materials which could be afforded by linking together metal centres with organic ligands into an infinite array, naming them 'coordination polymers'.[49] Early research into coordination polymers focused on their design as nets, using a metal of appropriate coordination geometry and ligands as rod-like connecting units, Figure 1.5.[50] It was hypothesised that through crystal engineering, coordination polymers could be designed and synthesised with large cavities which could be utilised for a range of applications, and a myriad of examples have shown this to be true.[51]

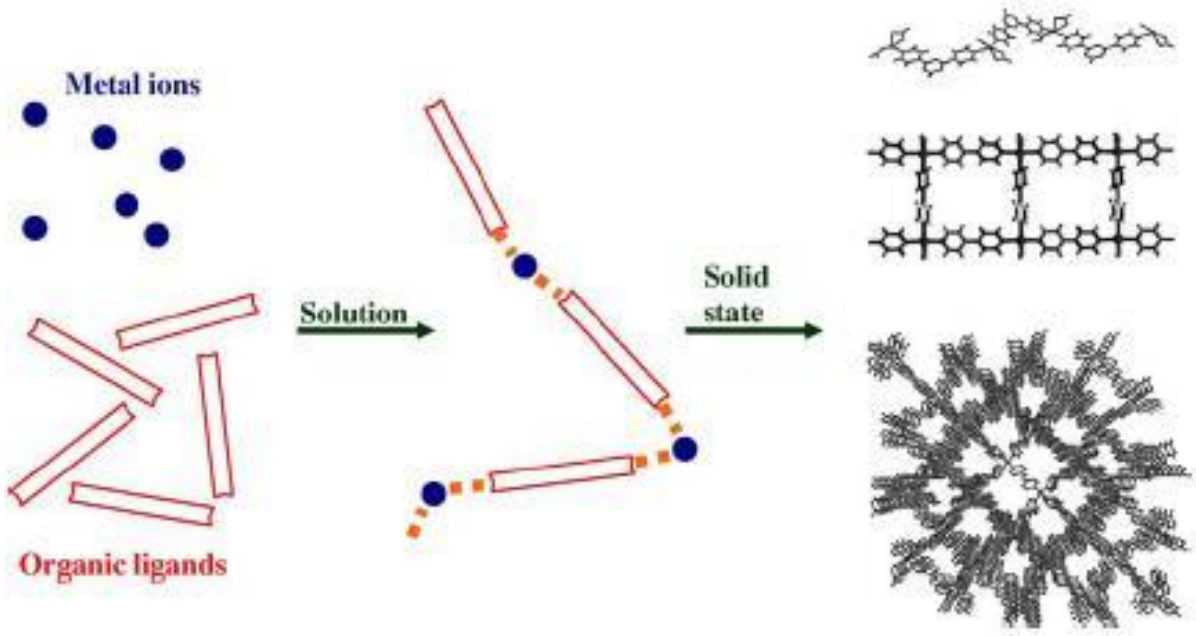

Figure 1.5. Schematic of the formation of 1D, 2D and 3D coordination polymers from metal ions and organic ligands. Reprinted from, Coordination Chemistry Reviews, 250, A.Y. Robin, K. M. Fromm, Coordination polymer networks with O- and N-donors: What they are, why and how they are made, 2127-2157, Copyright (2006), with permission from Elsevier.

1.3.1 Metal-organic frameworks

The porous subset of coordination polymers have been named metal organic frameworks (MOFs).[52] Considering the potential properties, cavities and chemical environment of coordination polymers and MOFs, they have been investigated for applications in many areas including catalysis, gas sorption, gas separation, magnetism, luminescence, conductivity, drug delivery and sensing.[51, 53-60]

In addition to the initial net-based design strategy, multiple other design strategies for coordination polymers have been considered and implemented. Most predominant has been the approach by Yaghi *et al.* who initiated the research into metal-oxide clusters with predetermined coordination geometry, termed secondary building units (SBUs), Figure 1.6.[61] The combination of SBUs with ligands of identical geometry and coordinating groups but varying length was used to synthesise several series of MOFs with porosity dependent on the length of the ligand; this approach was termed “reticular synthesis”.[62]

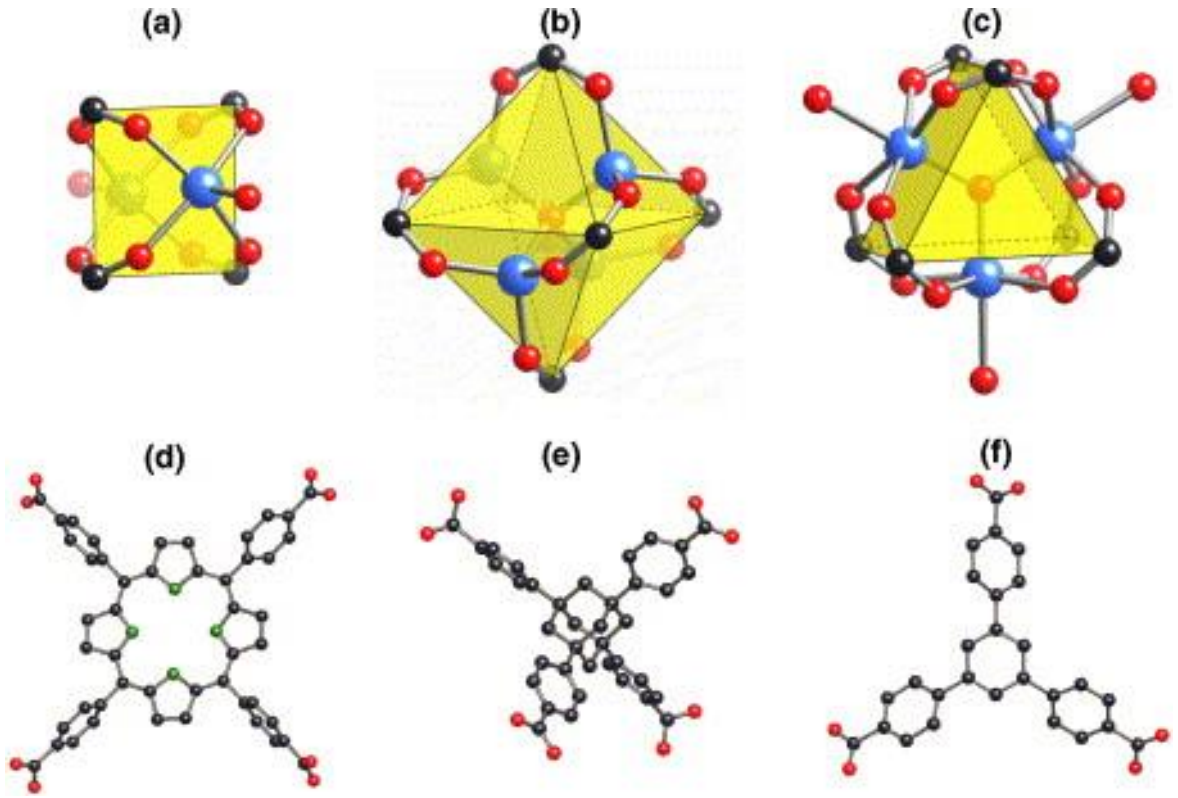

Figure 1.6. Examples of SBUs, (a) square planar "paddlewheel" motif, (b) octahedral "basic zinc acetate" motif, (c) trigonal prismatic trimer, and examples of ligands used in MOF synthesis, (d) square planar tetrakis(4-carboxyphenyl)porphyrin, (e) tetrahedral adamantine-1,3,5,7-tetracarboxylic acid and (f) trigonal ligand 1,3,5-tris(4-carboxyphenyl)benzene. Reprinted from Microporous and mesoporous materials, 73, J. L. C. Rowsell and O. M. Yaghi, Metal–organic frameworks: a new class of porous materials, 3-14, copyright 2004, with permission from Elsevier.

When MOFs are first synthesised their pores are typically filled with the solvent(s) in which they are synthesised, and removal of this solvent will often lead to degradation of the material. Therefore research into MOFs which are stable when desolvated became the forefront of MOF research in order to form materials that were viable for applications. Early work on coordination polymers and MOFs which were thermally stable once desolvated emerged in the 1990s from the groups of Fujita, Yaghi and Williams, Figure 1.7. Fujita *et al.* reported the reaction of 4,4′-bipy with Cd^{II} to form a 2D square network which was shown to encapsulate some aromatic guests with high shape selectivity and could act as a heterogeneous catalyst for cyanosilylation of aldehydes.[63] The Williams group reported the synthesis of HKUST-1, a 3D MOF with square-planar Cu^{II} paddlewheel SBUs with a trimesic acid ligand, which had open pores in the

[100] and [111] direction, giving a material displaying porosity of 40.7% of the total volume.[64] The same year HKUST-1 was first reported, Yaghi *et al.* reported the structure of MOF-5, a 3D cubic network of tetrahedral Zn-oxide clusters and terephthalate ligands, which had 55-61% solvent accessible void space.[65]

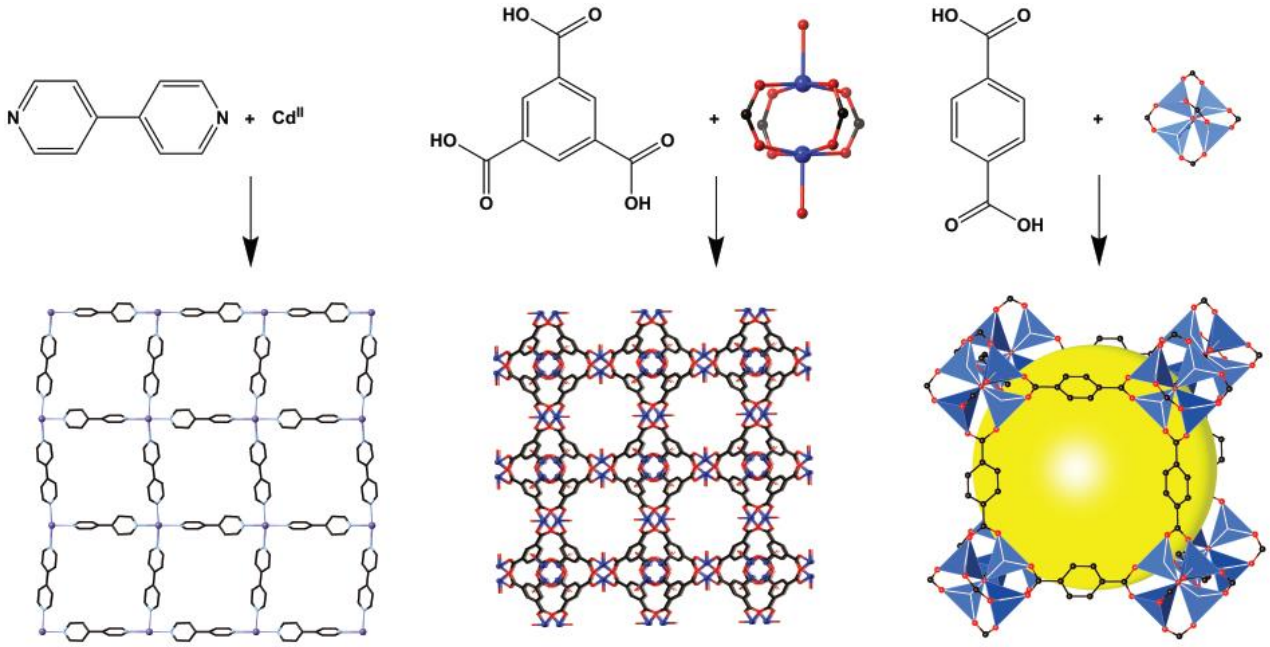

Figure 1.7. Examples of early coordination polymers, a square sheet reported by Fujita (left), HKUST-1 reported by Williams using square planar Cu^{II} paddlewheel SBUs (centre) and MOF-5 reported by Yaghi using the tetrahedral 'basic zinc acetate' SBU (right).[63-65]

Coordination polymers and MOFs may be mechanically interlocked, in which two or more networks are entangled in such a way that they cannot be separated without the breaking of covalent or coordination bonds, and is termed interpenetration. [66, 67] Interpenetration often occurs in coordination networks which have large open windows which another network may pass through.[68] Although interpenetration is often viewed in a negative light, as it can decrease the porosity of the material, it has also been shown to stabilise the networks.[69] Interpenetration can also create smaller pores which enable more ligand to guest interactions, improving the efficiency of many applications of MOFs, including catalysis and separations.[69, 70]

Interpenetration can occur in various topologies dependent on the dimensionality of the networks involved and if the networks interpenetrate in a parallel or inclined manner, Figure 1.8. 1D coordination polymers may be 1D→1D parallel interpenetrated, alternatively inclined or parallel interpenetration can occur in a

1D→2D or 1D→3D manner.[71-73] In a similar way, 2D coordination polymers can be 2D→2D parallel interpenetrated or have 2D→3D parallel or inclined interpenetration.[74-77] Naturally, 3D coordination polymers can only be 3D→3D interpenetrated.[78-80] Interpenetration may also occur between networks of different dimensionalities.[81]

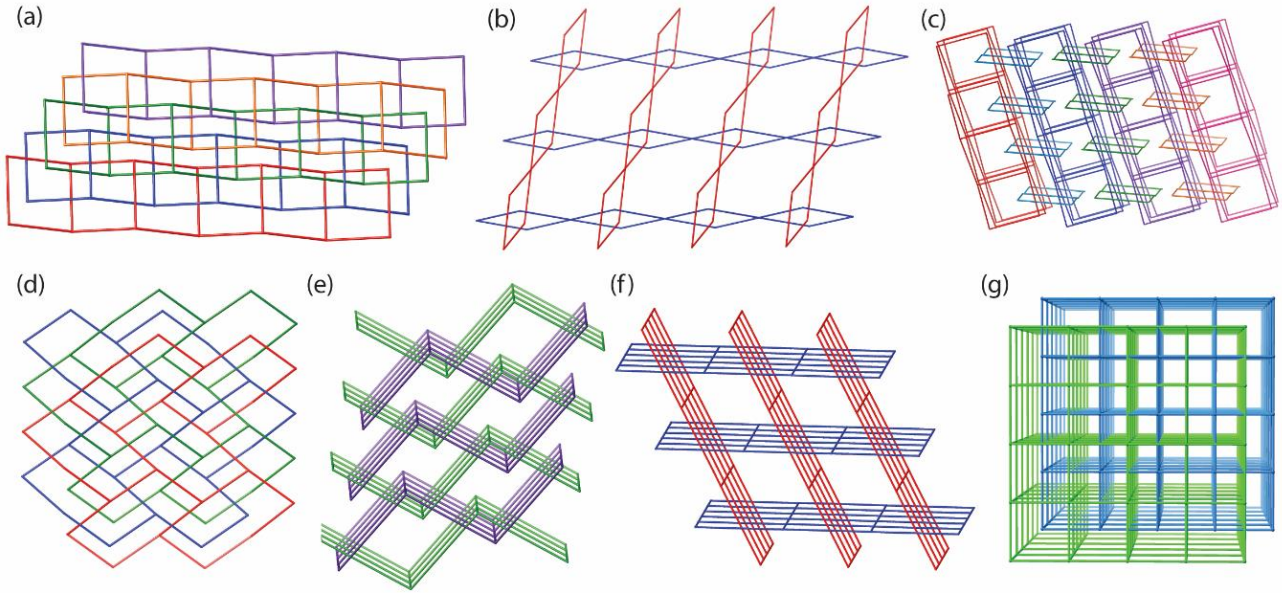

Figure 1.8. Topological diagrams of different modes of interpenetration. a) 1D→2D parallel, b) 1D→2D inclined, c) 1D→3D, d) 2D→2D parallel, e) 2D→3D parallel, f) 2D→3D inclined, and g) 3D→3D interpenetration.

As MOFs consist of both organic and inorganic components, the possibility arises to modify or exchange one or both of these components after the synthesis of the material, a process which is termed post synthetic modification (PSM).[82] PSM has become a commonplace tool in the synthesis of MOFs, as it can enhance or add to their physical and chemical properties. For a process to be considered PSM it must occur in a single-crystal-to-single-crystal manner which maintains the crystallinity, porosity and overall structure of the MOF. The potential application of PSM on MOFs for catalysis was outlined by Robson in the first report of coordination polymers, in which he stated that *"they may, after appropriate functionalisation of the rods, provide tailor-made materials for the heterogeneous catalysis of a wide range of transformations"*.[49] Since then, PSM has been developed to add or modify catalytic metal sites or functional groups on ligands in order to achieve catalysis of a large range of reactions.[83-85] There are multiple different

classes of PSM, including post synthetic deprotection (PSD) in which a protecting group on the ligand is removed so that the functional group is available for chemical reactions within the MOF.[86, 87] Ligands or metal ions on a MOF can also be exchanged from solution after the assembly of the material, a process called post synthetic exchange (PSE).[88, 89] A recently reported class of PSM is post synthetic insertion (PSI), in which additional ligands are inserted into preformed MOFs, either by adding new metal sites to SBUs, or the ligand coordinating to existing vacant metal sites.[90, 91] Also possible is post synthetic polymerisation (PSP), where the MOF is used to template a new material, such as a polymer monolith, in which the MOF ligands are connected together by additional organic groups and the metals are then removed, in order to produce a MOF-templated polymer.[92, 93]

1.3.2 Applications of MOFs and coordination polymers

The potential applications of coordination polymers and MOFs are vast and ever increasing. As such, only a brief summary of them will be discussed herein. Early work on the development of MOFs centred on their use as porous materials for gas sorption and storage, particularly hydrogen and carbon dioxide.[94, 95] MOFs are ideal candidates for gas separations and storage due to their large surface areas, adjustable surface properties and varying pore sizes. Gas capture and storage can occur in rigid MOFs by adsorbate-surface interactions, size/shape exclusion or a combination of both. Gas capture in flexible MOFs is more complex and can occur by size/shape exclusion or adsorbate-surface interactions involving a pore size or shape change, or by adsorbate-surface interactions which are only made possible by gate-opening or structural rearrangement, or by specific pressures which make selective adsorption possible.[56] Initial research into gas capture, storage and separation with MOFs involved sorption in bulk crystalline or pelletized materials, however it has recently moved to include MOF thin films which can be used to create ultrapermeable membranes with exceptional selectivity.[96, 97]

As stated briefly above in the context of post synthetic modification, MOFs are also ideal candidates to act as heterogeneous catalysts. The catalytically active sites of MOFs can exist in a series of classes, including coordinatively unsaturated metal sites, functional organic sites, metalloligands, and metal nanoparticles inserted into the MOF cavities.[98] Through these catalytic sites, MOFs have been shown to achieve catalysis

in a range of different reactions.[85, 99-104] MOFs have also been shown to display interesting optical properties which can be linker or metal based and be dependent on temperature, metal or guests,[105-107] with applications in sensors or switches.[53] MOFs are also being widely investigated for their potential magnetic applications, in which the magnetism is inherent in the system through paramagnetic metals or open-shell ligands, or introduced to the system by magnetic guests.[54] The inorganic-organic hybrid nature of MOFs can also be exploited for applications in drug delivery, as they combine the two current routes to drug delivery, the organic route which uses biocompatible macromolecules that can encapsulate a range of drug molecules, and the inorganic route utilising zeolites or mesoporous silicate materials of precise porosity.[108]

As can be seen, the relatively simple design and synthesis of coordination polymers and MOFs makes them excellent candidates for a broad range of applications. The field of MOFs and coordination polymers and their real-world applications is still in its infancy, and will continue to be investigated in the future.

1.3.3 Chiral coordination polymers

Chiral coordination polymers and MOFs are an exciting class of metallosupramolecular materials. They are being investigated to further the fundamental understanding of the addition, control and preservation of chirality in coordination chemistry and for their possible applications in chiral catalysis, separation and sensing.[109]

Chirality may be introduced to infinite coordination networks using similar routes as chiral host-guest supramolecular systems, as discussed in Section 1.2.3. Chirality can be incorporated by the use of a chiral ligand, by spontaneous resolution of a network with achiral ligands, the memory of chirality effect and induction of chirality by a network forming around a chiral guest.

The simplest approach is the first, the use of enantiopure chiral ligands that will produce homochiral coordination networks. The chiral pool strategy, in which naturally occurring enantiopure molecules are used as ligands or incorporated into ligands is the most straightforward route to chiral ligands and therefore chiral coordination networks, Figure 1.9.[110] The naturally occurring molecule camphoric acid is well suited to utilisation as a ligand, as it is ditopic with two carboxylic acid groups and it is a similar length to the classic MOF ligand, 1,4-benzenedicarboxylic acid. The Bu group has published a study into MOFs utilising

(*S*)- or (*R*)-camphoric acid ligands with In^{II}, Co^{II}, Ni^{II} and Mg^{II} to form six different MOFs incorporating three different homochiral features, namely that they crystallise as homochiral nets, they involve helicates and are synthesised from chiral ligands.[111] Camphoric acid been widely utilised as a ligand for the synthesis of homochiral MOFs for applications (*vide infra*). The functionalisation of naturally occurring tartaric acid with an additional pyridyl coordinating group was first reported in 2000 by Kim and co-workers, reaction of this ligand with Zn^{II} formed a porous homochiral MOF which displayed enantioselective encapsulation of cationic metal complexes and chiral catalysis of a transesterification reaction.[110] Amino acids or small peptide chains may also be used as chiral ligands, as demonstrated by Rosseinsky and co-workers, who used a Gly-Ser peptide ligand to synthesise a MOF with Zn^{II} which showed large solvent channels while solvated, however when the material was desolvated the cooperative hydrogen bonding of the peptide chain caused folding of the material into a non-porous state.[112]

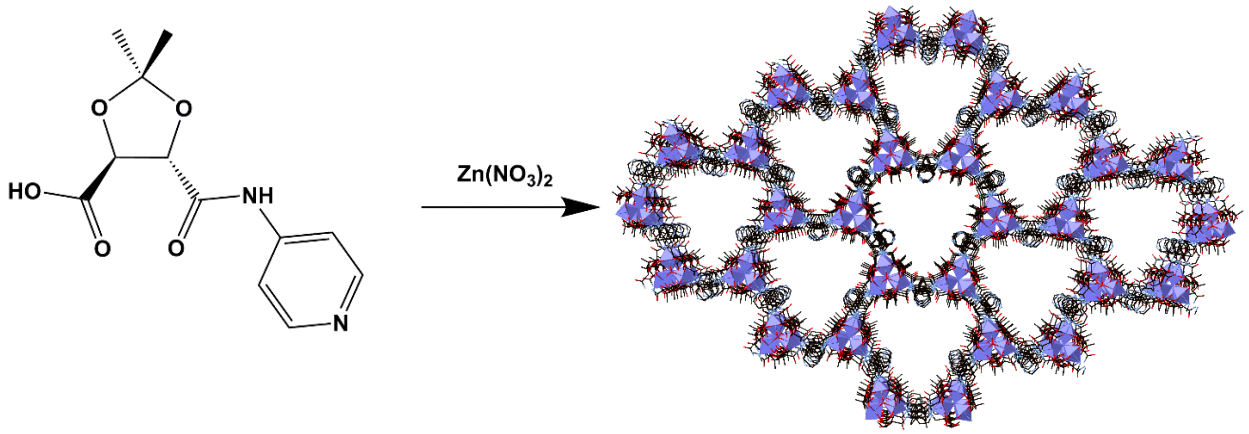

Figure 1.9. The tartaric acid derived pyridyl functionalised ligand used by Kim et al. (left), for the synthesis of a chiral MOF which showed enantioselective catalysis and separation (right).

The synthesis of chiral coordination polymers may also be achieved using exclusively achiral ligands. The use of exclusively achiral ligands will often form centrosymmetric networks. However they may also crystallise as non-centrosymmetric systems, removing the need for the synthesis of chiral ligands or the chiral pool strategy. The chirality in systems of exclusively achiral ligands may arise from chiral metal coordination or through the occurrence of a helicates within the network. Formation of a bulk homochiral sample by this approach can be difficult, as the crystals will usually form in a conglomerate.[113] In rare cases

of spontaneous resolution, the preferred crystallisation of one handedness will lead to a homochiral material, a process called second order spontaneous resolution.[114] Synthesis of homochiral MOFs with achiral ligands is also possible through seeding. If the crystals form as a conglomerate, a single crystal of one handedness may be used to seed the synthesis of a homochiral sample of the coordination polymer.[115] The memory of chirality effect is also a useful technique for the synthesis of homochiral coordination polymers and MOFs, as demonstrated by Morris and co-workers in 2007 when they reported the induction of chirality by (*S*)-aspartate into a network which involved only achiral building blocks.[116] The formation of a chiral coordination polymer with achiral ligands formed around a chiral guest can also be realised in the context of a chiral cation within the pores of the network. Train, Gruselle *et al*. reported the synthesis of the $[MnCr(oxalato)_3]^-$ network, which can be synthesised in both handednesses, based on the chirality of the alkyl side chain of the template cation.[117]

The chiral pool method can also be used for chiral induction of MOFs, as shown by the Bu group who reported the synthesis of MOFs with adamantane-1,3-dicarboxylic acid ligands and Mn^{II}, in which the chirality of the framework was controlled by the handedness of the camphoric acid which was used for chiral induction.[118] The amino acid proline has also been used to induce chirality in MOF-5 by distortion of the framework backbone, as the handedness of proline used in the reaction controlled the handedness of the framework, without being incorporated into the final structure.[116] Chiral ionic liquids have also been shown to induce chirality when used as the reaction medium for a MOF made of achiral ligands. The Morris group reported the reaction of 1,3,5-benzene tricarboxylic acid with Ni^{II} in a chiral ionic liquid which formed a homochiral MOF which did not incorporate any of the chiral ion in pores of the framework.[116]

In addition to the classical methods for chiral induction in infinite coordination networks, chirality can also be introduced by post synthetic modification. PSM may be used to add chiral functionality to a MOF, in order to increase its stereoselective applications. In 2009 Kim *et al.* demonstrated post synthetic insertion to create a chiral MOF by adding (*S*)-proline to the open metal sites of MIL-101, to produce a chiral MOF which showed catalytic activity in asymmetric aldol reactions.[119]

Chiral coordination polymers and MOFs have also been shown to have applications in nonlinear optics. Solid state second-order nonlinear optical materials, which are a class of materials which have the ability to double the frequency of an intense beam of laser light, only exist in non-centrosymmetric or polar materials.[120] The use of chiral ligands allows the engineering of coordination polymers into non-centrosymmetric environments, capable of nonlinear optics.[121]

1.3.4 Applications of chiral coordination polymers

Chiral MOFs have applications in three main areas, stereoselective catalysis, separation and sensing.[122] As chiral catalysis is one of the main avenues by which stereoselective synthesis can be achieved in organic chemistry, it has been major focus in the development of homochiral MOFs for applications. To be an effective chiral heterogeneous catalyst, the MOFs must have a stable framework and possess large and accessible pores, a catalytic centre and a chiral environment.[123] Homochiral MOFs for catalysis have been designed and synthesised using multiple classes of ligands including, but not limited to, amino acid and other chiral pool derived ligands, chiral molecules such as functionalised 1,1′-bi-2-naphthol (BINOL) ligands and metalloligands, as well as post-synthetic modification, which will be briefly reviewed herein.

As the coordination behaviour of amino acids is usually dominated by the chelate effect of the carboxylate and amine groups, they are not effective ligands for the synthesis of MOFs. Amino acids have therefore been combined with additional bridging ligands in order to form chiral MOFs. Such was the case with a series of MOFs incorporating aspartic acid and Cu^{II} or Ni^{II}, with dipyridyl coligands, either 4,4′-bipy or 1,2-di(4-pyridyl)ethylene (dpe). Protonation of the framework using HCl rendered a Brønsted acidic MOF which has modest catalytic activity, showing catalysis for methanolysis of *cis*-2,3-epoxybutane with up to 30% conversion and 17% ee.[124, 125] The advantages of the robust porosity of classical MOFs can be combined with the chirality of amino acids by adding the amino acids via PSM, as reported by Canivert *et al.* in 2015. The study was undertaken with three different MOFs, MIL-101, MIL-68 and UiO-66 which all traditionally use a terephthalic acid ligand, but in this case were synthesised with 2-aminoterephthalic acid to provide a site for PSM. Amino acids or short peptide chains were grafted to the MOF by microwave irradiation and the MOFs were shown to catalyse the aldol reaction of acetone and 4-nitrobenzaldehyde

with conversion up to 80% and 27% ee.[126] PSM with amino acids has also been shown by adding amino acids to metal centres, as demonstrated by Kim *et al.* in which proline was added to coordinatively unsaturated metal centres in a MOF to produce a chiral MOF that was capable of catalysing a stereoselective aldol reaction with up to 86% yield and 68% ee.[119] It is also possible to synthesise a chiral catalytic MOF by deprotecting the amino acid functionality in a MOF post synthetically, however the conditions necessary for deprotection of the amino acid will often lead to racemisation. To avoid this problem Telfer and co-workers reported a thermolabile approach to amino acid deprotection in which a Boc-protected proline on a biphenyl dicarboxylic acid ligand formed a chiral MOF with Zn^{II}. The Boc group could be removed in a single-crystal to single-crystal (SCSC) manner by heating in DMF under microwave radiation, maintaining an ee of 80% of the proline. The bulky protecting group was also shown to inhibit the interpenetration of the framework. The deprotected MOF catalysed the aldol reaction of acetone and 4-nitrobenzaldehyde with 29% ee.[127]

The axially chiral molecule BINOL has also been widely utilised as a ligand for chiral catalysis as it contains secondary functional groups and can be functionalised in multiple different positions to synthesise a range of ligands with varying coordinating groups and lengths. Such a highly functionalisable ligand is important for the synthesis of chiral MOFs with tuneable properties and pore sizes.[128] BINOL is also a well-known chiral auxiliary in organic chemistry for enantioselective homogenous catalysis.[129] Therefore the ability to place such a molecule into open channels of a porous framework is an important step towards the rational design and application of chiral molecules in enantioselective catalysis.[130]

The first BINOL containing MOF to catalyse chiral reactions was reported by Lin and co-workers. A phosphoric acid functionalised BINOL ligand formed a series of MOFs with lanthanide metal centres, and showed enantioselective catalysis for the reaction of benzaldehyde and cyanotrimethylsilane, affording mandelonitrile in a 69% yield. Unfortunately the product was essentially racemic, with an ee of < 5%. [131] Lin soon followed up the work with a 4-pyridyl functionalised BINOL ligand which formed a MOF with Cd^{II}. The MOF underwent PSM to bind a $[Ti(O^{i}Pr)_2]$ fragment to the BINOL hydroxyl groups which were lining the pores of the MOF, generating a MOF which was catalytically active for the addition of $ZnEt_2$ to

aromatic aldehydes to synthesise chiral secondary alcohols. The catalytic activity was investigated with a range of aromatic aldehydes, showing >99% yield and up to 93% ee.[132] The same group also reported an elegant study into the influence of pore size on the catalytic activity of BINOL MOFs, Figure 1.10. Four BINOL ligands of varying lengths that were functionalised with four carboxylate coordinating groups formed a series of four copper paddlewheel MOFs with identical structures and varying pore sizes. The MOFs could undergo PSM to incorporate a $[Ti(O^iPr)_2]$ fragment to form a series of eight functional chiral MOFs for asymmetric catalysis, four with $[Ti(O^iPr)_2]$ and four without. It was observed that with increasing pore size the post synthetically modified MOFs showed an increase in ee of 9%, 86%, 91% and 91% for the reaction of $ZnEt_2$ with aromatic aldehydes.[133] BINOL MOFs have also been used for many other reactions, as shown by Tanaka and co-workers with a copper paddle-wheel MOF utilising a dicarboxylic acid BINOL ligand, which showed up to a 54% yield and 45% ee for the enantioselective ring opening reactions of epoxides.[134] A different BINOL MOF, utilising a tetratopic carboxylate ligand, acted as an enantioselective catalyst for ring-opening of *meso*-epoxides with up to 89% ee. It was observed for this system that the yield and enantioselectivity of the MOF catalyst was highly sensitive towards the epoxide and aniline structures, as well as the reaction conditions.[135]

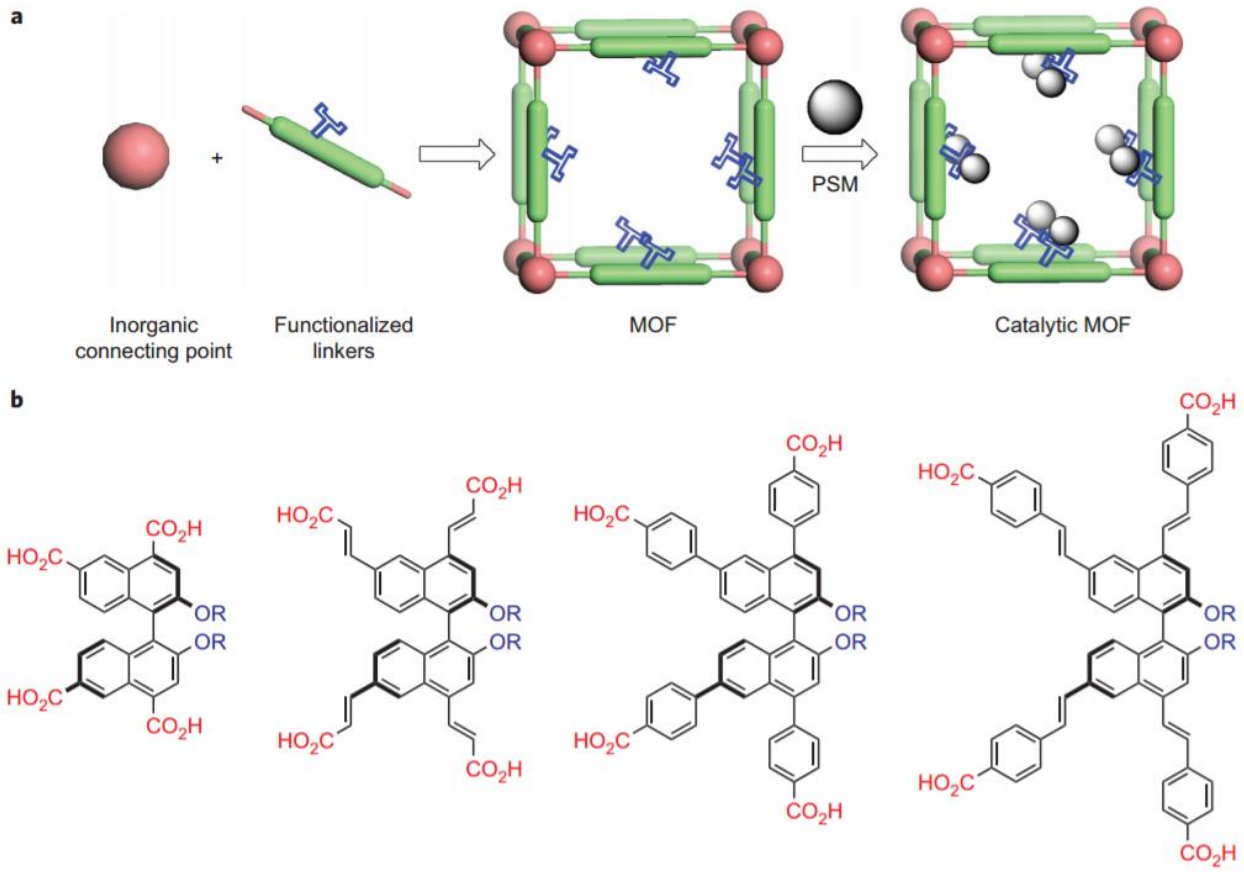

Figure 1.10. a) Schematic representation of the synthesis and PSM of the homochiral BINOL MOFs, b) the four ligands of varying lengths used for homochiral MOFs synthesis. Reprinted with permission from Macmillan Publishers Ltd: Nature Chemistry, 2, 838-846, 2010.

The pore size of MOFs has also been showed to have an influence on the enantioselectivity of reactions catalysed by BINOL containing MOFs. In 2016 the Tanaka group reported the synthesis of a dicarboxylic BINOL ligand that formed a 3D MOF when reacted with Cu^{II}. The MOF was shown to catalyse the Diels-Alder reaction between isoprene and *N*-ethyl maleimide with a yield of up to 81% and 75% ee.[136] The same group has also reported BINOL MOFs which show enantioselective aminolysis and alcoholysis of epoxides and sulfoxidation of sulfides with H_2O_2.[137-141] As can be seen, BINOL is a robust ligand for the synthesis of chiral MOFs that have been shown to have enantioselective catalytic properties for a range of reactions. Heterogeneous chiral catalysis may also be achieved with a MOF using catalytically active metal centres embedded within the ligands. This approach avoids the additional step of post synthetic modification of the MOF. The use of M(salen) metalloligands have been shown to be particularly effective for the synthesis of

chiral MOFs for stereoselective catalysis, catalysing a range of asymmetric organic transformations, including olefin oxidation, epoxidation and aziridination, cyclopropanation, sulphide oxidation and cyanosilation of aldehydes.[142-146] As the applications of M(salen) metalloligands is so broad, only a few examples will be discussed.

The Lin group reported an isoreticular series of MOFs with three Mn(salen)-based ligands of increasing length, which formed a series of five chiral MOFs, both interpenetrated and non-interpenetrated, with a range of pore sizes, Figure 1.11.[144] Although the MOFs underwent framework collapse upon removal of solvent, their porosity was confirmed by dye uptake experiments. All five MOFs acted as enantioselective catalysts for epoxidation reactions, with increased pore size leading to increased activity, suggesting that diffusion of the reactants into the pores strongly influences the reactivity. The catalytic activity of the two MOFs with the largest pore sizes rivalled that of the homogeneous control catalyst.[144] The catalytic activity of another M(salen) MOF has also been reported which displays superior catalytic activity to its homogenous equivalent. Two chiral MOFs with either VO(salen) or both VO(salen) and Cu(salen) metalloligands and Cd^{II} were reported that showed up to 99% conversion and 93% ee for the enantioselective cyanisation reaction between aldehydes and trimethylsilyl cyanide after oxidation of the VO(salen) ligand. Such remarkable stereoselectivity and yield was possible because the reaction was able to go through a VO-VO cooperative activation pathway due to the forced proximity of the VO(salen) moieties within the channels. The oxidised VO(salen) material was also utilised in a gram-scale synthesis of the natural products (*R*)- and (*S*)-tembamide.[147]

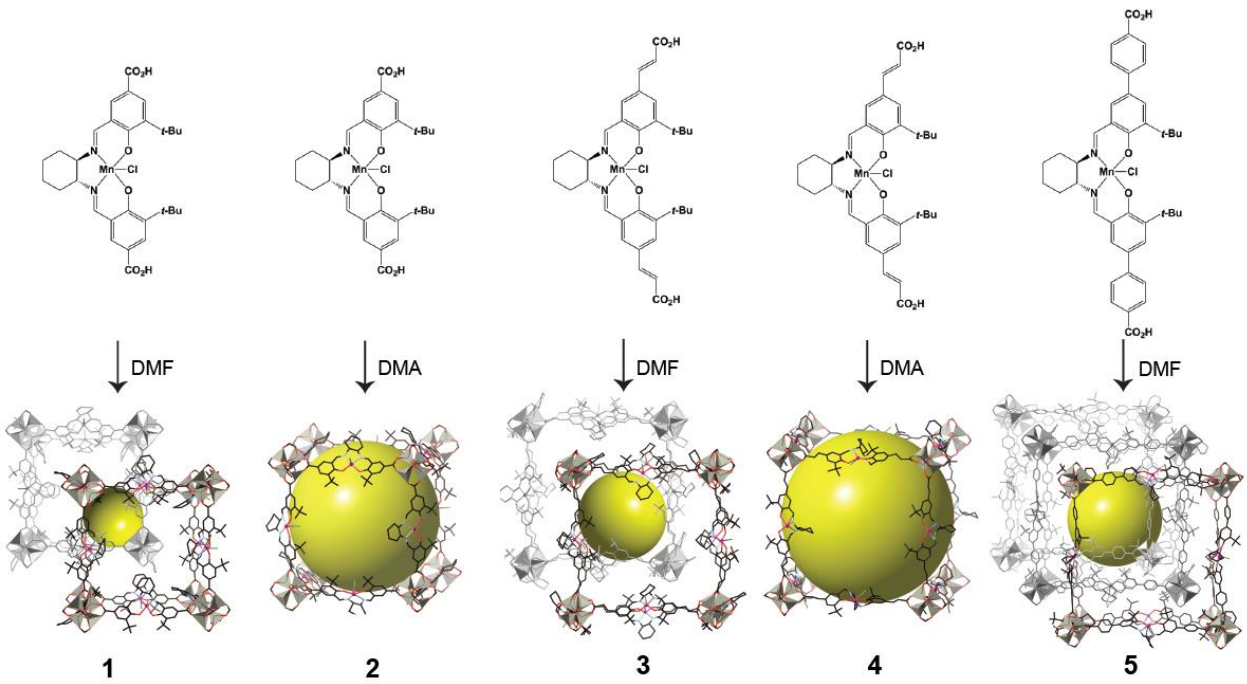

*Figure 1.11. The series of Mn(salen) MOFs reported by Lin. Materials **2** and **4** showed the highest catalytic activity due to their large pores.*

Although chiral catalysis is the preferred method for the synthesis of chiral molecules, it is not always practical and still may not lead to an enantiopure product. Chiral separation is therefore another important application of interest for chiral MOF materials. Chiral separation with homochiral MOFs may be achieved by enantioselective sorption, incorporating MOFs into membranes, growing chiral MOFs into thin films or by using the MOFs to make chiral stationary phases for HPLC or GC. Chiral MOFs may be an alternative to conventional HPLC or GC columns because they can be made to be stable, reliable and cost effective, and their tunability allows them to be tuned to the desired properties of the system.[148] Similar to chiral MOFs for catalysis, homochiral MOFs for separation have been developed with a range of ligands including cyclodextrins, amino acids and other chiral pool molecules, and BINOL and other ligands with axial chirality, among others which for the sake of brevity will be not discussed herein.[149, 150] Chiral MOFs have been shown to resolve racemic mixtures of many classes of molecules, including sulfoxides, *sec*-alcohols, β-lactams, benzoins, flavanones, epoxides, amines, alcohols, amino acids, bases and amides.[151-157]

Much of the early work in this area was investigating chiral MOFs for separation by enantioselective absorption. The combination of aspartic acid and 4,4′-bipy was shown by the Rosseinsky group to be a

suitable combination to make a family of chiral MOFs with Ni^{II} that could selectively adsorb one handedness of a chiral diol with up to 53% ee for the case of 2-methyl-2,4-pentanediol. Computational studies of the guest interactions with the pores showed that the mode of interaction is dependent on the pore surface and nature of the guest, rationalising the higher percentage ee achieved for 2-methyl-2,4-pentanediol in comparison to other short chain diols that were investigated.[124] Derivatives of amino acid may also be used as ligands, as was the case in a report by Zhang and co-workers in which either (*S*)- or (*R*)-proline was attached to 1,3-benzenedicarboxylic acid to make a ligand which formed MOFs with helical channels, the helicity of which depended on the handedness of the ligand. The chiral channels within the MOFs were a suitable size for separation of small chiral molecules, showing up to 68.3% ee for the separation of methyl lactate.[158] Post-synthetic modification is also a viable approach for the synthesis of chiral MOFs for enantioselective separation. The achiral MOF ZIF-8 was reported to undergo post-synthetic ligand substitution to incorporate the amino acid (*R*)-histidine. The water stability of ZIF-8 combined with its inherent chirality from the (*R*)-histidine enabled the material to be used to separate the amino acids alanine and glutamic acid from water/ethanol mixtures with 78% and 79% ee, respectively.[159] Although enantioselective sorption with chiral MOFs acts as proof-of-concept that chiral MOFs can enantioselectively interact with chiral guests, in order to be scaled up for real-world applications it is much more suitable for MOFs to be incorporated into HPLC or GC columns or membranes.[160, 161] The chiral pool method has been extensively employed in the synthesis of porous MOFs for chiral resolution by chromatography, including the use of amino acids, lactic acid, mandelic acid and camphoric acid.[160, 162] The first reported enantioselective separation employing a column made of a chiral MOF used the chiral pool method, namely the synthesis of a MOF with (*S*)-lactic acid and 1,4-benzenedicarboxylic acid with Zn^{II} which was packed into a 33 cm glass tube. The column showed baseline separation of D/L-methyl phenyl sulfoxide, and some separation of other sulfoxides.[163] (*S*)-Leucine was used to induce chirality in a 4,4′-biphenyldicarboxylic acid MOF with Cd^{II} and this MOF was used as a chiral stationary phase in a steel column which showed separation of a range of racemic molecules including alcohols, ketones, flavone, phenol, bases and amides. [164, 165]

Camphoric acid has been widely utilised for the synthesis of homochiral MOFs for use in columns for HPLC and GC. A series of isoreticular MOFs with (*R*)-camphoric acid and pyridyl coligands of varying lengths, namely diazabicyclo[2.2.2]octane (dabco), 4,4′-bipy and 1,4-di(4-pyridyl)benzene (dpb), had increasing void volume with increasing coligand length and were therefore used to investigate the influence of pore size on enantioselective separation D/L-limonene. The MOFs were grown into thin films by layer-by-layer liquid-phase epitaxy, and are referred to as SURMOFs (surface mounted MOFs).[166] It was observed that the MOF with medium sized pores showed the best enantioselectivity, as the pore is a similar size to the analyte, maximising the interaction of the analyte with the chiral functionality of the ligand whilst still allowing the analyte to move within the pores.[167] SURMOFs of [Cu_2((*S*)-cam)$_2$(L)] (L=4,4′-bipy or dabco) mounted on a polymer from a natural marine organism, 3,4-dihydroxy-l-phenylalanine, have also been used to make a column for GC, showing baseline separation of D/L-methyl lactate.[168] These results, among others not discussed herein, establish that the use of SURMOFs for HPLC and GC columns is a promising alternative to traditional columns.[169]

As with chiral catalysis, BINOL-derived ligands have been widely used for the synthesis of chiral MOFs for enantioselective separation applications. A dicarboxylate functionalised BINOL ligand was reported that formed a MOF-silica composite material when reacted with Cu^{II} and monodisperse silica gel. [170] The MOF-silica composite was packed into a steel column, and its chiral resolution properties were tested with various chiral sulfoxides, showing efficient separation of 11 different racemates.[170] The chiral resolution of sulfoxides has been extensively investigated because they are a class of valuable chiral auxiliaries for asymmetric synthesis and important ligands for enantioselective catalysis.[170] The Tanaka group followed up this work with the synthesis of three homochiral MOFs with the same BINOL ligand and Cu^{II} or Zn^{II}, which were packed into columns and showed remarkable chiral recognition towards a range of racemates including sulfoxides, benzoins, epoxides, β-lactams and flavanones. The variety of racemates that could be separated by these columns demonstrates that chiral HPLC with a chiral MOF stationary phase is indeed a viable design strategy.[154]

The isophthalate functionalised 1,1′-biphenol molecule, which has axially chirality, has been shown to form MOFs capable of enantioselective adsorption and separation when reacted with Mn^{II}. These homochiral MOFs were first investigated for enantiosorption of racemic 1-phenylethylamine and showed enantioselective sorption of the (*R*) enantiomer with up to 91% ee. Amines were investigated because they are key intermediates in the synthesis of many pharmaceutical compounds. The MOFs also showed enantioselective sorption of benzyl amine and ten of its derivatives. Encouraged by these results, a HPLC column was prepared from the most promising MOF material. All attempts at separating 1-phenylethylamine were unsuccessful, due to its high affinity for the column. Acylation of the amines was therefore carried out to improve the selectivity and separation of these compounds on the chiral MOF column, showing baseline separation for three different analytes.[171]

Cyclodextrin (CD) MOFs have also been shown to be a versatile separation medium. The Stoddart group reported the synthesis of a MOF made from γ-cyclodextrin and alkali metal salts.[172, 173] As CD is chiral, having 40 stereocentres per CD γ-torus, this CD-MOF was shown to separate a large range of organic compounds, including haloaromatics, pinenes, terpines, limonene and 1-phenylethanol.[174] The variety of routes to the synthesis of chiral MOFs capable of enantioselective separation and the large range of chiral analytes that have been resolved by these materials demonstrates that this is an important area of research that is likely to be scaled up into real-world applications in the future.

Chiral MOFs have also been shown, to a lesser extent to that of separation and catalysis, to have applications as fluorescent sensors. The Lin group reported a MOF with a tetrabenzoic acid BINOL derived ligand and Cd^{II} which shows fluorescence. However the fluorescence was quenched by the addition of chiral amino alcohols, as they hydrogen-bond with the binaphthol moieties of the BINOL ligands which are lining the pores of the MOF.[175] A chiral fluorescent MOF was also reported that was an enantioselective sensor for histidine. The MOF was formed from a tetralactic acid substituted pyrene ligand with Zn^{II}, and was found to be highly fluorescent with a quantum yield of 46%. The fluorescence was quenched by histidine, with more effective quenching of (*R*)-histidine than (*S*)-histidine, and was therefore the first chiral MOF capable of differentiating between enantiomers through fluorescence.[176]

The production of enantiopure compounds is crucial to the pharmaceutical, agrochemical, flavour and fragrances industries, leading to a huge demand for chiral molecules. [177]

1.4 Discrete coordination complexes

Coordination polymers and MOFs are a readily tuneable class of materials that have found applications in a broad range of areas. Their polymeric structure however leads to their properties being applicable only in the solid state. Discrete coordination compounds, particularly cage complexes, have also garnered much interest, as they may be utilised in the solid state or in solution, drastically increasing the modes by which they may be used for different applications. The design of discrete coordination compounds is similar to that of coordination polymers and MOFs, in that the size, shape and functionality of the ligand and the charge and coordination geometry of the metal must all be taken into account. However their design and synthesis differ somewhat in that the ligand, metal and synthesis must all be considered to inhibit the formation of polymeric materials, and lead to the formation of discrete coordination compounds of desired structure and properties.

There are several different design strategies for the rational design and synthesis of discrete coordination assemblies, however they all rely on the precise control of ligand geometry and binding sites, and the geometry and available coordination sites of the metal ions involved.[178] The metal ions utilised may have all their coordination sites occupied by the ligands that bridge them together to form cage complexes, or they may be cis-protected, in the case of square planar Pt^{II} and Pd^{II}, in order to give them convergent coordination geometry. The seminal studies by the Fujita group into the rational synthesis of molecular squares used the cis-protected metal approach, to cap Pd^{II} ions to give a cis coordination geometry and allow them to be bridged into a square by linear bidentate 4,4′-bipy ligand, Figure 1.12.[179] These design strategies have been utilised over recently years to synthesise a plethora of discrete metallosupramolecular complexes.[180-182]

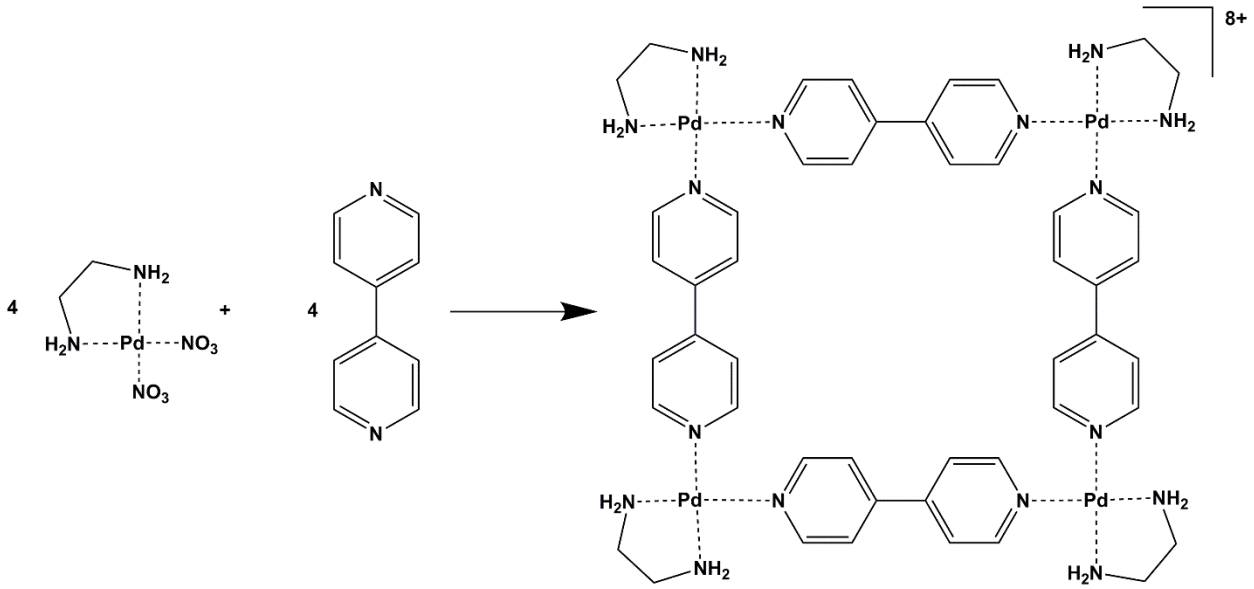

Figure 1.12. The rational synthesis of a square complex utilising cis-protected Pd^{II} and 4,4'-bipy.

1.4.1 Coordination cage complexes

Early work on discrete coordination assemblies by Lehn and Sauvage, Nobel Prize winners in the field, focused on the utilisation of supramolecular self-assembly principles for the synthesis of complexes such as catenanes, rotaxanes, knots, rings and related species.[1, 14, 183-187] Over recent years this area of discrete coordination complexes has led to the synthesis of metallosupramolecular cage complexes as "molecular flasks", cage complexes which may encapsulate guest molecules.[188-192] Coordination cage complexes may take the form of Platonic solids, which have faces of one type of polygon, Archimedean solids, which have faces of two or more regular polygons with identical vertices, or Johnson solids, which have faces of two or more regular polygons and different vertices.[182] Metallosupramolecular cage complexes have found applications in a variety of areas such as catalysis,[31, 193, 194] separation,[195, 196] gas sequestration[197-199] and stabilisation of reactive species.[200]

The simplest platonic solid, the tetrahedron, may be assembled through different metal-ligand stoichiometries, M_4L_6 and M_4L_4. In both M_4L_6 and M_4L_4 cages the metals form the vertices of the cage. In the case of M_4L_6 cages the ligands form the edges, and in the case of M_4L_6 cages the ligands form the faces of the tetrahedron. M_4L_6 cages may also be formed in which the ligands form the faces and the metals

occupy each of the edges of the cage.[201] The first metallosupramolecular tetrahedron was serendipitously synthesised by Saalfrank and co-workers, which was a M_4L_6 tetrahedra with Mg^{II} corners, bridged by a malonic acid based ligand.[202] Following on from this work, the groups of Raymond,[203-205] McCleverty,[206, 207] Ward,[208-211] Nitschke,[195, 212-214] Lindoy,[215, 216] Stang[217-219] and Severin[220, 221] have reported a number of tetrahedral cages of different forms.

Cubic cage complexes may be formed by two different methods, those of edge-directed self-assembly, in which 12 ditopic ligands form the edges of the cube and eight tritopic 90° metal units form the corners, or face-directed self-assembly, in which six tetratopic units form the faces of the cube and 12 ditopic 90° units are on the edges, leaving the corners empty.[222-224] The higher order platonic solids of octahedra and dodecahedra are more difficult to form, as they require the combination of a larger number of ligands and metal ions and often form with a high degree of void space. Reports of higher order polyhedra are therefore much rarer in the literature than tetrahedral cage complexes.[225-230]

An example of a tetrahedral cage with octahedral metal centres and bis-bidentate ligands has been reported by Lindoy and co-workers, Figure 1.13.[215] The combination of aryl-linked bis-β-diketonato ligands with Fe^{III} metal centres formed a $[Fe_4L_6]$ edge capped tetrahedral cage was shown by its single crystal X-ray structure to encapsulate four THF molecules. A prominent example of an octahedral coordination cage was reported by the Fuijta group. [225] The cage, with a 12+ charge, was formed with four rigid tris-pyridyl ligands occupying alternating faces of the octahedron, and six square planar Pd^{II} metal centres which were cis protected with ethylene diamine, forming the vertices of the octahedron, Figure 1.13.

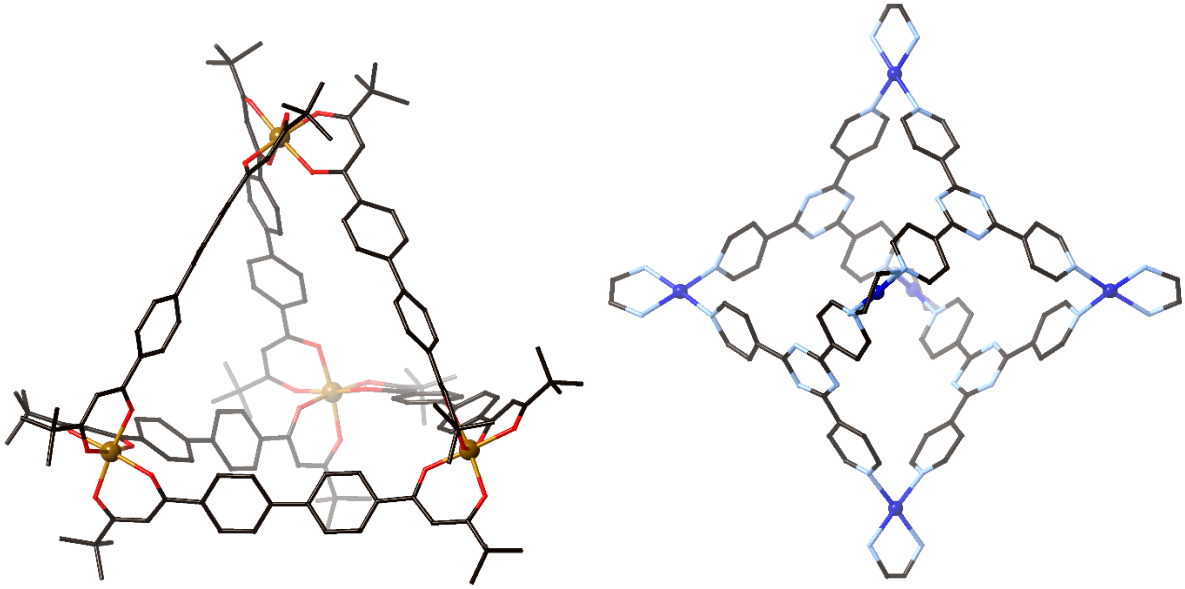

Figure 1.13. The [Fe_4L_6] edge capped tetrahedral cage reported by Lindoy and co-workers (left),[215] and the octahedral face capped coordination cage reported by the Fuijta group (right).[225]

Coordination cages may be cationic, anionic or neutral, depending on the combination of charges of the ligands and metal centres. Early examples of anionic tetrahedral cages were reported by the Raymond group, which used metal ions such as Ga^{III}, Al^{III}, In^{III} and Fe^{III}, with octahedral coordination geometry, with bis-catechol- and bis-hydroxamate-based ligands.[203, 204] Anionic cages have been shown to accommodate cationic guests, and in some case may only form in the presence of templating anionic guests.[231, 232] Cationic tetrahedral cages have been reported widely by the McCleverty, Ward and Nitschke groups, containing dipyridyl- or bis-diimine- based ligands which may vary widely through the ligand spacers between the coordianting groups. The combination of these neutral bis-bidentate ligands with metal ions that adopt an octahedral coordination geometry has led to the synthesis of a plethora of cationic tetrahdral cages that have been shown to have many interesting properties and applications.[195, 206, 209] Neutral tetrahedral cages have been reported by the Lindoy group, through the combination of Fe^{III} metal centres and bis-β-diketonato ligands (*vide supra*).[215, 233] The majority of the reported higher order polyhedral cages have been cationic, as they are formed by the combination of metal cations and neutral ligands[143, 208, 223, 234] with a few notable exceptions, such as the neutral cages formed by the combination of paddlewheel SBUs and carboxylate

ligands.[228, 235] Neutral coordination cages have been reported to a lesser extent than cationic or anion cages, as they require the selection of suitable ligands and metal centres in order to achieve charge balance.

Cage complexes which are not platonic or archimedean solids include trigonal bipyramids, double squares, adamantanoids, trigonal prisms, tetragonal prisms, molecular boxes and molecular spheres. Trigonal bipyramids are M_3L_2 complexes which combine two tritopic, tetrahedral donors and three ditopic 90° units.[236] The same combination of metal and ligands may form M_6L_4 double square complexes, when more flexible ligands are used.[237] Adamantanoids are similar to tetrahedra, as they both have edges kinked at 109.5° at their point of bisection, and maintain their overall symmetry. The combination of six 120° ditopic units and four 109.5° units can lead to the self-assembly of an adamantanoid cage.[238, 239] For the sake of brevity, the synthesis and structure of trigonal prisms,[240, 241] tetragonal prisms,[242] molecular boxes[241] and molecular spheres[243] will not be discussed in detail.

1.4.3 Applications of coordination cage complexes

In a similar manner to coordination polymers and MOFs, a variety of applications are possible for cage complexes. Due to their discrete nature, coordination cage complexes may be utilised for applications in solution, as well as in the solid state. The majority of properties and applications of coordination cage complexes arise from the void space within the cage.[244]

The cavity within coordination cage complexes enables them to have selective guest binding properties. The selectivity of cage complexes is due to an interplay between the guest and host, and based on the size, shape, bonding and electronic factors inherent in both.[189] There are a myriad of reported examples of cage complexes with selective and reversible guest encapsulation in solution.[245-251] Coordination cages that are made with neutral ligands will be cationic, due to the charge of the metal ions. Cationic coordination cages have been shown to have a range of anion binding properties, including strong and selective anion binding in competitive environments such as water, and anion exchange through the windows of the cage.[252] The selectivity of the cages may also be changed based on the pH of the solution, as shown by the Ward group in the report of a cubic cage complex which would bind three different guests based on the pH of the solution and therefore the charge of the guests.[253] The Rebek group have also shown that it is possible to

control the encapsulation of guests with light, as photoisomerisation of the guest causes it to be "ejected" from the cage due to shape incompatibility of the guest.[254]

The thoughtful selection of metal ions for coordination cages can lead to interesting properties such as luminescence and magnetism. The use of a Ru^{II}-pyridyl functionalised ligand for the synthesis of a Pd_2L_4 cage formed a luminescent coordination cage complex with an exceptionally high quantum yield of 66%.[255] The selection of appropriate metal centres, such as Fe^{II}, can also form cage complexes which display spin crossover properties, examples of which include reports by the Kruger group with tetrahedral cages, and the Batten group with nanoball complexes.[198, 256]

The selective guest binding of cage complexes enables them to have applications in separations, selective guest binding, drug delivery and catalysis.[31, 194, 257-260] An exciting application of coordination cages which has emerged in the last few years is the binding of chemical warfare agents.[261, 262] The Ward group reported a luminescent cubic coordination cage which showed luminescent quenching upon binding of chemical warfare agent simulants.[263] Metallosupramolecular cage complexes may also be used in stabilisation of reactive species. In 2009 the Nitschke group reported a tetrahedral metallosupramolecular cage which encapsulated white phosphorus molecules, making these highly air-sensitive molecules air-stable and water-soluble, as the cages were too small to allow for formation of the oxidised species of white phosphorus.[264]

Coordination cages have also been shown to catalyse reactions on the interior of the cages in such a way that different products form than if the reaction took place outside the cage. The Fujita group reported the Diels-Alder reaction of malemides with anthracene molecules, in which the addition of the malemides occurred at the terminal rather than central position of the anthracene molecule when carried out in a Pd^{II} cage.[265] The Ward group have also reported a multifunctional water-soluble cubic cage, which was shown to catalyse a Kemp elimination reaction with very high rate enhancement of the reaction inside the cage in comparison to the reaction carried out in the absence of the cage.[266]

Metallosupramolecular cages have also been used as drug delivery vectors, as they may increase solubility, regulate drug release and overcome drug resistance mechanisms, which are common issues in medicine.

[257, 267, 268] Cisplatin, the preferred drug to treat many types of cancers, has poor solubility, requiring intravenous administration. Encapsulation of cisplatin in a water soluble cage may overcome this issue. Crowley reported a $[Pd_2L_4]^{4+}$ cage with pyridyl ligands which encapsulated two molecules of cisplatin. Unfortunately, release of the guest was achieved only through disassembly of the cage by addition of a competing ligand.[269] The Ward group reported a pH dependent-cationic cubic cage which strongly binds the neutral drug molecules aspirin, amantadine and nicotine. Decrease in pH leads to protonation of the guest, decreasing its binding affinity and leading to release of the guest from the cage.[269] Additional metallosupramolecular cages have been reported for encapsulation of drug and prodrug molecules.[246, 247]

The post synthetic modification of cages has been used to introduce new functionality, change solubility, trap species out of equilibrium and construct interlocked species and polymers.[270-272] The Zhou group reported a series of cuboctahedron coordination cages which incorporated copper paddlewheel nodes and ligands which decorated the outside of the cage with alkene groups. The cages could be post synthetically modified by click chemistry in order to make them water soluble, and they showed controlled drug release of the anti-cancer drug 5-fluorouracil.[273]

1.4.2 Chiral coordination cage complexes

As with chiral coordination polymers and MOFs, coordination cage complexes may also be designed with chiral functionality. Chirality may be added by the same techniques utilised for chiral host-guest complexes, coordination polymers and MOFs (see Section 1.2.3). The design and synthesis of chiral macrocyclic complexes and hydrogen-bonded cages and their applications are well established,[274-278] and are beyond the scope of this discussion.

In the formation of chiral coordination cages, the most commonly utilised method is the use of achiral ligands with bidentate coordinating groups, which coordinate to an octahedral metal, inducing chirality around the metal centre. Tetrahedral cages synthesised by this method have four metal centres, at the corners of the tetrahedron, and may form as chiral cages with either ΛΛΛΛ or ΔΔΔΔ configuration, displaying *T*-symmetry, due to stereochemical communication between the metal centres through the ligands.[201] The tendency for all of the metal centres within the cage to be the same handedness depends on

the number, nature and geometry of ligands, statistical probability, encapsulated anions and stereochemical coupling between ligands.[201, 279, 280] Tetrahedral cages may also form with a mixture of Δ and Λ metal centres, with ΛΛΛΔ or ΔΔΔΛ metal centres, displaying C_3-symmetry, or with ΛΛΔΔ metal centres, displaying S_4-symmetry. The lower symmetry tetrahedra require the ligands to be in more than one conformation within the assembly. Chiral tetrahedral cages have been widely reported by Nitschke,[195, 281] Raymond,[282, 283] Ward[284] and others.[233, 285] Higher order polyhedral cages may also be formed with achiral ligands, with the added complexity of the increase in number of metal nodes leading to an increase in possible combinations of chiral centres.[29, 143, 286-288] As with coordination polymers and MOFs however, even when the cages form with metal centres of like handedness, the use of achiral ligands for synthesis of chiral cages will commonly form a racemic mixture of the cages. Although enantiopure cages may be formed with achiral ligands, resolution of the cages in order to access a homochiral sample is difficult. Apart from the rare phenomenon of spontaneous resolution,[289] other reported processes to separate chiral cages include cocrystalisation with a chiral counterion[290] or chromatographic separation.[291]

The most reliable method for the synthesis of homochiral coordination cages is the use of enantiopure ligands. Chiral ligands for the synthesis of chiral coordination cages have been reported with many sources of chirality, including BINOL based ligands with axial chirality,[292-294] ligands functionalised with amino acids and other chiral pool molecules,[295, 296] metalloligands with tris-bidentate metal coordination,[297] as well as other ligands with stereogenic centres, Figure 1.14.[298-300] In the case of tetrahedral cages with octahedral metal centres and bidentate ligands, adding chiral functionality to the periphery of the ligands can force the metal centres to be all the same handedness, and therefore form homochiral cages.[300-302]

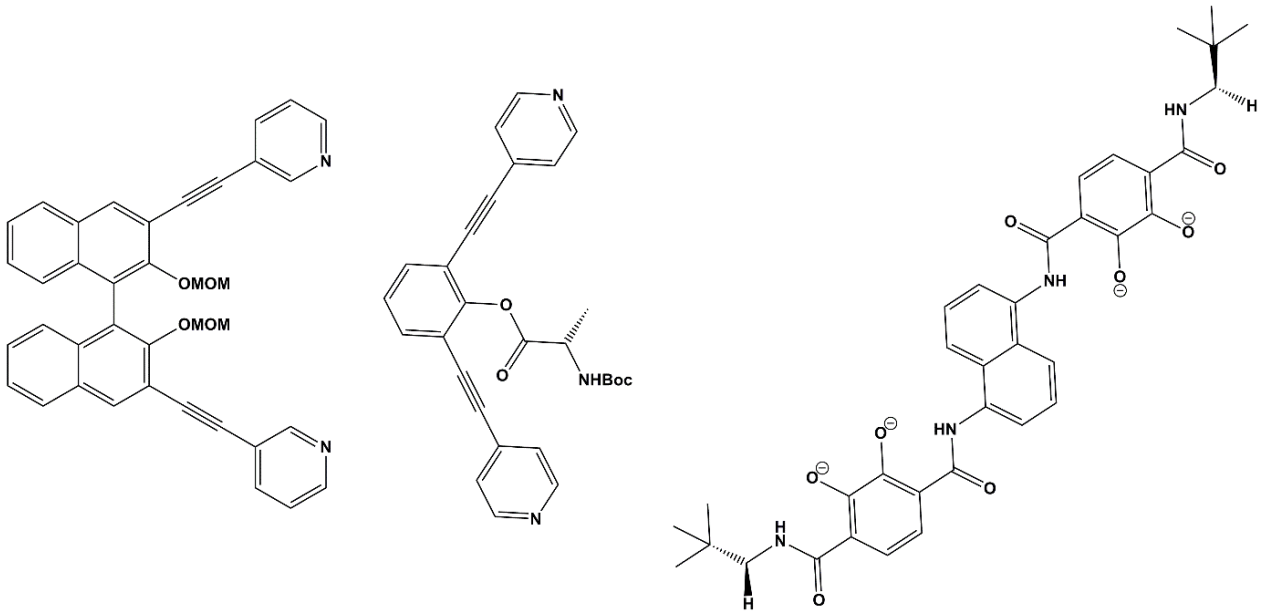

Figure 1.14. Selected examples of enantiopure ligands which have been reported in the synthesis of homochiral coordination cages. A BINOL group functionalised with pyridyl coordinating groups (left), a bent dipyridyl ligand functionalised with N-protected (S)-alanine (centre) and a bis-catechol ligand with pendant chiral groups, in which three catechol groups coordinate to each octahedral metal centre, inducing chirality around the metal (right).

An additional class of chiral coordination compounds that were not discussed in the context of infinite systems is that of helicates[303] Helicates possess chirality by the ligands twisting around a central axis as they bridge between metal centres.[304] Helicates may be formed by chiral ligands, or through spontaneous resolution of achiral ligands.[305, 306] The Raymond group reported the chiral induction of dinuclear triple-stranded helicates from achiral ligands by chiral cations.[307] However the use of achiral ligands also risks the formation of achiral mesocates instead of helicates, or the formation of a racemic mixture of helicates of opposite handedness.[308]

There are selected examples of inducing chirality in a coordination cage through alternative methods to those discussed above. It is possible to induce chirality in a cage by using chiral auxiliary ligands. The first example of this was by the group of Stang in 2006, in which a tetrahedral cage was synthesised with tritopic pyridyl ligands and Pd^{II} or Pt^{II} metal centres, in which the metal coordination sphere was completed by coordination of chiral BINAP ligands, which led to the formation of the chiral cages with *T* symmetry.[309]

It has also been observed that tetrahedral cages with octahedral metal centres and achiral bidentate ligands may selectively form with all metal centres of the same handedness, depending on the anion encapsulated within them.[310] The chiral memory effect has also been observed for chiral coordination cages. The first example of this was reported by the Raymond group, in which a tetrahedral cage was formed in an enantiopure form by crystallisation with a chiral counterion. The chirality of the cage was maintained after the exchange of the chiral counterion for an achiral counterion.[311] The memory of chirality effect was also demonstrated by the Nitschke group, in which a homochiral M_4L_4 tetrahedral cage which was synthesised with chiral ligands maintained its chirality upon replacement of the chiral ligands with achiral ligands.[302]

1.4.3 Applications of chiral coordination cage complexes

As there as several techniques for the synthesis of chiral coordination cages that incorporate a chiral void within them, chiral coordination cages are a class of materials which are suitable for investigation for applications in areas such as enantioselective recognition and guest binding, chiral catalysis, chiral separation, non-linear optics and chiral sensing.[182, 312]

Chiral recognition is the preferential binding of one enantiomer to a chiral host which is based on the difference in stability of the diastereoisomeric complexes formed between the different enantiomers and the host. As discussed in the context of chiral host-guest chemistry (*vide supra*), chiral recognition usually requires three simultaneous interactions, with at least one being stereochemically dependent.[25] Chiral recognition is a pre-requisite for the application of chiral coordination cages in chiral separation or sensing. Enantioselective guest binding has been observed by the Raymond group with a chiral $[Ga_4L_6]^{12-}$ tetrahedral cage. Encapsulation of a chiral ruthenium complex was observed to occur in an enantioselective manner due to the chiral cavity within the cage, as monitored by ^{1}H-NMR spectroscopy.[313]

Chiral sensing by chiral coordination cages is often measured by the fluorescent output of the cage complex. An elegant example of this was reported by the Cui group in 2012 in which an enantiopure pyridyl functionalised ligand formed a fluorescent quadruple stranded helicate cage with Zn^{II}, with a chiral amphiphilic cavity. The cage exhibited enantioselective fluorescence enhancement with amino acids in solution. This work was followed up by the same group with a report of the fluorescence enhancement of

this cage by saccharides in solution, with enantioselectivity factors of 2.4 – 4.9, and enantioselectivity factors of 1.3 – 3.6 upon interaction with chiral amines in the solid state.

Although enantioselective recognition of chiral molecules by chiral coordination cages has been well established, the enantioseparation of chiral molecules by chiral cages remains a challenge, with only a few reported examples. In 2004 the Raymond group reported a chiral water-soluble $[Ga_4L_6]^{12-}$ tetrahedral cage with a hydrophobic cavity which could encapsulate small hydrophobic molecules. The encapsulation of the chiral molecules was monitored by the signals of the host-guest diastereomers by ^{1}H-NMR spectroscopy and showed diastereomer excesses (de) of up to 54% in the case of fenchone, Figure 1.15.[314] The Cui group also reported the synthesis of a chiral tetrahedral cage made from functionalised chiral 1,1′-biphenyl ligand, which showed enantioselectivity of up to 99.5% when used as a host in the crystallisation of racemic alcohols.[315] Recently a homochiral octahedral complex with chiral Ru^{II} stereocentres has been reported which shows enantioseparation of atropisomeric molecules in solution, with the highest ee of 62% for the resolution of 1,1′-spirobiindane-7,7′-diol.[316] These reports represent proof of concept for the separation of small chiral molecules using chiral coordination cages, providing impetus for further research into this area in order to achieve complete resolution of racemic mixtures of chiral molecules.

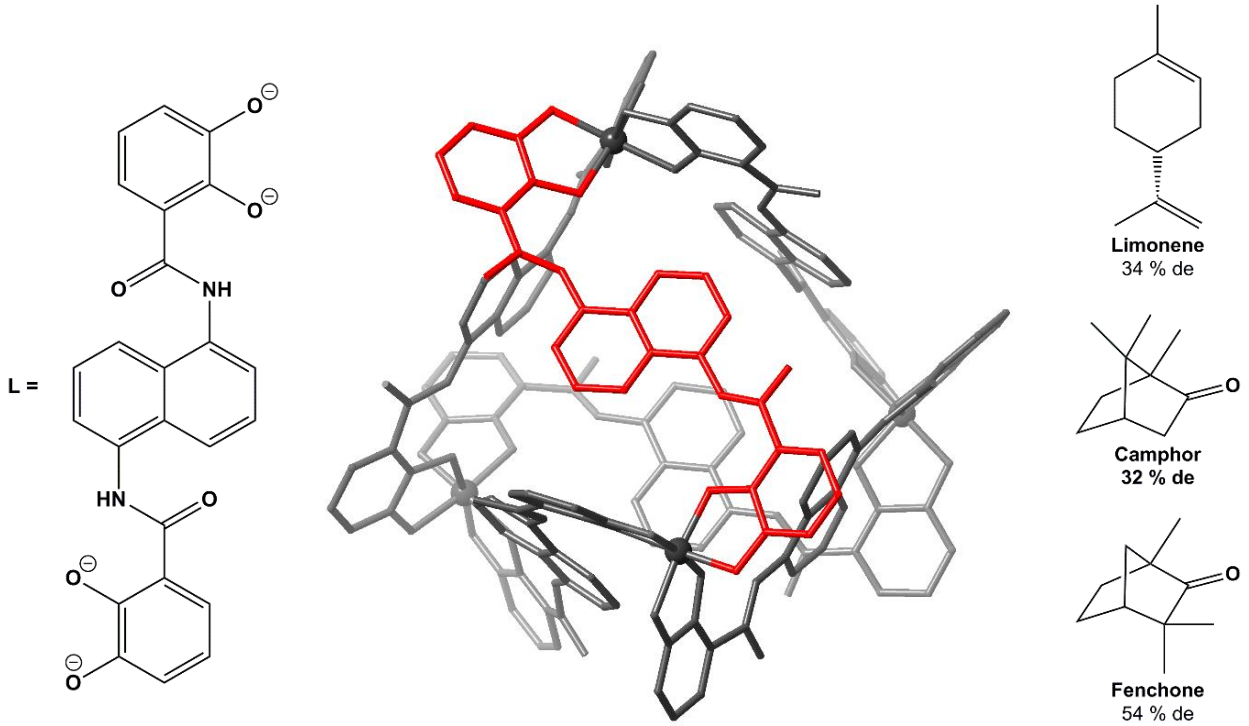

Figure 1.15. An example of the $[Ga_4L_6]^{12-}$ cages reported by Raymond, which showed enantioselective separation of small chiral molecules by encapsulation within the cage. The ligand (left), the cage shown as stick model (with the exception of the metals). All hydrogen atoms are omitted for clarity (centre). The chiral molecules which were separated through interaction with cage, and the diastereomer excesses which were observed (right).

The application of chiral coordination cages in enantioselective catalysis has been well developed in recent years. The encapsulation of starting materials may lead to the progress of the reaction in an enantioselective manner, or may form products which are not possible in the absence of the cage. The $[Ga_4L_6]^{12-}$ chiral cage reported by Raymond has been shown to catalyse a 3-aza-Cope rearrangement, leading to enantioselective formation of chiral aldehydes.[317, 318] This chiral $[Ga_4L_6]^{12-}$ cage is an outstanding compound, as it has been used in the catalysis of many enantioselective reactions, such as the Nazarov cyclisation of pentenediols, acid-catalysed hydrolysis of orthoformates, isomerisation of allylic alcohols and intramolecular hydroalkoxylation of allenes.[319-323] The Pd^{II} octahedral cage reported by Fuijta has been functionalised with chiral diamine capping ligands and shows up to 50% ee in [2 + 2] olefin cross coupling reactions between fluoranthene and maleimide derivatives.[324]

1.5 Ligands utilised in this study

1.5.1 Ditopic ligands

Rigid, ditopic carboxylate linkers have been well studied since the beginning of the MOF field.[65, 325] The use of rigid ligands will increase predictability in the formation of MOFs,[65] in contrast to flexible ligand that may adopt multiple different conformations and therefore tend to form MOFs with less predictability.[326] Depending on the metal node used and the ligands length, flexibility and substitution, an exceptional range of coordination polymers and MOFs can be formed.[327, 328] For example, a 4-connected paddlewheel cluster formed with two metal cations and four carboxylate groups may form 1D, 2D or 3D networks, depending on the relative angle between the two coordinating carboxylate groups.[329] The combination of copper paddlewheel clusters and ditopic linkers has also been shown to form a range of metal organic polyhedra (MOPs) in which the size of the cage is increased in conjunction with the increase in length of the ligand, providing that the dihedral angle of the ligand is maintained.[329] Using rigid, ditopic carboxylate ligands is advantageous due to the formation of predictable coordination compounds. In the synthesis of new materials, semi-rigid ligands have an advantage of being able to adopt different geometries as necessary in order to form a coordination network, dependent on the reaction conditions.[327]

1.5.2 Mixed ligand coordination networks

Early development in field of coordination chemistry focused on the synthesis of coordination compounds with one type of ligand, however the field has also advanced to include coordination polymers incorporating more than one type of ligand, as they may form coordination compounds which are otherwise unobtainable.[330] The combination of carboxylate and pyridyl linkers is the most appropriate and reliable combination of ligand classes for the synthesis of a wide range of coordination networks, as they are a good balance of charge balance and multiple coordinating groups which will fit around a metal centre. The combination of multiple carboxylate ligands would lead to an excess of negatively charged groups, and the combination of multiple pyridyl groups would be too bulky to fit around a single metal centre. Commonly the carboxylate ligands form a 2D sheet, and the metal nodes in the sheets are pillared by the dipyridyl

ligands into a 3D network.[331, 332] The advantage of these pillared networks is that the material can be functionalised using dipyridyl linkers with additional functional groups, while maintaining the same network topology. Increasing the ligand length will act to increase the size of the pores, as shown by the Cao group in 2011, when they reported a series of isostructural 3D coordination polymers in which 2D sheets of $[Cd_4(L)]$ (L = tetrakis[(3,5-dicarboxyphenoxy)methyl]methane) were pillared by dipyridyl ligands.[333] The dipyridyl ligands utilised were 4,4′-bipyridine, 4,4′-azopyridine and 2,4-bis(4-pyridyl)ethane, and increasing the length of the ligand correlated with increased pore size of the material, Figure 1.16. Functionalisation of the pyridyl ligand can also act to change the properties of the material, such as the flexibility and hydrophobicity of the pores.[334] Pillared-layer MOFs have been shown to have properties including selective guest encapsulation, structural flexibility, gas sorption, luminescence and catalysis.[332, 333, 335-338]

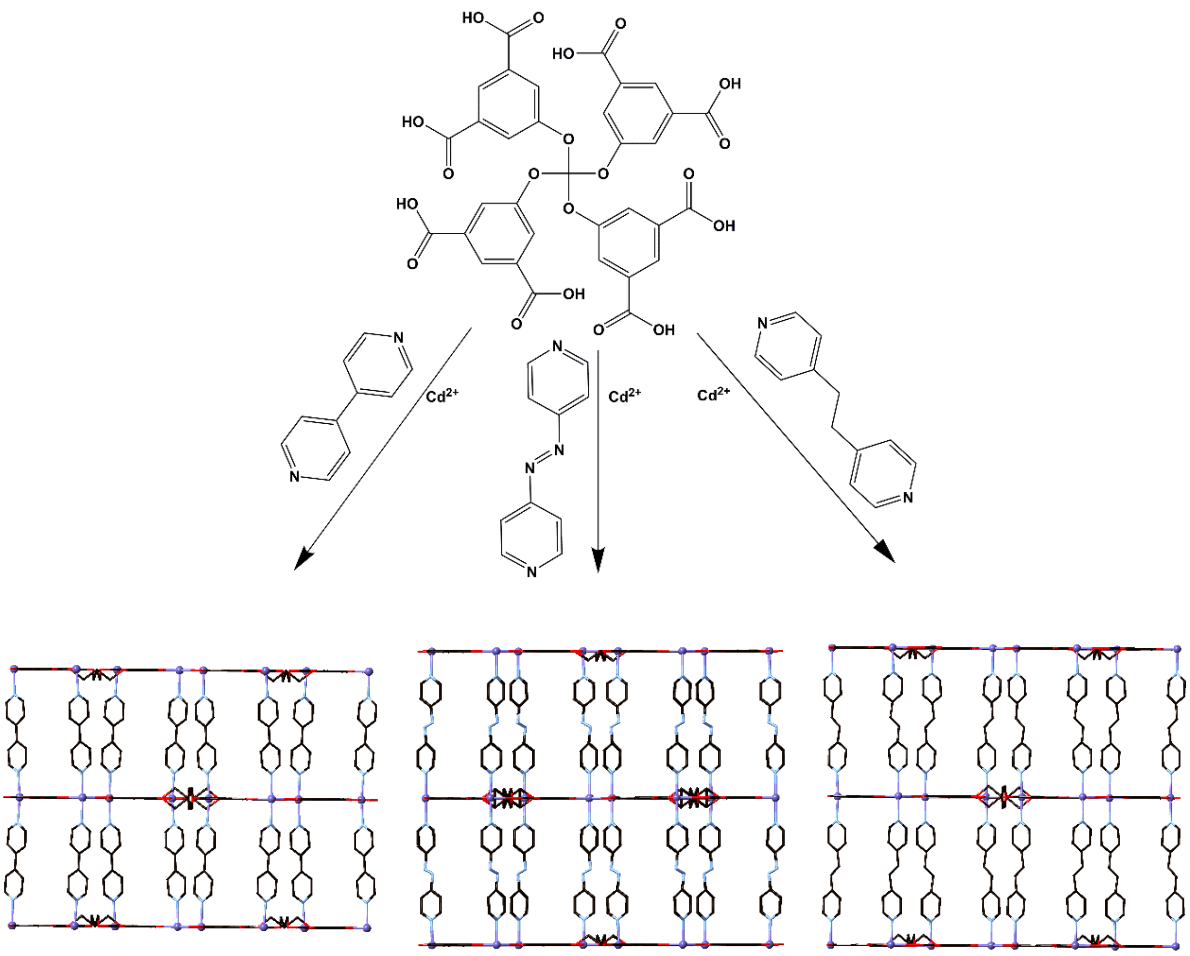

Figure 1.16. A series of isostructural 3D coordination polymers made by the pillaring method, involving 2D sheets of metal-carboxylate which are pillared by 4,4'-bipyridine (left), 4,4'-azopyridine (centre) and 2,4-bis(4-pyridyl)ethane (right), with increasing length of dipyridyl ligand correlating with increased pore size.

1.5.3 Diimide ligands

Ditopic ligands with imide groups present an opportunity for a class of ligands that have a range of core groups that may be functionalised through the imides with a variety of coordinating groups. There are some examples of the use of this class of ligands in crystal engineering and MOF synthesis. Aromatic core groups, such as pyromellitic, perylene, naphthalene, oxydiphthalic and norbornene diimide have been shown to form coordination compounds when functionalised with pyridyl, benzoic acid, isophthalic acid, aminoquinoline, pyrazole, phosphanyl alkyl thioether, ethylthiol and amino acid coordinating groups.[71, 339-

[352] Despite the variety of diimide ligands used thus far, there is still large scope for the development of this class of ligands.

Diimide ligands are suitable for investigation as ligands in metallosupramolecular chemistry because they are synthetically accessible through the imidation of a dianhydride with amines. The size and shape of the diimide core can range from linear and rigid to bent and flexible, and the imide may be formed with amines with a variety of coordinating groups. Diimide ligands are limited only by imagination and the synthetic complexity of the dianhydride and amine starting materials.

The substitution of amino acids onto dianhydride molecules to form diimide ligands for the synthesis of chiral coordination compounds is still in its infancy.[350, 352-354] Therefore this class of ligands was chosen to be investigated in the course of this work, as they may be easily substituted with amino acids to make enantiopure ligands for the formation of homochiral coordination compounds with the view to investigating these materials for applications such as enantioselective sensing, catalysis and separation.

There were four different diimide core groups investigated in this work, two of which were linear and therefore predisposed to forming coordination polymers, and two which have a significant bend in the core and are therefore more likely to form discrete coordination complexes.[71, 344, 348, 355, 356] Investigation of these ligands showed that such a generalisation is not sufficient to rationalise the coordination behaviour of these ligands as the metal centres, ligand flexibility and reaction conditions also played important roles in the structures of the coordination compounds which were formed.

1.5.4 Amino acid based ligands

In the design and synthesis of chiral coordination compounds for targeted applications, the most reliable method for the synthesis of bulk chiral materials is the use an enantiopure chiral ligand. The utilisation of the chiral pool method, the incorporation of naturally occurring chiral molecules into ligands, such as amino acids, lactic acid and camphoric acid, has proven to be a versatile and successful method for the synthesis of homochiral coordination compounds (*vide supra*).

Amino acids were selected for use in the following work based on their functionality on the α-carbon. The carboxylate group provides a suitable coordinating group for the synthesis of coordination compounds, the

amine group may readily react with an anhydride to form a diimide ligand, and the broad range of amino acid side chains is able to form ligands which vary in steric bulk and functionality. A series of amino acid substituted diimide ligands will therefore all have carboxylate coordinating groups, but will vary in the steric bulk of the amino acid side chain. The coordination behaviour of these ligands may therefore be investigated to determine the influence of the side chain on the coordination compounds formed.

1.6 Project aims

The present study aims to exploit the ease with which chiral ligands may be formed by substitution of amino acids onto diimide core groups in order to form a library of chiral ligands and explore their behaviour in the synthesis of coordination compounds, and investigate the properties of the resulting chiral coordination compounds.

Diimide ligands were chosen because they represent a class of synthetically versatile ligands which have not yet been widely utilised in the metallosupramolecular field. A range of diimide ligands were used which varied in size, shape, and flexibility of the core group, in order to investigate the influence which the core may have on the coordination polymers and complexes which were formed. The amino acids used were chosen because their side chains represent a range of steric bulk and functionality.

In order to gain further understanding of the influence of amino acid side chain on the formation of coordination polymers with transition metals and dipyridyl ligands, the alanine, leucine and phenylalanine substituted NDI ligands were explored in Chapter 2. The amino acid substituted biphenyl diimide ligands, with a slightly longer and more flexible core than the NDIs, were explored in Chapter 3, in order to investigate how the change in the ligand core influences the coordination compounds which are formed.

As NDIs have often been shown to have interesting luminescent properties, the fluorescent properties the (*S*)-leucine substituted NDI in solution were explored in Chapter 4, in the form of the carboxylic acid ligand precursor as well as when incorporated into coordination complexes.

Diimide ligands with a bent core were investigated in Chapter 5, in order to determine how the bend in the ligand core will influence the coordination compounds which are formed. The influence of the change in

handedness or the removal of chirality of the ligand was also investigated. The utilisation of rhodium metal centres in chiral coordination compounds in order to form enantioselective catalysts was also explored. Finally in Chapter 6 the combination of copper paddlewheel SBUs with the rigid leucine substituted NDI ligand is explored for the synthesis of coordination compounds and the properties of the resulting material was examined.

Chapter 2: Coordination polymers with naphthalene diimide ligands

2.1 Introduction

The prediction and control of the structure of coordination polymers and MOFs has been the aim of supramolecular chemistry for many years.[327, 357, 358] Due to the variation of strength and directionality in the interactions which influence the formation of coordination polymers, such as coordination bonds, hydrogen-bonds and π-interactions, the structure of coordination polymers can be difficult to design and predict.[359] The change in metal, synthetic conditions, or small changes in the ligand can be sufficient to drastically change the structure of the coordination polymer obtained.[360, 361] As the properties and therefore applications of coordination polymers are heavily reliant on their structure, the ability to predict and design the structure of coordination polymers is an important area of research.

2.1.1 Naphthalene diimides

Naphthalene diimide ligands have been shown to be versatile molecules in supramolecular chemistry due to the ease by which they can be functionalised to incorporate a variety of functional groups.[362-364] NDIs have been integrated into a number of discrete supramolecular complexes, including catenanes and polyhedra.[342, 365] MOFs have also been synthesised using NDI ligands,[366, 367] some of which have interesting optical properties.[106, 368, 369] Coordination polymers incorporating NDI ligands usually involve face-to-face π-interactions**,** often leading to entanglement of the networks. The most commonly encountered mode of entanglement is interpenetration, in which two or more coordination polymers within a system are interlocked such that they are not chemically bonded together but cannot be broken without breaking chemical bonds. [17] Interpenetration can be considered as coordination polymers involving polycatenane motifs.[66, 67] Other modes of entanglement include polythreading, which can be considered as an extended analogue of a molecular pseudo-rotaxane, in which a coordination polymer 'thread' passes through a series

of 'loops' of a separate coordination polymer in the same system.[370] Polyknotting is also possible, otherwise known as self-penetration, in which a single coordination polymer net contains rings through which another thread of the same network passes.[67, 371] The study into interpenetration and related phenomena, and understanding how these complex self-assembly processes may be designed and predicted, is of importance because of the influence they have on the properties of the coordination polymers.[372] Although interpenetration is often seen as a disadvantage to creating MOFs, with the desired void space being partially or fully occupied, it can often have a stabilising influence on the material.[373]

Naphthalene diimide ligands have been synthesised by the Turner group in which each imide site is subsituted with an amino acid. The carboxylic acid of each amino acid provides a coordinating group, and the chirality of the ligand guarantees the formation of enantiopure coordination networks. The amino acid substituted NDI ligands were also of interest because they had limited degrees of freedom. The only flexibility of the ligands is the relative orientation of the amino acids, in that they can adopt an "S" shape, meaning that the carboxylate groups are in a *trans* configuration across the NDI plane, or a "U" shape, a *cis* configuration. NDIs are also very π-rich, leading to a prevalence of π-interactions in their coordination polymers. The combination of the rigidity of the ligands and their predisposition to π-interactions, means that these NDI ligands are good candidates for the synthesis of coordination polymers with a good degree of predictability and design.

A secondary ligand has also been used in coordination polymer and MOF synthesis, in order to increase the dimensionality of the networks and lead to new topologies. In this study, linear dipyridyl ligands were used alongside the amino acid subsituted NDI ligands, to aid in the formation of higher dimensionality networks and to investigate the different π-interactions which would be possible upon the introduction of different aromatic ligands.

2.1.2 Previous work with naphthalene diimide ligands

Previous work on coordination polymers by the Turner group with NDIs has included initial results with amino acid substituted ligands and Cd^{II} metal centres, Figure 2.1. The AlaNDI ligand, with a non-bulky methyl side chain, formed a 1D chain of conjoined $\{Cd_2(AlaNDI)_2\}$ metallomacrocycles. The NDIs in the

macrocycle are ~ 7.2 Å apart, the optimum distance for an aromatic group to thread through the macrocycle with face-to-face π-interactions, which typically occur at 3.2 – 3.8 Å.[12] The 1D chains are interpenetrated into a 2D sheet by catenane motifs between the macrocycles, facilitated by face-to-face π-interactions.[352] The LeuNDI ligand formed analogous 1D metallomacrocycle chains, however the bulky isobutyl side chain of the (*S*)-leucine appeared to inhibit the interpenetration of the macrocycles. The combination of LeuNDI with Cd^{II} and the linear dipyridyl ligand 4,4′-bipyridine (4,4′-bipy) formed 1D chains of alternating $\{Cd_2(LeuNDI)_2\}$ metallomacrocycles and 4,4′-bipy ligands. Interpenetration occurred in these chains by a rotaxane motif of 4,4′-bipy passing through the macrocycle of perpendicular chains, forming a 1D → 3D polyrotaxane, Figure 2.1.[71] The PheNDI ligand, which has a phenyl side chain, when reacted with 4,4′-bipy and Cd^{II}, formed chains with bimetallic nodes of conjoined $\{Cd_2(PheNDI)_2\}$ macrocycles which were bridged into a 2D sheet by double pillars of 4,4′-bipy, as the 4,4′-bipy was coordinated to the axial positions of the Cd^{II}. The 2D sheets did not interpenetrate, as the double pillars of 4,4′-bipy would not fit through the macrocycles, instead a separate 1D chain of [Cd(4,4′-bipy)(solv.)] was threaded through the macrocycles, forming a 1D + 2D → 3D polythreaded structure.[355]

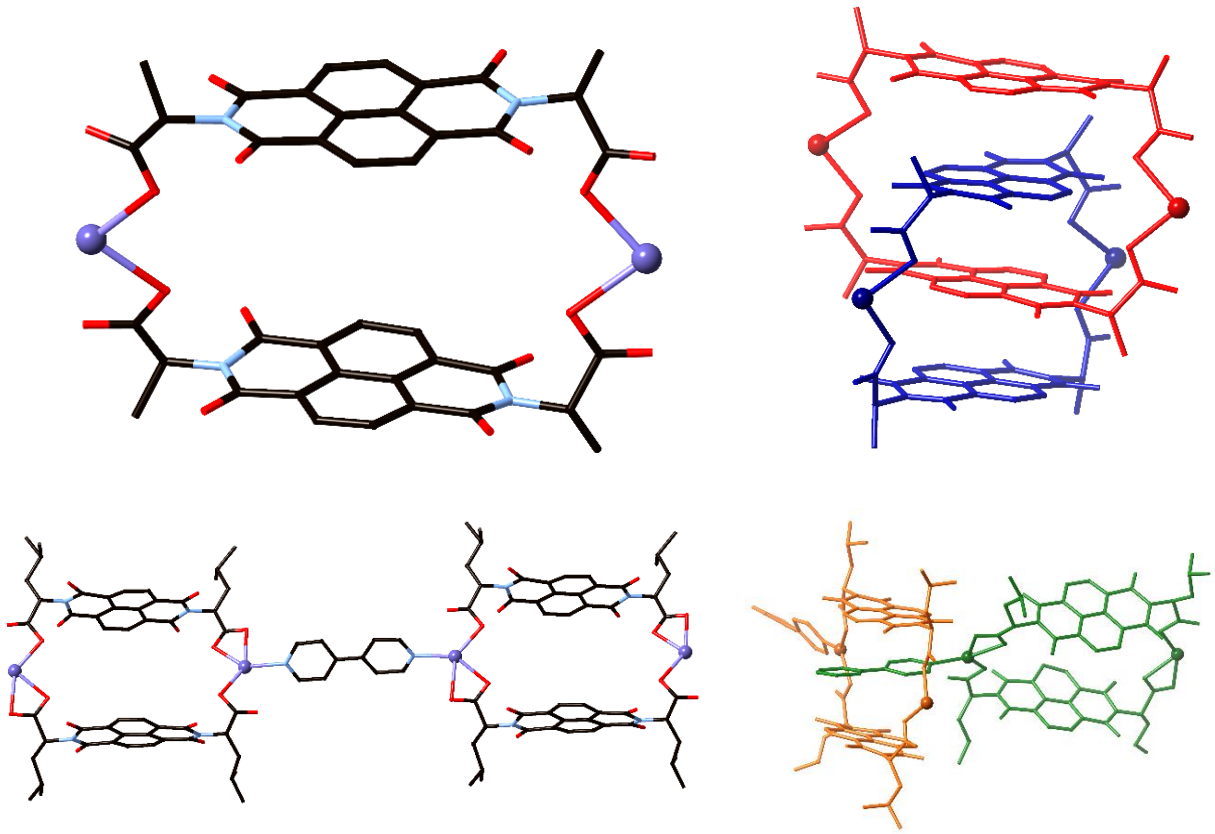

Figure 2.1. The {Cd_2(AlaNDI)$_2$} metallomacrocycle in which the planes of the NDIs are ~7.2 Å apart (top left) and the catenane motifs of the metallomacrocycles (top right).[352] *The 1D chain of alternating {Cd_2(AlaNDI)$_2$} metallomacrocycles and 4,4'-bipy dipyridyl ligands (bottom left) and the rotaxane motifs in which the dipyridyl ligands thread through the metallomacrocycles (bottom right).*[71] *For clarity all solvent molecules and hydrogen atoms have been omitted.*

2.2 Ligands utilised in this study

The initial results suggested a correlation between the bulkiness of the amino acid side chain of the NDI ligand, and the interpenetration of the network formed. Therefore study into the coordination behaviour of AlaNDI, LeuNDI and PheNDI ligands with transitions metals was continued with a range of dipyridyl ligands.

2.2.1 Synthesis of naphthalene diimide ligands

The amino acid substituted NDIs, H_2AlaNDI, H_2LeuNDI and H_2PheNDI molecules have been previously synthesised by the Turner group in order to be utilised in the synthesis of homochiral coordination

polymers, Figure 2.2.[352, 355, 374] The H_2AlaNDI, H_2LeuNDI and H_2PheNDI species were all synthesised by reaction of 1,4,5,8-naphthalene tetracarboxylic acid dianhydride and the respective amino acids in DMF at 90 °C overnight, Figure 2.2. Racemisation of the amino acid was observed if the reaction was conducted above 90 °C in DMF. Although H_2GlyNDI was previously reported by reaction of 1,4,5,8-naphthalene tetracarboxylic acid dianhydride with glycine in acetic acid under microwave irradiation,[375] the reaction was attempted under identical conditions which were developed for the synthesis of H_2AlaNDI, H_2LeuNDI and H_2PheNDI, achieving a pure product of H_2GlyNDI in which the analysis was concordant with the literature. In all cases, following the reaction in DMF, the hot reaction solution was poured over ice. In the case of H_2GlyNDI and H_2AlaNDI the clean product precipitated from the water/DMF solution and could be recovered by filtration with yields of 71% and 55%, respectively. The H_2LeuNDI and H_2PheNDI compounds did not precipitate from the water/DMF solution, and required extraction from the solution with diethyl ether in the case of H_2LeuNDI and ethyl acetate in the case of H_2PheNDI, with yields of 94% and 65%, respectively. The formation of all the products were confirmed by ^{1}H-NMR and ^{13}C-NMR spectroscopy, mass spectrometry, infrared spectroscopy and microanalysis. The presence of a ^{1}H-NMR signal for the hydrogen atom on the alpha-carbon of the amino acid at approximately 4 – 5 ppm was indicative of the formation of the product.

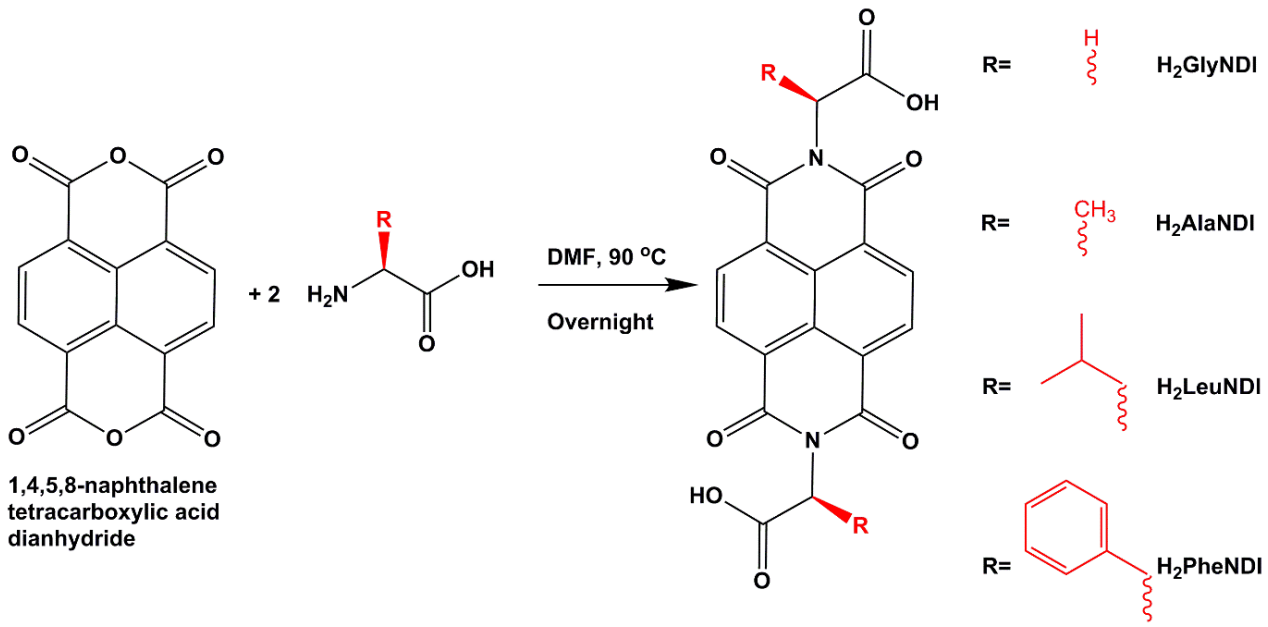

Figure 2.2. The synthetic scheme for the formation of the amino acid substituted NDI molecules.

The AlaNDI, LeuNDI and PheNDI ligands were chosen because they represent a range of side chains (methyl, isobutyl and phenyl group, respectively). The variation in the bulkiness and nature of the amino acid side chain is shown to have a distinct influence on the interpenetration of the coordination polymers obtained.

The dipyridyl ligands used in this study were 4,4′-bipyridine (4,4′-bipy), 1,2-di(4-pyridyl)ethylene (dpe), 1,4-bis-(4-pyridyl)benzene (bpb) and N,N′-bis(4-pyridyl)-1,4,5,8-naphthalene tetracarboxylic diimide (4PyNDI), Figure 2.3. The presence of dipyridyl ligands represents an interesting case, as the NDI ligands have the potential to form either self-complementary catenane motifs or rotaxanes which incorporate the secondary ligand. The coordination polymers of this study will be discussed in order of increasing bulkiness of the amino acid side chain, beginning with AlaNDI, followed by LeuNDI, then PheNDI. The metal ions used were exclusively Cd^{II}, Zn^{II} and Mn^{II} as they proved to be most suitable for the ligands being studied.

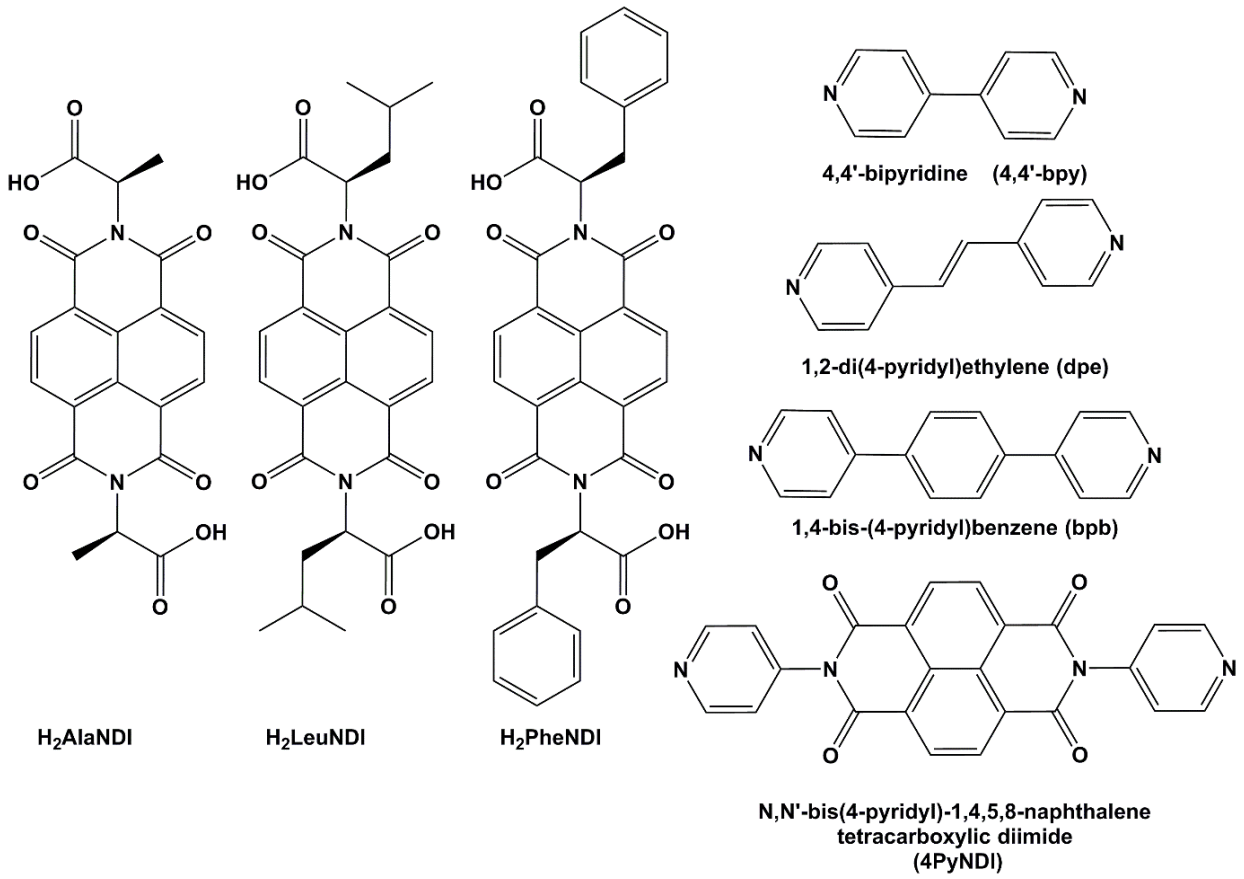

Figure 2.3. The amino acid substituted NDI ligands H_2AlaNDI, H_2LeuNDI and H_2PheNDI (left) and dipyridyl ligands (right) utilised in this study.

2.3 Coordination polymers with the non-bulky AlaNDI ligand

Previous results with AlaNDI have shown that it is possible to form catenane motifs with conjoined $\{Cd_2(AlaNDI)_2\}$ macrocycles, although the ligand is also able to adopt a divergent conformation which does not form the cyclic motif.[348, 352]

The structure of the coordination polymer with AlaNDI and Cd^{II} has been previously reported by the Turner group (*vide supra*), therefore its coordination chemistry with dipyridyl ligands is explored herein. The reaction of H_2AlaNDI, $Cd(NO_3)_2$ and 4,4′-bipyridine (4,4′-bipy) in DMF at 100 °C yielded orange crystals containing the 1D coordination polymer *poly*-[$Cd_2(AlaNDI)_2$(4,4′-bipy)(solv.)], **2.1**. The two crystallographically unique Cd^{II} ions, as parts of two unique 1D chains in the structure, exist as monometallic nodes, both with pentagonal bipyramidal coordination geometries, Figure 2.4. The equatorial positions are occupied by one 4,4′-bipy ligand and two chelating AlaNDI carboxylate groups. The solvent

ligands coordinated at the axial sites differ for the two unique metal centres. The axial sites of Cd(1) are both occupied by DMF ligands, while the axial sites of Cd(2) are both occupied by disordered water and DMF ligands (50:50). As has been previously observed with coordination polymers involving amino acid NDI ligands, the structure of **2.1** involves $\{Cd_2(AlaNDI)_2\}$ metallomacrocycles in which the naphthalene groups are almost parallel and form a suitably sized space in which to accommodate an aromatic guest with face-to-face π-interactions (with shortest inter-NDI C···C distances of 7.411(7) Å and 7.129(10) Å). The metallomacrocycles are bridged by the 4,4′-bipy ligands into a 1D chain of alternating rings and threads, Figure 2.4. The structure contains two crystallographically unique 1D chains that are perpendicular and co-planar. The intersection of these chains involves a rotaxane motif in which the 4,4′-bipy of one polymer is threading through the metallomacrocycle of another, which leads to a 1D → 2D polyrotaxane, Figure 2.4. The 4,4′-bipy ligand and the macrocycle interact by π-interactions with closest C···C contacts of 3.402(12) and 3.461(12) Å. The 2D polyrotaxane sheets pack by virtue of π-interactions between the exterior faces of the metallomacrocycles, with closest C···C contacts of 3.435(15) and 3.481(11) Å.

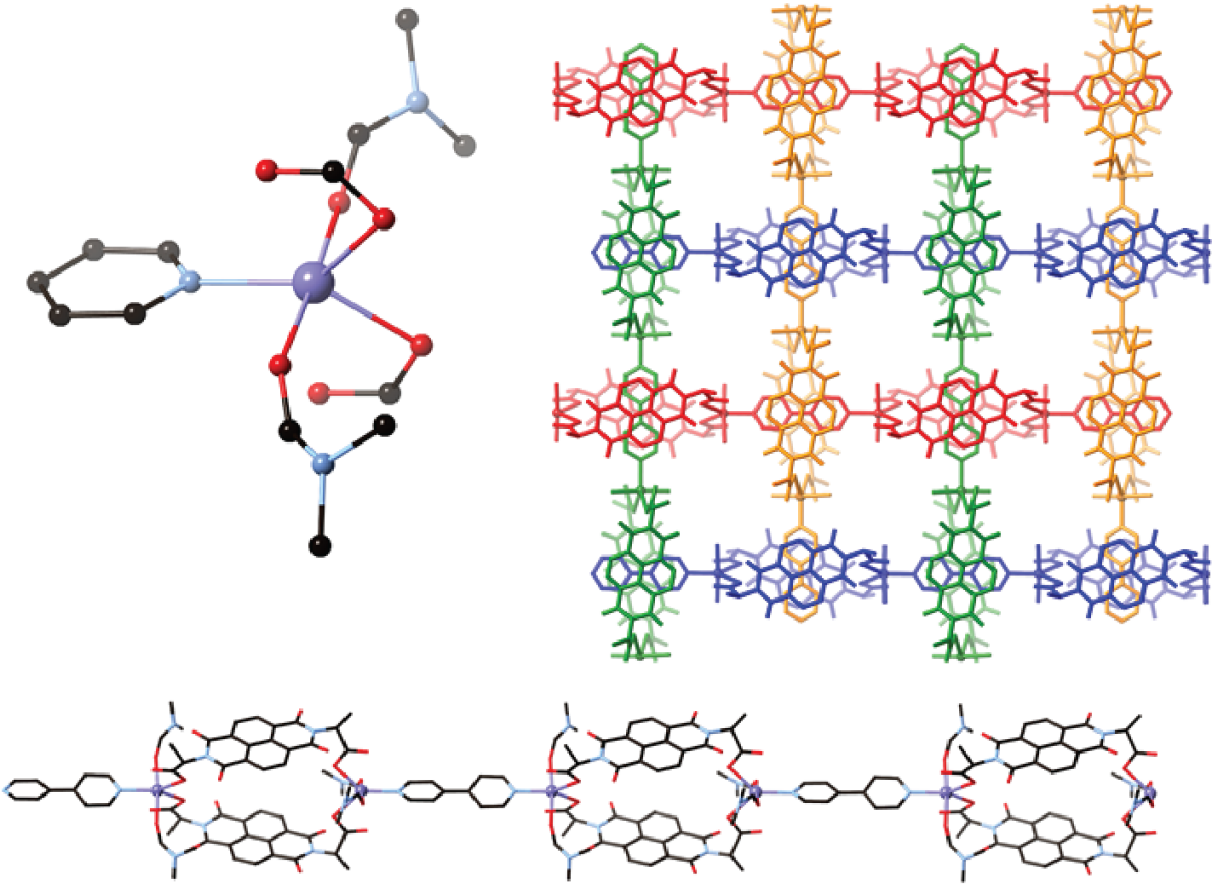

*Figure 2.4 The metal coordination environment of Cd(1) in **2.1** (left), a single chain of **2.1** which involves Cd(1) (bottom) and interpenetrating perpendicular 1D chains of **2.1**, featuring the 4,4′-bipy ligands threading through metallomacrocycles to form a 1D → 2D polyrotaxane (right). All hydrogen atoms are omitted for clarity.*

The structure of **2.1** highlights the reproducibility of polyrotaxane motifs in amino acid-NDI systems, with strong similarities to the structure of the previously reported coordination polymer *poly*-[Cd_2(LeuNDI)$_2$(4,4′-bipy)(DMF)$_3$(OH_2)] which forms a 1D → 3D polyrotaxane.[71] The cause of the difference in interpenetration topology between these two structures lies in the relative orientation of the 4,4′-bipy and the metallomacrocycle in the 1D chain, and is presumably brought about by the change in steric bulk of the amino acid side chain. In the 1D → 3D polyrotaxane, the 4,4′-bipy is twisted by approximately 35° with respect to the NDI macrocycle. The twist of the 4,4′-bipy leads to the 1D chains forming a 3D polyrotaxane, while in the structure of **2.1** the 4,4′-bipy and NDIs are parallel, leading to a 2D polyrotaxane, Figure 2.5. This could be rationalised in terms of packing, with the less bulky AlaNDI

ligands allowing 2D polyrotaxane sheets to stack, whereas this is disallowed for the bulkier LeuNDI analogue and hence an alternative packing motif is formed.

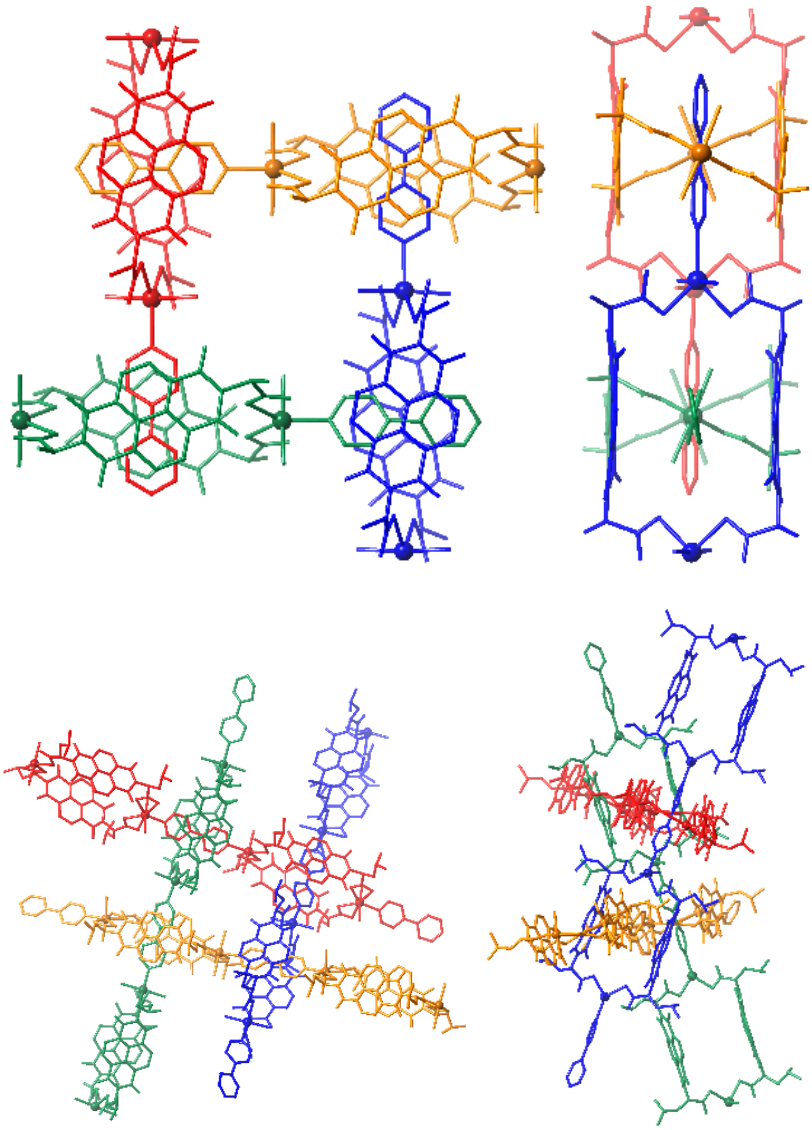

Figure 2.5. The 1D → 2D polyrotaxane of ***2.1*** *with AlaNDI, shown front- and side-on (top) and the previously reported poly-[Cd_2(LeuNDI)$_2$(4,4′-bipy)(DMF)$_3$(OH_2)] which is a 1D → 3D polyrotaxane, shown front- and side-on (bottom), which are different topologies due to the twist of the 4,4′-bipy in relative to the plane of the NDI. For the sake of clarity, only coordinated oxygen atoms of coordinated solvent molecules are shown and all hydrogen atoms are omitted.*

It is well documented that reaction conditions can influence products in self-assembly syntheses, herein demonstrated by reacting H_2AlaNDI, 4,4′-bipy and $Cd(NO_3)_2$ in DMF: methanol: water (2:1:1) at 85 °C to

concomitantly form *poly*-[Cd_4(AlaNDI)$_4$(4,4′-bipy)(DMF)$_4$(OH_2)$_2$]·5H_2O·4DMF, **2.2** and *poly*-[Cd(AlaNDI)(4,4′-bipy)(OH_2)]·3.5H_2O·0.5DMF, **2.4** . Whilst **2.4** could be isolated in a pure form by using the exact stoichiometry of metal and ligands present in the product, numerous attempts to isolate **2.2** as a pure material by a variety of synthetic alterations failed to yield the clean product.

The asymmetric unit of **2.2** contains one bimetallic Cd^{II} node coordinated by four halves of unique AlaNDI ligands, half of a 4,4′-bipy ligand, two DMF molecules and an aqua ligand. Each metal adopts a distorted octahedral geometry, Figure 2.6, in which the equatorial sites of each are occupied by one chelating carboxylate and two carboxylate groups bridging between the two metals in μ-1κO,2κO′ coordination modes. The formally non-coordinating oxygen atoms of the monodentate carboxylates have weak interactions at Cd···O distances of 2.717(6) Å and 2.962(5) Å. The axial sites of Cd(1) are occupied by a DMF ligand and a 4,4′-bipy ligand, and the axial sites of Cd(2) are occupied by a DMF and an aqua ligand. The 4,4′-bipy exhibits rotational disorder and is modelled over two positions, with the planes of these two dipyridyl positions offset by 70.3(13)°. The bimetallic nodes are bridged by pairs of AlaNDI ligands forming the anticipated conjoined metallomacrocycles in the same manner as the previously reported 1D chain *poly*-[Cd(AlaNDI)(DMF)$_2$].[42] The 4,4′-bipy ligands are aligned perpendicular to the metallomacrocycle chains, in which one 4,4′-bipy ligand bridges between two nodes of adjacent chains, to form a (6,3) sheet, Figure 2.6 (taking the macrocycle to be a 2-connector between nodes).

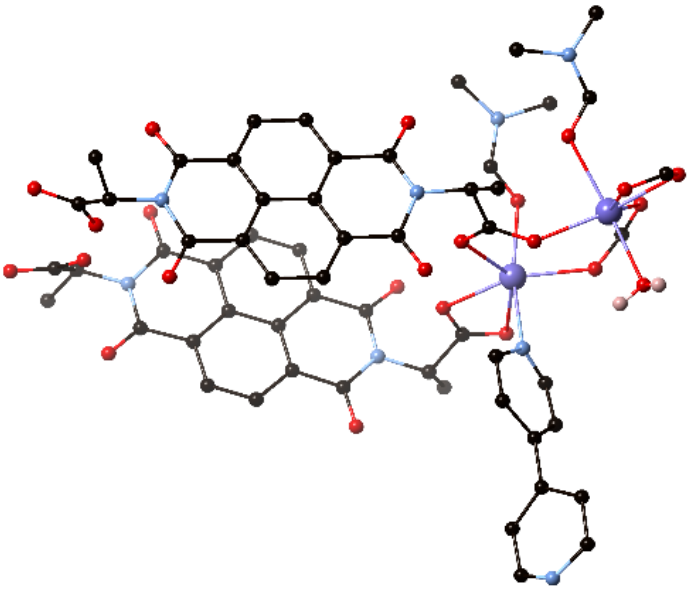

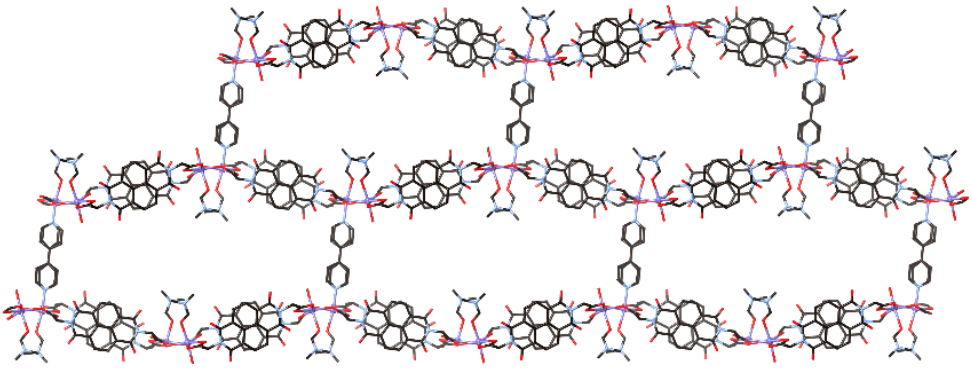

*Figure 2.6. The metal coordination environment in the structure of **2.2** (top), with only one part of the rotational disorder of the 4,4'-bipy ligand shown. The (6,3) sheet formed by the bridging of 4,4'-bipy between bimetallic nodes of metallomacrocycle chains in **2.2** (bottom). All hydrogen atoms are omitted for clarity.*

The individual 2D sheets in the structure of **2.2** interpenetrate in a 2D → 2D manner with catenane motifs between NDI metallomacrocycles, involving parallel face-to-face π-interactions with the closest C⋯C distances of 3.520(8) Å and 3.491(9) Å, Figure 2.7. The interpenetrating layers pack by face-to-face π-interactions between the surfaces of the NDI ligands external to the metallomacrocycles, with the closest C⋯C distance being 3.4069(7) Å. Whilst an individual network in **2.2** can be described as having (6,3) topology, the loops cannot be simplified as a single linker in the overall structure due to the interpenetration,

therefore the topology of this coordination polymer is described by the Schäfli symbol $2^2 \cdot 6^8$. It would appear that the 4,4′-bipy exhibits disorder because it is not involved in π-interactions. It may be reasonably assumed that the catenane motif forms when sterically allowed by the ligands in order to maximise interactions between the large NDI π-surfaces. It is also possible for the AlaNDI/4,4′-bipy system to form rotaxane motifs, as shown in **2.1**, however it appears that the shape of the individual frameworks plays a significant role in the formation of a catenane or rotaxane motif. Interpenetration of the polymers must be self-complementary, such that the macrocyclic groups are parallel, and there is no ligating solvent preventing interpenetration from occurring. In the case of **2.2** the macrocycles are aligned in a favourable orientation to interpenetrate by catenane motifs.

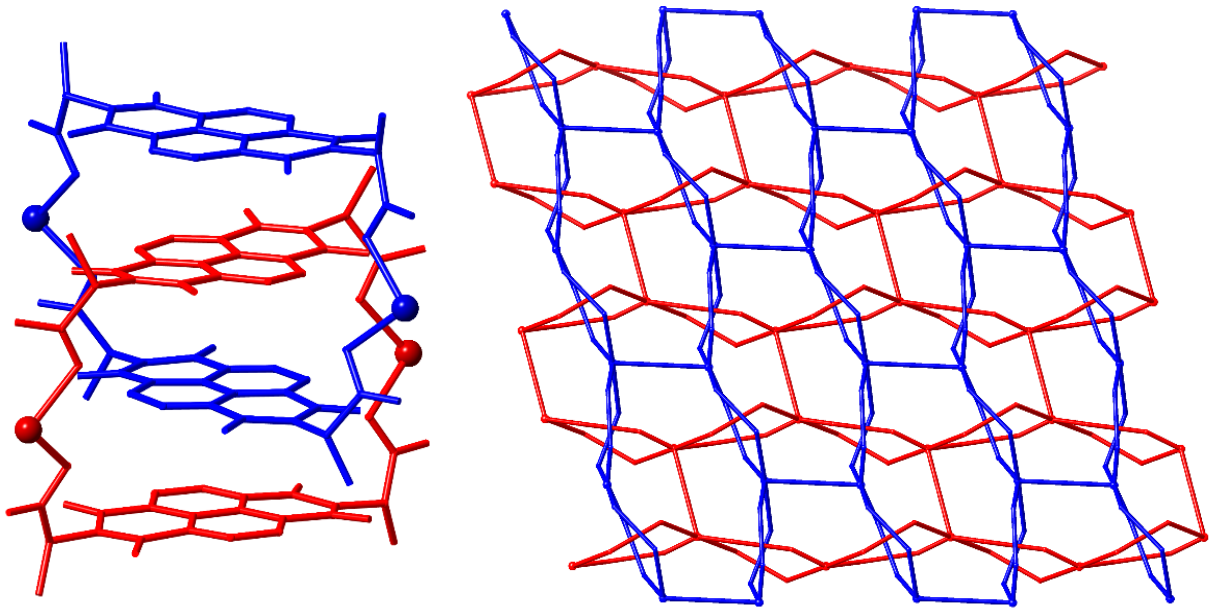

*Figure 2.7. The catenane motif of **2.2** by which two perpendicular sheets are interpenetrated (left), with all hydrogen atoms and coordinated solvent omitted for clarity. The interpenetrating sheets in which 4,4′-bipy ligands are shown as rods and NDI macrocycles are shown as loops (right).*

A reaction conducted under identical reaction conditions to those for **2.2**/**2.4** using Mn^{II} yielded a coordination polymer of the formula *poly*-$[Mn_4(AlaNDI)_4(4,4'\text{-bipy})(DMF)_4(OH_2)_2]\cdot 2DMF\cdot 5.5H_2O$, **2.3**, which is essentially isostructural to **2.2**, with the exception of a lack of rotational disorder of the 4,4′-bipy ligand and a slight difference in the metal coordination environments. The two metals in the asymmetric

unit of **2.3** form a bimetallic node. Mn(1) adopts a distorted octahedral geometry, with the equatorial positions occupied by one chelating carboxylate group and two carboxylate groups which bridge the two metal centres in a μ-1κO,2κO′ coordination mode, analogous to both Cd^{II} ions in **2.2**. The difference lies in the coordination environment of Mn(2), which adopts a trigonal bipyramidal geometry. The equatorial sites are occupied by a monodentate carboxylate group and the two carboxylates which bridge between the metal centres. The axial sites are occupied by a 4,4′-bipy ligand and disordered aqua/DMF site (50:50). In the same manner as **2.2**, 1D chains of $\{Mn_2(AlaNDI)_2\}$ metallomacrocycles are bridged by 4,4′-bipy ligands to form a (6,3) sheet with 2D → 2D interpenetration by a catenane motif between the $\{Mn_2(AlaNDI)_2\}$ metallomacrocycles involving π-interactions between the NDI planes (closest C⋯C distance = 3.523(6) Å).

As mentioned above, forming concomitantly with compound **2.2** is *poly*-[Cd(AlaNDI)(4,4′-bipy)(OH_2)]·3.5H_2O·0.5DMF, **2.4**. Although **2.4** involves the same components as **2.2**, the ratios of their components, and subsequently their structures, are different. The structure of **2.2** is a 2D → 2D interpenetrated coordination polymer, while the structure of **2.4** is an interpenetrated 3D network. The asymmetric unit of **2.4** contains one Cd^{II} metal centre, an AlaNDI ligand, a 4,4′-bipy ligand and an aqua ligand. The Cd^{II} adopts a distorted pentagonal bipyramidal coordination geometry, the equatorial sites are occupied by two chelating carboxylate groups and an aqua ligand, and the axial sites are occupied by two 4,4′-bipy ligands. The AlaNDI ligand adopts an "S" shape, i.e. *trans* configuration, unlike the "U" shape in all the other AlaNDI coordination polymers discussed herein, and therefore does not form analogous metallomacrocycles.

The "S"-shaped NDI ligands in **2.4** form 1D chains by bridging between the monometallic Cd^{II} nodes, with the carboxylate groups coordinated to the same face of each node, and the 4,4′-bipy ligands bridge between these chains in two directions, forming a 3D network. Given the relative rigidity of the AlaNDI ligands it is a geometric requisite around the metal centre that in this configuration they still maintain a distance of ca. 7 Å between their NDI planes and therefore maintain potential for face-to-face π-interactions between networks, Figure 2.8. The structure is 2-fold interpenetrated, as two networks stack together with the 1D NDI chains being intertwined (closest C⋯C distance = 3.305(6) Å) and the 4,4′-bipy ligands also arranged

in an infinite stack (closest C···C distance = 3.429(6) Å). Small channels remain in the structure, into which the aqua ligands are protruding, containing unresolved electron density associated with solvent molecules. Common between the structures of **2.2** and **2.4** is the fact that the NDI ligands are exclusively involved in π-interactions with other NDIs, rather than with the 4,4′-bipy ligands. This implies that even in the absence of the macrocyclic motif in the case of **2.4** (and therefore absence of the catenane motif) that these homo-interactions are preferred.

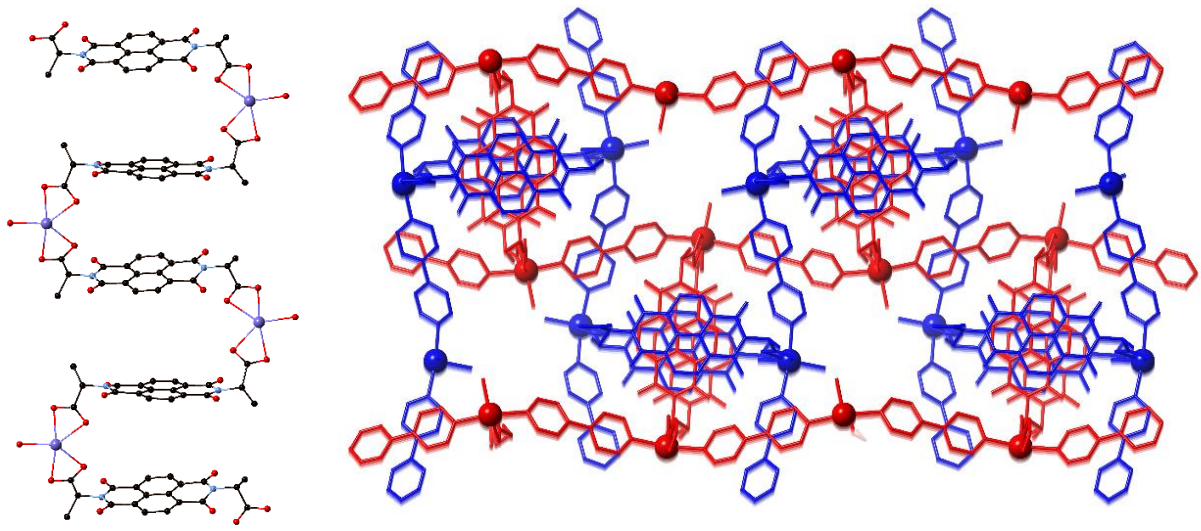

*Figure 2.8. The {Cd(AlaNDI)} chains formed by the "S" shaped AlaNDI ligands in the structure of **2.4**; the 4,4′-bipy ligands coordinate to the metal into and out of the page (left). (b) The two-fold 3D → 3D interpenetrated networks with one network shown in blue and one shown in red, looking down the NDI chains, showing the face-to-face π-stacking of the NDI ligands and of the 4,4′-bipy ligands (right). All hydrogen atoms are omitted for clarity.*

In order to further explore the robustness of the $\{M_2(AlaNDI)_2\}$ macrocycle, the AlaNDI/4,4′-bipy system was investigated using Zn^{II}, which has a smaller ionic radius than Cd^{II}. Reaction conditions analogous to those used in the synthesis of the **2.2**/**2.4** mixture yielded a material with the formula *poly*-$[Zn_2(AlaNDI)_2(4,4'\text{-bipy})_2]\cdot 0.3MeOH\cdot 0.7H_2O$, **2.5**. The two Zn^{II} centres in the asymmetric unit adopt distorted tetrahedral coordination geometries, with two monodentate carboxylate groups and two 4,4′-bipy ligands in the coordination sphere of each monometallic node. The AlaNDI ligands are "U" shaped, bridging between two monometallic nodes to form a $\{Zn_2(AlaNDI)_2\}$ metallomacrocycle. The metallomacrocycles are bridged by 4,4′-bipy ligands in two directions to form T-shaped nodes, leading to

a (6,3) sheet (if the macrocycles are considered as a single linker), which contain a 1D chain of alternating macrocycles and 4,4′-bipy, similar to that in **2.1**. The sheets interpenetrate in a 2D → 2D parallel manner, with the 4,4′-bipy ligands within the 1D chain motif threading through a perpendicular metallomacrocycle, forming a rotaxane motif, Figure 2.9. The rotaxane motif involves near parallel face-to-face π-interactions (closest C···C distance = 3.476(8) Å and 3.539(7) Å, interplanar angles 7.01(12)° and 6.80(12)°). The structure is quite similar to that of **2.1**, and can be visualised as interpenetrating perpendicular chains that are connected by an additional 4,4′-bipy. There are also near parallel face-to-face π-interactions between the 2D sheets involving the external faces of the NDI ligands (closest C···C distances = 3.472(13) Å and 3.488(8) Å, interplanar angle 9.98(14)° and 0.86(13)°, respectively). Despite the smaller ionic radius, and therefore lower coordination number of Zn^{II} in the structure of **2.5**, in comparison to Cd^{II} in the structures of **2.1**, **2.2** and **2.4**, the metallomacrocyclic motif persists, demonstrating a resilience to the change in nature of the metal ion.

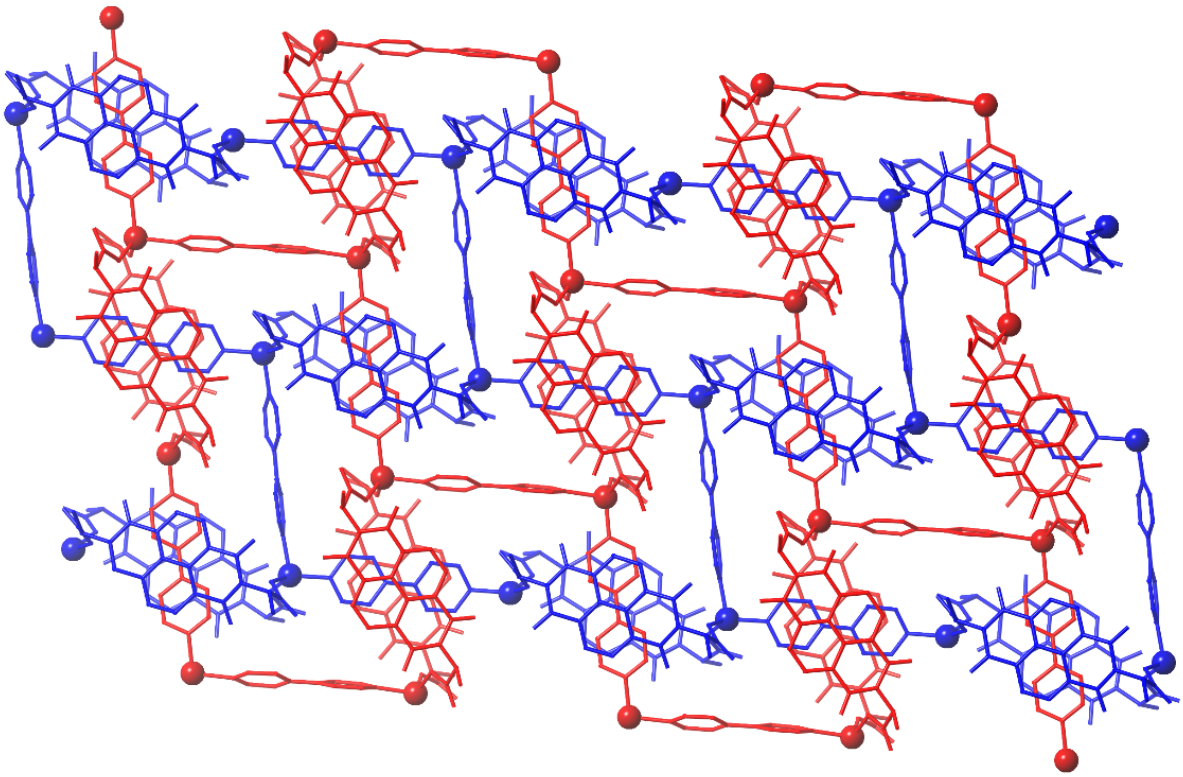

Figure 2.9. The 2D → 2D interpenetration of the sheets of ***2.5****, showing the 4,4′-bipy ligands threading through the metallomacrocycles. All hydrogen atoms are omitted for clarity.*

The coordination behaviour of AlaNDI alongside dipyridyl ligands was further explored by using 1,2-di(4-pyridyl)ethylene (dpe), in order to investigate the influence which a slightly longer dipyridyl ligand would have on the structure of the coordination polymers observed. The reaction of H_2AlaNDI, dpe and $Mn(NO_3)_2 \cdot 4H_2O$ was again carried out under identical reaction conditions to **2.2** – **2.5**, to yield crystals of the formula *poly*-[Mn(HAlaNDI)$_2$(dpe)], **2.6**. The structure of **2.6** is unlike those discussed thus far, as only one of the two carboxylic acid groups on H_2AlaNDI is deprotonated. The asymmetric unit of the structure contains one Mn^{II} ion, two HAlaNDI ligands, and a dpe ligand. The Mn^{II} metal centre adopts a distorted octahedral geometry, with the equatorial sites occupied by two monodentate carboxylate groups and two carboxylic acid groups, and the axial sites occupied by two dpe ligands. There are hydrogen bonds between the O–H groups of the coordinating carboxylic acids and the uncoordinated oxygen atom of the carboxylate groups (O-H···O distances = 1.612(4) Å and 1.566(4) Å), Figure 2.10. The HAlaNDI ligands are "U" shaped, forming a continuous 1D chain of metallomacrocycles connected by monometallic Mn^{II} nodes. The dpe ligands bridge between pairs of metal nodes of adjacent chains to form a (4,4) sheet, if the macrocycle is considered as a single linker. These sheets interpenetrate in a 2D → 2D manner, with the dpe ligands threaded through the metallomacrocycles with face-to-face π-interactions between the two ligands (closest C···C distance = 3.357(7) Å), Figure 2.10. The interpenetrated layers stack by π-interactions between the external faces of the HAlaNDI ligands (closest C···C distance = 3.312(7) Å). The difference in the protonation state of the ligand has a significant influence on the structure of the coordination polymer, contrasted with those containing the dianionic AlaNDI species. Although the metallomacrocycles are maintained, they involve monometallic, rather than bimetallic nodes, for charge balance. The structure is a (4,4) sheet, in contrast to the (6,3) sheets of **2.1**, **2.2**, **2.3** and **2.5**, presumably because the macrocycles cannot be spaced out by the dipyridyl ligand (as in **2.5**) without forming a cationic network. Despite numerous attempts, a coordination polymer containing Mn^{II}, dpe and fully deprotonated AlaNDI could not be isolated.

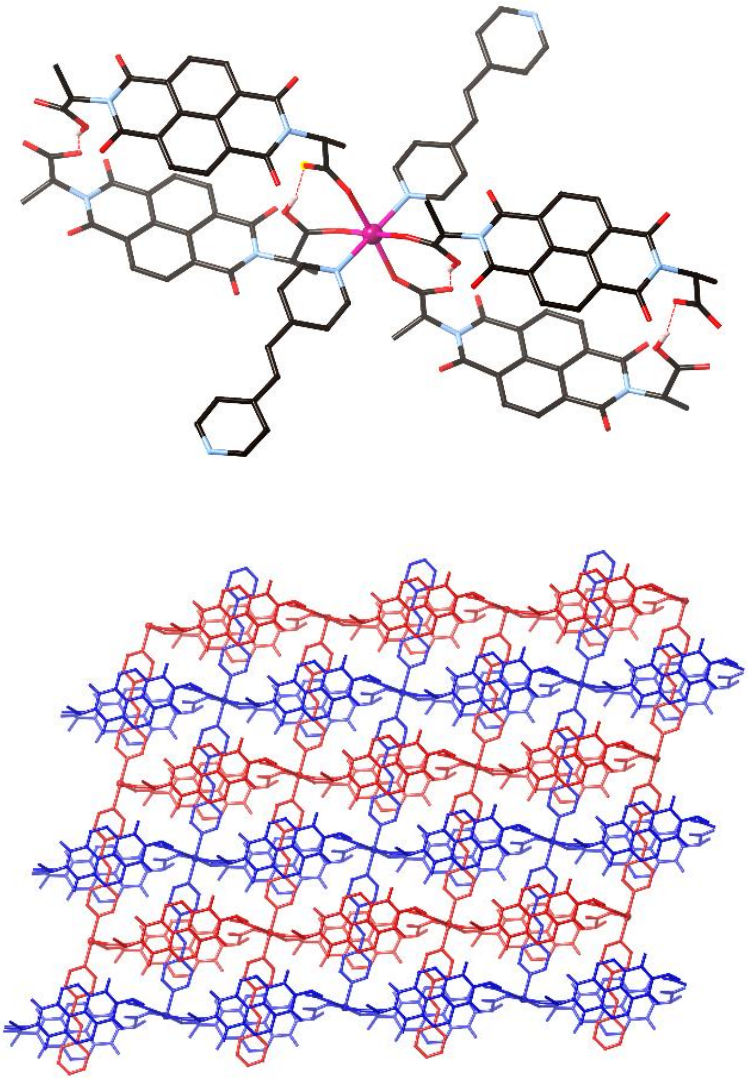

*Figure 2.10. The metal coordination environment in the structure of **2.6** (all hydrogen atoms not participating in hydrogen bonding are omitted for clarity) with hydrogen bonding shown in dashed red lines (top). The 2D → 2D parallel interpenetration of the sheets of **2.6** (bottom).*

The longer and more π-rich dipyridyl ligand, *N*,*N′*-bis(4-pyridyl)-1,4,5,8-naphthalene tetracarboxylic diimide (4PyNDI) was also used in combination with AlaNDI. The reaction of H_2AlaNDI, 4PyNDI and $Cd(NO_3)_2{\cdot}4H_2O$ under the same reaction conditions as **2.2**–**2.6** yielded concomitant crystals of three coordination polymers, *poly*-$[Cd_2(AlaNDI)_2(4PyNDI)_2]{\cdot}4DMF$, **2.7**, *poly*-$[Cd_2(AlaNDI)_2(OH_2)_2(4PyNDI)_2]{\cdot}DMF{\cdot}H_2O$, **2.8** and *poly*-$[Cd_2(AlaNDI)_2(DMF)_2(OH_2)_2(4PyNDI)]{\cdot}DMF{\cdot}4H_2O$, **2.9**, as confirmed by PXRD. Despite many attempts at subtly varying the

reaction conditions, a pure phase of each compound was unable to be synthesised, demonstrating that while the occurrence of the macrocyclic motif may be somewhat predictable, the overall structures of the materials that form are less easy to foretell.

Poly-[Cd_2(AlaNDI)$_2$(4PyNDI)$_2$]·4DMF, **2.7**, is a 2D sheet which contains bimetallic Cd^{II} nodes, similar to those in the structure of **2.2**, in which each of the metal ions adopts a distorted octahedral geometry. The equatorial sites are each occupied by a chelating carboxylate group and two carboxylate groups bridging between the metals in a μ-1κO,2κO′ coordination mode, giving rise to a chain of conjoined metallomacrocycles similar to the previously reported [Cd(AlaNDI)(DMF)$_2$],[42] and the structures of **2.2** and **2.4**. All four of the axial sites in the bimetallic node are occupied by 4PyNDI ligands, Figure 2.11. The 4PyNDI form 'double pillars' which bridge the 1D metallomacrocycle chains into 2D sheets. These pillars contains near parallel face-to-face π-interactions between the naphthalene groups (closest C···C distance = 3.328(10) Å, interplanar angle 2.0414°), and between the dipyridyl groups (3.7222(8) Å and 3.4138(7) Å, 6.405(3)° and 30.328(9)°, respectively). The 2D sheets are not interpenetrated as these 'double pillars' are too bulky to thread through the AlaNDI metallomacrocycles. The parallel arrangement of the 4PyNDI ligands is not a motif that is observed for the AlaNDI ligands; this is presumably due to the steric bulk of the methyl group in AlaNDI which prevents such a spatial arrangement. It appears that the macrocycles are filled by solvent (by SQUEEZE analysis) although this could not be modelled. The sheets pack in an offset manner with the 4PyNDI ligands involved in π-interactions with the AlaNDI ligands of adjacent sheets (closest C···C distances = 3.3493(7) Å and 3.3847(7) Å, interplanar angle 1.47(16)° and 2.86(15)°).

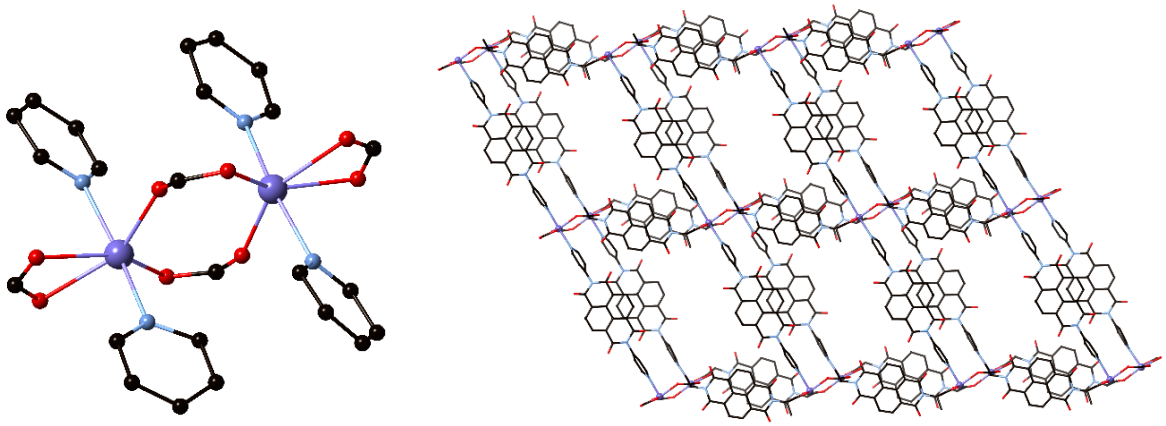

*Figure 2.11. The metal coordination environment in the structure of **2.7** (left) and one 2D sheet (right). All hydrogen atoms are omitted for clarity.*

Compound **2.8** is also a 2D coordination polymer with the same ratio of metal and ligands as **2.7**, yet a very different structure. *Poly*-[Cd_2(AlaNDI)$_2$(OH_2)$_2$(4PyNDI)$_2$]·DMF·H_2O, **2.8**, contains one formula unit in its asymmetric unit. Each metal centre adopts a distorted octahedral geometry in which the equatorial positions are occupied by one chelating and one monodentate carboxylate groups and a 4PyNDI ligand, and the axial positions are occupied by a 4PyNDI ligand and an aqua ligand. The structure of a single network of this coordination polymer is similar to that of **2.4**, involving 1D chains of alternating {Cd_2(AlaNDI)$_2$} metallomacrocycles and 4PyNDI ligands, that are bridged by perpendicular 4PyNDI ligands, to form (6,3) sheets with T-shaped monometallic nodes, Figure 2.12. The sheets are interpenetrated in a 2D → 2D manner by a rotaxane motif with the 4PyNDI which is perpendicular to the metallomacrocycle containing chains threaded through the metallomacrocycles (closest C···C distances = 3.38(3) Å and 3.43(3) Å, interplanar angle 1.5(3)° and 0.8(5)°, respectively). There are also π-interactions between the parallel sheets, involving the external faces of the AlaNDI macrocycles and the 4PyNDI ligands which are not threaded (closest C···C distance = 3.34(3) Å and 3.40(3) Å, interplanar angle 9.8(3)° and 11.1(4)°, respectively). The plane of the dipyridyl groups of each of the 4PyNDI ligands are rotated with respect to the plane of the naphthalene core by 69.67(3)° and 77.91(3)° for the non-interpenetrating ligands and by 58.583(19)° and 49.072(17)° for the interpenetrating ligands, and so are not involved in any π-interactions. In contrast to

2.7, the structure of **2.8** shows that 4PyNDI can engage in π-interactions with AlaNDI and form rotaxane motifs in a similar manner to those occurring in **2.5** and **2.6**.

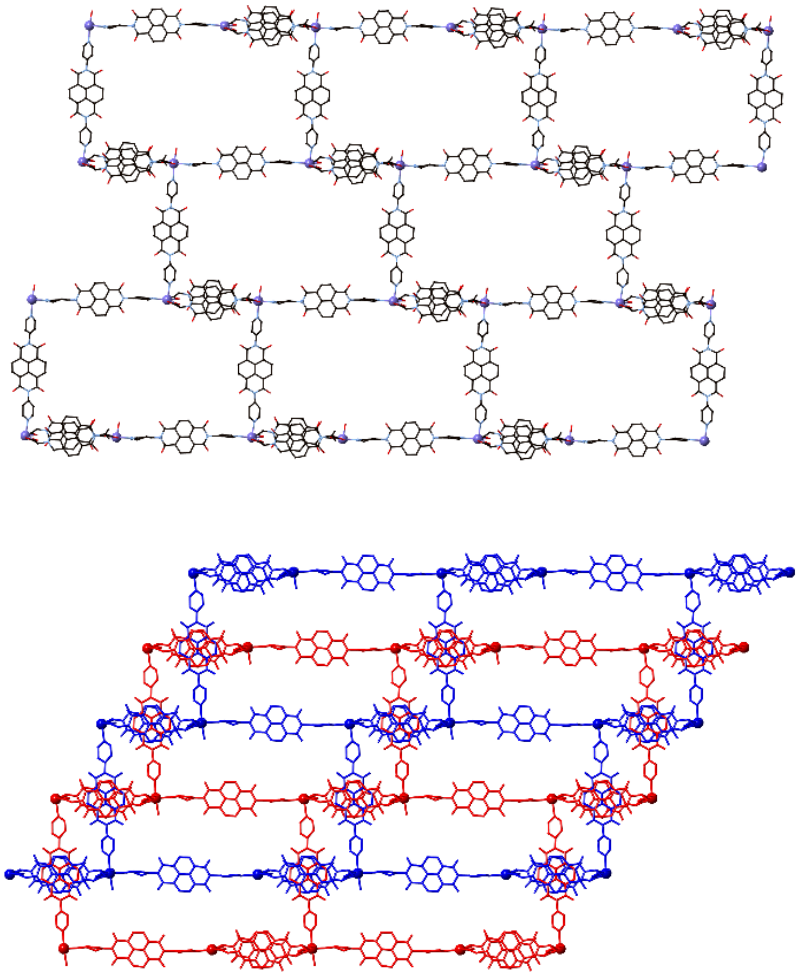

*Figure 2.12. A single (6,3) sheet in the structure of **2.8** (top), and the 2D → 2D interpenetration of the sheets involving a rotaxane motif (bottom). All hydrogen atoms are omitted for clarity.*

The third concomitant product containing 4PyNDI, *poly*-$[Cd_2(AlaNDI)_2(DMF)_2(OH_2)_2(4PyNDI)]\cdot DMF\cdot 4H_2O$, **2.9**, is considerably different to **2.7** and **2.8**, being a non-interpenetrated 1D coordination polymer. The asymmetric unit contains one formula unit which comprises significantly more coordinated solvent than compounds **2.7** and **2.8**, limiting connectivity of the polymer. Both unique Cd^{II} ions adopt a distorted pentagonal bipyramidal geometry in which the equatorial sites are occupied by two chelating carboxylate groups of the AlaNDI ligands, and a 4PyNDI ligand, and

the axial sites are occupied by a coordinated DMF and an aqua ligand. The $\{Cd_2(AlaNDI)_2\}$ metallomacrocycles with monometallic nodes are bridged by 4PyNDI ligands to give a 1D chain, Figure 2.13, very similar to the chains of **2.1**, which form a 1D → 2D polyrotaxane, or the previously reported *poly*-$[Cd_2(LeuNDI)_2(4,4'\text{-bipy})(DMF)_3(OH_2)]$ 1D → 3D polyrotaxane.[71] Unlike the previous systems involving 4,4′-bipy, the chains in the structure of **2.9** do not form a polyrotaxane. The space inside each metallomacrocycle is filled with one water and one DMF molecule (with the former involved in hydrogen bonds to the latter and a carboxylate) Figure 2.13. Non-parallel face-to-face π-interactions exist between the AlaNDI ligands and 4PyNDI ligands of adjacent chains (closest C···C distance = 3.366(11) Å and 3.424(11) Å, inter-planar angle 26.08(7)° and 25.80(7)°, respectively). It is somewhat surprising that this rotaxane motif does not occur, as it is demonstrated herein to be a favourable motif with 4,4′-bipy, and it is certainly possible for a 4PyNDI to pass through the metallomacrocycle, as in the structure of **2.8**. It is possible, given 4PyNDI is longer than 4,4′-bipy, that the chains may not be able to pack in a favourable way to be compatible with a rotaxane motif. The structures of **2.7**, **2.8** and **2.9** show that a variety of coordination polymers can form concomitantly with the same components, highlighting the unpredictability of these systems, despite the prevalence of the metallomacrocyclic synthon.

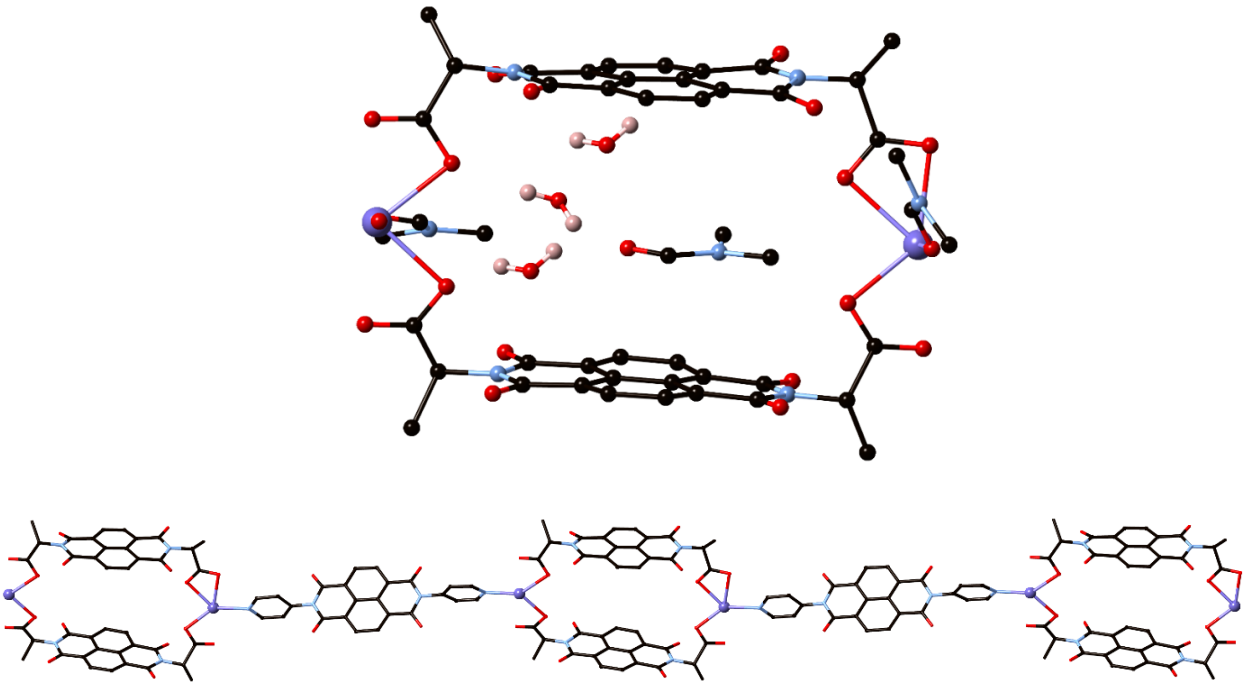

*Figure 2.13. One macrocycle in the structure of **2.9** showing the coordinated and non-coordinated solvent (top), all but O-H hydrogen atoms are omitted for clarity. The 1D chains of alternating {$Cd_2(AlaNDI)_2$} metallomacrocycles and 4PyNDI in the structure of **2.9** (hydrogen atoms and coordinated solvent are omitted for clarity).*

The AlaNDI ligand displays a strong tendency to form interpenetrated coordination polymers featuring an M_2L_2 metallomacrocyclic motif when used in combination with dipyridyl ligands. Whilst changes in metal ion, dipyridyl ligand and synthetic conditions influenced the overall structure of the coordination polymers and the nature of the interpenetration, the cyclic motif persisted in all but one of the nine examples reported herein. Interpenetration occurs in one of two ways; by a catenane motif between two metallomacrocycles, or a rotaxane motif with a dipyridyl ligand threaded through a macrocycle. In both cases the interpenetration is mediated by face-to-face π-interactions allowed by the favourable distance between the NDIs within the metallomacrocycle (ca. 7.2 Å).

There is a degree of unpredictability in this system, which is highlighted by two syntheses that resulted in concomitant formation of multiple crystalline products. Interpenetration is also not guaranteed in the self-assembly process, as eight of the nine coordination polymers reported with AlaNDI contain the macrocyclic motif, and of these eight, two are not interpenetrated. Compound **2.7** is sterically restricted from

interpenetrating due to the 'double pillars' of 4PyNDI which could not fit through the metallomacrocycle. Unexpectedly, the 1D chain of **2.9** is also not interpenetrated, despite the chain being very closely related to that of **2.1**.

The AlaNDI coordination polymers which are interpenetrated contain chains of either conjoined macrocycles (**2.2**, **2.3** and **2.6**) or chains of alternating macrocycles and dipyridyl ligands (**2.1**, **2.5** and **2.8**). Compounds **2.2** and **2.3**, which are essentially isostructural, are the only compounds reported herein that contain the catenane motif. The macrocycle:4,4′-bipy ratio is higher in **2.2** and **2.3** than others reported, and as such the (6,3) sheets interpenetrate in a more efficient manner through catenation than would be possible through a rotaxane motif. Compounds **2.1** and **2.6** both have a 1:1 macrocycle:L ratio (L = 4,4′-bipy and dpe, respectively), leading to close packed structures in which every macrocycle is involves in a rotaxane motif. Compounds **2.5** and **2.8** have a 1:2 macrocycle:L ratio (L = dpe and 4PyNDI, respectively) and both form (6,3) sheets in which each 6-membered ring contains two macrocycles and four dipyridyl ligands. Once again the interpretation involves co-planar networks with a rotaxane motif, with half of the dipyridyl ligands not taking part in the interpenetration. Therefore the ratio between macrocycle and dipyridyl ligand has a significant impact on the type of interpenetrated network formed. While the complete control of the ratio which crystallises remains somewhat unpredictable under self-assembly conditions, the macrocycle motif has proved itself as a reproducible supramolecular synthon.

2.4 Coordination polymers using the bulky LeuNDI ligand

As discussed above, the AlaNDI ligand formed a wide range of interpenetrated coordination polymers, most likely due to the non-bulky methyl side chain of the ligand. The LeuNDI ligand was also explored, in order to investigate the influence of its more bulky and somewhat flexible isobutyl side chain. Initial results by the Turner group with LeuNDI and Cd^{II} included a non-interpenetrated 1D chain of conjoined $\{Cd_2(AlaNDI)_2\}$ macrocycles of formula *poly*-$[Cd(AlaNDI)(DMF)_2]$ and a 1D → 3D polyrotaxane, *poly*-$[Cd_2(LeuNDI)_2(4,4'\text{-bipy})(DMF)_3(OH_2)]$, in which interpenetration occurred by a rotaxane motif (discussed in Section 2.1.2). It was hypothesised that interpenetration occurred by a rotaxane motif due to the bulky isobutyl side chain of the LeuNDI ligand, disallowing interpenetration by a catenane motif.[71] This

hypothesis was supported by the series of interpenetrated coordination polymers which could be formed by with AlaNDI, via either a catenane or a rotaxane motif. The coordination behaviour of LeuNDI was therefore further explored using Zn^{II} and Mn^{II}, and with the dipyridyl ligands dpe and 1,4-bis-(4-pyridyl)benzene (bpb).

The coordination chemistry of LeuNDI was first explored with Zn^{II} in the absence of dipyridyl ligands. The reaction of H_2LeuNDI and $Zn(OAc)_2$ in DMF/water produced crystals which were analysed to reveal a coordination polymer of the formula *poly*-$[Zn_8(DMF)_3(LeuNDI)_6(\mu_3\text{-}OH)_4(OH_2)_3]\cdot 2DMF\cdot 10H_2O$, **2.10**. The structure of **2.10** is quite different to those of all other NDI coordination polymers reported herein, as it does not involve mono- or bi-metallic nodes, but tetrametallic nodes, and the nodes are bridged not by two NDI ligands, but three, to form a 1D chain.

The structure of **2.10** is modelled in the chiral space group $P2_1$ and the asymmetric unit involves eight Zn^{II} ions, six LeuNDI ligands, four μ_3-OH ions, three ligated DMF molecules and three aqua ligands. Each tetranuclear node involves four Zn^{II} ions, six LeuNDI carboxylate groups, two μ_3-OH and three coordinated solvent molecules, either DMF or water. There are multiple different metal coordination environments within the nodes, Figure 2.14. Three of the metal centres, Zn(1), Zn(4) and Zn(5) are tetrahedral, coordinated to one monodentate carboxylate group, a μ_3-OH ion and two bridging carboxylate groups in a μ-1κO,2κO′ coordination mode. Zn(2) adopts an octahedral coordination geometry with two bridging μ-1κO,2κO′ carboxylate groups, two μ_3-OH ions, a coordinated DMF and an aqua ligand. The axial positions are occupied by the bridging carboxylate groups, and the equatorial positions are occupied by *cis* μ_3-OH ions and the DMF and aqua ligand *cis* arrangement. The geometry of Zn(3) is trigonal bipyramidal, in which the equatorial positions are occupied by a DMF molecule, a μ_3-OH ion and a bridging μ-1κO,2κO′ carboxylate group, and the axial positions are occupied by a μ_3-OH ion and a bridging μ-1κO,2κO′ carboxylate group. Zn(6) is similar to Zn(2) as they both adopt an octahedral coordination geometry, however their coordinating groups differ. The equatorial positions of Zn(6) are occupied by two *cis* μ_3-OH ions, a DMF and a bridging μ-1κO,2κO′ carboxylate, and the axial positions are occupied two bridging μ-1κO,2κO′ carboxylate groups. Zn(7) and Zn(8) are both trigonal bipyramidal with the equatorial positions

occupied by a bridging μ-1κO,2κO′ carboxylate, a μ_3-OH ion and an aqua ligand. The axial positions of Zn(7) and Zn(8) are occupied differently, with a bridging μ-1κO,2κO′ carboxylate and a μ_3-OH in the axial positions of Zn(7) and two bridging μ-1κO,2κO′ carboxylate groups in the axial positions of Zn(8).

The non-coordinating oxygen atom of the monodentate carboxylate group on Zn(1) is hydrogen bonding to the water molecule coordinated to Zn(2), O···H-O distance 2.04(11) Å, and the monodentate carboxylate group coordinated to Zn(4) is hydrogen bonding with the μ_3-OH ion bridging between Zn(2)-Zn(4), O-H···O distance 2.09(3) Å. In the second tetranuclear node there is also hydrogen bonding between the monodentate carboxylate group coordinated to Zn(5) with the μ_3-OH ion bridging between Zn(5)-Zn(7), O···H-O distance 2.23(3) Å.

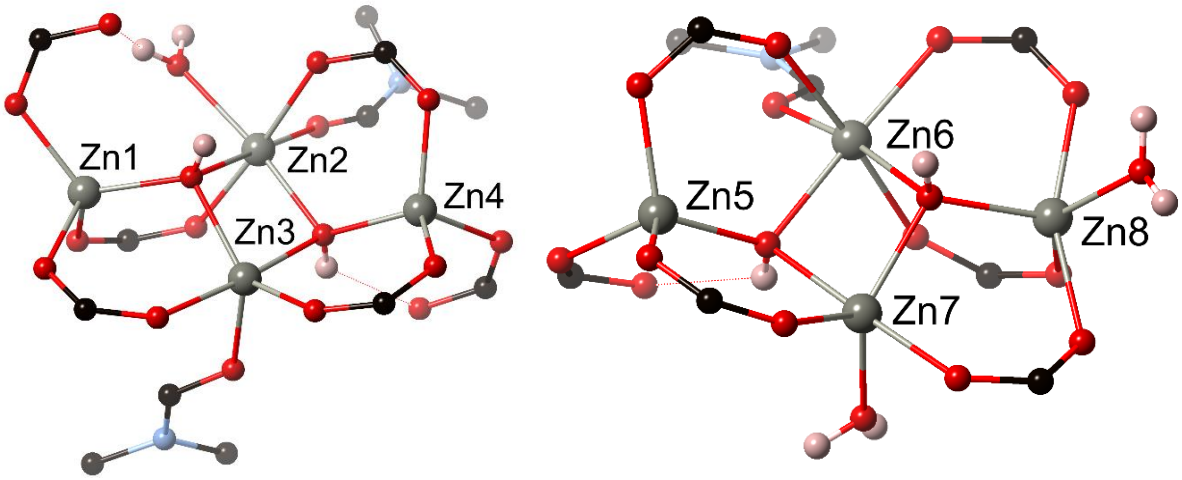

*Figure 2.14. The two crystallographically independent tetranuclear Zn^{II} nodes in the structure of **2.10**. Hydrogen bonding shown as dotted red line. Only O-H hydrogen atoms are shown for clarity.*

As there are three instead of two LeuNDI ligands bridging pairs of metal nodes, the metallomacrocycles which were observed in the structures of **2.1 - 2.3** and **2.5 - 2.9** are not present. It appears that the flexibility in the coordination environment of Zn^{II} allows it to adopt these tetranuclear nodes, which are bridged by three ligands. The 1D chains are not interpenetrated, as the tri-ligand links do not have space within them to allow the formation of catenane motifs, as was the case with the $[M_2(NDI]_2$ metallomacrocycles. There are face-to-face π-interactions between two NDI ligands of neighbouring chains, with a minimum C···C

distance of 3.369(17) Å. There is only one LeuNDI ligand engaged in π-interactions in each tri-ligand linker, and they alternate in direction between nodes, Figure 2.15.

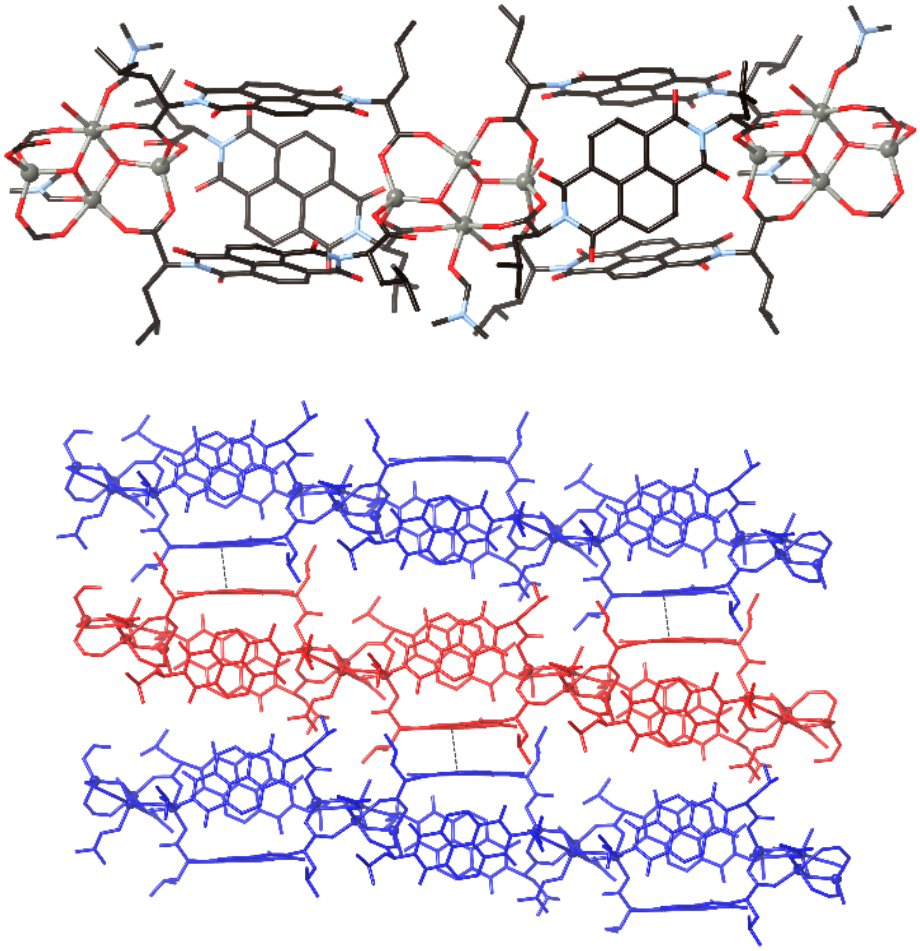

*Figure 2.15. The 1D chains of **2.10**. Two tri-ligand linkers bridging the tetranuclear nodes (top). The chains aligned with one another, with π-interactions between alternating tri-ligand linkers shown in black dashed lines (bottom).*

The coordination behaviour of LeuNDI was further explored by the reaction of H_2LeuNDI with $MnCl_2 \cdot 4H_2O$ and dpe. The reaction formed a crystalline product of the formula *poly*-[Mn(HLeuNDI)$_2$(dpe)]·MeOH, **2.11**. The structure of **2.11** is modelled in the chiral space group $P2_1$ and the asymmetric unit contains a Mn^{II} ion, two HLeuNDI ligands and a dpe ligand. The material also includes one methanol molecule per asymmetric unit which could not be modelled in the crystal structure but was assigned through microanalysis and TGA. The Mn^{II} adopts a distorted octahedral geometry, in which the equatorial positions are occupied by two *trans* monodentate carboxylate groups and two monodentate

carboxylic acid groups of the HLeuNDI ligand, and the axial positions are occupied by dpe ligands. Hydrogen bonding occurs between the carboxylic acid groups and the non-coordinating oxygen atoms of the carboxylate groups, (O-H···O distances = 1.663(4) Å and 1.619(4) Å). The structure of **2.11** is very similar to **2.6**, both involving 1D chains of conjoined $\{Mn(HLeuNDI)_2\}$ metallomacrocycles with monometallic nodes, which are bridged into (4,4) sheets by the dpe ligands occupying the axial positions of the octahedral Mn^{II}, Figure 2.16. The compounds of **2.6** and **2.11** were synthesised by identical reaction conditions. In the same manner as **2.6** the sheets are 2D → 2D interpenetrated by a rotaxane motif of the dpe ligands threading through the macrocycles, engaging in face-to-face π-interactions, in this case at the closest C···C distance of 3.358(9) Å.

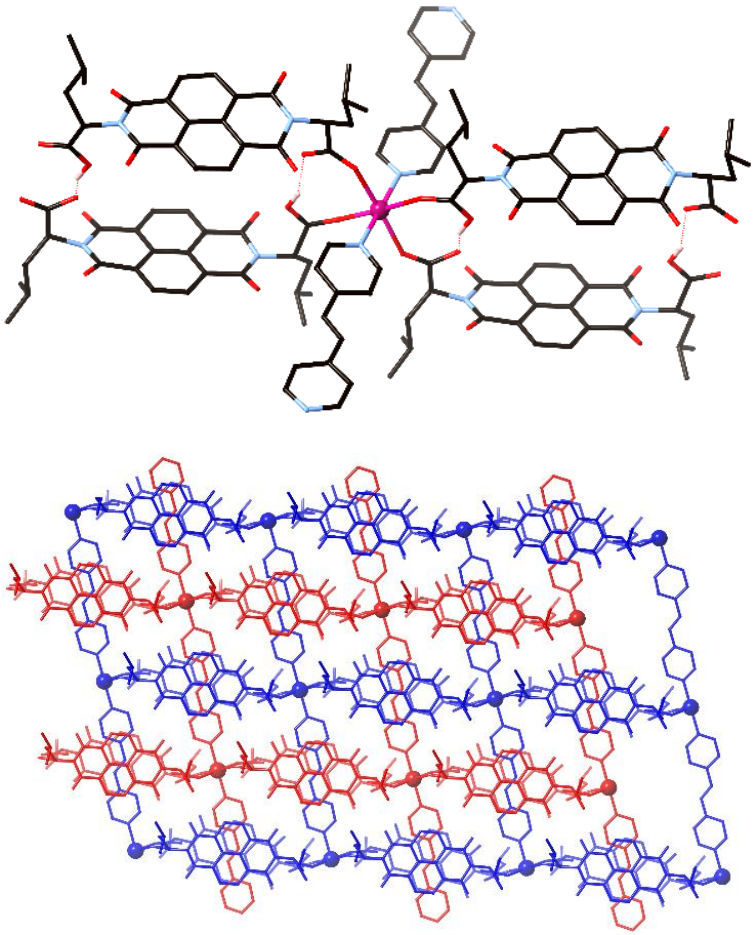

*Figure 2.16. The metal coordination environment in the structure of **2.11** (top) with the hydrogen bonding shown in red dashed lines. The 2D → 2D interpenetration by a rotaxane motif of the dpe ligands threading through the metallomacrocycles (bottom). All hydrogen atoms which are not engaged in hydrogen bonding are omitted for clarity.*

The structures of **2.6** and **2.11** both involve face-to-face π-interactions between the NDI and dpe ligands in the rotaxane motif. In the structure of **2.6** there are also π-interactions between the external faces of the NDI ligands of adjacent sheets (*vide supra*). The bulky isobutyl side chain of HLeuNDI appears to prohibit π-interactions between the sheets of **2.11**. The unit cells of the structures of **2.6** and **2.11** are very similar, with the exception of the *b*-axis which is longer in **2.11** to account for the greater height of the HLeuNDI ligand due to the isobutyl side chains in comparison to the methyl side chains of HAlaNDI ligand, Figure 2.17. The $\{Mn(HAlaNDI)_2\}$ macrocycles of **2.6** are only slightly offset from each other as they are engaged in π-interactions. In contrast, the $\{Mn(HLeuNDI)_2\}$ macrocycles of **2.11** are offset from each other, as the isobutyl side chains sit above the NDIs of adjacent sheets which are not engaged in π-interactions between sheets. The structures of **2.6** and **2.11** demonstrate that AlaNDI and LeuNDI may form very similar coordination polymers with a rotaxane motif, however the bulkiness of the side chain can change their packing.

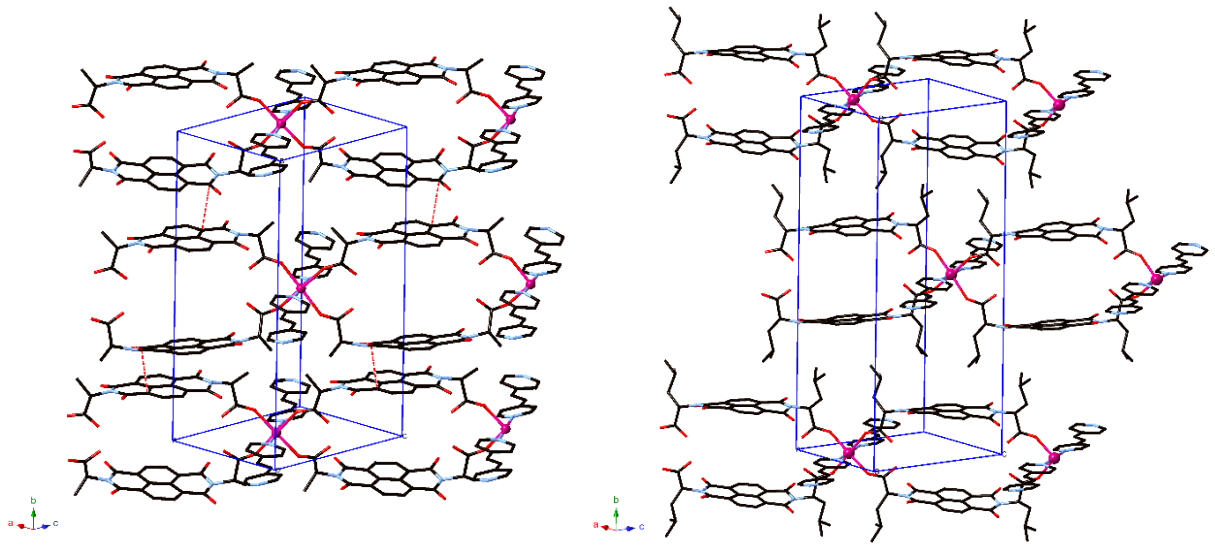

*Figure 2.17. The packing within the unit cells of **2.6** (left) and **2.11** (right). The π-interactions in **2.6** are shown as red dashed lines. All hydrogen atoms are omitted for clarity.*

The coordination behaviour of LeuNDI with Mn^{II} was further explored using 1,4-bis-(4-pyridyl)benzene (bpb), a dipyridyl ligand which is longer than 4,4′-bipy and dpe. The reaction of H_2LeuNDI, $Mn(NO_3)_2{\cdot}4H_2O$ and bpb was carried out under identical reaction conditions to those which formed

compounds **2.2** – **2.9** and **2.11**, yielding a crystalline product of a coordination polymer with formula *poly*-$[Mn_4(LeuNDI)_4(dpb)_2(DMF)_2(OH_2)_2]\cdot DMF\cdot 4.5H_2O$, **2.12**. The structure of **2.12** is modelled in the chiral space group *P*1 and the asymmetric unit contains four Mn^{II} ions, four LeuNDI ligands, two bpb ligands, two aqua ligands and two ligated DMF molecules as well as two non-coordinated water molecules, one of which is modelled at half occupancy, and a non-coordinated DMF molecule. The material also contains three water molecules which could not be modelled crystallographically, but were assigned through TGA, SQUEEZE and microanalysis.

The Mn^{II} ions from bimetallic nodes which are bridged by two LeuNDI ligands, forming 1D chains of $\{Mn_2(LeuNDI)_2\}$ metallomacrocycles, analogous to those of **2.2**, **2.3** and **2.7**. All four of the Mn^{II} ions adopt a distorted octahedral geometry in which the axial positions are occupied by a chelating carboxylate and two carboxylate groups bridging between the metals of the bimetallic node in a μ-1κO,2κO′ coordination mode. The axial positions of each Mn^{II} are occupied by one bpb ligand and a solvent molecule, water molecules in the case of Mn(1) and Mn(2) and DMF molecules for Mn(3) and Mn(4). The two bpb ligands on the bimetallic nodes are pointing in opposite directions to each other, bridging the 1D metallomacrocycle chains into a (4,4) sheet by single pillars of bpb, Figure 2.18.

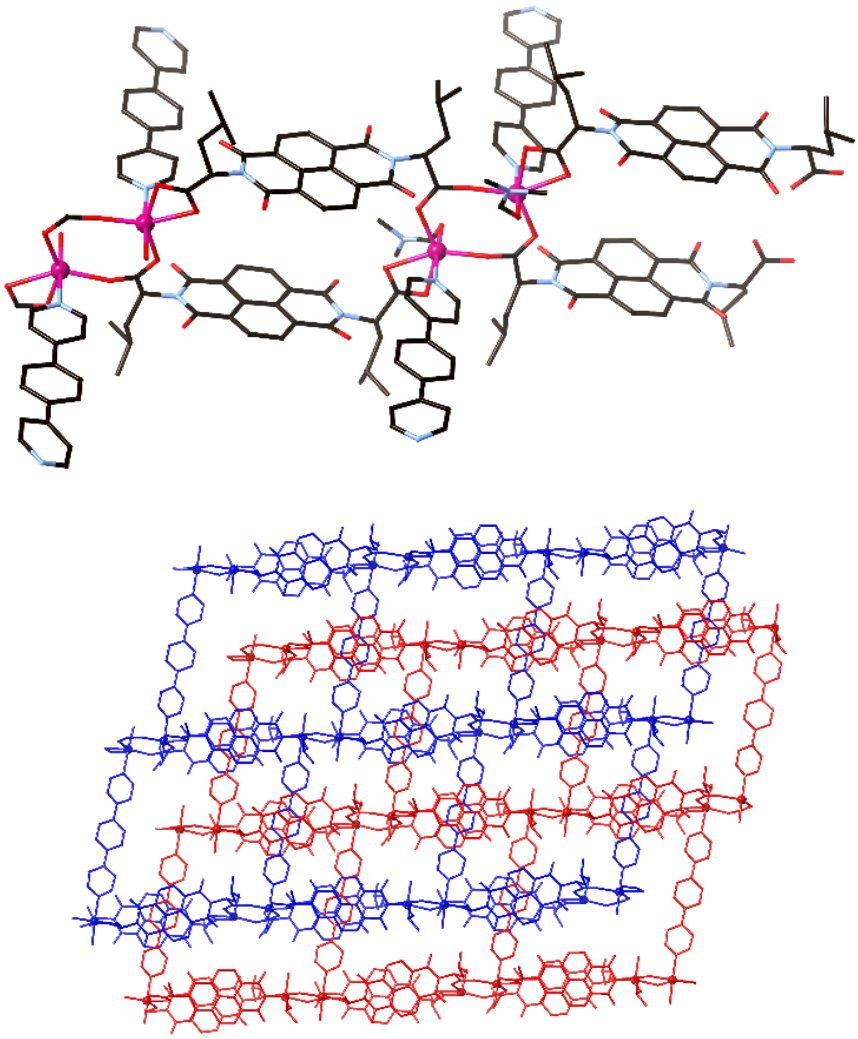

*Figure 2.18. The metal coordination environments present in **2.12** (top) and the 2D → 2D parallel interpenetration by a rotaxane motif (bottom).*

The 2D sheets of **2.12** are very similar to those of **2.6** and **2.11**, with the exception that they involve bimetallic nodes to allow for charge balance of the fully deprotonated LeuNDI ligand, and there is only one dipyridyl ligand coordinated to each metal centre, in comparison to the two dipyridyl ligands coordinated to each Mn^{II} in **2.6** and **2.11**, allowing the bpb ligands to act as single pillars in order to bridge the NDI macrocycle chains into sheets. As with **2.6** and **2.11** the 2D sheets are interpenetrated by a rotaxane motif in which the dipyridyl ligand, in this case bpb, threads through the metallomacrocycle, engaging in π-interactions with minimum C···C distance of 3.2889(14) Å and 3.3665(14) Å. If both axial positions of the

Mn^{II} were occupied by dipyridyl ligands, they would form double pillars, which would be too wide to fit through the macrocycle and would therefore inhibit interpenetration, as was the case in the structure of **2.7**. The structure of **2.12** may also be compared to those of **2.2** and **2.3** which also involve 1D chains of conjoined $\{M_2(NDI)_2\}$ macrocycles which are bridged into a 2D sheet by dipyridyl ligands. However this is where the similarities between these compounds end. Of the total of four axial positions of the bimetallic nodes in **2.2** and **2.3**, only one is occupied by a dipyridyl ligand, which leads to the 1D chains being bridged into a (6,3) sheet, compared to the two dipyridyl ligands on each bimetallic node of **2.12** leading to a (4,4) sheet. The interpenetration of **2.2** and **2.3** occurs via a catenane motif between macrocycles of chains which are perpendicular to one another. In contrast, the interpenetration of **2.12**, as well as **2.6** and **2.11**, occurs by a rotaxane motif, allowing the NDI chains to be aligned parallel to one another.

The use of bpb with LeuNDI was further investigated by their reaction with $Cd(NO_3)_2{\cdot}4H_2O$ in DMF, which yielded a crystalline product which was analysed to reveal a material of the formula *poly*-$[Cd_4(bpb)_2(DMF)_8(LeuNDI)_4]{\cdot}6H_2O{\cdot}0.5DMF$, **2.13**. The structure of **2.13** is modelled in the chiral space group *P*1 and contains in its asymmetric unit four Cd^{II} ions, four LeuNDI ligands, two bpb ligands and eight coordinated DMF molecules. Microanalysis and thermogravimetric analysis, with SQUEEZE analysis of the voids in the structure, were used to assign an additional six water molecules and half a DMF molecule per formula unit. Each of the Cd^{II} ions adopts a distorted octahedral geometry in which the equatorial positions are occupied by one chelating and one monodentate carboxylate group and a bpb ligand, and the axial positions are occupied by DMF ligands, Figure 2.19. The LeuNDI ligands form $\{Cd_2(LeuNDI)_2\}$ metallomacrocycles with monometallic nodes which are bridged into a 1D chain by bpb ligands. The chains are interpenetrated by a rotaxane motif in which the bpb ligands thread through the macrocycles of perpendicular chains, forming a 1D → 2D polyrotaxane, Figure 2.19. There are face-to-face π-interactions between the NDIs and bpb, with closest C···C distances of 3.373(13) Å and 3.361(15) Å.

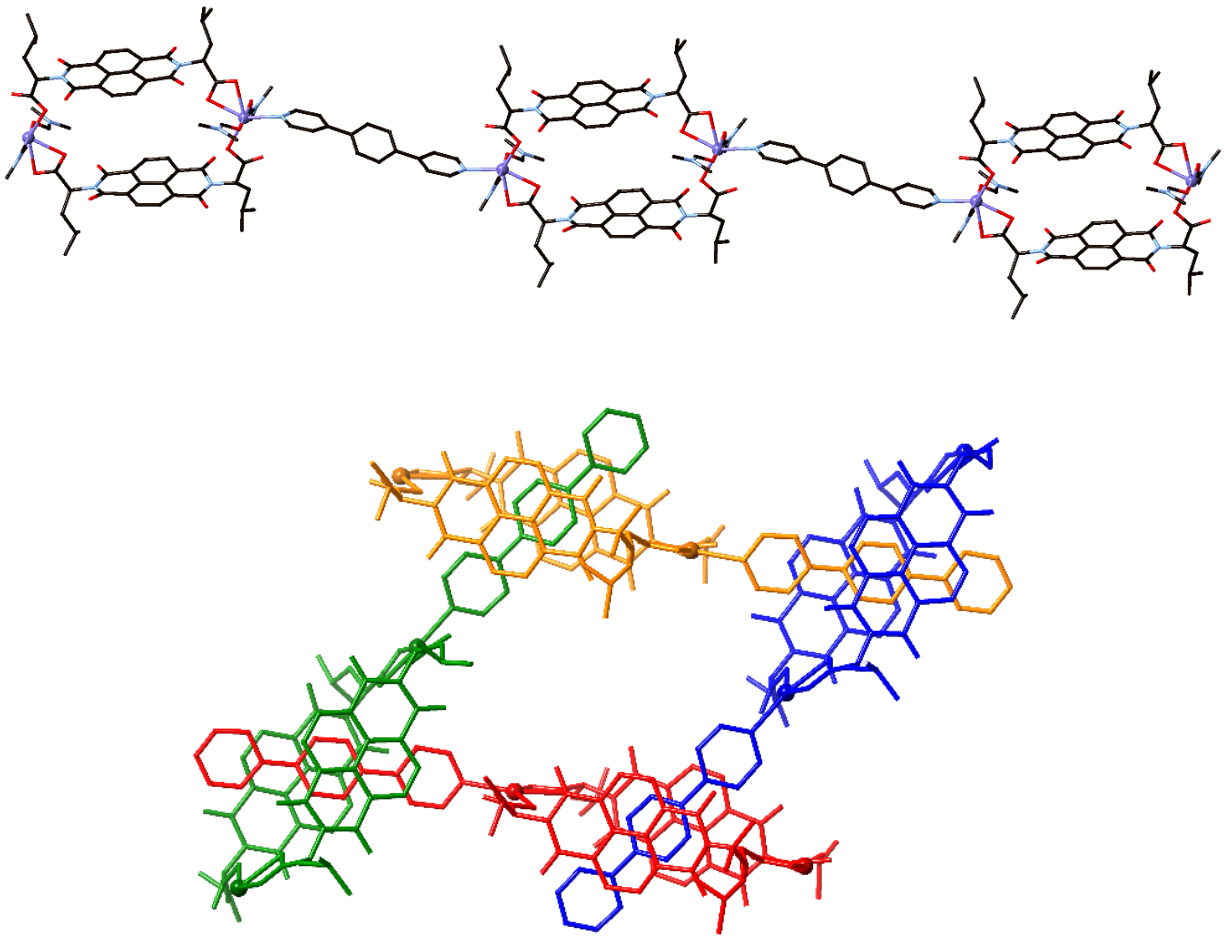

*Figure 2.19. The 1D chain in **2.13** involving metallomacrocyclic motifs which is bridged by bpb ligands (top) and the 1D → 2D interpenetration of the 1D chains by a rotaxane motif (bottom). For clarity all hydrogen atoms are omitted, and coordinated solvent is omitted from the packing diagram.*

The 1D chains of **2.13** are very similar to the chains present in **2.1**, **2.9** and the chains in the previously reported coordination polymer *poly*-[Cd_2(LeuNDI)$_2$(4,4′-bipy)(DMF)$_3$(OH_2)] which is a 1D → 3D polyrotaxane. In the same manner as **2.1** the 1D chains of **2.13** form a 1D → 2D polyrotaxane. The 1D → 3D polyrotaxane adopts this topology presumably because this is the most efficient packing arrangement for chains of alternating {Cd_2(LeuNDI)$_2$} macrocycles and 4,4′-bipy due to the bulkiness of the isobutyl side chain, the length of 4,4′-bipy and the π-interactions between the NDI macrocycles and 4,4′-bipy. In **2.1**, **2.13** and the 1D → 3D polyrotaxane there are face-to-face π-interactions between the macrocycle and the dipyridyl ligand threading through them. Due to the bulky isobutyl side chain of the LeuNDI ligand in

2.13 and the 1D → 3D polyrotaxane, there are no π-interactions between the external faces of the NDI macrocycles, instead the isobutyl groups of the LeuNDI of neighbouring chains sit above the NDI macrocycles. The chains of alternating $\{Cd_2(LeuNDI)_2\}$ and bpb present in **2.13** form a 1D → 2D polyrotaxane most likely because the extra length of the bpb compared to 4,4′-bipy allows this topology to form the most efficient packing of the chains.

The formation of a 1D → 2D polyrotaxane of **2.13** may also be explained in terms of the difference in the arrangement of the NDIs and the bpb ligand within the chains, in comparison to **2.1** and the 1D → 3D polyrotaxane. In the chains of alternating $\{Cd_2(AlaNDI)_2\}$ and 4,4′-bipy in **2.1** the planes of the NDIs and 4,4′-bipy are co-planar, forming completely straight chains which form a 1D → 2D polyrotaxane, Figure 2.20. In the of case the 1D → 3D polyrotaxane, the 4,4′-bipy is twisted by 35° with respect to the plane of the NDI macrocycle, leading to a 3D polyrotaxane, Figure 2.20. However in the case of **2.13** the chains are not straight in relation to the plane of the NDIs, as the bpb is offset by ~ 18° away from the plane of the NDIs, Figure 2.20. It appears that this difference in the arrangement of the macrocycles and bpb in the chains may allow a 1D → 2D polyrotaxane to form, despite the bulky side chains of the LeuNDI ligand. It also appears that using a longer and wider dipyridyl ligand will inhibit the formation of a polyrotaxane, as was the case with **2.9** which consists of 1D chains of alternating $\{Cd_2(AlaNDI)_2\}$ macrocycles and 4PyNDI ligand which had no interpenetration.

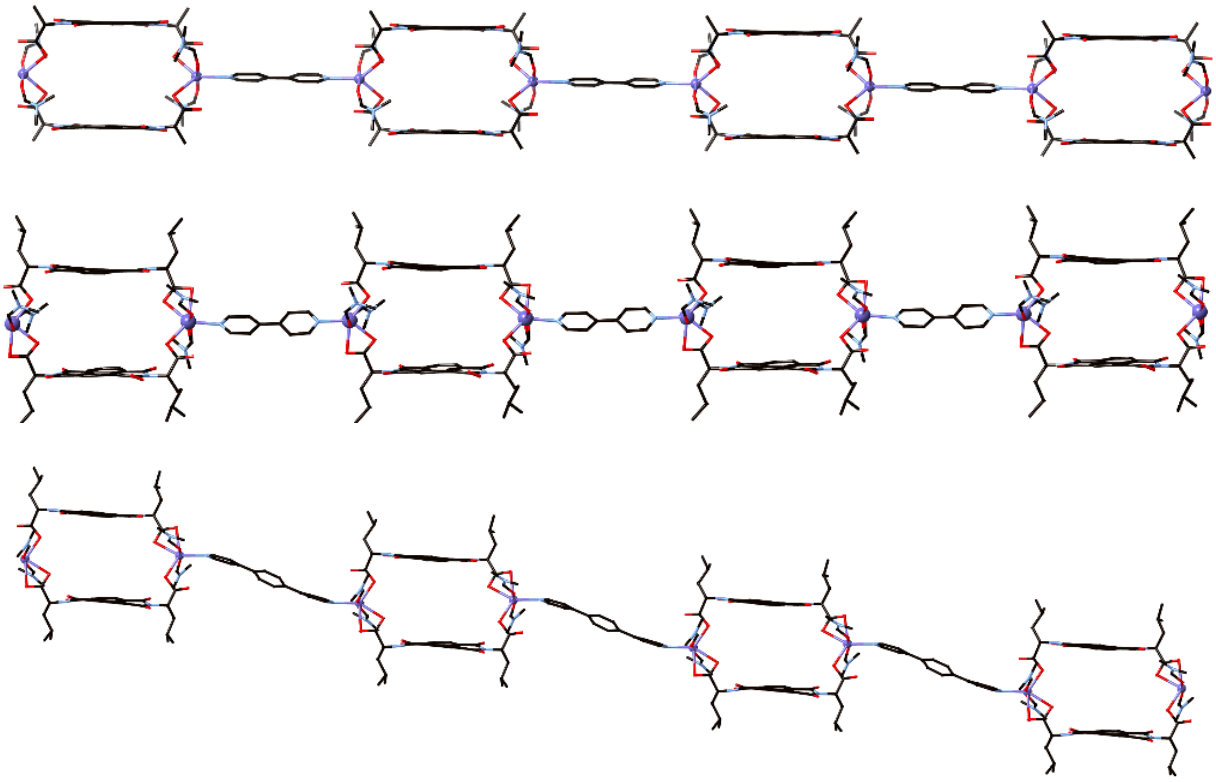

*Figure 2.20. The straight 1D chains of **2.1** (top) which form a 2D polyrotaxane, the chains of previously reported poly-[Cd_2(LeuNDI)$_2$(4,4′-bipy)(DMF)$_3$(OH_2)] which from a 3D polyrotaxane (centre) and the chains of **2.13** in which the bpb ligand is offset from the NDI plane and forms a 2D polyrotaxane (bottom).*

The chains in **2.1**, **2.13** and the 1D → 3D polyrotaxane are also slightly different in how the dipyridyl ligand threads through the macrocycle. In the case of **2.1** and the 3D polyrotaxane, the 4,4′-bipy intersects with the macrocycle at ~ 90°, however in the case of **2.13** the bpb intersects the macrocycle at ~ 59°. The change in how the dipyridyl ligand threads through the macrocycle is possibly due to the increased length of bpb in comparison to 4,4′-bipy. The shorter 4,4′-bipy dipyridyl ligand is forced to take the shortest route through the macrocycle, due to the steric effects of the neighbouring NDI ligands, however the longer bpb dipyridyl ligand has more flexibility in how it threads through the macrocycle, allowing the 1D chains to be rotated in relation to the macrocycles.

The structures of **2.12** and **2.13** demonstrate that a slight increase in the length of a dipyridyl ligand coupled with {M_2(NDI)$_2$} macrocycles can lead to unexpected interpenetration topologies. In the case of **2.12** an interpenetrating (4,4) sheet is formed with single dipyridyl ligand pillars between chains of conjoined NDI

macrocycles with bimetallic nodes, while this topology had only previously been observed with NDI ligands which were not fully deprotonated and therefore formed chains with monometallic nodes. In the case of **2.13** 1D chains of alternating $\{M_2(NDI)_2\}$ macrocycles and dipyridyl ligand formed a 1D → 2D polyrotaxane, despite analogous chains with 4,4′-bipy forming a 3D polyrotaxane in the case of LeuNDI and a 2D polyrotaxane in the case of AlaNDI.

2.5 Coordination polymers utilising the PheNDI ligand with a bulky aromatic side chain

Previous work using AlaNDI and LeuNDI ligands revealed that both were capable of forming an $\{M_2(NDI)_2\}$ metallomacrocyclic motif when incorporated into coordination polymers (*vide supra*).[71, 352, 356] In the case of the {Cd(AlaNDI)} macrocycles, catenation of these rings usually occurs, whereas this is not the case for the more sterically encumbered {Cd(LeuNDI)} macrocycles. The phenylalanine-containing H_2PheNDI is also bulky, with the added 'complication' of phenyl rings which can compete with NDI···NDI interactions.

A coordination polymer with PheNDI was sought in the absence of any dipyridyl ligands, to explore the coordination behaviour of the ligand. The reaction of H_2PheNDI with $MnCl_2{\cdot}4H_2O$ at 70 °C in a solvent mixture of DMF, MeOH and H_2O (2:1:1) yielded yellow crystals that were structurally characterized to reveal the material *poly*-$[Mn(DMF)_2(HPheNDI)_2]{\cdot}MeOH{\cdot}H_2O$, **2.14**. Whereas most of the coordination polymers which were previously reported by the Turner group, and those discussed above, contain fully deprotonated amino acid ligands, with the exception of **2.6** and **2.11**, only one of the carboxylic acids of each ligand in **2.14** is deprotonated. The Mn^{II} ion has a distorted octahedral geometry in which the equatorial sites are occupied by two monodentate carboxylate groups and two monodentate carboxylic acid groups, and the axial sites are occupied by two DMF ligands, Figure 2.21. Each carboxylic acid group forms a hydrogen bond with a carboxylate group coordinated to the same metal ion. Each HPheNDI ligand bridges between two metal nodes, forming a (4,4) sheet, Figure 2.21. The combination of the π-rich naphthalene core and the phenyl side chain of the ligand leads to π-π interactions within the structure. There are two near-parallel face-to-face π-interactions between a phenyl group of an HPheNDI ligand with the

naphthalene core of a neighbouring ligand within the windows of the 2D sheets (closest C···C distances = 3.376(3) and 3.4355(9) Å). Two unique non-parallel π-interactions exist between adjacent sheets (closest C···C distances = 3.2789(5) and 3.3959(7) Å, inter-planar angles 32.148(7) and 33.197(9)°, respectively). Despite repeated attempts, coordination polymers of the form [M(PheNDI)] could not be isolated.

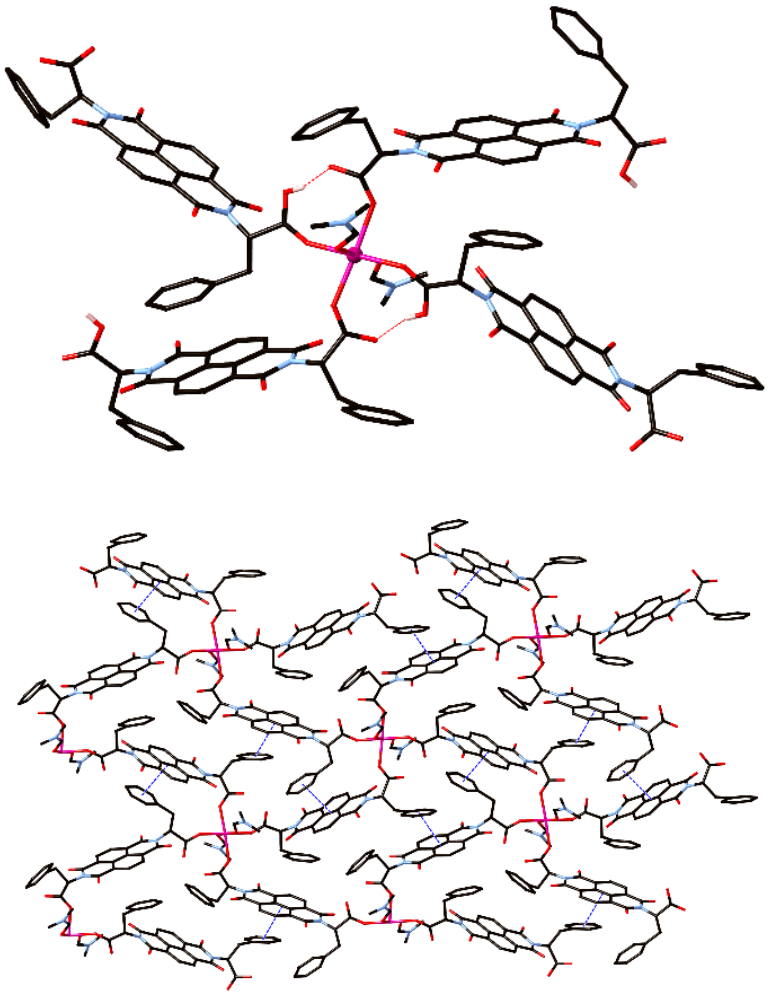

Figure 2.21. The metal coordination environment in the structure of ***2.14****, showing hydrogen bonding as red dashed lines (top). The 2D sheet of* ***2.14*** *showing π-π interactions within the sheet between the NDI core and the phenyl side chain as blue dashed lines (bottom). Hydrogen atoms are omitted for clarity.*

In a similar manner to **2.6** and **2.11** which involved mono-deprotonated NDI ligands, the structure of **2.14** also contains mono-metallic nodes, to account for charge balance. They all involve hydrogen bonding between the carboxylic acids and the non-coordinating carboxylate oxygen atoms. The structure of **2.14** is

quite different to that of **2.6** and **2.11** in that it does not include a dipyridyl ligand, and is not interpenetrated. The interpenetration in **2.6** and **2.11** is through a rotaxane motif of the dipyridyl ligand with the $\{M_2(NDI)_2\}$ macrocycle. It appears that **2.14** is not interpenetrated because the PheNDI ligands do not form a macrocycle and so cannot interpenetrate by a catenane motif, and **2.14** does not have a dipyridyl ligand which could be interpenetrate by a rotaxane motif. It is possible for NDI ligands which do not form the common macrocycle motif to be interpenetrated, as was shown by the structure of **2.4** which was 3D → 3D interpenetrated and a previously reported coordination polymer, *poly*-[Ca(AlaNDI)$(DMF)_2$], which was 2D → 3D interpenetrated, both of which involve face-to-face π-interactions of the NDIs of the entangled networks.[348] However it appears that the sheets of **2.14** are not interpenetrated due to the bulky phenyl side chain, which act to block the interpenetration and compete for π-interactions with the NDIs, as can be seen by the prevalence of these interactions within and between the sheets of **2.14**.

PheNDI was also explored with the addition of dipyridyl ligands to explore if the phenyl side chain would change the coordination and interpenetration of the coordination polymers obtained, in comparison to the AlaNDI and LeuNDI ligands. H_2PheNDI, $Cd(NO_3)_2{\cdot}4H_2O$ and 4,4'-bipy were reacted at identical conditions which yielded **2.2** – **2.9**, **2.11** and **2.12**. The reaction yielded crystals which were analysed by X-ray crystallography to reveal a coordination polymer of the formula *poly*-[Cd(4,4′-bipy)(OH_2)(PheNDI)]$\cdot 3.5H_2O\cdot$DMF, **2.15**. The Cd^{II} ion adopts a distorted pentagonal bipyramidal geometry, with two chelating carboxylate groups and an aqua ligand occupying the equatorial sites and the nitrogen donor atoms of two 4,4′-bipy ligands occupying the axial sites, Figure 2.22. The PheNDI ligands adopt a "U-shaped" geometry and form $\{Cd_2(PheNDI)_2\}$ metallomacrocycles which have been shown to be almost ubiquitous in the NDI coordination polymers discussed thus far. The $\{Cd_2(PheNDI)_2\}$ metallomacrocycles are bridged into a ladder-like 1D chain by the 4,4′-bipy ligands forming an apparent 'tube' of metallomacrocycles that propagates parallel to the *c*-axis. The plane of the naphthalene core of the PheNDI ligand is approximately perpendicular (84°) to the plane of the 4,4′-bipy ligands, which allows π-π stacking between these two ligands of adjacent chains (closest C⋯C distance = 3.353(11) Å), Figure 2.22. In addition to the face-to-face π-interactions with the NDI core, the 4,4′-bipy is also nestled between

the flanking phenyl side chains, with CH···π interactions from the 4,4′-bipy to the phenyl rings (CH···centroid distances = 2.7216(4) and 2.9890(4) Å).

Although the planes of the NDIs within the metallomacrocycles in **2.15** are 7.621(3) Å apart, a suitable distance for π-interactions to occur with an aromatic guest to form a polyrotaxane or polycatenane, the metallomacrocycle remains 'empty'. The structure of **2.15** exhibits 24.6% void volume (as calculated using Mercury),[376] corresponding to the channels through the metallomacrocycles in which no solvent was able to be modelled from the diffraction data. The solvent in the channels was assigned as 3.5 water molecules and one DMF molecule through TGA, microanalysis and residual electron density. Based on previous results of coordination polymers involving NDI metallomacrocycles, such as **2.1**, **2.5** and previously reported 1D → 3D polyrotaxane, *poly*-[Cd_2(LeuNDI)$_2$(4,4′-bipy)(DMF)$_3$(OH_2)], it was expected that the 4,4′-bipy ligand may thread through the metallomacrocycle, given the potential for favourable π-interactions. However, the configuration of the phenyl side chains on the PheNDI ligand seems to generate too much steric bulk for two NDIs to approach closely to each other, as demonstrated by the excellent size fit of the 4,4′-bipy ligands between the phenyl rings. In a similar manner to the previously reported 1D → 3D polyrotaxane, *poly*-[Cd_2(LeuNDI)$_2$(4,4′-bipy)(DMF)$_3$(H_2O)], in which the isobutyl side chain of the LeuNDI ligand was too bulky to allow polycatenation of the NDI metallomacrocycles and there were π-interactions between the NDI and the 4,4′-bipy, the structure of **2.15** demonstrates that the addition of 4,4′-bipy to an NDI ligand with a bulky side chain will lead to π-interactions between the 4,4′-bipy and NDI ligands.

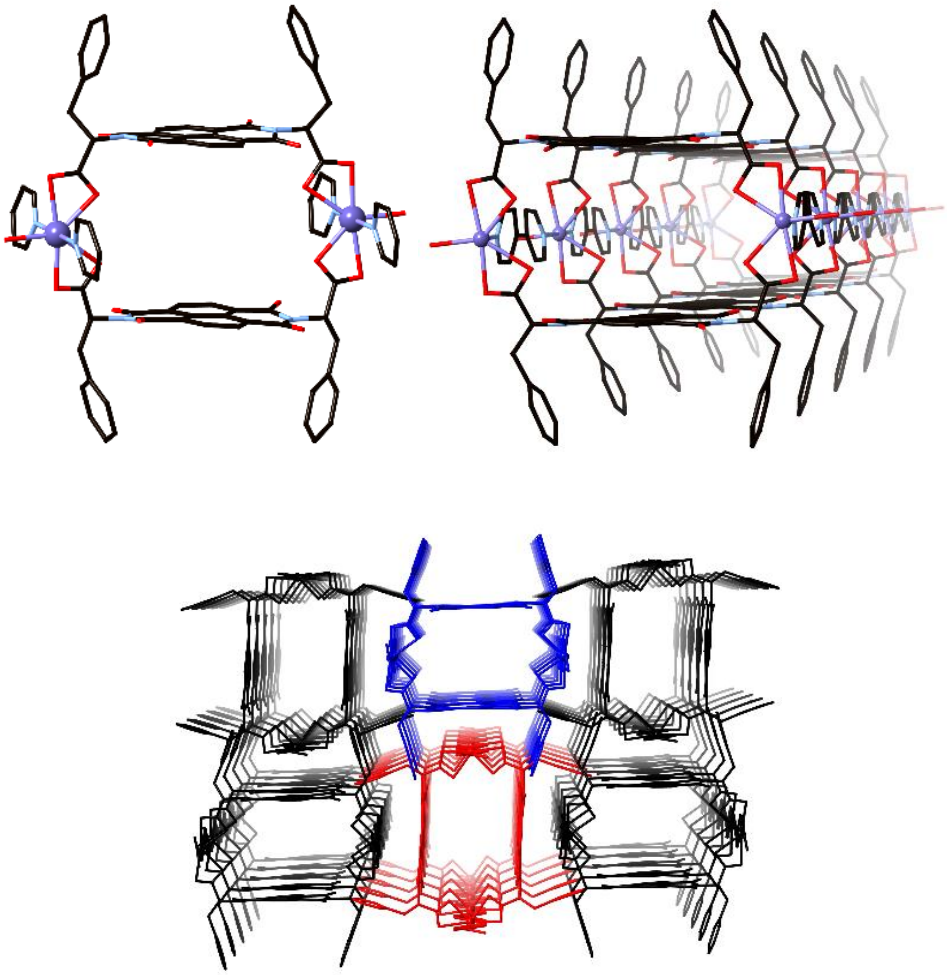

*Figure 2.22. The {Cd_2(PheNDI)$_2$} metallomacrocycle motif in the structure of **2.15**, showing the coordinated 4,4′-bipy ligands and the aqua ligand (left). The 1D chain of **2.15** showing the plane of the NDI perpendicular to the plane of the 4,4′-bipy (right). The packing of the 1D chains by π-interactions between the 4,4′-bipy ligands of one chain with the NDIs of the adjacent chains (bottom). All hydrogen atoms, and the aqua ligands in the case of the packing diagram, have been omitted for clarity.*

Based on previous results, it is conceivable that in the absence of the phenyl side chain, **2.15** may interpenetrate by either a catenane or rotaxane motif. In the same way as the structure of **2.14**, the structure of **2.15** also shows a lack of interpenetration in a coordination polymer which would have been expected to be interpenetrated if it had a less sterically demanding side chain. The structure of **2.15** demonstrates that the phenyl side chain in its bulkiness and aromaticity, is likely to inhibit interpenetration by steric effects and by competing for π-interactions.

The influence of synthetic conditions and metal ion on the structure of coordination polymers is demonstrated by the reaction of H_2PheNDI, $Mn(NO_3)_2{\cdot}4H_2O$ and 4,4′-bipy at 70 °C in a DMF/H_2O mixture (2:1) which yielded orange crystals of the formula *poly*-{[Mn_2(PheNDI)$_2$(4,4′-bipy)$_2$][Mn(4,4′-bipy)(DMF)$(NO_3)_2$]·0.5DMF·7H_2O}, **2.16**. The structure of **2.16** is similar to that which was previously reported with Cd^{II}, *poly*-{[Cd_2(4,4′-bipy)$_2$(PheNDI)$_2$][Cd(4,4′-bipy)(DMF)$_{1.5}(NO_3)_2(OH_2)_{0.5}$]·DMF}. The structure of **2.16** involves two different entangled coordination polymers, namely a 2D sheet, [Mn_2(4,4′-bipy)$_2$(PheNDI)$_2$] and a 1D chain [Mn(4,4′-bipy)(DMF)$(NO_3)_2$], Figure 2.23. The 2D sheet is structurally similar to the 1D 'tubes' with monometallic nodes in the structure of **2.15** and can be seen as tubes that are connected side-by-side through bimetallic nodes. The {Mn_2(PheNDI)$_2$} metallomacrocycles bridge between bimetallic nodes which have one carboxylate chelating to each metal and two carboxylates that bridge the metals in a μ-1κ*O*,2κ*O*′ coordination mode, thereby forming a continuous chain of metallomacrocycles similar to those present in **2.2**, **2.3**, **2.7**, **2.12** and previously reported coordination polymers with AlaNDI in *poly*-[Cd_2(AlaNDI)$_2$(DMF)$_4$], LeuNDI in *poly*-[Cd_2(LeuNDI)$_2$(DMA)$_4$] and PheNDI in *poly*-{[Cd_2(4,4′-bipy)$_2$(PheNDI)$_2$][Cd(4,4′-bipy)(DMF)$_{1.5}(NO_3)_2(OH_2)_{0.5}$]}·DMF.[71, 352, 355] The Mn^{II} ion in the 2D sheet adopts a distorted octahedral geometry with the bridging and chelating carboxylates in the equatorial sites and the 4,4′-bipy ligands in the axial sites. Axial coordination of the 4,4′-bipy ligands on each Mn^{II} of the bimetallic node allows formation of 'double pillars' between the bimetallic nodes to bridge the metallomacrocycle chains into a (4,4) sheet, Figure 2.23. The metal centre of the 1D chain adopts a distorted pentagonal bipyramidal geometry in which the axial positons are occupied by two 4,4′-bipy ligands and the equatorial positions are occupied by a DMF molecule and two chelating nitrate ions, to account for charge balance.

The asymmetric unit also includes a DMF molecule which is modelled as half occupancy, as well as void space in which no solvent could be modelled. The solvent in the voids was assigned as an additional half occupancy DMF molecule, and seven water molecules, by TGA, microanalysis and residual electron density.

In a similar manner to the 'double pillars' present in the structure of **2.7**, the 'double pillars' of 4,4′-bipy in **2.16** are too wide to fit through the macrocycle and therefore the sheets do not interpenetrate by a rotaxane motif. Although the double pillars of dipyridyl ligands are too wide to take part in interpenetration, the macrocycles remain a suitable shape for an aromatic group to pass through and engage in π-interactions. The 1D chains of [Mn(4,4′-bipy)(DMF)$(NO_3)_2$] thread through the metallomacrocycles, with near-parallel π-interactions between the 4,4′-bipy of the chains and PheNDI ligands of the metallomacrocycles, at a closest C···C distance of 3.369(10) Å. The combination of the 2D sheet with empty macrocycles and 1D chains forms a 1D + 2D → 2D polythreaded coordination polymer. The structure of **2.16** demonstrates that an aromatic group threading through the macrocycles is a favourable interaction for these coordination polymers, however in this case the 'double pillars' of 4,4′-bipy inhibit interpenetration between the sheets, and therefore an additional 1D chain forms which threads through the macrocycles to give a polythreaded coordination polymer.

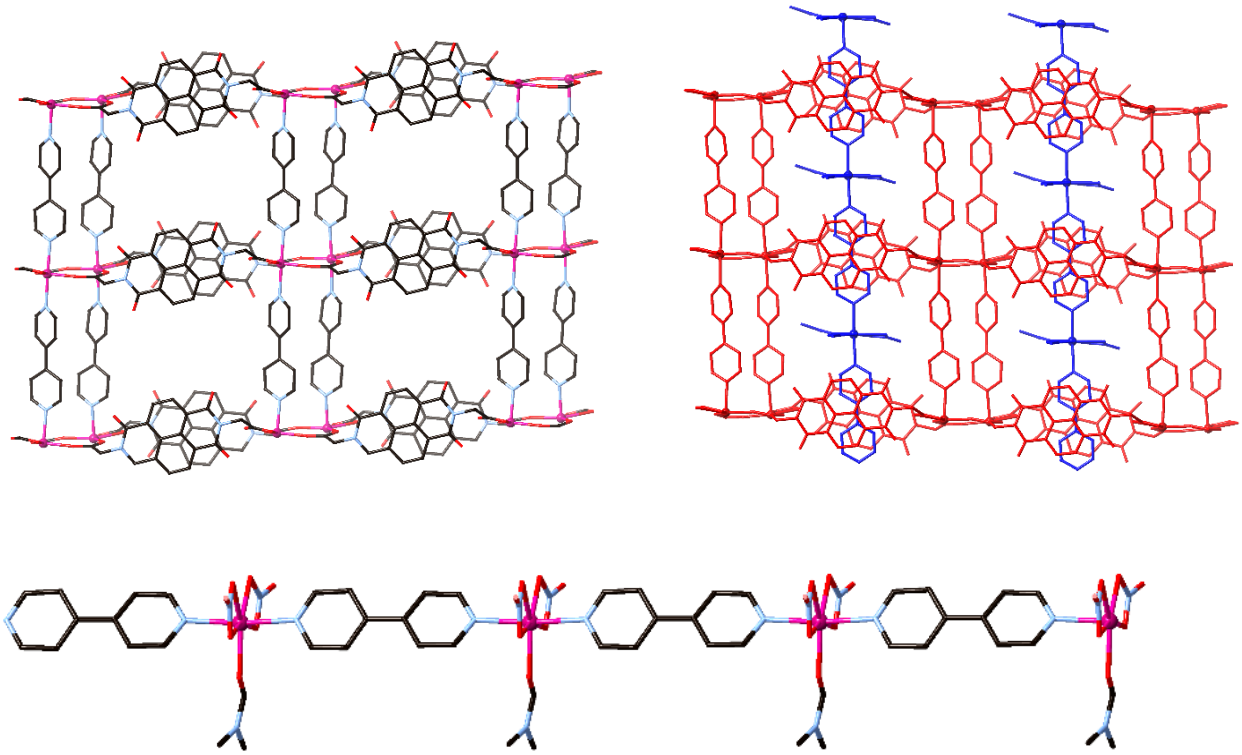

Figure 2.23. The [Mn_2(4,4′-bipy)$_2$(PheNDI)$_2$] 2D sheet (left) and the [Mn(4,4′-bipy)(DMF)(NO_3)$_2$] 1D chain (bottom) in the structure of ***2.16****. The 1D + 2D → 2D polythreaded structure formed by the 1D chain and the 2D sheet (right). All hydrogen atoms and phenyl side chains have been omitted for clarity.*

Following on from the results obtained with 4,4′-bipy, the different dipyridyl ligand, dpe, was employed in order to investigate the influence of a different dipyridyl ligand on the structure of coordination polymers with PheNDI. The reaction of H_2PheNDI, $Cd(NO_3)_2{\cdot}4H_2O$ and dpe under identical reaction conditions which formed **2.2** – **2.9**, **2.11**, **2.12** and **2.15** yielded orange crystals which were structurally analysed to show a coordination polymer of the formula *poly*-[Cd_4(DMF)(dpe)$_2$(OH_2)$_2$(PheNDI)$_4$]·10H_2O·0.5DMF, **2.17**. The asymmetric unit contains four PheNDI ligands, four dpe ligands, four Cd^{II} ions, two aqua ligands, and one DMF ligand, Figure 2.24. The four Cd^{II} ions form two crystallographically unique bimetallic nodes in the asymmetric unit of the structure, each of which is part of a crystallographically unique 2D sheet. The structure also includes void space in which no solvent could be modelled, but was assigned as ten water and 0.5 DMF molecules per asymmetric unit by TGA, microanalysis and residual electron density.

The four metal centres making up the two bimetallic nodes in **2.17** all have different coordination environments, Figure 2.24. Cd(1) has a distorted pentagonal bipyramidal coordination geometry. The equatorial sites of Cd(1) are occupied by five oxygen donor atoms from three different carboxylate groups; one carboxylate solely chelates to Cd(1), another carboxylate bridges between Cd(1) and Cd(2) in a μ-1κ*O*,2κ*O′* coordination mode and the third chelates to Cd(1) whilst also bridging to Cd(2) in an overall μ-1κ^2*O*,*O′*,2κ*O* coordination mode. The axial sites of Cd(1) are occupied by a dpe ligand and a DMF ligand. Cd(2) has a distorted trigonal bipyramidal geometry. The equatorial sites of Cd(2) are occupied by a monodentate carboxylate group and the aforementioned two bridging carboxylate groups. Similarly to Cd(1), the axial sites of Cd(2) are occupied by a dpe ligand and a solvent molecule, in this case water. In the second bimetallic node, the coordination environment of Cd(3) is distorted octahedral with the equatorial sites occupied by one chelating carboxylate group and two carboxylate groups which bridge between the metals of the bimetallic node in a μ-3κ*O*,4κ*O′* coordination mode; the axial sites are occupied by a dpe ligand and an aqua ligand. Cd(4) adopts a distorted square pyramidal geometry in which the basal sites are occupied by carboxylate groups in the same coordination modes as Cd(3), and the apical site is occupied by a dpe ligand.

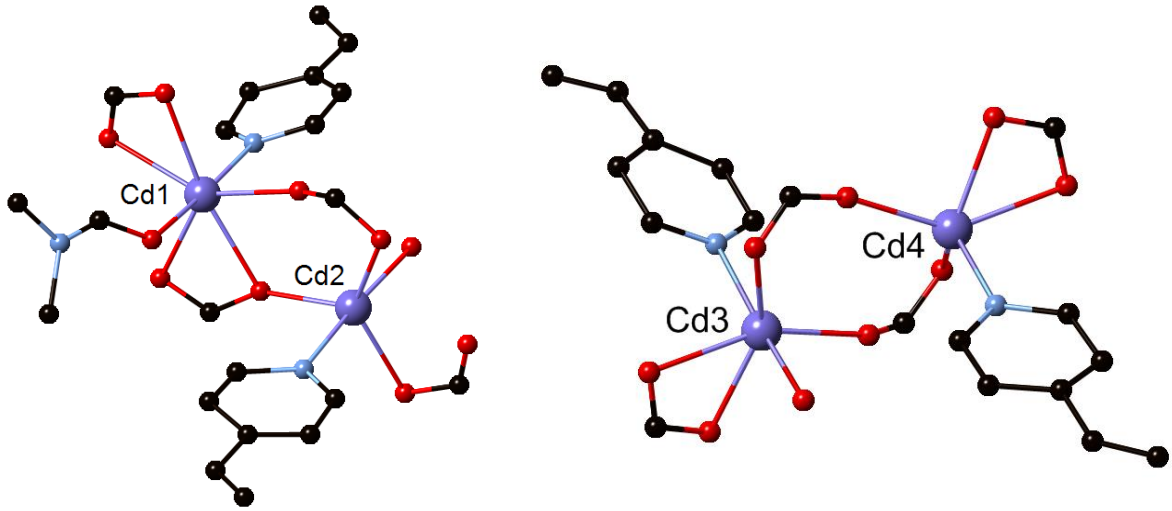

*Figure 2.24. The coordination environments of the two crystallographically unique nodes in the structure of **2.17**. Hydrogen atoms have been omitted for clarity.*

In a similar manner to the structures of **2.2**, **2.3**, **2.7**, **2.12** and **2.16**, the $\{Cd_2(PheNDI)_2\}$ metallomacrocycles in the structure of **2.17** are connected through the bimetallic nodes to form 1D chains, and these chains are bridged by dipyridyl ligands to form 2D sheets, Figure 2.25. (Note, this topological description refers to an isolated sheet, defining a macrocycle as a single linker). The structure of **2.17** is very similar to **2.12**, as they both involve 1D chains of conjoined NDI metallomacrocycles with bimetallic nodes in which one dipyridyl ligand on each metal centre bridges the chains the chains into a (4,4) sheet. In the same manner as **2.12**, the 2D sheets of **2.17** are interpenetrated by a rotaxane motif of the dipyridyl ligand, in this case dpe, threading through the metallomacrocycles and engaging in face-to-face π-interactions, with closest C⋯C distances of 3.2993(7) Å and 3.2911(11) Å, Figure 2.25. The structure of **2.17** is also similar to **2.12** in that there are no π-interactions with the external faces of the NDI metallomacrocycles, due to the bulkiness of the side chains of the amino acid substituted NDI ligands, and the side chains sit above the NDI planes of the interpenetrated sheets.

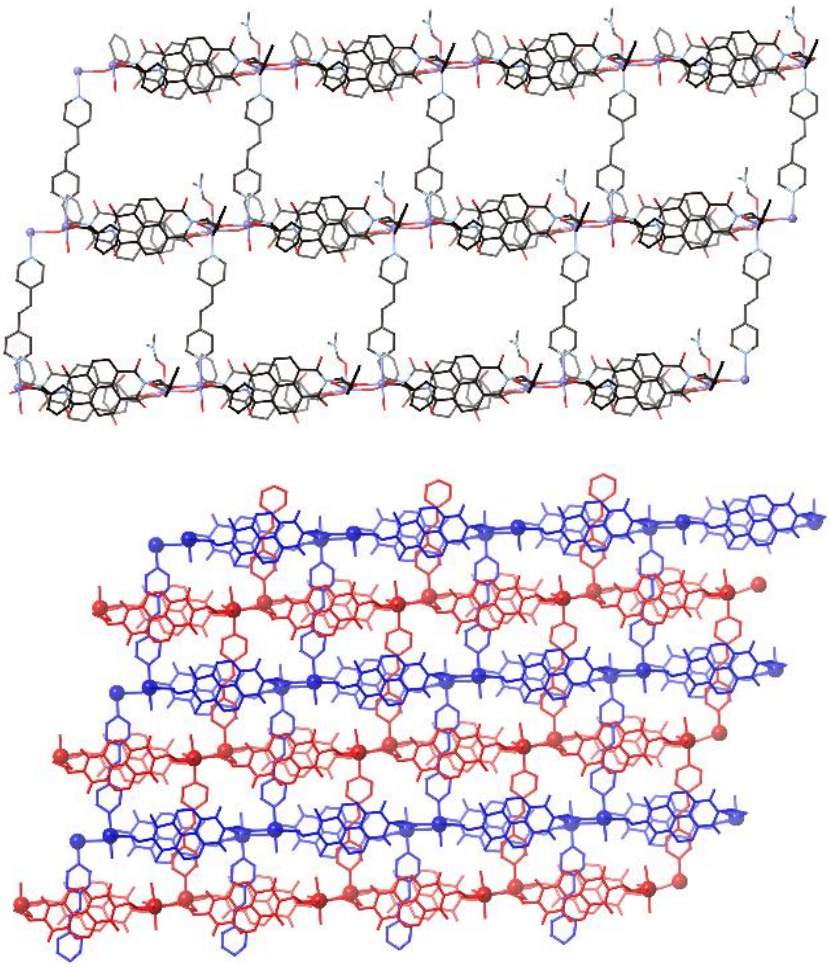

Figure 2.25. One of the two crystallographically unique 2D sheets, which are topologically identical, in the structure of ***2.17*** *(top), all hydrogen atoms are omitted for clarity. The 2D → 2D interpenetration of the two unique sheets by a rotaxane motif between the dpe ligand and the macrocycles (bottom). For clarity the hydrogen atoms and phenyl side chains are omitted.*

The coordination polymers formed with PheNDI and a wider dipyridyl ligand, 4PyNDI, were also investigated. 4PyNDI has a naphthalene core group and so is a much more π-rich system than 4,4′-bipy, bpb or dpe, although is sterically more demanding. The reaction of H_2PheNDI, $Cd(NO_3)_2$ and 4PyNDI was carried out under the same conditions which formed **2.2** – **2.9**, **2.11**, **2.12**, **2.15** and **2.17**, and yielded yellow crystals which were structurally characterized to reveal a coordination polymer of formula *poly*-$[Cd_2(PheNDI)_2(4PyNDI)_2]\cdot 6H_2O\cdot 2DMF\cdot MeOH$, **2.18**. The asymmetric unit of **2.18** contains two Cd^{II} metal centres, two PheNDI ligands, two 4PyNDI ligands and one non-coordinated DMF (other lattice

solvent molecules were assigned by analytical methods, see experimental section). The structure of **2.18** contains bimetallic nodes in a similar manner to those reported in the structures of compounds **2.2**, **2.3**, **2.7**, **2.12**, **2.14** and **2.17**. The two Cd^{II} ions in the structure of **2.18** adopt different coordination environments, very similar to Cd(1)/(2) in the structure of **2.17**. Cd(1) has a distorted octahedral geometry with the equatorial sites occupied by three different carboxylate groups; one carboxylate solely chelating to Cd(1), one carboxylate bridging between Cd(1) and Cd(2) in a μ-1κO,2κO′ coordination mode and the third bridging between Cd(1) and Cd(2) whilst also chelating to Cd(2) in an overall μ-1κO,2κ^2O, O′ coordination mode. The axial sites of Cd(1) are occupied by the nitrogen donor atoms of two 4PyNDI ligands. Cd(2) has a distorted pentagonal bipyramidal coordination geometry in which the equatorial sites are occupied by three different carboxylate groups, one chelating to Cd(2) and two bridging carboxylates as described above. The axial sites of Cd(2) are occupied by two 4PyNDI ligands. The 4PyNDI ligands occupy the axial sites of each metal in the bimetallic node to form double pillars of the dipyridyl ligand in a similar manner to that in the structures of **2.7** and **2.16**.

The 2D sheets in the structure of **2.18** are very similar to those in the structure of **2.14**. Both form (4,4) sheets which involve face-to-face π-interactions between the ligands within the sheets. The sheets in **2.14** are slightly different, as the ligand is only mono-deprotonated, and therefore the sheet has monometallic nodes, to account for charge balance.

Unlike the structures of **2.2**, **2.3**, **2.7**, **2.12**, **2.16** and **2.17**, the structure of **2.18** does not involve $\{M_2(NDI)_2\}$ metallomacrocycles, instead the PheNDI ligands bridge between bimetallic nodes to form (4,4) sheets, Figure 2.26. The 4PyNDI double pillars bridge between the bimetallic nodes to link these sheets into a 3D network which is a distorted *pcu* topology, Figure 2.26. Due to the presence of two different NDI-based ligands the structure of **2.18** is heavily influenced by face-to-face π-π interactions. Within the (4,4) sheets there are π-interactions between the cores of two PheNDI ligands across the 4-membered ring (closest C···C distance = 3.34(2) Å). The close approach of two PheNDI ligands is seemingly allowed as they adopt a different conformation to those in all other structures. In the structure of **2.18** the phenyl groups are oriented away from the central core whilst in **2.15 - 2.17** the phenyl groups are positioned directly over the core

thereby sterically inhibiting interaction with another NDI group. In the structure of **2.14** one phenyl group is over the core, and the other is facing outwards. The phenyl groups in the structure of **2.18** are not involved in any face-to-face interactions, but do act as acceptors to CH⋯ π interactions from NDIs. The two 4PyNDI ligands in the double pillars are involved in face-to-face π-π interactions with each other (closest C⋯C distance = 3.54(3) Å).

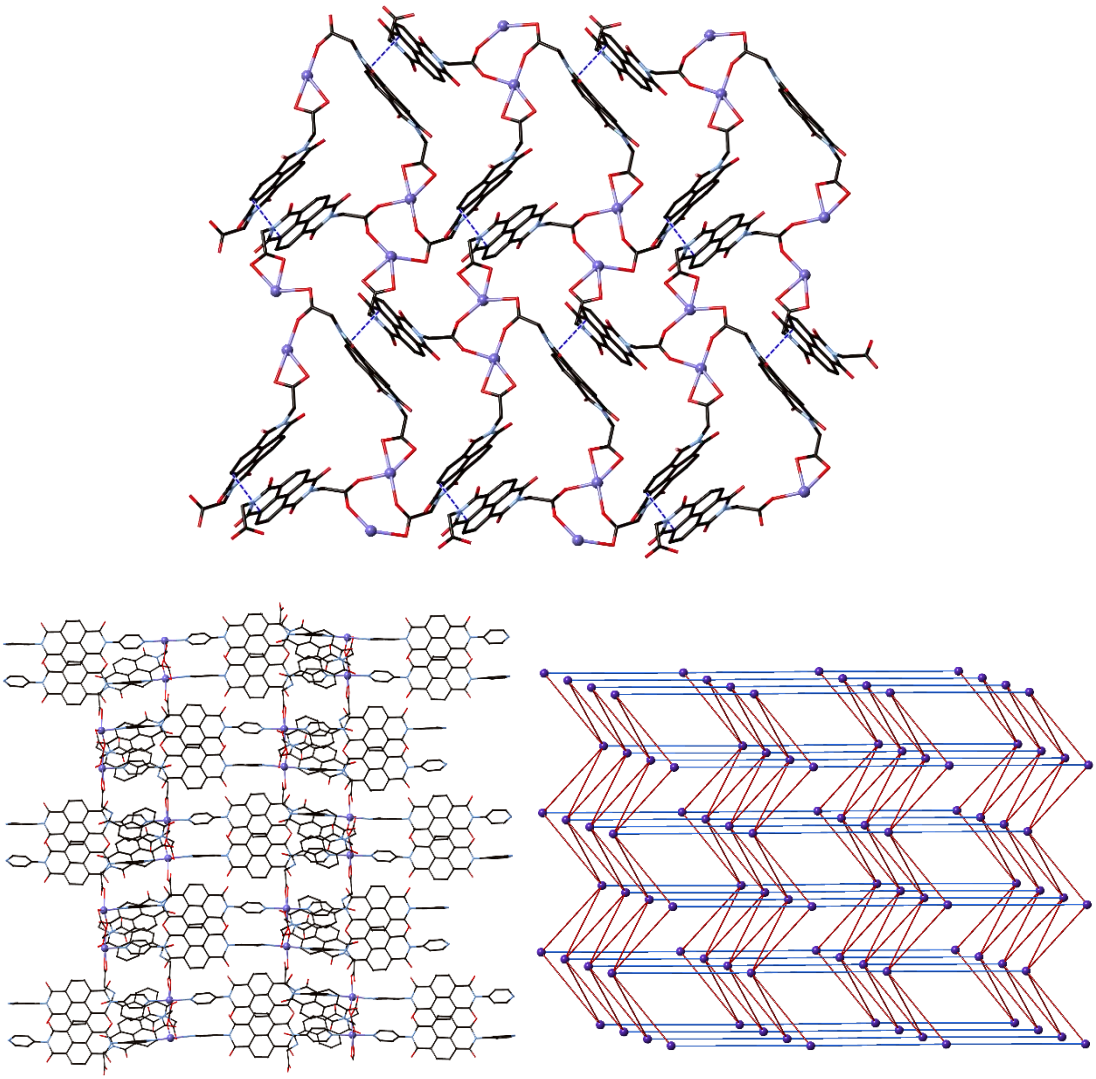

*Figure 2.26. The (4,4) sheet formed by the PheNDI ligands and bimetallic Cd^{II} nodes in the structure of **2.18**, with the face-to-face π-interactions between the ligands shown as blue dotted lines, phenyl groups and hydrogen atoms omitted for clarity (top). The 3D network of **2.18** with the {Cd(PheNDI)} sheets going into the page in molecular form (bottom left) and topologically (bottom right) showing the centroid of the bimetallic node in purple, PheNDI ligands in red and double ladders of 4PyNDI in blue.*

The ligand combination of PheNDI and 4PyNDI was also investigated with $Mn(NO_3)_2{\cdot}4H_2O$ under identical reaction conditions to those under which **2.2** – **2.9**, **2.11**, **2.12**, **2.15**, **2.17** and **2.18** were formed. The reaction yielded orange crystals of the formula *poly*-$[Mn_2(PheNDI)_2(4PyNDI)_2]{\cdot}3DMF{\cdot}2MeOH{\cdot}H_2O$, **2.19**. The structure of **2.19** is almost identical to the structure of **2.18**, with some differences induced by the incorporation of a smaller metal ion. The asymmetric unit of the structure of **2.19** is half that of **2.18** and contains one Mn^{II} ion, one PheNDI ligand and one 4PyNDI coligand, as well as non-coordinated solvent molecules. The Mn^{II} adopts a distorted octahedral geometry in which the equatorial sites are occupied by carboxylate groups; one carboxylate is chelating solely to Mn(1) and two carboxylates are bridging between Mn(1) and its symmetry equivalent in a μ-1κ*O*,2κ*O′* coordination mode. The structures of **2.18** and **2.19** are modelled in different space groups, $P2_12_12_1$ and $P2_12_12$, respectively, and the unit cell of **2.19** is half that of **2.18** (along the *c*-axis). Although the overall connectivity and topology of the structures of **2.18** and **2.19** are identical, the structural difference can be understood by the slightly different metal coordination geometries, with the symmetry of the node broken in **2.18** by the bridging carboxylates, Figure 2.27. The comparison of **2.18** and **2.19** show a structural tolerance with a change in metal ion having no influence on the coordination polymers which were synthesized with the same ligands under identical synthetic conditions.

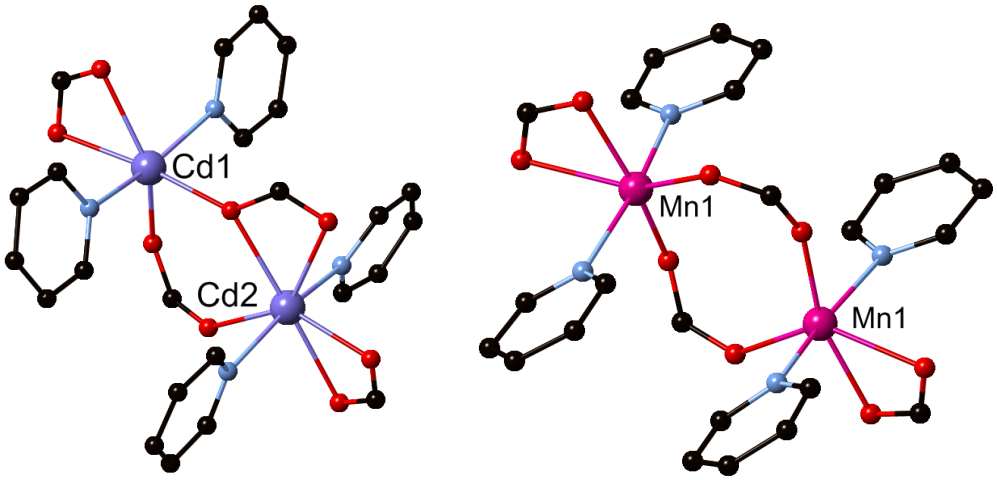

*Figure 2.27. The difference in the coordination environment within the bimetallic nodes in the structures of **2.18** (left) and **2.19** (right), leading to a change in space group despite the overall structure remaining the same. Hydrogen atoms are omitted for clarity.*

2.6 Conclusions

The topology and interpenetration of coordination polymers is often difficult to predict or control, due to the many interactions of various strengths which determine and control the structure that is obtained. It has been observed through the series of coordination polymers reported herein which utilised amino acid substituted NDI ligands, that these ligands have a strong tendency to form a M_2L_2 metallomacrocyclic motif. Of the 19 coordination polymers discussed herein, 14 of them involve this motif. Of all the coordination compounds reported by the Turner group using amino acid substituted NDI ligands, herein and in previous work, 73% involve this metallomacrocyclic motif, and a further 73% of these that involve macrocycles are interpenetrated by an aromatic group threading through the macrocycle. The M_2L_2 metallomacrocyclic motif is therefore a remarkably reproducible building block in crystal engineering. The prevalence of this motif allows the coordination polymers with amino acid substituted NDI ligands to be synthesised with some degree of predictability.

Interpenetration has been demonstrated to occur in these coordination polymers in two ways; by a catenane motif between metallomacrocycles, or a rotaxane motif between a metallomacrocycle and a linear dipyridyl ligand. The NDIs of the macrocycle are arranged such that the planes of the NDIs are at a suitable distance (~7.2 Å) to incorporate an aromatic guest which is engaged in face-to-face π-interactions. The interpenetration is aided by the favourable π-interactions between the macrocycle motifs and the aromatic guest within them, be it another macrocycle or a dipyridyl ligand.

The occurrence and type of interpenetration was shown to be somewhat dependent on the nature of the amino acid side chain of the ligand which was utilised. The AlaNDI ligand, with a methyl side chain, tended towards forming interpenetrated coordination polymers involving the metallomacrocyclic motif. The lack of steric bulk of AlaNDI allowed the coordination polymers to be interpenetrated by a catenane motif, shown in the structures of **2.2** and **2.3**. Interpenetration of AlaNDI coordination polymers was also seen with a rotaxane motif, in the cases of **2.1** and **2.5**, **2.6** and **2.8**. The smaller amino acid side chain of AlaNDI also allowed face-to-face π-interactions between ligands of neighbouring networks, which was not observed in the coordination polymers with ligands of bulkier side chains. The LeuNDI ligand, with a bulkier isobutyl

side chain compared to AlaNDI, was not able to interpenetrate by a catenane motif, but was shown to interpenetrate by a rotaxane motif, in the structures of **2.11** – **2.13**. The PheNDI ligand, with a bulky and aromatic phenyl side chain, was less likely to be interpenetrated due to the steric bulk of the side chain, as well as the phenyl group competing for π-interactions with the naphthalene core groups. The non-interpenetrated coordination polymers in the structures of **2.14, 2.15, 2.18** and **2.19** showed how the phenyl side chain also took part in π-interactions with the aromatic dipyridyl ligands or the NDI naphthalene core group. Only one PheNDI coordination polymer was interpenetrated, **2.17**, which was interpenetrated by a rotaxane motif with a dpe dipyridyl ligand. The favourability of π-interactions in coordination polymers with PheNDI despite the bulky side chain was shown by a 1D + 2D → 2D polythreaded coordination polymer, in which a dipyridyl ligand containing chain was threaded through the metallomacrocycles, engaged in π-interactions with the NDIs.

The importance of face-to-face π-interactions in the packing of coordination polymers with amino acid substituted NDI ligands was also shown by those which were not interpenetrated by a catenane or rotaxane motif. The structure of **2.4** involved 3D → 3D interpenetration, in which the "S"-shaped NDI ligands were involved with π-interactions of the NDI ligands of the interpenetrating network. The use of the π-rich dipyridyl ligand 4PyNDI alongside AlaNDI and LeuNDI led to the formation of five coordination polymers, four of which were not interpenetrated. It appears that the 4PyNDI ligands are more likely to engage in π-interactions with other 4PyNDI ligands, as shown in the structure of **2.7**, **2.18** and **2.19**, in contrast to the smaller dipyridyl ligands of 4,4′-bipy, dpe or bpb, which took part in π-interactions with NDI ligands. The structure of **2.8** was an exception, as it formed a 2D sheet which was interpenetrated by a rotaxane motif.

An interesting pattern was observed in the coordination polymers with NDI macrocycles and dipyridyl ligands which formed interpenetrating 2D sheets. The only structures to interpenetrate by the catenane motif, **2.2** and **2.3**, had a ratio of macrocycle to dipyridyl ligand of 2:1. The lower ratios, of 1:1, in the structures of **2.1**, **2.6**, **2.11**, **2.12**, and **2.17** and ratio of 1:2 in the structures of **2.5**, **2.8**, and **2.13** all interpenetrated by a rotaxane motif. The (6,3) sheets of **2.2** and **2.3** interpenetrate most efficiently by a

catenane motif, however the structures which involve more dipyridyl ligands will interpenetrate most efficiently by a rotaxane motif, as interpenetration by a catenane motif would leave surplus dipyridyl ligands which were not engaged in the π-interactions of passing through the NDI macrocycle.

The coordination behaviour of AlaNDI, LeuNDI and PheNDI was explored primarily with Cd^{II} and Mn^{II}, with a few examples incorporating Zn^{II}. It was observed that coordination polymers of identical components, with the exception of the use of Cd^{II} or Mn^{II}, formed coordination polymers of the same topology and interpenetration, varying only in the coordination sphere of the metal. The use of Zn^{II} in the structure of **2.5** formed a 2D → 2D interpenetrated sheet, very similar to others observed with Cd^{II} and Mn^{II}. However Zn^{II} was shown to behave quite differently in the structure of **2.10**, forming 1D chains with tetrametallic nodes, in contrast to the mono- or bimetallic nodes present in the Cd^{II} and Mn^{II} coordination polymers. The tetrametallic nodes were also bridged by three NDI ligands, in contrast to the two ligands bridging the Cd^{II} or Mn^{II} nodes of the common metallomacrocycle motif, which inhibited interpenetration of the chains by a catenane motif.

The utilisation of the reproducible the M_2L_2 metallomacrocyclic motif in coordination polymers with AlaNDI, LeuNDI and PheNDI ligands with transition metals and dipyridyl ligands has been shown to have clear merit in crystal engineering. The nature of the amino acid side chain appears to play a key role in the interpenetration of the networks. The non-bulky methyl side chain of AlaNDI allowed interpenetration by a catenane or rotaxane motif. The bulky isobutyl side chain of LeuNDI allowed interpenetration only by a rotaxane motif. The bulky and aromatic phenyl side chain of PheNDI inhibited interpenetration in all but one example.

Despite variations in the amino acid side chain of these NDI ligands, as well as synthetic conditions, metal ion and dipyridyl ligand, it is clear from the work reported herein that amino acid substituted NDI ligands form with some degree of reproducibility and may therefore be used in the design of coordination polymers with specific interactions and topologies. The driving force in this reproducibly appears to be the tendency for these ligands to form coordination polymers dominated by π-interactions and featuring a M_2L_2 metallomacrocyclic motif.

Chapter 3: Coordination compounds with biphenyl diimide ligands

3.1 Introduction

Early research into the design and synthesis of coordination polymers and MOFs focused on the use of rigid ligands which would form predictable networks.[22] However, the networks and topologies which are possible through this method are limited, and therefore the field has evolved to also include the use of more flexible ligands. The advantage of flexible ligands is access to architectures which are not possible with rigid ligands, and to achieve serendipitous networks for which the ligands may not have necessarily been designed. The obvious disadvantage to the use of flexible ligands is that they may adopt conformations which are not conducive to the formation of coordination polymer networks with interesting structures or properties.[377]

3.1.1 Biphenyl diimide ligands

In response to the highly reproducible metallomacrocyclic motif formed using amino acid substituted NDI ligands and transition metals, as detailed in Chapter 2, the coordination behaviour of a different amino acid substituted diimide ligand was investigated. Although the NDI coordination polymers could be formed with some degree of predictability and reproducibility, they did not form porous coordination polymers which could be utilised as solid state chiral materials for chiral separation or catalytic applications, as was the fundamental aim of this work. Therefore, amino acid substituted biphenyl diimide (BDI) ligands were investigated. The BDI core has two phthalimide groups which may rotate in relation to each other, giving it more flexibility than the rigid NDI core. The BDI core is also longer than the NDI, with N···N distances of ~ 7 Å and ~ 10.5 Å in the NDI and BDI ligands, respectively. The BDI core was chosen because it could be functionalised with amino acids on the imide groups by the same strategy as the NDI ligands, in order

to synthesise enantiopure chiral ligands, but it is slightly longer and more flexible and may therefore lead to the formation of coordination networks which were not possible with NDI ligands.

Ligands with a biphenyl core have previously been utilised in the synthesis of coordination polymers and MOFs, with different substitution and functionality on the rings, leading to a range of networks. In early MOF syntheses 4,4′-biphenyldicarboxylic acid (BPDC) was used as an extension of the classical MOF precursor, 1,4-benzenedicarboxylic acid, which forms MOF-5 with the octahedral $Zn_4O(CO_2)_6$ SBU, in an attempt to synthesise analogous networks with larger void volume. The use of H_2BPDC with reaction conditions which typically give MOF-5 formed a different network, in which an infinite Zn-carboxylate chain was bridged by BPDC ligands into a 3D network, Figure 3.1.[378] It was believed that this network formed instead of the expected analogous MOF-5 network because of the increased length of the BPDC ligand.

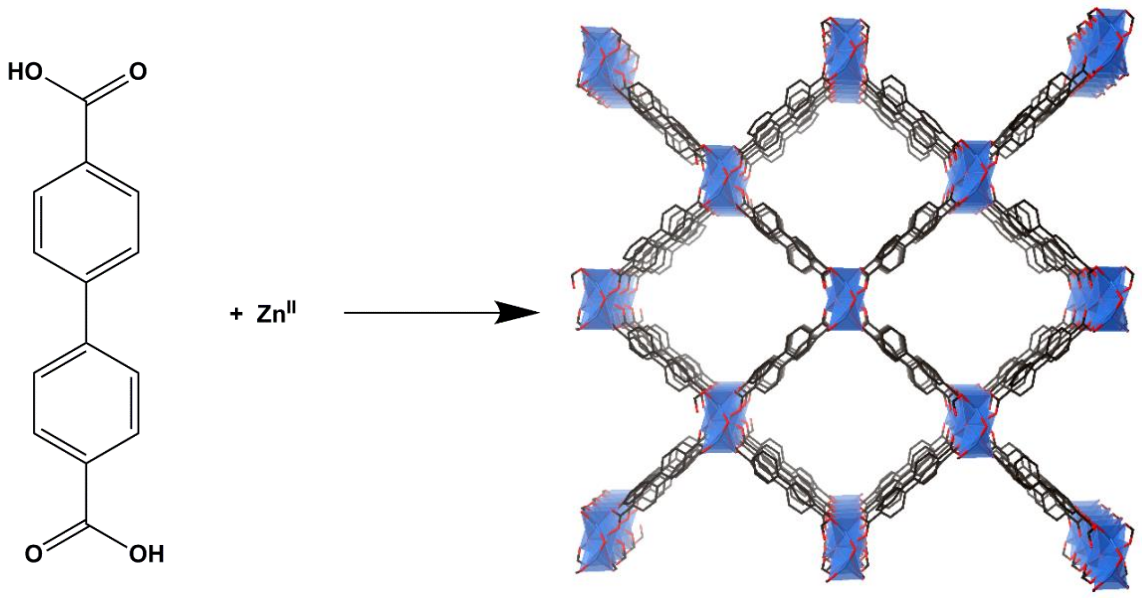

Figure 3.1. The synthesis and structure of [$Zn_3(OH)_2(BPDC)_2$] (4,4′-biphenyldicarboxylic acid), shown with the infinite Zn-carboxylate chains going into the page. All hydrogen atoms are omitted for clarity.

Although there are several examples of functionalised biphenyl cores being utilised as ligands, there is only one reported example of a biphenyl diimide (BDI) molecule being used as a ligand in coordination polymer synthesis. The BDI ligand, which was substituted through the imide groups with 3-methylpyridyl groups,

was reported to form a 2D coordination polymer when reacted with Cd^{II}, in which the ligand could be arranged in a "U" or "S" shape due to the flexibility of the methylene groups separating the imide and pyridyl groups of the ligand,[379] in a similar manner to the amino acid substituted NDI ligands which were also shown to be arranged in a "U" or "S" shape. This previous result with a BDI ligand suggests that amino acid substituted BDI ligands may behave similarly to the amino acid substituted NDI ligands, however the change in ligand length, aromaticity and flexibility are likely to lead to significant changes in the networks obtained. The BDI core has also been used as a polymer precursor, forming polymers with cyclohexane functionalised aromatic amines. The resulting polymers could be synthesised with high molecular weight and were readily soluble in common organic solvents.[380]

3.1.2 Isophthalic acid substituted diimide ligands

The use of ligands with multiple coordinating groups, such as several carboxylate groups, have been investigated as a strategy to increase the dimensionality of the coordination polymers and MOFs which are formed. Isophthalate functionalised ligands are an example of such a design strategy. Isophthalic acid substituted NDI (IsoNDI) has been used in coordination polymer synthesis, as it combines the rigidity of the NDI core with a high number of carboxylate groups, and is therefore more likely to form high dimensionality coordination networks than analogous ligands which have less coordinating groups.

A 3D porous MOF has been reported with IsoNDI and Zn^{II} nodes, which features an unprecedented 1D + 2D → 3D self-interpenetrated array. The pores of the network are lined with carbonyl groups and a carboxylic acid group which was not deprotonated during the synthesis, and showed good drug release properties with ibuprofen, as ibuprofen has a carboxylic acid group which can interact with the pores of the MOF through hydrogen bonding.[381] Several other instances of IsoNDI have been reported for the synthesis of 3D coordination polymers and MOFs, some of which include additional carboxylate ligands.[367, 369, 382, 383]

The high number of coordinating groups in IsoNDI leads to higher dimensionality networks, as well as the possibility of non-coordinating carboxylate and carboxylic acid groups which when lining the pores will lead to interactions with guests. The BDI core substituted with isophthalate groups has not yet been reported

as a ligand for the synthesis of coordination networks, and would be an interesting candidate as it involves four carboxylate groups, which are likely to lead to the formation of a 3D network, but has a slightly more flexible core than the IsoNDI analogue.

3.2 Ligands utilised in this study

Amino acid substituted BDI molecules have not been previously reported for use as ligands in metallosupramolecular chemistry. Their synthesis was achieved by the reaction of 3,3′,4,4′-biphenyltetracarboxylic dianhydride (BDA) with the amino acids glycine, (*S*)-alanine, (*S*)-leucine and (*S*)-phenylalanine, Figure 3.2.

The formation of similar biphenyl diimide ligands previously reported were conducted mainly by reaction of BDA with amino acids in acetic acid, under microwave reaction at 120 °C or under reflux.[384, 385] Due to the success of the synthesis of the amino acid substituted NDI ligands in DMF at 90 °C, the synthesis of the amino acid substituted BDI ligands was attempted by all three of these methods. The highest yielding reaction which gave a pure product was utilised for the bulk synthesis of the product. In all cases, following the reaction the solutions were poured over ice and the product was recovered by filtration.

The (*S*)-alanine substituted 3,3′,4,4′-biphenyl diimide molecule (H_2AlaBDI) was synthesised in a microwave reactor in acetic acid at 120 °C in 75% yield. The glycine, (*S*)-leucine and (*S*)-phenylalanine derived molecules (H_2GlyBDI, H_2LeuBDI and H_2PheBDI) were synthesised in DMF at 90 °C in yields of 70%, 75% and 91%, respectively, Figure 3.2. The formation of the pure product was confirmed by ^{1}H-NMR and ^{13}C-NMR spectroscopy, mass spectrometry, infrared spectroscopy and microanalysis. In the same manner as the synthesis of the NDI ligands, presence of a ^{1}H-NMR signal for the hydrogen atom on the alpha-carbon of the amino acid at approximately 4 – 5 ppm was indicative of the formation of the product.

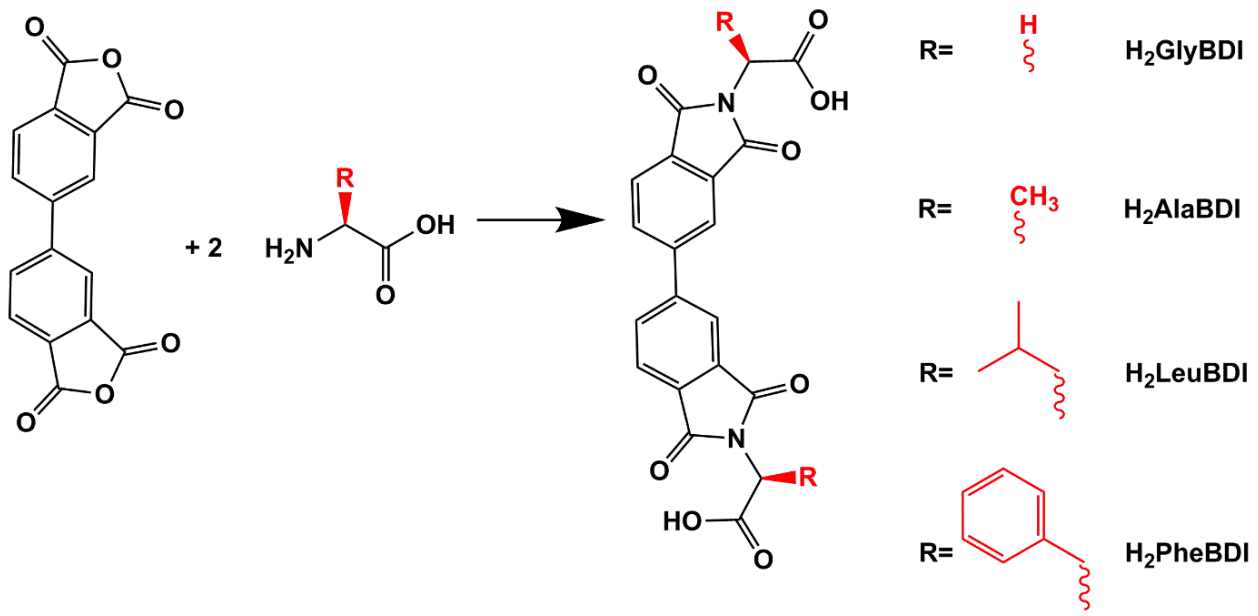

Figure 3.2. The reaction scheme for amino acid substituted BDI compounds.

The isophthalic acid substituted BDI molecule was also synthesised in order to investigate the BDI ligand with four coordinating groups. The H_4IsoBDI compound was synthesised in DMF at 120 °C in a 47% yield, Figure 3.3. Due to the insolubility of the product, the tetra-acid precipitated out of the reaction solution upon cooling, and was recovered by vacuum filtration. The synthesis of the product was again confirmed by ^{1}H-NMR and ^{13}C-NMR spectroscopy, mass spectrometry, infrared spectroscopy and microanalysis.

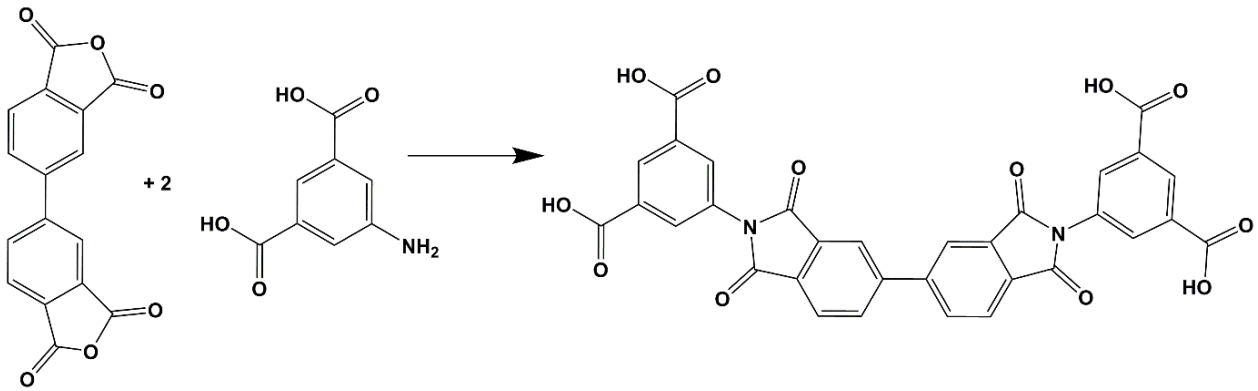

Figure 3.3. The synthetic scheme for the formation of H_4IsoBDI.

The amino acid ligands synthesised were H_2AlaBDI and H_2LeuBDI, which have a methyl and isobutyl side chain, respectively, Figure 3.4. The H_2GlyBDI and H_2PheBDI ligands were also synthesised, however

attempts at forming crystalline coordination compounds with H_2GlyBDI or H_2PheBDI and various metal salts led only to amorphous products, despite employing an exhaustive range of reaction techniques. H_4IsoBDI was also synthesised because, although it is not chiral, it presents the opportunity to investigate BDI ligands with four carboxylate coordinating groups, in contrast to the two coordinating groups in the amino acid substituted BDI ligands.

Dipyridyl ligands were used alongside the Ala- and LeuBDI ligands in order to explore their influence on increasing the dimensionality of the coordination polymers obtained. The dipyridyl ligands used were 4,4′-bipyridine (4,4′-bipy) and N,N′-bis(4-pyridyl)-1,4,5,8-naphthalene tetracarboxylic diimide (4PyNDI), Figure 3.4. The metal ions used were exclusively Cd^{II}, Zn^{II} and Cu^{II} as they proved to be the most suitable for the BDI ligands.

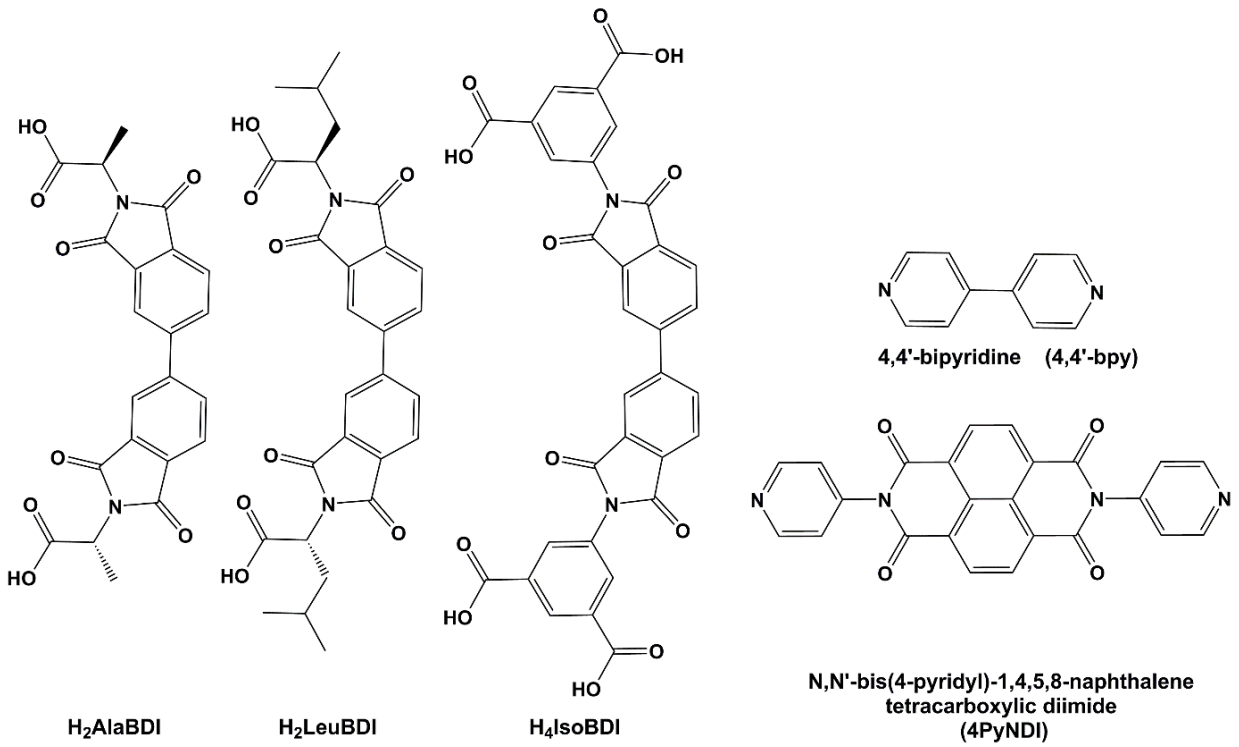

Figure 3.4. The amino acid substituted BDI ligands H_2AlaBDI, H_2LeuBDI, H_4IsoBDI (left) and the dipyridyl ligands 4,4′-bipy and 4PyNDI (right) used in this study.

3.3 Discrete macrocycles containing BDI ligands

The following will give a report on the coordination complexes, both discrete and polymeric, which were formed with amino acid and isophthalic acid substituted BDI ligands upon reaction with transition metals.

The BDI ligands were chosen because they are more flexible, longer and less π-rich than NDIs and therefore less likely to form coordination polymers of the same form, which were dominated by a macrocyclic motif and face-to-face π-interactions.

To explore the coordination behaviour of AlaBDI and LeuBDI, these ligands were first reacted with Cd^{II} in the absence of dipyridyl ligands. The reaction of H_2AlaBDI with $Cd(OAc)_2$ in DMSO at 100 °C formed colourless crystals containing the coordination compound $[Cd_2(AlaBDI)_2(DMSO)_6]\cdot 1.5H_2O$, **3.1**. The structure of **3.1** is modelled in the chiral space group *P*1 and the asymmetric unit contains two Cd^{II} ions, two AlaBDI ligands and coordinated solvent of six DMSO molecules. Both Cd^{II} ions adopt a distorted pentagonal bipyramidal coordination geometry, in which the equatorial positions are occupied by two chelating carboxylate groups and a DMSO ligand, and the axial positions are occupied by two more DMSO ligands. The coordinating carboxylate groups and coordinating solvent molecules have an average $Cd^{II}\cdots O$ distance of 2.315 Å. The non-coordinated oxygen atoms of the carboxylate groups have weak interactions with the Cd^{II}, with Cd···O distances of 2.501(5), 2.656(6), 2.458(5) and 2.474(6) Å. The structure also involves some residual electron density which could not be modelled crystallographically, however was assigned as 1.5 water molecules per asymmetric unit by TGA and microanalysis.

In a similar manner to the recurring metallomacrocycle motif of the NDI coordination polymers discussed in Chapter 3, the BDI ligands of **3.1** are "U" shaped, in a *cis* configuration, and form a $[Cd_2(AlaBDI)_2]$ metallomacrocycle, Figure 3.5. Although the same M_2L_2 metallomacrocycles are formed, they have monometallic nodes and are discrete complexes in which the metal ions are capped by solvent molecules, rather than forming 1D chains of conjoined macrocycles with bimetallic nodes, as was often observed with AlaNDI, LeuNDI and PheNDI. It is possible to form discrete NDI macrocycles through the use of the convergent dipyridyl ligands 2,2′-bipyridine and 1,10-phenanthroline, as shown in the structures of **4.1** and **4.2**. Despite employing various solvents, the crystals of **3.1** could not be dissolved in order to prove their existence in solution by mass spectrometry or ^{1}H-NMR spectroscopy.

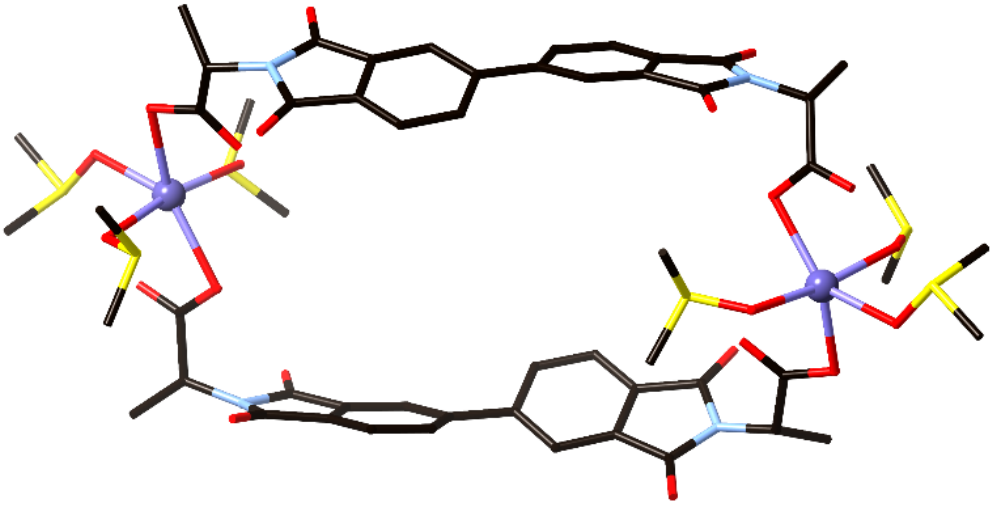

*Figure 3.5. The [$Cd_2(AlaBDI)_2(DMSO)_6$] macrocycles of the structure of **3.1**. All hydrogen atoms are omitted for clarity.*

Due to the increased length of BDI ligands compared to NDIs and the flexibility inherent in the core of the BDI ligands, the macrocycles are a slightly different size to the NDI macrocycles observed previously. The BDI ligands in the macrocycle have a plane a minimum C···C distance of 7.607(9) Å, compared to the NDI···NDI distance of ~ 7.2 Å. The BDI core group is also more flexible than the NDI core, demonstrated by the fact that the two phthalimide groups do not lie in the same plane. The planes of the phenyl rings are offset by 37.92(18)° and 23.71(19)°, leading to the ligands being less prone to engage in face-to-face π-interactions. In contrast to the various forms of interpenetration which occurred by a guest passing through the macrocycles of coordination polymers incorporating NDI ligands, the greater space between ligands of the macrocycle present in **3.1**, the flexibility of the core and the smaller aromatic surface of the ligand all appear to lead to a lack of catenation of the macrocycles. In the absence of catenation of the macrocycles, the space between BDI ligands in the macrocycles is filled with the coordinating DMSO molecules of two neighbouring complexes, Figure 3.6.

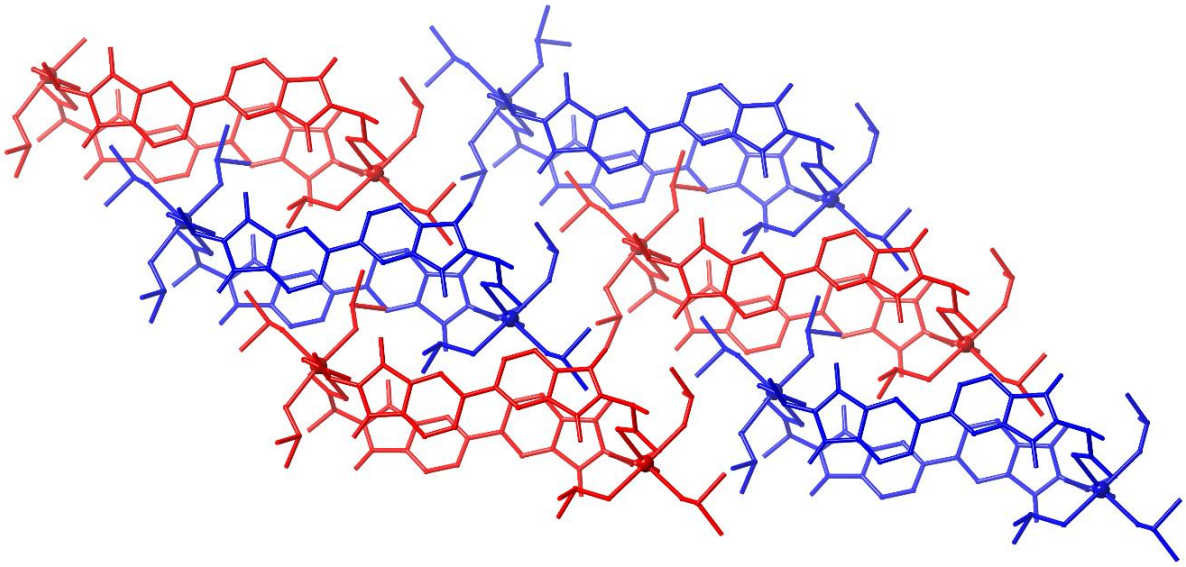

*Figure 3.6. The packing of the macrocycles of **3.1**, with the DMSO ligands of neighbouring macrocycles sitting between the BDI ligands. All hydrogen atoms are omitted for clarity.*

The reaction of H_2LeuBDI with $Cd(OAc)_2$ yielded a discrete macrocycle which is analogous to **3.1**, although the reaction took place in a solvent mixture of DMSO and DMF, forming a coordination compound of the formula $[Cd_2(LeuBDI)_2(DMSO)_3(DMF)_2(OH_2)]\cdot DMSO\cdot DMF$, **3.2,** Figure 3.7. The formation of the discrete macrocycle complexes was also confirmed by ^{1}H-NMR spectroscopy in d_6–DMSO, which showed an upfield shift in the signal for the hydrogen group on the α-carbon from 4.81 ppm of the free ligand, to 4.58 ppm in the complex. The coordinated DMF was also present in the ^{1}H-NMR spectrum. Due to the limited solubility of the complex, the ^{1}H-NMR analysis was carried out in d_6–DMSO and therefore the signals of the coordinated DMSO and water could not be distinguished from the residual solvent resonances.

The structure of **3.2** is modelled in the chiral space group $P2_1$ and the asymmetric unit contains one complete formula unit. The two crystallographically unique Cd^{II} ions adopt slightly different coordination geometries. The coordination geometry of Cd(1) is distorted octahedral, with the equatorial positions occupied by a monodentate carboxylate, a chelating carboxylate and a DMF molecule, and the axial positions are occupied by two DMSO ligands. The coordination geometry of Cd(2) is analogous to that of both Cd^{II} ions in the structure of **3.1**, adopting a distorted trigonal bipyramidal geometry, in which the axial

positions are occupied by two monodentate carboxylate groups and a solvent molecule, in this case a DMF molecule, and the axial positions occupied by two solvent molecules, in the case of **3.2** a DMSO ligand and a coordination water molecule. There is also hydrogen bonding of the aqua ligand with the non-coordinating DMF molecule, with an H···O distance of 2.01(4) Å.

The structure of **3.2** is analogous to that of **3.1**, in that it is a $\{Cd_2(BDI)_2\}$ macrocycle with monometallic nodes which are capped by solvent molecules. The flexibility of the BDI core group is demonstrated again, as the phthalimide groups are twisted in relation to one another, with interplanar angles of 37.9(2)° and 9.3(2)°. The BDI macrocycles of **3.2** are slightly more compact than those of **3.1**, with a minimum C···C distance of 6.510(11) Å, whereas the minimum C···C distance of **3.1** is 7.607(9) Å. Similar to **3.1**, the macrocycles do not form a catenane. In the case of **3.2** the space between the BDI ligands is occupied by the DMF molecules coordinating to the equatorial positions of the Cd^{II} of neighbouring complexes, Figure 3.7. The DMF ligands sitting within the macrocycles are aligned approximately with the plane of the BDI ligands at interplanar angles of ~8°. As DMF is a planar molecule, and DMSO is a more sterically demanding molecule, it appears that the space within the macrocycles of **3.2** is smaller due to the less sterically demanding guest molecules within them, while the larger DMSO molecules within the macrocycles of **3.1** force the BDI ligands to sit further apart to accommodate the guest molecules. The difference in size of the macrocycles of **3.1** and **3.2** demonstrates that the BDI ligands are more flexible than NDI ligands and can accommodate larger, non-aromatic guests within them.

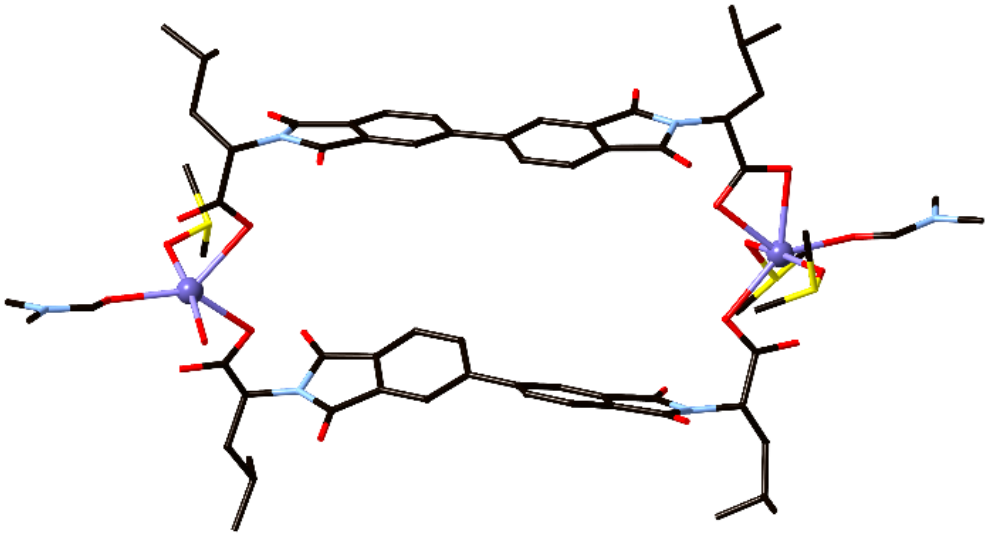

Figure 3.7. The [Cd_2(LeuBDI)$_2$(DMSO)$_3$(DMF)$_2$(OH_2)] macrocycle in the structure of ***3.2.*** *All hydrogen atoms are omitted for clarity.*

The alignment of the DMF molecules within the macrocycles leads to the complexes packing into a 2D sheet of macrocycles, Figure 3.8. The space above the plane of the BDI ligand of the macrocycle is occupied by the non-coordinating DMF molecules and the isobutyl side chains of the complexes of the neighbouring macrocycle sheets, in a similar manner to the LeuNDI coordination polymers. The structure **3.2** shows that although the BDI and NDI macrocycles have some significant differences in their structure and interpenetration, the bulky isobutyl group has the same influence on the packing of the complexes.

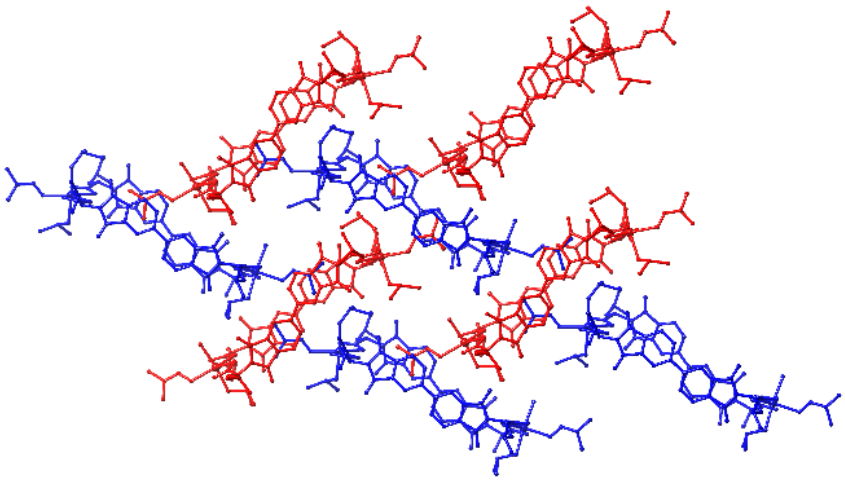

Figure 3.8. The packing of the macrocycles with the coordinated DMF ligands of two neighbouring macrocycles sitting between the BDI ligands (right). All hydrogen atoms are omitted for clarity.

3.4 Coordination complexes containing BDI and dipyridyl ligands

Due to the formation of discrete macrocycles with AlaBDI and LeuBDI when reacted with Cd^{II}, H_2AlaBDI and H_2LeuBDI were also reacted with dipyridyl ligands and transition metals, in an attempt to form coordination polymers. The reaction of H_2AlaBDI, $ZnCl_2{\cdot}6H_2O$ and 4,4′-bipy in DMF produced a crystalline product of the formula $(NH_2(CH_3)_2)_2[Zn_2(AlaBDI)_2(4,4'\text{-bipy})Cl_2]$, **3.3**. The structure of **3.3** is modelled in the chiral space group *C*2. The asymmetric unit contains one complete formula unit. Both the Zn^{II} ions adopt a tetrahedral coordination geometry, in which the coordination sphere is occupied by two monodentate carboxylate ligands, a 4,4′-bipy and a chloride ligand. In a similar manner to the structure of **3.1**, the AlaBDI ligands are "U-shaped", forming a metallomacrocycle motif. Surprisingly, the 4,4′-bipy ligands do not bridge the macrocycles into a 1D chain, instead the 4,4′-bipy is bridging between the Zn^{II} ions within the macrocycle, Figure 3.9. The difference in metal coordination geometry in **3.3** in comparison to **3.1** and **3.2** in which the Cd^{II} ions adopted distorted trigonal bipyramidal and octahedral geometries is likely due to the smaller ionic radius of Zn^{II} in comparison to Cd^{II}, allowing Zn^{II} to adopt a tetrahedral geometry. The complex has a 2- charge, and is charge balanced by the presence of two dimethylammonium

ions, formed by the hydrolysis of DMF during the reaction. The dimethylammonium ions form hydrogen bonds with the non-coordinated oxygen atoms of the monodentate carboxylate groups.

The AlaBDI ligands are again shown to be quite flexible in the structure of **3.3**. The phthalimide groups are twisted with interplanar angles of 21.8(8)° and 15.2(5)° in relation to each other. The 4,4′-bipy ligands are flexible in a similar manner, as the two pyridyl groups have an interplanar angle of 34.6(5)°. Despite the presence of an aromatic dipyridyl ligand in the middle of the macrocycle, there is still an absence of face-to-face π-interactions of the BDI ligands and the 4,4′-bipy, likely due to the flexibility of the ligands involved. There are also no π-interactions in the 3D packing of the macrocycles.

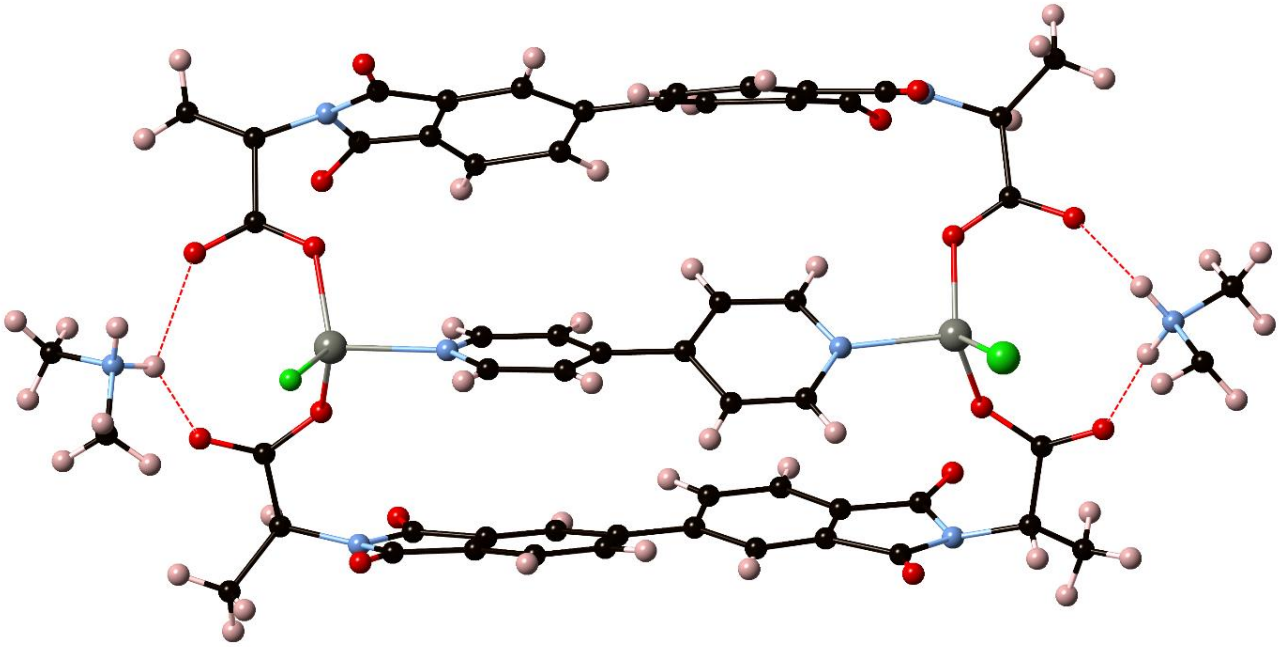

*Figure 3.9. The structure of **3.3** in which a 4,4′-bipy ligand bridges between the Zn^{II} ions of the $\{Zn_2(AlaBDI)_2\}$ macrocycle. Hydrogen bonds are shown as dashed red lines.*

The structure of the macrocycle in **3.3** is significantly different to those of **3.1** and **3.2**, due to the presence of the 4,4′-bipy within the macrocycle and the change in metal ion. The M···M distances within the macrocycle in the structures of **3.1** and **3.2** are 15.173(4) Å and 16.108(5) Å, respectively. The macrocycle is slightly more elongated in the structure of **3.2** due to the presence of planar DMF molecules within the macrocycle allowing the BDI ligands to sit closer together. In the structures of **3.1** and **3.2**, all the oxygen atoms of the carboxylate groups are coordinated or have a weak interaction with the Cd^{II} ions. The M···M

distance within the complex of **3.3** was significantly shorter, at 11.208(3) Å. The non-coordinating oxygen atoms of the monodentate carboxylate groups are not interacting with the Zn^{II}, as they have very long $Zn^{II}\cdots O$ distances of 3.090(17), 3.213(17), 3.033(11) and 3.307(8) Å. The observed difference in metal coordination and M···M distance within the macrocycle appears to be due to the metal ions of **3.3** being closer together to allow for the bridging of the 4,4′-bipy, and is allowed by the smaller ionic radius of Zn^{II} in comparison to Cd^{II}. The change in shape of the macrocycles of **3.3** again demonstrates how the flexibility of BDI ligands allows the formation of coordination complexes which would not be possible with rigid NDI ligands.

As the use of 4,4′-bipy was unsuccessful in forming coordination polymers with BDI ligands, a longer and more π-rich dipyridyl ligand, 4PyNDI, was engaged. The reaction of H_2AlaBDI, 4PyNDI and $Cd(NO_3)_2\cdot 4H_2O$ was carried out in DMF at 100 °C, forming crystals of a coordination polymer of the formula *poly*-[Cd(LeuBDI)(4PyNDI)]·$11H_2O$·2DMF, **3.4**. The structural determination of **3.4** revealed that the Cd^{II} ions form $\{Cd_2L_2\}$ macrocycles linked together by bimetallic nodes of the same form prevalent in the coordination polymers reported with NDI ligands. The asymmetric unit contains two Cd^{II} ions, two LeuBDI ligands and two 4PyNDI ligands and is modelled in the chiral space group *P*1. Both of the Cd^{II} ions adopt a distorted octahedral geometry. The two Cd^{II} ions in the bimetallic node are bridged by two carboxylate groups in a μ-1κ*O*,2κ*O′* coordination mode and the remaining equatorial sites are occupied by a chelating carboxylate group on each Cd^{II}. The axial positions are occupied by 4PyNDI ligands, forming "double pillars" of 4PyNDI ligands, which bridge the 1D metallomacrocycle chains into a 2D sheet, very similar to the structure of **2.7**, Figure 3.10. The structure also includes voids in which no solvent could be modelled, but was assigned as 11 water and two DMF molecules per asymmetric unit, by TGA, microanalysis and residual electron density.

The combination of LeuBDI with a π-rich dipyridyl ligand, 4PyNDI, in the structure of **3.4** leads to multiple instances of face-to-face π-interactions within the network. The 4PyNDI ligands in the double pillars are engaged in face-to-face π-interactions with each other through the naphthalene core, at a minimum C···C distance of 3.350(12) Å. There are also π-interactions between the sheets, in which the 4PyNDI ligands are

interacting with the external face of the $\{Cd_2(LeuBDI)_2\}$ macrocycles of the adjacent sheet, at minimum C···C distances of 3.250(13) and 3.293(11) Å. It can be observed from the structures of **3.1** – **3.3** that the BDI ligands are not predisposed to forming coordination networks in which face-to-face π-interactions have a significant influence on the packing of the compound, however upon addition of a π-rich dipyridyl ligand in the structure of **3.4**, π-interactions are a dominant interaction in the network which is formed.

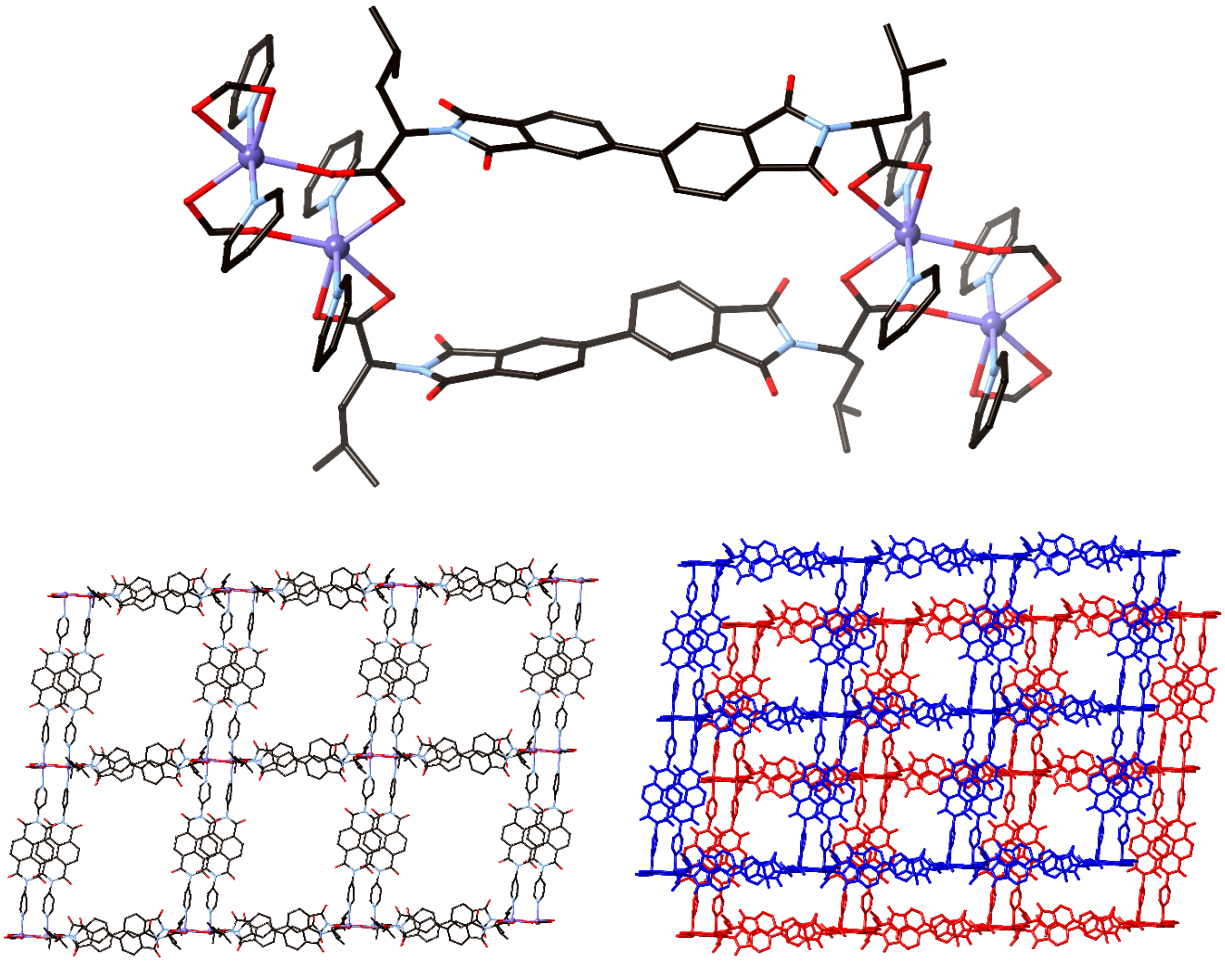

*Figure 3.10. The macrocycle present in the structure of **3.4**, showing the bimetallic nodes in which the equatorial positions are occupied by carboxylate groups and the axial positions are occupied by the dipyridyl groups of 4PyNDI (top). The 2D sheet formed by the chains of conjoined macrocycles being bridged by double pillars of 4pyNDI ligands in the structure of **3.4** (left). The packing of the 2D sheets in which there are π-interactions between the 4PyNDI ligands and the external faces of the LeuBDI ligands of the macrocycles (right). All hydrogen atoms are omitted for clarity.*

The structure of **3.4** is analogous to the structure of **2.7**, in that they both involve 1D chains of conjoined macrocycles with bimetallic nodes, which are bridged into 2D sheets by double pillars of 4PyNDI ligands. It was observed in the coordination polymers involving LeuNDI ligands, that there was a lack of interpenetration by a catenane motif and no instances of π-interactions with the external face of the $\{M_2(LeuNDI)_2\}$ macrocycles, due to the steric bulky of the isobutyl side chain crowding the naphthalene core. However, due to the added length of the BDI ligand in comparison to the NDI ligand, with N⋯N distances of ~7 Å and ~10.5 Å in the NDI and BDI ligands, respectively, it is possible for a 4PyNDI ligand to engage in π-interactions with the external face of the $\{M_2(LeuBDI)_2\}$ macrocycle. Comparison of the structure of **3.4** with that of **2.7** demonstrates that BDI and NDI ligands may form equivalent macrocycle motifs, and that the increase in the size of the LeuBDI ligand allows π-interactions to occur which were not possible with LeuNDI coordination polymers, however that π-interactions with BDI ligands will only occur in the presence of a π-rich dipyridyl ligand.

3.5 Discrete Cu^{II} square complexes incorporating BDI ligands

All the coordination complexes discussed thus far have involved BDI or NDI ligands with Zn^{II}, Cd^{II} or Mn^{II} metal centres. The use of Cu^{II} with BDI ligands was also explored, as it presents the potential to form copper paddlewheel SBUs when reacted with the carboxylate groups of the AlaBDI and LeuBDI ligands. A copper paddlewheel cluster involves two Cu^{II} ions with a square pyramidal coordination geometry, in which the equatorial sites of each Cu^{II} are occupied by oxygen atoms of carboxylate groups and each of the carboxylate groups bridging between the Cu^{II} ions in a μ-O,O′ bridging mode. The apical positions of the Cu^{II} are often occupied by solvent molecules, however they can also be occupied by additional monodentate ligands, thus functioning as an octahedral SBU.[386, 387] Copper paddlewheels may also be used in the synthesis of discrete metal organic polyhedral (MOPs). In the instances that the copper paddlewheel functions as a square planar node, the formation of a discrete MOP or a polymer is determined by the shape of the ligand used.[329, 388-390]

The reaction of H_2AlaBDI with $Cu(OAc)_2$ in a solvent mixture of DMF and DMSO formed a clear blue solution. After sitting at room temperature for one month, blue crystals formed, which were analysed by X-

ray diffraction to reveal a coordination complex of the formula $[Cu_8(LeuBDI)_8(DMSO)_4(OH_2)_4]\cdot$solv., **3.5**. The structure involves a $\{Cu_8(AlaBDI)_8\}$ complex in which four copper paddlewheels form the corners of a square, which are each bridged by two AlaBDI ligands to form the edges of the square, Figure 3.11. The structure of **3.5** is modelled in the chiral space group $P4_22_12$ and the asymmetric unit contains half of a $\{Cu_8(AlaBDI)_8\}$ square complex; four Cu^{II} ions, four AlaBDI ligands, coordinated solvent of two DMSO and two water molecules, and non-coordinated solvent of four DMSO molecules modelled at half occupancy, and two water molecules, one of which is modelled at half occupancy. The structure also contained significant void volume (47% as calculated by Mercury[376]) in which no solvent could be modelled.

The flexibility of the BDI core is shown again by the two phthalimide groups, which are twisted in relation to each other at 43.8(15), 40.6(9), 38.3(14) and 43.2(11)°. The twist in the ligands allows the ligands to form an "S" shape as they bridge between the paddlewheel motifs. The ligands are twisted at angles of 86.7(6), 76.2(6), 86.0(5) and 84.8(6)°, between planes of the coordinating carboxylates of each ligand. The (*S*)-alanine groups coordinated to the paddlewheel force the groups into a propeller motif, giving the paddlewheel chirality with a Λ configuration. The flexibility and chirality of the AlaBDI ligand allows the ligands to twist in the appropriate geometry in order to from this square complex.

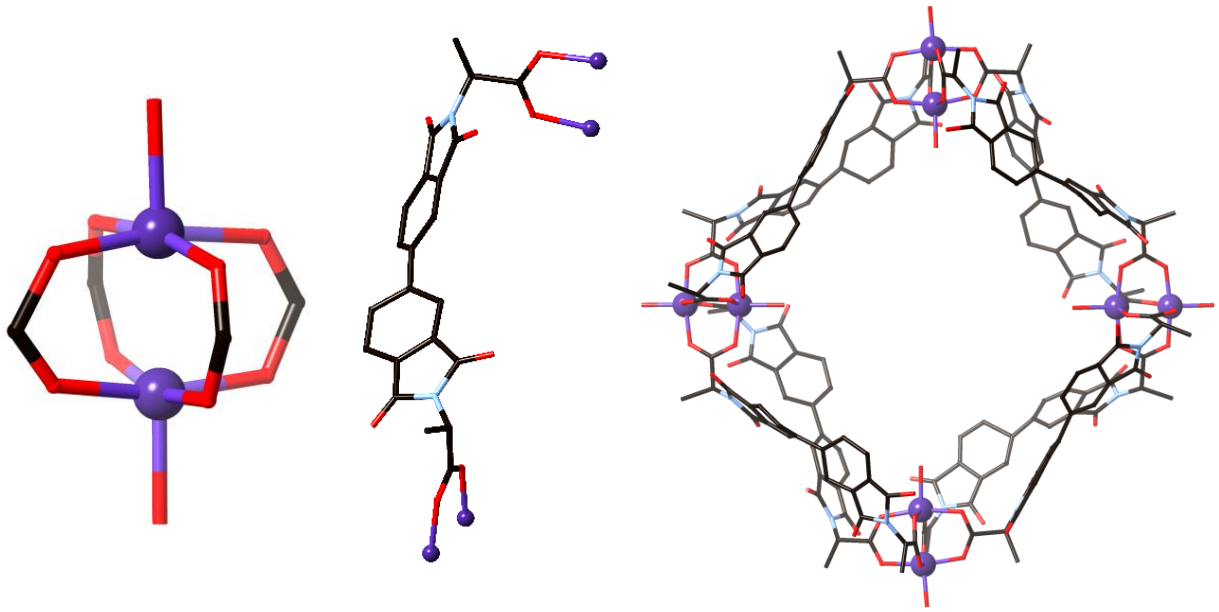

*Figure 3.11. The Cu^{II} paddlewheel cluster, showing only the oxygen atoms of the solvent atoms coordinated to the apical positions of the Cu^{II} (left), the coordination and "S" shape of each AlaBDI ligand made possible by the flexibility of the ligand, (centre) and the discrete coordination square of **3.5**, (right). All hydrogen atoms are omitted for clarity.*

The LeuBDI ligand was also reacted with Cu^{II} to assess to reproducibility of the square complex of **3.5**. The reaction of H_2LeuBDI and $Cu(OAc)_2$ was conducted in DMSO and formed blue crystals in one month, the crystals were analysed to reveal a coordination complex of the formula $[Cu_8(LeuBDI)_8(OH_2)_8]\cdot$solv., **3.6**. The structure of **3.6** is analogous to that of **3.5** in which four copper paddlewheels form the corners of a square which are bridged by two BDI ligands to form each edge of the square. The structure of **3.6** is modelled in the chiral space group $P2_1$ and the asymmetric unit contains an entire $[Cu_8(LeuBDI)_8(OH_2)_8]$ complex. The structure also contained significant void volume (39% as calculated by Mercury[376]) in which no solvent could be modelled.

The lower symmetry of the model of **3.6** in comparison to **3.5** is likely due to the flexibility of the isobutyl side chain of LeuBDI lowering to symmetry of the system. Similar to the structure of **3.6**, the flexibility of the core of the BDI ligand allows them to form this square complex. The phthalimide groups of each ligand are twisted in relation to each other by 43.4(6), 38.7(5), 45.3(6), 38.1(5), 46.2(6), 38.7(4), 39.8(6) and 35.7(4)°. The ligands form an "S" shape, twisting at angles of 85.5(3), 86.2(3), 94.9(2), 82.2(2), 82.0(2),

85.8(2), 89.0(2), 99.7(3)° in order to bridge between the paddlewheels. The chirality of the (*S*)-leucine groups on the ligand forces the paddlewheel into a propeller motif, giving it a Λ configuration, similar to that observed in **3.5**. The solid-state packing of the complexes of **3.6** involves some non-parallel π-interactions between the complexes, with closest C···C distance of 3.36(2) Å and interplanar angle of 18.6(5)°, and closest C···C distance of 3.39(2) Å and interplanar angle of 18.4(5)°, Figure 3.12.

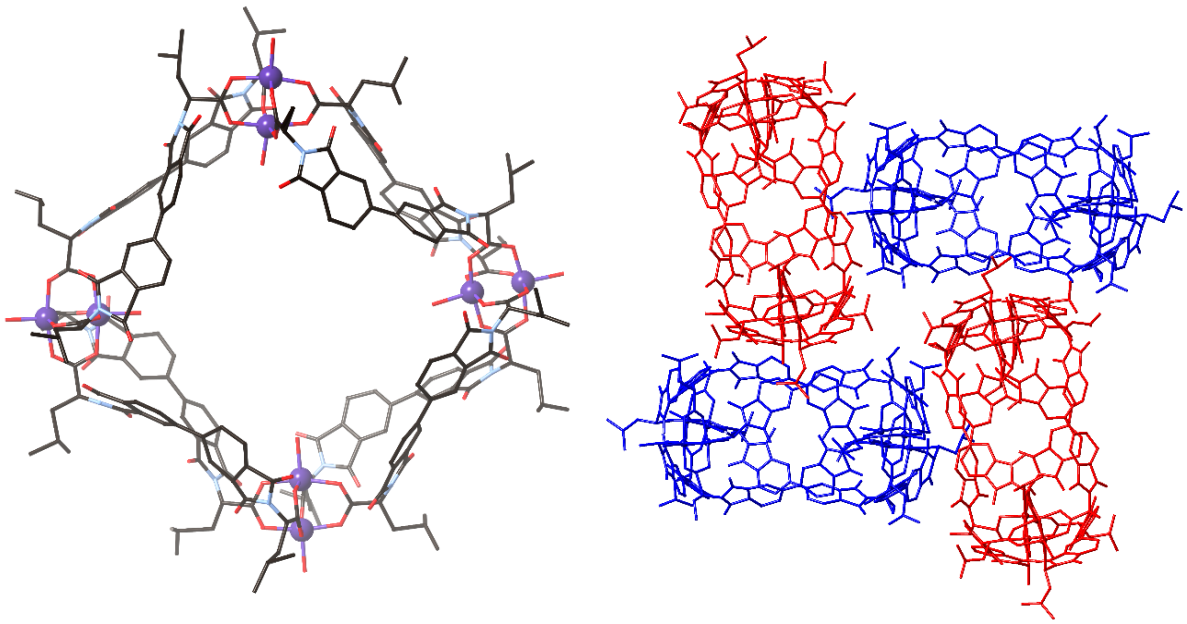

*Figure 3.12. The square complex of **3.6** (left) and the packing of the complex of **3.6** with some non-parallel π-interactions between the phenyl groups of the ligand (right). All hydrogen atoms are omitted for clarity.*

The square complexes of **3.5** and **3.6** form with a large void in their centre and the packing of the complexes also leads to large voids between them, leading to solvent accessible void space within the solid state structures of 47% and 39%, respectively. Due to this inefficient packing and the high porosity of the complexes, the crystals were highly unstable out of solution. It was observed that removing the crystals from solution led to the rapid loss of solvent and consequently loss of crystallinity. As a result, the bulk characterisation technique of powder X-ray diffraction was unable to be used for the bulk characterisation of the solid state structures of **3.5** and **3.6**.

The structure of **3.5** and **3.6** show that engaging Cu^{II} instead of Zn^{II}, Cd^{II} and Mn^{II} with amino acid substituted diimide ligands allows the formation of a copper paddlewheel SBU, leading to the formation of

discrete coordination complexes which would not have been possible with the previously utilised transition metals.

3.6 Infinite networks with IsoBDI ligand

The isophthalic acid substituted BDI ligand, despite its lack of chirality, was also investigated, to determine how the presence of four carboxylate coordinating groups would influence the coordination compounds formed. As the IsoBDI ligand has twice as many coordinating groups than the AlaBDI or LeuBDI ligands, it is more likely to form infinite coordination networks.

The reaction of H_4IsoBDI with $ZnCl_2 \cdot 6H_2O$ in DMF formed colourless crystals, which were structurally characterised to show a 3D coordination polymer with formula *poly*-$[Zn_4(IsoBDI)_2(DMF)(OH_2)_4] \cdot DMF \cdot 9H_2O$, **3.7**. The structure of **3.7** involves four Zn^{II} ions, two IsoBDI ligands, four water ligands and a ligated DMF molecule in the asymmetric unit, as well as additional void space in which no ordered solvent molecules could be modelled. The non-coordinated solvent was assigned as one DMF and nine water molecules per asymmetric unit, by residual electron density, as well as TGA and microanalysis.

There are two bimetallic nodes in the structure of **3.7**, in which the two Zn^{II} ions within the nodes are bridged by three carboxylate groups in μ-1κ*O*,2κ*O′* coordination modes, Figure 3.13. One node involves Zn(1) and Zn(2), and the other involves Zn(3) and Zn(4). Zn(1) adopts a tetrahedral geometry, in which three of the sites are occupied by the bridging carboxylates, and the remaining site is occupied by a ligated DMF molecule. Zn(2) and Zn(3) both adopt a trigonal bipyramidal geometry in which the equatorial positions are occupied by a monodentate carboxylate and two bridging carboxylates, and the axial positions are occupied by the remaining bridging carboxylate and a water molecule. Zn(4) is also in a trigonal bipyramidal geometry, with the equatorial positions occupied by two water molecules and a bridging carboxylate, and the axial positions are occupied by two bridging carboxylate groups.

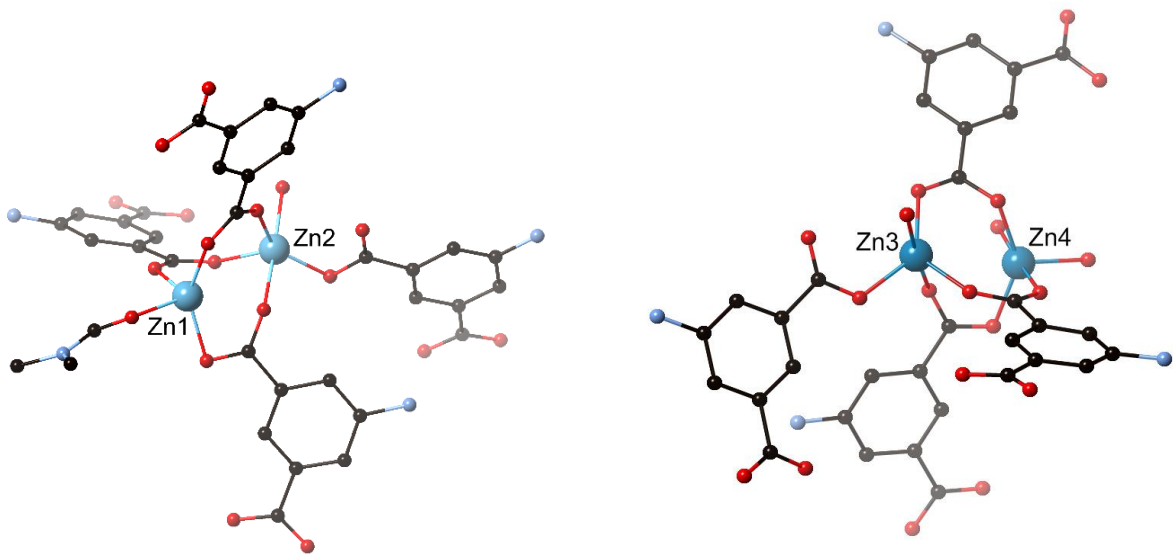

*Figure 3.13. The two bimetallic nodes, entailing four crystallographically unique Zn^{II} ions, in the structure of **3.7**. All hydrogen atoms are omitted for clarity.*

The four carboxylate groups on the ligand enables it to act as a four connecting node bridging between the four connecting bimetallic Zn^{II} nodes. The topology of the coordination polymer can be described by a Schläfli symbol of $(4^2.6^2.8^2)_4$. The aromaticity of the ligands allows face-to-face parallel π-interactions to occur between the ligands. There are two crystallographically unique IsoBDI ligands in the structure, which engage in three different instances of π-interactions. One isophthalate group of each ligand is engaged in face-to-face π-interactions with the phthalimide groups of neighbouring ligands, with closest C⋯C distances of 3.381(11) Å and 3.419(11). There are also π-interactions between two neighbouring phthalimide groups, with closest C⋯C distance of 3.411(11) Å. The remaining isophthalate groups are twisted in relation to the core of the ligand and not engaged in π-interactions. The structure of **3.7** packs in such a way to leave 36% of the material as void space. The voids are in the form of intersecting 1D channels, when viewed down the **b**- and **c**-axis, Figure 3.14.

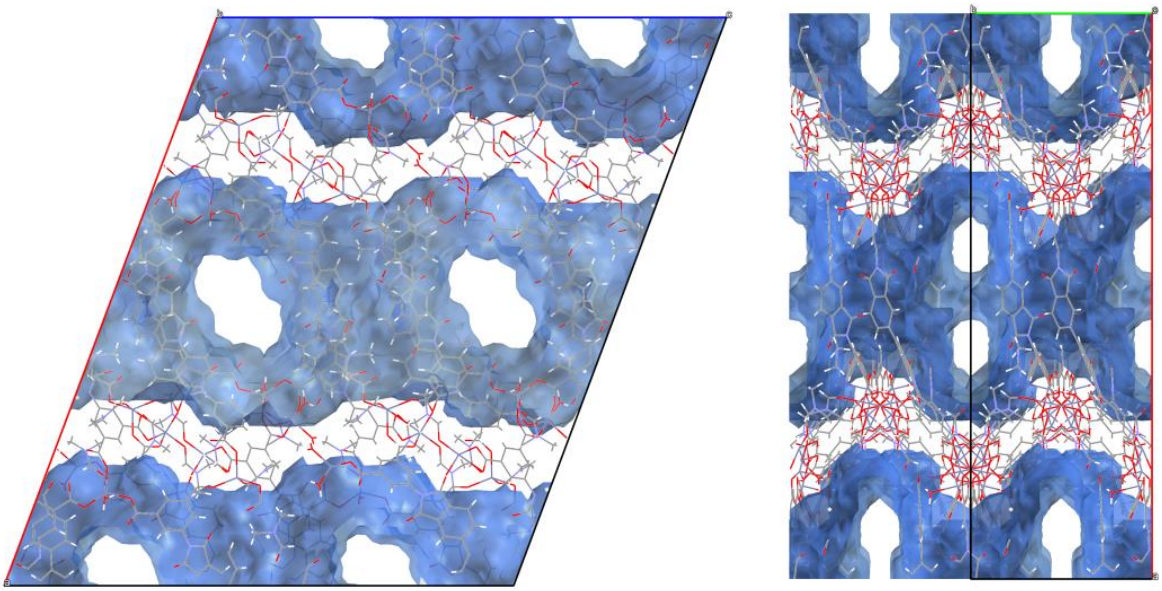

*Figure 3.14. The 1D solvent channels present in the structure of **3.7**, viewed along the **b**- and **c**-axis, respectively.*

Due to the solvent channels present in the structure of **3.7** the material was investigated for permanent porosity with the view to test this material for gas storage applications. Thermogravimetric analysis (TGA) of the fully solvated material showed a steady loss of solvent between 25 – 150 °C, Figure 3.15. The material was soaked in dichloromethane, acetonitrile and methanol to evacuate the non-volatile DMF from the pores and investigate the stability of the desolvated material. The TGA of the soaked samples showed the loss of the majority of the solvent between 25 – 100 °C, Figure 3.15. The desolvated samples were analysed by powder X-ray diffraction, which showed that the desolvation of the sample led to the loss of crystallinity of the material. The material was therefore not investigated for permanent porosity via gas sorption measurements.

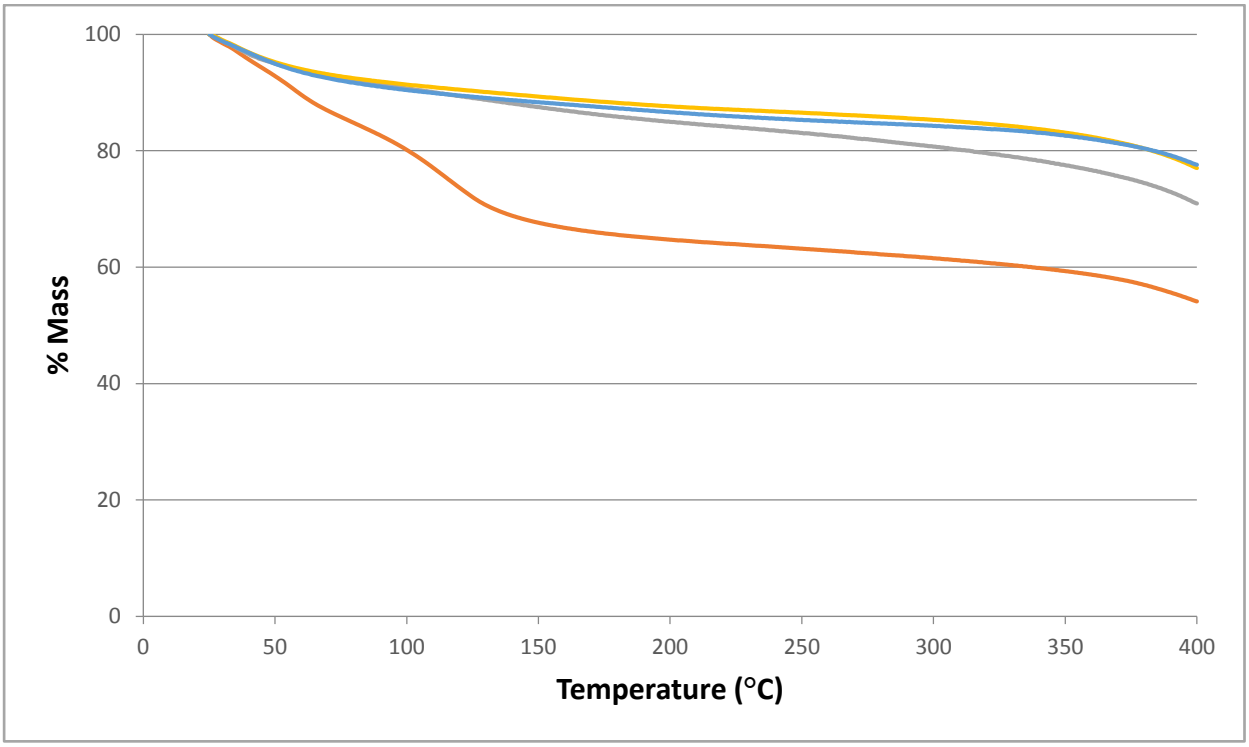

Figure 3.15. The thermogravimetric analysis of the freshly synthesised ***3.7*** *from DMF (orange), and after soaking in dichloromethane (grey), acetonitrile (yellow) and methanol (blue).*

In a similar manner to the amino acid substituted BDI and NDI ligands, the reaction of H_4IsoBDI with transition metals was also investigated with the addition of dipyridyl ligands. The reaction of H_4IsoBDI, 4PyNDI and $Cd(NO_3)_2{\cdot}4H_2O$ yielded yellow crystals which were structurally characterised to show a coordination polymer of the formula *poly*-[Cd(IsoBDI)$_{0.5}$(4PyNDI)]·2.5DMF·4H_2O, **3.8**. The structure of **3.8** is modelled in the centrosymmetric space group *C*2/*c* and the asymmetric unit contains one Cd^{II} ion, half an IsoBDI ligand and a 4PyNDI ligand. The Cd^{II} ions form a bimetallic node and adopt a distorted octahedral geometry in which the equatorial positions are occupied by one chelating carboxylate and two carboxylates which are bridging between the metals in a μ-1κO,2κO′ coordination mode, and the axial sites are occupied by 4PyNDI ligands. The IsoBDI ligands act as a four connecting node, bridging the bimetallic Cd^{II} nodes into a (4,4) sheet. The 4PyNDI ligands act as double pillars, in a similar manner to that observed in the structures of **2.7**, **2.18**, **2.19** and **3.4**. The 2D sheets are bridged into a 3D network by the double pillars of 4PyNDI. The bimetallic nodes act as a 6-connecting node and the IsoBDI ligand acts as a 4-

connecting node, and the network can be described by a Schläfli symbol of $(4^4.6^8.8)(4^4.6^2)$ and has an **fsc** topology, Figure 3.16.

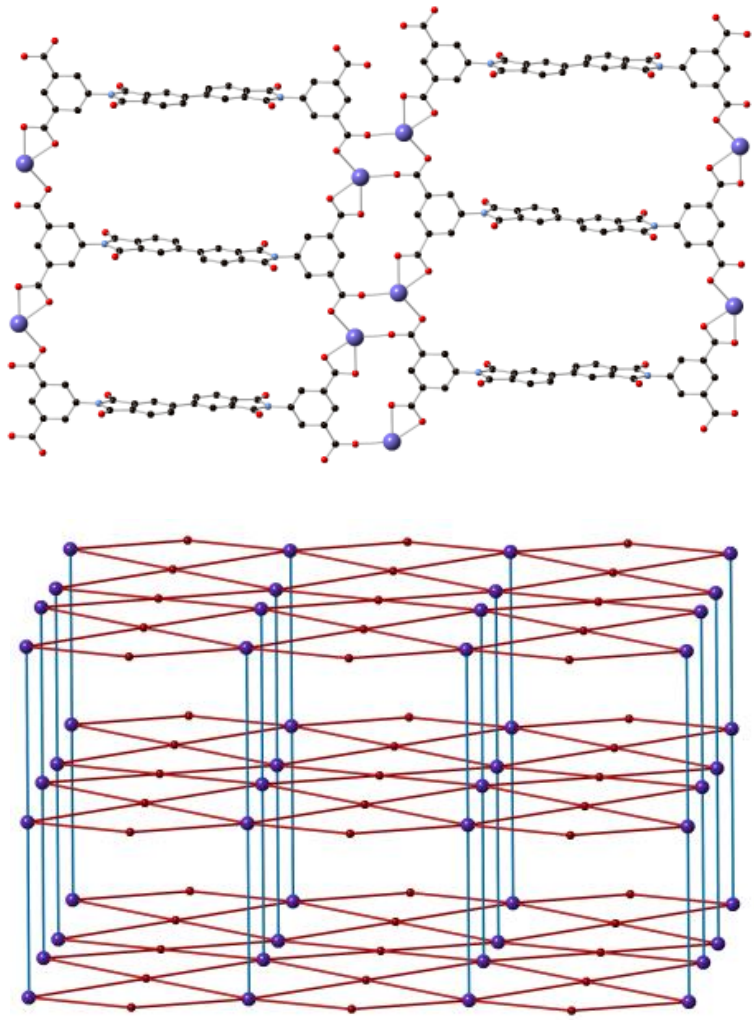

*Figure 3.16. The 2D sheet within the structure of **3.8** (top), the 4PyNDI ligands bridge these sheets together to form a 3D network. All hydrogen atoms omitted for clarity. The topology diagram of the 3D network (bottom). The ligands are represented by red spheres and rods, the metal spheres are represented by purple spheres, and the double pillars are represented by blue rods.*

The isophthalate groups are twisted in relation to the BDI core group at an interplanar angle of 77.259(4)°. The two phthalimide groups of the BDI core are co-planar. The network of **3.8** is 2-fold interpenetrated, as the double pillars of 4pyNDI ligands pass through the windows between IsoBDI ligands, Figure 3.17. The arrangement of the IsoBDI ligands allows parallel π-interactions between the BDI core and the

interpenetrating 4PyNDI ligands, with closest C···C distances of 3.900(6) and 3.4067(7) Å. The 4PyNDI ligands also have parallel π-interactions with each other through the NDI cores, with closest C···C distance of 3.3893(7) Å. The dipyridyl groups of the 4PyNDI ligand are also engaged in offset parallel π-interactions, with closest C···C distances of 3.4832(18) and 3.6955(19) Å. As was previously observed with the NDI ligands and the structure of **2.4**, the π-rich 4PyNDI ligand facilitates π-interactions within the network.

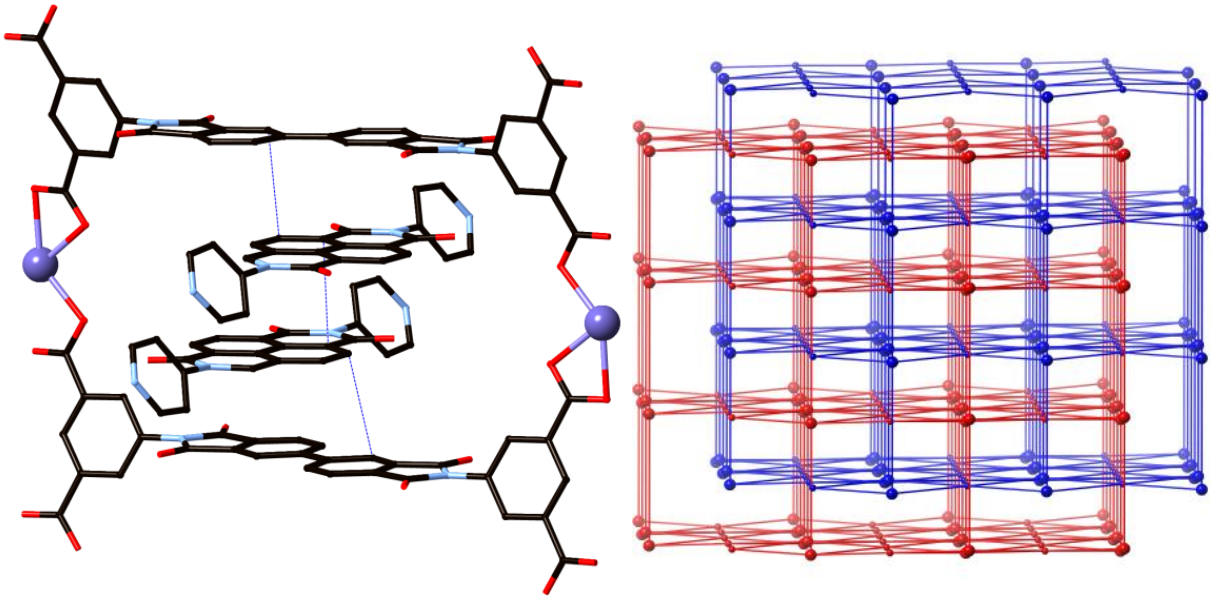

*Figure 3.17. The interpenetration of the two 3D networks of **3.8**, by the double pillars of 4PyNDI threading through the {Cd_2(IsoBDI)$_2$} loop and engaging in π-interactions, shown as blue dashed lines (left). All hydrogen atoms are omitted for clarity. The interpenetrating networks as shown by their topology diagrams, shown in red and blue (right).*

Despite the 2-fold interpenetration of the network of **3.8**, the structure still shows potential for porosity. The structure contains intersecting 1D solvent channels, when viewed down the **b**- and **c**-axes, Figure 3.18, giving the material 35% void space, as calculated by Mercury.[376] Solvent could not be modelled in the single crystal X-ray structure of **3.8**, however TGA, microanalysis and residual electron density suggested that the voids contained four water and 2.5 DMF molecules per asymmetric unit.

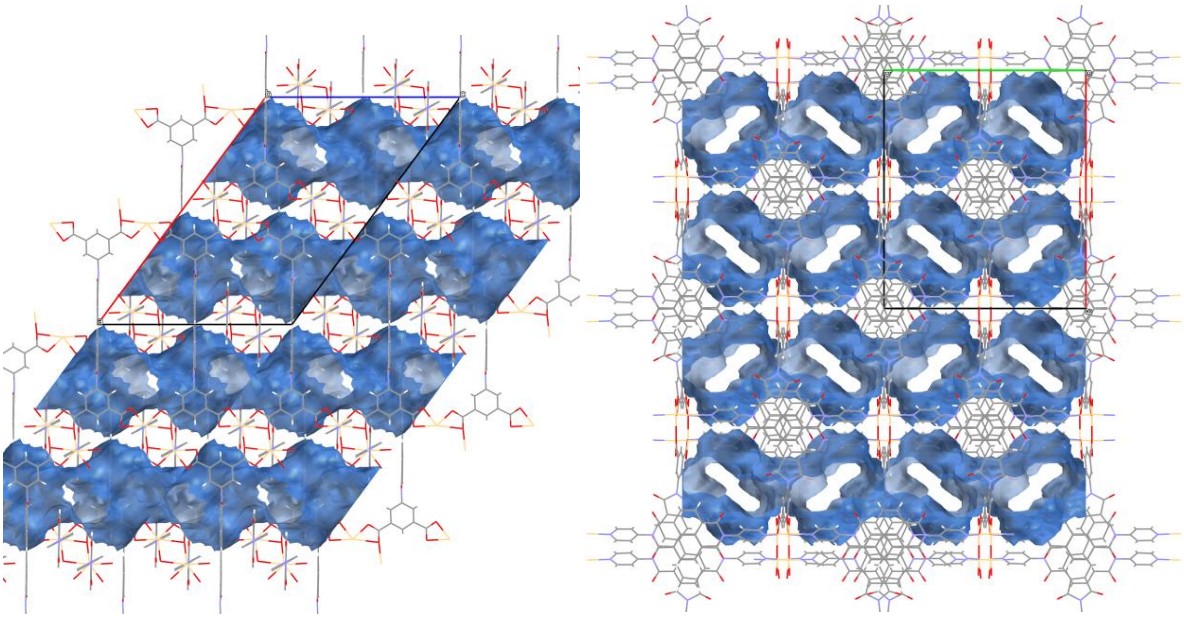

*Figure 3.18. The 1D channels in the structure of **3.8**, viewed down the **b**- (left) and **c**-axes (right).*

As the structure of **3.8** showed solvent filled channels, the material was investigated for permanent porosity. The evacuation of the pores was first investigated by soaking the material in acetonitrile and dichloromethane, in order to exchange the non-volatile DMF from the pores. The TGA of the unactivated sample showed solvent loss between 25 – 175 °C. The TGA of the acetonitrile and dichloromethane soaked samples showed rapid solvent loss between 25 – 70 °C, Figure 3.19.

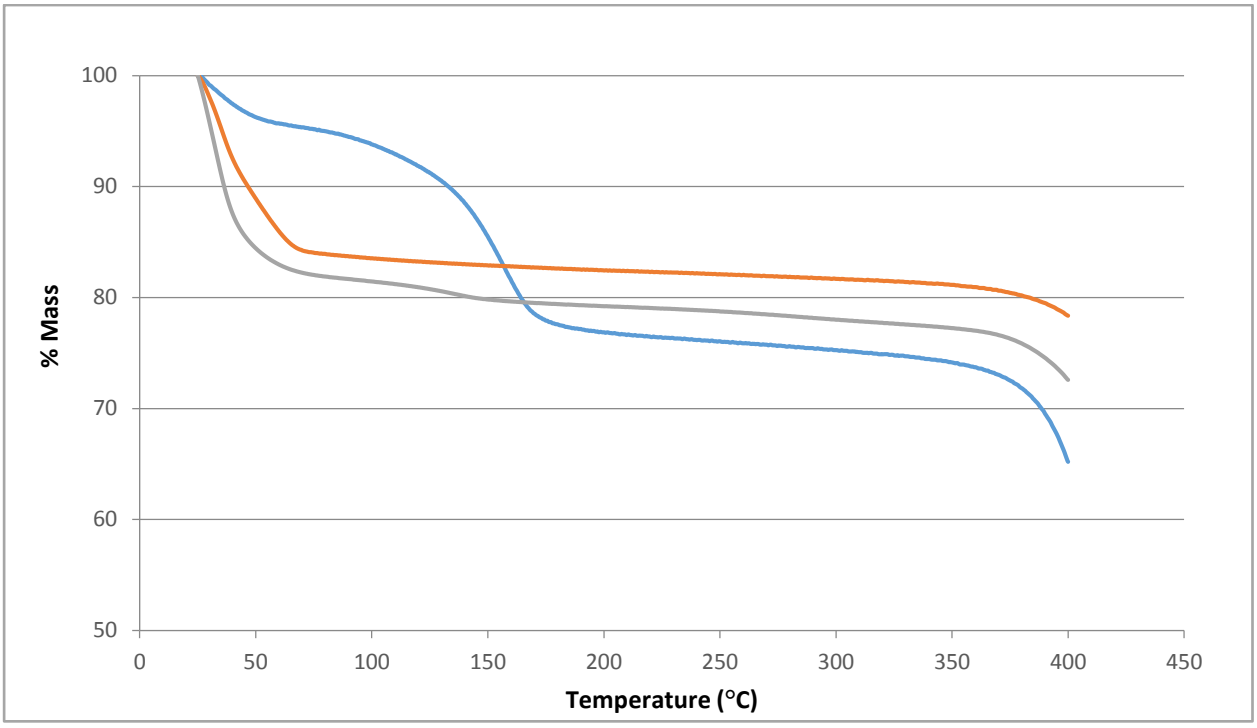

*Figure 3.19. The TGA of **3.8** freshly synthesised from DMF (blue) and after soaking in acetonitrile (orange) and dichloromethane (grey).*

The most efficient solvent exchange was observed for the sample which was soaked in acetonitrile, as it plateaued from 70 °C, while the dichloromethane sample showed most of the mass loss by ~ 60 °C and then another step of solvent loss until 150 °C. Therefore a bulk sample of **3.8** was soaked in acetonitrile and activated for gas sorption measurements to analyse if the material had permanent porosity. Unfortunately, the material did not display any indication of gas sorption.

The coordination polymers obtained containing IsoBDI showed the influence of increasing the number of coordinating groups of a ligand from two carboxylate groups to four. The higher number of coordinating groups, also coupled with dipyridyl ligands in one case, led to the formation of 3D networks. Both of the coordination polymers obtained with IsoBDI showed solvent channels in their structure, however neither showed permanent porosity and so could not be investigated for gas storage applications.

3.7 Conclusion

All the coordination complexes reported with amino acid substituted BDI ligands have shown that these ligands form $[M_2L_2]$ metallomacrocycle motifs in a similar manner to those reported with amino acid

substituted NDI ligands. As the core of the BDI ligand is not a fused aromatic system, as was the case for the NDI ligands, the BDI core is somewhat flexible and forms coordination compounds which are much less likely to be dominated by π-interactions.

In the absence of a dipyridyl ligand, the reaction of AlaBDI or LeuBDI with Cd^{II} formed discrete macrocycle complexes, **3.1** and **3.2**, similar to those reported as forming in the coordination polymers involving NDI ligands. The use of a small dipyridyl ligand, 4,4′-bipy, alongside AlaBDI and Zn^{II} did not form a polymeric coordination compound as was expected, but a discrete macrocycle in which the 4,4′-bipy bridged the metals within the macrocycle. It was only upon the reaction of a longer and π-rich dipyridyl ligand, 4PyNDI, with LeuBDI and Cd^{II}, that a coordination polymer, **3.4**, was formed. The use of Cu^{II} with AlaBDI or LeuBDI led to two analogous $\{Cu_8(BDI)_8\}$ square complexes, **3.5** and **3.6**, in which four copper paddlewheel SBUs form the corners of the square and two BDI ligands form each edge of the square. Although these square complexes were unable to be analysed in bulk, they are an interesting example of discrete complexes formed with copper paddlewheels and amino acid substituted diimide ligands, which are further explored with different ligands in Chapters 5 and 6.

The coordination complexes **3.1** – **3.6** were much less dominated by π-interactions than those involving amino acid NDI ligands, most likely due to the BDI ligands being more flexible and less π-rich. The structures of **3.1** – **3.3** did not involve any discernible π-interactions. The π-rich 4PyNDI ligand used in **3.4** led to face-to-face π-interactions both within and between the 2D sheets of the structure. The structures of **3.5** and **3.6** involved some non-parallel face-to-face π-interactions between the complexes in their solid-state packing.

The change from amino acid substituted BDI ligands to an isophthalic acid substituted ligand, IsoBDI, which has four coordinating carboxylate groups, led to the formation of two different 3D coordination polymers. The network with Zn^{II} metal centres, **3.7**, showed solvent filled channels accounting for 36% of the unit cell. The use of IsoBDI with Cd^{II} and 4PyNDI formed a 3D network which showed solvent filled channels which accounted for 35% of the unit cell, **3.8**. Both **3.7** and **3.8** were investigated for permanent

porosity, but showed loss of crystallinity or no gas absorption, and therefore it was concluded that they did not display permanent porosity.

The amino acid substituted BDI ligands reported herein have been shown to form similar $[M_2L_2]$ macrocycle motifs as those which were observed to be ubiquitous with amino acid substituted NDI ligands. As the BDI ligands were not as π-rich as the NDI ligands, their coordination compounds were much less dominated by π-interactions, and formed with less predictability. These results demonstrate that amino acid substituted diimide ligands, both with an NDI or a BDI core group, are reliable tectons for the synthesis of coordination polymers with $[M_2L_2]$ metallomacrocycle motifs.

Chapter 4: Fluorescent properties of naphthalene diimides

4.1 Introduction

Luminescence is the emission of light by any substance resulting from radiative relaxation (i.e emission of a photon) from an excited state to a lower energy state. This transition is often from a higher electronic state to the ground state.[391] In an electronically excited species, the excited electron may be in an excited singlet state, in which the electron is spin paired to a second electron in the ground state, or it may change spin, a process called intersystem crossing, to a triplet state, in which it is not spin paired with an electron in the ground state. Photoluminescence is the excitation of a sample by photons, followed by the emission of photons from the excited state.

Photoluminescence can be divided into two categories, depending on the nature of the excited state. The transition from a singlet to the ground state is classified as fluorescence. As this transitions between singlet to ground state is spin-allowed, the transition is quite fast, typically occurring on a time scale of nanoseconds. The transition from triplet to ground state is called phosphorescence. As the transition from triplet to ground state is not spin-allowed, the transition is much slower, resulting in emission lifetimes of microseconds through to seconds.

4.1.1 Fluorescence

Fluorescence is a widely utilised tool for analysing the structure and interactions of matter, due to the specificity of fluorescent characteristics of the emitting molecule due on its microenvironment.[392] There are multiple highly sensitive techniques which may be utilised based on the fluorescence output of a material.[393] A molecule which is fluorescent is called a fluorophore, of which there are multiple different types. Fluorophores which have different forms have certain advantages over one another. Commonly investigated fluorophores include small-molecule dyes, which have fluorescent properties which are tuned by their structure, [394, 395] quantum dots, which have fluorescent characteristics tuned by size,[396, 397] and

naturally occurring fluorescent proteins, which have led to the advancement of biological imaging [398-400] Small molecule dyes are commonly studied fluorophores because many may be designed to be non-toxic and insensitive to pH and temperature, and may be functionalised for a specific purpose and incorporated into larger structures.

An area which fluorescent compounds find a broad range of applications is that of sensing, due to the sensitivity which fluorescence has to the environment of the compound. Fluorescent sensors have found applications in the detection of toxic metals such as lead, cadmium and mercury.[401] Fluorescence has been used in the sensing of cations, and offers significant advantages over other cation sensing techniques, as it is minimally invasive, highly sensitive, relatively inexpensive, allows continuous monitoring and does not require a large amount of sample.[402]

Fluorescent compounds may also have applications in enantioselective sensing, an example of which is a chiral boronic acid molecule which was observed to have highly enantioselective fluorescence when interacting with sugar esters.[403] Chiral MOFs may also act as enantioselective fluorescent sensors, as reported by the Lin group. A chiral BINOL functionalised ligand formed a 3D MOF with 57% void space, which showed fluorescence emission when suspended in acetonitrile. The addition of chiral amino alcohols acted to quench the fluorescence of the MOF, by the preconcentration of the guest molecules in the pores. The different handednesses of amino alcohol guest which were incorporated into the pores led to different quenching efficiencies, making this MOF an enantioselective fluorescent sensor material.[175]

Fluorophores may sometimes interact with each other in solution, which leads to a change in their emission.[391] A well know example of this is pyrene, which at low concentration shows emission which is vibrationally structured and a mirror image of its absorbance, however at higher concentration it emits at a longer or lower energy wavelength, which is due to the formation of excited state dimers (excimers) in solution. Excimers form when a monomer (M) interacts with another monomer which is in an excited state (M*), forming an excited state dimer, which will then emit a photon and dissociate, Equation 4.1. Excited state complexes (exciplexes) may also form between a fluorophore in an excited state (A*) and another molecule (B), which emits a photon when the complex dissociates, Equation 4.2.

$$2M \xrightarrow{h\nu} M + M^* \rightarrow D^* \xrightarrow{h\nu'} 2M \quad (\textit{Equation 4.1})$$

$$A + B \xrightarrow{h\nu} A^* + B \rightarrow [AB]^* \xrightarrow{h\nu'} A + B \quad (\textit{Equation 4.2})$$

4.1.2 Physical properties of naphthalene diimides

NDIs have attracted much attention in a variety of fields because they are a class of compounds with properties which can be highly dependent on their substitution. The ease of functionalisation of NDIs while maintaining their basic structure has led to their investigation into a variety of fields for applications in areas such as organic electronic devices,[404, 405] photovoltaics,[406] flexible display devices,[407] dyes,[408] fluorescence sensors,[409] medicine and biology[410, 411] and semiconductors.[412]

The electron deficient nature of NDIs has enabled them to be utilised within supramolecular chemistry for the formation of various supramolecular architectures, including rotaxanes, catenanes, nanotubes and foldamers, typically through the combination of the electron deficient NDI with an electron rich aromatic alkoxy molecule. [365, 413-418] Outside the field of metallosupramolecular chemistry NDIs have been the subject of investigation in many other areas of chemistry and materials science.[363]

As was observed in their solid state coordination compounds, NDIs readily form face-to-face π-interactions, which contributed to the reproducibility of the $\{M_2L_2\}$ metallomacrocyclic motif in the coordination polymers discussed in Chapter 2. The π-rich naphthalene core of NDIs may also be used to facilitate the formation of low-molecular weight gels.[419] In 2006 the Shinkai group reported an efficient and versatile NDI based organogelator which formed a robust 1D gel superstructure, facilitated by a combination of π-π stacking, hydrogen-bonding and van der Waals forces. The organogel could be used as a colourmetric detection system for naked-eye differentiation between several positional isomers of dihydroxynaphthalene.[419] It was the propensity of the NDI core to form π-interactions which led to the formation of such an efficient gel, demonstrating that the π-rich core of the NDI is useful in materials chemistry as well as in reproducibility in supramolecular chemistry.

The fluorescence properties of NDIs can be tuned depending on the substitution of the molecule. Therefore NDIs have been investigated widely for their fluorescent properties. Functionalisation of NDIs through

only their diimide nitrogen sites typically has minimal influence on the weakly fluorescent nature of the NDI core, and shows absorption spectra with structured bands in the range of 300-400 nm, indicative of π-π* transitions. The emission spectra of imide substituted NDIs usually mirrors that of the absorption spectra, with a small Stokes shift. The increased solubility of NDIs in comparison to the other larger rylene diimides, perylene diimide (PDI) and terylene diimide (TDI), make them much more attractive for fluorescence studies in a variety of solvents and concentrations.[420] The core substitution of NDIs with electron donating groups such as amines produces molecules of variable absorption and fluorescent properties, dependent on the substitution. Core substituted NDIs therefore have broad applications as readily tuneable dyes.[420-423] Although NDIs which are not core-substituted are usually weakly fluorescent, they have also been shown to have excimer- or exciplex-like emission. The presence of an NDI excimer or exciplex can be identified by a broadening of the characteristic absorption spectrum and emission spectrum around 300-400 nm, and a broad and unstructured emission band at longer wavelength ~ 400 – 600 nm, with maxima around 480 – 550 nm.[393] An example of such exciplexes is through solvent dependent emission of an NDI which showed typical NDI emission maxima at 386 nm when dissolved in acetonitrile, and showed broad emission with maxima at 436, 481 and 522 nm when dissolved in benzene, toluene and *p*-xylene, respectively.[424] The shifted and broadened emission of the NDI when dissolved in aromatic solvents could be attributed to the formation of exciplexes between the NDI and aromatic solvent molecules. An NDI-based chemosensor utilising the phenomenon of NDI-NDI excimers has also been reported for the sensing of the biologically important molecule pyrophosphate (PPi). The NDI chemosensor forms a 2 + 2 type excimer with the PPi molecule, which brings the NDI groups into close proximity, allowing favourable π-interactions between the NDIs, Figure 4.1. The formation of the excimer is indicated by a broad emission peak at 490 nm.[411]

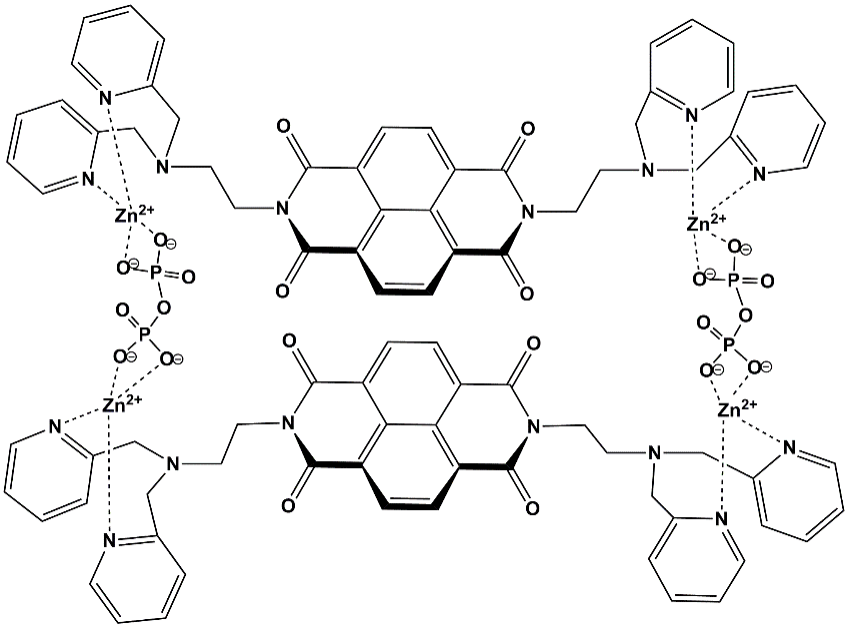

Figure 4.1. The NDI chemosensor in which two NDIs, two PPi ions and two Zn^{II} ions form a complex in which the NDIs are engaged in face-to-face π-interactions and form excimers, shown by emission at 490 nm.

The formation of NDI exciplexes with aromatic solvent molecules has also been observed with solid state materials which incorporate NDI functionality. An asymmetrically functionalised NDI which was substituted through the imide positions, with a butyl group and an alanine methyl ester, was shown to form a 2D layered nanomaterial which displayed tunable fluorescence emission, dependent on aromatic solvents.[425] The emission maxima changed to 450, 487 to 523 nm with benzene, toluene and xylene, respectively. An NDI based MOF was also shown to be a fluorescent chemical sensor. The MOF showed instant and reversible solvatochromic behaviour based on the presence of solvents of varying polarity, and exhibited selective detection of amines by photoluminescence quenching.[369] This previous work establishes the viability of designing NDIs to form exciplexes with aromatic solvents or NDI excimers which may form in solution.

4.2 Fluorescence of the leucine substituted NDI

Due to the many applications of NDIs outside the area of metallosupramolecular chemistry owing to their interesting physical properties, the amino acid substituted NDI ligands which were utilised in this work for

coordination chemistry were also investigated for their photophysical properties. The fluorescence properties of H_2LeuNDI were investigated in detail due to its solubility in a range of organic solvents.

As the fluorescence of NDIs has previously been shown to be solvent dependent, the fluorescence properties of H_2LeuNDI were investigated in a range of solvents. The non-polar aromatic solvents used were toluene and *o*-, *m*- and *p*-xylene. The non-aromatic solvents chloroform and acetonitrile were also investigated. These solvents were chosen because they represented a good range of polarity, size and aromaticity through which to investigate the solvent dependent fluorescent properties of H_2LeuNDI.

4.2.1 Fluorescence of H_2LeuNDI in non-aromatic solvents

The spectra of H_2LeuNDI in acetonitrile and chloroform showed absorption and emission which is typical for NDIs which are not substituted at the core positions, Figure 4.2. The absorbance spectra show peaks at 361 and 380 nm and a shoulder at 345 nm in chloroform, and at 358 and 378 nm with a shoulder at 342 nm in acetonitrile, attributed to π-π* transitions of the NDI core.[424] The emission spectra are mirror images of the absorbance, with peak maxima at 411 and 407 nm in chloroform and acetonitrile, respectively, and a shoulder at 390 nm. Emission spectra which are mirror images of the absorbance are typical of imide substituted NDIs. The fluorescence of H_2LeuNDI in chloroform and acetonitrile is very weak, with quantum yields of 0.0014 and 0.0016, respectively.

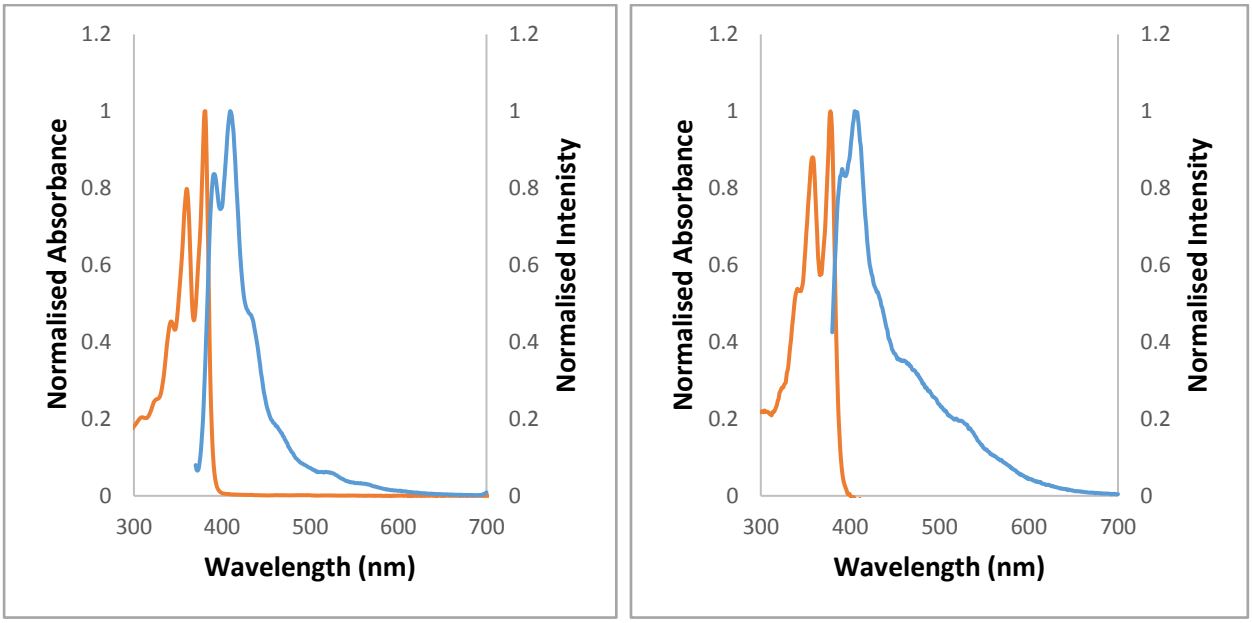

Figure 4.2. Normalised absorption (orange) and emission (blue) spectra of H_2LeuNDI at 30 µmol/L in chloroform (left) and acetonitrile (right), showing absorbance peaks at ~360 and 380 nm and emission maxima at ~410 nm, typical of NDIs which are not substituted at the core positions. Unnormalised absorptions of H_2LeuNDI in chloroform and acetonitrile at 30 µmol/L were 0.51 and 0.09, respectively.

The fluorescence emission of H_2LeuNDI was also measured with varying concentrations, in order to analyse if an increase in concentration would encourage aggregation of the molecules and the occurrence of excited state dimers (excimers). The emission was measured in solutions of H_2LeuNDI in chloroform at concentrations ranging from 10 – 150 µmol/L, Figure 4.3. The emission intensity increased with higher concentration, with the exception of the solution at a concentration of 150 µmol/L, which shows decreased intensity compared to the solution at 100 µmol/L. It is likely that the emission intensity decreased with increased concentration due to the inner filter effect, in which molecules in the sample absorb light which is emitted by other molecules within the sample, due to high concentration. The emission peak at 390 nm decreases in relation to the peak at 410 nm upon increasing concentration, due to the inner filter effect, as the molecules absorb to a much greater extent at 390 nm than 410 nm. The increase in concentration does not lead to any new emission peaks, which could be attributed to the presence of excimers, suggesting that the H_2LeuNDI molecules are not forming excimers in chloroform solutions. The ^{1}H-NMR of solutions of H_2LeuNDI of increasing concentration from 10 – 80 mmol/L were also measured, as interaction of the NDI

cores in solution would likely lead to a shift in the signal of the NDI core. The increase in concentration does not lead to a shift in the ^{1}H-NMR signal of the NDI core, Figure 4.3. The absence of new peaks in the emission spectra of H_2LeuNDI upon increasing concentration and the lack of shift in the ^{1}H-NMR signal for the NDI core both suggest that the NDIs are not aggregating and therefore not interacting in solution through the aromatic NDI cores.

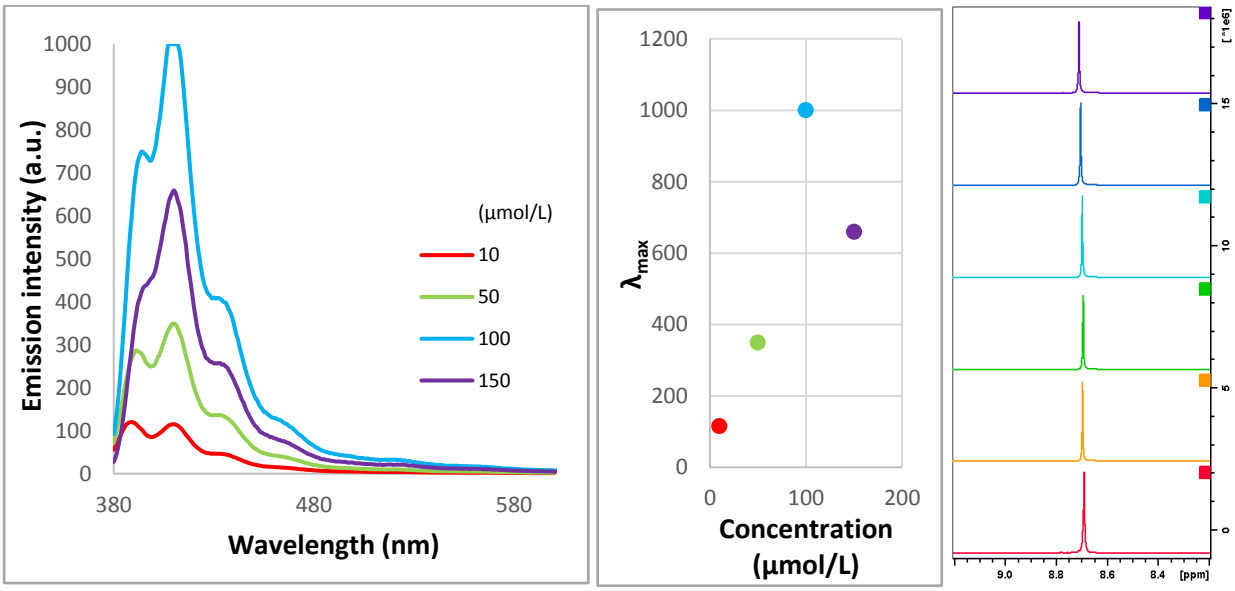

Figure 4.3. Emission of H_2LeuNDI in chloroform at increasing concentrations (left). The highest concentration leads to decreased emission intensity due to the inner filter effect. The maximum emission of H_2LeuNDI in chloroform at each concentration, showing an increase in emission intensity with concentration up to 100 umol/L, after which the inner filter effect causes a decrease in the emission intensity. (centre). The ^{1}H-NMR signal for the NDI core of H_2LeuNDI in chloroform at concentrations of 10 mmol/L (red), 30 mmol/L (green), 40 mmol/L (light blue), 60 mmol/L (dark blue) and 80 mmol/L (purple) (right), showing that increased concentration does not shift the ^{1}H-NMR signal for the NDI core, suggesting that the H_2LeuNDI molecules do not aggregate in solution, despite elevated concentration.

4.2.2 Fluorescence of H_2LeuNDI in aromatic solvents

The absorbance and emission spectra of H_2LeuNDI were also measured in the aromatic solvents *o*-, *m*- and *p*-xylene, and toluene, Figure 4.4. The absorbance spectra of H_2LeuNDI were very similar for all aromatic solvents, showing twin peaks at ~ 360 and ~ 380 nm, with a shoulder at ~340 nm. Similar to the absorbance

in non-aromatic solvents, the absorbance peaks all show the typical peaks which are characteristic of π-π* transitions of the NDI core.

The fluorescence emission in aromatic solvents was very different to that of H_2LeuNDI in chloroform and acetonitrile, Figure 4.4. The emission spectra of H_2LeuNDI in aromatic solvents all show a broad and unstructured red shifted band in the range 450 – 700 nm. H_2LeuNDI in toluene has an emission maximum at 503 nm, *o*- and *m*-xylene have emission maxima at 520 nm, and *p*-xylene is even more red-shifted, emitting with maximum at 539 nm. The fluorescence of H_2LeuNDI in aromatic solvents was more intense than in acetonitrile or chloroform, although still very weak, with quantum yields of 0.037, 0.052, 0.025 and 0.018 for toluene, *o*-, *m*- and *p*-xylene, respectively.

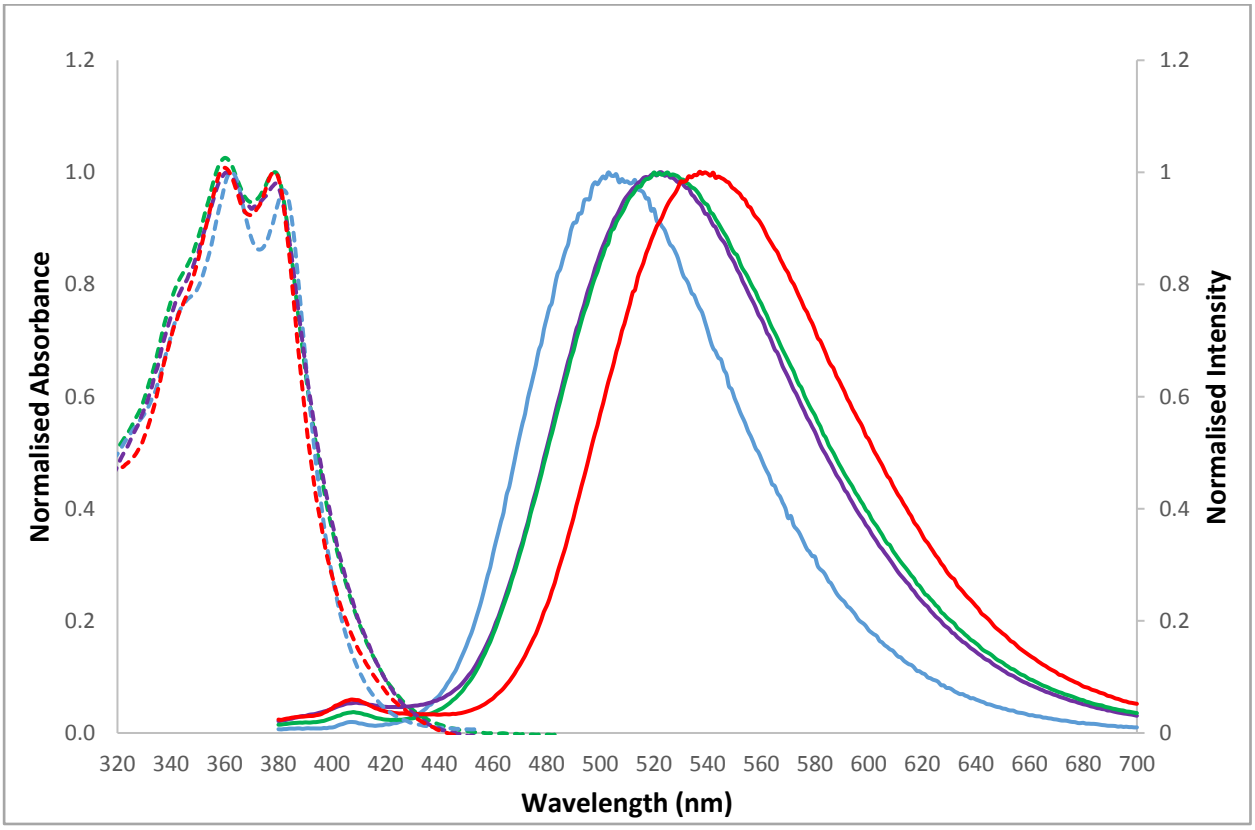

Figure 4.4. Normalised absorbance (dashed lines) and emission upon excitation at 360 nm (solid lines) spectra of H_2LeuNDI in toluene at 30 µmol/L (blue) and o-xylene (purple), m-xylene (green) and p-xylene (red) at 20 µmol/L. The absorbance maximum for all solutions were between 0.2 and 0.35.

The emergence of broad peaks at such long wavelengths may be explained by the formation of excited state complexes (exciplexes) of the NDI with the aromatic solvent, facilitated by face-to-face π-interactions. The lack of these red-shifted peaks in non-aromatic solvents suggests that the solvent must be aromatic in order to form these exciplexes. There is some precedent for the formation of exciplexes of N-substituted NDIs with aromatic solvents, showing emission ~ 450-500 nm (*vide supra*).[393, 424, 425] The dependence of the emission maximum of H_2LeuNDI on the aromatic solvent in which it is dissolved suggests that the emission is due to the presence of NDI-solvent exciplexes. The exciplex emission with *m*- and *o*-xylene are likely quite similar because these molecules have similar shapes. The added hindrance of the methyl groups in *p*-xylene may lead to the *p*-xylene interacting with the NDI core in a different way to the toluene, *o*-xylene or *m*-xylene molecules, leading to the difference in fluorescence emission.

The relative shifts in emission maxima of H_2LeuNDI in toluene and *o*-, *m*- and *p*-xylene may be indicative of the stability of the exciplexes in solution. The longer emission wavelength of H_2LeuNDI with *p*-xylene could be attributed to a lower energy and therefore more stable exciplex than those of H_2LeuNDI with *o*- or *m*-xylene, which are in turn more stable than the exciplexes formed with toluene.

4.2.3 Fluorescence titration of H_2LeuNDI in chloroform and aromatic solvents

The influence of an aromatic solvent on the formation of NDI-solvent exciplexes was investigated by a fluorescence titration of H_2LeuNDI in chloroform, with increasing proportions of the aromatic solvents toluene and *o*-, *m*- and *p*-xylene. These solvents were chosen because the emission of H_2LeuNDI in chloroform was simply a mirror image of the absorbance, and aromatic solvents appeared to facilitate the formation of NDI exciplexes. The experiment was conducted with a series of 30 μmol/L solutions of H_2LeuNDI in chloroform, with aromatic solvents at 0%, 1%, 10%, 20%, 50% and 100% by volume. The emission spectra showed a decrease in the typical NDI emission peaks at 390 and 410 nm upon the increase in proportion of aromatic solvent. The increase in the proportion of aromatic solvent also led to the appearance and subsequent increase of the broad emission band at 510 nm, Figure 4.5. Based on the emission in toluene and xylenes (*vide supra*) which suggested the formation of NDI-solvent exciplexes, these results suggest that addition of a small amount of aromatic solvent in a non-aromatic solvent is

sufficient to initiate the formation of exciplexes. The addition of as little as 1% aromatic solvent in chloroform was enough to show a change in the emission spectrum, with a decrease in the peaks at 390 and 410 nm and the appearance of a broad peak at ~ 510 – 540 nm.

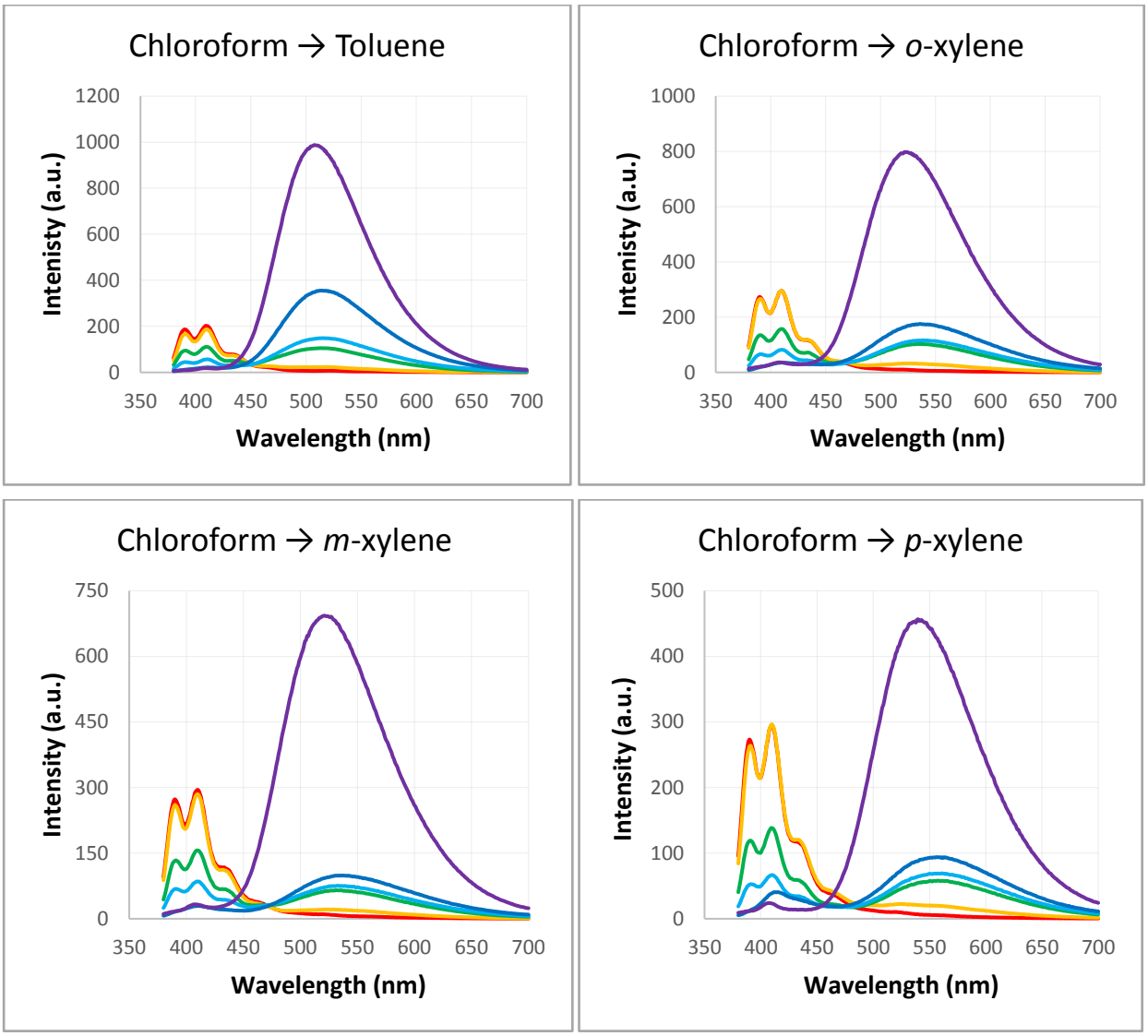

Figure 4.5. Emission spectra of H_2LeuNDI at 30 umol/L in chloroform with aromatic solvent proportions of 0% (red), 1% (orange), 10% (green), 20% (light blue), 50% (dark blue) and 100% (purple) upon excitation at 360 nm.

As the emission of H_2LeuNDI with toluene and other aromatic solvents showed broad emission at ~510 – 540 nm, and increased concentration of H_2LeuNDI in non-aromatic solvents did not lead to the emergence

of broad emission around this wavelength, it may be deduced that the emission at ~510 – 540 nm is due to the formation of exciplexes of NDIs with aromatic solvents.

4.2.4 ^{1}H-NMR studies of H_2LeuNDI exciplex formation

The formation of exciplexes of H_2LeuNDI with aromatic solvent molecules in chloroform solution was also investigated by ^{1}H-NMR, as it was hypothesised that if the aromatic solvent is interacting with the NDI core to form exciplexes, the ^{1}H-NMR signal of the NDI core should shift upon increased concentration of aromatic solvent. The ^{1}H-NMR experiments were conducted with a standard concentration of 10 mmol/L of H_2LeuNDI with the same solvent ratios which were used for the fluorescence emission experiments, 0%, 1%, 10%, 20%, 50% and 100% in the case of toluene in chloroform, and 0%, 1%, 10%, 20% and 50% in the case of *o*-, *m*- and *p*-xylene, as deuterated xylenes could not be obtained. The ^{1}H-NMR experiment shows an upfield shift in the signal of the NDI core upon the increase in proportion of aromatic solvent in the chloroform solution, Figure 4.6. In a pure chloroform solution of H_2LeuNDI, the NDI core showed an ^{1}H-NMR signal at 8.69 ppm. In a similar manner to that observed with the fluorescence emission, 1% aromatic solvent was enough to cause a small shift in the NDI signal, to 8.68 ppm for all aromatic solvents. The increase of aromatic solvent to 10% shifted the NDI signal to 8.60 ppm in the case of toluene and *o*-xylene, and 8.61 ppm in the case of *m*- and *p*-xylene. In the solutions with 20% and 50% aromatic solvent the NDI signal was observed at 8.52 and 8.30 ppm, respectively. The 100% toluene solution showed the NDI signal at 8.03 ppm.

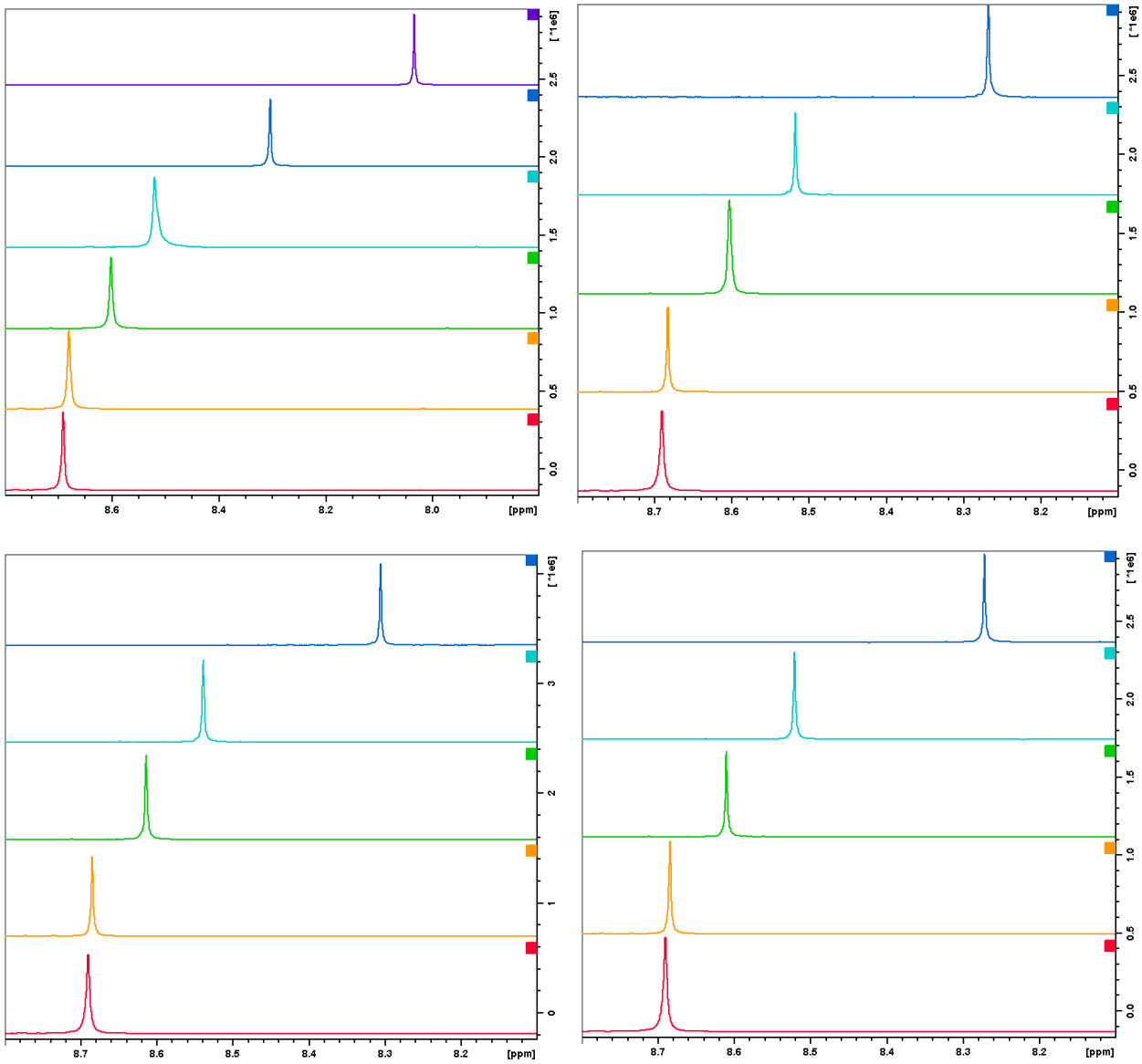

Figure 4.6. The ^{1}H-NMR titrations of H_2LeuNDI in chloroform with toluene (top left), o-xylene (top right), m-xylene (bottom left) and p-xylene (bottom right) proportions of 0% (red), 1% (orange), 10% (green), 20% (light blue), 50% (dark blue) and 100% (purple). The 100% aromatic solvent experiment could not be conducted with the xylenes because the deuterated solvents were unable to be obtained.

The change in ^{1}H-NMR signal upon an increase in the proportion of aromatic solvent suggests that there is an interaction with the core of the NDI ligand with the aromatic solvent. The ^{1}H-NMR results therefore strongly support the hypothesis that the fluorescence emission of H_2LeuNDI in other aromatic solvents was due to interaction between the NDI core and the solvent. The fact that this emission at ~ 500 nm was only present in aromatic solvents suggests that the exciplex formation is dependent on the ability of the solvent

to engage in π-interactions with the core of the NDI molecule. The change in fluorescence emission and shift in NMR signal of the NDI core in a chloroform solution with only 1% aromatic solvent also suggests that the formation of exciplexes is a favourable interaction for this system.

4.2.5 Time resolved fluorescence studies of H_2LeuNDI

Time correlated single photon counting was used to further investigate the influence of the aromatic solvent on the fluorescence emission of H_2LeuNDI. The fluorescence lifetimes in all aromatic solvents were fitted with more than one exponential decay function, suggesting that there is more than one fluorescent molecule or exciplex present in solution, Figure 4.7 and Table 4.1.

Toluene was the most complex decay profile, and was modelled with three exponential decay functions. The emission lifetime of toluene was modelled with a very rapid lifetime of 0.3 ns, another rapid lifetime of 1.8 ns and a longer lifetime of 6.6 ns, with proportions of 52, 36 and 12%, respectively. The emission of H_2LeuNDI in *o*-xylene was also modelled with three exponential decay functions, showing a short lifetime of 0.9 ns, a longer lifetime of 4.3 ns and a much longer lifetime of 9.4 ns, with proportions of 36, 49 and 15%, respectively. The emission in *m*-xylene and *p*-xylene were slightly less complex, and were able to be modelled with a di-exponential decay function. The emission in *m*-xylene showed a short lifetime of 1.6 ns, and a longer lifetime of 8.4 ns, with proportions of 10 and 90%, respectively. The emission in *p*-xylene had a short lifetime of 2.9 ns and a longer lifetime of 6.4 ns, with proportions of 15 and 85%, respectively. The emission lifetimes of H_2LeuNDI in aromatic solvents required modelling with multiple exponential functions likely due to a distribution of exciplexes present in solution. A single NDI may form an exciplex with a single solvent molecule. Alternatively exciplexes may form with three species, such as two solvent molecules sandwiching an NDI molecule, or two NDI molecules which sandwich a solvent molecule. Regardless of the type of exciplex formed, it appears that exciplexes only form with aromatic solvent molecules, as evidenced by the long lived emission lifetimes of H_2LeuNDI in aromatic solvents. The formation of exciplexes with aromatic solvents strongly suggests that π-interactions play an important role in the formation of exciplexes containing H_2LeuNDI in solution. However further study is required to fully

characterise the excited state behaviour of these exciplexes, as the time resolved experiments suggest a distribution of exciplexes in solution.

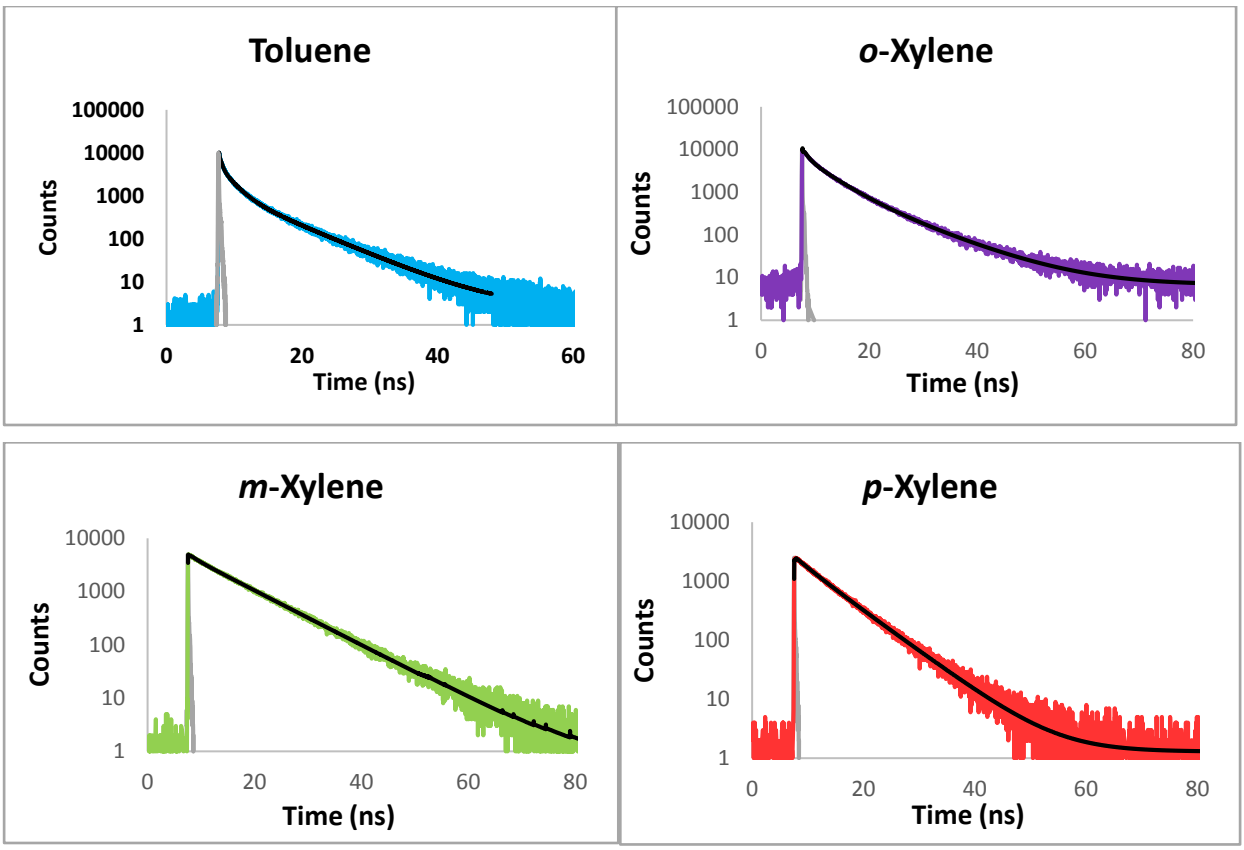

Figure 4.7. The time correlated single photon counting decay histograms and fitted exponentials decay functions (black) of H_2LeuNDI in toluene (blue), o-xylene (purple), m-xylene (green) and p-xylene (red). IRF (grey) is instrument response function.

Table 4.1. Summary of emission lifetimes and proportions thereof of H_2LeuNDI in aromatic solvents. All were collected with an excitation wavelength of 375 nm.

	$\lambda_{detection}$ (nm)	Conc. (µmol/L)	Lifetime 1 (ns)	Proportion 1 (%)	Lifetime 2 (ns)	Proportion 2 (%)	Lifetime 3 (ns)	Proportion 3 (%)
Toluene	510	30	0.3	52	1.8	36	6.6	12
o-Xylene	530	10	0.9	36	4.3	49	9.4	15
m-Xylene	530	20	1.6	10	8.4	90	-	-
p-Xylene	530	20	2.9	15	6.4	85	-	-

4.3 Discrete LeuNDI coordination complexes

As the results obtained with H_2LeuNDI in solution suggested that π-interactions of the NDI with aromatic solvent molecules were leading to the formation of exciplexes, attempts were made to form discrete coordination complexes with fixed NDI conformations which could be analysed for their fluorescence properties in solution. By forming a coordination complex in which the NDIs were essentially "locked together" by coordination bonds, the fluorescence behaviour of these complexes could be analysed and rationalised based on the known structure, and therefore compared to the fluorescence of the H_2LeuNDI compounds in solution.

The presence of the $\{M_2NDI_2\}$ metallomacrocyclic motif in 73% of the coordination polymers with amino acid substituted NDI ligands discussed in Chapter 2 and in previous work by the Turner group[352] suggested that it would be possible to form a discrete $\{M_2NDI_2\}$ macrocycle. It was thought that a single $\{M_2NDI_2\}$ macrocycle would have a space between the NDI planes, in which an aromatic guest could be inserted, and therefore change the fluorescence properties of the system. Given the frequency of interpenetration of these $\{M_2NDI_2\}$ based NDI coordination polymers by a catenane motif between the macrocycles, it was also thought that a discrete NDI [2]-catenane also could be formed in which the NDIs were locked into face-to-face π-interactions, and the fluorescence emission of the catenane could be analysed in order to investigate the influence which π-interactions have on the emission of the NDIs.

The formation of discrete LeuNDI coordination complexes requires capping of the metals in such a fashion as to block the formation of coordination polymers. As the coordination polymers reported in Chapter 2 often involved divergent dipyridyl ligands such as 4,4′-bipyridine, it was hypothesised that convergent dipyridyl ligands could be suitable for capping the metals of the $\{M_2NDI_2\}$ macrocycle in order to form discrete complexes. The convergent dipyridyl ligands selected were 2,2′-bipyridine (2,2′-bipy) and 1,10-phenanthroline (1,10-phen). Cd^{II} was selected as the metal centre for investigation into the synthesis of these products, as it was prolific in LeuNDI coordination polymers.

4.3.1 Discrete metallomacrocycle with LeuNDI

A crystalline product was isolated by the reaction of H_2LeuNDI, $Cd(NO_3)_2 \cdot 4H_2O$ and 1,10-phen in a solvent mixture of DMF, water and methanol at 85 °C, very similar conditions to those utilised for the formation of coordination polymers with Cd^{II} and LeuNDI. The composition of the crystals was determined to be $[Cd_2(1,10\text{-phen})_2(\text{LeuNDI})_2(OH_2)_2] \cdot 2H_2O \cdot \text{DMF}$, **4.1**$\cdot 2H_2O \cdot$DMF. The structure was modelled in the chiral space group *C*2 and the asymmetric unit contains two Cd^{II} ions, two LeuNDI ligands, two 1,10-phen ligands, two aqua ligands and a non-coordinated water molecule, in addition to void space with residual electron density in which no solvent could be modelled. As was expected, the LeuNDI ligands are "U" shaped and bridge between two monometallic Cd^{II} nodes to form a $\{Cd_2(\text{LeuNDI})_2\}$ macrocycle, Figure 4.8. Each of the Cd^{II} ions adopt a distorted octahedral geometry in which the equatorial positions are occupied by one chelating and one monodentate carboxylate groups of the LeuNDI ligands, and one of the nitrogen atoms of the 1,10-phen ligand. The axial sites are occupied by the remaining 1,10-phen nitrogen atoms, and an aqua ligand.

In a similar manner to the $\{M_2NDI_2\}$ macrocycles present in the NDI coordination polymers reported previously and in Chapter 2, the planes of the NDIs are parallel and at a suitable distance for an aromatic guest to sit between them and engage in face-to-face π-interactions. The mean interplanar distance of the NDIs is 6.890(6) Å and the closest C···C distance is 6.747(8) Å, which represents a slightly narrower macrocycle than those observed in the NDI coordination polymers, which generally have interplanar distances in the range 7 – 7.2 Å. It is possible that the NDI planes in the macrocycle of **4.1** is narrower because it does not have an aromatic guest passing through it. In contrast to many of the NDI coordination polymers, the macrocycle of **4.1** is not interpenetrated by either a catenane or rotaxane motif. Instead of an NDI threading through the macrocycle, the 1,10-phen ligands of adjacent macrocycles are sitting partially within the space between the NDIs of the macrocycle, with face-to-face π-interactions, at closest C···C distances of 3.404(18) and 3.413(19) Å, Figure 4.8. The formation of **4.1** shows that the $\{M_2(\text{NDI})_2\}$ metallomacrocycle motif which was so prevalent in coordination polymers is also possible in discrete coordination complexes.

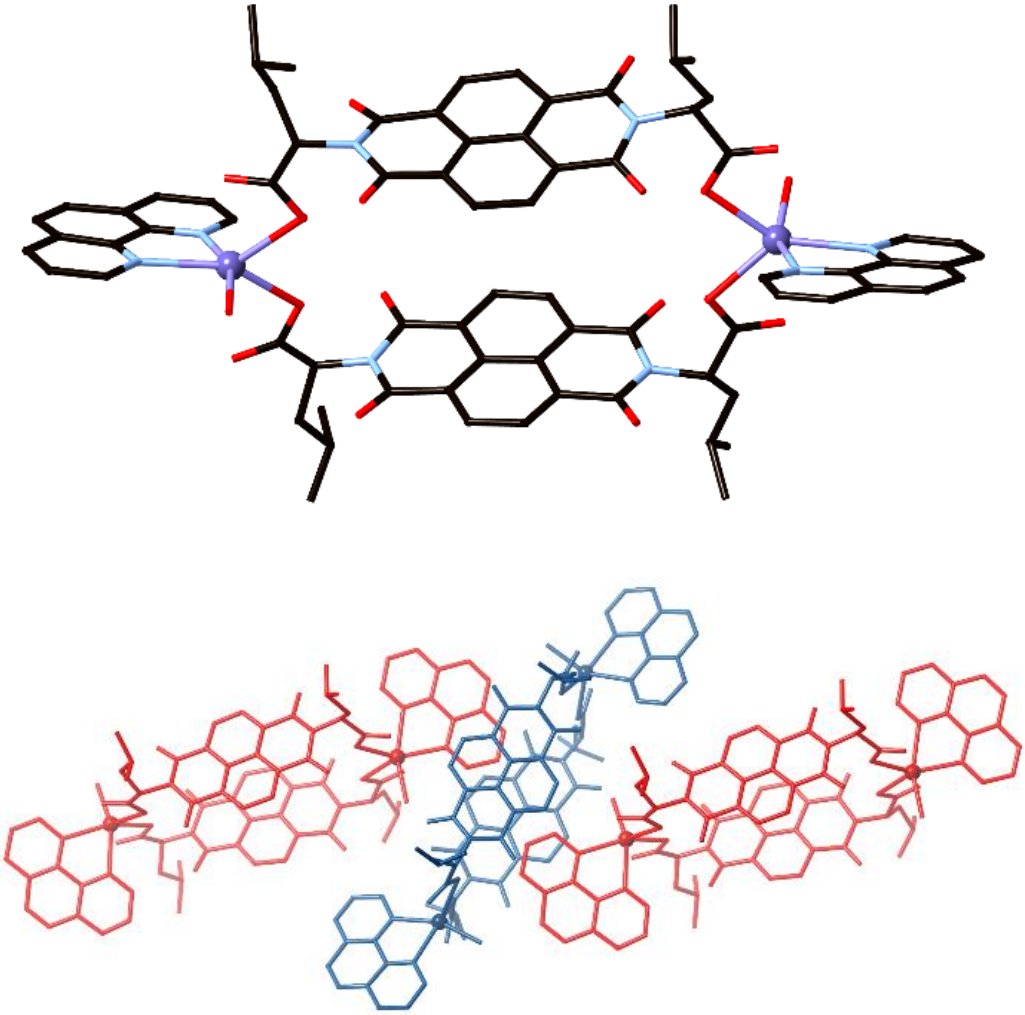

*Figure 4.8. The discrete macrocycle of **4.1** (left) and the packing of the macrocycles in which the 1,10-phen of adjacent macrocycles sit between the NDIs of the macrocycle (right). All hydrogen atoms are omitted for clarity.*

4.3.2 Discrete [2]-catenane with LeuNDI

The formation of a discrete catenane in which the NDIs are locked into face-to-face π-interactions was achieved by the reaction of H_2LeuNDI with $Cd(NO_3)_2 \cdot 4H_2O$ and 2,2′-bipy in a solvent mixture of DMF and water at 85 °C to form a crystalline product. The crystals were of the composition $\{[Cd_2(LeuNDI)_2(2,2'\text{-bipy})_2(OH_2)_2]\}_2 \cdot 2DMF \cdot 5H_2O$, **4.2**$\cdot 2DMF \cdot 5H_2O$, which is a [2]-catenane of two $\{Cd_2(LeuNDI)_2\}$ macrocycles, Figure 4.9. The structure of **4.2** is modelled in the chiral space group $C222_1$ and the asymmetric unit contains two half macrocycles, in the form of four half LeuNDI ligands, two 2,2′-bipy ligands, two Cd^{II} ions and two aqua ligands, as well as void space with residual electron density in which

no solvent could be modelled. The metal centres have the same coordination environment as those in **4.1**; a distorted octahedral geometry with one chelating and one monodentate carboxylate and an aqua ligand, and the remaining two sites occupied by the chelating dipyridyl ligand. The macrocycles are of the same form as those observed in the NDI coordination polymers, with NDIs at interplanar distances of 7.3219(14) and 7.2279(14) Å. The macrocycles of **4.2** form a [2]-catenane in which the NDIs are engaged in face-to-face π-interactions, with closest C···C distances of 3.5141(7), 3.5690(7) and 3.4699(7) Å, Figure 4.9. The 2,2′-bipy ligands also have non-parallel face-to-face π-interactions with the 2,2′-bipy ligands of neighbouring catenanes, with closest C···C distance of 2.9116(6) Å and interplanar angle of 13.802(4)°. In a similar manner as the coordination polymers with LeuNDI, the bulkiness of the isobutyl side chain of the ligand inhibits face-to-face π-interactions between the NDIs of neighbouring complexes, Figure 4.9. The structure also includes void space in which no solvent could be modelled crystallographically, but was assigned as two DMF and five water molecules per asymmetric unit, by TGA, microanalysis and residual electron density.

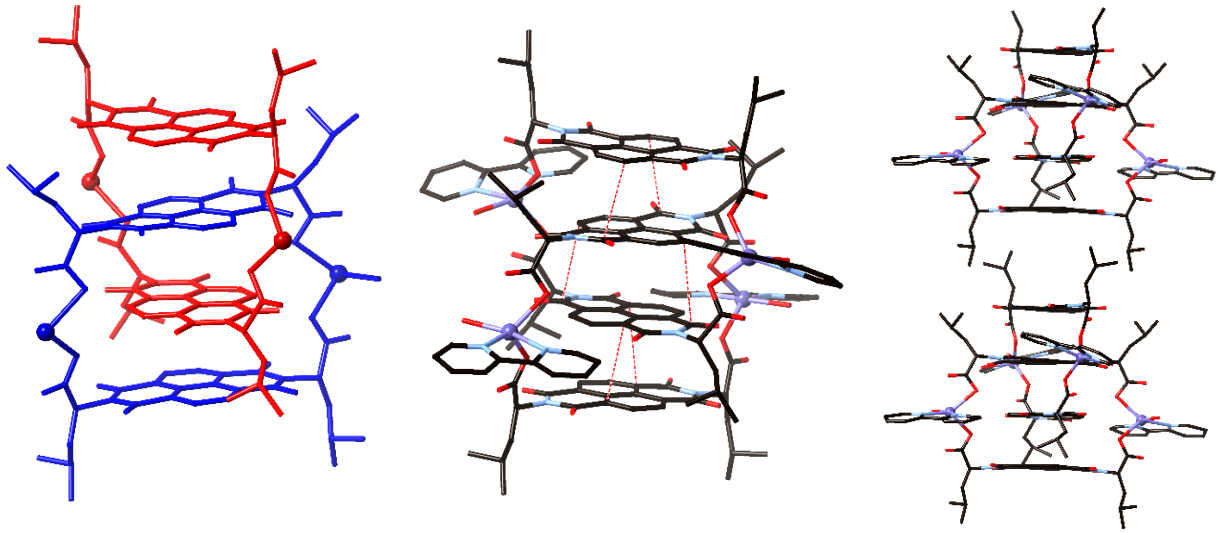

*Figure 4.9. The [2]-catenane of **4.2** with the two different macrocycles shown in red and blue, and the aqua ligands and 2,2′-bipy omitted for clarity (left). The [2]-catenane of **4.2**, showing the π-interactions by the closest C···C distances as red dashed lines (centre). The packing of the catenanes in which the bulkiness of the isobutyl side chains inhibit π-interactions between NDIs of neighbouring catenanes (right). All hydrogen atoms omitted for clarity.*

It is somewhat surprising that the macrocycles of **4.2** form a catenane, as this was never observed for coordination polymers with the LeuNDI ligand. The AlaNDI ligand, with a methyl side chain, did form catenane motifs in coordination polymers, and therefore the lack of catenation of $\{M_2(LeuNDI)_2\}$ macrocycles was attributed to the bulkiness of the isobutyl side chain. It did not seem possible for an NDI of an interpenetrating macrocycle to sit between the bulky isobutyl chains of the macrocycle through which it was interpenetrating. In the previously reported 1D chains of *poly*-$[Cd(LeuNDI)(DMF)_2]$ which are $\{M_2(LeuNDI)_2\}$ macrocycles conjoined by bimetallic nodes, the isobutyl groups are forced to face towards the NDI core, Figure 4.10.[71] If the isobutyl groups were rotated away from the NDI core and instead were situated over the metal node, they would clash with the isobutyl groups of neighbouring macrocycles. In the case of **4.2** however, the macrocycles are not conjoined, and the isobutyl groups are free to face away from the NDI core, therefore being further apart and allowing space for an interpenetrating NDI to sit above the NDI core and fit between the two isobutyl groups, Figure 4.10. At the distance above the NDI macrocycle which an interpenetrating NDI would sit, ~ 3.5 Å, the isobutyl groups in the 1D chains are ~ 8.5 Å apart (as measured between the closest carbon atoms of the isobutyl groups), which is not sufficient space to fit an NDI ligand, which is ~ 6.5 Å wide, when taking into account van der Waals radii of the atoms. In the catenane of **4.2** however, the isobutyl groups are ~ 11.2 Å apart, a much more suitable space through which an NDI ligand may fit. The difference which allows this catenation of the $\{M_2(LeuNDI)_2\}$ macrocycles in **4.2** appears to be the fact that they are discrete complexes, in contrast to polymers, and the isobutyl groups are free to orient themselves away from the NDI core in order to allow for catenation of the macrocycles.

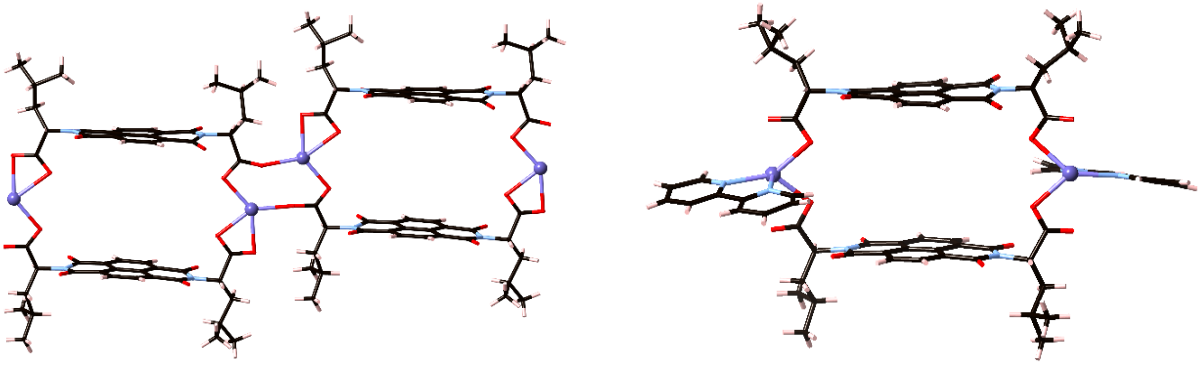

*Figure 4.10. Two conjoined macrocycles in the 1D chain of previously reported poly-[Cd(LeuNDI)(DMF)$_2$], in which the isobutyl groups are too close to allow for catenation of the macrocycles (left). The discrete macrocycle in the structure of **4.2**, in which the isobutyl groups are free to rotate away from the NDI plane and therefore allow catenation of the macrocycles (right). All coordinated solvent molecules are omitted for clarity.*

4.3.3 Fluorescence properties of LeuNDI macrocycle (4.1) and catenane (4.2)

Compounds **4.1** and **4.2** provided suitable samples to probe the influence which face-to-face π-interactions may have on the fluorescence emission properties of the LeuNDI ligand. In the empty macrocycle **4.1** the NDI ligands are locked at 7 Å apart, so that they may not engage by π-interactions with one another, and would therefore not form intramolecular excimers. The macrocycles of **4.1** may only form excimers if they form between two different macrocycles in solution. The catenane of **4.2** involves the NDIs locked together such that they are engaged in face-to-face π-interactions. The comparison of the fluorescence emission of these two systems, as well as their solvent and concentration dependent absorbance and fluorescence emission, will therefore provide information as to the influence of π-interactions on the NDI ligands forming exciplexes with aromatic solvent molecules or with other NDI ligands forming excimers. The fluorescence properties of **4.1** and **4.2** may provide information as to the type of interactions which are responsible for the broad emission of H_2LeuNDI at ~500 – 520 nm which was observed in aromatic solvents.

The macrocycle and catenane, **4.1** and **4.2**, respectively, had very limited solubility, and could only be dissolved in chloroform, despite attempts with many other solvents. Therefore only solutions of the complexes in chloroform were analysed by fluorescence spectroscopy. The chloroform solutions of **4.1** and

4.2 could be doped with up to 50% toluene, in order to investigate the influence of an aromatic solvent on the fluorescence emission of the systems.

The absorbance of **4.1** in chloroform is similar to that of H_2LeuNDI, with peaks at 355 and 376 nm, and a shoulder at 350 nm, Figure 4.11. The emission of **4.1** is also similar to H_2LeuNDI, being a mirror image of the absorbance with peaks at 391 and 410 nm. The fluorescence emission of **4.1** in chloroform does however show broad emission at ~480 nm, which was not observed in the emission of H_2LeuNDI in chloroform.

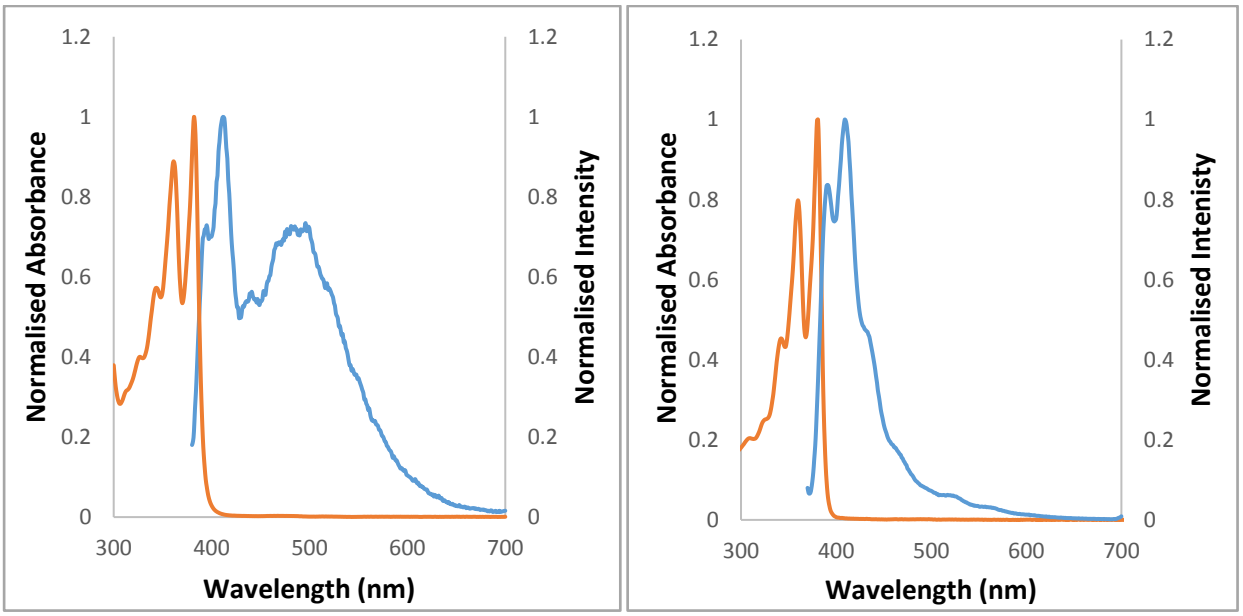

*Figure 4.11. The absorbance (orange) and emission (blue) spectra of **4.1** in chloroform at 25 µmol/L upon excitation at 360 nm (left) and the H_2LeuNDI ligand in chloroform at 30 µmol/L upon excitation at 355 nm (right).*

In order to prove that the macrocycles of **4.1** exist in solution, a chloroform solution of **4.1** was analysed by mass spectrometry. The macrocycle was shown to exist in solution, by the detection of the $[Cd_2(LeuNDI)_2(1,10\text{-phen})_2(H_2O)_2)+H]^+$ ion. However the mass spectrometry also shows fragments of the macrocycle in solution, that of $[Cd(LeuNDI)(1,10\text{-phen})+H]^+$ and $[Cd(LeuNDI)(1,10\text{-phen})(H_2O)+H]^+$. It is possible that the fragments were formed under the conditions required to ionise the complex in the mass spectrometer, or it is also possible that the macrocycle fragmented when dissolved in chloroform. The ^{1}H-NMR of **4.1** could not be analysed, due to the very poor solubility of the complex.

As the proposed exciplexes of aromatic solvents with H_2LeuNDI in solution are characterised by emission at ~500 nm, NDI-NDI excimers may also emit at a similar wavelength, as demonstrated by literature precedent with similar NDI systems.[393, 411, 424] As the solutions of **4.1** in chloroform do not contain any aromatic solvents, the broad emission at ~480 nm may be attributed to intermolecular NDI-NDI excimers in solution. The NDI-NDI excimers in a solution of **4.1** could be due to two macrocycles interacting via the external NDI surfaces of the macrocycles. It is also possible that fragments of the macrocycle, as observed by mass spectrometry, are interacting with the macrocycle in solution, leading to the observation of broad emission at ~500 nm, attributed to NDI-NDI excimers.

The concentration dependence of the fluorescence emission of **4.1** was also investigated. If the broad emission at ~450 – 550 nm is due to NDI-NDI excimers, increased concentrations would lead to an increase in this emission at those wavelengths. Increase in concentration of **4.1** in chloroform shows similar emission intensity of the typical NDI emission peaks at 390 and 410 nm, and an increase in emission at ~480 nm, Figure 4.12. The increased concentration of **4.1** leading to increased emission at ~480 nm suggests that this emission is due to NDI-NDI excimers, as increasing the concentration of **4.1** leads to aggregation of the macrocycles in solution to form intermolecular excimers.

The nature of excimers is that two excited state molecules interact to form an excited state dimer, which has different emission to the molecules on their own. Increased concentration increases the likelihood of an excited state NDI interacting with another NDI to form an excimer. As these NDIs have such short lifetimes, and the macrocycles of **4.1** are larger than the free ligand, and therefore will diffuse slower than the ligand, the fluorescence of NDI-NDI excimers between NDIs of **4.1** macrocycles will be very weak.

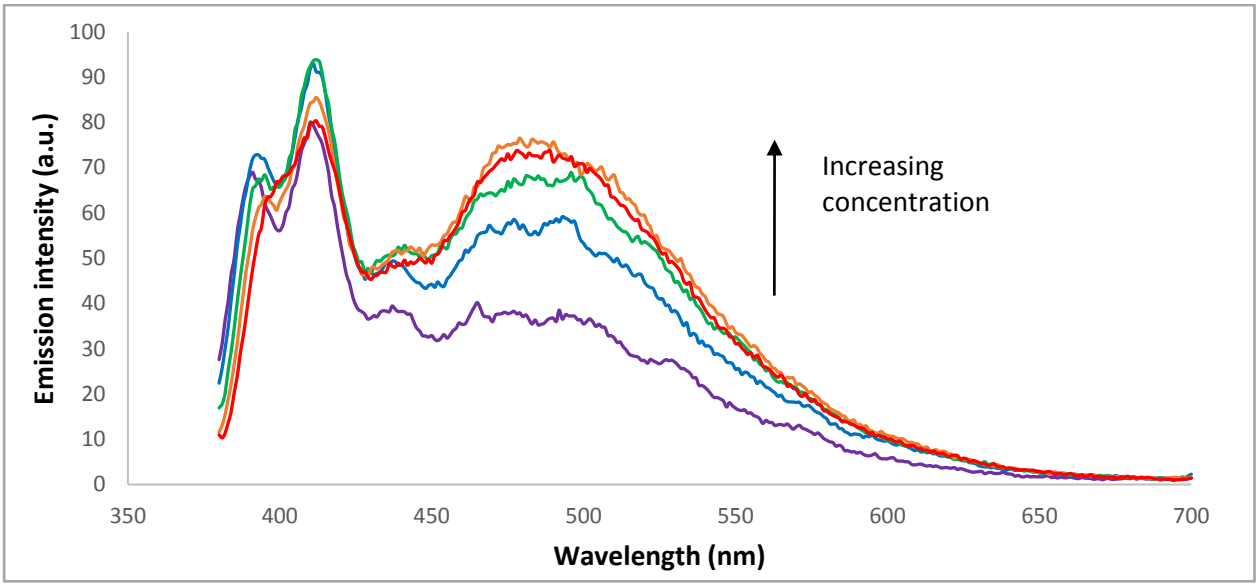

*Figure 4.12. The emission of **4.1** in chloroform with concentrations of 10 (purple), 20 (blue), 30 (green), 40 (orange) and 50 (red) µmol/L.*

The fluorescence of H_2LeuNDI in chloroform does not show emission at ~480 nm, even at high concentrations. Therefore it appears that to form NDI-NDI excimers, at least one of the NDIs must be locked into a "U-shape", as they are in the macrocycle structure of **4.1**. It is possible that the free rotation around the alpha-carbon of the leucine groups of H_2LeuNDI means that the free ligands in solution cannot form excimers with each other, as the ligand may adopt various conformations. By being locked into the "U" confirmation, the ligands in **4.1** are able to form excimers in solution. Although it is also possible that some [Cd(LeuNDI)(phen)] fragments of **4.1**, as observed by mass spectrometry, are interacting with the macrocycles of **4.1** in solution and forming excimers.

As the emission of **4.1** in chloroform was similar to H_2LeuNDI in chloroform, a similar titration was attempted, in which the fluorescence emission of **4.1** was measured in chloroform solutions with increasing proportions of toluene, Figure 4.13. Due to the poor solubility of **4.1**, the emission of **4.1** in a 100% solution of toluene was unable to be measured. The fluorescence emission titration of **4.1** showed a similar pattern to that of H_2LeuNDI (*vide supra*). The increase in toluene proportion between 0 – 1% was investigated in 0.2% increments. The small increases in toluene proportions leads to little change in emission at 390 and 410 nm, but a small increase in the broad emission at ~480 nm. Further increase in the toluene proportion

leads to a decrease in the typical NDI emission at 390 and 410 nm, and shift in the maxima of the broad emission to ~500 nm for 10%, ~505 nm for 20% and ~510 nm for 50%. Although direct comparison is not possible between the H_2LeuNDI titration and this titration with **4.1**, due to different concentrations, the shift in emission maxima seems to suggest that the emission moves from NDI-NDI excimers to being dominated by NDI-toluene exciplexes, as the NDI-toluene exciplexes with H_2LeuNDI had emission maxima around 510 nm.

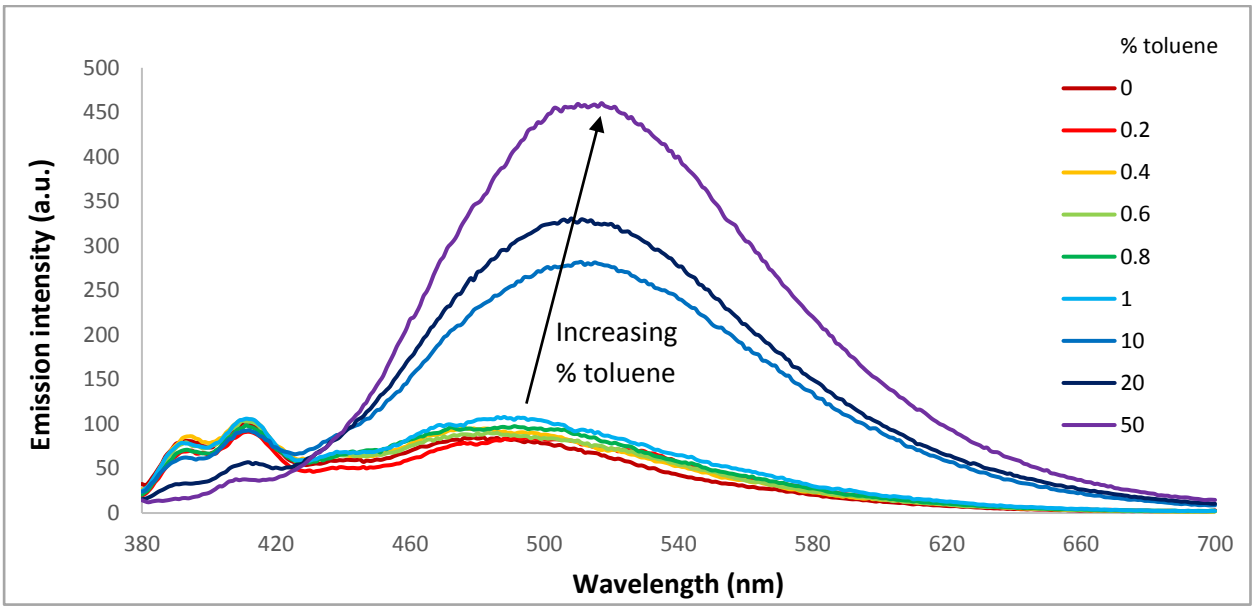

*Figure 4.13. The fluorescence emission titration of **4.1** in chloroform at 25 µmol/L upon excitation at 360 nm, with increasing proportions of toluene.*

The fluorescence emission of **4.2**, the $[Cd_2(LeuNDI)_2(2,2'\text{-bipy})_2(OH_2)]_2$ catenane, was also studied. As with **4.1**, **4.2** was analysed only in chloroform, due to the limited solubility. The absorbance spectrum shows peaks at 362 and 381 nm, characteristic of the π-π* transitions of the NDI core, Figure 4.14. The emission of **4.2** in chloroform upon excitation at 360 nm is similar to that of H_2LeuNDI in toluene and xylenes, with a small peak at 410 nm, and a broad peak with maxima at ~480 nm, Figure 4.14. However if the same solution is excited at 400 nm, the emission shows a broad peak at 480 nm, which is much more intense than the emission at 480 nm observed upon excitation at 360 nm. Based on the observed fluorescence emission of **4.1**, the emission at 480 nm may be attributed to NDI-NDI excimers. The difference in emission

dependent on excitation wavelength suggests that exciting the sample at 400 nm excites the excimers to a greater extent than if light of 360 nm is used.

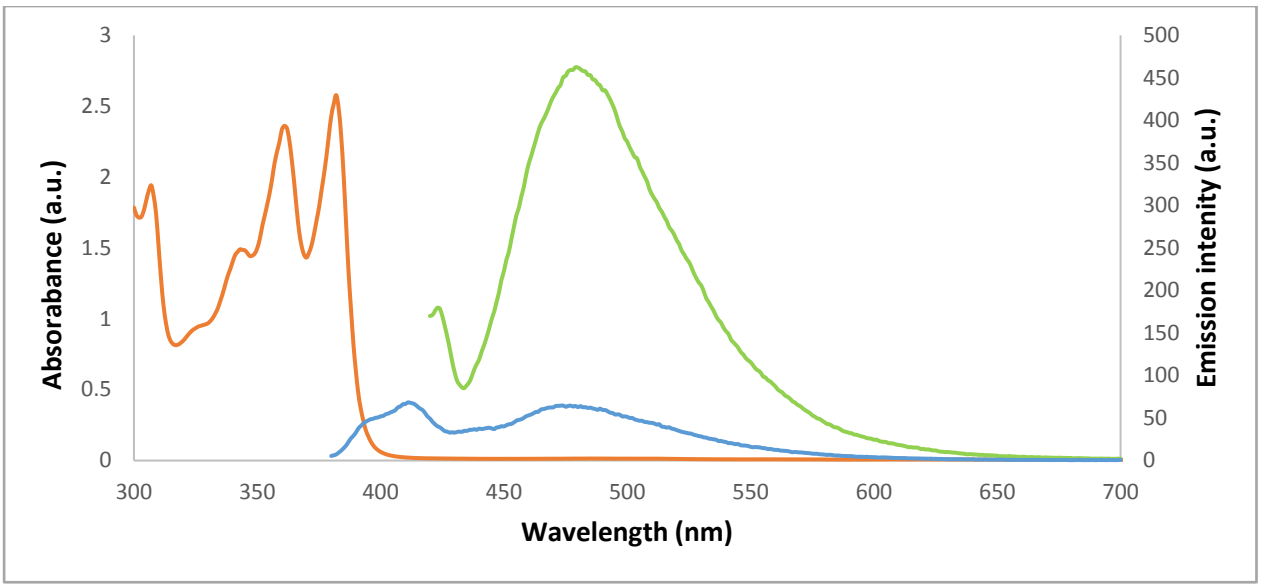

*Figure 4.14. The absorbance (orange) and emission, upon excitation at 360 nm (blue) and 400 nm (green) of **4.2** in chloroform at 70 µmol/L.*

In the same manner as **4.1**, mass spectrometry was used in order to determine if the catenane of **4.2** existed in solution. The mass spectrometry of a chloroform solution of **4.2** showed a $[Cd_4(LeuNDI)_4(2,2'\text{-bipy})_4(OH_2)(CHCl_3)(CH_3COOH)+2H]^{2+}$ fragment, confirming that the catenane of **4.2** does exist in solution. However a fragment was also detected with the formula $[Cd_2(LeuNDI)_2(2,2'\text{-bipy})_2(OH_2)(CHCl_3)(CH_3COOH)+H]^{+}$, suggesting that a macrocycle may also be formed by this system. It is possible that this fragment formed during the mass spectrometry, or that the system is somewhat labile in solution, and the catenane has broken apart and formed macrocycles. A small amount of acetic acid was used to protonate the compounds in the mass spec, and was found to have associated with the compound when charged. The ^{1}H-NMR of **4.2** could not be analysed, due to the very poor solubility of the complex.

In a similar manner to **4.1**, the fluorescence emission of **4.2** was also measured at a range of concentrations in chloroform, in order to investigate if an increase in concentration will change the emission of the compound in solution. The fluorescence emission of **4.2** in chloroform with excitation at 360 nm shows an interesting behaviour upon increasing concentration, Figure 4.15. At low concentrations (5 and 10 µmol/L)

the emission is dominated by structured bands at 390 and 410 nm. Increase in concentration, from 40 – 100 µmol/L, showed a decrease in the structured bands at 390 and 410 nm and an increase in broad emission at 480 nm. The emission of **4.2** at increasing concentration in chloroform upon excitation at 360 nm suggests that at low concentration the emission is dominated by NDI emission, and the increase in concentration leads to the emission being dominated by NDI-NDI excimer emission.

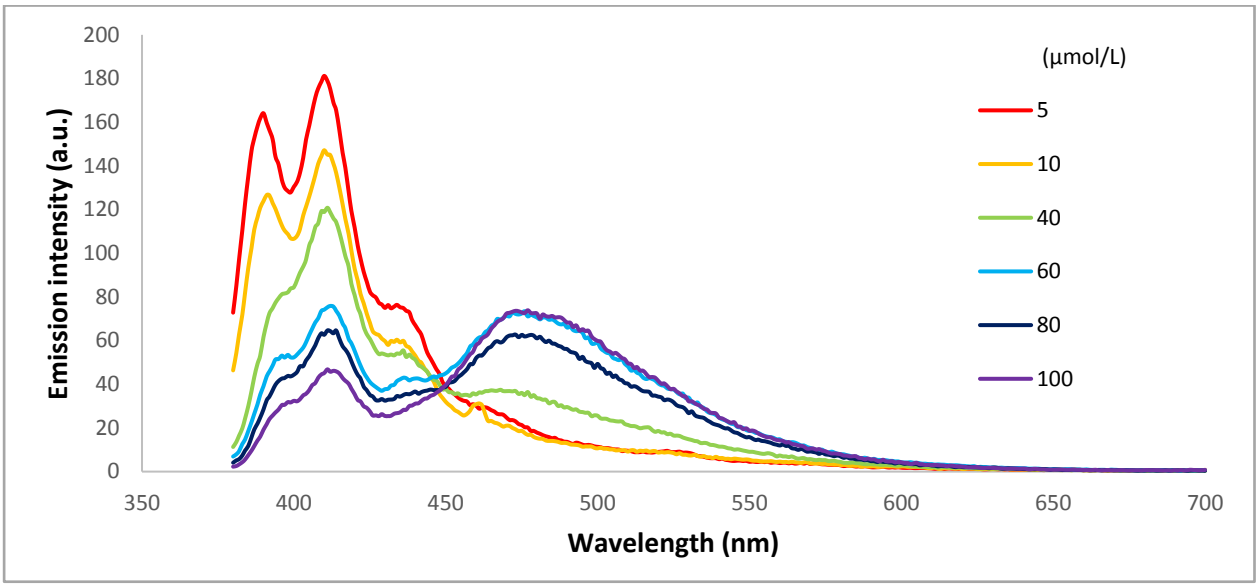

*Figure 4.15. Fluorescence emission of **4.2** at increasing concentration in chloroform upon excitation at 360 nm.*

The fluorescence emission of **4.2** upon excitation at 400 nm with increasing concentration in chloroform showed a similar pattern to that with excitation at 360 nm, Figure 4.16. As the emission spectra upon excitation at 400 nm can only be measured from 420 nm, it is impossible to determine how this excitation wavelength influences the emission at 410 nm. The concentration dependence of the emission at 480 nm, attributed to NDI-NDI excimers, suggests that the excimers are forming both within the catenanes, and between separate catenanes via the external NDI faces of the catenanes. As the mass spectrometry also shows [Cd_2(LeuNDI)$_2$(2,2′-bipy)$_2$(solv.)] fragments in solution, it is also possible that these fragments interact with each other or with the catenane of **4.2** in solution, leading to the observation of emission at 480 nm, attributed to NDI-NDI excimers.

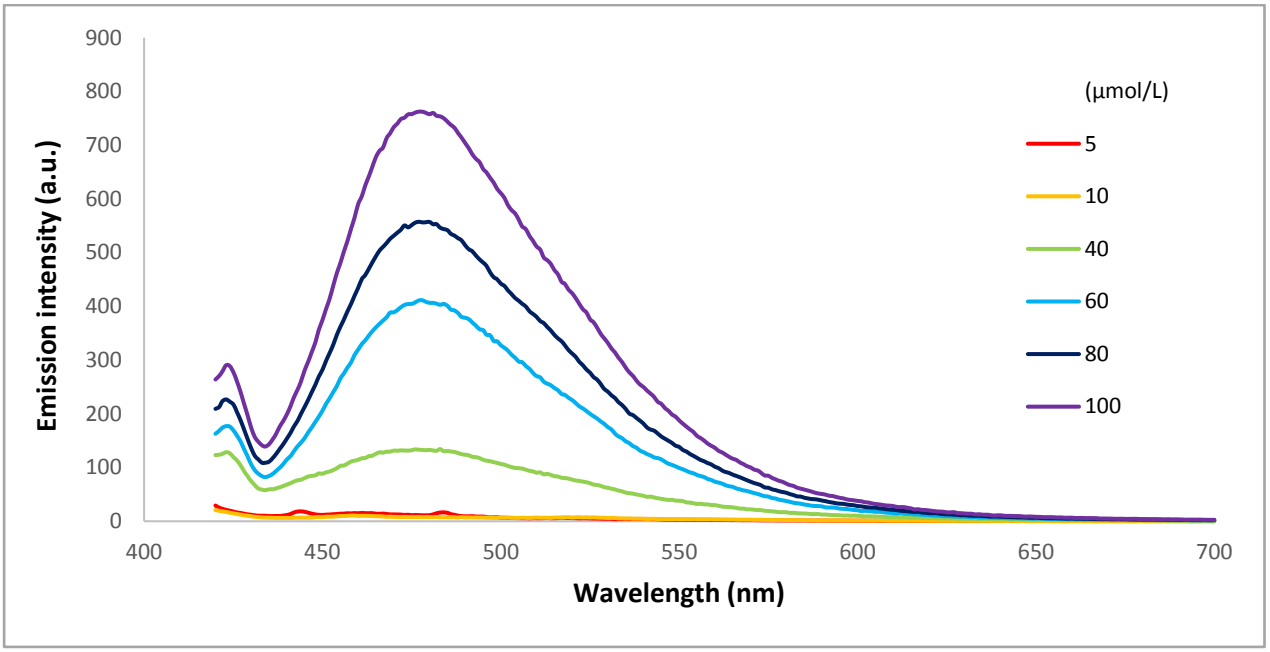

*Figure 4.16. Fluorescence emission of **4.2** at increasing concentration in chloroform upon excitation at 400 nm.*

The emergence of the broad emission at 480 nm upon increased concentration may be attributed to the formation of NDI-NDI excimers between the external faces of the NDI catenane of **4.2**. As the H_2LeuNDI does not show the same emergence of broad emission at increased concentration, this suggests that the LeuNDI ligand must be locked in a "U-shape" in order to form an excimer. It is surprising that **4.2** does not show excimer-like emission at low concentrations in chloroform, as it suggests that the NDIs within **4.2** are not forming intramolecular excimers, but rather will only form intermolecular excimers when the complexes aggregate at increased concentration.

The absorbance and fluorescence emission of **4.2** was also investigated in solvent mixtures of chloroform and toluene. A series of chloroform solutions of **4.2** with a constant concentration and varying proportion of toluene were prepared, with toluene proportions of 0, 1, 10, 20 and 50%. As **4.2** was not soluble in pure toluene, the emission and absorbance of the 100% toluene solution could not be measured.

The absorbance of the chloroform solutions of **4.2** with increasing proportions of toluene showed an interesting trend, Figure 4.17. The absorbance of the 100% chloroform solution showed the typical NDI absorbance peaks of 360 and 380 nm, and a shoulder at 340 nm, and the absorbance only occurs at

wavelengths below 400 nm. The incorporation of 1% toluene also shows typical structured NDI absorbance, but also shows a slight broadening of the absorbance around 400 nm, indicative of ground state interactions, such as the formation of aggregates of NDIs with toluene. The increase to 10% toluene shows a decrease in the sharpness of the structured NDI peaks at 360 and 380 nm, and broadening of the absorbance at 400 nm. Further increase to 20 and 50% toluene shows a broadening of the absorbance at 360 and 380 nm to be much less structured, and increased absorbance at 400 nm. Overall the effect of increasing the proportion of toluene in chloroform solutions of **4.2** leads to the broadening of the absorbance spectrum to include absorbance at 400 nm and decrease the absorbance of the typical NDI peaks of 360 and 380 nm.

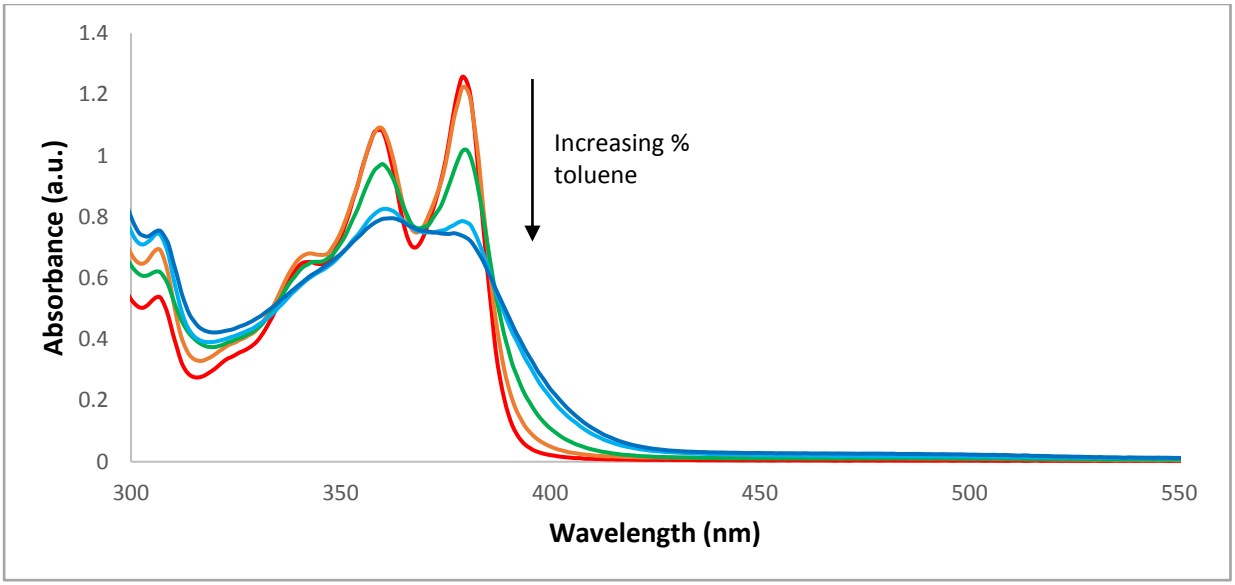

*Figure 4.17. The absorbance of **4.2** in chloroform with varying proportions of toluene at 0% (red), 1% (orange), 10% (green), 20% (light blue) and 50% (dark blue).*

As the emission of **4.2** was shown to be dependent on the wavelength of excitation, the emission of the chloroform solutions with increasing proportions of toluene was measured with excitation wavelengths of 360 and 400 nm. The emission of **4.2** in 100% chloroform upon excitation at 360 nm shows the typical NDI emission peaks at 390 and 410 nm, and a broad emission at ~480 nm. The incorporation of 1% of toluene into the chloroform solution of **4.2** showed similar emission peaks at 390 and 410 nm as that of **4.2** in pure chloroform, with excitation at 360 nm. The 1% toluene solution of **4.2** with excitation at 360 nm also shows a small increase in broad emission at ~480 nm. The emission of **4.2** with increasing proportions of toluene

upon excitation at 360 nm shows a red shift in the emission maxima from 480 nm at 1% toluene, to 505 nm at 10%, 510 nm at 20% and 515 nm at 50% toluene, and also shows a dramatic increase in the emission intensity upon increase in proportion of toluene in the solution.

Overall, the fluorescence emission behaviour of **4.2** upon excitation at 360 nm with increasing proportions of toluene shows similar behaviour to the fluorescence emission titration of a chloroform solution of **4.1** with toluene, showing an increase in intensity and red-shift of the broad emission peaks from ~480 to ~510 nm, Figure 4.18. The similarity between the emission of **4.1** and **4.2** in chloroform solutions with increasing proportions of toluene, in comparison to the emission of H_2LeuNDI in chloroform and toluene, suggests that both **4.1** and **4.2** in chloroform/toluene solutions involve NDI-NDI excimers with emission maxima at ~480 nm and NDI-toluene exciplexes with emission maxima at ~520 nm.

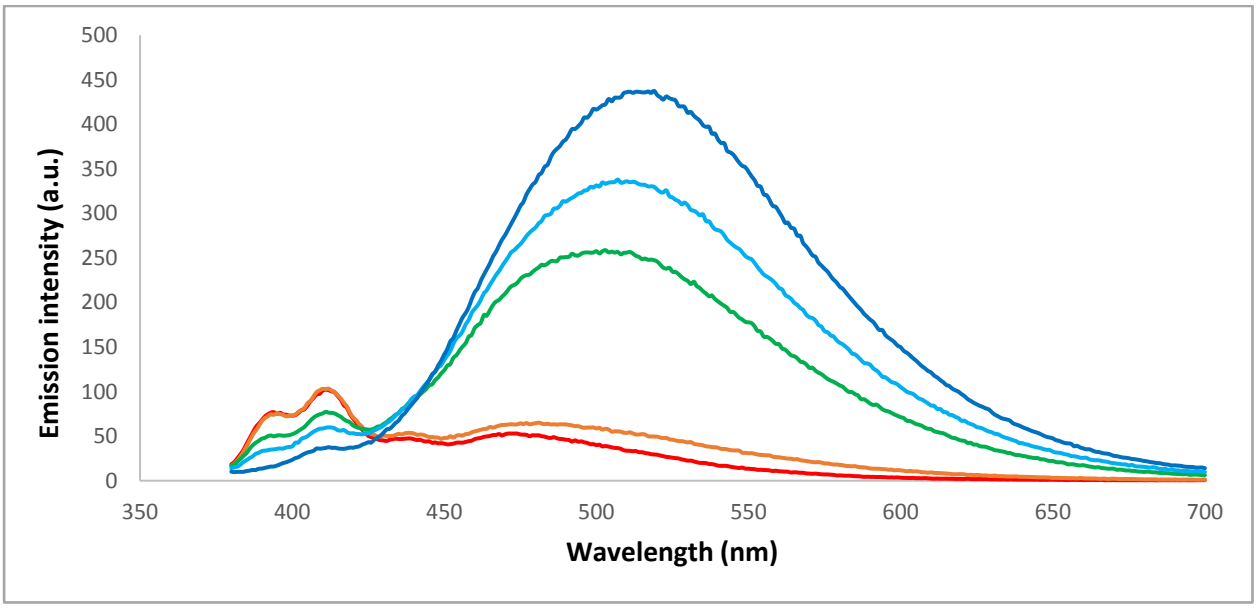

*Figure 4.18. The fluorescence emission titration of **4.2** in chloroform at 25 µmol/L upon excitation at 360 nm, with increasing proportions of toluene; 0% (red), 1% (orange), 10% (green), 20% (light blue) and 50% (dark blue).*

The fluorescence emission of **4.2** in chloroform with increasing proportions of toluene was also investigated with an excitation wavelength of 400 nm, Figure 4.19. The emission of **4.2** in 100% chloroform shows broad emission at 480 nm, attributed to NDI-NDI excimers in solution. The incorporation of 1% toluene appears to show a slight decrease in emission at ~480 nm, and a broadening of the peak. The increase in

proportion of toluene to 10, 20 and 50% in chloroform solutions of **4.2** shows an increase in the emission intensity. The emission of the solutions of **4.2** in chloroform upon excitation of 400 nm shows a slight blue shift with the increase in proportion of toluene, with maxima at 477 nm for 0% and 1%, 483 nm for 10%, 487 nm for 20% and 492 nm for 50% toluene.

Excitation at 400 nm excites predominantly the NDI-NDI excimers, which form more readily with increased proportions of toluene because of the decrease in solubility, helping them to aggregate together to form excimers. There is a slight shift in the emission maxima upon excitation at 400 nm upon incorporation of toluene, from exciplexes which form between toluene and the NDIs in the catenane under these conditions.

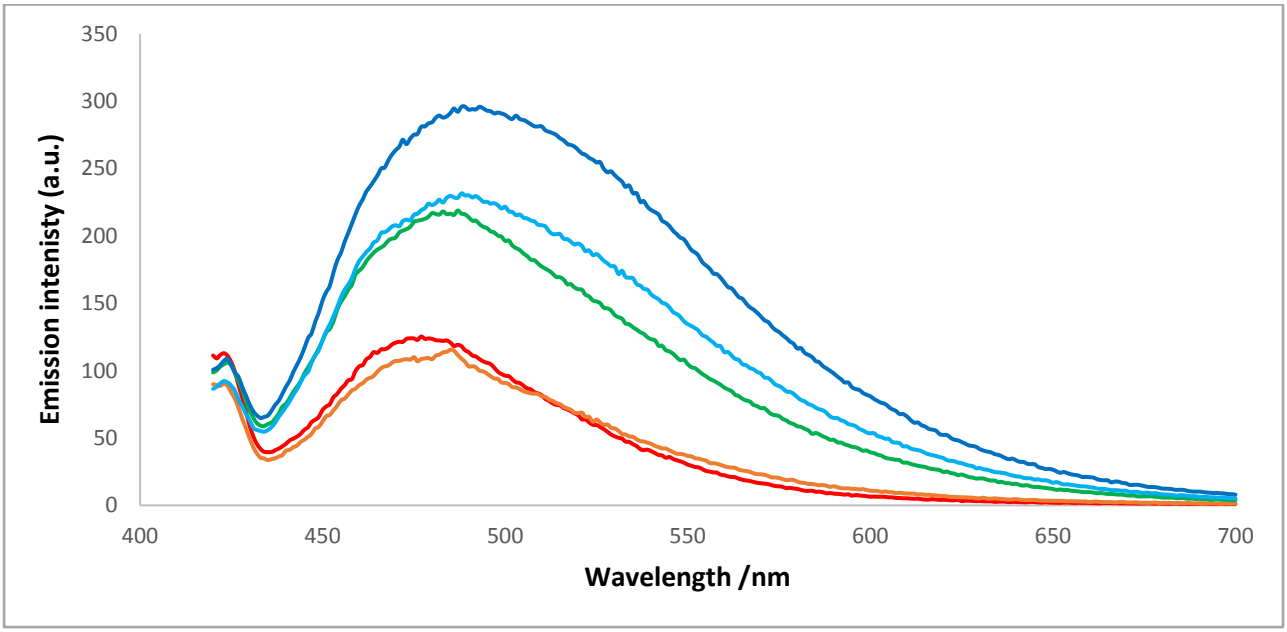

*Figure 4.19. The fluorescence emission titration of **4.2** in chloroform at 25 µmol/L upon excitation at 400 nm, with increasing proportions of toluene; 0% (red), 1% (orange), 10% (green), 20% (light blue) and 50% (dark blue).*

The dramatic increase in intensity of the broad emission of **4.2** with increasing toluene proportions upon excitation at 360 nm, coupled with the red-shift of the broad emission, suggests that this emission is predominantly from NDI-toluene exciplexes. Increase in the emission upon excitation at 400 nm when toluene is increased is in agreement with the broadening of the absorbance to include absorbance at 400 nm upon increase in toluene proportion. The solutions with higher proportion of toluene showed increased

emission at ~480 nm when excited at 400 nm. The emission maxima of the catenane solutions with increasing toluene at excitation of 400 nm shifts from 480 nm at 0% toluene, to 490 nm at 50% toluene, a much smaller shift than that observed for the same solutions when excited at 360 nm, showing that excitation at 400 nm predominantly excites the NDI-NDI excimers.

4.4 Conclusion

The (*S*)-Leucine-substituted naphthalene diimide molecule has been shown to have intriguing, albeit weak, fluorescence properties, in which the π-rich nature of the NDI core forms exciplexes with aromatic solvent molecules. The fluorescence emission of H_2LeuNDI in the non-aromatic solvents acetonitrile and chloroform showed two peaks at 391 and 410 nm. The fluorescence emission of H_2LeuNDI in the aromatic solvents toluene and *o*-, *m*- and *p*-xylene showed a broad emission peak at ~500 nm, which suggested that the NDI core and the aromatic solvent formed exciplexes, leading to the change in emission. The degree of solvent dependence on the emission of H_2LeuNDI was investigated by a fluorescence titration of chloroform and aromatic solvents, which showed the decrease in the emission at 391 and 410 nm and the increase in the emission ~ 500 nm upon the increase of aromatic in the solution. ^{1}H-NMR titrations of H_2LeuNDI in chloroform with increasing proportions of aromatic solvent showed an upfield shift in the ^{1}H-NMR signal of the NDI core, upon increase in proportion of aromatic solvent. The results from the fluorescence and ^{1}H-NMR titrations suggest that exciplexes of NDIs and aromatic solvent molecules were causing the emission at ~500 nm.

In order to investigate the fluorescence properties of LeuNDI in known configurations, discrete coordination complexes with LeuNDI and Cd^{II} were synthesised. Convergent dipyridyl ligands were used to cap the metal centres and inhibit the formation of coordination polymers. A discrete macrocycle, **4.1**, was synthesised which involved an empty space between the NDIs, in which the Cd^{II} metal centres were capped with 1,10-phen. A discrete catenane, **4.2**, was also synthesised in which the Cd^{II} metal centres are capped with 2,2′-bipy, in which two macrocycles are interlocking and engaged in face-to-face π-interactions.

The fluorescence of **4.1** in chloroform showed similar emission to that of H_2LeuNDI in non-aromatic solvents, with an additional broad emission peak at ~480 nm, which increased in intensity with increasing concentration, showing that there could be a small amount of excimer formed between NDIs in solution. The titration of **4.1** in chloroform with increasing proportions of toluene showed similar behaviour to that of the same titration of H_2LeuNDI, with a decrease in the NDI emission at 391 and 410 nm, and an increase in the emission at ~ 500 nm, upon increase in the proportion of toluene. The similar behaviour of **4.1** and H_2LeuNDI showed that the LeuNDI in a coordination complex has similar fluorescence properties to the free ligand in solution, and both appear to be forming exciplexes with aromatic solvent molecules.

The fluorescence emission of **4.2** in chloroform was shown to be dependent on concentration and excitation wavelength. Excitation at 360 nm showed the typical NDI emission peaks at 390 and 410 nm. Increase in concentration of **4.2** showed the emergence of a broad emission peak at ~480 nm. The emission at ~480 nm was therefore attributed to NDI-NDI excimers. The titration of **4.2** in chloroform with increasing proportions of toluene showed similar emission to that of H_2LeuNDI in aromatic solvents, however the emission maxima shifted from ~480 nm to ~520 nm. The emission at ~480 nm could be attributed to NDI-NDI excimers, and the shift of the emission maxima to ~520 nm upon increase in proportion of toluene suggests the formation of NDI-toluene exciplexes.

Although there is some precedent for the observation of excimers or exciplexes with N-substituted NDIs in solution, there are only a handful of examples. Therefore the investigation into the solvent dependent fluorescence emission of H_2LeuNDI and the fluorescence of the LeuNDI coordination compounds of an empty macrocycle and a catenane represent a significant contribution to the understanding of this relatively unknown area.

Chapter 5: Helicate and mesocate cage complexes

5.1 Introduction

The linear amino acid substituted NDI and BDI ligands formed a series of coordination polymers and discrete coordination compounds that were dominated by an M_2L_2 metallomacrocyclic motif. Diimide ligands with a significant bend in the core were also utilised, to investigate how this change in ligand geometry would influence the coordination compounds which were formed.

5.1.1 Helicates in metallosupramolecular chemistry

A helicate is a discrete or one-dimensional complex which involves the wrapping of a strand around a central axis. Helices are essential in nature, as DNA is a double-helix, and are also relatively common in metallosupramolecular chemistry.[303] The formation of a helicate requires some flexibility in the building blocks, as they must twist around in order to form a helical structure. In metallosupramolecular chemistry, helicates usually consist of metal nodes and bridging ligands that are twisted in order to generate a helical sense. Discrete metallosupramolecular helicates may also be formed in which two or more metal nodes are bridged by ligands that are twisted to form a helicate. Helicates are described by the number of ligands which are joining the metals together, and most often form as single, double, triple or quadruple stranded, in which one, two, three or four ligands bridge the metals nodes, respectively.[426] The term helicate was first introduced by Lehn in 1987 with the report of dinuclear helicates with Cu^{I} and ligands with either two or three 2,2′-bipyridine units.[427] Since then there has been a substantial amount of research into the synthesis and control of helicates.[210, 303, 304, 428-434]

5.1.2 Helicate cage complexes

Helicates are inherently chiral entities, as when they are viewed down the helical axis they will rotate in a clockwise or anticlockwise fashion, giving them Δ and Λ configuration, respectively, due to chirality in the

metal coordination environment.[435] The chirality of the metal centres must both be of the same handedness, either ΛΛ or ΔΔ in a dinuclear helicate, in order to be considered as a helicate. A dinuclear complex with two metal centres of opposite handedness, ΛΔ, is not chiral, and is termed a mesocate, because although it may have a twist in the ligand, the twist does not carry through to the helicity of the complex.[308, 436] The use of achiral ligands will generally form either mesocates, or will form helicates in a racemic mixture, although spontaneous resolution is possible.[305, 437-439] The use of enantiopure chiral ligands will selectively form helicates of one handedness.[377, 440, 441]

As discussed in Chapter 1, functional chiral coordination cages are a synthetic target for metallosupramolecular chemists due to their potential applications in chiral catalysis and separations. Helicates may form as cages if the ligands twist in such a way as to form a void space between the metals centres. Helicate cage complexes therefore represent an approach by which a range of chiral coordination cages may be synthesised. Helicate cages that are designed with the view to be utilised for applications such as chiral catalysis and separation are most often triple or quadruple stranded, in order to generate an isolated cavity within the cage.[433, 442] In general, single or double stranded helicate cages would not be useful for applications because they do not form an enclosed internal cavity.[426, 440, 443] The first dinuclear quadruple stranded helicate was reported in 1998 and was designed with square planar Pd^{II} metal centres and flexible pyridyl ligands, in order to form a discrete helical cage complex, Figure 5.1.[432] Since then there have been multiple quadruple stranded helicate cages reported utilising Pd^{II} metal centres and pyridyl ligands.[444-446] Dinuclear quadruple stranded helicate cages are most often synthesised with "banana-shaped" ligands, to allow the ligand to twist between two metal centres and generate helicity within the complex.[447] Variation in the position of coordinating groups and flexibility of the ligands has been shown to form quadruple stranded helicate cages, as well as tetrahedral and octahedral cages.[448] Quadruple stranded helicates are also possible in which two helical hemispheres are joined together by metals to form a helical cage complex.[449]

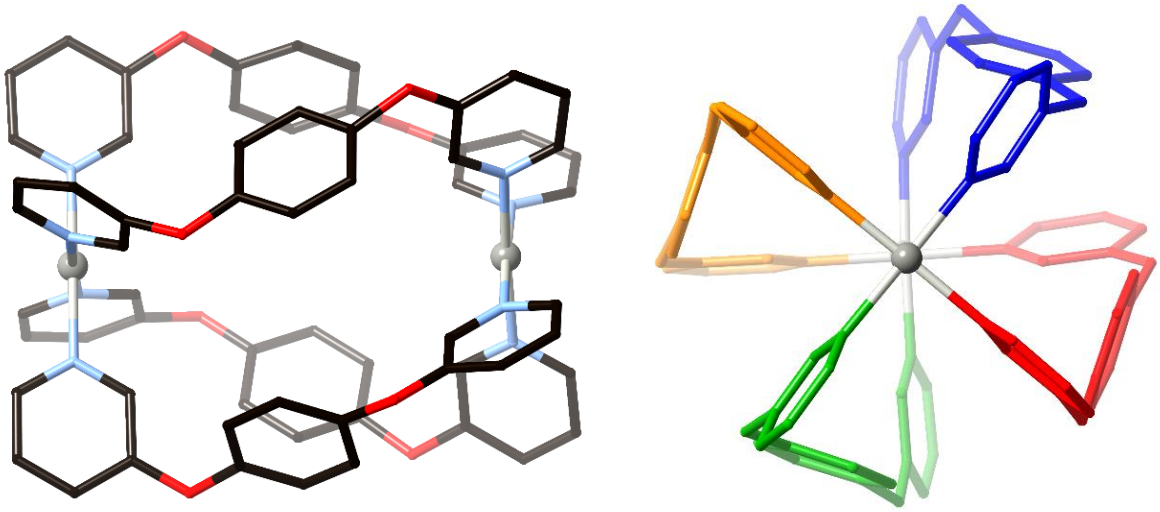

Figure 5.1. The first reported dinuclear quadruple stranded helicate cage complex,[432] side view (left) and view down metal axis with ligands in different colours, showing the twist in the ligands (right). All hydrogen atoms are omitted for clarity.

The use of achiral ligands in M_2L_4 cage complexes may lead to the formation of mesocates or helicates, and if helicates are formed they will most often be a racemic mixture of the Δ and Λ cages.[269, 450-452] The use of chiral ligands for the synthesis of M_2L_4 cages is very likely to form helical complexes.[292, 449] Therefore the most reliable method for the synthesis of homochiral helicate cages for applications is the use of enantiopure ligands. As previously discussed in relation to the synthesis of homochiral coordination polymers and MOFs, functionalising ligands with amino acids provides a simple route to the synthesis of enantiopure ligands with carboxylate coordinating groups.

5.1.3 Chiral paddlewheel motifs

Helicate cage complexes may be made using paddlewheel SBUs and carboxylate ligands.[442] These cages present some advantages over the cationic cages made with Pd^{II} and pyridyl ligands, because they are neutral and therefore may be used for encapsulation of a larger variety of guest molecules. The paddlewheel SBU has been shown to be a versatile building unit in the synthesis of MOFs and coordination cages.[273, 329] The copper paddlewheel complexes reported in Chapter 3 with AlaBDI and LeuBDI showed that the chirality of the ligand forces the paddlewheel into a chiral propeller motif. The copper paddlewheel has been extensively utilised in the synthesis of MOFs, and paddlewheels may also formed with Rh^{II}, which

has remarkable catalytic properties.[453, 454] The incorporation of rhodium paddlewheels into chiral coordination complexes therefore presents the opportunity for the synthesis of chiral catalytic coordination compounds. Several chiral "bowl-shaped" coordination complexes have been synthesised with chiral imide ligands and rhodium paddlewheels, some of which involving amino acid substituted imide ligands, Figure 5.2. These chiral rhodium paddlewheel bowl complexes have been shown to have asymmetric catalytic properties for cyclopropanation reactions.[455-459] In a similar manner to the copper paddlewheels reported with amino acid BDI ligands in Chapter 3, the chirality of the rhodium paddlewheels is induced by chirality of the imide ligands forcing the ligands into a propeller motif.

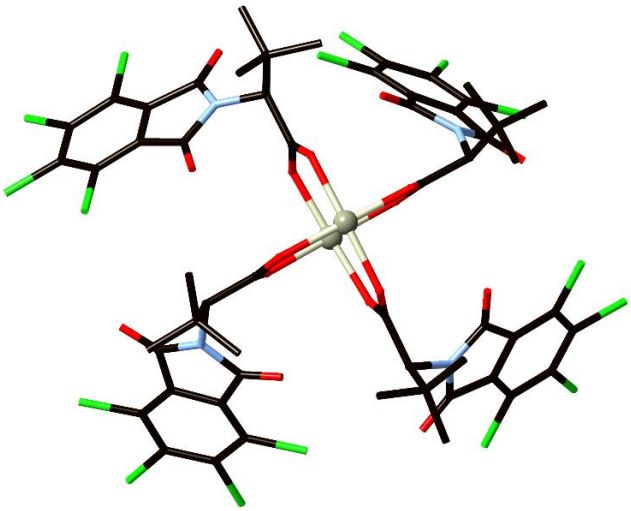

Figure 5.2. An example of a "bowl-shaped" chiral rhodium paddlewheel complex made with phthalimide ligand functionalised with an amino acid, showing the propeller motif around the paddlewheel.

5.1.4 Transition-metal-catalysed cyclopropanation reactions

The first transition-metal-catalysed enantioselective reaction reported was a cyclopropanation reaction between an alkene and diazoester.[460] This reaction has remained prevalent in the field of asymmetric catalysis because of its use in both natural-product-based and synthetic drugs.[461] The transition-metal-catalysed decomposition of diazo precursors for cyclopropanation reactions has been established to have a metallocarbene intermediate. Metallosupramolecular complexes that incorporate rhodium paddlewheels have been investigated for their selectivity in cyclopropanation reactions.[462-465] It has been determined that

in the case of chiral rhodium paddlewheels made from amino acid derived ligands, enantioselectivity arises from control of the carbene-transfer step of the metal to the alkene, which is possible due to the exposed axial sites of the rhodium paddlewheel.[461]

Copper(I) complexes have also been shown to be effective chiral catalysts for cyclopropanation reactions.[466, 467] It was shown that a copper paddlewheel will be decomposed by the reactants of the cyclopropanation reaction,[389] therefore rhodium paddlewheels are preferable due to their increased stability. Dirhodium catalysts are very versatile for cyclopropanation reactions because the reaction may be carried out under very mild conditions, and the reaction may be tuned by the suitable selection of ligands.[468] The products of a cyclopropanation reaction of an alkene with a diazoacetate will have two stereocentres. Therefore the diastereoselectivity, as well as the enantioselectivity of each stereocenter, may be investigated for the reaction. The chiral rhodium paddlewheel complexes which have shown good enantioselectivity are limited to three general forms, Figure 5.3.[455, 469-472] The enantioselectivity of the reactions has been shown to be highly sensitive to the structure of the diazoester, with larger substituents leading to higher enantioselectivity and diastereoselectivity. Rhodium paddlewheel catalysed cyclopropantion reactions have been reported with 99% enantiomeric excess (ee) and >95:5 diastereomeric ratio (dr) using complexes with amino acid substituted phthalimide ligands.[470]

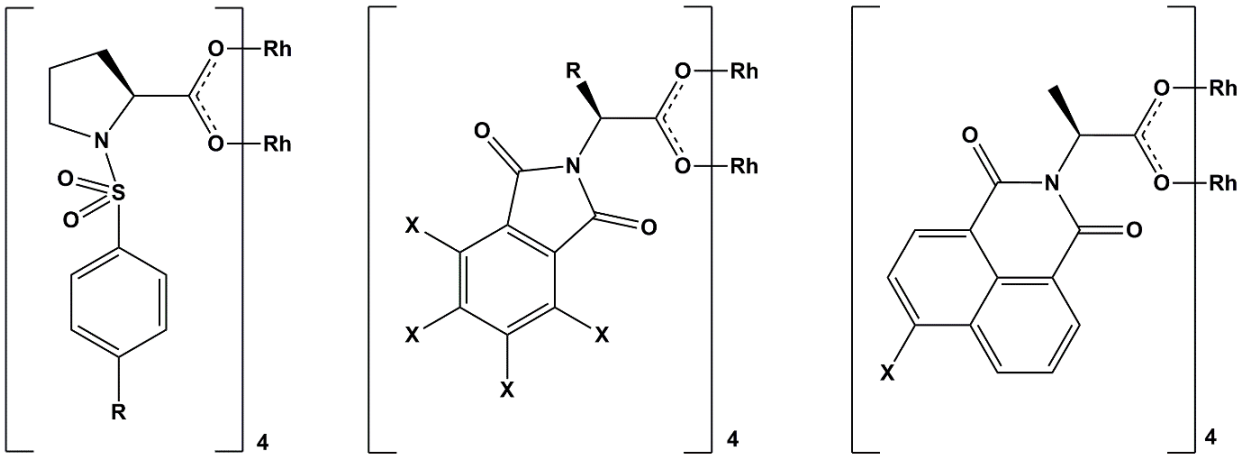

Figure 5.3. Chiral rhodium paddlewheel complexes which have shown enantioselective catalytic properties for cyclopropanation reactions. X denotes a halide or hydrogen atom.[459]

5.1.5 Bent diimide ligands

The use of amino acid functionalised banana-shaped ligands for the synthesis of homochiral helicates has been reported once before, simultaneous to the present study, in which amino acid substituted bicyclooctene diimide ligands formed homochiral quadruple stranded helicates with copper paddlewheels, and the configuration of the cage was shown to be dependent on the chirality of the ligand.[442] Pyridyl functionalised achiral bicyclooctene ligands have previously been reported to form triple and quadruple stranded mesocates with Zn^{II} and Cu^{II} metal centres, respectively, showing that bicyclooctene has a suitable shape for forming binuclear mesocate and helicate cages.[473]

In this study two different diimide molecules with a bent core were selected, 3,3′,4,4′-biphenylsulfone diimide (BPSD) and 9,10-dimethyl-9,10-ethanoanthracene-2,3,6,7-diimide (EADI), as they can be functionalised with amino acids, and have a bend in the core which may be conducive to the formation of helical cage complexes. Both the 3,3′,4,4′-biphenylsulfone dianhydride and 9,10-dimethyl-9,10-ethanoanthracene-2,3,6,7-dianhydride molecules have been reported previously as polymer precursors, but neither have been utilised as precursors to diimide ligands in metallosupramolecular chemistry.[474-476] There is some precedent for the formation of helicates with the BPSD ligand, as functionalised biphenyl sulfone molecules have been reported to form hydrogen bonded helicates.[477, 478]

The biphenyl sulfone diimide ligand core has not been previously used for the synthesis of coordination compounds. However the biphenyl sulfone core has been functionalised with carboxylate, amine and imidazole groups to synthesise coordination polymers with transition metals and lanthanides.[479-487] The biphenyl sulfone group has also been used in organic macrocycles, due to the significant bend through the sulfone group facilitating the formation of cyclic compounds.[488-490] There are also many reports of organic polymers which incorporate the BPSD fragment.[491-493]

The 9,10-dimethyl-9,10-ethanoanthracene-2,3,6,7-diimide class of ligands was investigated because they have a similar bend in the core to the BPSD molecules, but are longer and are therefore likely to form larger helicate cage complexes. The EADI molecule has only been reported twice in the literature, both as part of

permeable polymers.[494, 495] The use of the EADI ligand in metallosupramolecular chemistry is therefore unprecedented.

5.2 Synthesis of biphenyl sulfone diimides

The amino acid substituted BPSD series of molecules were synthesised by the same method as the BDI and NDI molecules, (see Chapters 2 and 3) in which the 3,3′,4,4′-biphenylsulfone tetracarboxylic dianhydride was reacted with the respective amino acids to form the diimide. The glycine, (*S*)-alanine, (*S*)-leucine and (*S*)-phenylalanine BPSD derivatives were synthesised, Figure 5.4. The three different synthetic methods of heating in DMF overnight, heating overnight in acetic acid and microwave synthesis in acetic acid were attempted for the BPSD compounds. The synthetic method that gave the pure product in the highest yield was utilised for the bulk synthesis.

The glycine substituted molecule (H_2GlyBPSD) was synthesised by heating the starting materials in DMF at 100°C overnight, giving a clean product with a 52% yield. The (*S*)-alanine substituted molecule ((*S*)-H_2AlaBPSD) was synthesised by heating the starting materials in acetic acid overnight, giving the product in a 58% yield. The (*S*)-leucine and (*S*)-phenylalanine substituted compounds ((*S*)-H_2LeuBPSD and (*S*)-H_2PheBPSD) were synthesised in a microwave reactor in acetic acid at 120 °C, with yields of 72 and 86%, respectively.

For the purposes of investigating the influence that the handedness of the ligand could have on the chirality of the coordination complexes formed, H_2LeuBPSD was also synthesised with the unnatural handedness of the leucine, (*R*)-leucine. (*R*)-H_2LeuBPSD was synthesised by microwave irradiation at 120 °C, with a 79% yield. The achiral version of H_2LeuBPSD, which was substituted with one (*R*)-leucine and one (*S*)-leucine, (*S*,*R*)-H_2LeuBPSD, was also synthesised, by reacting a 1:1 ratio of (*R*)-leucine and (*S*)-leucine with 3,3′,4,4′-biphenylsulfone tetracarboxylic dianhydride, also in a microwave reactor at 120 °C. The reaction would have formed a statistical mixture (25:50:25) of (*S*,*S*)-, (*S*,*R*)- and (*R*,*R*)-H_2LeuBPSD, and formed with a 90% yield. The reaction of this statistical mixture with Cu^{II} fortuitously formed metallosupramolecular products with the (*S*,*R*)-LeuBPSD ligand as desired (*vide infra*), and therefore the mixture was not purified to isolate (*S*,*R*)-H_2LeuBPSD. The successful synthesis of the BPSD molecules

was confirmed by ^{1}H-NMR and ^{13}C-NMR spectroscopy, mass spectrometry, infrared spectroscopy and microanalysis. In the same manner as the synthesis of the NDI and BDI ligands, presence of a ^{1}H-NMR signal corresponding to the hydrogen atom on the alpha-carbon of the amino acid at ~4.8 ppm was indicative of the formation of the product.

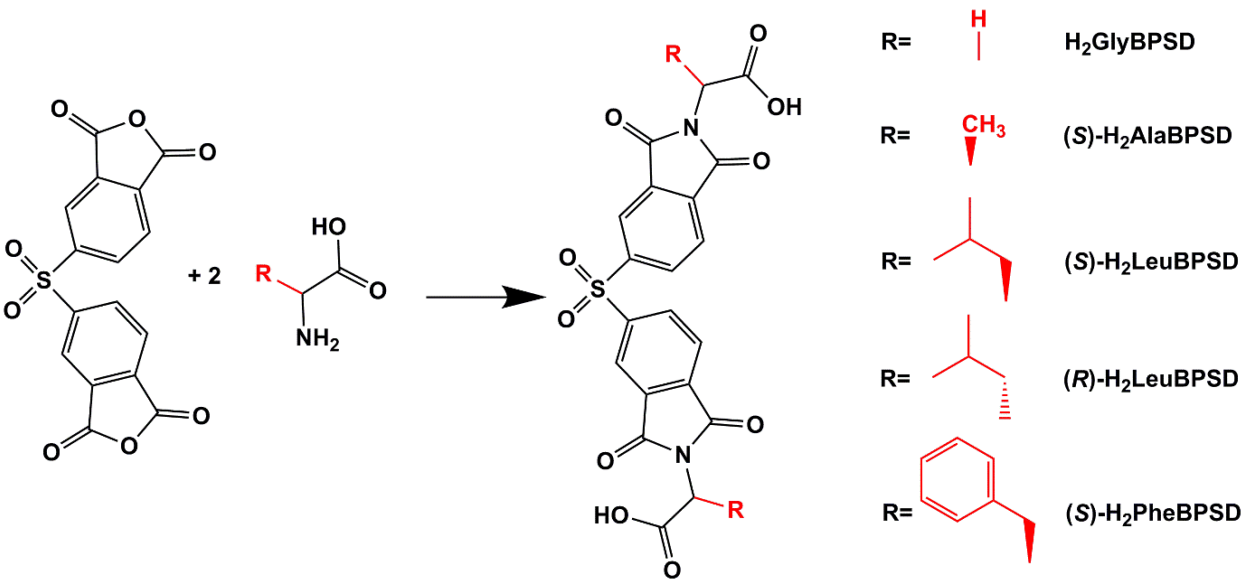

Figure 5.4. The reaction scheme for the synthesis of the amino acid substituted BPSD compounds.

5.3 Quadruple stranded helicate and mesocate cages

In addition to the numerous coordination polymers that were formed with the linear NDI and BDI ligands, the coordination chemistry BPSD and EADI ligands which have a bent core were investigated. The syntheses of both copper and rhodium paddlewheel complexes with amino acid substituted bent diimide ligands were investigated, with the aim of synthesising homochiral coordination cage complexes with enantioselective catalytic properties. The first class of ligands investigated for this purpose were the amino acid substituted BPSD ligands.

5.2.1 Homochiral quadruple stranded helicate cages

Enantiopure (*S*)-H_2LeuBPSD was reacted with $Cu(NO_3)_2{\cdot}3H_2O$ in DMA at 100°C, which yielded only a blue solution. After two months sitting at room temperature, blue crystals formed that were analysed to reveal a coordination compound of the formula $[Cu_4((S)\text{-LeuBPSD})_4(OH_2)_4]{\cdot}2DMA$, [**Λ,Λ-**

5.1(OH_2)]·2DMA, which is a helical cage, Figure 5.5. The structure of **Λ,Λ-5.1** is modelled in the space group *P*1, with one cage complex and some non-coordinated solvent in the asymmetric unit. The complex consists of two {$Cu_2(O_2C)_4$} paddlewheel motifs which are bridged by the four (*S*)-LeuBPSD ligands, with aqua ligands coordinated to the apical positions of the paddlewheels on the interior and exterior of the cage. The C-S-C angle in the BPSD ligands have a bend of 103.1(7), 100.8(8), 102.6(8) and 100.1(9)°, giving the ligand sufficient bend to form a dinuclear cage complex. The internal Cu^{II} atoms are separated by 7.233(3) Å and the cage has an internal void volume of *ca*. 350 $Å^3$, with the absence of internal coordinated solvent. When the cage is viewed down the axis connecting all four Cu^{II} ions, the paddlewheels have a negligible offset with regard to each other. However the ligands do not bridge to the paddlewheel site directly below them, instead each ligand is twisted ~ 90° as they bridge between the paddlewheels, giving the cage complex a helical sense. The four (*S*)-Leucine groups around each paddlewheel force the substituents into a propeller motif, therefore inducing chirality around the metal centre and making the cage a quadruple stranded helicate with Λ,Λ configuration, Figure 5.5.

As the initial synthesis of **Λ,Λ-5.1** was extremely slow, new synthetic methods were explored to synthesise the material in bulk. A method was developed in which (*S*)-H_2LeuBPSD and $Cu(NO_3)_2$ were dissolved in a solvent mixture of DMA/MeOH, and a solution of triethylamine and methanol (1:1) was added slowly to the solution to deprotonate of the carboxylic acids, in order to induce coordination to the metals and formation of the complex. This method produced a crystalline sample of the complex in 56% yield overnight.

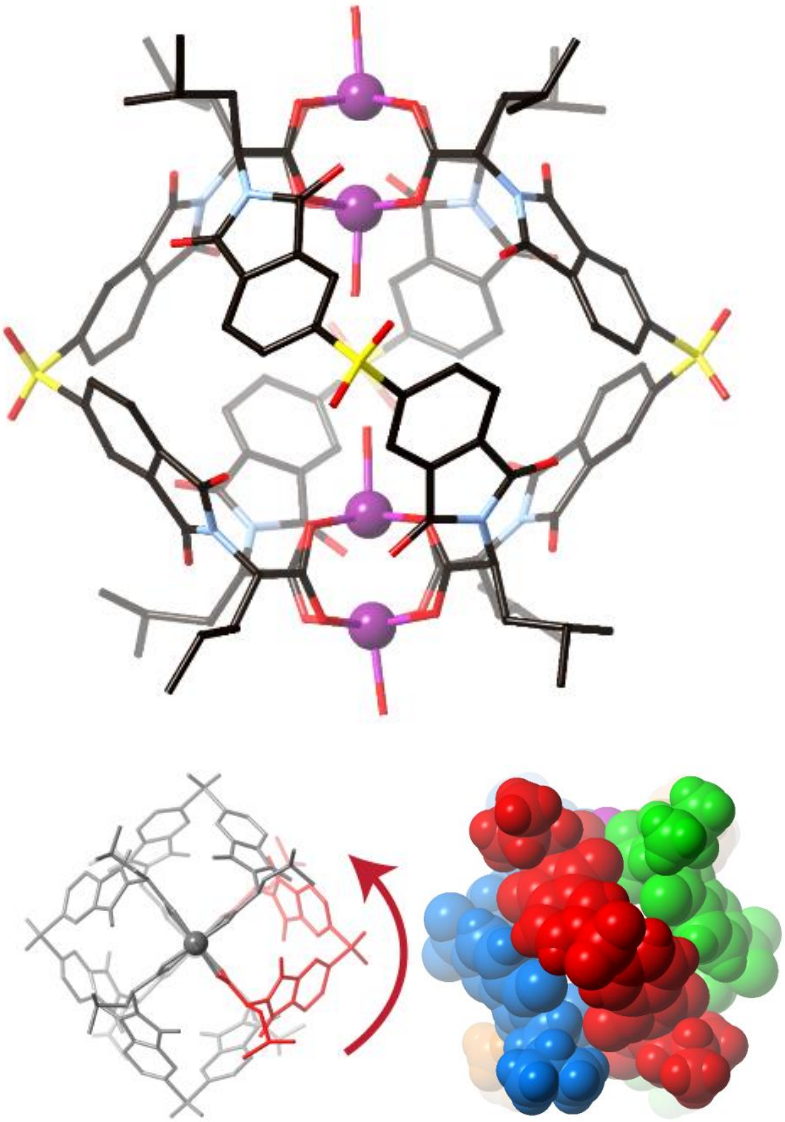

*Figure 5.5. The homochiral quadruple stranded helicate cage of **Λ,Λ-5.1**. Shown as a stick model (with the exception of the metal ions) from the side view (top) and the top view looking down the axis connecting all four Cu^{II} ions (left), showing the twist in the ligands. Hydrogen atoms are omitted for clarity. The cage also shown as a space filling diagram, to further illustrate the twist in the ligands (right).*

Since it was observed that the (*S*)-LeuBPSD ligand caused a helical sense around the copper paddlewheels of the **Λ,Λ-5.1** cage complex, the behaviour of the opposite handedness ligand, (*R*)-LeuBPSD with Cu^{II} was also explored. (*R*)-H_2LeuBPSD was also reacted with $Cu(NO_3)_2$ in DMA/MeOH using triethylamine as a base, to yield a pure sample of $[Cu_4((R)\text{-LeuBPSD})_4(OH_2)(MeOH)_{2.5}(HNMe_2)_{0.5}]\cdot 4DMA$, $[\mathbf{\Delta,\Delta 5.1}\cdot(OH_2)(MeOH)_{2.5}(HNMe_2)_{0.5}]\cdot 4DMA$ in 54% yield. Employing the (*R*)-LeuBPSD ligand with Cu^{II}

forms a quadruple stranded helicate analogous to that of **Λ,Λ-5.1**, with two copper paddlewheels connected by four LeuBPSD ligands. However in the case of the (*R*)-LeuBPSD in **Δ,Δ-5.1** the change in handedness of the amino acid in the ligand induces a swap in the handedness of the propeller motif around the copper paddlewheel, leading to the formation of the opposite handedness helicate, the Δ,Δ configuration, Figure 5.6. The (*R*)-LeuBPSD ligands in **Δ,Δ-5.1** are arranged in the same way as the (*R*)-LeuPBSD ligands in **Λ,Λ-5.1**, C-S-C angles of 102.1(5), 103.1(4), 100.9(3) and 101.2(4)°. The cages are the same shape, with an internal Cu···Cu distance of 7.3069(14) Å and void volume of 366 Å^3 in the structure of **Λ,Λ-5.1**, in comparison to 7.233(3) Å and 353 Å^3 in the structure of **Δ,Δ-5.1**. These two helical cage complexes demonstrate that the handedness of the ligand employed will force the chirality around the metal centre and therefore control the supramolecular chirality of the cage complexes obtained.

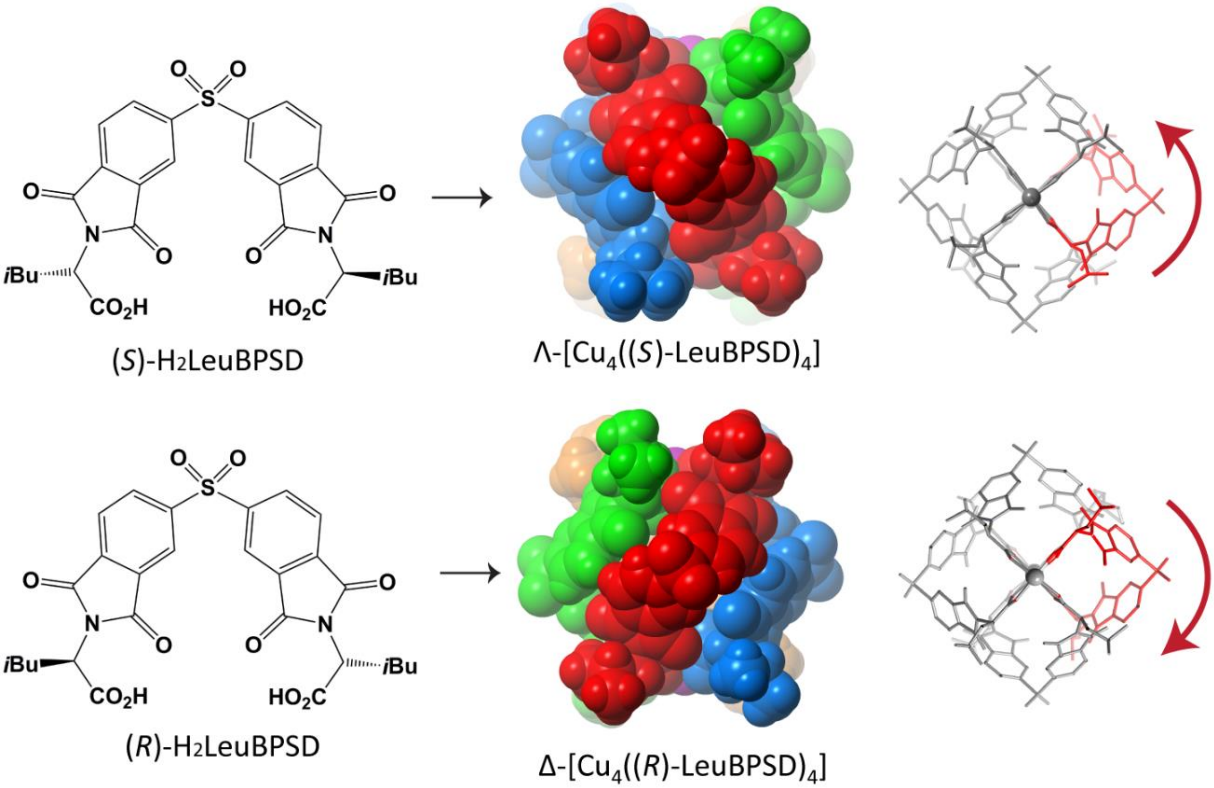

*Figure 5.6. The two opposite handedness LeuBPSD ligands (left) and the two opposite handedness quadruple stranded helicate cage complexes which they form with Cu^{II}, shown in space packing (centre). The view down the Cu^{II} axis of **Λ,Λ-5.1** and **Δ,Δ-5.1**, showing the twist of the ligands as they bridge between the copper paddlewheels (right). Hydrogen atoms and coordinated solvent are omitted for clarity.*

The solution stability of these complexes as well as their helicity is confirmed by solution circular dichroism studies. Circular dichroism (CD) spectra of the **Λ,Λ-5.1** and **Δ,Δ-5.1** cage solutions in acetonitrile showed opposite Cotton effects, which are greatly enhanced with respect to the ligands alone, indicating that the structure and helicity of the cages is maintained in solution, Figure 5.7. The solution stability of the complexes is also confirmed by the observation of *m/z* peaks corresponding to the [**M** + H]$^+$ ion for both cage complexes.

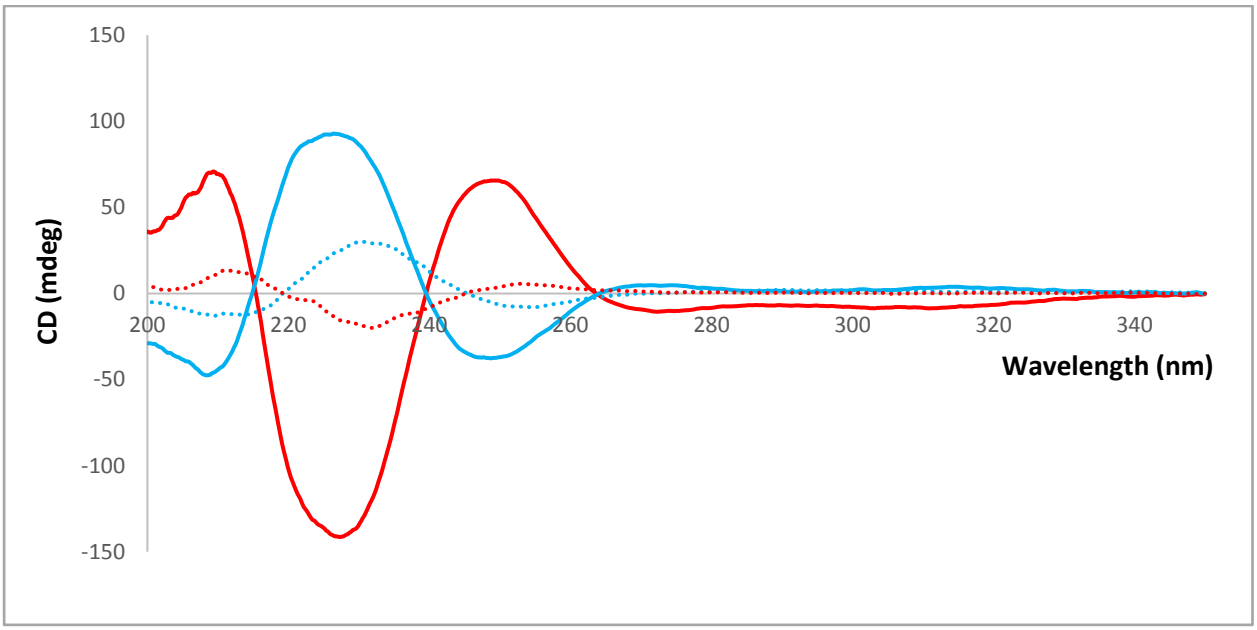

*Figure 5.7. The circular dichroism spectra of **5.1** and LeuBPSD. **Λ,Λ-5.1** shown as solid blue line, and the (S)-H_2LeuBPSD ligand shown in dotted blue line, and the opposite handedness **Δ,Δ-5.1** shown as solid red line, the (R)-H_2LeuBPSD ligand shown as a dashed red line. The CD of the cage complexes and ligand solutions were conducted in acetonitrile at concentrations of 6 µmol/L and 60 µmol/L, respectively.*

The solvent coordinated to the apical positions of the copper paddlewheels in **Λ,Λ-5.1** and **Δ,Δ-5.1** is very difficult to assign crystallographically, most likely due to rotational disorder along the Cu-O bond and variation in coordinated solvent between cages within each crystalline sample. The best model of the coordinated solvent in the crystal structure of **Λ,Λ-5.1** is four aqua ligands. The coordinated solvent that could be best modelled in the structure of **Δ,Δ-5.1** was more complex. The apical sites of the paddlewheels in **Δ,Δ-5.1** on the exterior of the cage are occupied by methanol molecules. One of the interior sites is occupied by an aqua ligand and a methanol molecule that share the coordinated oxygen atom (fixed

occupancies 50:50), and the methanol molecule is modelled over two positions (fixed occupancies 25:25), and the remaining interior site is occupied by a dimethylamine molecule, presumably from hydrolysis of the DMA used in the reaction, and an aqua ligand (fixed occupancies 50:50).

As these cages have some internal void volume, the accessibility of the pores in solution is of interest to gauge whether these cages maybe used for solution guest binding. Unfortunately since **5.1** involves paramagnetic Cu^{II} the solution guest binding interactions could not be easily investigated by ^{1}H-NMR spectroscopy. However a serendipitous crystalline sample was obtained from a solution of **Λ,Λ-5.1** in d_6-DMSO, which was then replicated on a larger scale. The crystals were found to contain the complex $[Cu_4((S)\text{-LeuBPSD})_4(DMSO)_2(OH_2)_4]$, ($[$**Λ,Λ-5.1(DMSO)**$_2(OH_2)_2]\cdot 2DMSO$). The structure of **Λ,Λ-5.1(DMSO)**$_2$ is identical to that of **Λ,Λ-5.1** with the exception of the coordinated solvent molecule. There are two DMSO molecules which are coordinated to the Cu^{II} sites on the interior of the cage, Figure 5.8, demonstrating that it is possible for the solvent on the inside of the cage to exchange in solution. The coordinated DMSO molecules are disordered over two positions (free occupancies 53:47). The external apical positions are occupied by aqua ligands.

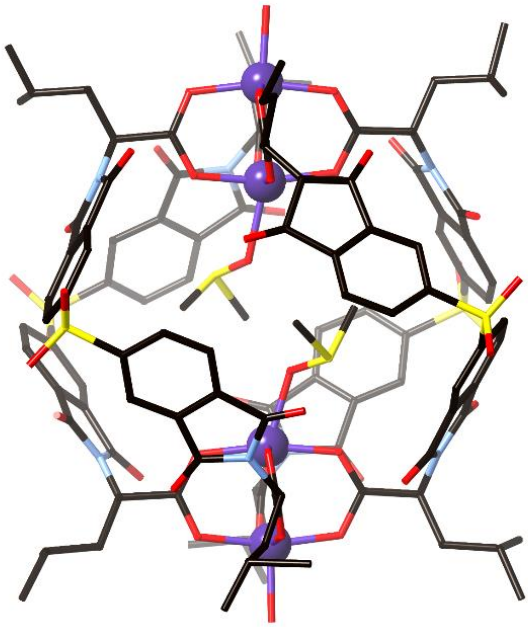

*Figure 5.8. The structure of **Λ,Λ-5.1(DMSO)**$_2$ in which the solvent coordinated to the interior Cu^{II} sites have exchanged for DMSO. For clarity only one of the confirmations of the disordered DMSO is shown and hydrogen atoms are omitted.*

5.2.2 Self-selection of homochiral quadruple stranded helicate cages

In order to explore the supramolecular self-selectivity of the (*S*)-H_2LeuBPSD and (*R*)-H_2LeuBPSD for formation of homochiral quadruple stranded helicate cages, a reaction was carried out with a 50:50 mixture of (*S*)- and (*R*)-H_2LeuBPSD and $Cu(NO_3)_2 \cdot 3H_2O$. The crystalline product was analysed by single crystal X-ray diffraction to reveal a centrosymmetric structure (space group *C*2/*c*) in which the asymmetric unit contains a quadruple stranded helicate with the ligands all of the same handedness, **Λ,Λ-5.1/Δ,Δ-5.1**·DMA, Figure 5.9. The helicate of opposite handedness, containing the other ligand, is generated by inversion symmetry in the crystal structure. Powder X-ray diffraction (PXRD) shows the presence of crystalline **Δ,Δ-5.1** and **Λ,Λ-5.1** in addition to **Λ,Λ-5.1/Δ,Δ-5.1**, indicating that the homochiral crystals of enantiopure cages form alongside the centrosymmetric crystals of **Λ,Λ-5.1/Δ,Δ-5.1**. In the structure of **Λ,Λ-5.1/Δ,Δ-5.1** the LeuBPSD ligands only form cage complexes with ligands of like handedness, demonstrating that these ligands display narcissistic self-selection to form helical cage complexes.

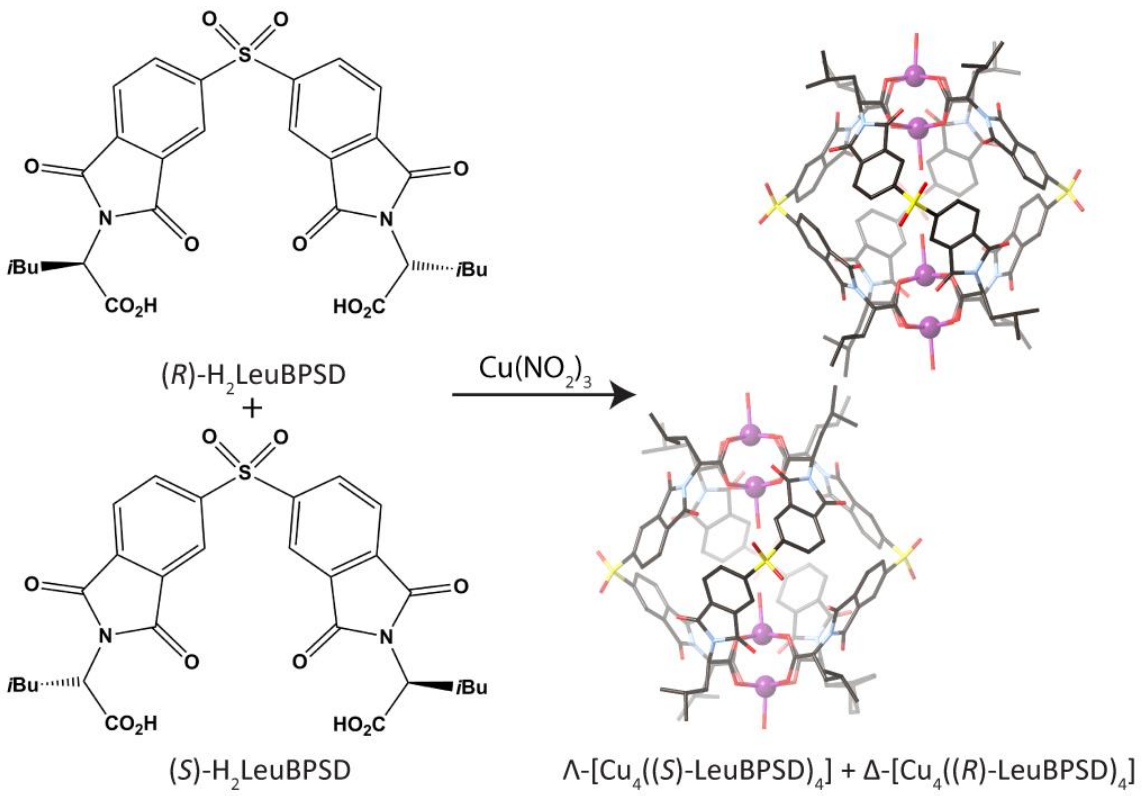

*Figure 5.9. The synthesis of **Λ,Λ-5.1/Δ,Δ-5.1** with both handedness of helicate cage in a single crystal, demonstrating that the LeuBPSD ligands display narcissistic self-selection.*

5.2.3 Mesocate cage complexes

The self-selection of the LeuBPSD ligands prompted the exploration of how the chirality of these cage complexes may be removed. It was shown that this may occur through two different methods, the use of a (*S,R*)-LeuBPSD ligand which involves two leucine amino acids of opposite handedness in the ligand, and the use of the achiral GlyBPSD ligand.

The (*S,R*)-LeuBPSD ligand was prepared by reacting a 50:50 mixture of (*R*)- and (*S*)-Leucine with the 3,3′,4,4′-biphenylsulfone dianhydride (*vide supra*). As each LeuBPSD ligand contains two amino acid groups, this reaction would most likely form the (*S,S*)-, (*S,R*)- and (*R,R*)-H_2LeuBPSD ligands in a statistical mixture (25:50:25). Due to the statistical prevalence of (*S,R*)-H_2LeuBPSD, the mixture was reacted without purification with $Cu(NO_3)_2 \cdot 3H_2O$ by analogous reaction conditions to those which formed bulk samples of **Λ,Λ-5.1** and **Δ,Δ-5.1**. A crystalline product was formed which was analysed by single crystal X-ray diffraction to reveal a coordination complex of the form $[Cu_4((S,R)\text{-LeuBPSD})_4(MeOH)_2(OH_2)_2]$, $[\mathbf{5.2}(OH_2)_2(MeOH)_2] \cdot 2DMA$. The PXRD of the bulk crystalline sample containing **5.2** showed that **Λ,Λ-5.1**, **Δ,Δ-5.1** and **Λ,Λ-5.1/Δ,Δ-5.1** were also present, due to the presence of the (*S*)-LeuBPSD and (*R*)-LeuBPSD ligands in the reaction mixture. Complex **5.2** crystallises in the centrosymmetric space group $P\bar{1}$ with half of the complex in the asymmetric unit. In a similar manner to **5.1** the structure of **5.2** involves two copper paddlewheels which are bridged by four LeuBPSD ligands. The ligands in **5.2** are exclusively (*S,R*)-LeuBPSD, and are arranged such that one of the paddlewheels is exclusively coordinated by the (*S*)-leucine terminal groups and the other paddlewheel is exclusively coordinated by the (*R*)-leucine terminal groups, further demonstrating the self-selection of the enantiomers. Due to the orientation around each metal, and the mixed chirality of each ligand, the ligands are not twisted between the metal centres, forming a mesocate cage, Figure 5.10. As the ligands are not twisted between the metal centres, the copper paddlewheels are further apart than the helicates of **5.1**, with an internal Cu···Cu distance of 9.015(4) Å (*cf* 7.2 Å). The longer Cu···Cu distance leads to a much larger internal void volume of ~ 610 $Å^3$, almost double that of **5.1** with voids of ~ 350 $Å^3$. The cores of the ligands also have slightly different conformations, with C-S-C angle of

106.23(17) and 101.01(17)°, compared to the ligands in **5.1** which had C-S-C angles of ~101°, demonstrating that the BPSD ligands have some degree of flexibility.

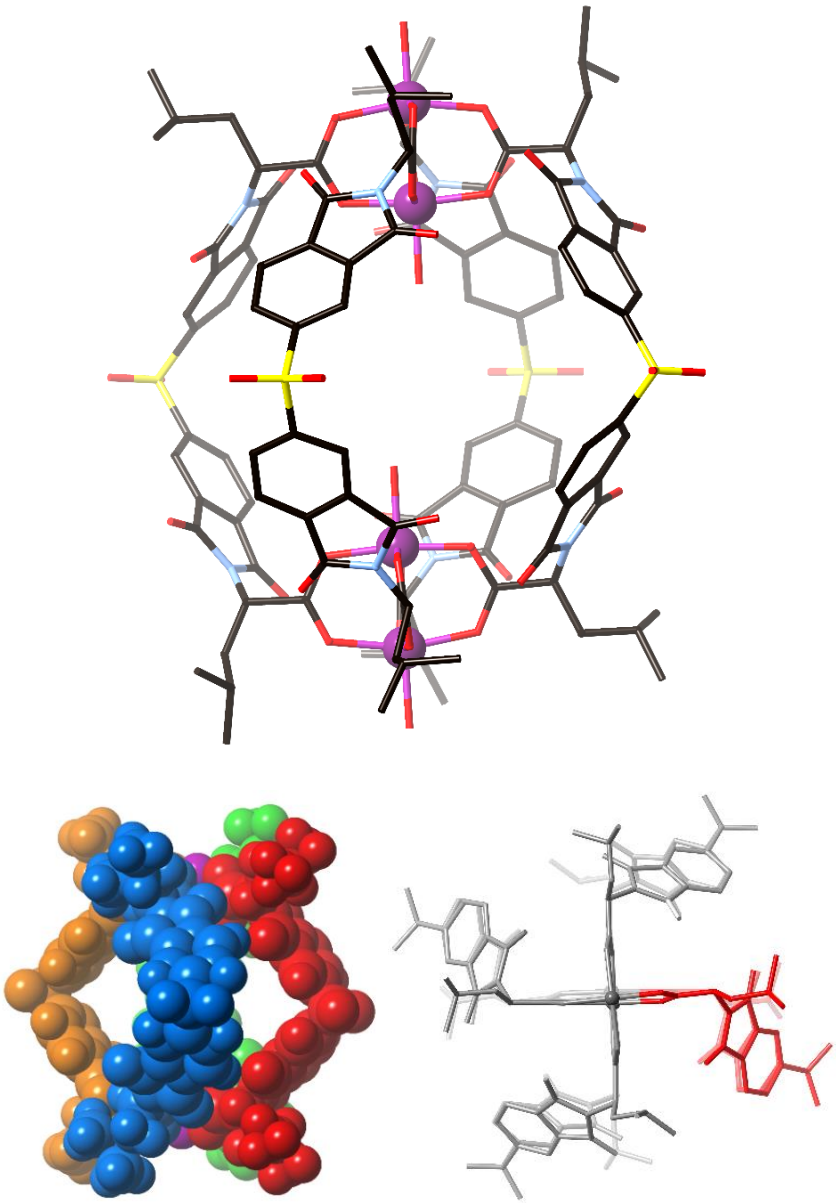

*Figure 5.10. The structure of **5.2** shown with stick bonds (top) and space packing (left). View looking down the Cu···Cu showing the ligands aligned with each other to form a mesocate (right).*

Using achiral H_2GlyBPSD, [Cu_4(GlyBPSD)$_4$(MeOH)$_3$(OH_2)], [**5.3**(MeOH)$_3$(OH_2)]·3.5DMA·1.5MeOH, was isolated as a pure crystalline phase. The cage structure is very similar to that of **5.2** in that it is a mesocate in which the ligands bridge between the copper paddlewheels in a non-helical arrangement,

Figure 5.11. The structure of **5.3** is modelled in the centrosymmetric space group $P2_1/n$ with one copper paddlewheel and two GlyBPSD ligands in the asymmetric unit. The two crystallographically unique apical Cu^{II} sites are occupied by methanol ligands. The methanol coordinated to the external Cu^{II} site is disordered over two positions (fixed occupancies 25:75), sharing the coordinated oxygen atom. In the asymmetric unit there are also non-coordinated solvent molecules of two methanol molecules modelled as 25% and 50% occupancy, and DMA molecules. There are two DMA molecules modelled at half occupancy, and another DMA molecule which is modelled as disordered over two positions (fixed occupancies 25:50).

Despite the lack of stereocentres in GlyBPSD, the amino acids around each paddlewheel are arranged in a propeller motif, seemingly due to the steric requirements of the ligand. As is the case in the structure of **5.2**, the propeller motifs are of opposite direction for each paddlewheel. The internal Cu···Cu distance of **5.3** is 9.311(3) Å, slightly longer than that of **5.2** due to a slight difference in the arrangement in the ligands. In the structure of **5.2** the ligands are approximately evenly spaced around the cage, as can be seen by the S···S distances of 10.179(5) Å and 12.547(3) Å between neighbouring ligands. In comparison, in **5.3** the complex is 'pinched' in one direction, with S···S distances 9.561(2) Å and 13.767(3) Å, elongating the cage slightly. The elongation of the mesocate cages in comparison to the helicate cages leads to much larger void volumes within the cages, with internal void volumes in **5.2** and **5.3** of 610 $Å^3$ and 670 $Å^3$, respectively, in the absence of internally coordinated solvent (*cf.* 350 $Å^3$ in **5.1**). The cages **5.2** and **5.3** also have larger windows between the ligands than the **5.1** cages, as can be seen in the structure of **5.3** which reveals well-ordered, partial occupancy DMA solvent molecules within the windows. The lack of twist in the ligands of the mesocate cages allows larger windows and void volumes. The ligands in the structure of **5.3** also show a slightly different bend than those of **5.1** and **5.2**, with C-S-C angle of 105.1(2) and 103.7(3)°. The variation in ligand arrangement between **5.2** and **5.3** demonstrates that these cages are somewhat flexible.

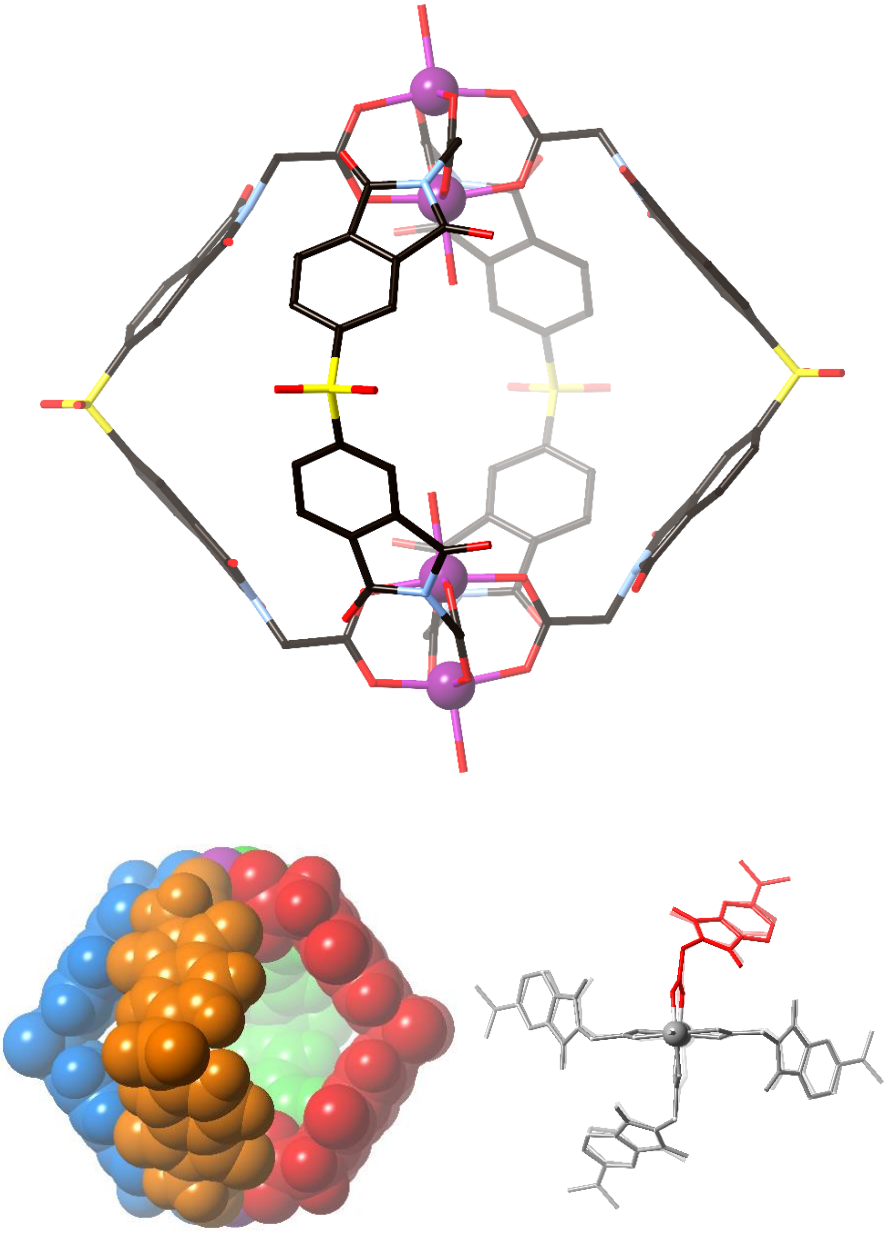

*Figure 5.11. The structure of **5.3**. shown as stick model (top), in space packing (left) and looking down the Cu···Cu axis to shown that the ligands are not twisted, therefore forming a mesocate (right).*

5.2.4 Retention of helicity upon incorporation of achiral ligand

Considering that homochiral helical cages **Λ,Λ-5.1** and **Δ,Δ-5.1** were obtained from chiral BPSD ligands, and the mesocate cages **5.2** and **5.3** were obtained from achiral BPSD ligands, it was considered of interest whether the helicity of the cages could be maintained upon incorporation of a proportion of achiral ligand,

or if incorporation of any amount of achiral ligand would "switch off" the helicity of the cage complexes. Circular dichroism (CD) was considered an appropriate technique to investigate this system, as it is indicative of the concentration of chiral complex present in solution.

As a control experiment, a series of solutions were made with a constant concentration of Cu^{II} and decreasing concentrations of (*S*)-H_2LeuBPSD. The (*S*)-H_2LeuBPSD:Cu^{II} ratios of the solutions ranged from 8:8 to 0:8, consistent with removal of half an equivalent of ligand for each cage, considering the M_4L_4 nature of the cage complexes. The solutions were diluted to an appropriate concentration and analysed by CD. The CD signal of the solutions was measured between 240-350 nm, showing a strong Cotton effect between 240-265 nm. The maximum signal at 250 nm decreases with the decrease in (*S*)-H_2LeuBPSD concentration, consistent with a decrease in the concentration of helicate complex in solution. A graph of the CD signal at 250 nm shows a linear relationship between the (*S*)-H_2LeuBPSD concentration and the CD signal of the solution, Figure 5.12. A linear trendline was calculated from the graph, demonstrating that the decrease in (*S*)-H_2LeuBPSD with a constant concentration of Cu^{II} shows a linear decrease in CD signal.

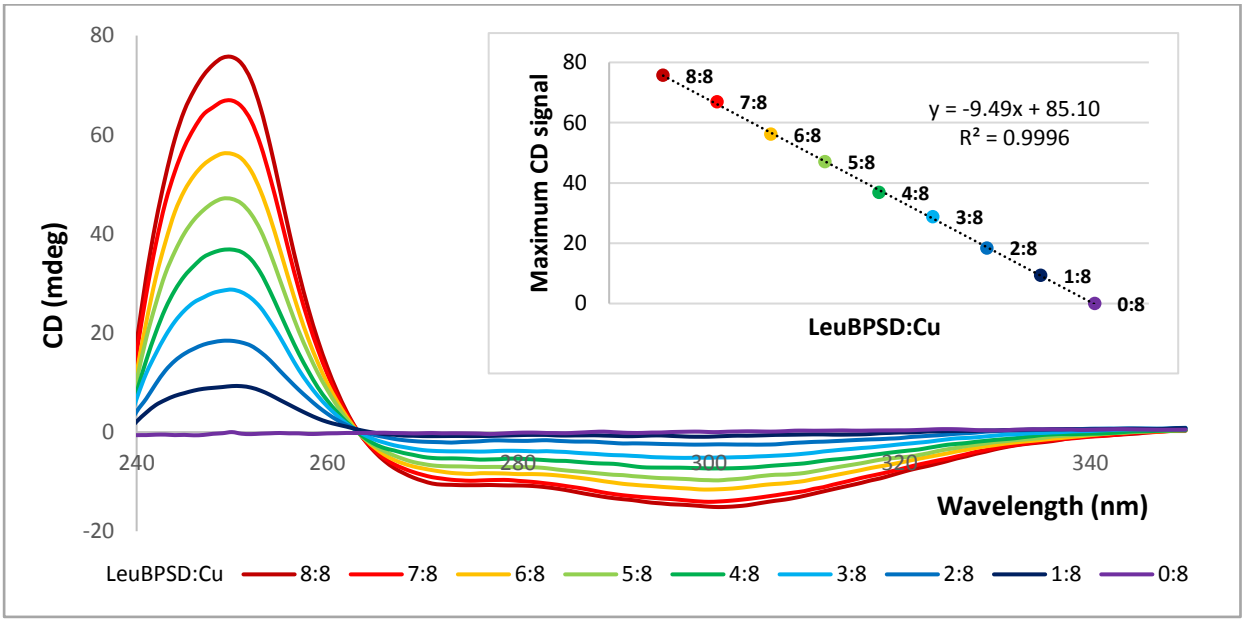

Figure 5.12. The control CD experiment showing a linear relationship between the decrease in (S)-LeuBPSD concentration and the maximum CD signal of the system, consistent with a linear decrease in the concentration of helicate cage in the solution.

In order to investigate the influence of substituting GlyBPSD for (*S*)-LeuBPSD, a new experiment was undertaken in which a series of nine solutions were made with varying (*S*)-H_2LeuBPSD:H_2GlyBPSD ratios and a constant concentration of Cu^{II}. The total concentration of BPSD ligands was maintained in a 1:1 ratio with Cu^{II}, and the (*S*)-H_2LeuBPSD:H_2GlyBPSD ratios varied between solutions. The (*S*)-H_2LeuBPSD:H_2GlyBPSD ratios ranged from 8:0 to 0:8, and as there are four ligands in one cage complex, this was a substitution of half an equivalent of (*S*)-LeuBPSD for GlyBPSD in subsequent reaction solutions. The experiment was designed to investigate if a GlyBPSD ligand could be substituted for an (*S*)-LeuBPSD ligand whilst maintaining the helicity of the cage and therefore maintaining the CD signal.

As would be expected, the solution of 8:0 made with (*S*)-H_2LeuBPSD:H_2GlyBPSD shows the strongest Cotton effect. However the signal does not decrease in a linear fashion upon the incorporation of GlyBPSD, Figure 5.13. The graph of the maximum CD signal, at 250 nm, shows that the solutions of (*S*)-Leu:Gly ratios 8:0 to 5:4 all show the same signal. The solutions of (*S*)-Leu:Gly ratios 4:4 to 0:8 show a steady decrease in CD signal as the proportion of GlyBPSD increases. If the GlyBPSD was not incorporated into the cages, or if it “switched off” the helicity of the cages, the CD would show a decrease in the signal upon any increase in the GlyBPSD. Instead the CD signal is maintained upon addition of GlyBPSD, suggesting that achiral ligands can be incorporated into the cages without removal of their helicity.

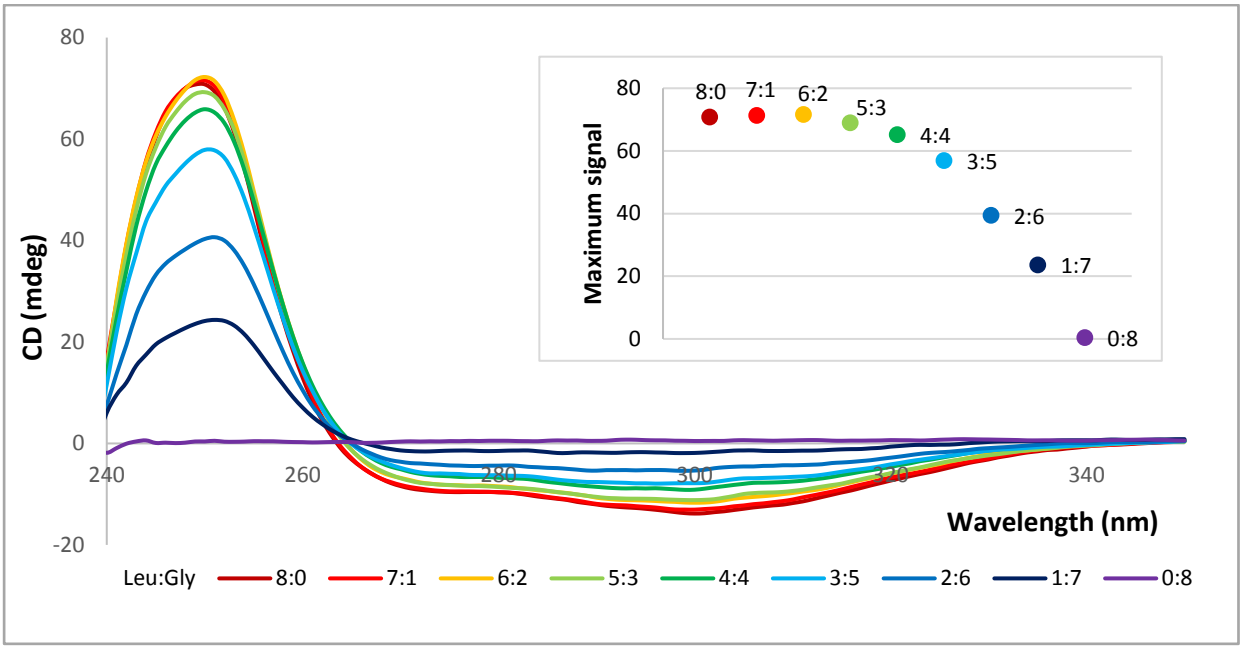

Figure 5.13. The CD results obtained by replacing (S)-LeuBPSD with GlyBPSD with a standard concentration of Cu^{II}. The maximum CD signal of each solution (inset).

The composition of each solution of varying (*S*)-LeuBPSD:GlyBPSD ratio with a constant concentration of Cu^{II} was analysed by HPLC, via monitoring at 280 nm, Figure 5.14. It was observed that the [Cu_4((*S*)-LeuBPSD)$_4$(solv.)$_4$] complex eluted at a retention time of 4.1 minutes, as this was the only signal observed for the solution of 8:0 (*S*)-LeuBPSD:GlyBPSD and Cu^{II}. The [Cu_4(GlyBPSD)$_4$(solv.)$_4$] complex eluted first, with a retention time of 1.1 minutes. There were also three different peaks observed in the HPLC between 1.1 and 4.1 minutes, which it is assumed correlate to the [Cu_4L_4] complexes with (*S*)-LeuBPSD:GlyBPSD ratios of 1:3, 2:2 and 3:1.

The three HPLC peaks which elute between the [Cu_4(GlyBPSD)$_4$] and [Cu_4((*S*)-LeuBPSD)$_4$] complexes elute at retention times of 1.2, 1.6 and 2.4 minutes. These HPLC signals can be assigned as [Cu_4(GlyBPSD)$_3$((*S*)-LeuBPSD)], [Cu_4(GlyBPSD)$_2$((*S*)-LeuBPSD)$_2$] and [Cu_4(GlyBPSD)((*S*)-LeuBPSD)$_3$]. The increased bulkiness of the presence of the (*S*)-LeuBPSD ligand in the cage complex would lead to longer retention times. Therefore the peaks may be assigned as [Cu_4(GlyBPSD)$_3$((*S*)-LeuBPSD)] eluting at 1.2 minutes, [Cu_4(GlyBPSD)$_2$((*S*)-LeuBPSD)$_2$] eluting at 1.6 minutes and [Cu_4(GlyBPSD)((*S*)-LeuBPSD)$_3$] eluting at 2.4 minutes, with increasing (*S*)-LeuBPSD composition correlating with increased retention time.

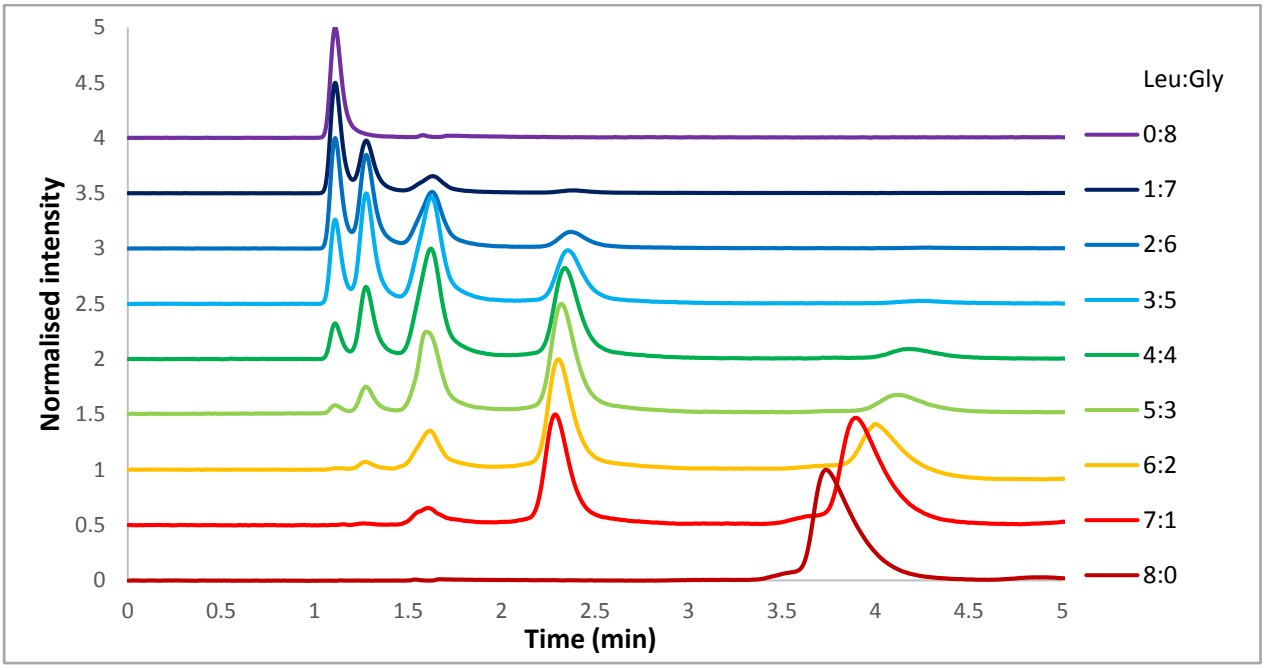

Figure 5.14. The HPLC traces of each (S)-LeuBPSD:GlyBPSD + Cu^{II} mixture. All intensities are normalised.

Mass spectroscopy of each peak extracted from the HPLC was attempted, in order to unequivocally assign the composition of each peak in the HPLC, however the concentration of the cage complex in each HPLC fraction was too low for the complex to be detected. Mass spectrometry of the 4:4 (*S*)-LeuBPSD:GlyBPSD reaction solution showed peaks correlating to the $[Cu_4(GlyBPSD)_3((S)\text{-}LeuBPSD)(OH_2)_4\text{-}H]^-$, $[Cu_4(GlyBPSD)_2((S)\text{-}LeuBPSD)_2\text{-}H]^-$ and $[Cu_4(GlyBPSD)((S)\text{-}LeuBPSD)_3(OH_2)]\text{-}H]^-$ species, confirming that the mixed ligand cages do exist in solution, and that all three mixed ligand cages exist in one reaction solution, as was also shown by the HPLC of this reaction.

The difference in the composition of cages in the solutions may be expressed by calculating the relative area of each peak in the HPLC. Figure 5.15 shows how the change in the (*S*)-LeuBPSD:GlyBPSD ratio from 8:0 to 0:8 shows the decrease in the relative concentration of $[Cu_4((S)\text{-}LeuBPSD)_4]$ (shown as red column), the appearance and then decrease in the mixed ligand cages, and the appearance of the $[Cu_4(GlyBPSD)_4]$ cage (shown as a purple column). The incorporation of half an equivalent of GlyBPSD per cage, the 7:1 solution, shows the proportion of the $[Cu_4((S)\text{-}LeuBPSD)_4]$ complex decrease to 60%, and the appearance of the $[Cu_4((S)\text{-}LeuBPSD)_3(GlyBPSD)]$ cage (shown as orange column) accounting for 35%

of the solution, and the appearance of a small amount of the [Cu_4((*S*)-LeuBPSD)$_2$(GlyBPSD)$_2$] complex (shown as green column) making up 5% of the solution. The 6:2 solution, with one equivalent of GlyBPSD per cage, shows the [Cu_4((*S*)-LeuBPSD)$_4$] cage decrease to 35% of the total solution, the increase in the relative concentrations of the [Cu_4((*S*)-LeuBPSD)$_3$(GlyBPSD)] and [Cu_4((*S*)-LeuBPSD)$_2$(GlyBPSD)$_2$] complexes to 48 and 15%, respectively, and the appearance of 2% of the [Cu_4((*S*)-LeuBPSD)(GlyBPSD)$_3$] complex (shown as blue column).

Further increase in the proportion of GlyBPSD in the 5:3 solution shows the first mixture which contains all five different cage complexes. The [Cu_4((*S*)-LeuBPSD)$_4$] complex decreases to 9% of the solution, the [Cu_4((*S*)-LeuBPSD)$_3$(GlyBPSD)] cage maintains a similar proportion to the 6:2 solution, at 49% of the mixture, the [Cu_4((*S*)-LeuBPSD)$_2$(GlyBPSD)$_2$] complex shows a marked increase, accounting for 35% of the solution. The 5:3 solution also shows an increase in concentration of the [Cu_4((*S*)-LeuBPSD)(GlyBPSD)$_3$] complex, accounting for 6% of the mixture, and the [Cu_4(GlyBPSD)$_4$] complex first appears, making up 1% of the solution.

The CD of these first four solutions shows that 100% of the complexes in solutions are helicates, which based off the composition of the solutions from HPLC, suggests that the [Cu_4((*S*)-LeuBPSD)$_3$(GlyBPSD)], [Cu_4((*S*)-LeuBPSD)$_2$(GlyBPSD)$_2$] and [Cu_4((*S*)-LeuBPSD)(GlyBPSD)$_3$] cages are all helicates. Therefore it appears that only one (*S*)-LeuBPSD ligand is required per [Cu_4L_4] cage in order to induce the chirality of the cage and form a helicate. Although the HPLC of the 5:3 solution shows 1% of the [Cu_4(GlyBPSD)$_4$] complex, this is unlikely to lead to a discernible decrease in CD signal.

Consistent with the lower CD signal observed for the 4:4 mixture, the HPLC of this solution shows an increase in the proportion of the [Cu_4(GlyBPSD)$_4$] complex, to 5% of the mixture. The 4:4 mixture also contains 17% of the [Cu_4((*S*)-LeuBPSD)(GlyBPSD)$_3$] complex, 39% of the [Cu_4((*S*)-LeuBPSD)$_2$(GlyBPSD)$_2$], 34% of the [Cu_4((*S*)-LeuBPSD)$_3$(GlyBPSD)] and 5% of the [Cu_4((*S*)-LeuBPSD)$_4$] complex. If the cages were forming a purely statistical mixture, the 4:4 solution should show equal proportions of the [Cu_4((*S*)-LeuBPSD)$_4$] and [Cu_4(GlyBPSD)$_4$] complexes, which is observed, as they both account for 5% of the mixture. However the [Cu_4((*S*)-LeuBPSD)(GlyBPSD)$_3$] and [Cu_4((*S*)-

LeuBPSD)$_3$(GlyBPSD)] cages do not form in equal proportions, as the [Cu$_4$((*S*)-LeuBPSD)$_3$(GlyBPSD)] is more dominant, accounting for 34% of the mixture, while the [Cu$_4$((*S*)-LeuBPSD)(GlyBPSD)$_3$] cage accounts for 17% of the mixture.

As would be expected upon the increase in GlyBPSD concentration to being in excess of (*S*)-LeuBPSD, the 3:5 solution shows an increase proportion of the [Cu$_4$(GlyBPSD)$_4$] complex, to 14%. The 4:4 solution is also the last observation of the [Cu$_4$((*S*)-LeuBPSD)$_4$] cage, accounting for 1% of the mixture. The 4:4 solution also shows an increase in the proportion of the [Cu$_4$((*S*)-LeuBPSD)(GlyBPSD)$_3$] complex, to 26%, the maintaining of the proportion of the [Cu$_4$((*S*)-LeuBPSD)$_2$(GlyBPSD)$_2$] complex, at 39%, and the decrease in the [Cu$_4$((*S*)-LeuBPSD)(GlyBPSD)$_3$] complex, to 20% of the mixture. The 6:2 solution shows a further increase in the proportion of the [Cu$_4$(GlyBPSD)$_4$] complex, to 28% of the mixture, and an increase in the [Cu$_4$((*S*)-LeuBPSD)(GlyBPSD)$_3$] complex, to 33%. The proportion of the [Cu$_4$((*S*)-LeuBPSD)$_2$(GlyBPSD)$_2$] and [Cu$_4$((*S*)-LeuBPSD)$_3$(GlyBPSD)] complexes decreases in the 6:2 solution, to 31 and 33%, respectively.

The 1:7 solution shows the last observation of the [Cu$_4$((*S*)-LeuBPSD)$_3$(GlyBPSD)] complex, accounting for 2% of the mixture. The [Cu$_4$((*S*)-LeuBPSD)$_2$(GlyBPSD)$_2$] complex also shows a marked decrease in the 1:7 solution, to 13% of the solution. The remaining 1:7 solution is accounted for my 34% of the [Cu$_4$((*S*)-LeuBPSD)(GlyBPSD)$_3$] complex, and 51% of the [Cu$_4$(GlyBPSD)$_4$] complex. As would be expected, the 0:8 solution contains 100% of the [Cu$_4$(GlyBPSD)$_4$] complex.

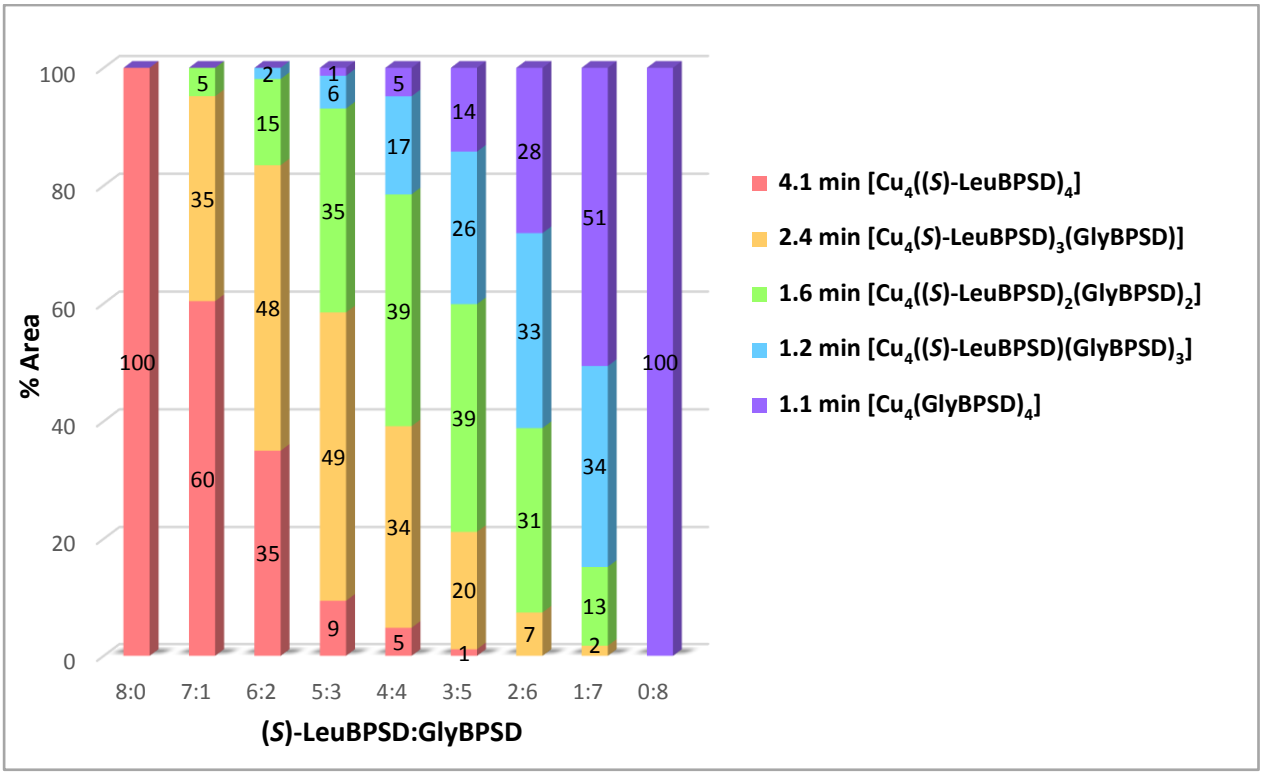

Figure 5.15. The relative composition of each solution of varying (S)-LeuBPSD:GlyBPSD ratio with a constant concentration of Cu^{II}, as analysed by HPLC.

Comparison of the compositions of each solution in this series appears to suggest that the [Cu_4((*S*)-LeuBPSD)$_4$] helicate forms with greater dominance than that of the [Cu_4(GlyBPSD)$_4$] mesocate. The incorporation of the (*S*)-LeuBPSD ligand into the [Cu_4(GlyBPSD)$_4$] cage also appears to occur more readily than the incorporation of GlyBPSD into the [Cu_4((*S*)-LeuBPSD)$_4$] cages, shown by the greater proportions of the [Cu_4((*S*)-LeuBPSD)$_3$(GlyBPSD)] complex in comparison to the [Cu_4((*S*)-LeuBPSD)(GlyBPSD)$_3$] complex.

The proportion of each complex in solution was calculated from the HPLC data, and then compared with the CD results, in order to determine which of the mixed ligand cage complexes are helicates. Based on the total amount of ligand and Cu^{II} added to the reactions, each solution should have had a concentration of 19.2 mmol/L of cage. Therefore it was assumed that if all the peaks in the HPLC account for this total concentration, the relative areas of the HPLC peaks may be used to calculate the concentration of each cage complex in solution, Table 5.1.

Based on the maximum CD signal of the 8:0 (*S*)-LeuBPSD:GlyBPSD ligand solution, which contained purely the [Cu_4((*S*)-LeuBPSD)$_4$] helicate, and assuming a linear relationship between CD signal and helicate concentration, the helicity of the mixed ligand cages may be determined by the predicted CD signal based on concentrations obtained from HPLC. The CD signal was predicted based on the concentrations of each complex from HPLC assuming that all but the [Cu_4(GlyBPSD)$_4$] cage complex formed helicate cages, and these CD signals may be compared with the experimental values, Figure 5.16.

Table 5.1. The concentration (mmol/L) of each cage complex as calculated by the HPLC results, and the predicted CD signal for each solution if all but the [Cu_4(GlyBPSD)$_4$] complexes are helicate cages.

	Cage concentration based on HPLC (mmol/L)							
(*S*)-LeuBPSD:GlyBPSD	**4:0**	**3:1**	**2:2**	**1:3**	**0:4**	**Total mesocate**	**Total helicate**	**Predicted CD signal**
8:0	19.2	0	0	0	0	0	19.2	71
7:1	11.6	6.7	0.9	0	0	0	19.2	71
6:2	6.7	9.3	2.8	0.4	0	0	19.2	71
5:3	1.8	9.4	6.6	1.1	0.3	0.3	18.9	70.1
4:4	0.9	6.6	7.6	3.2	0.9	0.9	18.3	67.6
3:5	0.2	3.9	7.4	5.0	2.7	2.7	16.5	60.9
2:6	0	1.4	6.0	6.4	5.4	5.4	13.8	51.1
1:7	0	0.3	2.6	6.6	9.7	9.7	9.5	35.0
0:8	0	0	0	0	19.2	19.2	0	0

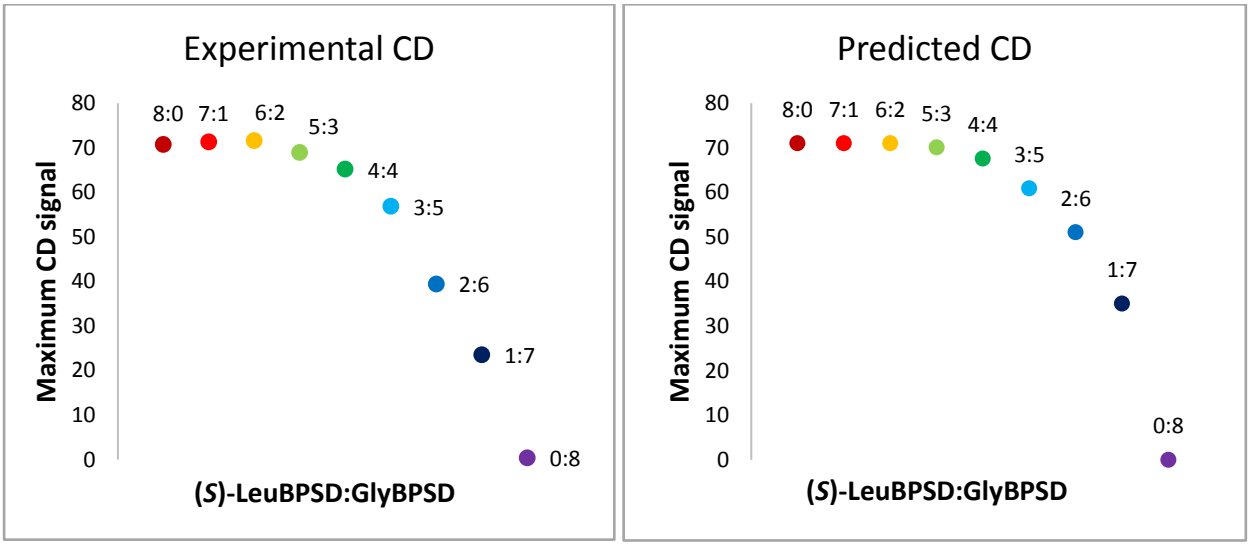

Figure 5.16. The experimental (left) and predicted (right) maximum CD signal of the reaction of solutions of varied (S)-LeuBPSD:GlyBPSD ratios.

Based on the comparison between the experimental CD results and the predicted CD signal from the HPLC results, it appears that the assumption that all the mixed ligand cages are quadruple stranded helicates is correct. It appears that it is only the [Cu_4(GlyBPSD)$_4$] cage complex which is a mesocate, and only one (*S*)-LeuBPSD ligand per [Cu_4(BPSD)$_4$] cage is enough to induce the chirality of the cage, as the CD signals are consistent with the [Cu_4((*S*)-LeuBPSD)$_4$], [Cu_4((*S*)-LeuBPSD)$_3$(GlyBPSD)], [Cu_4((*S*)-LeuBPSD)$_2$(GlyBPSD)$_2$] and [Cu_4((*S*)-LeuBPSD)(GlyBPSD)$_3$] cages all being helicates. A quadruple stranded helicate is therefore a very favourable conformation for these ligand systems.

The total concentration of each ligand in solution was calculated based on the mixed cage compositions from the HPLC results. These calculations were able to confirm that the assignment of the peaks of the mixed ligand systems in the HPLC was correct. There is a small discrepancy between the calculated total concentration of each ligand based on the HPLC data and the concentration of each ligand put into the reaction, with the calculated concentration of (*S*)-LeuBPSD being slightly higher and the concentration of GlyBPSD being slightly lower than the concentration of the ligands put into each reaction mixture, Table 5.2.

Table 5.2. The concentration of (S)-LeuBPSD and GlyBPSD ligands in each reaction mixture, based on the HPLC results and the reaction concentration, and the difference between them. All concentrations shown in mmol/L.

(*S*)-LeuBPSD: GlyBPSD	**Calculated concentration**		**Reaction concentration**		**Concentration difference (reaction – calculated)**	
	LeuBPSD	**GlyBPSD**	**LeuBPSD**	**GlyBPSD**	**LeuBPSD**	**GlyBPSD**
8:0	76.8	0	76.8	0	0.0	0.0
7:1	68.3	8.5	67.2	9.6	-1.1	1.1
6:2	60.8	16.0	57.6	19.2	-3.2	3.2
5:3	49.8	27.0	48.0	28.8	-1.8	1.8
4:4	41.8	35.0	38.4	38.4	-3.4	3.4
3:5	32.2	44.6	28.8	48.0	-3.4	3.4
2:6	22.7	54.1	19.2	57.6	-3.5	3.5
1:7	12.7	64.1	9.6	67.2	-3.1	3.1
0:8	0	76.8	0	76.8	0.0	0.0

The discrepancy between concentration of ligands based on the HPLC results and the reaction mixture is consistent with the higher proportions observed in HPLC of the [Cu_4((*S*)-LeuBPSD)$_4$] and [Cu_4((*S*)-

LeuBPSD)$_3$(GlyBPSD)] cages in comparison to the [Cu$_4$((*S*)-LeuBPSD)(GlyBPSD)$_3$] and [Cu(GlyBPSD)$_4$] cages. It may be that the GlyBPSD ligands are less readily incorporated into [Cu$_4$(BPSD)$_4$] complexes, and will stay in solution as free ligands instead of coordinating to the Cu^{II} to form a cage complex. As the free ligands were not observed in the HPLC, even when blank solutions of H$_2$GlyBPSD and (*S*)-H$_2$LeuBPSD with no metal were analysed, it is possible that there is free H$_2$GlyBPSD in the reaction solutions which is not observed by the HPLC, and also not observed by CD.

These results suggest that a [Cu$_4$(BPSD)$_4$] homochiral quadruple stranded helicate may be formed with only one chiral (*S*)-LeuBPSD ligand and three achiral GlyBPSD ligands, showing that a helicate is a robust supramolecular species for this ligand system. Helicates may also be formed with (*S*)-LeuBPSD:GlyBPSD ratios of 2:2 and 3:1, in the form of [Cu$_4$((*S*)-LeuBPSD)$_2$(GlyBPSD)$_2$] and [Cu$_4$((*S*)-LeuBPSD)$_3$(GlyBPSD$_3$] complexes. The tendency for a helicate to be formed with a small amount of chiral ligand was demonstrated through a combination of circular dichroism, HPLC and mass spectrometry in order to analyse the composition of each of the mixed ligand reactions and assign them to the formula of the supramolecular cage complex which was formed.

5.4 A larger helicate complex utilising a larger ligand

Due to the relatively small void volume in chiral cages **Λ,Λ-** and **Δ,Δ-5.1**, attempts were made to synthesise a longer chiral diimide ligand with the necessary angle to produce large chiral cage complexes in order to achieve chiral separation or catalysis within them. As outlined in Section 5.1.5, homochiral quadruple helicate cages have been prepared utilising amino acid substituted bicyclooctene diimide ligands, as the bicyclooctene group provides the necessary bend in the ligand to form a bi-paddlewheel cage complex.

5.4.1 Synthesis of larger diimide ligand

The compound chosen to be a longer analogue of the BSPD ligands, was the (*S*)-leucine substituted 9,10-dimethyl-9,10-dihydro-9,10-ethanoanthracene-2,3,6,7-diimide (EADI) molecule, Figure 5.17.

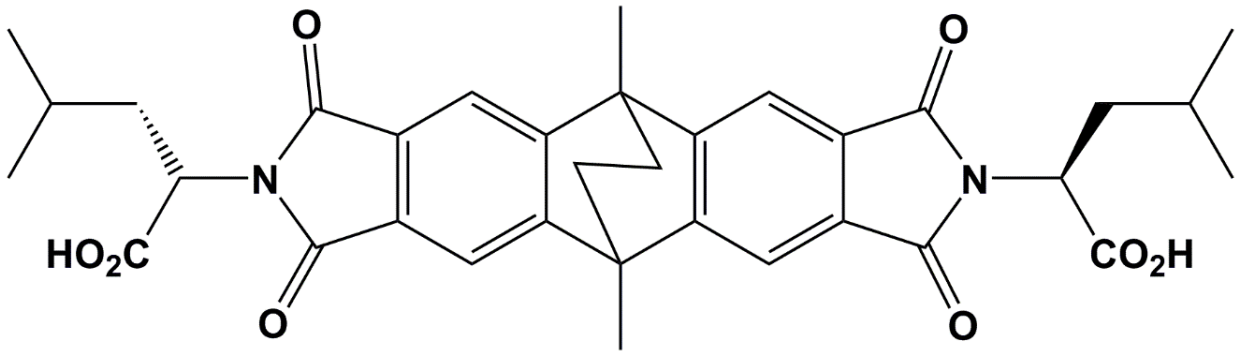

Figure 5.17. (S)-H_2LeuEADI, with a similar bend in the core as the bicyclooctene ligands which have been shown to form quadruple stranded helicates with copper paddlewheels.

9,10-Dimethyl-9,10-ethanoanthracene-2,3,6,7-tetracarboxylic acid was synthesised in three steps by a literature procedure, Figure 5.18.[476] The first step was a Grignard reaction with 2,5-hexanedione and two equivalents of 4-bromo-1,2-dimethylbenzene. The second step was a cyclisation reaction using aluminium trichloride in order to form the 9,10-dimethyl-9,10-ethanoanthracene core. The four terminal methyl groups were then oxidised using potassium permanganate in a pyridine and water mixture in order to form 9,10-dimethyl-9,10-ethanoanthracene-2,3,6,7-tetracarboxylic acid. The tetra-acid was reacted with (*S*)-leucine in acetic acid under reflux for four nights, and the H_2LeuEADI product was isolated as a pale yellow solid by pouring the reaction mixture into ice and recovered by vacuum filtration. The synthesis of H_2LeuEADI was confirmed by ^{1}H-NMR, ^{13}C-NMR, mass spectrometry, infrared spectroscopy and microanalysis.

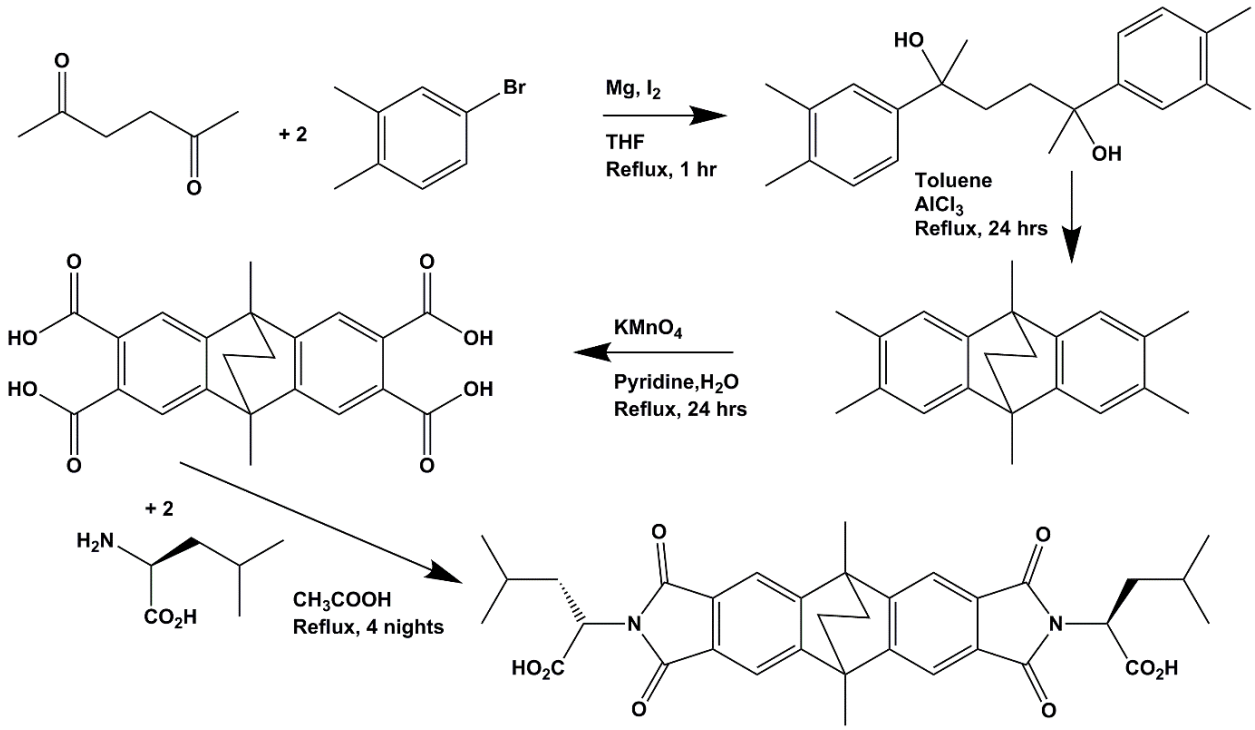

Figure 5.18. The synthetic scheme for the synthesis of H_2LeuEADI.

5.4.2 Quadruple stranded helicate with EADI ligand

As the leucine analogues of the BPSD ligands had been so successful in the synthesis of quadruple stranded helicate cages, the (*S*)-LeuEADI ligand was utilised for the attempted synthesis of larger homochiral helicate cages. Λ,Λ-[Cu_4((*S*)-LeuEADI)$_4$(OH_2)$_3$(DMF)]·3.5DMF·9.5H_2O, [**5.4**(DMF)(OH_2)$_3$]·3.5DMF·9.5H_2O, a homochiral quadruple stranded helicate cage, was successfully synthesised from (*S*)-H_2LeuEADI and Cu(OAc)$_4$ in DMF. The structure of **Λ,Λ-5.4** is similar to that of **5.1** in that it involves two copper paddlewheels which are bridged by four ligands into a cage complex, Figure 5.19. The ligands once again twist ~ 90° between the metal centres to generate the helicity of the cage, Figure 5.19. The bulky isobutyl (*S*)-leucine side chains of the ligand force the ligands around the metal centre to adopt the same propeller motif as **Λ,Λ-5.1**.

The structure of **Λ,Λ-5.4** is modelled in the space group $C222_1$. The asymmetric unit contains one copper paddlewheel, a complete (*S*)-LeuEADI ligand and two half (*S*)-LeuEADI ligands, in addition to coordinated solvent molecules. Both external Cu^{II} coordination sites are occupied by aqua ligands, and the internal sites are occupied by a disordered DMF and aqua ligand (fixed occupancy 50:50) sharing the coordinated oxygen

atom. The cage has a Cu···Cu distance of 9.225(3) Å, a similar distance to the mesocate cages of **5.2** and **5.3**, and longer than the helicate cages of **5.1** (*cf* 7.2 Å). The internal cavity of the cages of **Λ,Λ-5.4** is ~ 380 $Å^3$ (in the absence of coordinated solvent), a 25% increase in void volume compared to **5.1**. The core of the EADI ligand has a slightly different shape to the BPSD ligand, with mean plane angles of 121.315(8) and 121.459(12)°, as measured by the angle between the planes of the bicyclooctane group, compared to the C-S-C angle of ~100 – 109° in the BPSD ligands.

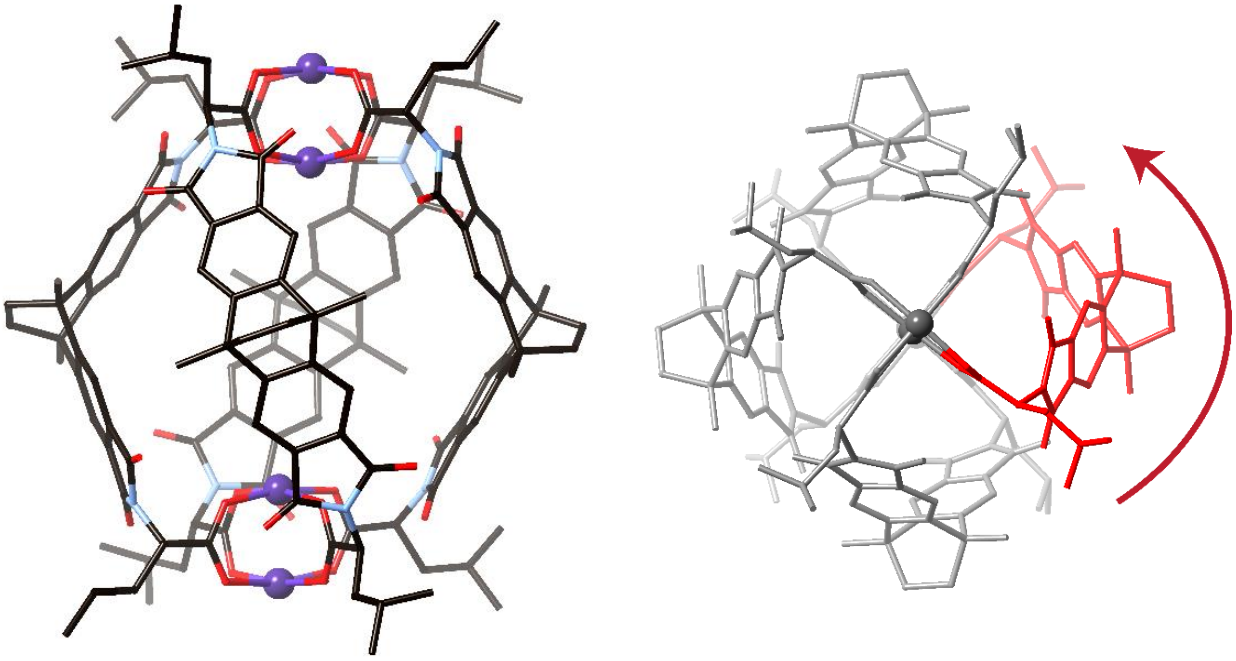

*Figure 5.19. The structure of **Λ,Λ-5.4** shown as a stick model (left) and looking down the Cu···Cu axis to show the twist of the ligands which generate the helicity of the cage (right). Hydrogen atoms and coordinated solvent have been omitted for clarity.*

The solution stability of **Λ,Λ-5.4** and helicity of cages were confirmed by mass spectrometry and circular dichroism, Figure 5.20. The circular dichroism of **Λ,Λ-5.4** showed a similar Cotton effect as that observed for **Λ,Λ-5.1**, which is to be expected as they are both helicate cages of Λ,Λ confirmation. The mass spectroscopy of an acetonitrile solution of **5.4** showed ions of $[\mathbf{5.4}+H]^+$ and $[\mathbf{5.4}(OH_2)(MeCN)+H]^+$, confirming that the cages persist in solution, and that there is some exchange of the coordinated solvent in solution or during the ionisation of the complexes.

Unfortunately due to the multi-step synthesis of the ligand, these cages were not able to be investigated for enantioselective catalysis and separation properties. The synthesis of **Λ,Λ-5.4** showed that homochiral quadruple stranded helicate cages with amino acids substituted bent diimide ligands are a favourable product with copper paddlewheel motifs.

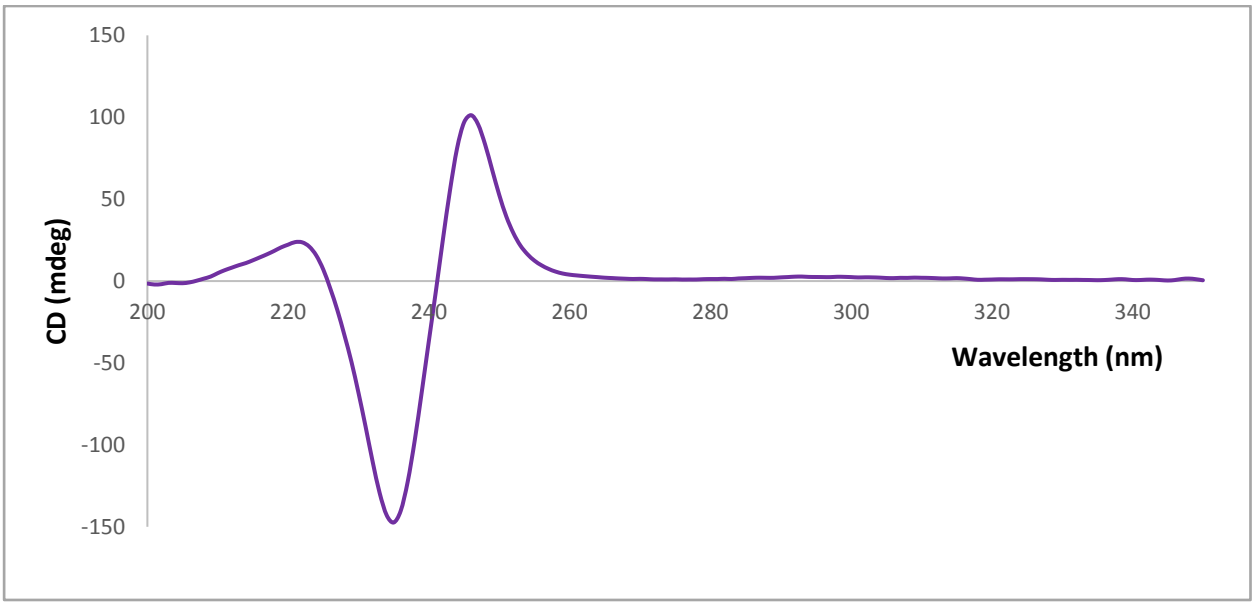

*Figure 5.20. The circular dichroism spectrum of **Λ,Λ-5.4** in acetonitrile at 11 μmol/L.*

5.5 Helicate cages with rhodium metal centres

The chiral cages **5.1** and **5.4** presented an opportunity for the investigation into their potential applications in enantioselective catalysis. However due to the paramagnetic copper paddlewheels in the cages, it was not possible to monitor chiral guest encapsulation or catalysis within or around the cages through solution ^{1}H-NMR spectroscopy studies. As outlined in Section 5.1, there are some examples of chiral copper complexes which have achieved enantioselective catalysis and separation.[442] However the use of other metal centres, such as rhodium, in complexes involving chiral paddlewheels for enantioselective catalysis, has been explored to a greater extent.[458, 462, 496, 497] Rhodium has the advantage of being diamagnetic, enabling ^{1}H-NMR studies to be conducted, and forms more stable complexes than copper, increasing the stability of the chiral cage complexes that could be synthesised.

5.5.1 Homochiral helicate cage with Rhodium paddlewheels

Due to the slow kinetics of Rh^{II}, helicate cages with Rh^{II} could not be synthesised by the same methods as **5.1 – 5.4**. However a synthesis was developed in which $Rh_2(OAc)_4$ was heated with (*S*)-H_2LeuBPSD in chlorobenzene and crystallised from chloroform by vapour diffusion with methanol. The crystals formed had the formula $[Rh_4((S)\text{-}H_2LeuBPSD)_4(OH_2)_4][Rh_4((S)\text{-}H_2LeuBPSD)_4(OH_2)_2(MeOH)_2]\cdot 4MeOH\cdot 10H_2O$, $[\mathbf{5.5}(solv.)_4]\cdot 4MeOH\cdot 10H_2O$. The structure of **5.5** is analogous to that of **Λ,Λ-5.1**, with two paddlewheels bridged by four ligands, in which the chirality of the ligands forces a propeller motif around the paddlewheel and the twist of the ligands form a quadruple stranded helicate cage. In the same manner as **Λ,Λ-5.1**, the structure of **5.5** is a helicate cage of Λ,Λ-configuration.

The structure of **5.5** is modelled in the chiral space group *C*2, and the asymmetric unit includes two $[Rh_4((S)\text{-}H_2LeuBPSD)_4(solv.)_4]$ complexes, Figure 5.21. The presence of two crystallographically unique cages of **5.5** is due to slight structural differences between them. In the helicate cages of **5.1** and **5.4** the paddlewheels had a negligible offset from each other when viewed down the Cu···Cu axis, with the ligands twisted by 90°, generating the helicity of the cages. In the case of **5.5**, the ligands once again twist between the paddlewheels to form a helicate, however the angle of the twist in the (*S*)-LeuBPSD ligands are different for the two crystallographically unique cages. In the cage involving Rh(1)-Rh(4), cage **5.5a**, the ligands twist at an average angle of 58.6° between the paddlewheels. In the cage with Rh(5)-Rh(8), cage **5.5b**, the ligands have an average twist angle of 68.5°, Figure 5.21. The difference in the twist of the ligand leads to a difference in the internal Rh-Rh distances in **5.5a** and **5.5b** which are 9.7751(17) Å and 9.1051(16), respectively. As was the case with the comparison between the copper paddlewheel helicates and mesocates, **5.1** – **5.4** the smaller twist angle leads to a longer internal M···M distance.

The difference in the twist of the ligands in the two crystallographically unique cages of structure of **5.5** is quite fascinating, as it shows that these cages are somewhat flexible. The difference in the twist of the ligands in **5.5** compared to the twist in the BPSD ligands in **5.1**, also shows that these ligands are flexible. It is worth noting that it is the solid state structure of the cages of **5.1** and **5.5** which has been described

herein, however given these results it is highly probably that the cages exist with a range of twist angles when in solution.

The difference in the twist of the ligands leads to the two crystallographically unique cages having different internal void volumes. The cage of **5.5a** is larger due to the smaller twist angle of the ligands, with a void volume of 611 Å^3, and **5.5b** is smaller, due to the greater twist in the ligands, leading to a smaller void volume of 501 Å^3.

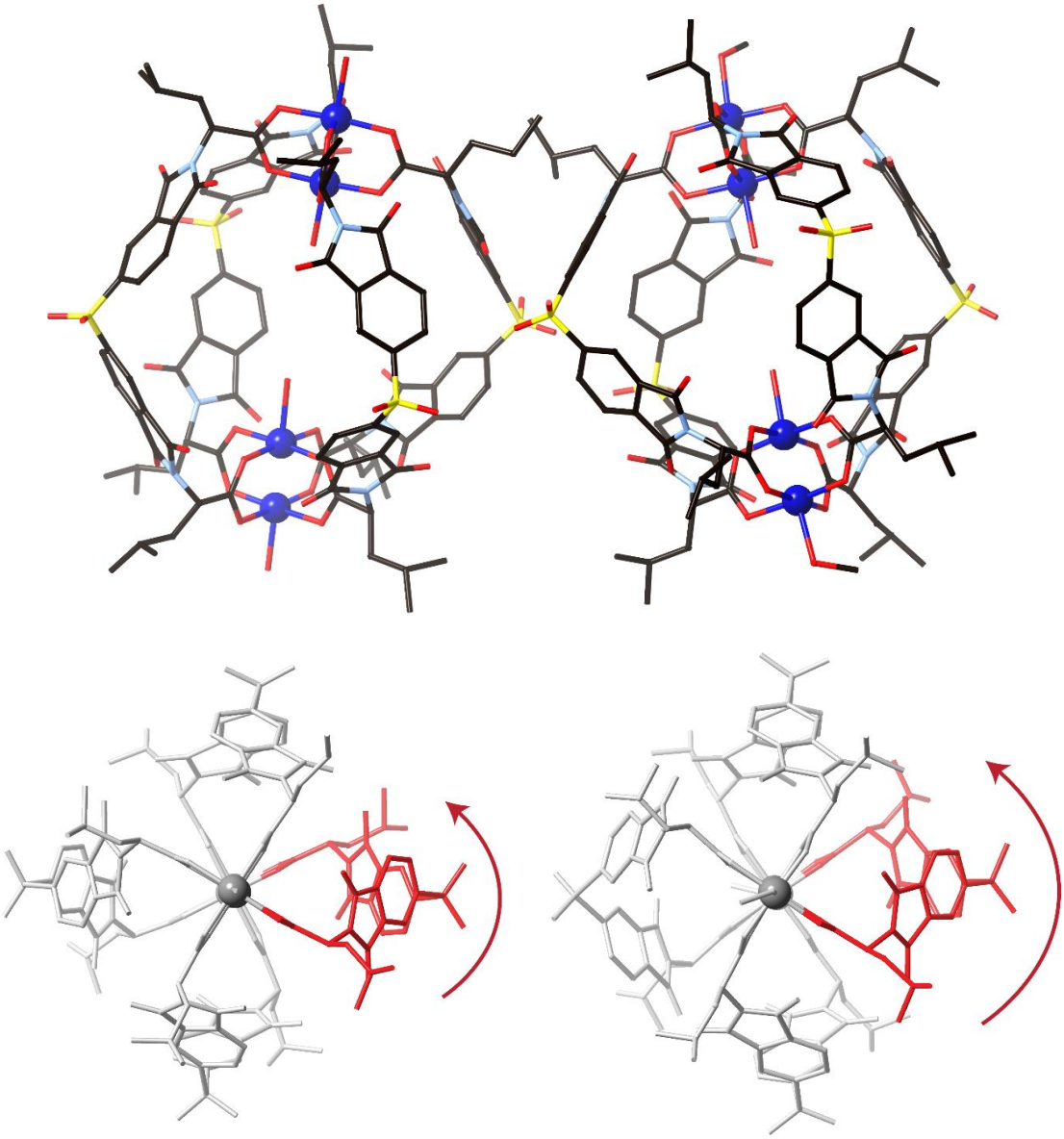

*Figure 5.21. The two crystallographically unique [Rh$_4$((S)-LeuBPSD)$_4$(solv.)$_4$] cages **5.5a** (left) and **5.5b** (right), showing the difference in the angle at which the ligands twist between paddlewheels. Hydrogen atoms are omitted for clarity.*

The two unique cages of **5.5** have different coordinated solvent molecules. All the apical Rh^{II} positions in **5.5a** are occupied by aqua ligands. The internal apical Rh^{II} positions in **5.5b** are occupied by aqua ligands, and the external positions are occupied by methanol molecules. As the crystals were grown from chloroform, there are also five chloroform molecules which could be modelled in the structure, two of which are modelled at 50% occupancy. The helicity of the **5.5** cages was also confirmed by circular dichroism, Figure 5.22. The CD of **5.5** showed similar cotton effects to that of Λ,Λ-**5.1** and **5.4**, as would be expected as they are all helicates of Λ,Λ-configuration.

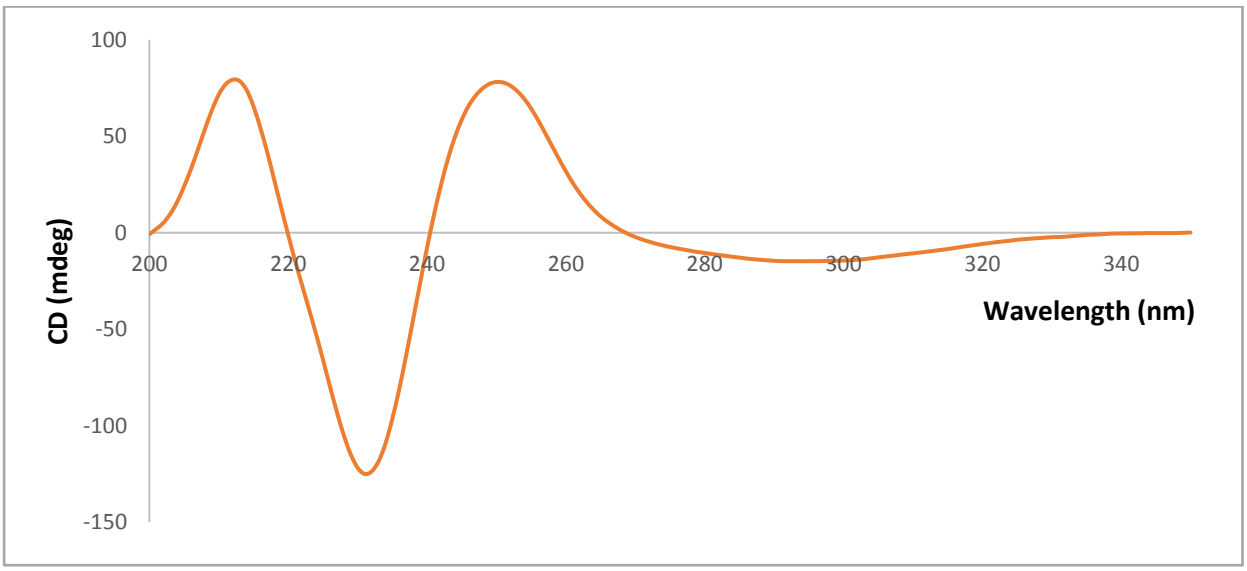

*Figure 5.22. Circular dichroism spectrum of **5.5** in acetonitrile.*

The smaller angle at which the ligands twist in the structure of **5.5** in comparison to **5.1** leads to larger windows between ligands. The apparent flexibility in the cages means that they may exist with the ligands twisting at a range of angles. A smaller twist angle in the ligand leads to cages with larger windows, making guest exchange more likely. The flexibility of the cages and the presence of Rh^{II} metal centres in **5.5** led to this material being investigated for enantioselective catalytic properties.

5.5.2 Enantioselective catalysis with rhodium(II) helicate cages

Cyclopropanation reactions have been used to probe the enantioselective catalytic properties of chiral rhodium(II) paddlewheel complexes.[454] The $[Rh_2L_4]$ complex in which the ligand is an amino acid substituted phthalimide molecule, which is effectively half of the cage of **5.5**, have been shown to be an

effective catalyst in these reactions.[455, 470, 498] One such example is the [Rh_2(*S*-PTTL)$_4$] complex (L= (*S*)-tert-leucine substituted phthalimide).[470] The cyclopropanation reactions of α-alkyldiazo compounds with styrene catalysed by [Rh_2(*S*-PTTL)$_4$] were shown to have improved diastereoselective ratio (dr) and enantioselectivity (ee) with increasing steric bulk of the α-alky substituent, Figure 5.23.

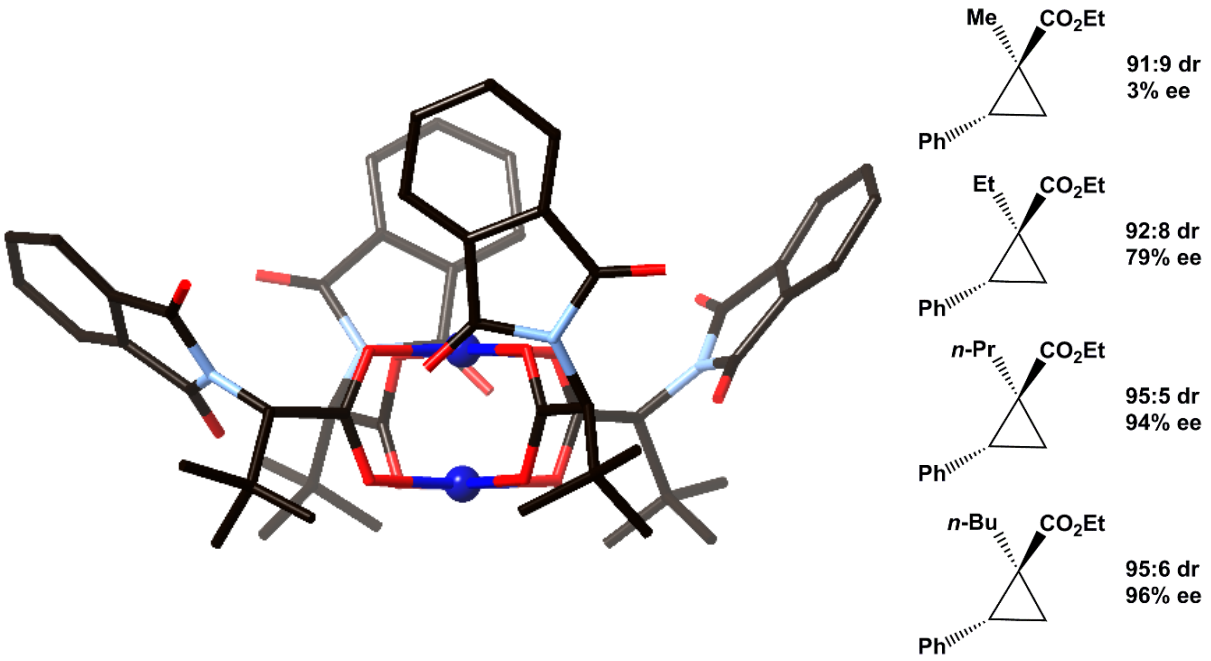

Figure 5.23. The [Rh_2(S-PTTL)$_4$] complex, which is effectively half of the cage of **5.5** *(left). All hydrogen atoms and coordination solvent molecules are omitted for clarity. The enantioselective catalysis of α-alkyldiazo compounds with styrene by [Rh_2(S-PTTL)$_4$], showing that increasing steric bulk of the α-alkyl substituent leads to higher dr and % ee (right).*

The enantioselective catalysis properties of **5.5** were investigated using the cyclopropanation reaction of ethyl diazoacetate (EDA) and styrene, as the product has two chiral centres and the reaction will not proceed in the absence of a catalyst, Figure 5.24. The presence of two stereocentres in the product means that the diastereoselectivity as well as the enantioselectivity of each could be determined. The four products formed were *cis*- and *trans*-ethyl-2-phenylcyclopropanecarboxylate. The position bearing the ester functionality is designated as position 1 on the cyclopropane ring, therefore the two *cis* products are the 1*R*,2*S* and 1*S*,2*R* isomers, and the *trans* products are the 1*S*,2*S* and 1*R*,2*R* isomers.

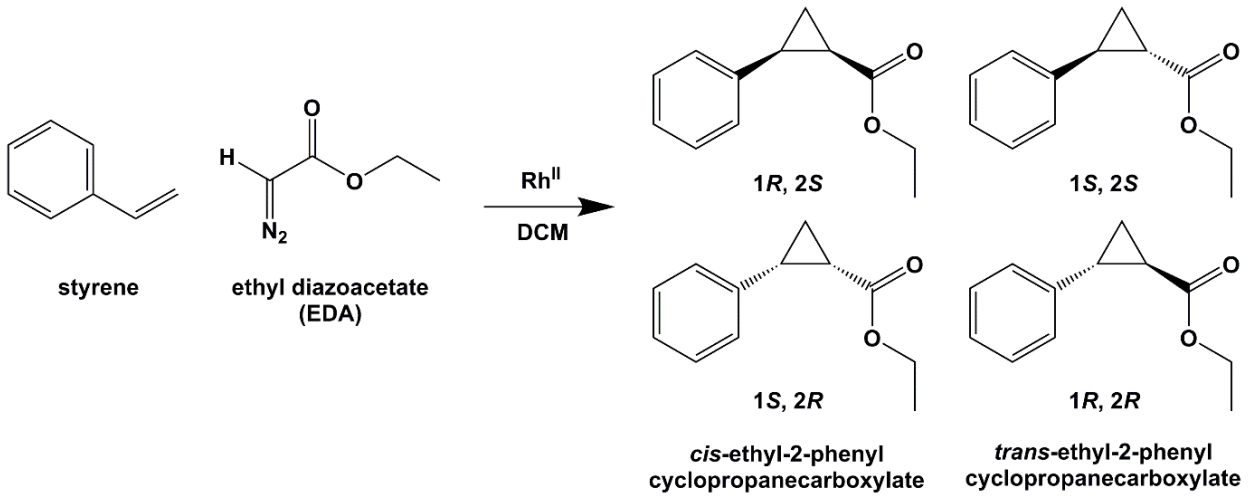

Figure 5.24. Cyclopropanation reaction of styrene with ethyl diazoacetate which are catalysed by rhodium paddlewheel complexes.

To act as a comparison to the catalytic activity of **5.5**, two other rhodium(II) paddlewheel complexes were used to catalyse the cyclopropanation reaction. $[Rh_2(CH_3COO)_4]$, which is an achiral Rh^{II} paddlewheel was used as a comparison that should not show any diastereoselectivity or enantioselectivity. The rhodium(II) paddlewheel substituted with four (*S*)-leucine phthalimide ligands (LeuPI), $[Rh_2(LeuPI)_4]$, was also used as it is a "bowl-shaped" complex which is half of the helicate cage of **5.5**. There is some disagreement in the literature in regards to the conformation of $[Rh_2L_4]$ complexes in solution. Crystal structures of the complexes have shown the ligands to be "all-up", forming a "bowl-shaped" complex.[469, 470] However it has also been postulated that in solution is it possible that the complexes may be a mixture of the four different possible symmetries, Figure 5.25.[499] In the case of **5.5**, the cage is essentially two "bowl-shaped" complexes fused together, and therefore all of the rhodium paddlewheels are locked in the "all-up" conformation. The enantioselective catalytic properties of **5.5** may therefore be better rationalised based on the known conformation of the chiral paddlewheels.

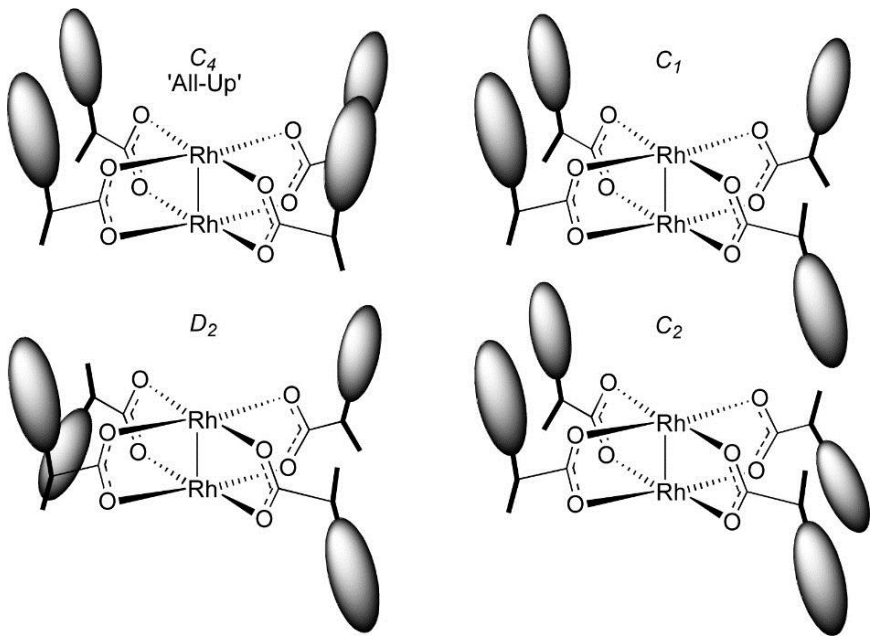

Figure 5.25. The four possible conformations of a [Rh₂L₄] complex. Reprinted with permission from V. N. G. Lindsay, W. Lin and A. B. Charette, J. Am. Chem. Soc., 2009, 131, 16383-16385. Copyright 2009 American Chemical Society.

The cyclopropanation reactions were undertaken by slow addition of a DCM solution of styrene to a DCM solution of the rhodium catalyst and EDA. The catalyst was used in a loading of 0.8% of Rh^{II} metal centres. The removal of the DCM from the reaction mixture left the products, unreacted starting materials, and the catalyst. The Rh^{II} catalysts could not be recovered after the reaction, is it appeared that they were soluble in the products and starting materials. The reaction mixture was analysed by ^{1}H-NMR spectroscopy to determine the % conversion of the reaction, and by GC to determine the diastereomeric ratio (dr) and the % enantioselectivity (% ee).

The ^{1}H-NMR spectra of the reaction solutions after removal of the DCM showed that the reactions had not gone to completion. Comparison of the integration of the signals of the products and starting materials was used to calculate the % conversion of the reaction. The cyclopropantion reaction catalysed by **5.5** showed 22% conversion to the products. The reactions catalysed by $[Rh_2(CH_3COO)_4]$ and $[Rh_2(LeuPI)_4]$ showed 28 and 18% conversion, respectively. Analysis of the products by GC was used to determine the diastereoselectivity of the reaction, Table 5.3. Analysis was conducted in collaboration with the Marriott group at Monash University. The catalysis with **5.5** gave the *cis* and *trans* products in a ratio of 49:51.

Interestingly, the reactions catalysed by [$Rh_2(CH_3COO)_4$] and [$Rh_2(LeuPI)_4$] gave the *cis* and *trans* products in ratios of 37:63 and 53:47, respectively.

The % ee of for the *cis* and *trans* products was also analysed for each reaction, Table 5.3. The reaction catalysed by **5.5** showed a 8% ee of the *cis* product, with the 1*S*,2*R* enantiomer in excess, and a 13% ee for the *trans* product, with the 1*S*,2*S* enantiomer in excess. The reaction catalysed by [$Rh_2(CH_3COO)_4$] shows a lower % ee for both the *cis* and *trans* products, Table 5.3. The reaction catalysed by [$Rh_2(LeuPI)_4$] shows similar results to the reaction catalysed by **5.5**, with a 2% ee of the cis product, again with the 1*S*,2*R* enantiomer in excess and a 15% ee of the trans product, with the 1*S*,2*S* diastereomer in excess.

Comparison of the [$Rh_2(LeuPI)_4$] results with that of the previously reported [Rh_2(*S*-PTTL)$_4$] complex, further demonstrates that an increase in steric bulk will lead to improved dr and %ee. The α-alkyldiazo starting material in this case, EDA, is less sterically demanding than the previously reported α-alkyldiazo compounds and leads to an even lower dr and %ee.

Table 5.3. Enantioselective catalysis results using Rh^{II} paddlewheel of the cyclopropanation reaction of styrene and EDA.

Catalyst	**Diasteromeric ratio *cis* : *trans***	**cis % ee**	**Excess enantiomer**	**trans % ee**	**Excess enantiomer**
5.5	49:51	8	1*S*,2*R*	13	1*S*,2*S*
[$Rh_2(CH_3COO)_4$]	37:63	2	1*R*,2*S*	8	1*S*,2*S*
[$Rh_2(LeuPI)_4$]	53:47	2	1*S*,2*R*	15	1*S*,2*S*

It has been previously established that catalysing cyclopropanation reactions with [$Rh_2(CH_3COO)_4$] would lead to the formation of the *trans* product preferentially, due to how the starting materials form the metallocarbene transition state around the paddlewheel.[462, 500] It has also been observed that increase in steric bulk of the ligands around the rhodium paddlewheel correlates with a decrease in diastereoselectivity,[471] explaining why catalysis with [$Rh_2(CH_3COO)_4$] gave a dr of 37:63 with the *trans* product in preference, while **5.5** and [$Rh_2(LeuPI)_4$] give a dr of 49:51 and 53:47, respectively.

The chirality of **5.5** and [$Rh_2(LeuPI)_4$] appears to lead to some enantiomeric enrichment of each of the *cis* and *trans* products, in contrast to the achiral [$Rh_2(CH_3COO)_4$] complex. The observed enantioselectivity of

the catalysts is very low however, with maximum ee of 13 and 15% for the *trans* product formed by catalysis with **5.5** and [$Rh_2(LeuPI)_4$], respectively. Based on these results, and previous work with other rhodium paddlewheel catalysts, there are multiple alterations to the reaction that may be attempted in order to improve the enantioselectivity of this reaction when catalysed by **5.5** or analogous [Rh_4L_4] chiral cages. The solvent in which the reaction is carried out may be changed, as similar reactions have shown improved enantioselectivity when the solvent was changed to hexane or acetone. [23, 53] The conversion may also be improved by increasing the catalyst loading or reaction time. It has previously been reported that increasing the steric bulk of the ligands can lead to a drecease in the diastereoselectivity of the reaction, therefore the use of a less bulky amino acid side chain, such as a methyl group in the case of (*S*)-alanine, may increase the diastereomeric ratio of the products. The substituents of the azide and ethylene starting materials have also been shown to have a large impact on the enantioselectivity of the reaction, therefore the use of different starting materials may also lead to higher enantioselectivity of the reaction.[470] It is clear that the enantioselective catalytic properties of **5.5** are quite poor for the reaction which was studied. However **5.5** does show some enantioselective catalytic activity, and therefore warrants further study in order to develop the optimum reaction conditions and substrates to achieve high diastereoselectivity and enantioselectivity. The enantioselective catalytic properties of **5.5** could also be investigated with other reactions that have been shown to be catalysed by rhodium paddlewheels, such as intramolecular C-H insertion, amination and 2,3-sigmatropic rearrangement.

5.6 Conclusion

The series of helicate and mesocate cages discussed herein show remarkable control of helicity through the control of the chirality of the ligands. Each ligand contained two amino acid groups substituted onto a diimide core group, with a sufficient bend in the core of the ligand to allow the ligands to form an [M_4L_4] cage complex with copper paddlewheel nodes. Chirality of the ligand around the coordinating carboxylate groups forced the Cu^{II} paddlewheels into a propeller motif, and the ligands into forming a helicate cage complex. The removal of chirality of the ligand led to the removal of the chirality of the cage. A change in handedness of the LeuBPSD ligand was observed to change the handedness of the helicate that was formed.

These cages showed narcissistic self-selection, as the reaction of a racemic mixture of (*S*)-LeuBPSD and (*R*)-LeuBPSD with Cu^{II} formed a racemic mixture of helicate cages, each containing ligands of like handedness. It was also shown through a "sergeants and soldiers" experiment, in which chiral ligands were replaced with achiral ligands, that only one chiral ligand per cage was required in order to force the cage into a helicate conformation. A quadruple stranded helicate is therefore shown to be a robust supramolecular species for the copper paddlewheel and BPSD ligands system.

A different amino acid substituted diimide ligand with a bent core was also investigated. The reaction of the (*S*)-LeuEADI ligand with Cu^{II} formed an analogous quadruple stranded helicate cage. [Cu_4((*S*)-LeuEADI)$_4$(solv.)$_4$] demonstrated that the helicate cages are somewhat flexible, as the core of the BPSD ligand has a bend of 101-105° compared to the EADI ligand with a bend of ~121°. A [Cu_4((*S*)-LeuEADI)$_4$(solv.)$_4$] quadruple stranded helicate showed the reproducibility of copper paddlewheel based helicate cages with amino acid substituted diimide ligands with a bent core.

A quadruple stranded helicate cage with (*S*)-LeuBPSD was also formed with Rh^{II} paddlewheels, in order to form a catalytically active chiral cage complex. The [Rh_4((*S*)-LeuBPSD)$_4$(solv.)$_4$] helicate cage complex showed a small degree of enantioselective catalytic activity in the cyclopropantion of styrene and ethyl diazoacetate. The enantioselective catalytic properties of **5.5** warrants further study in order to find the optimum reaction conditions to achieve high enantioselectivity.

The series of cages reported herein form with two different ligand core groups, BPSD and EADI, and two different metal nodes, Cu^{II} and Rh^{II} paddlewheels, demonstrating the reproducibility of forming dinuclear quadruple stranded helicate cages with amino acid substituted diimide ligands with a bent core.

Chapter 6: A chiral octahedral cage complex

6.1 Introduction

Polyhedral coordination cage complexes have attracted research interest due to their aesthetically pleasing structures, the increased understanding which they provide on the control of self-assembly of elaborate structures and their host-guest chemistry with small molecules or anions.[208, 501-505] The work on supramolecular coordination cage complexes predominantly features the synthesis and properties of tetrahedral cages. The design and synthesis of higher order polyhedral cages is more challenging, however impetus into their research is provided by their larger and more complex void volumes. Increase in the order of polyhedra may be brought about by a change in the bend of the ligand, as illustrated by the Fujita group when they synthesised a series of coordination polyhedra using square planar Pd^{II} centres and bent dipyridyl ligands.[180] Increase in the bend angle of the ligand led to the increase in the order of the polyhedra, leading to an M_6L_{12} cube, $M_{12}L_{24}$ cuboctahedron, $M_{24}L_{48}$ rhombicuboctahedron and $M_{30}L_{60}$ icosidodecahedron.[180, 506] Coordination cage complexes are of interest because they have been utilised for applications in catalysis, drug delivery, magnetism, luminescence and stabilising reactive species. [256, 257, 261, 264, 265, 267, 268, 273]

6.1.1 Chiral higher order polyhedral cages

The design and synthesis of chiral higher order polyhedral cage complexes has also attracted attention due to their possible applications in chiral sensing, catalysis and separations (see Chapter 1).[507-510] Chiral supramolecular cages may be designed with chiral or achiral ligands via multiple methods, including incorporation of multiple metals of different geometry or combination of different ligands with varied geometry.[201] A variety of synthetic approaches has led to the synthesis of multiple types of higher order polyhedral coordination cages, including M_6L_9 trigonal prisms,[511] M_8L_6 cube,[512] M_8L_{12} cube,[222, 513, 514] $M_{10}L_{15}$ pentagonal prism,[515, 516] $M_{12}L_{12}$ icosahedron,[517] $M_{12}L_{18}$ hexagonal prism,[293, 518] $M_{12}L_{12}L_4$ mixed ligand cuboctahedra,[519] truncated tetrahedra,[520-522] and stellated systems.[523, 524]

6.1.2 Chiral octahedral cages

The synthesis of octahedral cage complexes has been reported less than other higher order polyhedral cage complexes, and very few chiral octahedral cage complexes have been reported. Octahedral cage complexes have only been reported with metal nodes as the vertices and ligands forming either the edges or faces of the cage. As yet there are no examples of octahedral coordination cages with ligands forming the vertices and metal nodes forming the edges or faces. A very early example of a supramolecular octahedral cage complex was by Fujita and co-workers in the report of an octahedral cage with Pd^{II} nodes in which four triptopic pyridyl ligands occupy alternate faces of the octahedron, and the Pd^{II} sites are capped by convergent ethylenediamine ligands.[225] Since then, multiple octahedral cage complexes have been reported.[228, 235, 525-529]

Octahedral coordination cages may be synthesised with monometallic or paddlewheel nodes, and the ligand may form the edges or the faces of the octahedron. Similar to the synthesis of other chiral polyhedral cages, chiral octahedral cages are synthesised by two main strategies, the use of chiral ligands, and the use of bidentate achiral ligands which generate chirality through coordination to an octahedral metal centre. Due to the synthetic challenges in the formation of chiral octahedral cages, such as the design of ligands of appropriate shape and coordination, there are only a handful of reported chiral octahedral cage complexes.[316, 530-532] The Nitschke group, who have reported widely on the synthesis of chiral tetrahedral cages with bidentate ligands which induce chirality around an octahedral metal centre, have also reported two chiral octahedral cages by the same synthetic strategy, in which a $[Zn_6L_4]^{12+}$ octahedral cage was synthetised with Zn^{II} metal centres and a ligand with three phenanthroline coordinating groups, Figure 6.1.[531] In a similar manner to the octahedral cage reported by Fujita and co-workers in 1995,[225] the ligands occupy alternate faces of the octahedron. The octahedral cages were synthesised with two ligands with slightly different core groups, and had internal void volumes of 282 $Å^3$ and 423 $Å^3$, as calculated by VOIDOO.[533] The octahedra were shown to bind a range of neutral and anionic guests within the voids. The crystal structure of the octahedral complexes shows a racemic mixture of the all-Δ,Δ and all-Λ,Λ

configurations, demonstrating that although achiral ligands may form chiral cages, it is almost impossible for achiral ligands to form as an enantiomerically pure bulk product.

A face-capped chiral octahedral cage has also been reported with a trimesoyltri((*S*)-alanine) ligand (TMTA) and copper paddlewheel nodes, $[Cu_{12}(TMTA)_8(OH_2)]$,[530] Figure 6.1. This cage has an internal void volume of 1224 Å^3, as calculated by PLATON.[534] The cage showed antiferromagnetic interactions between the Cu^{II} ions in the paddlewheels. The porosity of the solid state sample of this chiral octahedral cage was investigated by gas sorption experiments and showed selective adsorption of H_2 and CO_2 gas over CH_4. Unfortunately this cage has not been reported as being investigated for any applications which utilise its chirality.

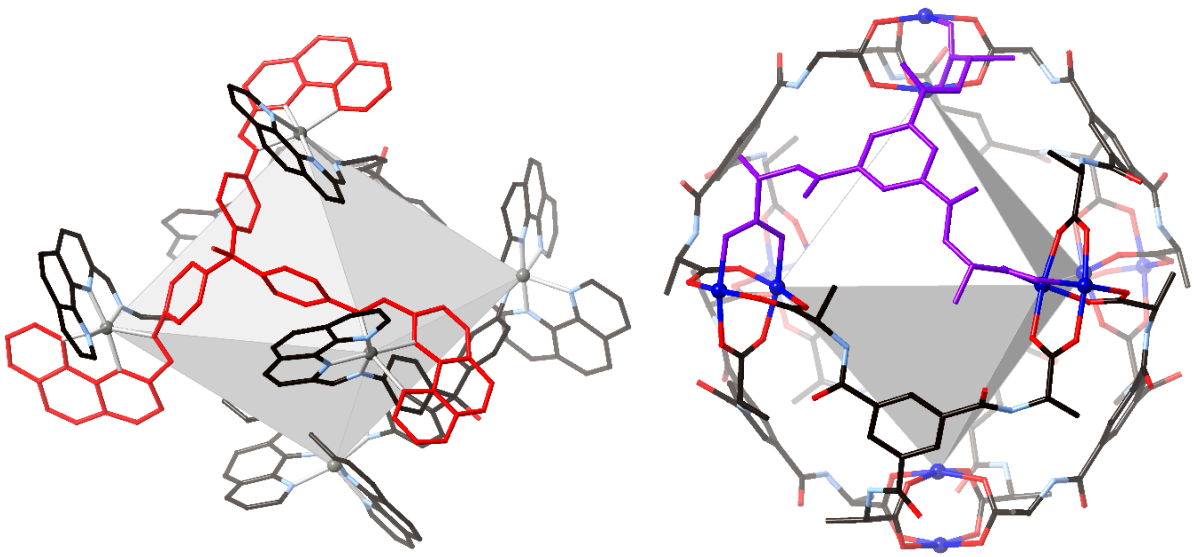

Figure 6.1. Examples of chiral face capped octahedral complexes. The $[Zn_6L_4]^{12+}$ complex in which chirality is induced by metal coordination (left).[531] The $[Cu_{12}L_{12}]$ complex which utilises a chiral ligand (right).[530]

A chiral octahedral cage complex has been reported which exploited the chirality of three bidentate ligands coordinated to an octahedral metal centre in order to form chiral metalloligands. The metalloligands were synthesised from Ru^{II} coordinated to three phenanthroline ligands, which were resolved into the Λ,Λ and Δ,Δ forms in order to form a robust chiral ligand. The chiral metalloligands were functionalised with pyridyl groups and their reaction with Pd^{II} formed homochiral octahedral cages, $[Pd_6(RuL_3)_8]$, with an internal void volume of 2895 Å^3, as calculated by VOIDOO.[533] These cages showed enantioselective separation of

atropisomeric compounds.[316] The same cage has also recently been reported for regio- and enantioselective photoinduced coupling of naphthols.[532]

6.2 Chiral octahedral complex

Considering the multitude of infinite coordination compounds which are formed with amino acid substituted NDI ligands, and the discrete cages obtained with amino acid substituted BPSD and EADI ligands and copper paddlewheel SBUs, it is worth considering the behaviour of chiral amino acid substituted NDI ligands in coordination compounds which utilise Cu^{II} metal centres. Given the results with BPSD, EADI and BDI ligands in combination with Cu^{II}, it was envisioned that reacting NDI ligands with Cu^{II} would form a chiral complex with copper paddlewheels. However, the rigidity of the NDI backbone in comparison to the BPSD, EADI and BDI ligands meant that it was unlikely to form analogous coordination compounds to those discussed previously.

The coordination behaviour of (*S*)-LeuNDI with Cu^{II} was investigated by reacting (*S*)-H_2LeuNDI with $Cu(NO_3)_2 \cdot 3H_2O$ in DMF at 120 °C. In a similar manner to the initial synthesis of cage **5.1**, the reaction produced only a blue solution. However after a week at ambient temperature, blue crystals formed from the reaction mixture. The crystals were analysed to reveal a coordination complex of the formula $[Cu_{12}((S)\text{-LeuNDI})_{12}(OH_2)_{12}] \cdot 22H_2O \cdot 30DMF$, **6.1**$\cdot 22H_2O \cdot 30DMF$. Unlike all of the coordination compounds discussed with (*S*)-LeuNDI and transition metals in Chapter 2, **6.1** is a discrete coordination complex. The complex consists of six copper paddlewheels and twelve (*S*)-LeuNDI ligands, forming an octahedral complex in which the paddlewheels form the vertices and the ligands form the edges of the octahedron, Figure 6.2. Due to the shape of the (*S*)-LeuNDI ligand, it is not able to form helicate cages with two copper paddlewheel motifs as in the case of **5.1** – **5.5**, or square complexes similar to **3.5** and **3.6**, instead it forms a larger octahedral complex. Given the examples of octahedral coordination complexes discussed in the introduction to this chapter, this is the first example of a chiral edge capped octahedral coordination complex.

The crystal structure of **6.1** is modelled in the chiral space group *P*23, with one third of the cage in the asymmetric unit. There are two crystallographically unique copper paddlewheels and four (*S*)-LeuNDI

ligands, as well as four coordinated water molecules. In the same manner as the cages of **5.1** – **5.5** and the square complexes of **3.5** and **3.6**, the paddlewheel is formed by four carboxylate groups of the amino acid ligands, with solvent coordinated to the apical positions. In the case of **6.1** all the apical positions of the paddlewheel are occupied by aqua ligands. The isobutyl side chains of (*S*)-LeuNDI force the paddlewheel into a propeller motif, similar to **Λ,Λ-5.1**, demonstrating that (*S*)-leucine substituted imide ligands will force paddlewheel motifs into a Λ,Λ-configuration, due to the steric requirements of the side chain. When viewed down the copper paddlewheels of opposite vertices of the octahedron, the coordinating groups are offset, at an average offset of 58.8°, Figure 6.2. Due to the chirality of **6.1**, the cage does not strictly have octahedral symmetry, as it does not have any mirror planes. Instead, **6.1** is best described as having D_4 symmetry. Unlike the majority of the coordination polymers with NDI ligands reported in Chapter 2, the structure of **6.1** is not dominated by face-to-face π-interactions. The cages pack in such a way that the isobutyl side chains of the LeuNDI ligands sit above the NDI core groups of adjacent cages.

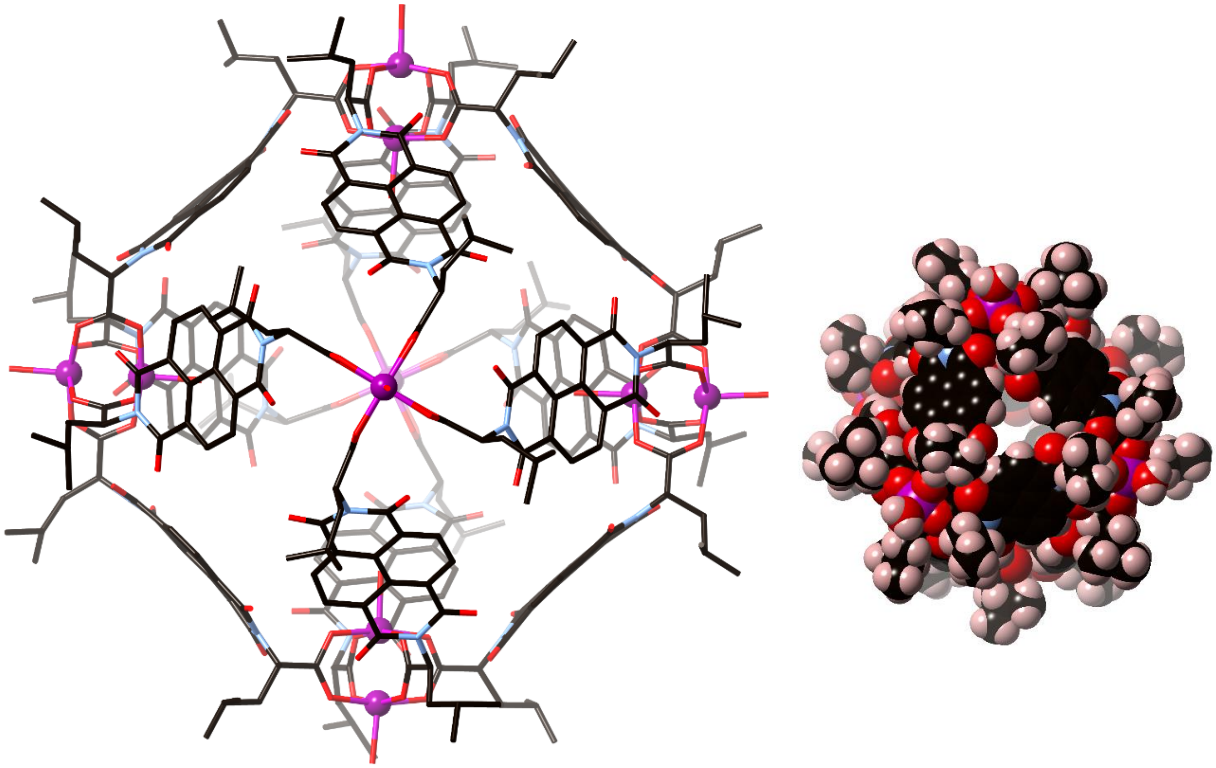

*Figure 6.2. The structure of **6.1** looking down one of the Cu···Cu axes (left), all hydrogen atoms are omitted for clarity. A space packing diagram of the cage showing the windows into the internal void (right).*

The cages of **6.1** have a large internal void volume of ~2100 Å^3. The internal void of **6.1** is significantly larger than the $[Zn_6L_4]^{12+}$ and $[Cu_{12}(TMTA)_8(OH_2)]$ chiral octahedral cages (*cf.* 282 Å^3, 423 Å^3 and 1224 Å^3),[530, 531] although it is ~60% of the size of the void of the $[Pd_6(RuL_3)_8]$ octahedral cage[316] discussed in section 6.1.2. The packing of the cages in the solid state also leads to the formation of solvent filled channels between the cages, of ~2500 Å^3 per cage, and solvent filled spheres between the vertices of the cages of ~1000 Å^3 per cage. The channels between the cages are connected to the voids within the cages by windows with a width of ~5 Å (porosity discussed further in section 6.4). There was no non-coordinated solvent which could be modelled in the structure of **6.1**, however the solvent is the voids was assigned as 22 water and 30 DMF molecules per cage complex through TGA, microanalysis and residual electron density.

The persistence of the cages in acetonitrile solution is shown by mass spectrometry. During the mass spectrometry experiment, 1% acetic acid was added to the acetonitrile solution in the ESI process, in order

to protonate the cages during droplet desolvation and ion formation. The [**6.1**+2H]$^{2+}$ and [**6.1**+3H]$^{3+}$ ions were observed, in which it is likely that some of the imide nitrogen atoms are protonated during ion formation, Figure 6.3. Additional 2+ and 3+ fragments were also observed with coordinated water and acetonitrile molecules (refer to Chapter 8). The dissolution of the as synthesised material in acetonitrile appears to have exchanged some of the ligated water molecules with acetonitrile molecules.

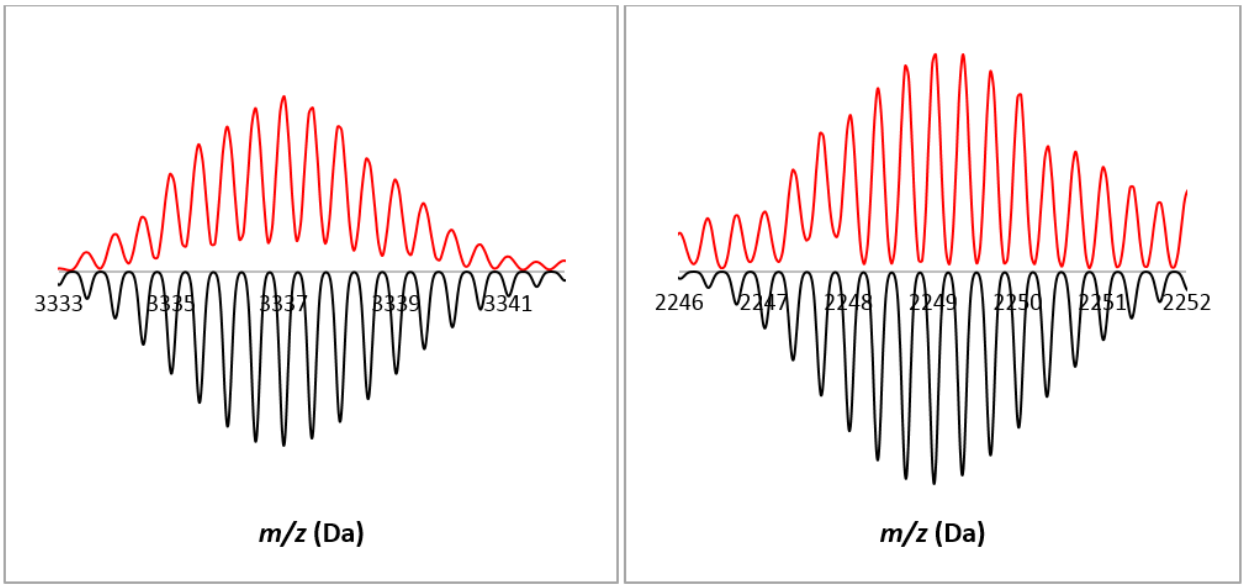

*Figure 6.3. The comparison of the experimental (red) and predicted (black) mass spectra of [**6.1**+2H]$^{2+}$ (left) and [**6.1**+3H]$^{3+}$ (right) ions, confirming the solution stability of the complexes.*

The structure of **6.1** shows that using the relatively rigid amino acid substituted NDI ligand, a discrete chiral coordination complex may be synthesised which has a significantly different geometry than the discrete coordination complexes formed with the other diimide ligands. The bend in the core of the BPSD and EADI ligands leads to the formation of M_4L_4 helicate cages. The linear but slightly flexible BDI ligands form M_8L_8 square complexes. The rigid and linear NDI ligands form an $M_{12}L_{12}$ octahedral complex. These results show the propensity of amino acid substituted diimide ligands to form discrete complexes with paddlewheel metal nodes.

6.3 Achiral copper coordination polymer with GlyNDI ligands

The achiral GlyNDI ligand was also investigated with Cu^{II}, in order to determine how the removal of the chirality of the ligand would influence the coordination complex formed. As was discussed in Chapter 5, the substitution of the achiral GlyBPSD ligand for the chiral LeuBPSD acted to remove the helicity of the complex and form a quadruple stranded mesocate. Although considering that **6.1** is not a helical complex, but an octahedral complex with defined edges formed by rigid ligands, it was unclear how the removal of the chirality of the ligand may influence the formation of a coordination complex of GlyNDI and Cu^{II}.

6.3.1 Synthesis of H_2GlyNDI

The synthesis of H_2GlyNDI has been reported once previously for use as a ligand in metallosupramolecular chemistry.[375] The reported synthetic method was the reaction of 1,4,5,8-naphthalene tetracarboxylic acid dianhydride with glycine in acetic acid under microwave irradiation.[375] However due to the success of the synthesis of the H_2AlaNDI, H_2LeuNDI and H_2PheNDI compounds in DMF at 90 °C overnight, the synthesis of H_2GlyNDI was attempted using identical conditions, Figure 6.4. The reaction achieved a pure product of H_2GlyNDI in which the analysis was concordant with the literature. The product was isolated by pouring the hot reaction mixture over ice, leading to the precipitation of the pure product from solution, which was recovered by filtration with a 71% yield. The formation of the product was confirmed by ^{1}H-NMR spectroscopy.

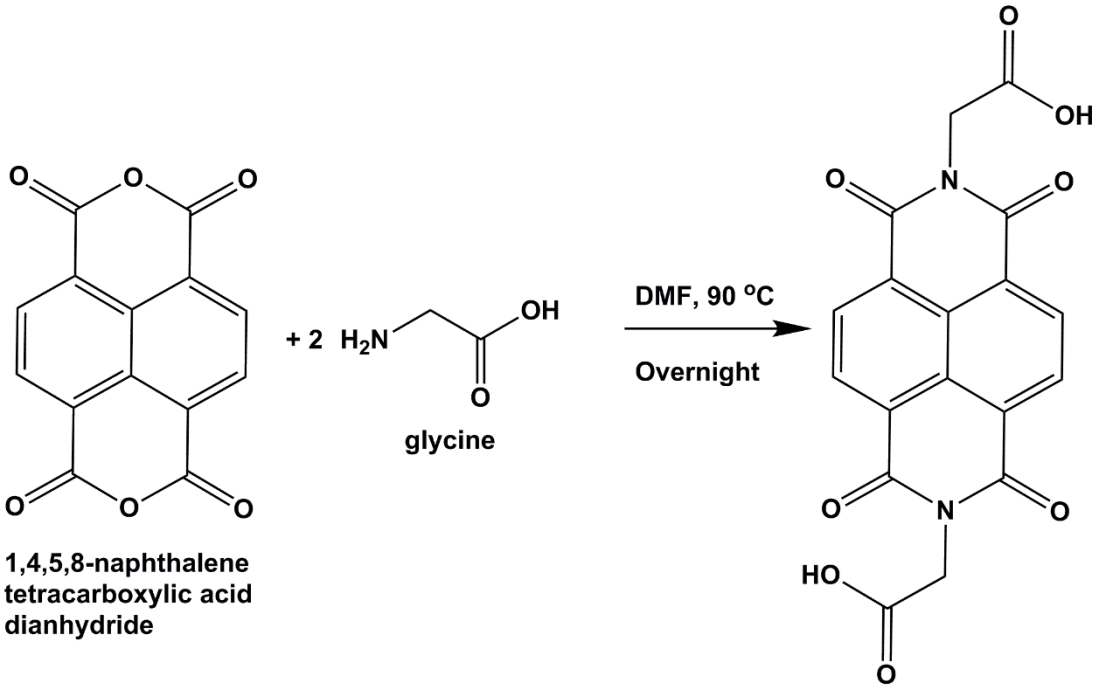

Figure 6.4. The synthetic scheme for the formation of H_2GlyNDI.

6.3.2 Synthesis of an achiral coordination polymer with GlyNDI

The reaction of H_2GlyNDI with $CuCl_2 \cdot 3H_2O$ in DMA at 120 °C yielded blue crystals within 24 hours. The crystals were analysed to reveal a coordination polymer of formula *poly*-$[Cu_2(GlyNDI)_2(DMA)_2] \cdot DMA$, **6.2**. The structure of **6.2** is modelled in the centrosymmetric space group *Pna*2_1 and the asymmetric unit contains two Cu^{II} ions, two GlyNDI ligands, two ligated DMF molecules and one non-coordinated DMF molecule. The Cu^{II} forms paddlewheels with the carboxylate groups of the amino acid, however in the case of **6.2** the ligands are "S-shaped". The ligands in the structures of **6.1, 5.1** – **5.5** and **3.5** – **3.6** are all "U-shaped" and form a "bowl" of which the paddlewheel is the centre, Figure 6.5. In the structure of **6.2** the ligands do not coordinate to the paddlewheel in such a way as to form a "bowl" shape. Of the four ligands coordinating to each paddlewheel, two ligands are coordinated to the paddlewheel in a *cis* fashion and are facing in one direction, and the remaining ligands, also coordinated to the paddlewheel in a *cis* fashion, face in the opposite direction, leading to the formation of a polymeric 2D sheet instead of a discrete cage complex, Figure 6.5.

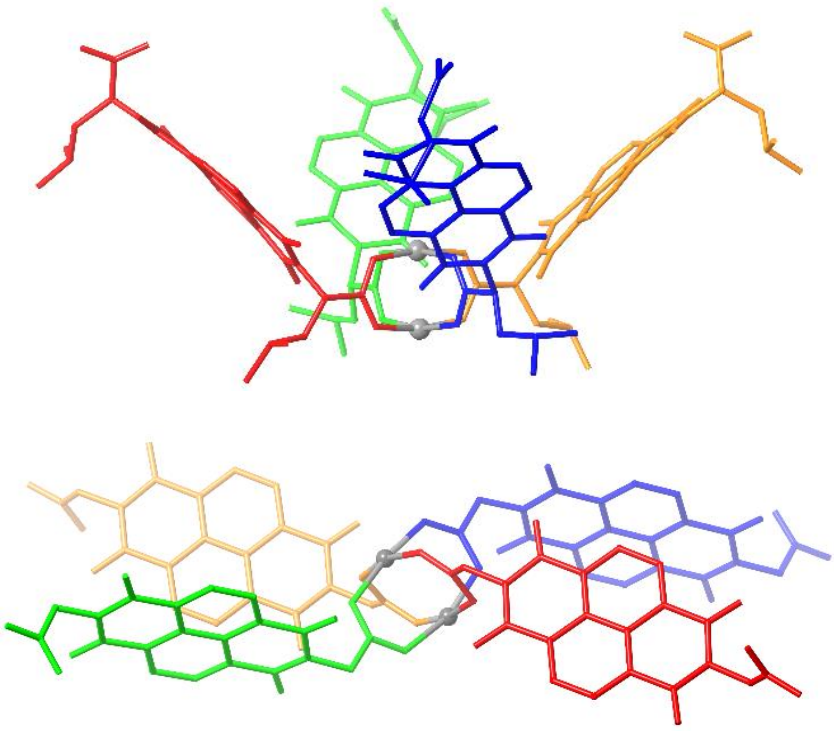

*Figure 6.5. The difference in the arrangement of ligands around the copper paddlewheels in the structures of **6.1** and **6.2**. A single paddlewheel in **6.1** showing the bowl shape of the "U-shaped" LeuNDI ligands around the paddlewheel, forming a discrete cage complex (top). A single paddlewheel in **6.2** showing the arrangement of the "S-shaped" GlyNDI ligands around the paddlewheel, forming a polymeric 2D sheet instead of a discrete cage complex (bottom). All hydrogen atoms and solvent molecules are omitted for clarity.*

The coordination of the GlyNDI ligands acts to bridge the paddlewheels into a polymeric network, instead of a discrete cage, as was observed for all previous amino acid diimide ligands with copper paddlewheels. The structure of **6.2** is a (4,4) sheet, in which the copper paddlewheels are the nodes and the ligands are the linker, Figure 6.6. Unlike the paddlewheels in **6.1** and those discussed with BDI and BPSD ligands, the paddlewheels are not forced into a propeller motif by the chirality of the ligand. It appears that the combination of achiral ligands which do not force the paddlewheels into a propeller, and a rigid ligand backbone which does not allow the ligands to bend between metal centres, leads to a polymer rather than a cage complex. Similar to the previously reported polymers with NDI ligands, the structure of **6.2** is dominated by π-interactions which occur in an offset parallel manner between the sheets, Figure 6.6, where the π-interactions have closest C⋯C distances of 3.375(7) and 3.429(7) Å.

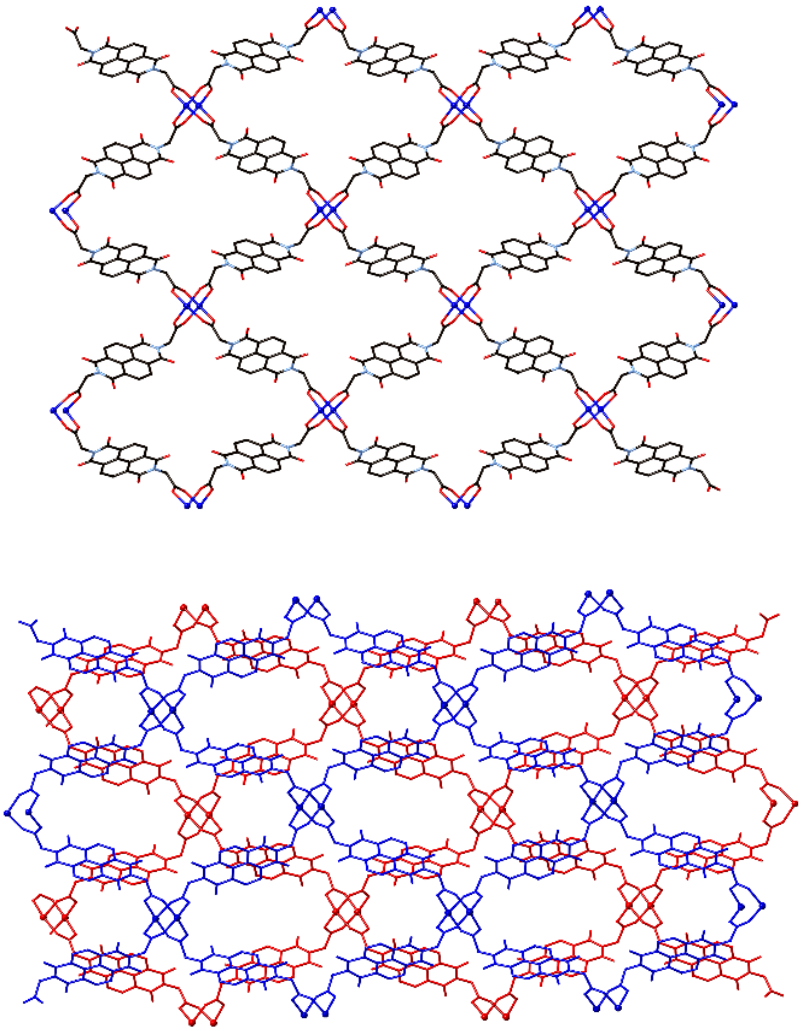

*Figure 6.6. The 2D sheet of the structure of **6.2** (top) and the packing of the 2D sheets of **6.2**, with offset parallel π-interactions between the NDIs of adjacent sheets (bottom). All hydrogen atoms and solvent molecules are omitted for clarity.*

6.4 Porosity of chiral octahedron

The cages of **6.1** have a significant internal void volume, and also pack in the solid state in such a manner as to form voids between the cages, Figure 6.7. The cages have an internal void of ~2100 Å^3, significantly larger than the voids in the cages of **5.1** - **5.5** (*cf.* 350 – 700 Å^3). The cages are packed by hexagonal close packing, occupying opposite corners of the unit cell, forming additional spherical voids of ~1000 Å^3 per cage at the remaining corners of the unit cell. There are also channels formed between the cages, which have a total volume of ~2500 Å^3 per cage. The narrowest point of the channels is between parallel NDI

planes of adjacent cages, with plane to plane distances for the four crystallographically unique NDIs of 7.6561(7), 7.4838(6), 7.5762(6) and 7.5599(7) Å. The channels between the cages are connected to the voids within the cages by windows with a width of ~ 5 Å. The packing of the cages is such that the spherical voids between the cages are blocked off from the channels, and therefore it is unlikely that this void will be available pore space within the material. The three different voids give the solid state structure of **6.1** a total void volume of 44%, as calculated by Mercury.[376]

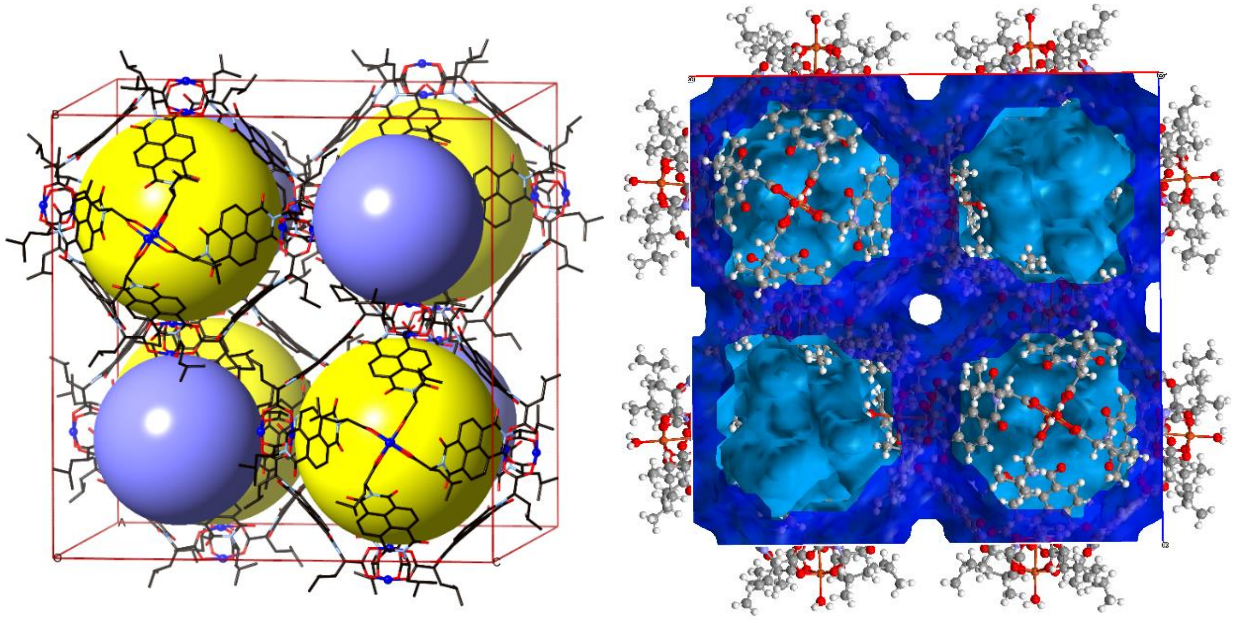

*Figure 6.7. The porosity of **6.1** shown as spheres, within the cages (yellow sphere) and between the cages at the corners of the unit cell (purple sphere). All hydrogen atoms are omitted for clarity (left). The contact surface of the solid state structure of **6.1** looking down the channels between the cages, showing the spherical voids within the cages, the spherical voids between the cages, and the channels between the cages (right).*

Due to the high degree of porosity of the cages in the solid state, the crystalline material was investigated for gas sorption properties. As **6.1** was synthesised in DMF, the voids of the as synthesised material are filled with DMF and water molecules, as shown by microanalysis. Thermogravimetric analysis showed the slow loss of solvent from 50 – 260 °C, due to the low volatility of DMF, and the narrow pore apertures. Solvent exchange was conducted by soaking the material in methanol overnight, and TGA showed the removal of all solvent by 50 °C with a plateau region in the range 50 – 200 °C, Figure 6.8.

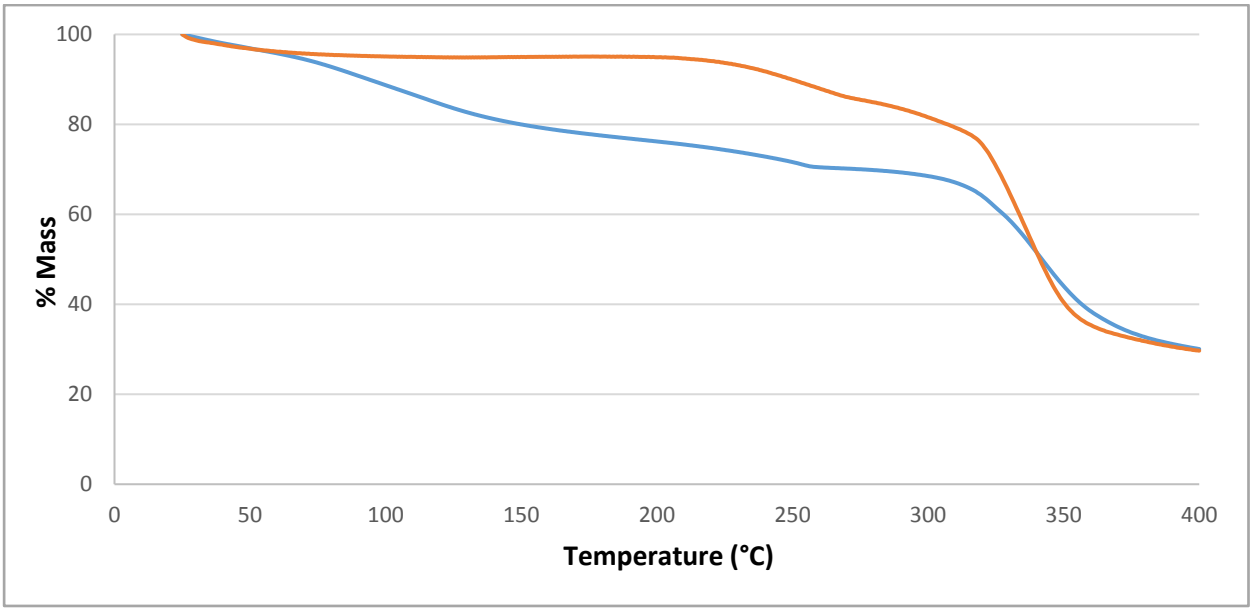

*Figure 6.8. The TGA of freshly grown crystals of **6.1** (blue) and after solvent exchange with methanol (orange).*

Activation of the sample for gas sorption measurements was conducted by heating the methanol exchanged sample under vacuum at 50 °C, in order to remove all solvent from the pores. There is some alteration in the PXRD of the material following activation, suggesting that the material may undergo some structural rearrangement when the solvent molecules are removed, Figure 6.9. As the solid state crystalline material of **6.1** is made up of discrete coordination cages, it is possible that the cages may rearrange slightly when the voids are emptied. The PXRD of the activated material and the material after the gas sorption experiments are very similar, showing that the gas sorption does not change the arrangement of the complexes in the solid state, Figure 6.9.

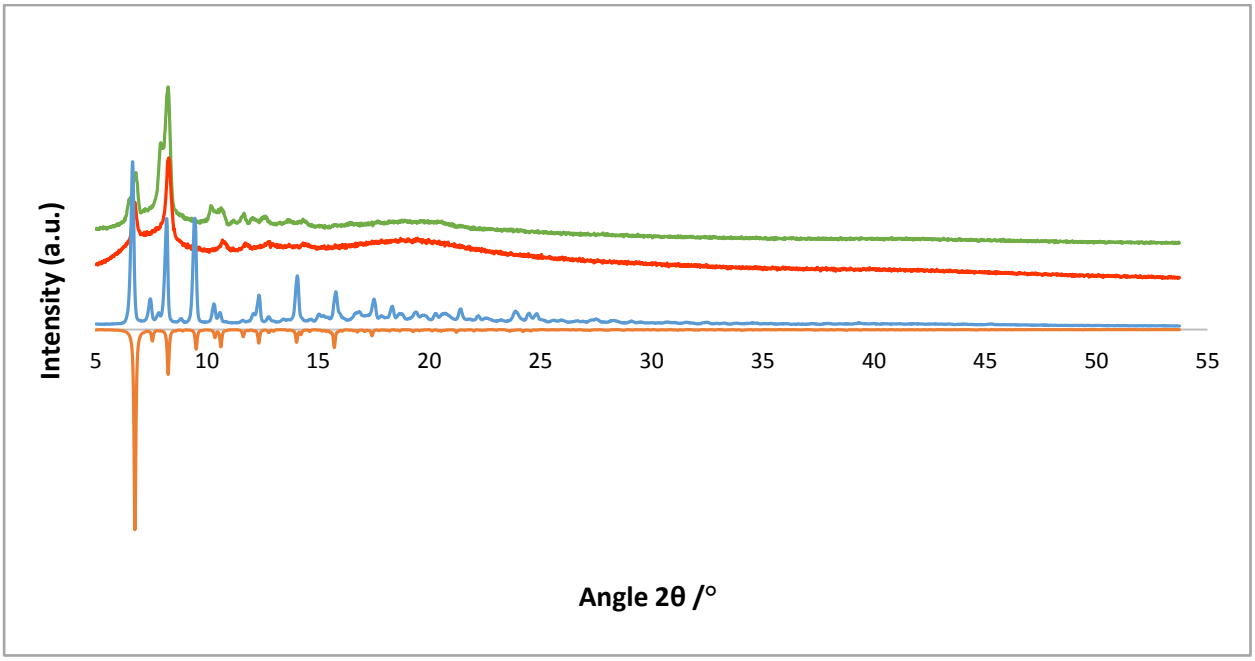

*Figure 6.9. Comparison of the calculated (orange) and experimental PXRD of **6.1** fresh (blue), activated (red) and post-gas sorption (green).*

The sorption isotherms of CO_2 (273 K) and N_2 (77 K) at 0 – 101 kPa show gas uptake into the material, with maximum adsorptions of 2.7 and 13.4 mmol/g, respectively, confirming the porosity of the material, Figure 6.10. The CO_2 isotherm appears to follow a type 1B adsorption isotherm,[535] although it does not reach a plateau, suggesting that the material will show higher uptake at increased pressure. The N_2 isotherm follows a type 2 adsorption isotherm,[535] which appears to almost plateau at approximately 50 kPa. The absorption of CO_2 and N_2 into the material corresponds to a maximum uptake volume of 28.2 $Å^3$ of CO_2 and 125.5 $Å^3$ of N_2 per cage, which is much smaller than the total voids of the material, suggesting that the gas has not filled the pores within the material at atmospheric pressure.

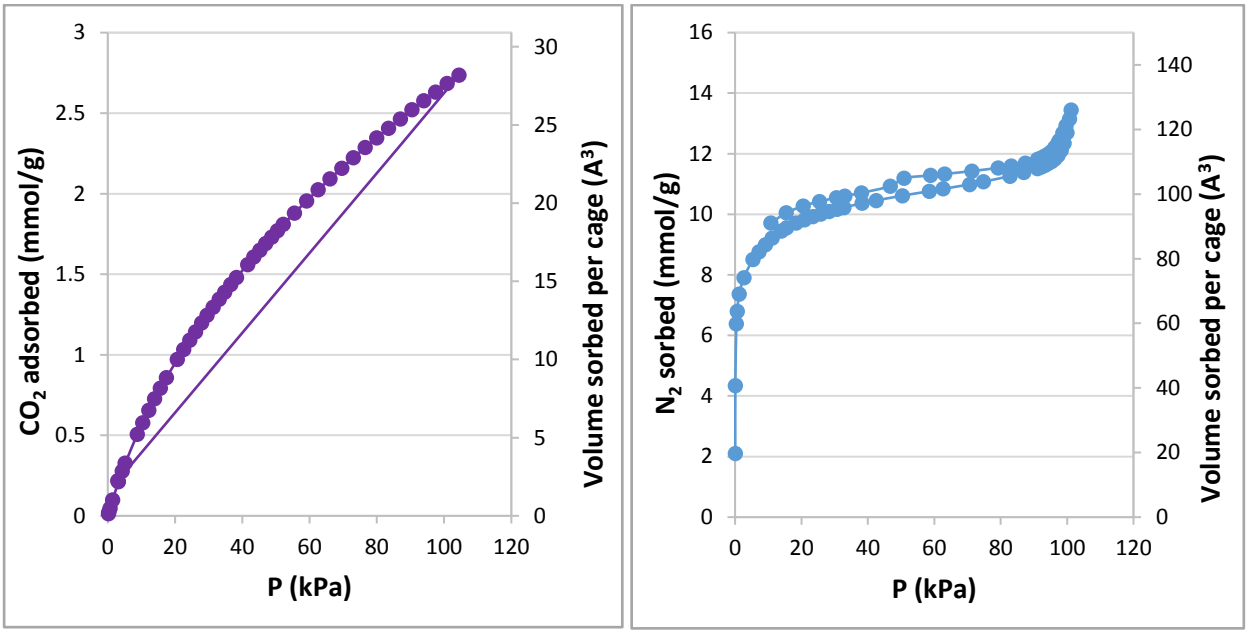

*Figure 6.10. The CO_2 (left) and N_2 (right) absorption isotherms of **6.1** at low pressure showing the uptake in gas absorbed (mmol/g) and in volume adsorbed per cage (Å^3).*

Given the small pore apertures in the material and the low pressure gas isotherms which show uptake consistent with partially filled pores, the gas sorption properties of **6.1** were also investigated at high pressure, with CO_2, H_2, CH_4, N_2 and N_2O over a range of temperatures, in collaboration with the Abrahams group at the University of Melbourne. The gas uptake was calculated in terms of the volume absorbed (cm^3/g) and total volume of gas per cage (Å^3), in order to determine if the gas was going only into the channels between the cages, into the voids within each cage, or into the spherical voids between cages, in order to gauge the accessibility of the voids within the solid state structure of **6.1**.

As the CO_2 uptake at low pressure did not show a plateau, and therefore may be likely to take up more gas at higher pressure, the CO_2 uptake was investigated at 1 – 2600 kPa. The CO_2 isotherms all follow a type 1B absorption isotherm,[535] Figure 6.11. Decreased temperature of the system leads to higher CO_2 uptake, with 137 cm^3/g adsorbed at 298 K, 162 cm^3/g adsorbed at 273 K and 187 cm^3/g adsorbed at 258 K. The volume of gas uptake may also be calculated in terms of volume of gas adsorbed per octahedral complex, which accounts for sorption of 2994 Å^3 at 298 K at 2630 kPa, 3549 Å^3 at 273 K at 2710 kPa and 4092 Å^3 at 258 K at 1810 kPa. The single crystal data of **6.1** shows total voids of ~5600 Å^3 per cage, with voids of

2100 Å^3 within the cage, 1000 Å^3 in the spheres between cages, and 2500 Å^3 in the channels between cages. The desorption isotherms each show a slight hysteresis.

The volume of CO_2 adsorbed at all temperatures suggests that the CO_2 is filling both the channels and the voids within cages, as the volume adsorbed is greater than the volume of the channels, showing the accessibility of the voids within the cages. The maximum uptake, of 4092 Å^3 at 258 K suggests that the channels and voids within the cages are almost completely filled with CO_2. The spherical voids between cages are very hindered, and so are likely to only be filled if there is some rearrangement of the cages in the solid state after activation of the material. There was some alteration in the PXRD of the activated material in comparison to the as-synthesised crystals, suggesting that there could be some rearrangement of the cages in the solid state, which may allow gas molecules into the spherical voids between the cages. The isosteric enthalpy of CO_2 adsorption was calculated in order to determine the strength of interactions between the CO_2 molecules and the surface of the pores. The sorption enthalpy was calculated to be ~28 kJ/mol, which falls into the physisorption range of adsorption behaviour.[535]

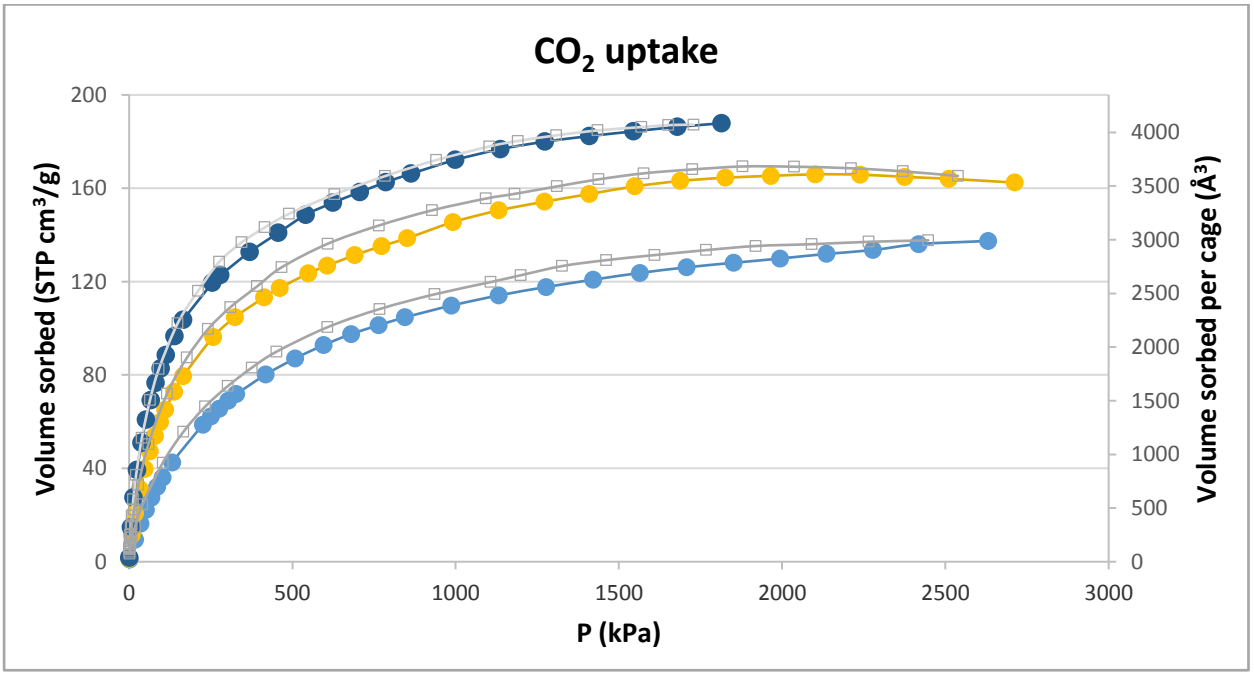

*Figure 6.11. The absorption (coloured lines) and desorption (grey lines) of CO_2 with **6.1** at 1 – 2600 kPa at 298 K (light blue), 273 K (yellow) and 258 K (dark blue). Expressed in volume absorbed in cm^3/g of material, and volume adsorbed per cage complex.*

The N_2 isotherm at low pressure followed a type 2 adsorption isotherm,[535] with a maximum uptake of 125 $Å^3$, by no means filling the pores of the material. Therefore the N_2 adsorption was also measured at high pressure of 1 – 2600 kPa and at temperatures of 298, 273 and 258 K, Figure 6.12. The adsorption at 298, 273 and 258 K showed maximum uptake of 29, 34 and 45 cm^3/g at 2400 kPa, respectively. The adsorption isotherms of N_2 at 298, 273 and 258 K correlate to sorption of 574, 686, and 881 $Å^3$ per cage, respectively. As the total void per cage in the single crystal structure of **6.1** is ~5600 $Å^3$, these sorption isotherms show that N_2 at these temperatures does not fill the pores. It is likely that N_2 shows less sorption than CO_2 because it is non-polar, and therefore has reduced interactions with the surface of the cage material.[536]

The absorption isotherm of N_2 was also measured at 77 K, between 1 – 101 kPa, and showed a maximum uptake of 205 cm^3/g, corresponding to 4068 $Å^3$ per cage. The volume of N_2 adsorbed by **6.1** is similar to the total volume of CO_2 adsorbed, which would account for the gas almost completely filling the channels between the cages and the voids within the cages, which are ~2500 $Å^3$ and ~2100 $Å^3$, respectively. The isosteric enthalpy of N_2 adsorption was calculated to determine the strength of interactions between the CO_2 molecules and the surface of the pores. The sorption enthalpy was calculated to be ~20 kJ/mol, which again falls into the physisorption range of adsorption behaviour.[535]

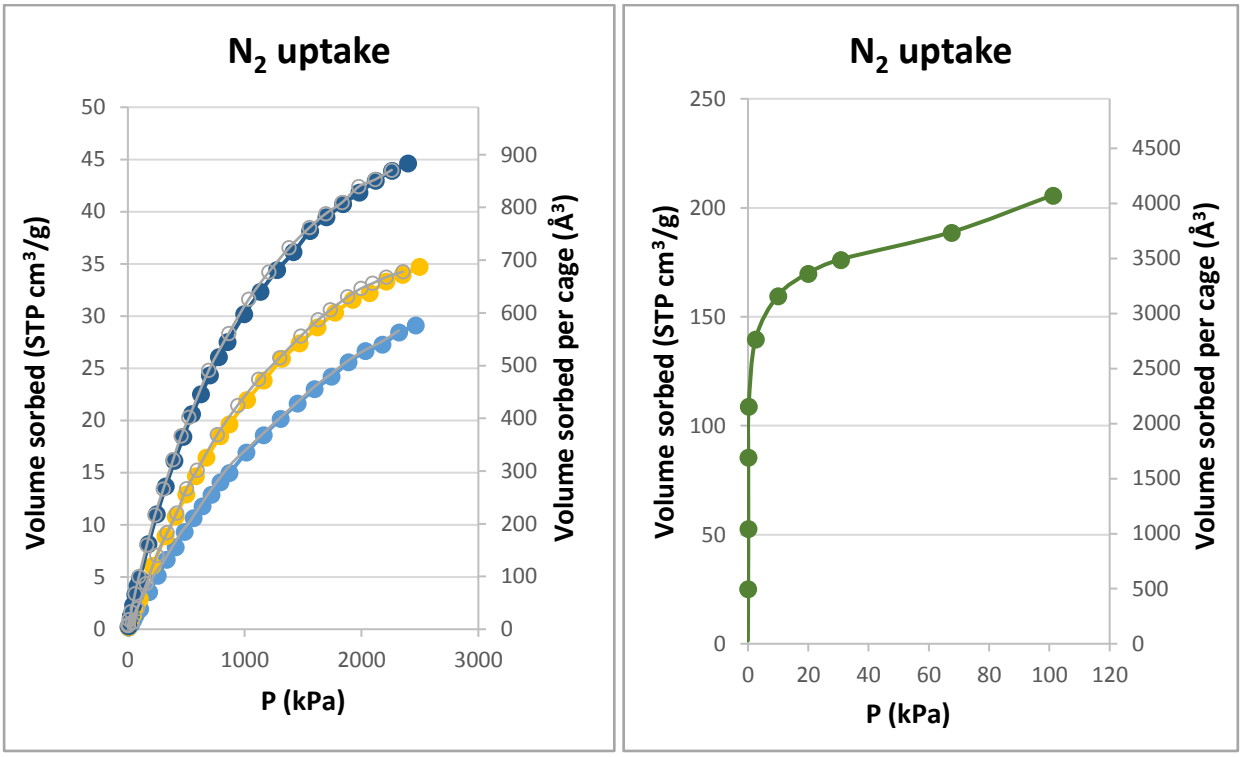

*Figure 6.12. The N_2 adsorption isotherms of **6.1** with N_2 at 1 – 2600 kPa at 298 (light blue), 273 (yellow) and 258 K (dark blue) (left) and at 77 K (green) (right). Expressed in volume absorbed in cm^3/g of material, and in volume adsorbed per cage complex.*

The gas sorption properties of **6.1** were also investigated with H_2 at 77 K from 1 – 1020 kPa and at 298 K from 1 – 1607 kPa, Figure 6.13. The absorption isotherm at 298 K showed low uptake of 6.1 cm^3/g, which corresponds to the sorption of 83 $Å^3$ of H_2 per cage. A much larger volume of H_2 was adsorbed at 77 K, a maximum of 172 cm^3/g, corresponding to 2348 $Å^3$ per cage. The maximum uptake of H_2 at 77 K corresponds to gas molecules partially occupying the channels between the cages and the voids within the cages. The adsorption of H_2 is lower than the maximum uptake of CO_2 or N_2, suggesting that H_2 has less affinity for the internal voids of the material.

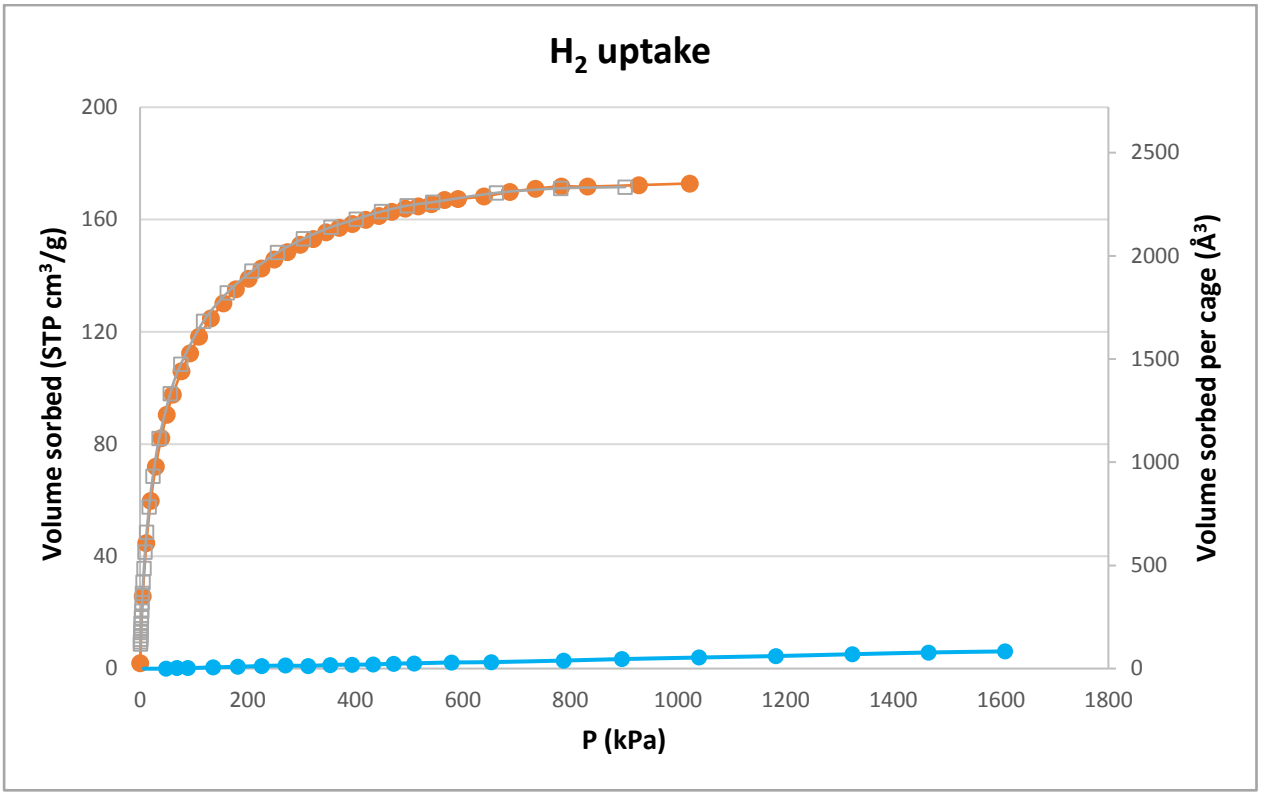

Figure 6.13. The adsorption isotherm of H_2 at 77 K from 1 – 1020 kPa (orange) and at 298 K from 1 – 1067 kPa (blue). Expressed in volume absorbed in cm^3/g of material, and in volume adsorbed per cage complex.

High pressure gas adsorption measurements of **6.1** were also undertaken with CH_4 gas, at 298, 273 and 258 K at pressures of 1 – 3100 kPa, Figure 6.14. The adsorption of CH_4 at 298, 273 and 258 K showed a maximum uptake of 70.5, 82.1 and 90.3 cm^3/g, respectively. The maximum uptake at 298, 273 and 258 K accounts for a total volume of 1539, 1792 and 1995 $Å^3$ of gas per cage, respectively. The maximum uptake of CH_4, 1995 $Å^3$ at 258 K, is smaller than the maximum sorption values of CO_2, N_2 and H_2, and is less than the volume of the channels between the cages (~2500 $Å^3$), suggesting that either CH_4 is not passing into the voids within the cages, or that both of these voids are partially filled with CH_4 gas molecules. As the windows between the channels and the voids within the cages are quite small (~5 Å), and the maximum volume of CH_4 is less than the volume of the channels per cage, it is likely that the CH_4 molecules are not passing into the voids within the cages, and are instead only populating the channels.

The isosteric enthalpy of adsorption was calculated for CH_4, in order to investigate the strength of interactions between the CH_4 molecules and the surface of the pores. The sorption enthalpy was calculated to be ~20 kJ/mol, consistent with physisorption of the gas molecules in the material.[535]

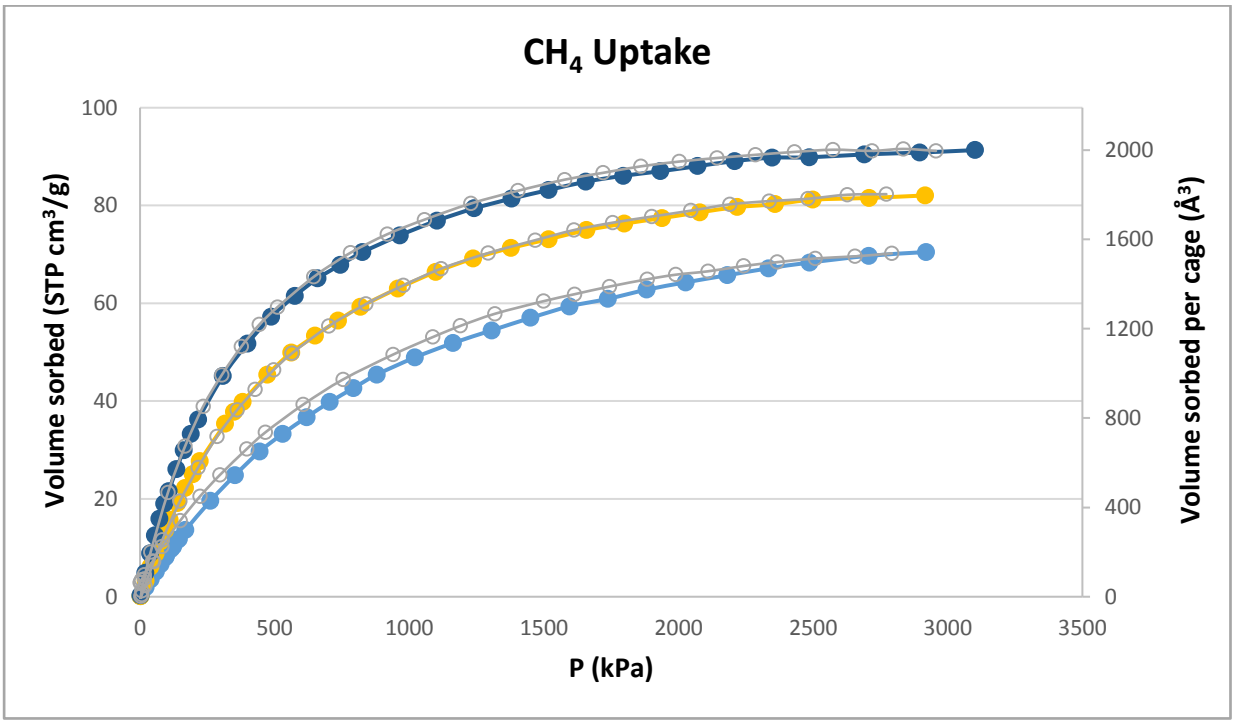

*Figure 6.14. The absorption (coloured lines) and desorption (grey lines) of CH_4 with **6.1** at 1 – 3100 kPa and at 298 K (light blue), 273 K (yellow) and 258 K (dark blue). Expressed in volume absorbed in cm^3/g of material, and volume adsorbed per cage complex.*

The adsorption of N_2O was also measured with the solid state material of **6.1**, at pressures of 1 – 2640 kPa and 298, 273 and 258 K, Figure 6.15. The maximum uptake of N_2O at 298 K was 143 cm^3/g at 2520 kPa, at 273 K was 189 cm^3/g at 2640 kPa and 258 K was 205 cm^3/g at 1510 kPa. The maximum volume of N_2O adsorbed per cage at 298, 273 and 258 K was calculated to be 3220, 4365 and 4624 $Å^3$, respectively. As the solid state structure of **6.1** contains a total void volume of the ~5600 $Å^3$ per cage, made up of three different voids; ~2100 $Å^3$ within the cage, ~1000 $Å^3$ in the spheres between cages, which are very hindered from the other voids, and ~2500 $Å^3$ in the channels between cages, it appears that the N_2O gas molecules are filling the channels between cages and also the voids within the cages.

The maximum uptake of N_2O by the material, that of 4624 $Å^3$ at 258 K slightly exceeds the volume of the voids within the cages and the channels between the cages, so it is possible that the spherical voids between

the cages may also be partially populated by N_2O molecules. As the PXRD of the activated and post-gas material is slightly different to the as-synthesised material, it is possible that the cages have rearranged slightly in the solid state in order to allow gas molecules to enter the voids between the cages.

Each of the adsorption isotherms with N_2O appear to follow a type 4 isotherm[535] with a point of inflection after adsorption of 2700 $Å^3$, 2900 $Å^3$ and 2500 $Å^3$ at 258 K, 273 K and 298 K, respectively. As the channels between the cages account for approximately 2500 $Å^3$ per cage, it appears that the step in the adsorption occurs when the channels have been filled, and the system is at a sufficient pressure for the gas molecules to populate the voids within the cages. The uptake of N_2O at 258 K is higher than any uptake observed for CO_2, N_2, H_2 or CH_4 at any temperature attempted. The higher uptake of N_2O in comparison to the other gases analysed is likely due to the polarity of N_2O leading to favourable interactions with the internal surface of **6.1**.

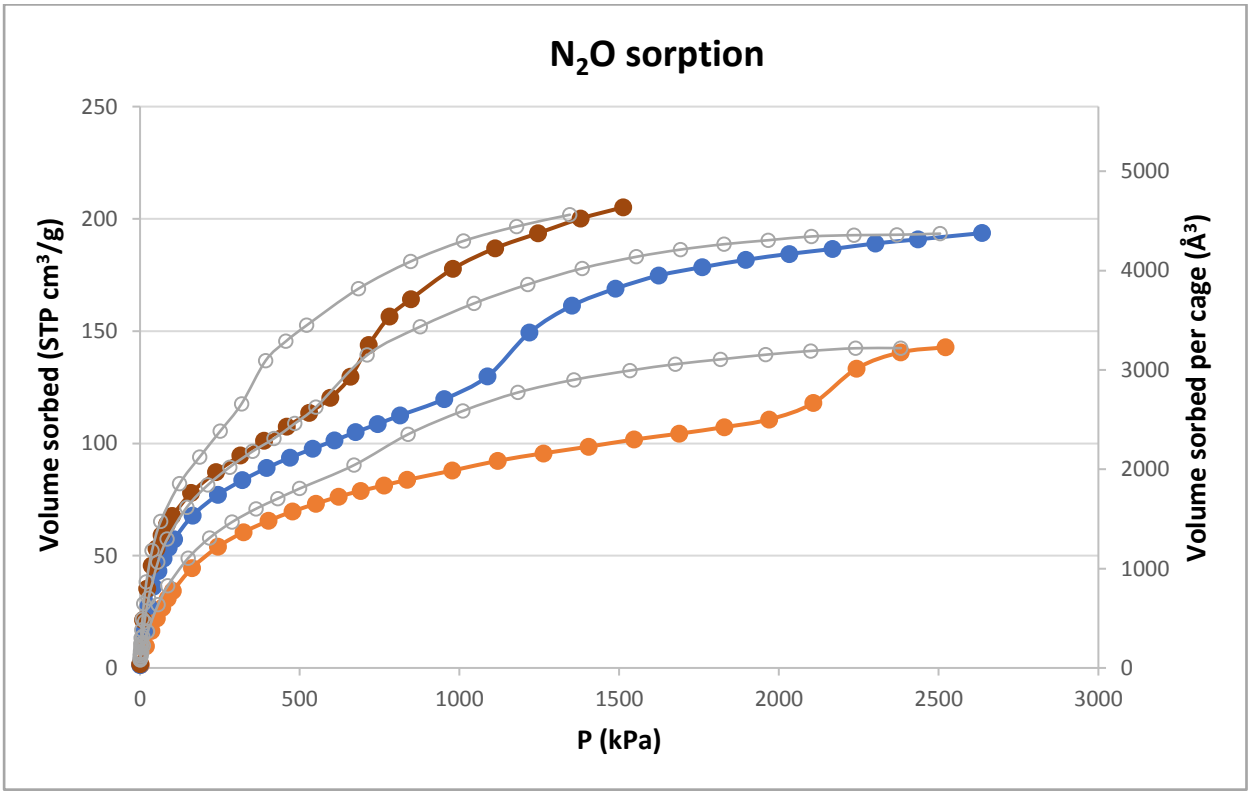

*Figure 6.15. The absorption (coloured lines) and desorption (grey lines) of N_2O with **6.1** at 1 – 3100 kPa at 298 K (orange), 273 K (blue) and 258 K (brown). Expressed in volume absorbed in cm^3/g of material, and in volume adsorbed per cage complex.*

The high pressure gas adsorption measurements of **6.1** confirm the porosity of the solid state material of this octahedral cage complex. Of the three different void spaces within the material, the channels between cages, the spherical voids within cages and the spherical voids between cages, it appears that the spherical voids between cages are generally too hindered to be populated by adsorbed gas molecules. The single crystal structure of **6.1** shows that the spherical voids between the cages are inaccessible from the other voids within the structure, due to the size, shape, and arrangement of the LeuNDI ligand in the cage complex. The maximum gas adsorption of **6.1** appeared to fill the channels between the cages and the voids within the cages, but only appeared in one instance for N_2O at 258 K, to be a large enough volume to suggest that the gas molecules may be populating all three voids within the solid state structure of **6.1**. As the PXRD of the activated solid state sample is slightly different to the as-synthesised sample, it is possible that during activation the cages rearrange slightly in order to allow gas molecules to populate the spherical voids between the cages.

6.5 Fluorescent properties of chiral octahedron

Based on the interesting fluorescent properties of H_2LeuNDI, and LeuNDI in the discrete macrocycle and catenane (see Chapter 4), the fluorescence of **6.1** was investigated. The solution stability of **6.1** was confirmed by mass spectrometry (see Chapter 8 for details). The complex was dissolved in chloroform, acetonitrile, toluene, *o*-, *m*- and *p*-xylene. The fluorescence intensity in the non-aromatic solvents of chloroform and acetonitrile was extremely weak, and therefore could not be analysed in detail. The fluorescence of **6.1** in aromatic solvents was also quite weak, however was sufficient for steady-state analysis. In a similar fashion to the fluorescence of H_2LeuNDI in aromatic solvents, the fluorescence of **6.1** in aromatic solvents showed broad emission around 450 – 510 nm, Figure 6.16. The emission of **6.1** in *o*-xylene is essentially indistinguishable from that of *m*-xylene, with emission maxima at 482 and 479 nm, respectively. In the same way as H_2LeuNDI, the emission of **6.1** is blue shifted relative to the *o*- and *m*-xylene, with emission maxima at 455 nm, and the solution of **6.1** in *p*-xylene is red shifted with the emission maxima at 507 nm.

The similar fluorescence emission of **6.1** and H_2LeuNDI in aromatic solvents suggests that the LeuNDI ligands within **6.1** are interacting with the solvent molecules in a similar fashion to when they are non-coordinated, i.e. free in solution. In a similar manner to H_2LeuNDI, **6.1** appears to be forming exciplexes with the aromatic solvent, evidenced by the broad emission at 450 – 510 nm and the shift in emission maxima with change in solvent. The much weaker fluorescence of **6.1** than H_2LeuNDI also suggests that the Cu^{II} to which the LeuNDI is coordinated was acting to quench the fluorescence of the ligands. These results are quite intriguing, as they demonstrate that H_2LeuNDI maintains its fluorescent properties when complexed, and that exciplex formation with aromatic solvents is still possible for coordinated LeuNDI ligands, occurring in a very similar manner to that of the free ligand.

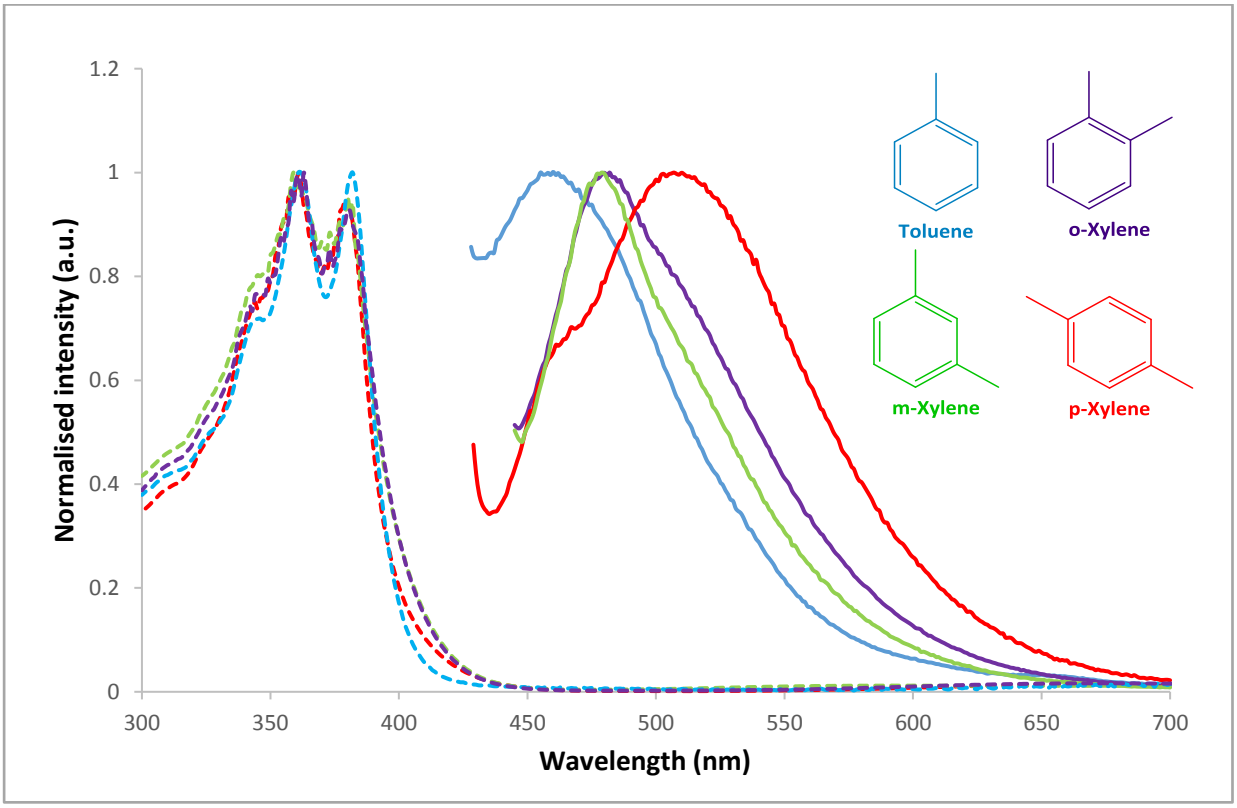

*Figure 6.16. Normalised absorbance (dashed lines) and fluorescence emission (solid lines) of **6.1** at 20 µmol/L in toluene excited at 390 nm (blue), o-xylene excited at 410 nm (purple), p-xylene excited at 395 nm (red) and m-xylene excited at 410 nm (green).*

The apparent formation of exciplexes of aromatic solvent molecules with the LeuNDI ligands within **6.1** led to the investigation of the fluorescent properties of **6.1** with larger aromatic molecules. Solutions of **6.1**

in toluene with the aromatic guest molecules naphthalene and triphenylene were prepared and their fluorescence emission analysed. The fluorescence emission of **6.1** was very weak, and the spectra were dominated by the emission of the guest molecules. Fluorescence emission spectra of the guest molecules in the absence of **6.1** showed much more intense fluorescence, suggesting that **6.1** was having the effect of quenching the fluorescence of the guest molecules.

In order to investigate the fluorescence quenching of naphthalene and triphenylene with **6.1**, a series of solutions were prepared in chloroform with a range of concentrations of **6.1** and a standard concentration of triphenylene and naphthalene. All solutions were prepared with concentration of 120 µmol/L of triphenylene or naphthalene and **6.1** at concentrations of 0, 3.2, 6.7, 10, 13.2 and 16.7 µmol/L. These concentrations were chosen because they represent LeuNDI:guest ratios of 0:12, 4:12, 8:12, 12:12, 16:12 and 20:12. The fluorescence of these samples showed a steady decrease in emission upon increase in concentration of **6.1**, Figure 6.17 and 6.18.

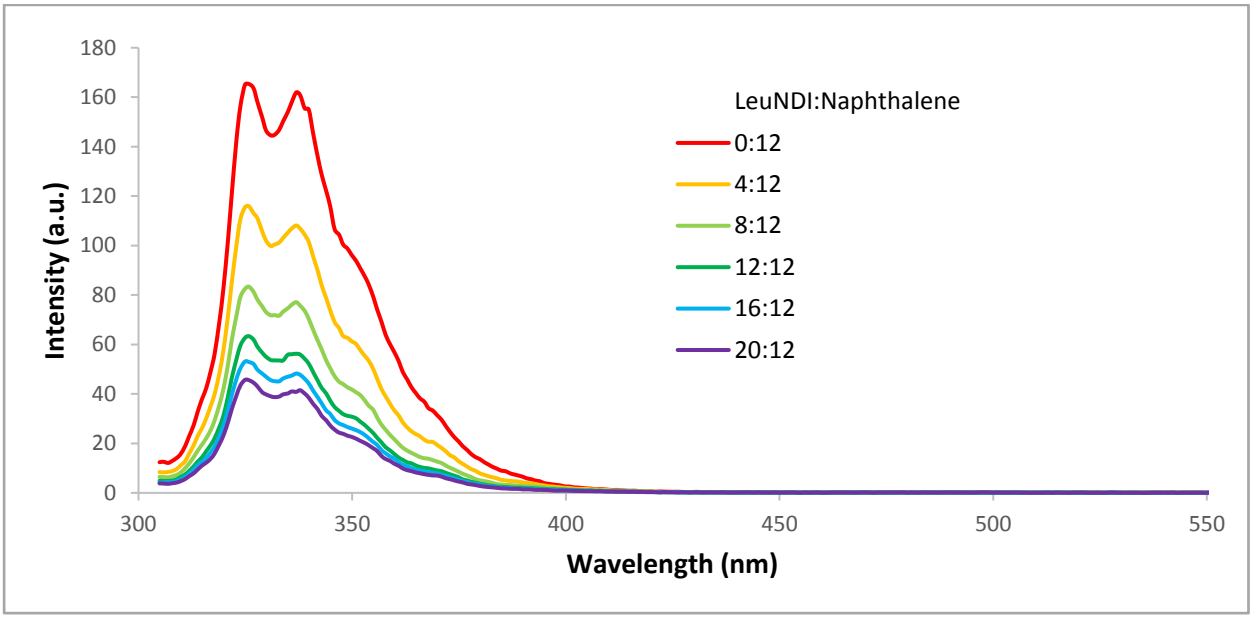

*Figure 6.17. Fluorescence emission of naphthalene upon excitation at 285 nm with variable concentrations of **6.1** showing the quenching of naphthalene by **6.1**.*

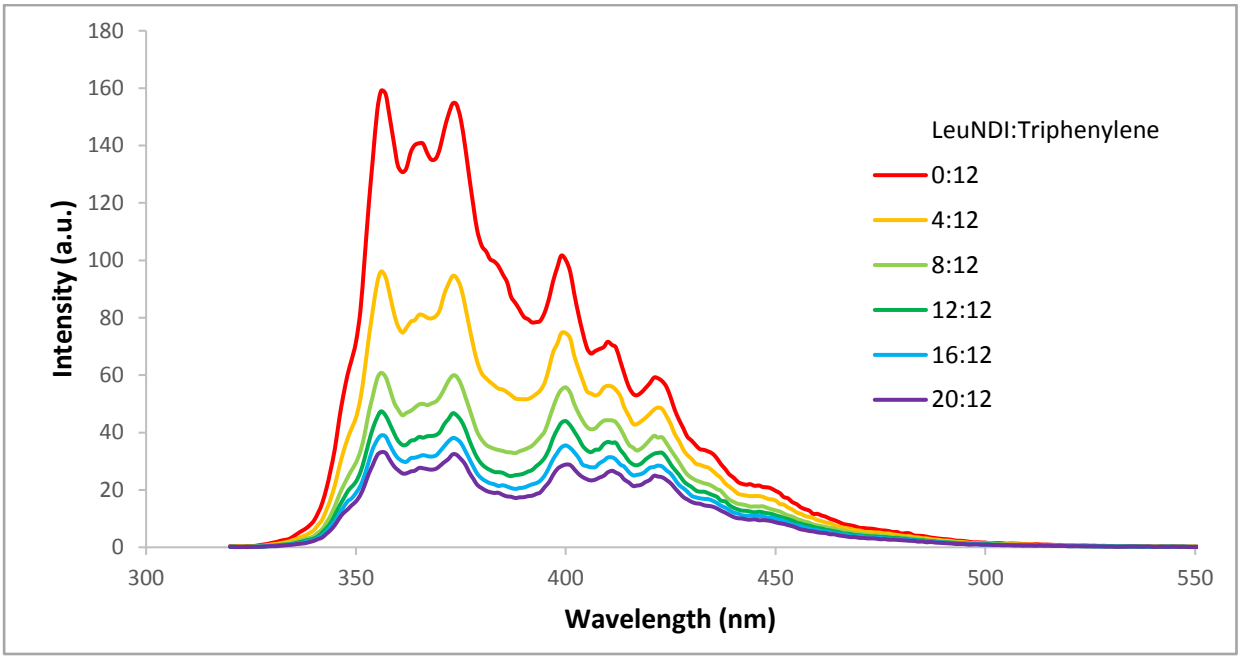

*Figure 6.18. Fluorescence emission of triphenylene upon excitation at 300 nm with variable concentrations of **6.1** showing the quenching of triphenylene by **6.1**.*

The change in fluorescence emission of naphthalene and triphenylene upon increase in concentration of **6.1** was analysed to see if it followed a Stern-Volmer relationship and therefore if **6.1** was acting to quench the fluorescence of the aromatic molecules. The maximum emission intensity of naphthalene and triphenylene in the absence of **6.1** (I_0) was divided by the maximum intensity for each concentration of **6.1** (I), and this ratio was graphed against the concentration of **6.1**, Figure 6.19. If this follows a liner relationship, then it may be concluded that **6.1** is acting to quench the fluorescence of triphenylene and naphthalene. As **6.1** absorbed light at ~320 – 390 nm, the quenching effect of the complex was somewhat altered by the inner filter effect, because triphenylene and naphthalene also emitted over that range. The majority of the emission of naphthalene was between 320 and 355 nm, with the maxima at 337 nm, therefore the quenching rate constant was measured at this maximum, as there were no local maxima outside the range in which the absorption of the light by **6.1** would not influence the calculations. The Stern-Volmer constant of **6.1** on naphthalene was calculated to be 1.82 x 10^5 M^{-1}. The quenching rate constant of triphenylene was calculated with a local maximum at 421 nm, showing Stern-Volmer constants of 8.4 x 10^5 M^{-1}. The quenching rate constant was calculated at 421 nm because the compound absorbs light at the emission maxima of 373 nm,

and therefore the quenching constant calculated from this maximum would not be accurate, due to the inner filter effect. The compound does not absorb light at 421 nm, and would therefore not be influenced by the inner filter effect. Both graphs show a linear relationship, confirming that **6.1** is acting to quench the fluorescence of naphthalene and triphenylene in solution. As **6.1** quenches the fluorescence of triphenylene and naphthalene, it can be concluded that the LeuNDI ligand is interacting with these aromatic molecules, further demonstrating that LeuNDI has interesting fluorescence properties both as a free ligand, H_2LeuNDI, as when in a metal complex such as **6.1**.

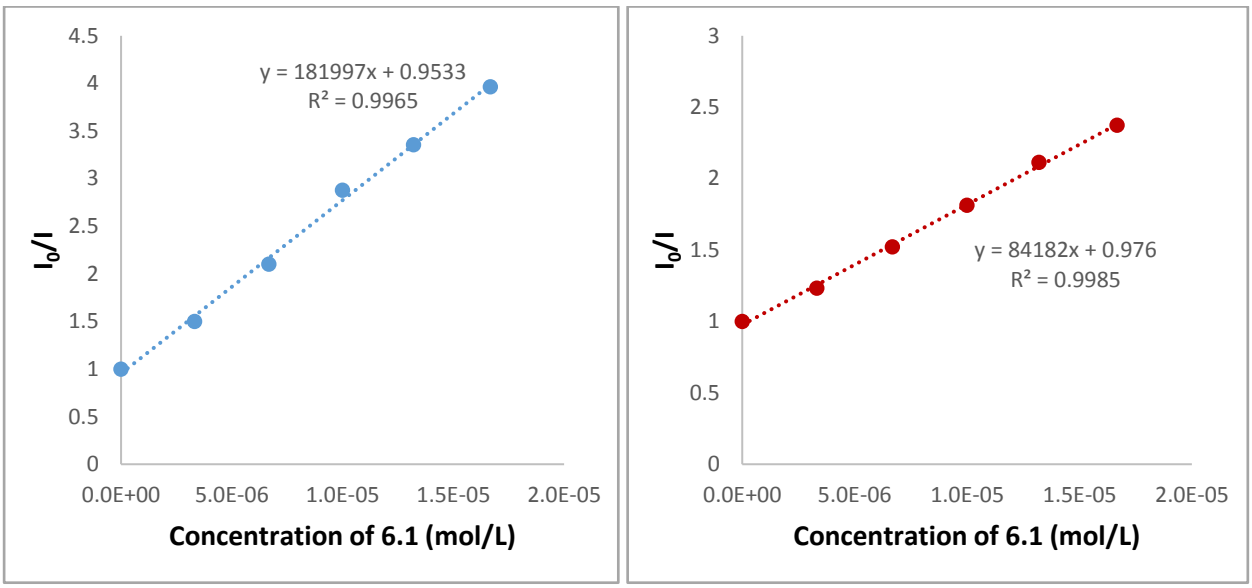

*Figure 6.19. Stern-Volmer graphs of the quenching effects of **6.1**. The Stern-Volmer graph of naphthalene (left) was calculated with the maximum peak at 337 nm (blue). The Stern-Volmer graph of triphenylene (right) was calculated with the local maxima at 421 nm (red).*

6.6 Chiral separation properties of chiral octahedron

As the structure of **6.1** is a chiral cage complex with a significant internal void volume, it was investigated for chiral resolution properties, in collaboration with the Hill group at Monash University. As outlined in Chapter 1, chiral coordination cages have been shown to have chiral resolution properties when used as both a heterogeneous or homogeneous separation medium. In the structure of **6.1** the chiral paddlewheel motifs form a chiral environment on the exterior of the cages by the arrangement of the isobutyl side chains of the (*S*)-LeuNDI ligand, and on the interior of the cage by the arrangement of the ligands in a propeller

motif. It is therefore possible that chiral separation may occur by interaction of a chiral analyte with the chiral paddlewheel motifs on either the inside or outside of the cage.

The heterogeneous chiral resolution properties of **6.1** were investigated by soaking a solid sample of as-synthesised **6.1** in a solvent in which it was not soluble, with a racemic sample of a soluble chiral analyte. Small chiral molecules were chosen, to increase the likelihood of them passing into the pores of the material. As the windows between the channels and the voids within the cages are ~5 Å wide, it is unlikely that the chiral guests will pass into the cages. The chiral molecules which were used were pantolactone, 2-methyl-2,4-pentanediol and 1-phenylethanol, Figure 6.20. These were chosen because they are all small chiral molecules which have a range of functional groups and each will therefore interact differently with **6.1**.

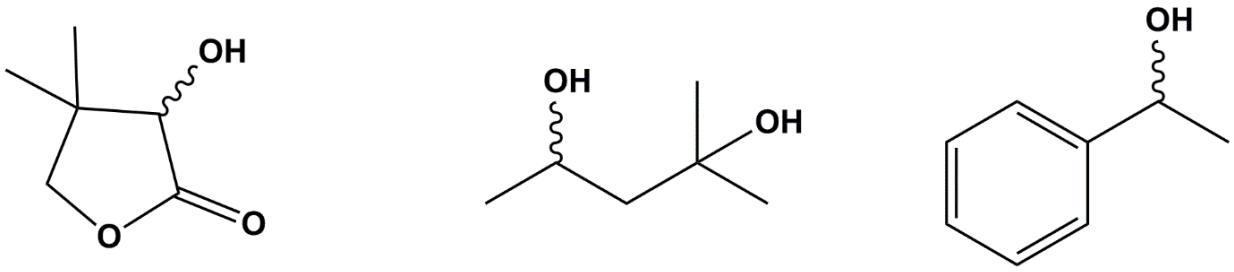

pantolactone **2-methyl-2,4-pentanediol** **1-phenylethanol**

*Figure 6.20. The small chiral molecules which were used to investigate the heterogeneous chiral resolution properties of **6.1**.*

The heterogeneous chiral separation properties of **6.1** were investigated by the following experiment: a mixture was prepared of **6.1** and the racemic chiral analyte in methanol or heptane. This mixture was left to soak for 24 hours to allow time for the analyte to interact and be adsorbed by the crystals of the cage complexes. After 24 hours the solid sample of **6.1** was recovered by filtration, washed slightly with methanol, and then soaked in methanol and left to sit for a further 24 hours, in order to desorb the analyte which had been trapped within the pores of the solid state material. The mixture was then centrifuged to isolate the solid state sample of **6.1**, and the supernatant was analysed by chiral GC in order to determine if there was an excess of either enantiomer. If **6.1** were to show chiral resolution properties, one enantiomer would be preferentially adsorbed into the material, and when the enantiomers are desorbed and analysed,

one enantiomer will be in excess compared to the other enantiomer. The results from these tests are summarised in Table 6.1.

*Table 6.1. The results of the chiral separation tests of **6.1** in the solid state.*

Analyte	**Solvent**	**ee%**
Pantolactone	Methanol	7%
2-methyl-2,4-pentanediol	Methanol	3%
2-methyl-2,4-pentanediol	Heptane	8%
1-phenylethanol	Methanol	13%
1-phenylethanol	Heptane	9%

Unfortunately the solid state separation with **6.1** achieved only very low enantioselectivity, with only one instance of an ee exceeding 10%. The separation of 1-phenylethanol gave the highest % ee for both solvents tested, at 13% in methanol and 9% in heptane. Pantolactone and 2-methyl-2,4-pentanediol both showed % ee of <10% in both methanol and heptane.

Examination of the solid state structure of **6.1** shows that all of the chiral groups on the exterior of the cage are facing into the smaller spherical voids which are isolated from the remaining voids within the structure. Therefore the chiral analyte molecules are unable to interact with the chiral paddlewheels on the exterior of the cage. The only remaining chiral environment is on the interior of the cage around the paddlewheel node, which the chiral analyte molecule may interact with in order to achieve enantioselective separation. However since the windows into the cage are too small to allow for the chiral guests to pass into the cage, it is unlikely that the guests are showing enantioselective absorption due to interactions with the inside of the cage.

The solid state material of **6.1** was shown to have quite poor enantioselective separation properties, most likely because the racemic chiral molecules are unable to interact with the chiral paddlewheel motifs on the exterior and interior of the cage. As **6.1** is a discrete coordination complex which shows some degree of solubility in a range of organic solvents, it would be very interesting to investigate the homogeneous enantioselective separation properties of **6.1** as future work.

6.7 Conclusion

The chiral octahedral coordination cage discussed herein is a remarkable material which displays a range of fascinating properties and structural features. It is the first reported example of an edge capped homochiral octahedral cage. The formation of the octahedral complex is possible through the combination of copper paddlewheel SBUs and the rigid chiral (*S*)-LeuNDI ligand. Using an achiral ligand, GlyNDI, with copper paddlewheels gives an infinite 2D sheet, suggesting that the octahedral cages will only form with a chiral ligand, as the chirality of the ligands force the groups around the paddlewheel into a propeller motif. The solid state material of **6.1** displays permanent porosity, as is confirmed by gas sorption experiments with a CO_2, H_2, CH_4, N_2 and N_2O over a range of pressures and temperatures. There are three distinct voids within the solid state structure of **6.1**; channels between the cages, spherical voids within the cages and spherical voids between the cages which were isolated from the channels, with volumes of approximately 2500, 2100 and 1000 $Å^3$, respectively. The volume of gas adsorbed into the material appears to show that the gas molecules may fill the voids within the cages and the channels between the cages, but is likely unable to access the spherical voids between the cages. The maximum gas adsorption was observed for CO_2 and N_2O, most likely because these molecules have a quadrupole moment and will therefore have improved interactions with the surface of the material in comparison to the molecules of H_2, CH_4 and N_2.

A crystalline sample of **6.1** was also investigated for chiral resolution properties. A series of small chiral molecules with varying functionality were tested to see if they would display enantioselective adsorption into a solid state sample of **6.1**. Unfortunately, **6.1** showed poor chiral resolution properties, with only one test showing an ee exceeding 10%, that of 1-phenylethanol in methanol. As **6.1** is a discrete complex and is solution stable, its chiral resolution properties in solution may also be investigated as part of future work.

As the H_2LeuNDI molecule has intriguing fluorescent properties (see Chapter 4), **6.1** was also investigated for its fluorescent properties, as it involves LeuNDI ligands. In a similar manner to the H_2LeuNDI ligand, it was observed that the fluorescence of **6.1** showed a broad emission peak at ~460 – 510 nm when dissolved in the aromatic solvents toluene and *o*-, *m*- and *p*-xylene. In the case of the H_2LeuNDI molecule this emission was attributed to the formation of exciplexes between the NDI and the aromatic solvent molecules,

facilitated by π-interactions. The similar emission of **6.1** to the H_2LeuNDI molecule suggests that the LeuNDI ligands within **6.1** are also forming exciplexes with aromatic solvent molecules. The LeuNDI ligands within **6.1** were also shown to interact with larger aromatic molecules, naphthalene and triphenylene, which are themselves fluorescent, in solution. The interaction of **6.1** with these molecules acted to quench the fluorescence of the naphthalene and triphenylene, following a Stern-Volmer relationship. The broad emission of **6.1** at ~460 – 510 nm when dissolved in aromatic solvents, and the quenching of fluorescence of larger aromatic molecules by **6.1** both suggest that the LeuNDI ligands within the complex will interact with other aromatic molecules in solution. These results confirm the solution stability of **6.1**, as well as show that the LeuNDI ligand still shows interesting fluorescent properties when incorporated into a coordination complex.

The chiral octahedral cage complex which is reported herein is a unique compound with varied and fascinating properties, which warrants further investigation to determine if it displays enantioselective guest binding or catalysis in solution.

Chapter 7: Conclusions

The aims of this research were to synthesise a series of chiral amino acid substituted diimide ligands, use them to form chiral coordination compounds with transition metals and subsequently investigate their properties. Four different diimide families were used, two of which had a linear core, the NDI and BDI ligands, and two which had bent cores, the BPSD and EADI ligands. The amino acids chosen were alanine, leucine and phenylalanine, as they vary in the steric bulk and aromatic functionality of their side chains. The achiral amino acid glycine was also used in order to explore the influence of removing the chirality of the ligand on the coordination compounds formed.

In Chapter 2 the amino acid substituted NDI ligands are shown to form a $\{M_2(NDI)_2\}$ metallomacrocyclic motif with remarkable reproducibility, forming in 73% of the coordination polymers discussed herein and in previous work by the Turner group. The coordination polymers obtained with the NDI ligands, dipyridyl ligands and transition metal centres tended towards interpenetration, either through a catenane motif between the $\{M_2(NDI)_2\}$ metallomacrocycles or by a rotaxane motif of the dipyridyl ligands threading through the $\{M_2(NDI)_2\}$ metallomacrocycles. The coordination polymers formed with NDI ligands are very likely to involve π-interactions, due to the π-rich aromatic core of the NDI.

In Chapter 3 the coordination behaviour of the BDI ligands were explored, as they are slightly longer and more flexible than their NDI counterparts. As the BDI core does not involve a fused aromatic system, unlike the NDI ligands, the coordination compounds with amino acid substituted BDI ligands did not involve π-interactions to the same extent as those with NDI ligands. The combination of AlaBDI or LeuBDI with Cd^{II} formed discrete macrocycles, in which the metal centres were capped with solvent molecules. Dipyridyl ligands were added in an attempt to form polymeric coordination networks, which was successful in the case of 4PyNDI, forming a 2D sheet with LeuBDI and Cd^{II}, however was not successful in the case of 4,4′-bipy, as it bridged between the Zn^{II} metal centres within a discrete $[Zn_2(AlaBDI)_2]$ macrocycle. The incorporation of copper paddlewheel SBUs with AlaBDI and LeuBDI formed $[M_8(BDI)_8]$ square complexes.

The fluorescent properties of the (*S*)-H_2LeuNDI molecule, in solution as a carboxylic acid and upon incorporation into discrete coordination complexes, were reported in Chapter 4. When (*S*)-H_2LeuNDI was dissolved in *o*-, *m*- or *p*-xylene or toluene, it formed exciplexes with these aromatic solvents. To further investigate this behaviour, two discrete coordination complexes were synthesised with Cd^{II} and LeuNDI, a macrocycle and a catenane, in which the metal centres were capped with the convergent dipyridyl ligands 1,10-phen or 2,2′-bipy, respectively. The fluorescence and absorption properties of the macrocycle and catenane were examined at varying concentrations and in chloroform solutions, as well as with varying proportions of toluene. By the comparison of the fluorescence emission properties of H_2LeuNDI and the macrocycle and catenane, it was determined that the NDI-NDI excimers will emit at ~ 480 nm and the exciplexes of NDIs with aromatic solvent molecules will emit at ~ 520 nm.

The behaviour of amino acid substituted diimide ligands with a bent core were discussed in Chapter 5. The BPSD ligands formed $[Cu_4(BPSD)_4]$ quadruple stranded helicate cages with chiral ligands, and quadruple stranded mesocates in the case of achiral ligands. In the BPSD system only one chiral ligand is required per $[Cu_4(BPSD)_4]$ cage, in order to induce the helicity of the cage, demonstrating that a quadruple stranded helicate is a robust supramolecular motif for this system of ligands with paddlewheel SBUs. The $[M_4(BPSD)_4]$ helicate cage was also synthesised with Rh^{II} paddlewheel nodes, which was investigated for chiral catalytic properties. Unfortunately, the cyclopropanation reaction catalysed by the $[Rh_4(LeuBPSD)_4]$ complex showed poor enantioselectivity, and therefore this system requires further study to determine the optimum reaction conditions to achieve higher enantioselectivity. A chiral EADI ligand was also synthesised as it has a similar bend in the core and is longer than the BPSD ligands. The EADI formed an analogous $[Cu_4(EADI)_4]$ quadruple stranded helicate cage to those formed with chiral BPSD, with a 25% increase in the internal void volume of the cage.

The combination of copper paddlewheel SBUs and the rigid LeuNDI ligand formed a chiral edge capped octahedral complex, which is discussed in Chapter 6, a class of complex that is unprecedented. The solid state octahedral cages are porous, demonstrated by both low and high pressure gas adsorption. The LeuNDI ligands in the octahedral cage complex maintained their fluorescent properties. Interaction with aromatic

solvent molecules shifted the emission maxima of the LeuNDI in the same manner as the H_2LeuNDI molecules in solution. The LeuNDI in the octahedral complex could also interact with larger aromatic molecules, triphenylene and naphthalene, demonstrated by the quenching of their fluorescence by the octahedral cage. The cage was also tested for chiral separation properties in the solid state with small chiral molecules, though this showed only low enantioselectivity. Future work will be directed towards optimising the conditions of separation and testing enantioselective separation properties of the compound in solution.

In conclusion, it was observed that in general the linear amino acid substituted diimide ligands will form coordination polymers, while the ligands with a bent core will form discrete coordination cage complexes. The exception to this rule was the combination of divergent dipyridyl ligands with linear NDI ligands which formed discrete coordination complexes with Cd^{II} metal centres. The other exception to this rule was in the coordination compounds incorporating copper paddlewheel SBUs, which formed discrete coordination complexes with the chiral linear BDI and NDI ligands.

The copper paddlewheel complexes present an interesting study of the influence of ligand structure on the coordination complexes formed. The diimide ligands with a significant bend in their core, BPSD and EADI, will form $[Cu_4L_4]$ helicate or mesocate complexes, with two metal nodes. The linear but slightly flexible and narrow BDI ligands formed $[Cu_8L_8]$ square complexes, with four copper paddlewheel nodes. Finally, the linear and rigid NDI ligand formed a $[Cu_{12}L_{12}]$ octahedral complex with six copper paddlewheel nodes in the case of the chiral (*S*)-LeuNDI ligand, and a 2D coordination polymer in the case of the achiral GlyNDI ligand. As the BDI and NDI ligands are both linear they are unable to form helicate or mesocate complexes, which would require the ligands to twist between two metal nodes. However, their difference in size and shape leads to their forming different coordination complexes with paddlewheel nodes. The flexibility of the core of the BDI ligand, in comparison to the rigid and wide NDI core, allows the BDI ligands to bend sufficiently in order to form $[Cu_8L_8]$ square complexes, and the narrow BDI core allows the ligands for form a complex in which two ligands form each edge of the square. The NDI ligands would not have sufficient flexibility and are too wide to be able to form analogous square complexes in which two ligands

form each edge, and instead form an octahedral complex in which each edge of the octahedron is occupied by a single NDI ligand.

The use of achiral ligands also has a different influence on the complexes obtained with copper paddlewheels, dependent on the ligand core. The achiral GlyNDI ligand forms a 2D coordination polymer with paddlewheel nodes, likely because the paddlewheel nodes are not forced into a propeller motif by the chirality of the ligand, giving more flexibility to the arrangement of the ligands around the paddlewheels and hence allowing formation of a coordination polymer. The achiral BPSD ligands have a different influence on the structure of the coordination complexes formed, as they still form $[Cu_4L_4]$ compounds, however the use of achiral ligands leads to the formation of an achiral complex, forming a mesocate instead of a helicate.

The work discussed herein shows an exploration of the coordination chemistry of amino acid substituted diimide ligands and the properties of some of the chiral coordination compounds which were formed. The core of the ligand, the bulkiness of the amino acid side chain, and the transition metal node utilised all had an influence on the coordination compounds formed, leading to an intriguing range of coordination complexes, including coordination polymers, helicate and mesocate complexes, and an unprecedented edge capped chiral octahedral complex. Some of the chiral coordination compounds formed warrant additional study, in order to further investigate their enantioselective catalysis and separation properties.

Chapter 8: Experimental

8.1 Materials and methods

Reagents

All starting materials, solvents and reagents were purchased from Sigma-Aldrich, TCI, Merck or Alfa Aesar and used as received. All chiral amino acid NDI compounds were synthesised according to literature procedures.[71, 352, 355] The 4PyNDI,[537] ethyl diazoacetate,[538] (*S*)-leucine phthalimide ((*S*)-leuPI),[539] [Rh_2((*S*)-leuPI)$_4$][496] and 9,10-dimethyl-9,10-dihydro-2,3,6,7-tetracarboxyl-9,10-ethanoanthracene[476] compounds were synthesised according to literature procedures.

Nuclear Magnetic Resonance (NMR) spectroscopy

Nuclear magnetic resonance spectra were collected using a Bruker DRX-400 spectrometer in d_6-DMSO with signals (reported in ppm) referenced against residual solvent peaks or TMS. ^{13}C-NMR spectra were collected at 100 MHz and ^{1}H-NMR spectra were collected at 400 MHz.

Mass Spectrometry

Low resolution mass spectrometry for the compounds was performed using a Micromass Platform Electrospray mass spectrometer in a DMSO/methanol solution as the mobile phase. The spectra were fitted with Agilent Multimode Source.

Mass spectrometry experiments of **4.1** and **4.2, 5.4** and **6.1** were performed by Dr W. Alex Donald at the University of New South Wales.

The mass spectroscopy of **5.4** and **6.1** were performed on a hybrid linear quadrupole ion trap and orbitrap mass spectrometer (Thermo LTQ Orbitrap XL) that is equipped with an electrospray ionisation (ESI) source. ESI solutions containing **5.4** and **6.1** in 99:1 acetonitrile:acetic acid were used. Acetic acid was added immediately before performing the measurement. For ion formation, a voltage of +5 kV was applied

to the ESI emitter relative to the capillary entrance of the mass spectrometer. Solutions were infused into the ESI source at 4 uL/min. The temperature of the capillary entrance to the mass spectrometer was 100°C.

Mass spectrometry experiments of **4.1** and **4.2**, were performed on a hybrid linear quadrupole ion trap and orbitrap mass spectrometer (Thermo LTQ Orbitrap XL) that was equipped with a custom external nanoelectrospray ionisation (nESI) source. Theta (dual chamber) were prepared by pulling borosilicate capillaries (theta capillaries, Harvard Apparatus, 1.5 mm o.d) to an inner orifice diameter of < 1 μm (Narishige PN-3 Glass Micropipette Puller, Narishige Scientific Instrument Labs, Tokyo, Japan). The electrospray capillaries were sputter-coated with a thin layer of Au and Pd (1:1 molar ratio) for 20 s (Scancoat Six, Edwards) operated at a pressure of 0.1 mbar in an Ar(g) atmosphere (1.25 kV, 30 mA). ESI solutions containing **4.1** and **4.2** in chloroform were loaded into a chamber of the theta capillary, with the other chamber containing acetonitrile with 1% acetic acid. For ion formation, a voltage of 1.5 kV was applied to the ESI emitter relative to the capillary entrance of the mass spectrometer. The temperature of the capillary entrance to the mass spectrometer is 50°C.

Mass spectrometry experiments of **Δ,Δ5.1**, **Λ,Λ5.1**, **5.2** and **5.3** were performed using an Agilent 6220 accurate mass LC-TOF system with Agilent 1200 Series HPLC, with an eluent of 0.3 mL/min of acetonitrile. The spectra were fitted with Agilent Multimode Source.

Mass spectrometry experiments of **5.5** and mixed ligand GlyBPSD:(*S*)-LeuBPSD complexes were performed using an Waters micromass ZQ QMS connected to an Agilent 1200 series HPLC system for automatic flow injections, with an eluent of 0.3 mL/min of methanol. The spectra were fitted with Agilent Multimode Source.

Infrared Spectroscopy

Infrared spectra were obtained using an Agilent Cary 630 diamond attenuated total reflection (ATR) spectrometer. MicroLab software was used to process the data.

Thermogravimetric Analysis

Thermogravimetric analysis (TGA) was conducted using a Mettler TGA/DSC 1 instrument. The temperature was ramped at 5 °C/min from room temperature to 400 °C under a dry N_2 supply of 10.0 mL/min. The data were analysed with the STARe program.

Microanalysis

Microanalyses were performed by either the Campbell Microanalysis Laboratory, Department of Chemistry, University of Otago, Dunedin, New Zealand or the Science Centre, London Metropolitan University, UK.

Circular Dichroism

Circular dichroism spectra were collected using a Jasco J-815 circular dichroism spectrophotometer. All spectra were collected from 200 – 350 nm in acetonitrile.

Powder X-Ray Diffraction

Powder X-ray diffraction (PXRD) data were collected at room temperature using a Bruker D8 Focus diffractometer equipped with Cu–Kα (λ = 1.5418 Å) radiation. The sample was mounted on a zero background silicon single crystal stage. Data were collected in the angle interval 2θ = 5 – 55° with a step size of 0.02°. The data was collected at 298 K and compared to predicted patterns based on the single crystal data (collected at 100 K).

Low Pressure Gas Sorption

The following relates to gas sorption studies undertaken on **6.1** at low pressure. In preparation for gas adsorption experiments, compound **6.1** was soaked in methanol overnight. The methanol was decanted from the samples, replaced with fresh methanol and left to soak for a further 24 hours. The sample was then recovered by filtration and loaded into a BET tube for sorption analysis, which was evacuated at 50 °C overnight using a Micromeritics Tristar VacPrep instrument (evacuated mass 0.1335 g of **6.1**). The sample was analysed for CO_2 and N_2 uptake, at 273 and 77 K, respectively, using a Micromeritics Tristar 3020

instrument. Temperature control was achieved using insulated iced water (273 K) or liquid nitrogen (77 K) baths. Ultra-high purity gasses (AirLiquide) were used for all analyses.

High Pressure Gas Sorption

The following relates to gas sorption studies undertaken on **6.1** at high pressure, which was undertaken by Dr. Keith White at the University of Melbourne. In preparation for gas adsorption experiments, compound **6.1** was soaked in methanol overnight. The methanol was decanted from the samples, replaced with fresh methanol and left to soak for a further 24 hours before being recovered by vacuum filtration. Prior to gas sorption measurements the methanol soaked sample of **6.1** was heated at 50 ˚C under dynamic vacuum for seven hours. The resultant solid of mass 0.1356 g underwent gas sorption experiments. The same sample of **6.1** was employed for each measurement, between gas sorption measurements the sample was heated at 50 ˚C under dynamic vacuum for at least one hour.

Gas sorption data were measured using a Sieverts-type BELsorp-HP automatic gas sorption apparatus (BEL Japan Inc.). 99.999% purity CO_2, N_2, He, H_2, and CH_4 and 99.9% purity N_2O were used for sorption studies. Non-ideal gas behaviour of each gas at each measurement and reference temperature was corrected for. Source data were obtained from the NIST fluid properties website.[540]

For isotherm measurements ranging from 258 – 298 K, sample compartment temperatures were controlled by a Julabo F25-ME chiller/heater that re-circulated fluid at +/- 0.1 °C through a capped, jacketed stainless steel flask housed within a polystyrene box. A calibrated external Pt 100 temperature probe monitored the flask temperature. Cryogenic temperatures were maintained with a BEL liquid N_2 level controller. Prior to gas sorption measurements, samples were held at the measurement temperature for a minimum of 1 hour to allow full thermal equilibrium to be attained before data collection.

Isosteric CO_2 and CH_4 sorption enthalpies were calculated using a least-squares fitting of a virial-type thermal adsorption equation that modelled ln(P) as a function of the amount of surface excess of gas sorbed at 258 and 273 K.[541] Optimised virial coefficients and R^2 values relating to CO_2 and CH_4 fitting are given in Table 8.1.

*Table 8.1: Optimised virial coefficients for modelling excess CO_2 and CH_4 on **6.1***

Gas	CO_2	CH_4
a0	-3496.25	-2351.61
a1	121.9241	-436.526
a2	-1.23584	701.4992
a3	-5.06492	-418.376
a4	1.301391	112.842
a5	-0.08698	-11.0367
b	15.39663	13.9544
$\mathbf{R^2}$	0.99966123	0.99698392

Quantum yields

The fluorescence quantum yield, Φ_{flu}, is the probability of an excited state resulting in fluorescence and is calculated by the ratio of photons emitted to the photons absorbed. The quantum yield is measured by comparing the emitted fluorescence with a standard of known quantum yield under identical conditions. The quantum yield is then calculated by the following equation:

$$\Phi_{flu} = \Phi_{ref} \frac{Area}{Area_{ref}} \cdot \frac{1-10^{-abs_{ref}}}{1-10^{-abs_{flu}}} \cdot \frac{\eta^2{}_{flu}}{\eta^2{}_{ref}}$$

where Φ_{flu} is the fluorescence quantum yield of the sample, *ref* is the standard reference, *Area* is the integrated area under the corrected emission spectrum, *abs* is the absorbance at the excitation wavelength and η is the refractive index of the solvent.

The standard material used for all measurements was quinine sulfate. All samples for quantum yield measurements were prepared with an absorbance of less than 0.1 at the absorption maximum, in order to avoid inner filter effects. Samples were degassed by bubbling N_2 gas through them for 10 minutes before measurement in order to reduce the effect of O_2 quenching.

Fluorescence lifetimes

Fluorescence lifetimes were measured using the method of time correlated single photon counting (TCSPC) on a set-up described previously.[542] The excitation source was a 375 nm pulsed diode laser (Picoquant, LDH-P-C-375) with a repetition rate of 5 or 10 MHz. The laser light was passed through a quarter waveplate (Thor labs) to ensure linear polarisaiton before being directed onto the sample. Emission was collected at

90° and passed through a polariser set to the magic angle (54.7°) to eliminate any photoselection bias. Detection wavelength selection was achieved using a monochromator (CVI, dk480) after which emission photons were focused onto a microchannel plate (Hamamatsu, R3809U-50) for detection. Photon emission times from the START (laser sync) and STOP (microchannel plate) signals were recorded using a photon timing device (PicoQuant, PicoHarp 300) and histogrammed to create a fluorescence decay profile. An instrument response function (IRF) was obtained by recording the decay profile of a scattering solution of dilute milk powder in water. Fluorescence lifetimes were determined by fitting the sample decay profile, by a sum of exponential functions convolved with the IRF, using a least-squares method based on the Levenberg-Marquardt algorithm (TRFA Global Analysis version 1.0, Scientific Software Technologies Centre). Goodness-of-fit was determined by the χ^2 parameter (values of ~$1.0 < \chi^2 < 1.2$ signifying a good fit) and inspection of the residuals (data minus fitted function) which should be randomly distributed about zero.

Absorbance and fluorescence emission

UV-Visible absorption measurements were taken with a Varian Cary 100 Bio UV-Visible spectrophotometer (Agilent) using solvent for baseline subtraction. Fluorescence excitation and emission spectra were recorded using a Varian Cary Eclipse fluorimeter (Agilent). All samples for steady state spectra were prepared in 1.0 cm path length quartz cuvettes. All solvents used for absorption and fluorescence measurements were of spectroscopic grade from Merck, TCI or Aldrich.

High performance liquid chromatography

HPLC was performed on an Agilent Infinity LC using a Symmetry C_{18} column of 3.9 x 150 mm dimensions with 5 μm particle size at a flow rate of 1 mL/minute of 100% acetonitrile. The output was measured at wavelengths of 220, 254 and 280 nm and the data were processed with Agilent Open Labs CDS Chemstation Editor software.

Chiral gas chromatography

The chiral separation properties of **6.1** were tested in collaboration with the Hill group at Monash University. Gas chromatographs were recorded on an Agilent 6890N fitted with a 7683B series

autosampler, Supelco Beta-Dex 120 column and FID detector. All injections were in methanol (1µl) with a 100:1 split ratio, the conditions for each analyte were as follows: 1-phenylethanol: 120 °C isothermal, injector 210°C, detector 200°C, He carrier gas 0.065MPa; pantolactone: 50°C (10 minutes) ramp at 5°C/minute to 200°C, injector 250°C, detector 250°C, He carrier gas 0.3 MPa. 2-methyl-2,4-pentanediol-100°C isothermal, injector 210°C, detector 200°C, He carrier gas 0.065 MPa. A temperature ramp to 170°C was completed for pantolactone and 1-phenylethanol methods to precondition the column for the next run, this was completed after each analyte had eluted. Enantiomeric excesses were calculated from the peak areas of each enantiomer of the analytes.

The products from the chiral catalysis tests with compound **5.5** were analysed by Dr Yada Nolvachai of the Marriott group at Monash University. The compounds were analysed with a Supelco Astec Chiraldex B-PM (30 m x 0.25 mm ID x 0.12 µm film thickness) with a DFS guard column (5 m x 25 mm ID), inlet temperature of 180 °C, FID temperature at 200 °C and acquisition rate of 5 Hz. The products from the reaction were diluted in acetonitrile (15 times dilution), 0.2 µL were injected with a split ratio of 100:1, with carrier gas of hydrogen at 1.5 mL/min at constant flow and temperature program of 100 °C to 180 °C (2 °C/min) and held at 180 °C for 60 minutes.

8.2 Synthesis of diimide compounds

8.2.1 Synthesis of naphthalene diimide compounds

<u>Synthesis of H_2GlyNDI</u>

A suspension of 1,4,5,8-naphthalene tetracarboxylic dianhydride (1.5 mmol, 400 mg) and glycine (3.1 mmol, 229 mg) in DMF (40 mL) was heated at 110 °C overnight, during which all solids were taken into solution. The reaction was poured onto approximately 100 mL of crushed ice, and allowed to stand until the ice had melted, resulting in precipitation of the product. H_2GlyNDI was collected by vacuum filtration and washed with water, before drying in a vacuum desiccator. Yield 408 mg, 71%. All analysis was consistent with the literature.[375] δ_H (400 MHz, d_6–DMSO), 4.79 (s, 4 H, H_2), 8.75 (s, 4 H, H_1), 13.21 (s, 2 H, H_3).

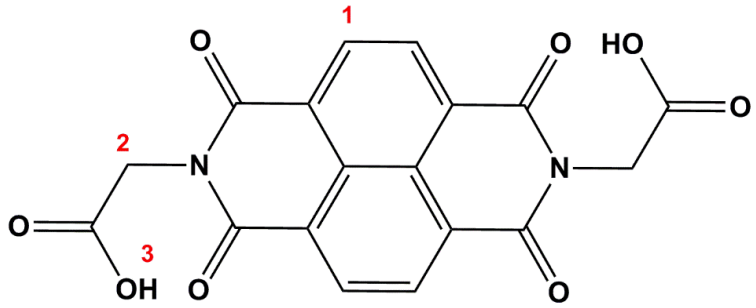

8.2.2 Synthesis of biphenyl diimide compounds

Synthesis of H_2GlyBDI

A suspension of 3,3′,4,4′-biphenyltetracarboxylic dianhydride (1.00 mmol, 294 mg) and glycine (2.10 mmol, 158 mg) in DMF (10 mL) was stirred at 100 °C overnight, during which all solids were taken into solution. The reaction was poured onto approximately 100 mL of crushed ice, and allowed to stand until the ice had melted, resulting in precipitation of the product. H_2GlyBDI was collected by vacuum filtration and washed with acetone (100 mL). Yield 273 mg, 70%. M.p. 329 – 330 °C. Found C, 56.60; H, 3.52; N, 7.06%; $C_{20}H_{12}N_2O_8 \cdot H_2O$ requires C, 56.34; H, 3.31; N, 6.57%. δ_H (400 MHz, d_6–DMSO), 4.32 (s, 4 H, H_4), 8.07 (d, J=7.8 Hz, 2 H, H_3), 8.34 (dd, ^3J=7.8, ^4J=1.5 Hz, 2 H, H_2), 8.38 (d, ^4J=1.5 Hz 2 H, H_1), 13.31 (s, 2 H, H_5). δ_C (100 MHz, d_6–DMSO), 40.33, 122.98, 124.56, 131.69, 132.98, 134.39, 145.01, 167.31, 169.328. υ_{max} /cm^{-1} 3193w, 2979w, 1767w, 1702s, 1655m, 1647m, 1637m, 1624m, 1619m, 1579w, 1430m, 1409m, 1388m, 1356m, 1306w, 1251m, 1227m, 1193m, 1182m, 1111m, 956s, 919m, 906w, 888w, 846m, 827m, 751s, 721m, 675m. *m/z* (ES$^-$) 363.0 ([M-COOH-H]$^-$ 100%, calculated for $C_{19}H_{11}N_2O_6^-$ 363.1); 407.0 ([M-H]$^-$, 41% calculated for $C_{20}H_{11}N_2O_8^-$, 407.1).

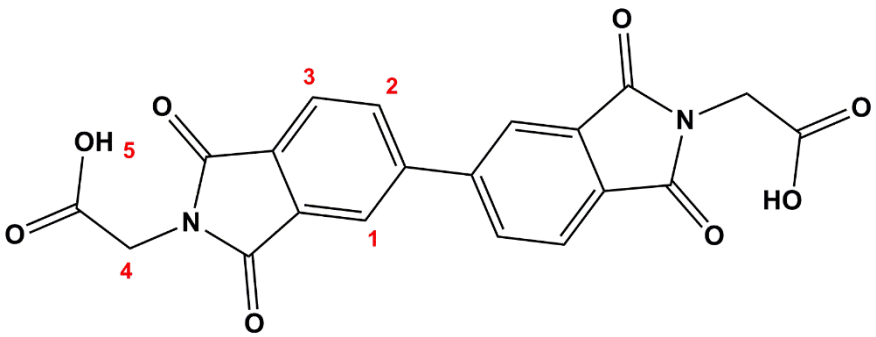

Synthesis of (*R*)-H_2 AlaBDI

A suspension of 3,3′,4,4′-biphenyltetracarboxylic dianhydride (1.00 mmol, 294 mg) and (*S*)-alanine (2.10 mmol, 187 mg) in acetic acid (5 mL) was heated by microwave irradiation for 5 minutes at 120 °C (power input 300 W). The reaction was poured onto approximately 100 mL of crushed ice and allowed to stand until the ice had melted, resulting in precipitation of the product. H_2AlaBDI was collected by vacuum filtration as a white powder and washed with water under all acid was removed. Yield 217 mg, 50%. M.p. 108 – 110 °C. Found C, 56.68; H, 4.23; N, 5.86%; $C_{22}H_{16}N_2O_8 \cdot 1.5H_2O$ requires C, 57.02; H, 4.13; N, 6.05. δ_H (400 MH, d_6–DMSO) 1.60 (d, *J*=7.3 Hz, 6 H, H_5), 4.92 (q, *J*=7.3, 2 H, H_4), 8.05 (d, *J*=7.8 Hz, 2 H, H_3), 8.32 (dd, ^3J = 7.8 Hz, ^4J=2.0 Hz, 2 H, H_2), 8.35 (s, 2 H, H_1), 12.01 – 14.09 (s, 2 H, H_6). δ_C (100 MHz, d_6–DMSO) 14.80, 47.13, 122.35, 124.00, 131.09, 132.36, 133.82, 144.51, 166.73, 166.75, 170.98, υ_{max} /cm^{-1} 3000w, 2920w, 1696s, 1618m, 1457w,1375m, 1241s, 1215m, 1144m, 1092m, 1019m, 920m, 887m, 779m, 741m, 972m. *m/z* (ES$^-$) 435.2 ([M-H]$^-$, calculated for $C_{22}H_{15}N_2O_8^-$, 435.1) 27%; 391.1 ([M-COOH-H]$^-$, calculated for $C_{21}H_{15}N_2O_6^-$, 391.1) 100%.

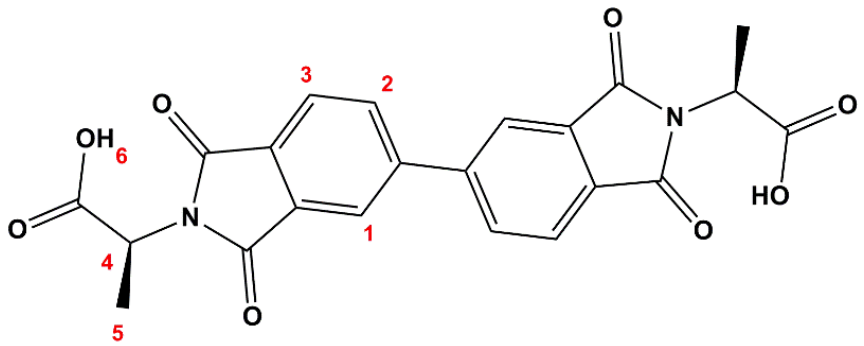

Synthesis of (*S*)-H_2LeuBDI

A suspension of 3,3′,4,4′-biphenyltetracarboxylic dianhydride (1.00 mmol, 294 mg) and (*S*)-leucine (2.10 mmol, 275 mg) in acetic acid (10 mL) was stirred at 120 °C overnight, during which all solids were taken into solution. The reaction was poured onto approximately 100 mL of crushed ice and allowed to stand until all the ice had melted, resulting in precipitation of the product. H_2LeuBDI was collected by vacuum filtration and washed with water until all acid was removed. Yield 448.5 mg, 86%. M.p. 267 – 273 °C. Found C, 62.03; H, 5.39; N, 5.23%; $C_{28}H_{28}N_2O_8 \cdot H_2O$ requires C, 62.45; H, 5.62; N, 5.20. δ_H (400 MH, d_6–DMSO) 0.91 (t, *J*=7.1 Hz, 12 H, H_8), 1.42 – 1.58 (m, 2 H, H_7), 1.89 (ddd, ^4J=4.4 Hz, ^3J=11.2 Hz, ^2J= 14.2

Hz, 1 H, H_5), 2.24 (ddd, ^3J=4.1, ^3J=10.3 Hz, ^2J= 14.2 Hz, 1 H, H_6), 4.85 (dd, J=4.4, 11.3 Hz, 2 H, H_4), 8.05 (d, J=7.8 Hz, 1 H, H_3), 8.32 (dd, ^3J=2.0 Hz, ^4J = 7.8 Hz, 1 H, H_2), 8.35 (s, 1H, H_1), 13.23 (br s, 2 H, H_9). δ_C (100 MHz, d_6–DMSO) 21.3, 23.5, 25.1, 37.2, 123.1, 124.6, 131.3, 132.6, 134.5, 145.5, 167.6, 171.2. υ_{max} /cm^{-1} 3588w, 3517w, 3471w, 3402w, 3202w, 3180w, 3073w, 2872w, 2650w, 1772m, 1707s, 1619w, 1468w, 1422m, 1377s, 1258m, 1202m, 1157m, 1098m, 1019m, 926m, 844m, 799w, 747s, 676m, *m/z* (ES$^-$) 475.2 ([M-COOH-H]$^-$, calculated for $C_{27}H_{27}N_2O_6^-$, 475.5), 100%.

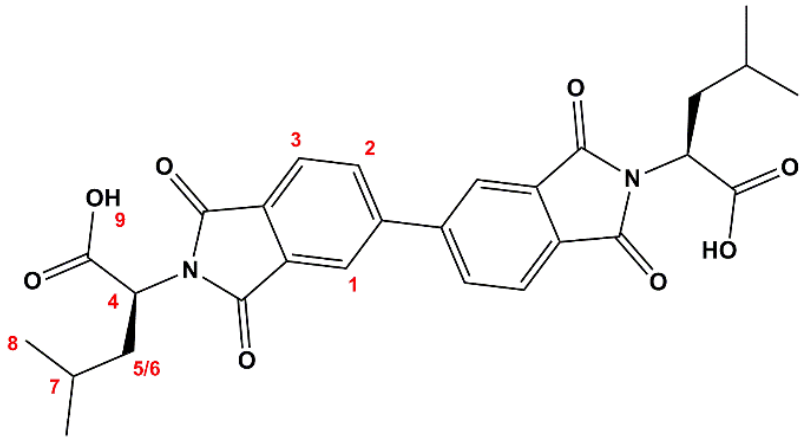

Synthesis of (*S*)-H_2PheBDI

A suspension of 3,3′,4,4′-biphenyltetracarboxylic dianhydride (1.00 mmol, 294 mg) and (*S*)-phenylalanine (2.10 mmol, 346 mg) in DMF (10 mL) was stirred at 90 °C overnight, during which time all solids were taken into solution. The reaction was poured over approximately 100 mL of crushed ice and allowed to stand until all the ice had melted. Concentrated hydrochloric acid was added dropwise to the solution which caused the precipitation of the product as a white powder, which was recovered by filtration and washed until all acid was removed. Yield 534 mg, 91%. M.p. 110-112 °C. Found C, 65.91; H, 4.36; N, 4.86%; $C_{34}H_{24}N_2O_8 \cdot 1.5H_2O$ requires C, 66.34; H, 4.42; N, 4.55. δ_H (400 MHz, d_6–DMSO) 3.38 (m, 2 H, $H_{5,6}$), 3.50 (m, 2 H, $H_{5,6}$), 5.14 (dd, J=11.7, 4.9 Hz, 2 H, H_4), 7.06 - 7.26 (m, 10 H, $H_{7,8,9}$), 7.93 - 7.98 (m, 2 H, H_3), 8.22 - 8.27 (m, 4 H, $H_{1,2}$). δ_C (100 MHz, d_6–DMSO) 34.4, 53.7, 123.0, 124.5, 127.1, 128.8, 129.2, 130.9, 132.9, 134.6, 137.8, 145.1, 167.2, 170.5. υ_{max} /cm^{-1} 3368s, 2604w, 2343w, 2101w, 1926w, 1883w, 1771m, 1702s, 1618s, 1497m, 1421m, 1378s, 1241m, 1186m, 1104s, 1029m, 999m, 949m, 913m, 843m,

740m, 697s. *m/z* (ES$^-$) 543.1 ([M-COOH-H]$^-$, calculated for $C_{33}H_{23}N_2O_6^-$, 100%); 587.1, ([M-H]$^-$, calculated for $C_{34}H_{22}N_2O_8^-$, 587.2) 78%.

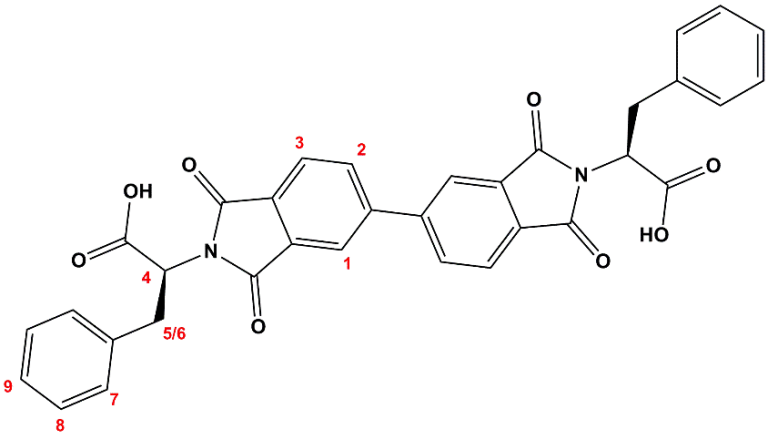

Synthesis of H_2IsoBDI

A suspension of 3,3′,4,4′-biphenyltetracarboxylic dianhydride (1.00 mmol, 343 mg) and 5-aminoisophthalic acid (2.10 mmol, 423 mg) in DMF (10 mL) was stirred at 120 °C overnight, during which time all solids were taken into solution. A white suspension formed when cooled and H_2IsoBDI was recovered by filtration and washed with water to remove all residual DMF. Yield 293 mg, 47%, M.p. >350 °C. Found C, 55.23; H, 3.13; N, 4.40%; $C_{32}H_{16}N_2O_{12}\cdot 4H_2O$ requires C, 55.50; H, 3.49; N, 4.05. δ_H (400 MHz, d_6–DMSO) 8.14 (d, *J*=7.7 Hz, 2 H, H_3), 8.33 (d, *J*=1.6 Hz, 4 H, H_4), 8.43 (dd, ^3J=7.81 Hz, ^4J=1.46 Hz, 2 H, H_2), 8.49 (d, *J*=1.3 Hz, 2 H, H_1), 8.53 (d, *J*=1.4, 2 H, H_5), 12.63 – 14.46 (br, 4 H, H_6). δ_C (100 MHz, d_6–DMSO), 122.9, 124.8, 129.6, 132.0, 132.22, 132.7, 133.1, 133.3, 134.3, 144.9, 166.5, 166.9. υ_{max} /cm^{-1} 3087m, 2876w, 2632w, 2093w, 2061w, 1998w, 1907w, 1849w, 1773m, 1719s, 1655m, 1601m, 1439m, 1415m, 1376s, 1282m, 1223s, 1090s, 1020m, 912m, 880w, 852w, 757s, 733s. 710s, 661m. *m/z* (ES$^-$) 309.0 ([M-2H]$^{2-}$, calculated for $C_{32}H_{14}N_2O_{12}^{2-}$, 309.0) 100%; 619.1 (M-H)$^-$, calculated for $C_{32}H_{15}N_2O_{12}^-$, 619.1) 9.1%.

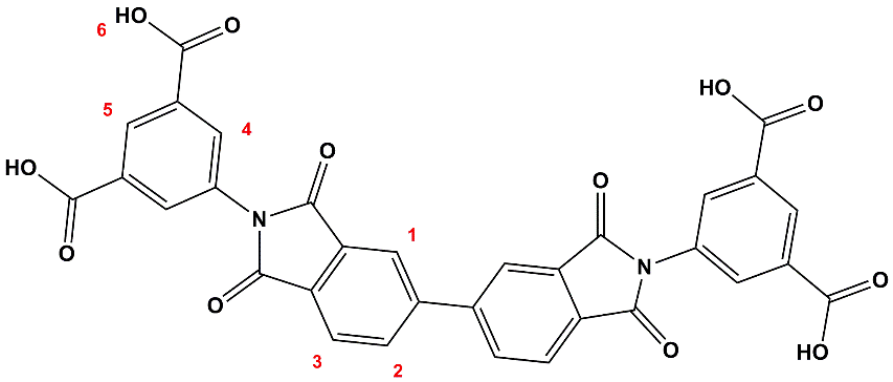

8.2.3 Synthesis of biphenyl sulfone diimide compounds

<u>Synthesis of H_2GlyBPSD</u>

A suspension of 3,3′,4,4′-biphenylsulfone tetracarboxylic dianhydride (1.00 mmol, 357 mg) and glycine (2.10 mmol, 158 mg) in DMF (10 mL) was heated at 100 °C overnight, during which time all solids were taken into solution. The reaction was poured onto approximately 100 mL of crushed ice and allowed to stand until all the ice had melted, resulting in precipitation of the product. H_2GlyBPSD was isolated as a white powder by vacuum filtration, washed with water (200 mL) and dried *in vacuo*. Yield 247 mg, 52%. M.p. 332 – 336 °C. Found C, 50.78; H, 2.65; N, 5.75%; $C_{20}H_{12}N_2O_{10}S$ requires C, 50.85; H, 2.56; N, 5.93%. δ_H (400 MHz, d_6–DMSO) 4.36 (s, 4 H, H_4), 8.18 (d, ^3J=7.8 Hz, 2 H, H_2), 8.62 (m, 4 H, H_1,H_3), 12.7 (br, 2 H, H_5). δ_C (100 MHz, d_6–DMSO) 40.5, 123.4, 125.5, 133.2, 135.1, 136.3, 145.3, 166.0, 166.2, 169.0. υ_{max} /cm^{-1} 3998w, 3950w, 3855w, 3713w, 3635w, 3493w, 2967w, 2900w, 2799w, 2725w, 2648w, 2546.4w, 2460 w, 2371w, 1782m, 1711s, 1528w, 1405s, 1314m, 1226m, 1146s, 1060m, 1008m, 963s, 926m, 883m, 852m, 755s, 671s.

m/z (ES$^-$) 470.9 ([M-H]$^-$, calculated for $C_{20}H_{11}N_2O_{10}S^-$, 471.0) 100%.

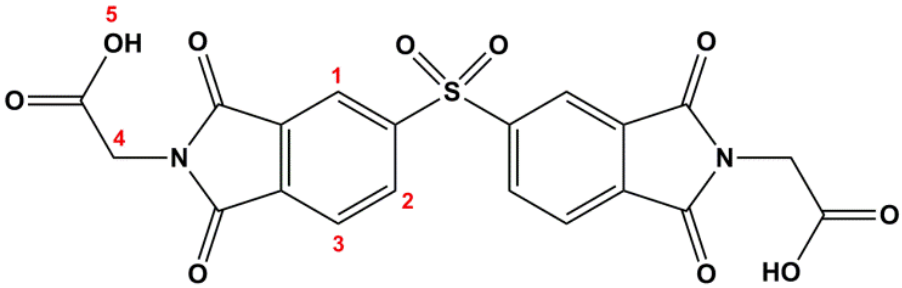

Synthesis of (*S*)-H_2AlaBPSD

A suspension of 3,3′,4,4′-biphenylsulfone tetracarboxylic dianhydride (1.00 mmol, 357 mg) and (*S*)-alanine (2.10 mmol, 187 mg) in acetic acid (15 mL) was stirred at 120 °C overnight, during which time all solids were taken into solution. The reaction was poured over approximately 100mL of crushed ice and allowed to stand until all the ice had melted, resulting in precipitation of the product. H_2AlaBSDI was recovered as a white powder by vacuum filtration and washed with water until all acid was removed. Yield 292.8 mg, 59%. M.p. 176 – 181 °C. Found C, 51.08; H, 3.48; N, 5.41%; $C_{22}H_{16}N_2O_{10}S$ requires C, 50.97; H, 3.50; N, 5.40%. δ_H (400 MHz, d_6–DMSO) 1.54 (d, *J*=7.4 Hz, 6 H, H_5), 4.91 (q, *J*=7.4 Hz, 2 H, H_4), 8.13 (d, *J*=8.3 Hz, 2 H, H_3), 8.57 (dd, ^4J= 1.5 Hz, ^3J= 5.9 Hz, 2 H, H_2), 8.58 (d, *J*=1.5 Hz, 2 H, H_1), 12.23 - 13.86 (br, 2 H, H_6). δ_C (100 MHz, d_6–DMSO), 15.1, 17.9, 123.3, 125.3, 133.2, 135.0, 136.2, 145.8, 165.9, 171.1. υ_{max} /cm^{-1} 3489w, 3305w, 3158w, 3085w, 3010w, 2934w, 2861w, 2656w, 2544w, 1782w, 1713s, 1614w, 1448m, 1422m, 1377s, 1351s, 1316s, 1269s, 1169m, 1145m, 1105m, 1064m, 1016m, 904m, 861m, 837m, 745m, 713m, 671s. *m/z* (ES$^-$) 411.1 ([M-O-CHCH$_3$COOH-H]$^-$, calculated for $C_{19}H_{11}N_2O_7S^-$ 411.0) 100%, 499.1 ([M-H]$^-$, calculated for $C_{22}H_{15}N_2O_{10}S^-$, 499.1), 91%.

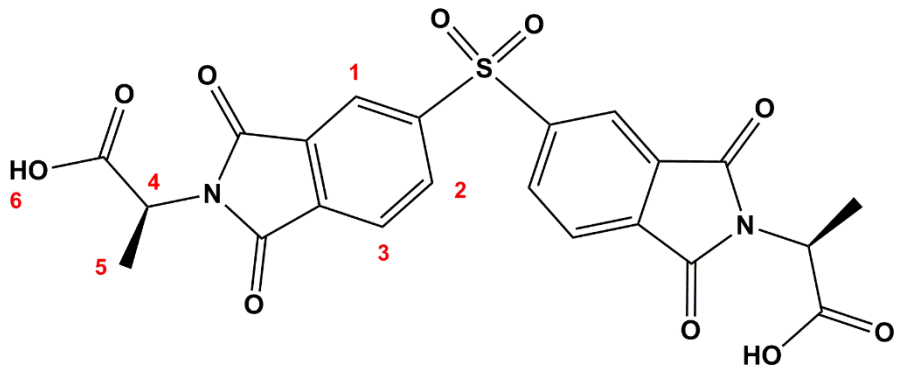

Synthesis of (*S*)-H_2LeuBPSD

A suspension of 3,3′,4,4′-biphenylsulfone tetracarboxylic dianhydride (1.00 mmol, 357 mg) and (*S*)-leucine (2.10 mmol, 275 mg) in glacial acetic acid (5 mL) was heated by microwave radiation at 120 °C for 10 minutes (power input 300 W). The solution was poured over approximately 100 mL of crushed ice and allowed to stand until the ice had melted, resulting in precipitation of the product. (*S*)-H_2LeuBPSD was isolated as a white powder which was recovered by vacuum filtration, washed with water until all acid was

removed and dried *in vacuo*. Yield 418 mg, 72%. M.p. 159 – 165 °C. Found C, 54.82; H, 5.05; N, 4.77%; $C_{28}H_{28}N_2O_{10}S{\cdot}1.5H_2O$ requires C, 54.99; H, 5.11; N, 4.58%. δ_H (400 MHz, d_6–DMSO) 0.89 (d, ^3J=7.0 Hz, 6 H, H_8,H_9), 0.91 (d, ^3J=7.0 Hz, 6 H, H_8,H_9), 1.48 (m, 2 H, H_7), 1.89 (ddd, ^2J=14.0 Hz, ^3J=10.9 Hz, ^3J=4.2 Hz, 2 H, $H_{5,6}$), 2.10 (ddd, ^2J=14.0 Hz, ^3J=10.9 Hz, ^3J=4.2 Hz, 2 H, H_5,H_6), 4.82 (dd, ^3J=10.9, ^3J=4.2 Hz, 2 H, H_4), 8.16 (d, ^3J=7.8 Hz, 2 H, H_2), 8.60 (m, 4 H, H_1, H_3). δ_C (100 MHz, d_6–DMSO) 21.3, 23.5, 24.8, 37.2, 51.0, 123.5, 125.5, 132.9, 135.2, 135.9, 145.9, 166.3, 166.5, 170.9. υ_{max} /cm^{-1} 3993w, 3928w, 3868w, 3823w, 3747w, 3682w, 3536w, 3516w, 3486w, 3344w, 3266w, 3169w, 3052w, 2871w, 2490w, 1780w, 1719s, 1637w, 1544w, 1469w, 1383s, 1323m, 1256m, 1146m, 1104w, 1059w, 934w, 860w, 745m, 672s. *m/z* (ES$^-$) 583.0 ([M-H]$^-$, calculated for $C_{28}H_{27}N_2O_{10}S^-$, 583.1) 100%.

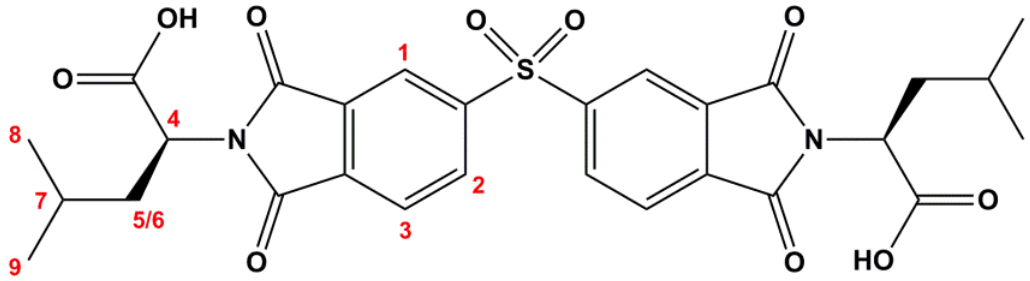

Synthesis of (*R*)-H_2LeuBPSD

A suspension of 3,3′,4,4′-biphenylsulfone tetracarboxylic dianhydride (1.00 mmol, 357 mg) and (*R*)-leucine (2.10 mmol, 275 mg) in acetic acid (5 mL) was heated by microwave radiation at 120 °C for 10 minutes (power input 300 W). The solution was poured over approximately 100 mL of crushed ice and allowed to stand until the ice had melted, resulting in precipitation of the product. (*R*)-H_2LeuBPSD was isolated as a white powder which was recovered by vacuum filtration, washed with water until all acid was removed. Yield 461 mg, 79%. M.p. 150 – 155 °C. Found C, 54.31; H, 4.97; N, 4.54%; $C_{28}H_{28}N_2O_{10}S{\cdot}2H_2O$ requires C, 54.19; H, 5.20; N, 4.51%. δ_H (400 MHz, d_6–DMSO) 0.84 (d, ^3J=7.1 Hz, 6 H, H_8,H_9), 0.86 (d, ^3J=7.1 Hz, 6 H, H_8,H_9), 1.48 (m, 2 H, H_7), 1.84 (ddd, ^2J=14.1, ^3J=10.8, ^3J=4.1, 2 H, H_5,H_6), 2.14 (ddd, ^2J=14.1, ^3J=10.8, ^3J=4.1, 2 H, H_5,H_6), 4.81 (dd, ^3J=11.2, ^4J=4.2, 2 H, H_4), 8.15 (dd, ^3J=7.8, ^4J=1.0, 2 H, H_2), 8.59 (m, 4 H, H_1,H_3). δ_C (100 MHz, d_6–DMSO), 21.3, 23.5, 24.8, 37.1, 51.0, 123.5, 125.5, 132.9, 135.2, 135.9, 145.9, 166.3, 166.5, 170.9. υ_{max} /cm^{-1} 2961w, 2875w, 2629w, 2506w, 1715s, 1618w, 1469w, 1383s, 1324m,

1256m, 1145m, 1059m, 932m, 861w, 746m, 671s. *m/z* (ES$^-$) 583.2 ([M-H]$^-$, calculated for $C_{28}H_{27}N_2O_{10}S^-$, 583.1) 100%.

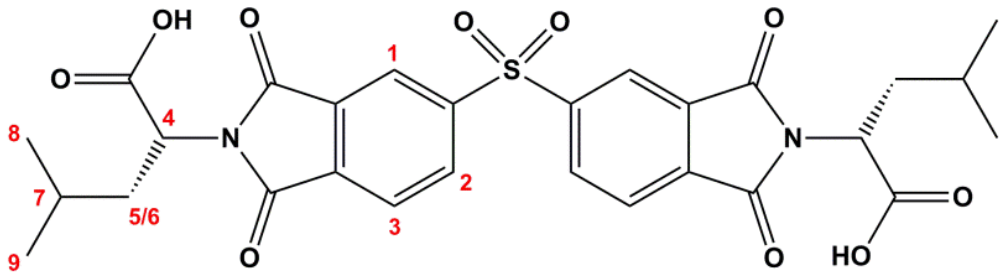

Synthesis of (*S*,*R*)-H_2LeuBPSD

A suspension of 3,3′,4,4′-biphenylsulfone tetracarboxylic dianhydride (1.00 mmol, 357 mg), (*R*)-leucine (1.05 mmol, 138 mg) and (*S*)-leucine (1.05 mmol, 138 mg) in acetic acid (5 mL) was heated at 120 °C with stirring overnight. The solution was poured over approximately 100 mL of ice and allowed to stand until the ice had melted, which caused the product to precipitate as a white powder. The product was recovered by vacuum filtration, washed with water until all acid was removed and dried *in vacuo*. Yield 526 mg, 90%. M.p. 153 – 157 °C. Found C, 57.39; H, 4.76; N, 4.74%; $C_{28}H_{28}N_2O_{10}S$ requires C, 57.52; H, 4.83; N, 4.79%. δ_H (400 MHz, d_6–DMSO) 0.85 (m, 12 H, H_8), 1.48 (m, 2 H, H_7), 1.85 (ddd, ^2J=14.2, ^3J=10.7, ^3J=4.0 Hz, 2 H, H_5, H_6), 2.15 (ddd, ^2J=14.2, ^3J=10.7, ^3J=4.0 Hz, 2 H, H_5, H_6), 4.81 (dd, ^3J=10.7, ^3J=4.0 Hz, 2 H, H_4), 8.15 (dd, ^3J=7.8, ^4J=1.0, 2 H, H_2), 8.59 (m, 4 H, H_1,H_3), 13.26 (br. s, 2 H, H_9). δ_C (100 MHz, d_6–DMSO), 21.3, 23.5, 24.8, 37.2, 51.0, 123.5, 125.5, 132.9, 135.2, 135.9, 145.9, 166.3, 166.5, 170.9. υ_{max}/cm^{-1} 2760w, 1780w, 1717s, 1616w, 1469w, 1422w, 1383s, 1323m, 1264w, 1146µ, 1103µ, 1059µ, 932w, 859w, 800w, 744m, 673s. *m/z* (ES$^-$) 583.1 ([M-H]$^-$, calculated for $C_{28}H_{27}N_2O_{10}S^-$, 583.1) 100%. It is likely that the product was a statistical mixture of the (*S*,*R*)-H_2LeuBPSD, (*S*,*S*)-H_2LeuBPSD and (*R*,*R*)-H_2LeuBPSD compounds.

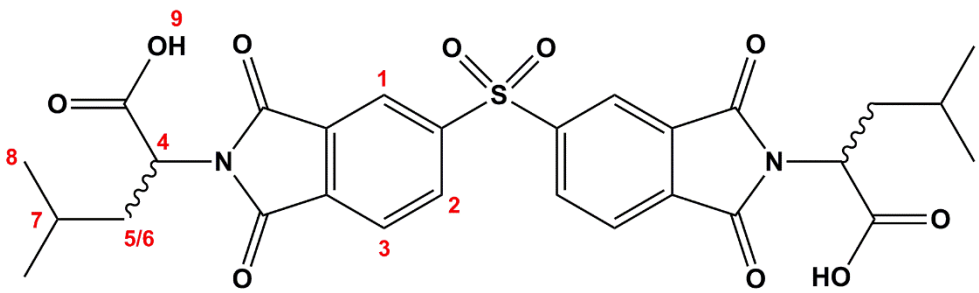

Synthesis of (*S*)-H_2PheBPSD

A suspension of 3,3′,4,4′-biphenylsulfone tetracarboxylic dianhydride (1.00 mmol, 357 mg) and (*S*)-leucine (2.10 mmol, 347 mg) in acetic acid (5 mL) was heated by microwave radiation at 120 °C for 10 min (power input 300 W). The solution was poured over approximately 100 mL of crushed ice and allowed to stand until the ice had melted, resulting in precipitation of the product. H_2PheBSDI was isolated as a white powder which was recovered by vacuum filtration and washed with water until all acid was removed. Yield 562 mg, 86%. M.p. 140 – 145 °C. Found C, 58.87; H, 4.00; N, 3.99%; $C_{34}H_{24}N_2O_{10}S\cdot2.5H_2O$ requires C, 58.53; H, 4.19; N, 4.02%. δ_H (400 MHz, d_6–DMSO) 3.27 (dd, ^2J=14.1 Hz, ^3J= 11.2 Hz, 2 H, $H_{5,6}$), 3.49 (dd, ^2J=14.1 Hz, ^3J= 4.9 Hz, 2 H, $H_{5,6}$), 5.15 (dd, ^3J=11.2 Hz, ^3J= 4.9 Hz, 2 H, H_4), 7.03 - 7.24 (m, 10 H, $H_{7,8,9}$), 8.07 (d, J=7.8 Hz, 2 H, H_3), 8.52 (d, J=1.5 Hz, 2 H, H_1), 8.54 (dd, ^4J=7.7 Hz, ^3J=1.5 Hz, 2 H, H_2), 13.15 - 13.64 (br, 2 H, H_{10}). δ_C (100 MHz, d_6–DMSO), 34.4, 53.9, 123.7, 125.5, 127.1, 128.8, 129.2, 132.3, 135.4, 135.5, 137.6, 145.9, 165.8, 170.1. υ_{max} /cm^{-1} 3596w, 3538w, 3517w, 3437w, 3402w, 3339w, 3258w, 3236w, 3161w, 3064w, 3029w, 2930w, 2749w, 2600w, 2516w, 1780m, 1717s, 1618w, 1497w, 1456w, 1420m, 1383s, 1323m, 1245m, 1178m, 1146s, 1105s, 1059m, 999m, 951m, 919m, 871m, 741s, 701m, 671s. *m/z* (ES$^-$) 651.1 ([M-H]$^-$, calculated for $C_{34}H_{23}N_2O_{10}S^-$, 651.1) 100%.

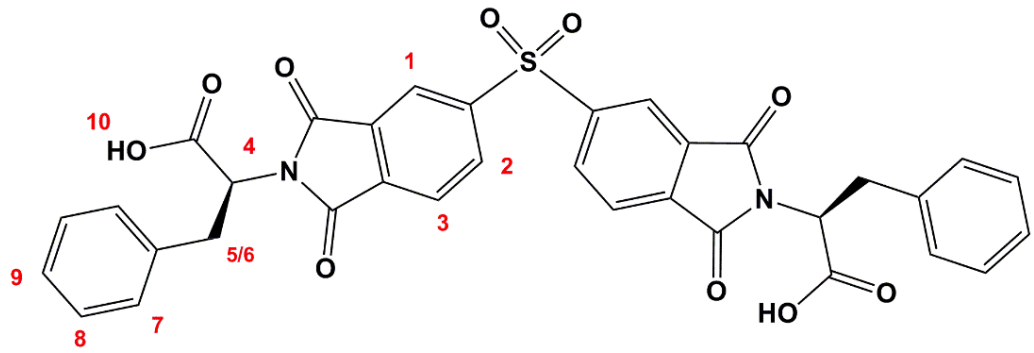

8.2.4 Synthesis of ethanoanthracene diimide molecule

Synthesis of (*S*)-Leucine-9,10-dimethyl-9,10-dihydro-2,3,6,7-diimido-9,10-ethanoanthracene

A suspension of (*S*)-Leucine (150 mg, 1.15 mmol) and 9,10-dimethyl-9,10-dihydro-2,3,6,7-tetracrboxyl-9,10-ethanoanthracene (190 mg, 0.463 mmol) were added to a RBF with acetic acid (20 mL) and heated at 120 °C for four nights, during which time all solids were taken into solution. After this time the light yellow

solution was poured over ice, forming a light yellow precipitate which was recovered by filtration, washed with water and dried *in vacuo*. Yield 172.5 mg, 62%, M.p. 195 – 198 °C. Found C, 63.56; H, 5.96; N, 3.99%; $C_{34}H_{36}N_2O_8$ requires C, 63.32; H, 6.15; N, 3.89%. δ_H (400 MHz, d_6–DMSO) 0.81 (m, 12 H, H_8), 1.36 (m, 2 H, H_7), 1.67 (s, 4 H, H_1), 1.8 (m, 2 H, H_5, H_6), 2.21 (s, 6 H, H_2), 2.16 (m, 2 H, H_5, H_6), 4.74 (dd, ^3J=12, ^3J=4.2 Hz, 2 H, H_4), 7.78 (s, 4H, H_3). δ_C (100 MHz, d_6–DMSO) 21.1, 23.5, 26.1, 37.1, 43.4, 44.3, 50.6, 116.6, 129.7, 152.8, 168.0, 171.3. υ_{max} /cm^{-1} 2958w, 2871w, 1841w, 17700m, 1702s, 1617m, 1534w, 1465w, 1442w, 1377s, 1321w, 1250m, 1205m, 1155m, 1088w, 991w, 911w, 869w, 752m. *m/z* (ES$^-$) 504.1 ([M-Leu+OH]$^-$, calculated for $C_{26}H_{26}NO_8^-$, 504.2), 100%, 599.2 ([M-H]$^-$, calculated for $C_{34}H_{35}N_2O_8^-$, 599.2) 93%.

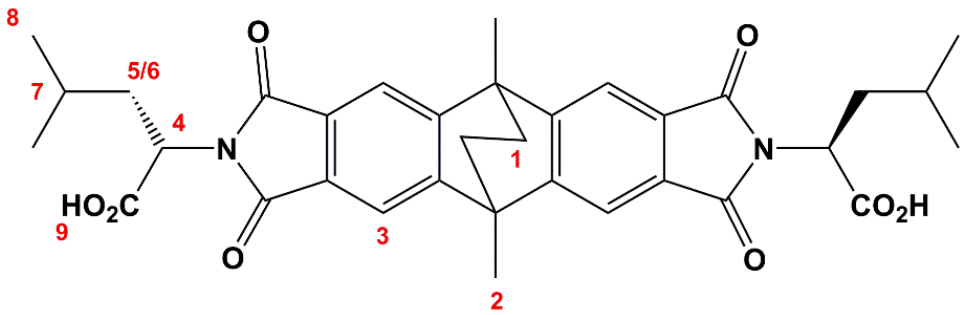

8.3 Synthesis of coordination complexes

Synthesis of *poly*-[Cd_2(AlaNDI)$_2$(4,4′-bipy)(DMF)$_3$(OH_2)][Cd_2(AlaNDI)$_2$(4,4′-bipy)(DMF)$_2$(OH_2)$_2$], 2.1

(*S*)-H_2AlaNDI (10.0 mg, 24.4 µmol), $Cd(NO_3)_2 \cdot 4H_2O$ (15 mg, 48.8 µmol) and 4,4′-bipyridine (1.9 mg, 12.2 µmol) were added to DMF (3mL) in a glass vial and sonicated to dissolve. The solution was heated at 100 °C in a dry bath incubator for 24 hours, during which time yellow needle-shaped crystals of **2.1** were formed, which were recovered by vacuum filtration. Yield 12.1 mg, 34%. Found C, 49.37; H, 4.03; N, 9.00%; $C_{59}H_{55}N_9O_{20}Cd_2$ ([Cd_2(AlaNDI)$_2$(4,4′-bipy)(DMF)$_3$(OH_2)]): requires C, 49.38; H, 3.86; N, 8.78%. υ_{max} /cm^{-1} 2934w, 1701w, 1646s, 1568s, 1449w, 1400m, 1375m, 1354m, 1331s, 1293m, 1244s, 1216m, 1193m, 1091m, 1060w, 1044w, 964w, 922w, 991w, 927w, 761m, 722w, 672m. TGA: On-set, 40 °C mass loss = 17.0% (calculated 16.5% for loss of one coordinated H_2O and three coordinated DMF molecules), decomp. 380 °C. Bulk purity was confirmed by PXRD.

Synthesis of *poly*-[Cd_4(AlaNDI)$_4$(4,4′-bipy)(DMF)$_4$(OH_2)$_2$]·5H_2O·4DMF, 2.2

(*S*)-H_2AlaNDI (10.0 mg, 24.4 μmol), $Cd(NO_3)_2·4H_2O$ (30.0 mg, 97.4 μmol) and 4,4′-bipyridine (3.8 mg, 24.4 μmol) were added to a mixture of DMF (2 mL), methanol (1 mL) and water (1 mL) and sonicated to dissolve. The solution was heated at 85 °C in a dry bath incubator for 24 hours, during which time yellow needle-shaped crystals of **2.2** were formed, which were recovered by vacuum filtration. Yield 13.5 mg. The X-ray diffraction data were processed with the SQUEEZE routine of PLATON[534] which showed voids of 786 Å^3 containing 211 e^- per formula unit, which would account for voids filled with five water molecules and four DMF molecules. Attempted synthesis of a pure phase of **2.2** was unsuccessful due to concomitant formation of **2.4**.

Synthesis of *poly*-[Mn_4(AlaNDI)$_4$(4,4′-bipy)(DMF)$_4$(OH_2)$_2$]·2DMF·5.5H_2O, 2.3

H_2AlaNDI (10.0 mg, 24.4 μmol), $Mn(NO_3)_2·4H_2O$ (12.0 mg, 97.6 μmol) and 4,4′-bipyridine (3.8 mg, 24.4 μmol) were added to a solvent mixture of DMF (2 mL), methanol (1 mL) and water (1 mL) and sonicated to dissolve. The solution was heated to 85 °C in a dry bath incubator overnight, to yield yellow crystals of **2.3** which were recovered by filtration. Yield 4.6 mg, 36%. Found C, 49.77; H, 3.82; N, 8.89%; $C_{96}H_{80}N_{12}O_{39}Mn_4$·2DMF·5.5$H_2O$: requires C, 49.87; H, 4.46; N, 8.62%. ν_{max}/cm^{-1} 2934w, 1699m, 1650s, 1579s, 1505w, 1442m, 1410m, 1373m, 1351s, 1323s, 1271m, 1240s, 1222m, 1099m, 1067w, 1038w, 995w, 967w, 921w, 883w, 844w, 805m, 760s, 728w, 675m. TGA: on-set, 25 °C mass loss = 10.7% (calculated 10.9% for loss of all coordinated DMF and H_2O, and 5.5 non-coordinated H_2O and two non-coordinated DMF molecules). Bulk purity was confirmed by PXRD. The X-ray diffraction data were processed using the SQUEEZE routine of PLATON, showing a total void space of 860 Å^3 containing 190 e^- per unit cell (430 Å^3 with 95 e^- per formula unit). The solvent assigned from the microanalysis which was not present in the crystal structure (1 DMF and 5.5 H_2O molecules) accounts for 95 e^- per formula unit.

Synthesis of *poly*-[Cd(AlaNDI)(4,4′-bipy)(OH_2)]·3.5H_2O·0.5DMF, 2.4

(*S*)-H_2AlaNDI (20.0 mg, 48.8 μmol), $Cd(NO_3)_2·4H_2O$ (15.0 mg, 48.8 μmol) and 4,4′-bipyridine (7.6 mg, 48.8 μmol) were added to a mixture of DMF (2 mL), methanol (1 mL) and water (1 mL) and sonicated to dissolve. The solution was heated at 85 °C in a dry bath incubator for four hours, during which time yellow

needle-shaped crystals of **2.4** were formed, which were recovered by vacuum filtration. Yield 9.5 mg, 28%. Found C, 47.58; H, 3.55; N, 7.95%; $C_{30}H_{22}N_4O_9Cd{\cdot}3.5H_2O{\cdot}0.5DMF$ ([Cd(AlaNDI)(4,4′-bipy)(OH_2)]·3.5H_2O·0.5DMF); requires C, 47.61; H, 4.12; N, 7.93%. υ_{max} /cm^{-1} 3359w, 2941w, 2365w, 2084w, 1705m, 1662s, 1572s, 1491w, 1448w, 1408s, 1365m, 1330s, 1246s, 1220m, 1200m, 1150w, 1095m, 1065m, 1008w, 967w, 922w, 879w, 858m, 812m, 765s, 728m. TGA: On-set, 65 °C mass loss = 14.9% (calculated 14.8% loss for loss of coordinated water and non-coordinated solvent of 3.5 water molecules and 0.5 DMF molecules), decomp. 350 °C. The X-ray diffraction data were processed with the SQUEEZE routine of PLATON[534] which showed voids of 232 Å^3, containing 73.5 e$^-$, per asymmetric unit. The solvent observed in the TGA and microanalysis which is not modelled in the voids of the crystal structure would account for 55e$^-$ per asymmetric unit, so it appears that a small amount of solvent may have been lost from the structure before microanalysis or TGA were conducted. Bulk purity was confirmed by PXRD.

Synthesis of *poly*-[Zn_2(AlaNDI)$_2$(4,4′-bipy)$_2$]·0.3MeOH·0.7H_2O, 2.5

(*S*)-H_2AlaNDI (10.0 mg, 24.4 µmol), $Zn(NO_3)_2{\cdot}6H_2O$ (19.2 mg, 97.6 µmol) and 4,4′-bipyridine (3.8 mg, 24.4 µmol) were added to a mixture of DMF (2 mL), methanol (1 mL) and water (1 mL) and sonicated to dissolve. The solution was heated at 85 °C in a dry bath incubator overnight to yield orange cube shaped crystals of **2.5**, which were recovered by vacuum filtration. Yield 9.3 mg, 30%. Found C, 56.85; H, 3.35; N, 8.64%; $C_{60}H_{40}N_8O_{16}Zn_2{\cdot}0.3MeOH{\cdot}0.7H_2O$, ([$Zn_2$(AlaNDI)$_2$(4,4′-bipy)$_2$]·0.3MeOH·0.7$H_2O$); requires C, 56.49; H, 3.35; N, 8.74%. υ_{max} /cm^{-1} 2957w, 1702m, 1667s, 1636s, 1577m, 1524w, 1447m, 1422m, 1370s, 1354s, 1372s, 1288m, 1240s, 1216s, 1201m, 1084m, 1068m, 1032w, 968w, 915w, 874w, 802s, 768s, 720m, 663m. TGA: On-set, 50 °C mass loss = 2.5% (calculated 2.0% for loss of uncoordinated 0.3 MeOH and 0.7 water molecules), decomp. 390 °C. Bulk purity was confirmed by PXRD.

Synthesis of *poly*-[Mn(HAlaNDI)$_2$(dpe)], 2.6

(*S*)-H_2AlaNDI (10.0 mg, 24.4 µmol), $Mn(NO_3)_2{\cdot}4H_2O$ (12.0 mg, 97.6 µmol) and 1,2-di(4-pyridyl)ethylene (4.4 mg, 24.4 µmol) were added to a solvent mixture of DMF (2 mL), methanol (1 mL) and water (1 mL) and sonicated to dissolve. The solution was heated at 85 °C in a dry bath incubator for two nights, to yield

yellow crystals of **2.6** which were recovered by filtration. Yield 5.1 mg, 10%. Found C, 59.15; H, 3.33; N, 7.87%; $C_{52}H_{36}N_6O_{16}Mn$, ([Mn(HAlaNDI)$_2$(dpe)]); requires C, 59.15; H, 3.44; N, 7.96%. υ_{max} /cm^{-1} 2943w, 1702m, 1657s, 1599m, 1578m, 1450w, 1420w, 1371w, 1353m, 1332s, 1246s, 1200m, 1138w, 1115m, 1086m, 1043m, 1010m, 965m, 924m, 887m, 841s, 805m, 773s, 760s, 723m, 650m. TGA On-set, 300 °C mass loss = 0%, decomp. 300 °C. Bulk purity was confirmed by PXRD.

Synthesis of *poly*-[Cd$_2$(AlaNDI)$_2$(4PyNDI)$_2$]·4DMA, 2.7, *poly*-[Cd$_2$(AlaNDI)$_2$(OH$_2$)$_2$(4PyNDI)$_2$]·DMF·H$_2$O, 2.8 and *poly*-[Cd$_2$(AlaNDI)$_2$(DMF)$_2$(OH$_2$)$_2$(4PyNDI)]·DMF·4H$_2$O, 2.9

(*S*)-H$_2$AlaNDI (10.0 mg, 24.4 µmol), Cd(NO$_3$)$_2$·4H$_2$O (30.0 mg, 97.4 µmol) and 4PyNDI (6.0 mg, 14.3 µmol) were added to a solvent mixture of DMF (2 mL), methanol (1 mL) and water (1 mL) and sonicated to dissolve. The solution was heated at 85 °C in a dry bath incubator for 24 hours, to yield yellow crystals which were recovered by filtration. Yield 21.1 mg. PXRD shows compounds **2.7**, **2.8** and **2.9** present in the bulk sample.

The X-ray diffraction data of **2.7** were processed with the SQUEEZE routine of PLATON[534] which showed voids of 727 Å^3, containing 162.5 e$^-$, per asymmetric unit, which could account for four DMF molecules. However as **2.7** could not be obtained as a pure phase, the solvent present in the pores could not be determined unequivocally by TGA and microanalysis.

Synthesis of *poly*-[Zn$_8$(DMF)$_3$(LeuNDI)$_6$(OH$_2$)$_3$(µ$_3$-OH)$_4$]·2DMF·10H$_2$O, 2.10

(*S*)-H$_2$LeuNDI (10 mg, 20.2 µmol) and Zn(OAc)$_2$ (3.7 mg, 20.2 µmol) were added to DMF (2 mL) and water (1 mL) in a glass vial and sonicated to dissolve. The solution was heated at 70 °C in a dry block incubator for four days, during which time yellow crystals of **2.10** were formed which were recovered by vacuum filtration. Yield 6.0 mg, 44%. Found C, 49.50; H, 5.10, N, 5.92%; $C_{165}H_{175}N_{15}O_{58}Zn_8$·2DMF·10H$_2$O, ([Zn$_8(DMF)_3$(LeuNDI)$_6$(OH$_2$)$_3(OH)_4$]·2DMF·10H$_2$O) requires C, 49.54; H, 5.08; N, 5.74%. υ_{max}/cm^{-1} 3089wm 2953w, 2870w, 1708m, 1659s, 1629s, 1580s, 1498w, 1450m, 1405m, 1376m, 1331s, 1246s, 1193m, 1105w, 991w, 877w, 849w, 772s, 728w. TGA: On-set, 62 °C, mass loss = 12.9% (calculated 12.8% for loss of all coordinated solvent, and non-coordinated solvent of 2 DMF and 10 H$_2$O molecules), decomp. 400 °C. Bulk phase purity was confirmed by PXRD. Data was treated

with the SQUEEZE routine of PLATON,[534] showing total solvent accessible voids of 499 Å^3 containing 144.5 e$^-$ per asymmetric unit, which would correspond to one DMF and 10 H_2O molecules which were not able to be modelled in the crystal structure.

Synthesis of *poly*-[Mn(HLeuNDI)$_2$(dpe)]·MeOH, 2.11

(*S*)-H_2LeuNDI (10 mg, 20.2 µmol), 1,2-di(4-pyridyl)ethylene (3.7 mg, 20.2 µmol) and $MnCl_2·4H_2O$ (8.0 mg, 40.4 µmol) were added to a solvent mixture of DMF (2mL), methanol (1 mL) and water (1 mL) in a glass vial and sonicated to dissolve. The solution was heated at 85 °C in a dry block incubator overnight, during which time yellow crystals of **2.11** were formed and were recovered by vacuum filtration. Yield 10.9 mg, 44%. Found C, 60.71; H, 4.65, N, 6.97%; $C_{64}H_{60}N_6O_{16}Mn·MeOH$ ([Mn(HLeuNDI)$_2$(dpe)]·MeOH) requires C, 60.60; H, 5.01; N, 6.52%. υ_{max} /cm^{-1} 3079w, 2955w, 1706m, 1654s, 1604m, 1577m, 1451m, 1372m, 1352m, 1329s, 1246s, 1194m, 1097m, 982m, 922w, 888w, 857m, 830m, 790s, 731m. TGA: On-set, 30 °C, mass loss = 4.5% (calculated 4.9% for loss of one non-coordinated MeOH), decomp. 330 °C. Bulk phase purity was confirmed by PXRD.

Synthesis of *poly*-[Mn$_4$(LeuNDI)$_4$(dpb)$_2$(DMF)$_2$(OH$_2$)$_2$]·DMF·4.5H$_2$O, 2.12

(*S*)-H_2LeuNDI (10 mg, 20.2 µmol), 1,2-di(4-pyridyl)benzene (4.7 mg, 20.2 µmol) and $Mn(NO_3)_2·4H_2O$ (10 mg, 40.4 µmol) were added to a solvent mixture of DMF (2mL), methanol (1 mL) and water (1 mL) in a glass vial and sonicated to dissolve. The solution was heated at 85 °C in a dry block incubator overnight, during which time yellow needle crystals of **2.12** were formed which were recovered by vacuum filtration. Yield 17.8 mg, 98%. Found C, 57.92; H, 4.93, N, 6.84%; $C_{142}H_{138}N_{14}O_{36}Mn_4·DMF·4.5H_2O$ ([Mn$_4$(LeuNDI)$_4$(dpb)$_2$(DMF)$_2$(OH$_2$)$_2$]·DMF·4.5H$_2$O) requires C, 57.23; H, 5.19; N, 7.03%. υ_{max} /cm^{-1} 2952w, 2869w, 1706m, 1661s, 1604s, 1577s, 1453m, 1414s, 1379m, 1330s, 1248s, 1198m, 1100w, 988w, 861w, 813m, 781s. TGA: On-set, 50 °C, mass loss = 11.0% (calculated 10.4% for loss of all coordinated solvent and non-coordinated solvent of one DMF and 4.5 water molecules), decomp. 400 °C. Bulk phase purity was confirmed by PXRD.

The structure showed small void spaces in which no data could be modelled, therefore the data were processed with the SQUEEZE routine of PLATON,[534] showing total voids of 201 Å^3 containing 44 e$^-$ per

formula unit. The solvent not assigned in the crystal structure which was present in the TGA and microanalysis is three water and 0.5 DMF molecules, which would account for 44 electrons per formula unit.

Synthesis of *poly*-[$Cd_4(bpb)_2(DMF)_8(LeuNDI)_4$]·$6H_2O$·0.5DMF, 2.13

(*S*)-H_2LeuNDI (10 mg, 20.2 µmol), 1,2-di(4-pyridyl)benzene (4.7 mg, 20.2 µmol) and $Cd(NO_3)_2$·$4H_2O$ (12 mg, 40.4 µmol) were added to DMF (3 mL) in a glass vial and sonicated to dissolve. The solution was heated at 100 °C in a dry block incubator for one week, during which time yellow orange shaped crystals of **2.13** were formed, which were recovered by vacuum filtration. Yield 5.7 mg, 31%. Found C, 53.69; H, 4.78; N, 8.16%; $C_{160}H_{176}N_{20}O_{40}Cd_4$·$6H_2O$·0.5DMF, ([$Cd_4(bpb)_2(DMF)_8(LeuNDI)_4$]·$6H_2O$·0.5DMF); requires C, 53.68; H, 5.34; N, 7.95%. υ_{max} /cm^{-1} 2952w, 1703m, 1660s, 1576s, 1450m, 1402m, 1330s, 1247sm 1193m, 1096w, 988w, 861w, 811s, 779s, 716m, 662m. TGA: On-set, 70 °C, mass loss = 14% (calculated 20.2% for loss of all coordinated DMF and non-coordinated solvent), decomp. 320 °C. Bulk phase purity was confirmed by PXRD. The microanalysis and TGA both show less solvent than is accounted for by SQUEEZE, likely because some of the non-coordinated solvent was lost before the TGA or microanalysis were conducted.

The X-ray structure showed voids in which no solvent could be modelled, therefore the data were processed with the SQUEEZE routine of PLATON,[534] showing a void of 956 $Å^3$ which was filled with 185 e^-. The solvent accounted for by the microanalysis which was not modelled in the crystal structure is six water molecules and 0.5 DMF molecules, which would account for 60 e^- per formula unit. It is likely that less solvent is shown by the microanalysis than would fit in the voids shown by SQUEEZE, because some solvent was lost before the microanalysis was conducted.

Synthesis of *poly*-[$Mn(DMF)_2(HPheNDI)_2$]·H_2O·MeOH, 2.14

(*S*)-H_2PheNDI (20.0 mg, 35.6 µmol) and $MnCl_2$·$4H_2O$ (21.0 mg, 106 µmol) were added to a solvent mixture of DMF (2 mL), methanol (1 mL), and H_2O (1 mL) in a glass vial and sonicated to dissolve. The reaction mixture was heated at 70 °C in a dry block incubator for 7 days, during which time yellow needles of **2.14** were formed, which were isolated by vacuum filtration. Yield 5.4 mg, 22%. Found C, 61.92; H, 4.32; N,

6.14%; $C_{70}H_{56}N_6O_{18}Mn\cdot H_2O\cdot MeOH$ ([Mn(HPheNDI)(DMF)$_2$]·H_2O·MeOH); requires C, 62.05; H, 4.55; N, 6.12%. υ_{max} /cm^{-1} 3612w, 2937w, 1330m, 1245s, 1185m, 1111m, 1062m, 991m, 931m, 872m, 827m, 746s, 701s. TGA: On-set, 75 °C, mass loss = 3.0% (calculated 2.9% for loss of MeOH and H_2O), decomp. 350 °C. Bulk phase purity was confirmed by PXRD.

Synthesis of *poly*-[Cd(4,4′-bipy)(OH$_2$)(PheNDI)]·3.5H$_2$O·DMF, 2.15

(*S*)-H_2PheNDI (20.0 mg, 35.6 μmol), $Cd(NO_3)_2\cdot 4H_2O$ (43.6 mg, 141 μmol), and 4,4′-bipyridine (2.8 mg, 17.8 μmol) were added to a solvent mixture of DMF (2 mL), methanol (1 mL), and H_2O (1 mL) in a glass vial and sonicated to dissolve. The solution was heated at 85 °C in a dry block incubator for two days, during which time yellow needle crystals of **2.15** were formed, which were isolated by vacuum filtration. Yield 17.8 mg, 98%. Found C, 54.98; H, 4.31; N, 7.13%; $C_{42}H_{30}N_4O_9Cd\cdot 3.5H_2O\cdot$DMF ([Cd(PheNDI)(4,4′-bipy)(H_2O)]·3.5H_2O·DMF); requires C, 54.97; H, 4.51; N, 7.12%. υ_{max} /cm^{-1} 1705m, 1655s, 1577s, 1499w, 1452m, 1413m 1376m, 1331s, 1277m, 1247s, 1219m, 1174m, 1098w, 1068w, 1042w, 988w, 939w, 911w, 872w, 837w, 814m, 783s, 747m, 697m, TGA: On-set, 60 °C, mass loss = 13.3% (calculated 13.8% for loss of one DMF and 3.5 H_2O), decomp. 350 °C. Bulk phase purity was confirmed by PXRD. The X-ray diffraction data were processed using the SQUEEZE routine of PLATON,[534] which showed a void space of 1219 Å^3 per unit cell, containing 328 e$^-$ per unit cell, (82 e$^-$ per asymmetric unit) corresponding to 0.5 DMF and 3.5 H_2O molecules per asymmetric unit.

Synthesis of *poly*-[Mn$_2$(4,4′-bipy)$_2$(PheNDI)$_2$][Mn(4,4′-bipy)(DMF)(NO$_3$)$_2$]·0.5DMF·7H$_2$O, 2.16

(*S*)-H_2PheNDI (20.0 mg, 35.6 μmol), 4,4′-bipyridine (5.6 mg, 17.8 μmol), and $Mn(NO_3)_2\cdot 4H_2O$ (18.0 mg, 71.2 μmol) were added to a solvent mixture of DMF (2 mL) and H_2O (1 mL) in a glass vial and sonicated to dissolve. The reaction mixture was heated at 70 °C in a dry block incubator for five nights, during which time orange crystals of **2.16** were formed, which were recovered by filtration. Yield 8.5 mg, 67%. Found C, 55.85; H, 3.70; N, 8.38%; $C_{97}H_{71}N_{13}O_{23}Mn_3\cdot$0.5DMF·7$H_2O$ ([Mn$_2$(PheNDI)$_2$(4,4′-bipy)$_2$][Mn(4,4′-bipy)(DMF)(NO$_3$)$_2$]·0.5DMF·7H_2O); requires C, 55.95; H, 4.22; N, 8.95%. υ_{max} /cm^{-1} 2934w, 1707s, 1666s, 1620s, 1602s, 1572, 1452m, 1412s, 1378m, 1333s, 1300s, 1248s, 1221m, 1173m, 1110m, 1088m,

1068m, 1044m, 991m, 916w, 878m, 853w, 812s, 781s, 752m, 731m, 700m, 678m. TGA On-set, 90 °C; mass loss = 7.0% (calculated 7.6% for loss of 0.5 DMF and 7 H_2O), decomp. 350 °C. Bulk phase purity was confirmed by PXRD. The X-ray diffraction data were processed with the SQUEEZE routine of PLATON,[534] which showed voids of 330 $Å^3$ containing 95 e^- per asymmetric unit, which would correspond to 7 H_2O molecules which are not modelled in the crystal structure.

Synthesis of *poly*-[Cd_4(DMF)(dpe)$_2$(PheNDI)$_4$(OH_2)$_2$]·10H_2O·0.5DMF, 2.17

(*S*)-H_2PheNDI (40.0 mg, 71.2 μmol), $Cd(NO_3)_2·4H_2O$ (87.2 mg, 142.4 μmol), and 1,2-di(4-pyridyl)ethylene (9.2 mg, 71.2 μmol) were added to a solvent mixture of DMF (4 mL), methanol (1.5 mL), and H_2O (1.5 mL) in a glass vial and sonicated to dissolve. The reaction mixture was heated at 85 °C in a dry block incubator for 12 h, during which time yellow crystals of **2.17** were formed, which were recovered by vacuum filtration. Yield 47.7 mg, 40%. Found C, 55.27; H, 3.83; N, 5.62%; $C_{155}H_{111}N_{13}O_{35}Cd_4·10H_2O·0.5DMF$ ([Cd_4(PheNDI)$_4$(dpe)$_4$(H_2O)$_2$(DMF)]·10H_2O·0.5DMF); requires C, 55.58; H, 4.01; N, 5.59%. υ_{max} /cm^{-1} 3334w, 3028w, 1991w, 1946w, 1771w, 1663s, 1573s, 1409m, 1331s, 1245m, 1174m, 1111w, 988m, 835m, 783s, 697m. TGA: On-set, 85 °C, mass loss = 7.0% (calculated 6.4% for loss of 0.5 DMF and 10 H_2O molecules), decomp. 390 °C. Bulk phase purity was confirmed by PXRD.

Synthesis of *poly*-[Cd_2(PheNDI)$_2$(4PyNDI)$_2$]·6H_2O·2DMF·MeOH, 2.18

(*S*)-H_2PheNDI (20.0 mg, 35.6 μmol), $Cd(NO_3)_2·4H_2O$ (43.6 mg, 141 μmol), and 4pyNDI (15.0 mg, 35.6 μmol) were added to a solvent mixture of DMF (2 mL), methanol (1 mL), and H_2O (1 mL) in a glass vial and sonicated to dissolve. The reaction mixture was heated at 85 °C in a dry block incubator for 48 hours, during which time yellow needle crystals of **2.18** were formed, which were recovered by vacuum filtration. Yield 32.3 mg, 39%. Found C, 57.57; H, 3.42; N, 8.19%; $C_{112}H_{64}N_{12}O_{24}Cd_2·6H_2O·2DMF·MeOH$ ([Cd_2(PheNDI)$_2$(4PyNDI)$_2$]· 6H_2O·2DMF·MeOH); requires C, 57.79; H, 3.83; N, 7.93%. υ_{max} /cm^{-1} 1705m, 1663s, 1577s, 1493w, 1448w, 1407w, 1379w, 1329s, 1245s, 1191m, 1146s, 1118s, 1092.4w, 1064w, 984w, 913w, 865w, 829w, 766s, 699.m, 658m. TGA: On-set, 53 °C, mass loss = 6.3% (calculated 6.7% for loss of two DMF), decomp. 380 °C. Bulk phase purity was confirmed by PXRD. The structure was processed with the SQUEEZE routine of PLATON,[534] showing voids of 435 $Å^3$ containing 138 e^- per

asymmetric unit, which corresponds to six H_2O and one DMF molecules more than the DMF and MeOH already modelled in the crystal structure (six H_2O, two DMF, and one MeOH in total). The MeOH and H_2O within the structure were likely lost before the TGA and microanalysis was conducted.

Synthesis of *poly*-[Mn_2(PheNDI)$_2$(4PyNDI)$_2$]·3DMF·2MeOH·H_2O, 2.19

(*S*)-H_2PheNDI (10 mg, 18 µmol), $Mn(NO_3)_2·4H_2O$ (9.0 mg, 36 µmol), and 4PyNDI (7.5 mg, 18 µmol) were added to a solvent mixture of DMF (2 mL), methanol (1 mL), and H_2O (1 mL) in a glass vial and sonicated to dissolve. The reaction mixture was heated at 85 °C in a dry block incubator for 24 hours, during which time yellow crystals of **2.19** formed, which were recovered by vacuum filtration. Yield 8.0 mg, 38%. Found C, 60.14; H, 3.46; N, 8.75%, ([Mn_2(PheNDI)$_2$(4PyNDI)$_2$]·3DMF·2MeOH·1H_2O); requires C, 60.61; H, 3.93; N, 8.62%. υ_{max} /cm^{-1} 3389w, 1659m, 1577s, 1439m, 1346s, 1241s, 1181m, 1096m, 1014w, 962w, 865w, 775m, 660s. TGA: On-set 50 °C; mass loss = 15.1% (calculated 14.9% for loss of three DMF, two MeOH, and one H_2O). decomp. 375 °C. Bulk phase purity wass confirmed by PXRD.

Synthesis of [Cd_2(AlaBDI)$_2$(DMSO)$_6$]·1.5H_2O, 3.1

(*S*)-H_2AlaBDI (100 mg, 0.229 mmol) and $Cd(OAc)_2$ (95.0 mg, 0.413 mmol) were added to DMSO (6 mL) and sonicated to dissolve. The solution was heated at 100 °C in a dry bath incubator for 48 hours to yield colourless crystals which were isolated by filtration. Yield 72.9 mg, 41%. M.p. 253-256 °C, Found C, 42.11; H, 4.20; N, 3.43%; $C_{56}H_{64}N_4O_{22}S_6Cd_2·1.5H_2O$ ([Cd_2(AlaBDI)$_2$(DMSO)$_6$]·1.5H_2O) requires C, 42.08; H, 4.29; N, 3.51.υ_{max} /cm^{-1} 2954w, 2928w, 2869w, 1769m, 1707s, 1642s, 1586s, 1497w, 1346w, 1253w, 1163w, 1105m, 1059m, 1014w, 964w, 934w, 859m, 775m, 742m, 667m, TGA: On-set, 95 °C, mass loss = 7.0% (calculated 6.6% for loss of one coordinated DMSO and 1.5 H_2O), 138 °C, mass loss = 21.5% (calculated 24.5% for loss of five coordinated DMSO), decomp. 375 °C. Bulk phase purity was confirmed by PXRD. Despite exhaustive attempts with various solvents, the crystalline sample of **3.1** could not be dissolved enough to confirm persistence in solution by mass spectrometry or NMR.

Synthesis of [Cd_2(LeuBDI)$_2$(DMF)$_2$(DMSO)$_3$(OH_2)]·DMF·DMSO, 3.2

(*S*)-H_2LeuBDI (20 mg, 38.4 µmol) and $Cd(OAc)_2$ (8.8 mg, 38.4 µmol) were added to a mixture of DMSO (1 mL) and DMF (0.5 mL) and sonicated to dissolve. The solution was heated at 100 °C for one week, and

then left to sit at room temperature. The product formed as a few colourless crystals after one month. Yield 12 mg, 32%. Found C, 47.84; H, 5.58, N, 5.42%; $C_{68}H_{86}N_4O_{16}Cd_2$·DMSO·DMF $[Cd_2(LeuBDI)_2(DMF)_2(DMSO)_3(OH_2)]$·DMSO·DMF requires C, 47.84; H, 5.58; N, 5.42%. δ_H (400 MHz, d_6–DMSO) 0.86 (d, ^3J=6.4, 24 H, H_8), 1.43 (m, 4 H, H_7), 1.92 (m, 4 H, $H_{5/6}$), 2.32 (m, 4 H, $H_{5/6}$), 2.73 (s, 6 H, $H_{10/11}$), 2.89 (s, 6 H, $H_{10/11}$), 4.58 (m, 4 H, H_4), 7.90 (d, 4 H, ^3J=7.7, 4H, H_3), 7.95 (s, 2H, H_9), 8.18 (s, 4 H, H_1), 8.21 (d, ^3J=7.7, 4 H, H_2). υ_{max} /cm^{-1} 2956w, 2929w, 2870w, 1767m, 1703s, 1651s, 1579s, 1467w, 1346s, 1258m, 1195w, 1163m, 1087m, 1005s, 955m, 935m, 858m, 774w, 742m, 703w, 669m. TGA: On-set, 90 °C, mass loss = 30.0% (calculated 30.5% for loss of all coordinated and non-coordinated solvent), decomp. 360 °C. Bulk phase purity was confirmed by PXRD. Despite multiple attempts, the presence of **3.2** could not be confirmed by mass spectrometry due to low solubility.

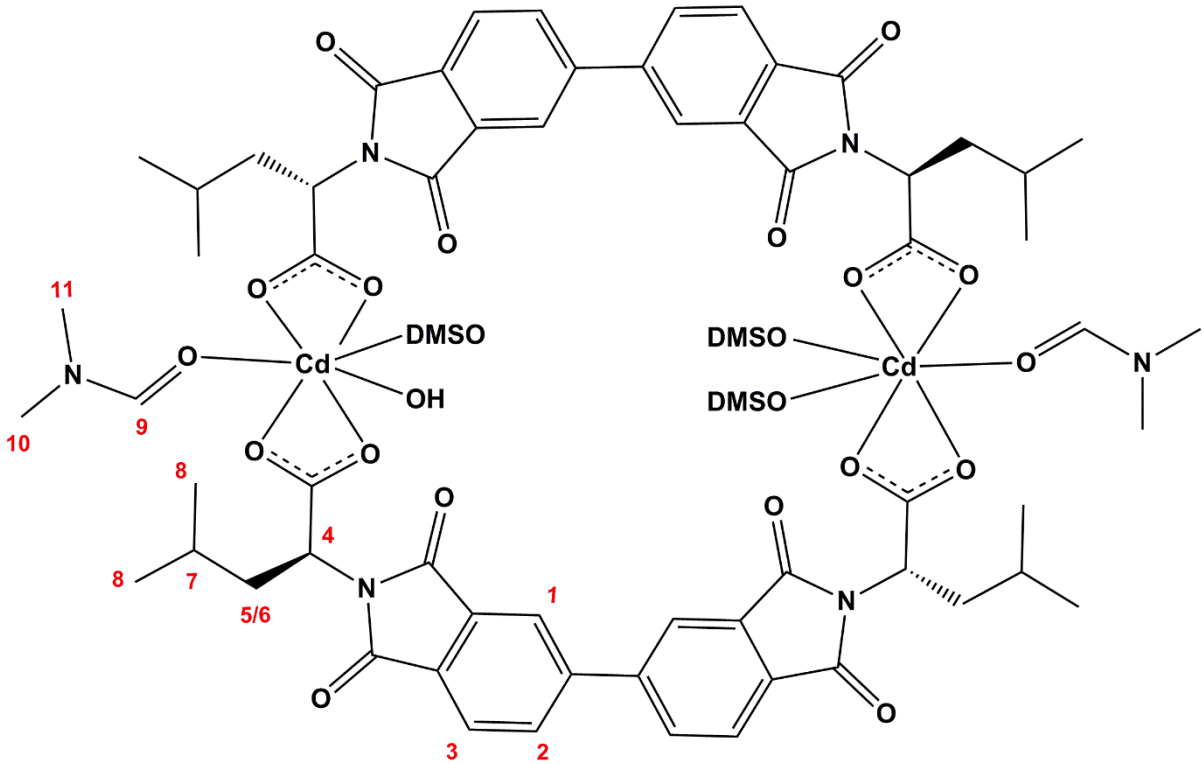

Synthesis of $(NH_2(CH_3)_2)_2[Zn_2(AlaBDI)_2(4,4'\text{-bipy})Cl_2]$, 3.3

(*S*)-H_2AlaBDI (10 mg, 23 µmol), 4,4′-bipyridine (7.1 mg, 45.5 µmol) and $ZnCl_2$·$6H_2O$ (6.2, 45.5 µmol) were added to DMF (3 mL) and sonicated to dissolve. The solution was heated at 60 °C for four nights,

then heated at 80 °C for one night and heated at 100 °C for three nights. After this time a few thin colourless needles of **3.3** were formed. All attempts at synthesising this material in bulk were unsuccessful.

Synthesis of *poly*-[Cd(LeuBDI)(4PyNDI)]·11H_2O·2DMF, 3.4

(*S*)-H_2LeuBDI (25.2 mg, 48.4 µmol), 4PyNDI (10.2 mg, 24.4 µmol) and $Cd(NO_3)_2·4H_2O$ (30.0 mg, 97.4 µmol) were added to DMF (3 mL) and sonicated to dissolve. The solution was heated at 100 °C for four nights, during which time yellow crystals of **3.4** were formed. Yield 15.7 mg, 26%. Found C, 55.34; H, 4.47, N, 7.27%; $C_{104}H_{70}N_{12}O_{24}Cd_2·9H_2O$ $[Cd_2(LeuBDI)_2(4PyNDI)_2]·9H_2O$ requires C, 55.15 ; H, 4.18 ; N, 7.27%. υ_{max} /cm^{-1} 1770w, 1705m, 1679m, 1577s, 1508m, 1424m, 1375s, 1342s, 1245s, 1193m, 1146m, 1094m, 1066m, 1019m, 982m, 857m, 827m, 766s, 741m 715m, 686m, 656m. TGA: On-set, 50 °C, mass loss = 14.7% (calculated 14.1% for loss of 11 H_2O and two DMF molecules), decomp 350 °C. Bulk phase purity was confirmed by PXRD.

The structure had solvent accessible voids in which no solvent could be modelled, so the data were processed with the SQUEEZE routine of PLATON[534] to show one large void of 961 Å^3 per formula unit, containing 194 e$^-$ which corresponds to 11 water and two DMF molecules. The microanalysis shows less solvent than accounted for by SQUEEZE or TGA, suggesting that some solvent was lost before the microanalysis was conducted.

Synthesis of $[Cu_8(AlaBDI)_8(DMSO)_4(OH_2)_4]$·solv., 3.5

(*S*)-H_2AlaBDI (10 mg, 22.9 µmol) was dissolved in DMSO (2 mL) and $Cu(OAc)_2$ (4.2 mg, 22.9 µmol) was dissolved in DMF (1 mL). The metal solution was added slowly to the ligand solution while stirring. The solution was left to sit at room temperature for one month, during which time blue crystals of **3.5** formed. Yield 6.5 mg, 51%. Found C, 41.52; H, 4.79; N, 3.73%; $C_{184}H_{144}N_{16}O_{72}Cu_8·55H_2O·4DMSO$ ($[Cu_8(AlaBDI)_8(DMSO)_4(OH_2)_4]·55H_2O·4DMSO$) requires C, 41.60; H, 5.06; N, 4.04%. υ_{max} /cm^{-1} 3058w, 1769m, 1703s, 1655m, 1596s, 1510m, 1459m, 1413m, 1370s, 1443s, 1289m, 1195w, 1156m, 1081m, 1016m, 915w, 887w, 866w, 845m, 779w, 743s. TGA: On-set, 70 °C, mass loss = 34% (calculated 28% for loss of all coordinated solvent molecules, all solvent assigned in the crystal structure of, four DMSO and three water molecules, and all unassigned lattice solvent), decomp. 330 °C. The data were processed with

the SQUEEZE routine of PLATON,[534] showing voids of 5104 Å^3 containing 1345 e$^-$ per formula unit, which is more than the solvent observed by the microanalysis and TGA results, suggesting that as the material was so porous that some of the solvent was lost before the TGA or microanalysis were conducted. The TGA shows more mass loss than would be expected based on the microanalysis, likely because some solvent was lost from the crystals before the microanalysis was conducted. The crystals were extremely fragile, and began to lose crystallinity immediately after being removed from the mother liquor, therefore the bulk purity could not be confirmed by PXRD.

Synthesis of [Cu$_8$(LeuBDI)$_8$(OH$_2$)$_8$]·solv., 3.6

(*S*)-H$_2$LeuBDI (70 mg, 134.4 µmol) was dissolved in DMSO (5 mL) in a glass vial and Cu(OAc)$_2$ (24.5 mg, 134.4 µmol) was dissolved in DMSO (16 mL) in a glass vial. The metal solution was added slowly to the ligand solution with stirring and then allowed to sit at room temperature, after one month a blue crystalline product of **3.6** formed which was recovered by vacuum filtration. The crystals were extremely fragile and PXRD or mass spectrometry data could not be obtained. Yield 50.1 mg, 29%. Found C, 40.55; H, 6.55; N, 3.01%; $C_{224}H_{225}N_{16}O_{72}Cu_8$·56H$_2$O·42DMSO ([Cu$_8$(LeuBDI)$_8$(OH$_2$)$_8$]·56H$_2$O·42DMSO) requires C, 40.68; H, 6.53; N, 2.47%. υ_{max} /cm^{-1} 2957w, 1770m, 1705s, 1649m, 1605m, 1390m, 1376s, 1320m, 1162w, 1103w, 1016m, 951m, 846s, 783w, 744m, 671m. TGA: On-set, 70 °C, mass loss = 48.2% (calculated 48.7% for loss of all coordinated water molecules and all lattice solvent of 42 DMSO and 56 H$_2$O molecules), decomp. 300 °C. The structure was highly porous, so was processed with the SQUEEZE routine of PLATON.[534] The SQUEEZE results suggest a void of 3765 Å^3 filled with 726 e$^-$ per unit cell. The solvent accounted for by TGA and microanalysis would account for 1652 e$^-$ per asymmetric unit, therefore it appears that the crystals contained a large amount of surface solvent which was not removed by filtration. The crystals were extremely fragile, and began to lose crystallinity when removed from the mother liquor, therefore the bulk purity could not be confirmed by PXRD.

Synthesis of *poly*-[Zn$_4$(IsoBDI)$_2$(DMF)(OH$_2$)$_4$]·DMF·9H$_2$O, 3.7

H$_4$IsoBDI (10 mg, 16.1 µmol) and ZnCl$_2$·6H$_2$O (4.4 mg, 32.3 µmol) were added to DMF (3 mL) and sonicated to dissolve. The solution was heated at 120 °C in a dry bath incubator for six nights to yield

colourless crystals of **3.7** which were isolated by filtration. Yield 3.3 mg, 17%. Found C, 44.26; H, 3.51; N, 4.24%; $C_{67}H_{39}N_5O_{29}Zn_4$·DMF·$9H_2O$ ([Zn_4(IsoBDI)$_2$(DMF)(OH_2)$_4$]·DMF·$9H_2O$) requires C, 41.97; H, 3.51; N, 4.20%. υ_{max} /cm^{-1} 3330w, 3084w, 2122w, 1924w, 1715m, 1559m, 1361s, 1234m, 1092m, 846m, 738s. TGA: On-set, 60 °C, mass loss = 33% (calculated 33.6% for loss of all coordinated solvent, and lattice solvent of six DMF and 14 H_2O molecules), decomp. 400 °C. Bulk phase purity was confirmed by PXRD. Processing the data with the SQUEEZE routine of PLATON[534] showed solvent accessible voids, giving a total of 8837 Å^3 filled with 3331 e$^-$ per unit cell, which corresponds to 1104 Å^3 filled with 416 e$^-$ per asymmetric unit. The solvent loss shown by the TGA accounts for 460 e$^-$ per asymmetric unit, which agrees with the SQUEEZE data. The microanalysis shows less solvent in the voids than SQUEEZE or TGA likely due to the loss of solvent before the microanalysis was conducted.

Synthesis of *poly*-[Cd(IsoBDI)$_{0.5}$(4PyNDI)]·2.5DMF·4H_2O, 3.8

H_4IsoBDI (20.0 mg, 32.2 µmol), 4PyNDI (13.4 mg, 31.9 µmol) and Cd(NO_3)$_2$·$4H_2O$ (19.8 mg, 64.3 µmol) were added to DMF (6 mL) and sonicated to dissolve. Concentrated nitric acid (4 drops) was added to the solution and the solution was heated at 85 °C for one week, during which time brown needle crystals of **3.8** were formed, which were isolated by filtration. Yield 24.8 mg, 41%. M.p. >350 °C Found C, 51.63; H, 3.82; N, 9.94%; $C_{40}H_{18}N_5O_{10}Cd$·2.5DMF·$4H_2O$ ([Cd(IsoBDI)$_{0.5}$(4PyNDI)]·2.5DMF·$4H_2O$) requires C, 51.63; H, 3.82; N, 9.59%. υ_{max} /cm^{-1} 1774w, 1721m, 1655s, 1605m, 1560m, 1508s, 1413m, 1375s, 1342s, 1278w, 1247w, 1193w, 1148w, 1096m, 1019w, 984w, 932w, 831w, 766m, 742s, 660m. TGA: On-set, 55 °C, mass loss = 24.5%, (calculated 23.3% for loss of non-coordinated solvent of 2.5 DMF and 4 H_2O), decomp. 380 °C. Bulk phase purity was confirmed by PXRD.

The structure showed significant void space in which no solvent could be modelled, therefore it was processed with the SQUEEZE routine of PLATON,[534] which showed voids of 975 Å^3 filled with 119 e$^-$ per asymmetric unit, which would account for the 2.5 DMF and four water molecules which were observed through the TGA and microanalysis.

Synthesis of $[Cd_2(1,10\text{-phen})_2(LeuNDI)_2(OH_2)_2]\cdot 2H_2O\cdot DMF$, 4.1·2H₂O·DMF

(*S*)-H_2LeuNDI (20 mg, 40.4 µmol), 1,10-phenanthroline (8.0 mg, , 20.2 µmol) and $Cd(NO_3)_2\cdot 4H_2O$ (25 mg, 80.8 µmol) were added to a solvent mixture of DMF (2 mL), methanol (1 mL) and water (1 mL) in a glass vial and sonicated to dissolve. The solution was heated at 85 °C in a dry block incubator overnight, during which time yellow crystals of **4.1** were formed, which were recovered by vacuum filtration. Yield 21.3 mg, 63%. Found C, 55.65; H, 4.26, N, 6.97%; $C_{76}H_{67}N_8O_{18}Cd_2\cdot 2H_2O\cdot DMF$, $[Cd_2(phen)_2(LeuNDI)_2(OH_2)_2]\cdot 2H_2O\cdot DMF$ requires C, 55.35; H, 4.59; N, 7.35%. υ_{max} /cm^{-1} 3070w, 2953w, 2116w, 1705m, 1660s, 1574s, 1515m, 1450m, 1376m, 1329s, 1246s, 1192m, 1145m, 1097m, 987m, 891w, 849m, 780s, 725s, 679m. *m/z* (ES$^+$) 787.13 $[Cd(LeuNDI)(phen)+H]^+$, (calculated for $C_{38}H_{33}CdN_4O_8^+$, 787.13), 823.11 $[Cd(LeuNDI)(phen)(H_2O)+H]^+$, (calculated for $C_{38}H_{37}CdN_4O_{10}^+$, 823.15), 1607.23 $[Cd_2(LeuNDI)_2(phen)_2(H_2O)_2)+H]^+$, (calculated for $C_{76}H_{69}Cd_2N_8O_{18}^+$, 1607.28). TGA: On-set, 60 °C, mass loss = 4.5% (calculated 4.2% for loss of one DMF and two water molecules, and two coordinated water molecules), decomp. 300 °C. Bulk phase purity was confirmed by PXRD.

The data was processed with the SQUEEZE routine of PLATON,[534] showing solvent accessible voids of 166 Å^3 containing 52 e$^-$ per asymmetric unit, which is accounted for by the solvent not modelled in the crystal structure, one DMF and two water molecules, which are also present in the microanalysis and TGA.

Synthesis of $[Cd_2(LeuNDI)_2(2,2'\text{-bipy})_2(OH_2)_2]_2\cdot 2DMF\cdot 5H_2O$, 4.2·2DMF·5H₂O

(*S*)-H_2LeuNDI (10 mg, 20.2 µmol), $Cd(NO_3)_2\cdot 4H_2O$ (12.5 mg, 40.4 µmol) and 2,2´-bipyridine (3.0 mg, 20.2 µmol) were added to DMF (2 mL) and water (1 mL) in a glass vial and sonicated to dissolve. The solution was heated at 85 °C in a dry block incubator for 2 nights, during which time yellow block crystals of **4.2** were formed which were recovered by vacuum filtration. Yield 5.1 mg, 16%. Found C, 55.34; H, 4.47, N, 7.27%; $C_{144}H_{136}N_{16}O_{36}Cd_4$, $[Cd_2(LeuNDI)_2(2,2'\text{-bipy})_2(OH_2)_2]_2$ requires C, 55.49; H, 4.40; N, 7.19%. υ_{max} /cm^{-1} 31.05w, 2953w, 2868w, 1705m, 1663s, 1591s, 1578s, 1491w, 1474w, 1438m, 1380m, 1328s, 1245s, 1193m, 1175w, 1154w, 1105w, 1060w, 1018w, 988w, 924w, 879w, 850w, 811w, 762s, 737m. *m/z* (ES$^+$) 1621.88 $[Cd_4(LeuNDI)_4(2,2'\text{-bipy})_4(OH_2)(CHCl_3)(CH_3COOH)+2H]^{2+}$ (calculated for $C_{147}H_{137}Cd_4Cl_3N_{16}O_{35}^{2+}$, 1621.73), 1631.42 $[Cd_2(LeuNDI)_2(2,2'\text{-bipy})_2(OH_2)_2(CH_3CN)+H]^+$, (calculated

for $C_{74}H_{72}Cd_2N_9O_{20}^+$, 1631.30). TGA: On-set, 50 °C, mass loss = 16.1% (calculated 15.2% for loss of five water and two DMF molecules, and two coordinated water molecules per asymmetric unit), decomp. 350 °C. Bulk phase purity was confirmed by PXRD.

The X-ray structure showed significant void space in which no solvent could be modelled, so the data were processed with the SQUEEZE routine of PLATON,[534] to show total void space of 534 Å^3 containing 131 e^- per asymmetric unit. This void may contain five water and two DMF molecules, accounting for 130 e^-, which could not be modelled in the structure. The TGA and SQUEEZE results show the same composition of non-coordinated solvent, and the microanalysis shows less solvent, as all but the coordinated solvent was lost before the microanalysis could be conducted.

Synthesis of Λ,Λ-[Cu_4((S)-LeuBPSD)$_4$(OH_2)$_4$]·2DMA ([Λ,Λ5.1(OH_2)$_4$]·2DMA)

Single crystals:

(*S*)-H_2LeuBPSD (10 mg, 17.1 µmol) and $Cu(NO_3)_2 \cdot 3H_2O$ (22 mg, 91.1 µmol) were added to DMA (3 mL) and sonicated to dissolve. The solution was heated at 100 °C for one week in a sealed vial. The solution was then left to sit at room temperature for two months, during which time a few blue crystals formed. The X-ray data was best modelled as Λ,Λ-[Cu_4((*S*)-LeuBPSD)$_4$(OH_2)$_4$]·2DMA. A different method was employed (see below) to synthesise a bulk sample in reasonable timeframe for which the PXRD matched that predicted for this crystalline sample.

Bulk powder sample:

(*S*)-H_2LeuBPSD (100 mg, 171 µmol) and $Cu(NO_3)_2 \cdot 3H_2O$ (220 mg, 911 µmol) were added to DMA (2.5 mL) and sonicated to dissolve. Methanol (4 mL) was added to the solution with stirring. A mixed solution of methanol (1 mL) and triethylamine (1 mL) was added dropwise (approx. four drops) to the metal/ligand solution with stirring until slight clouding remained. The reaction solution was left in a capped vial overnight during which time the product formed as a blue powder which was recovered by filtration and dried in air. PXRD confirmed this material to be the same crystalline phase as that isolated as single crystals (*vide supra*). Yield 64 mg, 56%. M.p. 282 – 284 °C. Found C, 51.45; H, 4.72; N, 5.22%;

$C_{112}H_{112}N_8O_{44}S_4Cu_4$·3.5DMA ([$Cu_4$((*S*)-LeuBPSD)$_4$($OH_2$)$_4$]·3.5DMA) requires C, 51.10; H, 4.89; N, 5.44%. υ_{max} /cm^{-1} 2954w, 1774w, 1711s, 1655m, 1610s, 1508m, 1467w, 1413m, 1377s, 1262w, 1178w, 1146m, 1102m, 1051m, 1020s, 947w, 895w, 861w, 784w, 732m, 671s. *m/z* (ES$^+$) 2586.25 (Λ,Λ-[**1**+H]$^+$, calculated for $C_{112}H_{105}Cu_4N_8O_{40}S_4^+$, 2585.25). TGA: On-set, 60 °C, mass loss = 12.7% (calculated 12.7% for loss of four coordinated H_2O molecules and 3.5 non-coordinated DMA molecules), decomp. 370 °C. The best structural model that could be fitted to the single crystal X-ray diffraction data was Λ,Λ-[Cu_4((*S*)-LeuBPSD)$_4$(OH_2)$_4$]·2DMA with significant void space in which no solvent could be modelled. The data was processed using the SQUEEZE routine of PLATON,[534] which showed a void space of 1039 Å^3 per unit cell (*i.e.* per cage), containing 339e$^-$. The best fit for the TGA and microanalysis suggests the presence of four coordinated water molecules and 3.5 non-coordinated DMA molecules, 1.5 DMA molecules which could not be modelled in the structure, which would lead to an expected 72 e$^-$ per cage. The greater electron count suggested by SQUEEZE compared to that expected based on the TGA and microanalysis results is likely due to solvent loss upon isolation prior to TGA or microanalysis being conducted.

Synthesis of Δ-[Cu_4((R)-LeuBPSD)$_4$(OH_2)(MeOH)$_{2.5}$($HNMe_2$)$_{0.5}$]·4DMA ([Δ5.1·(OH_2)(MeOH)$_{2.5}$($HNMe_2$)$_{0.5}$]·4DMA)

(*R*)-H_2LeuBPSD (100 mg, 171 µmol) and $Cu(NO_3)_2$·3H_2O (220 mg, 911 µmol) were added to DMA (2.5 mL) and sonicated to dissolve. Methanol (4 mL) was added to the solution with stirring. A mixed solution of methanol (1 mL) and triethylamine (1 mL) was added dropwise (approx. three drops) to the metal/ligand solution with stirring until slight clouding remained. The vial was capped and left to sit for one week, during which time the product formed as blue crystals which were recovered by filtration and dried in air. Yield 62 mg, 54%. M.p. 287–290 °C. Found C, 51.79; H, 5.05; N, 6.14%; $C_{115.5}H_{119.5}N_{8.5}O_{43.5}S_4Cu_4$·5DMA ([$Cu_4$((*R*)-LeuBPSD)$_4$($OH_2$)(MeOH)$_{2.5}$($HNMe_2$)$_{0.5}$]·5DMA) requires C, 51.8; H, 5.05; N, 6.14%. υ_{max} /cm^{-1} 2957w, 2871w, 1778w, 1711s, 1614s, 1469w, 1379s, 1264w, 1145s, 1103m, 1051m, 951w, 861m, 786m, 734m, 671s. Phase purity confirmed by PXRD. *m/z* (ES$^+$) 2646.28 (Δ,Δ-[**1**($NHMe_2$)(OH_2)+H]$^+$, calculated for $C_{114}H_{114}Cu_4N_9O_{41}S_4^+$, 2646.30). TGA: On-set, 50 °C, mass loss = 5.1% (calculated 4.5% for loss of one coordinated H_2O and 2.5 coordinated MeOH, and 0.5 coordinated $HNMe_2$), decomp. 350 °C. The best structural model that could be fitted to the single crystal X-ray diffraction data was Δ,Δ-[Cu_4((*R*)-

LeuBPSD)$_4$(OH$_2$)(MeOH)$_{2.5}$(HNMe$_2$)$_{0.5}$]·4DMA with significant void space in which no solvent could be modelled. The diffraction data was processed using the SQUEEZE routine of PLATON,[534] which showed a void of 479 Å^3 per unit cell (*i.e.* per cage) estimated to contain 47e$^-$. The best fit for the microanalysis suggests the presence of 2.5 coordinated methanol, one coordinated water molecule, 0.5 coordinated HNMe$_2$ and four modelled DMA molecules, which is one DMA molecule more than the model generated from X-ray data, which would lead to an expected 48e$^-$ per cage. The best fit for the TGA suggested mass loss for the coordinated solvent. The TGA shows less mass loss than would be expected based on the single crystal structure, SQUEEZE results and microanalysis, likely due to solvent loss before the TGA was conducted.

Synthesis of Λ,Λ-[Cu$_4$((S)-LeuBPSD)$_4$(OH$_2$)$_2$(DMSO)$_2$]·2DMSO ([Λ,Λ-5.1(DMSO)$_2$(OH$_2$)$_2$]·2DMSO)

An ^{1}H-NMR sample of Λ,Λ-[Cu$_4$((*S*)-LeuBPSD)$_4$(OH$_2$)$_4$] (5 mg) in d_6-DMSO (0.5 mL) was left to sit at room temperature. After one month blue crystals formed in the solution, from which X-ray diffraction data was collected. To replicate this synthesis, 83 mg of **Λ,Λ5.1** was dissolved in non-deuterated DMSO (1 mL) and left to sit at room temperature. After one month a microcrystalline product was found to have formed which was recovered by filtration. Found C, 45.74; H, 4.25; N, 3.69%; $C_{116}H_{120}N_8O_{44}Cu_4S_6$·15H$_2$O ([Cu$_4$((*S*)-LeuBPSD)$_4$(OH$_2$)$_2$(DMSO)$_2$]·15H$_2$O requires C, 45.72; H, 4.97; N, 3.68%. *m/z* (ES$^+$) 2685.26, ([**Λ,Λ5.1**(DMSO)+Na]$^+$, calculated for $C_{114}H_{110}Cu_4N_8O_{41}S_5Na^+$, 2685.25). υ_{max} /cm^{-1} 2733w, 1776w, 1713s, 1653m, 1616m, 1508w, 1465w, 1413m, 1379s, 1327m, 1260w, 1146m, 1101m, 1051s, 1019s, 948m, 894w, 863m, 786m,734m, 671s. TGA: On-set, 40 °C, mass loss = 23.5% (calculated 23.3% for loss of two coordinated H$_2$O and two coordinated DMSO, and seven DMSO and 15 H$_2$O), decomp. 350 °C. The best structural model that could be fitted to the single crystal X-ray diffraction data was Λ,Λ-[Cu$_4$((*S*)-LeuBPSD)$_4$(OH$_2$)$_2$(DMSO)$_2$]·2DMSO with significant void space in which no solvent could be modelled. The data was processed using the SQUEEZE routine of PLATON,[534] which showed a void space of 524 Å^3 per unit cell (*i.e.* per cage), containing 153e$^-$. The best fit for the TGA data suggests the presence of two coordinated DMSO and two coordinated water molecules, and 12 non-coordinated water molecules and eight non-coordinated DMSO molecules, which would give an expected electron count of 328e$^-$. The larger

expected electron count suggested by the TGA is likely due to the TGA being conducted soon after the sample was recovered by filtration and therefore a large amount of surface solvent still present on the crystals. The best fit for the microanalysis suggests the presence of the two coordinated DMSO and two coordinated water molecules, and 15 non-coordinated water molecules, likely due to the loss of solvent during transport.

Synthesis of Λ,Λ-[Cu_4((S)-LeuBPSD)$_4$(MeOH)$_2$(OH_2)$_2$]/Δ-[Cu_4((R)-LeuBPSD)$_4$(MeOH)$_2$(OH_2)$_2$]·DMA (Λ,Λ/Δ-[5.1(MeOH)$_2$(OH_2)]·DMA)

(*S*)-H_2LeuBPSD (50 mg, 171 µmol), (*R*)-H_2LeuBPSD (50 mg, 85.5 µmol) and $Cu(NO_3)_2 \cdot 3H_2O$ (220 mg, 911 µmol) were added to DMA (2.5 mL) and sonicated to dissolve. Methanol (4 mL) was added to the solution with stirring. A solution of methanol (1 mL) and triethylamine (1 mL) was added dropwise (approx. three drops) to the metal/ligand solution with stirring until slight clouding remained. The vial was capped and left to sit for one week, during which time the product formed as blue crystals which were recovered by filtration. Yield 36.1 mg, 31%. M.p. 285 – 288 °C. Found C, 51.79; H, 5.52; N, 6.84%; $C_{114}H_{116}N_8O_{44}S_4Cu_4 \cdot 8DMA$, ([$Cu_4$(LeuBPSD)$_4$(MeOH)$_2$($OH_2$)$_2$]·8DMA) requires C, 51.85; H, 5.61; N, 6.63%. υ_{max} /cm^{-1} 2957w, 2871w, 1778w, 1711s, 1611m, 1469w, 1379s, 1148m, 1103m, 1051m, 947m, 861w, 786w, 734s, 671s. Bulk phase purity was confirmed by PXRD. *m/z* (ES$^-$) 2619.22 (Λ,Λ/Δ,Δ-[**5.1**+Cl]$^-$, calculated for $C_{112}H_{104}Cu_4N_8O_{40}S_4Cl^-$, 2619.21), 2629.29 (Λ,Λ/Δ,Δ-[**5.1**($NHMe_2$)+H]$^+$, calculated for $C_{114}H_{112}Cu_4N_9O_{40}S_4^-$, 2628.29), 2646.28 (Λ,Λ/Δ,Δ-[**5.1**($NHMe_2$)(OH_2)+H]$^+$, calculated for $C_{114}H_{113}Cu_4N_9O_{41}S_4^-$, 2646.30). TGA: On-set, 40 °C, mass loss = 18.0% (calculated 18.4% for loss of two coordinated MeOH and two coordinated H_2O, and five non-coordinated DMA and one non-coordinated MeOH), decomp. 350 °C. The best structural model that could be fitted to the single crystal X-ray diffraction data was Λ,Λ-[Cu_4((*S*)-LeuBPSD)$_4$(MeOH)$_2$(OH_2)$_2$]/Δ,Δ-[Cu_4((*R*)-LeuBPSD)$_4$(MeOH)$_2$(OH_2)$_2$]·DMA (although it is likely that the composition of the coordinated solvent is more complicated) with significant void space in which no solvent could be modelled. The data was processed using the SQUEEZE routine of PLATON,[534] which showed a void space of 9264 Å^3 per unit cell (1158 Å^3 per cage), containing 300e$^-$ per cage. The mass spectrum shows two peaks corresponding to the cage containing one coordinated water molecule and one dimethylamine, and one dimethylamine. Although

$NHMe_2$ could not be modelled in the single crystal X-ray structure, dimethylamine was present from hydrolysis of DMA used in the reaction and is likely present in the crystalline sample with the cages containing various compositions of solvent and the average electron density not being sufficient to resolve this mixture, although Λ,Λ/Δ,Δ-[**5.1**($NHMe_2$)+H] and Λ,Λ/Δ,Δ-[**5.1**($NHMe_2$)(OH_2)+H] may represent two of the most stable ions which could be observed in the mass spectra. The best fit for the TGA analysis suggests the presence of two coordinated MeOH and two coordinated H_2O, and five non-coordinated DMA and one non-coordinated MeOH. The best fit for the microanalysis suggests the presence of two coordinated MeOH and two coordinated H_2O, and five non-coordinated DMA molecules, The solvent not modelled in the crystal structure which is observed in the TGA and the microanalysis corresponds to an electron count of 322e$^-$ and 336e$^-$, respectively, which is slightly more than that which is shown by the SQUEEZE results, likely due to some residual solvent when the TGA and microanalysis was conducted.

Synthesis of [Cu_4((S,R)-H_2LeuBPSD)$_4$(OH_2)$_2$(MeOH)$_2$]·2DMA, ([5.2(OH_2)$_2$(MeOH)$_2$]·2DMA)

(*S*,*R*)-H_2LeuBPSD (100 mg, 85.5 µmol) and $Cu(NO_3)_2·3H_2O$ (220 mg, 911 µmol) were added to DMA (2.5 mL) and stirred to dissolve. Methanol (4 mL) was added to the solution with stirring. A solution of methanol (1 mL) and triethylamine (1 mL) was added dropwise (approx. three drops) to the metal/ligand solution with stirring until slight clouding remained. The vial was capped and left to sit for four nights, during which time the product formed as blue crystals which were recovered by filtration. Yield 27.4 mg, 22%. M.p. 271 – 273 °C. Found C, 51.12; H, 4.70; N, 5.04%; $C_{114}H_{116}N_8O_{44}S_4Cu_4$·2.5DMA, ([$Cu_4$((*S*,*R*)-LeuBPSD)$_4$($OH_2$)$_2$(MeOH)$_2$]·2.5DMA requires C, 51.13; H, 4.81; N, 5.07%. υ_{max} /cm^{-1} 2200w, 1776w, 1717s, 1646m, 1608m, 1506w, 1467w, 1413m, 1381s, 1351m, 1323s, 1264w, 1142m, 1105m, 1057m, 1014w, 939w, 909w, 863w, 784m 745m, 671s. Bulk phase purity was confirmed by PXRD. *m/z* (ES$^+$) 2607.19 ([**2**+Na]$^+$, calculated for $C_{112}H_{104}Cu_4N_8O_{40}S_4Na^+$, 2607.23), 2685.40 ([**2**(MeOH)$_2$(OH_2)$_2$+H]$^+$, calculated for $C_{114}H_{117}Cu_4N_8O_{44}S_4^+$, 2685.32).TGA: On-set, 40 °C, mass loss = 23.3% (calculated 23.6% for loss of two coordinated H_2O and two coordinated MeOH, and eight DMA), decomp. 350 °C. The best structural model that could be fitted to the single crystal X-ray diffraction data was [Cu_4((*S*,*R*)-

$H_2LeuBPSD_4)(OH_2)_2(MeOH)_2]\cdot 2.5DMA$ with significant void space in which no solvent could be modelled. The data was processed using the SQUEEZE routine of PLATON,[534] which showed a void space of 1183 $Å^3$ per unit cell (*i.e.* per cage), containing $280e^-$ per cage. The best fit for the TGA data suggests the presence of the two coordinated methanol and two coordinated water molecules, and eight DMA molecules. The six non-coordinated DMA molecules suggested by the TGA would correspond to $264e^-$. The best fit for the microanalysis suggests the presence of the two coordinated methanol and two coordinated water molecules, and two non-coordinated DMA molecules. The greater electron count suggested by SQUEEZE compared to that which is expected based on the microanalysis results is likely due to solvent loss upon isolation prior to the microanalysis being conducted.

Synthesis of $[Cu_4(GlyBPSD)_4(MeOH)_3(OH_2)]\cdot 3.5DMA\cdot 1.5MeOH$ ($[5.3(MeOH)_3(OH_2)]\cdot 3.5DMA\cdot 1.5MeOH$)

Single crystals:

$H_2GlyBPSD$ (10 mg, 21.2 µmol) was dissolved in DMA (0.5 mL). $Cu(NO_3)_2\cdot 3H_2O$ (15.4 mg, 63.6 µmol) was also dissolved in DMA (0.5 mL) and combined with the ligand solution. Methanol (1 mL) was added to the combined metal/ligand solution with stirring. A solution of triethylamine (3 drops) in methanol (5 mL) was added dropwise to the metal/ligand solution with stirring, until the solution became cloudy (~0.5 mL). When the solution became cloudy the vial was capped and left to sit for one month, during which time a few blue crystals, suitable for X-ray diffraction were found to have formed. The X-ray data was best modelled as $[Cu_4(GlyBPSD)_4(MeOH)_3(OH_2)]\cdot 3.5DMA\cdot 1.5MeOH$. A different method was employed (see below) to synthesise a bulk sample in reasonable timeframe for which the PXRD matched that predicted for this crystalline sample.

Bulk powder sample:

$H_2GlyBPSD$ (30 mg, 63.6 µmol) and $Cu(NO_3)_2\cdot 3H_2O$ (46.2 mg, 190.7 µmol) were dissolved in a mixture of DMA (3 mL) and methanol (3 mL). A solution of triethylamine (3 drops) in methanol (5 mL) was added dropwise with stirring until the blue solution became slightly cloudy (approx. 2 mL). A blue powder was isolated by filtration after three nights, with PXRD confirming it to be the same crystalline phase as that isolated as single crystals. Yield 25.0 mg, 69%. M.p. >350 °C. Found C, 41.00; H, 2.87; N, 4.89%;

$C_{83}H_{54}N_8O_{44}S_4Cu_4 \cdot 4H_2O \cdot 6MeOH$ ($[Cu_4(GlyBPSD)_4(MeOH)_3\text{-}(OH_2)] \cdot 4H_2O \cdot 6MeOH$) requires C, 41.02; H, 3.07; N, 4.61%. υ_{max} /cm^{-1} 1775m, 1707s, 1593s, 1411s, 1372s, 1318s, 1198s, 1146s, 1061m, 1003m, 969s, 930m, 887w, 802w, 749s, 712s, 675s. *m/z* (ES$^+$) 2136.74 ([**5.3**+H]$^+$, calculated for $C_{80}H_{41}Cu_4N_8O_{40}S_4^+$, 2136.75), 2168.77 ([**3**+MeOH+H]$^+$, calculated for $C_{81}H_{45}Cu_4N_8O_{41}S_4^+$, 2168.77). TGA: On-set, 50 °C mass loss = 18.6% (calculated 18.6% for loss of three coordinated MeOH and one H_2O, and four non-coordinated H_2O, seven MeOH and two DMA), decomp. 350 °C. The best structural model that could be fitted to the single crystal X-ray diffraction data was $[Cu_4(GlyBPSD)_4(MeOH)_3(OH_2)] \cdot 3.5DMA \cdot 1.5MeOH$. There is some variation in the degree and composition of solvation in the single crystal structure and that suggested by TGA and microanalysis. This is likely due to the slight difference in synthetic conditions, some disorder associated with solvent molecules in the crystal structure (see X-Ray Crystallography Details) and handling methods for the various analyses. TGA suggests the presence of more solvent than the microanalysis results, with likely loss of solvent in transit.

Synthesis of $[Cu_4((S)\text{-LeuEADI})_4(DMF)(OH_2)_3] \cdot 3.5DMF \cdot 9.5H_2O$, [5.4 $DMF)(OH_2)_3] \cdot 3.5DMF \cdot 9.5H_2O$

(*S*)-LeuEADI (10 mg, 16.7 µmol) and $Cu(OAc)_4$ (6.0 mg, 33.3 µmol) were added to DMF (1 mL) and sonicated to dissolve. The solution was heated at 85 °C for two nights during which time light blue block shaped crystals formed, which were recovered by vacuum filtration. Yield 2.2 mg, 61%. Found C, 56.04; H, 5.58, N, 5.59%; $C_{139}H_{149}N_9O_{36}Cu_4 \cdot 3.5DMF \cdot 9.5H_2O$ $[Cu_4((S)\text{-LeuEADI})_4(DMF)(OH_2)_3] \cdot 3.5DMF \cdot 14H_2O$ requires C, 56.14; H, 6.02; N, 5.31%. υ_{max} /cm^{-1} 2955w, 2869w, 1771w, 1709s, 1637m, 1465w, 1411m, 1377s, 1351m, 1259w, 1204w, 1156w, 1101w, 1062w, 992w, 913w, 870w, 805w, 771w, 755m, 729w, 660m. *m/z* (ES$^+$) 2649.651 (**5.4**+H)$^+$, calculated for $C_{136}H_{136}Cu_4N_8O_{32}^+$, 2647.645), 2708.681 (**5.4**+H_2O+MeCN+H)$^+$, calculated for $C_{138}H_{141}Cu_4N_9O_{33}^+$, 2706.683). TGA: On-set, 70 °C, mass loss = 10% (calculated 11.8% for loss of two H_2O and 4.5 DMF non-coordinated molecules and all coordinated solvent), decomp, 350 °C.

The data showed significant void space, so was processed with the SQUEEZE routine of PLATON[534] to show void volume of 1269 Å^3 containing 292 e$^-$ per cage, which would correspond to 14 water and 3.5

DMF molecules per cage. The TGA and microanalysis show less than this, most likely due to solvent loss before TGA or microanalysis were conducted. Bulk phase purity was confirmed by PXRD.

Synthesis of $[Rh_4((S)\text{-LeuBPSD})_4(OH_2)_4]\cdot 4MeOH\cdot 10H_2O$, $[5.5(OH_2)_4]\cdot 4MeOH\cdot 10H_2O$

(*S*)-LeuBPSD (138 mg, 236 µmol) and $Rh_2(OAc)_4$ (60 mg, 236 µmol) were added to a dry RBF with a condenser attached and the system was degassed with nitrogen for 10 minutes. Chlorobenzene (50 mL) was added to the RBF and heated at reflux under nitrogen for 10 days. The solution was cooled to room temperature and the solvent removed under reduced pressure. Chloroform (20 mL) was added to the resulting green solid and the suspension was sonicated. The precipitate was removed by vacuum filtration leaving a green filtrate. The filtrate was placed in small glass vials (2 mL each) and these vials were placed in a large vial containing methanol (3 mL) and the large vials were capped. After one week green crystals had formed in the small vial, which were recovered by vacuum filtration. Yield 62.5 mg, 34%. Found C, 44.60; H, 4.51, N, 3.70%; $C_{112}H_{112}N_8O_{44}Rh_4\cdot 4MeOH\cdot 10H_2O$, $Rh_4((S)\text{-LeuBPSD})_4(OH_2)_4]\cdot 4MeOH\cdot 10H_2O$ requires C, 44.62; H, 4.78; N, 3.59%. δ_H (400 MHz, $CDCl_3$) 1.02 (m, 48 H, H_8), 1.36 (m, 8 H, H_7), 1.84 (m, 8 H, $H_{5,6}$), 2.07 (m, 8 H, $H_{5,6}$), 5.02 (m, 8 H, H_4), 8.07 (m, 8 H, H_2), 8.22 (m, 8 H, H_3), 8.57 (m, 8 H, H_1). υ_{max} /cm^{-1} 2959w, 2872w, 1777w, 1713s, 1601m, 1534w, 1466w, 1400m, 1378s, 1345m, 1326m, 1261w, 1236w, 1194w, 1176w, 1147m, 1101m, 1054m, 990w, 942w, 908w, 862w, 788m, 753w, 737m, 725m, 677s. *m/z* (ES^+) 2804.061 (**5.5**$(MeOH)_2$-H)$^-$, calculated for $C_{114}H_{112}N_8O_{42}Rh_4S_4^-$, 2804.194. TGA: On-set, 50 °C, mass loss = 12.5% (calculated 9.8% for loss of four non-coordinated methanol and 10 non-coordinated water molecules, calculated 2.3% for loss of four coordinated water molecules), decomp. 370 °C. Bulk phase purity was confirmed by PXRD.

The X-ray data were processed with SQUEEZE routine of PLATON,[534] suggesting voids of 1507 $Å^3$ which are filled with a total of 409 electrons per cage. As the solvent present in the structure would be chloroform, water and methanol, it is difficult to exactly assign the solvent composition in the structure, as these solvents are quite volatile. The voids shown by SQUEEZE fit for the presence of 20 chloroform, six methanol and 12 water molecules which could not be modelled in the structure. Much of this solvent would have been lost before the TGA and microanalysis was conducted.

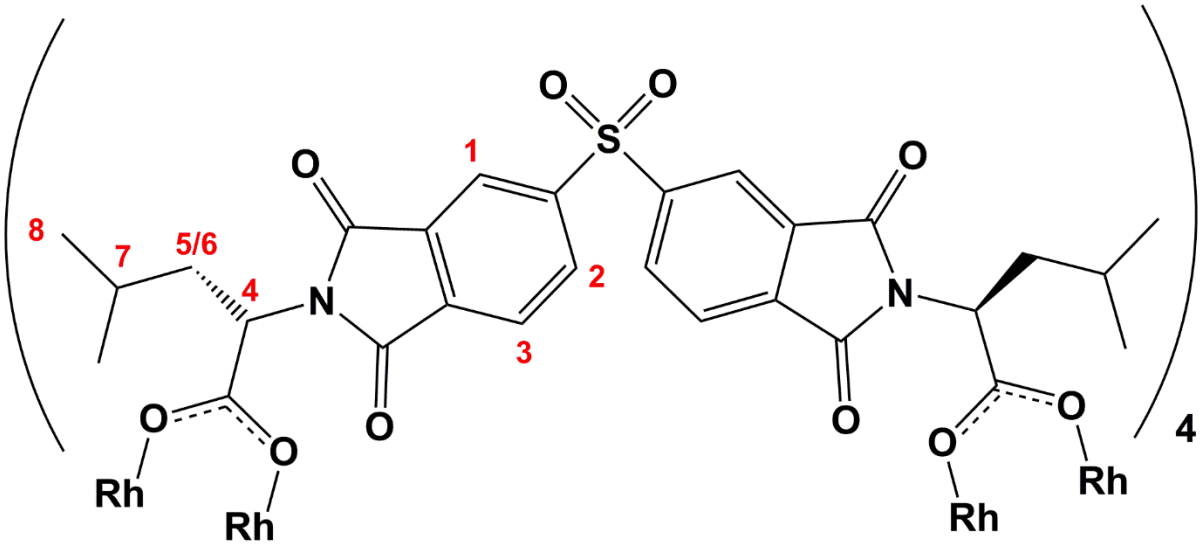

Synthesis of [Cu$_{12}$((S)-LeuNDI)$_{12}$(OH$_2$)$_{12}$]·22H$_2$O·30DMF, 6.1·22H$_2$O·30DMF

(*S*)-H$_2$LeuNDI (15 mg, 30.4 µmol) and Cu(NO$_3$)$_2$·3H$_2$O (7.0 mg, 30.4 µmol) were added to DMF (1 mL) in a glass vial and sonicated to dissolve. The solution was heated at 120 °C for 24 hours, and then left to sit for one week, during which time blue block crystals were found to have formed and were recovered by filtration. Yield 15 mg, 64%. M.p. 324 – 326 °C. Found C, 51.41; H, 6.01; N, 7.97%; C$_{312}$H$_{312}$N$_{24}$O$_{108}$Cu$_{12}$·22H$_2$O·30DMF: requires C, 50.94; H, 6.02; N, 7.98%. υ_{max} /cm^{-1} 2957w, 2863w, 1706m, 1664s, 1633s, 1578m, 1493w, 1449m, 1413m, 1414m, 1384m, 1326s, 1243s, 1198m, 1088m, 987w, 860m, 773s, 727m, 674m. TGA: On-set, 50 °C, mass loss = 29.4% (calculated 29.6% for loss of 12 coordinated H$_2$O and non-coordinated solvent of 22 H$_2$O and 30 DMF), decomp. 315 °C. Bulk phase purity was confirmed by PXRD. *m/z* (ES$^+$): calculated [Cu$_{12}$((*S*)-LeuNDI)$_{12}$+3H]$^{3+}$ (Cu$_{12}$C$_{312}$H$_{291}$N$_{24}$O$_{96}$$^{3+}$): 2225.007, measured 2225.006; calculated [Cu$_{12}$((*S*)-LeuNDI)$_{12}$(OH$_2$)$_3$+3H]$^{3+}$ (Cu$_{12}$C$_{312}$H$_{299}$N$_{24}$O$_{100}$$^{3+}$): 2249.021, measured 2249.022; calculated [Cu$_{12}$((*S*)-LeuNDI)$_{12}$(OH$_2$)$_5$+3H]$^{3+}$ (Cu$_{12}$C$_{312}$H$_{301}$N$_{24}$O$_{101}$$^{3+}$): 2255.025, measured 2255.006; calculated [Cu$_{12}$((*S*)-LeuNDI)$_{12}$(OH$_2$)$_{10}$(MeCN)+3H]$^{3+}$ (Cu$_{12}$C$_{314}$H$_{314}$N$_{25}$O$_{106}$$^{3+}$): 2298.718, found 2298.700; calculated [Cu$_{12}$((*S*)-LeuNDI)$_{12}$(OH$_2$)$_6$(MeCN)$_2$-CO$_2$+3H]$^{3+}$ (Cu$_{12}$C$_{315}$H$_{309}$N$_{26}$O$_{100}$$^{3+}$): 2273.716, measured 2273.684; calculated [Cu$_{12}$((*S*)-LeuNDI)$_{12}$+2H]$^{2+}$ (Cu$_{12}$C$_{312}$H$_{290}$N$_{24}$O$_{96}$$^{3+}$): 3337.007, measured 3337.005; calculated [Cu$_{12}$((*S*)-LeuNDI)$_{12}$(OH$_2$)$_4$+2H]$^{2+}$ (Cu$_{12}$C$_{312}$H$_{298}$N$_{24}$O$_{100}$$^{3+}$): 3373.028, measured 3373.026; calculated [Cu$_{12}$((*S*)-LeuNDI)$_{12}$(OH$_2$)$_6$(MeCN)$_2$-

CO_2+2H]$^{2+}$ ($Cu_{12}C_{315}H_{308}N_{26}O_{100}^{3+}$): 3410.071, measured 3410.016; calculated [Cu_{12}((*S*)-LeuNDI)$_{12}$(OH_2)$_2$($MeCN$)$_2$-CO_2+2H]$^{2+}$ ($Cu_{12}C_{315}H_{300}N_{26}O_{96}^{3+}$): 3374.549, measured 3374.490.

The structure was highly porous, so the data were processed with the SQUEEZE routine of PLATON,[534] showing one large void of 19365 Å^3 corresponding to the voids within the cages and channels between the cages, which were filled with 4874 e$^-$ and four smaller voids of 1035 Å^3, corresponding to the spherical voids between the cages, which were filled with 234 e$^-$ per unit cell, corresponding to voids of 4841.25 Å^3 with 1218.5 e$^-$ and 1035 Å^3 with 234 e$^-$ per cage (total 1452 e$^-$) , which would account for a total of 22 water molecules and 30 DMF molecules per cage (accounting for 1420 e$^-$).

Synthesis of *poly*-[Cu_2(GlyNDI)$_2$(DMA)$_2$]·DMA, 6.2

H_2GlyNDI (10 mg, 23.2 µmol) and $CuCl_2$·3H_2O (9.0 mg, 52.4 µmol) were added to DMA (2 mL) in a glass vial and sonicated to dissolve The solution was heated at 120 °C for 24 hours, and during which time small light blue crystals were formed, which were recovered by filtration. Yield 9.3 mg, 72%. M.p. >400 °C. Found C, 50.02; H, 3.48; N, 8.66%; $C_{44}H_{34}N_6O_{18}Cu_2$·DMA **(**[$Cu_2$(GlyNDI)$_2(DMA)_2$]·DMA); requires C, 50.17; H, 3.77; N, 8.53%. υ_{max} /cm^{-1} 2959w, 1713w, 1672m, 1640w, 1594m, 1505w, 1450w, 1422m, 1389m, 1350m, 1316s, 1243s, 1184m, 1118w, 1007s, 916w, 895w, 776s, 725m. TGA: On-set, 80 °C, mass loss = 22.9% (calculated 22.8% for loss of two coordinated DMA and one non-coordinated DMA), decomp. 280 °C. Bulk phase purity confirmed was by PXRD.

8.4 Enantioselective catalysis experiments

The enantioselective catalytic properties of **5.5** was investigated by the cyclopropanation reaction of styrene with ethyl diazoacetate. The reaction was also undertaken with [Rh_2(CH_2COO)$_4$]·2MeOH and [Rh_2((*S*)-LeuPI)$_4$] at catalysts, to act as comparisons to **5.5**.

<u>Cyclopropanation reaction with **5.5**</u>

A solution of ethyl diazoacetate (0.3 mL, 2.8 mmol) in DCM (5 mL) was added dropwise to a solution of styrene (0.5 mL, 4.4 mmol) and **5.5** (16.8 mg, 0.006 mmol, 0.024 mmol rhodium sites, 0.8 mol%) in DCM (5 mL) over a period of three hours. The solution was left to stir for a total of 24 hours, during which time the DCM was removed *in vacuo*.

Cyclopropanation reaction with [$Rh_2(OAc)_4$]

A solution of ethyl diazoacetate (0.3 mL, 2.8 mmol) in DCM (5 mL) was added dropwise to a solution of styrene (0.5 mL, 4.4 mmol) and [$Rh_2(OAc)_4$] (3 mg, 0.006 mmol, 0.024 mmol rhodium sites, 0.8 mol%) in DCM (5 mL) over a period of three hours. The solution was left to stir for a total of 24 hours, after which time the DCM was removed *in vacuo*.

Cyclopropanation reaction with [$Rh_2(LeuPI)_4$]

A solution of ethyl diazoacetate (0.3 mL, 2.8 mmol) in DCM (5 mL) was added dropwise to a solution of styrene (0.5 mL, 4.4 mmol) and [$Rh_2(LeuPI)_4$] (7.5 mg, 0.006 mmol, 0.024 mmol rhodium sites, 0.8 mol%) in DCM (5 mL) over a period of three hours. The solution was left to stir for a total of 24 hours, after which time the DCM was removed *in vacuo*.

The % conversion, *cis*/*trans* selectivity and % ee were calculated by ^{1}H-NMR and GC. The rhodium catalysts could not be recovered from the reaction solution, as they appeared to be soluble in the ethyl-2-phenylcyclopropanecarboxylate products.

8.5 Mixed ligand BPSD cage experiments

Standard experiment of constant Cu^{II} and variable (*S*)-H_2LeuBPSD

Standard solutions of $Cu(OAc)_2$ (43.4 mg, 240 mmol) in acetonitrile (30 mL) and (*S*)-H_2LeuBPSD (87.6 mg, 150 mmol) in DMA (1 mL) were prepared. The cage solutions were prepared by adding 160, 140, 120, 100, 80, 60, 40 and 20 uL of the (*S*)-LeuBPSD standard to individual glass vials and adding additional DMA (total 3 mL for each reaction mixture). The $Cu(OAc)_2$ standard (3 mL) was added to each solution of (*S*)-H_2LeuBPSD slowly with stirring, in order to make solutions with Cu : (*S*)-LeuBPSD molar ratios of 8:8, 8:7, 8:6, 8:5, 8:4, 8:3, 8:2, 8:1 and 8:0, and then left to sit for 24 hours at room temperature. Circular dichroism analysis was conducted on solutions in which 0.1 mL of each reaction solution was diluted to 5 mL with acetonitrile.

Substitution of H_2GlyBPSD for (*S*)-H_2LeuBPSD with constant Cu^{II}

Standard solutions of $Cu(OAc)_2$ (43.4 mg, 240 mmol) in acetonitrile (20 mL), and (*S*)-H_2LeuBPSD (87.6 mg, 150 mmol) in DMA (1 mL) and H_2GlyBPSD (70.8, 150 mmol) in DMA (1 mL) were prepared. The

reaction solutions were prepared by adding a total of 160 uL of BPSD standard solution to a volumetric flask (5 mL) and an additional 0.84 mL of DMA (1 mL total), Table 8.2. The $Cu(OAc)_2$ standard solution was added to each ligand solution (2 mL) slowly with stirring. Following the addition of the Cu^{II} solution, the volumetric flask was made up to the mark with acetonitrile and the solutions were left to sit at room temperature for 24 hours. Circular dichroism analysis was conducted on 0.1 mL of the reaction solutions diluted to 0.384 mmol/L with acetonitrile (5 mL). HPLC was carried out with 50 µL of the reaction solutions which was diluted to 1.92 mmol/L with acetonitrile (0.5 mL).

Table 8.2. The composition of each solution in the experiment in which (S)-H_2LeuBPSD was substituted for H_2GlyBPSD, with a constant concentration of Cu^{II}.

Sample code	H_2LeuBPSD equivalents (to 8 Cu^{II})	H_2LeuBPSD standard solution volume (µL)	H_2GlyBPSD equivalents (to 8 Cu^{II})	H_2GlyBPSD standard solution volume (µL)
A	8	160	0	0
B	7	140	1	20
C	6	120	2	40
D	5	100	3	60
E	4	80	4	80
F	3	60	5	100
G	2	40	6	120
H	1	20	7	140
I	0	0	8	160

8.6 Fluorescence experiments

Fluorescence emission titrations

All solutions of H_2LeuNDI in chloroform and acetonitrile were prepared at 30 µmol/L, with aromatic solvents toluene, *o*-xylene, *m*-xylene and *p*-xylene added at 0%, 1%, 10%, 20%, 50% and 100% by volume. All solutions of **4.1** and **4.2** were prepared at concentrations of 25 µmol/L in chloroform, with toluene at 0%, 1%, 10%, 20% and 50% by volume.

Quenching of aromatic molecules with 6.1

A series of six solutions were prepared with a constant concentration of naphthalene (120 μmol/L) and varying concentrations of the 6.1 complex (0, 3.3, 6.6, 10, 13.2, 16.6 and 20 umol/L). The fluorescence emission was measured with excitation at 285 nm.

A series of six solutions were prepared with a constant concentration of triphenylene (120 μmol/L) and varying concentrations of the 6.1 complex (0, 3.3, 6.6, 10, 13.2, 16.6 and 20 umol/L). The fluorescence emission was measured with excitation at 300 nm.

8.7 Chiral separation tests of compound 6.1

The chiral resolution properties of **6.1** in the solid state were tested in collaboration with The Hill group at Monash University.

Resolution of pantolactone

A 100mg/ml solution of D/L pantolactone in methanol was prepared, 1mL of this solution was then added to **6.1** (10 mg) and left to sit at room temperature for 24 hours. The solid sample of **6.1** was then recovered by filtration, washed slightly with methanol to remove any surface compounds, and then soaked in methanol (1 mL) for 24 hours at room temperature. The suspension was then centrifuged in order to isolate **6.1**, and the supernatant was analysed by chiral GC.

Resolution of 1-phenylethanol

To a sample of **6.1** (10 mg) in either methanol or heptane (0.3 mL) was added 1-phenylethanol (0.05 mL) left to sit at room temperature for 24 hours. The solid sample of **6.1** was then recovered by filtration, washed slightly with methanol to remove any surface compounds, and then soaked in methanol (1 mL) for 24 hours at room temperature. The suspension was then centrifuged in order to isolate **6.1**, and the supernatant was analysed by chiral GC.

Resolution of 2-methyl-2,4-pentanediol

To a sample of **6.1** (10 mg) in either methanol or heptane (0.3 mL) was added 2-methyl-2,4-pentanediol (0.05 mL) left to sit at room temperature for 24 hours. The solid sample of 6.1 was then recovered by

filtration, washed slightly with methanol to remove any surface compounds, and then soaked in methanol (1 mL) for 24 hours at room temperature. The suspension was then centrifuged in order to isolate 6.1, and the supernatant was analysed by chiral GC.

8.8 X-ray crystallography details

Data for H_2LeuNDI **4.1** was collected on an OXFORD Gemini Ultra diffractometer at 123 K. data were processed, including an empirical absorption correction, using proprietary software CrysAlisPro.[543] Data for **Λ,Λ5.1** was collected using a Bruker ApexII diffractometer at 123 K using graphite monochromated Mo-Kα radiation (λ = 0.71073 Å). Data collection and processing was conducted using the SAINT software suite.[544] Data for all remaining structures was collected using the MX1 or MX2 beamlines at the Australian Synchrotron. Data was collected at 100 K using an energy equivalent to Mo-Kα radiation (17.4 keV, λ = 0.7108 Å), with exception of **2.17**, which was collected using with energy at 13000 eV (λ = 0.9537 Å). Data collection at the Australian Synchrotron was controlled using the BluIce software package on the MX1 beamline operating at 17.4 keV (λ = 0.7108)[545] using the BluIce control software.[546] Data collection and processing were conducted using the program XDS.[547]

All structures were solved with SHELXT[548] using the dual-space method or SHELXS[549] using direct methods, and refined by least-squares methods using SHELXL-2016[550] within OLEX-2.[551] Non-hydrogen atoms were refined with anisotropic displacement parameters. Hydrogen atoms were placed in calculated positions and refined using a riding model with isotropic displacement parameters 1.2 or 1.5 times the isotropic equivalent of their carrier atoms. O-H hydrogen atoms were placed in calculated positions and refined using SHELX DFIX and DANG restraints to maintain their positions in the structures of **2.1**, **2.2**, **2.5**, **2.8**, **2.9**, **2.10**, **2.12**, **2.1**, **3.2**, **3.8**, **4.1**, **4.2**, **5.4** and **6.1**. The O-H hydrogen atoms were held in calculated positions by AFIX constraints in the structures of **2.3**, **2.4**, **2.6**, **2.11**, **2.13**, **2.14**, **2.15**, **2.16**, **2.17**, **2.18**, **2.19**, **3.3**, **3.4**, **3.5**, **3.6**, **3.7**, **Δ,Δ5.1**, **Λ,Λ5.1**, **Δ,Δ5.1**/ **Λ,Λ5.1**, **Λ,Λ/Δ,Δ5.1**, **5.2** and **5.5**.

The structures of **2.2**, **2.3**, **2.4**, **2.7**, **2.10**, **2.12**, **2.13**, **2.15**, **2.16**, **2.18**, **3.4**, **3.5**, **3.6**, **3.7**, **3.8**, **4.1**, **4.2**, **Δ,Δ5.1**, **Λ,Λ5.1**, **Δ,Δ5.1**/ **Λ,Λ5.1**, **Λ,Λ/Δ,Δ5.1**, **5.2**, **5.3**, **5.4**, **5.5** and **6.1** contained solvent accessible voids, and were processed with the SQUEEZE routine of PLATON.[534] Specific solvent contribution details are given in

section 8.3. Specific refinement details are discussed in Section 8.7.2. The CCDC numbers are provided for published data.

8.8.1 X-ray crystallographic information

Compound reference	**2.1**	**2.2**	**2.3**	**2.4**
Empirical formula	$C_{59}H_{55}Cd_2N_9O_{20}$	$C_{102}H_{88}Cd_4N_{14}O_{38}$ ·solvent	$C_{105}H_{95}Mn_4N_{15}O_{39}$ ·solvent	$C_{30}H_{22}CdN_4O_9$ ·solvent
Formula weight	1434.92	2567.46	2410.71	694.91
Crystal system	Tetragonal	Orthorhombic	Orthorhombic	Tetragonal
a/Å	16.984(2)	18.674(4)	18.324(4)	21.838(3)
b/Å	16.984(2)	23.894(5)	23.774(5)	21.838(3)
c/Å	21.780(4)	14.086(3)	14.040(3)	14.721(3)
α/°	90	90	90	90
β/°	90	90	90	90
γ/°	90	90	90	90
Volume/$Å^3$	6283(2)	6285(2)	6116(2)	7020(2)
Temperature /K	100(2)	100(2)	100(2)	100(2)
Space group	$P4_2$	$P2_12_12$	$P2_12_12$	$P4_32_12$
Z	4	2	2	8
Reflections measured	260223	105036	102704	71011
Reflections observed	11169	13033	13071	4960
Independent reflections	20299	14957	14521	5003
R_{int}	0.1306	0.0573	0.0538	0.0378
Final R1 values (I>=2σ (I))	0.0889	0.0417	0.0581	0.0235
Final wR(F2) values (I>=2σ (I))	0.2643	0.1112	0.1675	0.0622
Final R1 values (all data)	0.1420	0.0500	0.0653	0.0239
Final wR(F2) values (all data)	0.3113	0.1167	0.1770	0.0624
Flack parameter	0.024(12)	0.002(7)	0.031(3)	0.002(4)
CCDC Number	1537531	1537524	1537525	1537528
GooF	1.049	1.035	1.044	1.105
F_{000}	2912.0	2588.0	2484.0	2800.0
μ /mm^{-1}	0.758	0.746	0.487	0.673

Compound reference	**2.5**	**2.6**	**2.7**	**2.8**
Empirical formula	$C_{60.3}H_{42.6}N_8O_{17}Zn_2$	$C_{52}H_{36}MnN_6O_{16}$	$C_{88}H_{48}Cd_2N_{12}O_{24}$ ·solvent	$C_{91}H_{61}Cd_2N_{13}O_{28}$
Formula weight	1281.66	1055.81	1882.18	2009.32
Crystal system	Orthorhombic	Monoclinic	Monoclinic	Triclinic
a/Å	17.345(4)	9.1660(18)	15.369(3)	11.947(2)
b/Å	22.362(5)	21.819(4)	17.967(4)	13.534(3)
c/Å	13.817(3)	11.505(2)	18.470(4)	14.618(3)
α/°	90	90	90	81.85(3)
β/°	90	96.39(3)	107.96(3)	66.46(3)
γ/°	90	90	90	89.84(3)
Volume/Å^3	5359.2(19)	2286.6(8)	4851.6(19)	2141.2(9)
Temperature /K	100(2)	100(2)	100(2)	100(2)
Space group	$P2_12_12$	$P2_1$	$P2_1$	$P1$
Z	4	2	2	1
Reflections measured	89192	38240	121534	27891
Reflections observed	11756	9477	19973	9139
Independent reflections	12785	10778	22959	11796
R_{int}	0.0855	0.0521	0.0795	0.1358
Final R1 values (I>=2σ (I))	0.0616	0.0481	0.0488	0.0900
Final wR(F2) values (I>=2σ (I))	0.1749	0.1166	0.1358	0.2242
Final R1 values (all data)	0.0656	0.0574	0.0552	0.1100
Final wR(F2) values (all data)	0.1794	0.1220	0.1405	0.2444
Flack parameter	0.024(5)	0.020(7)	0.073(10)	0.21(3)
CCDC Number	1537526	1537527	1537532	1537529
GooF	1.041	1.046	1.062	1.051
F_{000}	2624.0	1086.0	1896.0	1017.0
μ /mm^{-1}	0.982	0.374	0.512	0.589

Compound reference	**2.9**	**2.10**	**2.11**	**2.12**
Empirical formula	$C_{73}H_{69}Cd_2N_{11}O_{29}$	$C_{168}H_{182}N_{16}O_{59}Zn_8$· solvent	$C_{64}H_{60}MnN_6O_{16}$	$C_{143.5}H_{144.5}Mn_4N_{14.5}O_{38}$
Formula weight	1789.19	3892.25	1224.12	2899.99
Crystal system	Triclinic	Monoclinic	Monoclinic	Triclinic
a/Å	8.3020(17)	17.903(4)	9.2140(18)	13.860(3)
b/Å	14.375(3)	27.001(5)	27.592(2)	15.990(3)
c/Å	17.195(3)	20.998(4)	11.553(2)	17.910(4)
α/°	66.80(3)	90	90	113.71(3)
β/°	88.82(3)	109.76(3)	97.20(3)	94.85(3)
γ/°	78.25(3)	90	90	93.80(3)
Volume/Å^3	1842.6(8)	9553(4)	2914.0(10)	3599.2(15)
Temperature /K	100(2)	100(2)	100(2)	100(2)
Space group	*P*1	$P2_1$	$P2_1$	*P*1
Z	1	2	2	1
Reflections measured	34 544	120868	49242	85185
Reflections observed	11894	25321	10793	16915
Independent reflections	12 148	54464	13794	27965
R_{int}	0.0402	0.1838	0.0710	0.1359
Final R1 values (I>=2σ (I))	0.0419	0.1163	0.0577	0.0867
Final wR(F2) values (I>=2σ (I))	0.1158	0.2981	0.1329	0.2302
Final R1 values (all data)	0.0428	0.1362	0.0825	0.1405
Final wR(F2) values (all data)	0.1166	0.3220	0.1493	0.2618
Flack parameter	0.045(6)	-0.003(16)	0.026(8)	0.075(14)
CCDC Number	1537530	-	-	-
GooF	1.093	1.027	1.039	1.056
F_{000}	912.0	4028.0	1278.0	1511.0
μ /mm^{-1}	0.673	1.071	0.304	0.426

Compound reference	**2.13**	**2.14**	**2.15**	**2.16**
Empirical formula	$C_{160}H_{176}Cd_4N_{20}O_{40}$	$C_{71}H_{60}MnN_6O_{20}$	$C_{42}H_{30}CdN_4O_9$	$C_{98.5}H_{74.5}Mn_3N_{13.5}O_{23.5}$
Formula weight	3468.80	1372.19	847.1	1988.03
Crystal system	Triclinic	Monoclinic	Orthorhombic	Monoclinic
a/Å	14.472(3)	8.3310(17)	18.928(4)	11.574(2)
b/Å	15.444(3)	25.564(5)	20.344(4)	27.811(6)
c/Å	21.130(4)	14.599(3)	11.804(2)	15.961(3)
α/°	82.80(3)	90	90	90
β/°	89.10(3)	96.14(3)	90	93.86(3)
γ/°	89.42(3)	90	90	90
Volume/$Å^3$	4684.7(17)	3091.4(11)	4545.4(16)	5125.9(18)
Temperature /K	100(2)	100(2)	100(2)	100(2)
Space group	*P*1	$P2_1$	$P2_12_12_1$	$P2_1$
Z	1	2	4	1
Reflections measured	78880	96739	57565	132448
Reflections observed	26569	17703	10123	20326
Independent reflections	31250	18060	10824	24382
R_{int}	0.0894	0.0566	0.0618	0.1106
Final R1 values (I>=2σ (I))	0.0573	0.0404	0.0599	0.0667
Final wR(F2) values (I>=2σ (I))	0.1530	0.1065	0.1638	0.1644
Final R1 values (all data)	0.0680	0.0412	0.0630	0.0809
Final wR(F2) values (all data)	0.1632	0.1071	0.1662	0.1738
Flack parameter	0.051(8)	0.018(3)	0.059(9)	0.044(5)
CCDC Number	-	1484835	1484836	1484838
GooF	1.024	1.068	1.065	1.052
F_{000}	1788.0	1426.0	1720.0	2046.0
μ /mm^{-1}	0.520	0.300	1.238	1.288

Compound reference	**2.17**	**2.18**	**2.19**	**3.1**
Empirical formula	$C_{155}H_{111}Cd_4N_{13}O_{35}$	$C_{115}H_{71}Cd_2N_{13}O_{25}$	$C_{60}H_{44}MnN_7O_{14.5}$	$C_{56}H_{64}Cd_2N_4O_{22}S_6$
Formula weight	3165.16	2259.64	1149.96	1562.27
Crystal system	Triclinic	Orthorhombic	Orthorhombic	Triclinic
a/Å	14.833(3)	13.852(3)	14.030(3)	9.0820(18)
b/Å	15.630(3)	19.665(4)	19.359(4)	12.597(3)
c/Å	16.029(3)	39.965(8)	19.915(4)	15.728(3)
α/°	90.55(3)	90	90	101.17(3)
β/°	106.95(3)	90	90	105.69(3)
γ/°	98.30(3)	90	90	105.32(3)
Volume/Å^3	3512.2(14)	10886(5)	5409.0(19)	1601.2(7)
Temperature /K	100(2)	100(2)	100(2)	100(2)
Space group	*P*1	$P2_12_12_1$	$P2_12_12$	*P*1
Z	1	4	4	1
Reflections measured	34160	92530	92183	52369
Reflections observed	9150	23716	9772	14230
Independent reflections	10997	25817	12900	14426
R_{int}	0.1013	0.0413	0.0826	0.0323
Final R1 values (I>=2σ (I))	0.0969	0.0961	0.0648	0.0366
Final wR(F2) values (I>=2σ (I))	0.2545	0.2479	0.1691	0.0990
Final R1 values (all data)	0.1118	0.1008	0.0892	0.0371
Final wR(F2) values (all data)	0.2702	0.2561	0.1893	0.0996
Flack parameter	-0.24(3)	0.019(5)	0.020(6)	0.030(4)
CCDC Number	1484839	1484840	1484841	-
GooF	1.032	1.192	1.067	1.073
F_{000}	1604.0	4592.0	2376.0	796.0
μ /mm^{-1}	0.682	0.470	1.412	0.939

Compound reference	**3.2**	**3.3**	**3.4**	**3.5**
Empirical formula	$C_{73}H_{99}Cd_2N_7O_{24}S_4$	$C_{58}H_{51}Cl_2N_8O_{16}Zn_2$	$C_{104}H_{76}Cd_2N_{12}O_{24}$	$C_{192}H_{174}Cu_8N_{16}O_{79}$ S_8·solvent
Formula weight	1811.63	1317.71	2102.56	4734.26
Crystal system	Monoclinic	Monoclinic	Triclinic	Tetragonal
a/Å	15.224(3)	22.805(5)	12.329(3)	32.195(5)
b/Å	14.661(3)	8.3750(17)	16.583(3)	32.195(5)
c/Å	20.163(4)	32.014(6)	17.491(4)	38.898(8)
α/°	90	90	63.30(3)	90
β/°	111.84(3)	96.64(3)	71.74(3)	90
γ/°	90	90	86.23(3)	90
Volume/Å^3	4177.4(16)	6073(2)	3022.0(14)	40318(14)
Temperature /K	100(2)	100(2)	100(2)	100(2)
Space group	$P2_1$	$C2$	$P1$	$P4_32_12$
Z	2	4	1	4
Reflections measured	95851	26435	89318	240968
Reflections observed	18156	8304	23655	12701
Independent reflections	19939	10663	27206	16092
R_{int}	0.0602	0.0833	0.0642	0.0649
Final R1 values (I>=2σ (I))	0.0567	0.0915	0.0573	0.0739
Final wR(F2) values (I>=2σ (I))	0.1498	0.2445	0.1599	0.2020
Final R1 values (all data)	0.0625	0.1137	0.0655	0.1007
Final wR(F2) values (all data)	0.1558	0.2669	0.1703	0.2502
Flack parameter	0.047(7)	0.042(12)	0.049(10)	0.043(5)
CCDC Number	-	-	-	-
GooF	1.020	1.048	1.069	1.085
F_{000}	1876.0	2708.0	1072.0	9720.0
μ /mm^{-1}	0.685	0.952	0.418	0.780

Compound reference	**3.6**	**3.7**	**3.8**	**4.1**	**4.2**
Empirical formula	$C_{224}H_{225}Cu_8N_{16}O_{72}$ ·solvent	$C_{134}H_{78}N_{10}O_{58}Zn_8$· solvent	$C_{40}H_{18}CdN_5O_{10}$·solvent	$C_{76}H_{69}Cd_2N_8O_{19}$	$C_{72}H_{68}Cd_2N_8O_{18}$
Formula weight	4801.51	3279.02	840.99	1623.19	1558.14
Crystal system	Monoclinic	Monoclinic	Monoclinic	Monoclinic	Orthorhombic
a/Å	23.022(5)	45.991(9)	29.453(6)	27.9956(5)	17.463(4)
b/Å	23.668(5)	13.810(3)	20.009(4)	14.8843(2)	30.555(6)
c/Å	29.937(6)	38.671(8)	20.281(4)	18.7743(2)	30.775(6)
α/°	90	90	90	90	90
β/°	106.48(3)	110.56(3)	126.55(3)	107.1577(17)	90
γ/°	90	90	90	90	90
Volume/$Å^3$	17001(6)	22997(9)	9601(4)	7475.0(2)	16421(6)
Temperature /K	100(2)	100(2)	100(2)	123.00(10)	100(2)
Space group	$P2_1$	*C*2/*c*	*C*2/*c*	*C*2	$C222_1$
Z	2	4	8	4	8
Reflections measured	103848	176152	81966	89995	176547
Reflections observed	25553	16709	10608	11774	11910
Independent reflections	36538	24775	13970	13273	16752
R_{int}	0.0942	0.0751	0.0994	0.0597	0.1271
Final R1 values (I>=2σ (I))	0.0626	0.0937	0.0951	0.0543	0.0865
Final wR(F2) values (I>=2σ (I))	0.1625	0.2799	0.2547	0.0616	0.1119
Final R1 values (all data)	0.0906	0.1264	0.1122	0.1380	0.2371
Final wR(F2) values (all data)	0.1889	0.3123	0.2654	0.1431	0.2682
Flack parameter	0.070(7)	-	-	0.040(5)	0.062(9)
CCDC Number	-	-	-	-	-
GooF	0.995	1.041	1.049	0.905	1.030
F_{000}	4978.0	6624.0	3368.0	3436.0	6368.0
μ /mm^{-1}	0.551	0.879	0.506	5.229	0.583

Compound abbreviation	**Λ,Λ5.1**	**Δ,Δ5.1**	**Λ,Λ5.1(DMSO)**	**Λ,Λ5.1/ Δ,Δ5.1**
Chemical formula	$C_{124}H_{139}Cu_4N_{11}O_{47}S_4$	$C_{130}H_{152}Cu_4N_{12}O_{48}S_4$	$C_{120}H_{108}D_{24}Cu_4N_8O_{46}S_8$	$C_{118}H_{125}Cu_4N_9O_{45}S_4$
Formula Mass	2917.85	3033.03	2957.12	2771.66
Crystal system	Triclinic	Triclinic	Triclinic	Monoclinic
a/Å	15.722(3)	15.702(3)	15.638(3)	33.892(4)
b/Å	15.738(3)	15.714(3)	15.8320(6)	15.712(3)
c/Å	18.629(4)	18.656(4)	18.4820(19)	62.235(8)
α/°	104.90(3)	113.620(3)	72.648(7)	90
β/°	114.87(3)	107.650(7)	65.229(3)	104.151(5)
γ/°	91.30(3)	90.700(7)	89.532(12)	90
Unit cell volume/$Å^3$	3996.1(17)	3971.6(9)	3929.5(17)	32135(8)
Temperature/K	123(2)	100(2)	100(2)	100(2)
Space group	*P*1	*P*1	*P*1	*C*2/*c*
Z	1	1	1	8
Reflections measured	86893	132655	101474	253460
Reflections observed	18730	31648	30085	31813
Independent reflections	31934	36094	36907	37475
R_{int}	0.0462	0.0525	0.0588	0.0754
Final R_1 values (I > 2σ(I))	0.0750	0.0596	0.0896	0.1151
Final $wR(F^2)$ values (I > 2σ(I))	0.1999	0.1667	0.2614	0.2819
Final R_1 values (all data)	0.1347	0.0670	0.1031	0.1249
Final $wR(F^2)$ values (all data)	0.2506	0.1749	0.2814	0.2876
Flack parameter	0.017(5)	0.023(3)	0.049(4)	-
CCDC number	1422157	1422158	1422159	1422160
GooF	1.012	1.031	1.037	1.020
F_{000}	1468.0	1592.0	1520.0	0.645
μ /mm^{-1}	0.651	0.661	0.715	1.146

Compound abbreviation	**5.2**	**5.3**	**5.4**	**5.5**
Chemical formula	$C_{122}H_{134}Cu_4N_{10}O_{46}S_4$	$C_{98.5}H_{88.5}Cu_4N_{11.5}O_{49}S_4$	$C_{139}H_{149}Cu_4N_9O_{36}$	$C_{230}H_{232}Cl_{12}N_{16}O_{88}Rh_8S_8$
Formula Mass	2858.78	1299.85	2775.82	6133.46
Crystal system	Triclinic	Monoclinic	Orthorhombic	Monoclinic
a/Å	14.751(3)	16.094(3)	17.052(3)	59.303(12)
b/Å	17.672(4)	20.448(4)	27.160(5)	17.345(4)
c/Å	19.460(4)	20.371(4)	37.010(7)	34.999(7)
α/°	102.82(3)	90	90	90
β/°	107.63(3)	101.20(3)	90	100.59(3)
γ/°	106.68(3)	90	90	90
Unit cell volume/Å^3	4358.1(19)	6576(2)	17140(6)	35387(13)
Temperature/K	100(2)	100(2)	100(2)	100(2)
Space group	$P\bar{1}$	$P2_1/n$	$C222_1$	$C2$
Z	1	2	4	4
Reflections measured	144847	61243	45853	91641
Reflections observed	15331	14130	7756	37723
Independent reflections	20739	15590	14407	50432
R_{int}	0.1208	0.0645	0.1457	0.0583
Final R_1 values (I > 2σ(I))	0.0884	0.0750	0.0861	0.1139
Final wR(F^2) values (I > 2σ(I))	0.2455	0.2253	0.2282	0.2937
Final R_1 values (all data)	0.1050	0.0790	0.1407	0.1357
Final wR(F^2) values (all data)	0.2594	0.2293	0.2606	0.3296
Flack parameter	-	-	0.065(14)	0.094(11)
CCDC number	1422161	1422162	-	-
GooF	1.032	1.069	0.942	1.356
F_{000}	1484.0	2670.0	5800.0	12480.0
μ /mm^{-1}	0.597	0.786	0.554	0.568

Compound abbreviation	**6.1**	**6.2**
Chemical formula	$C_{312}H_{312}Cu_{12}N_{24}O_{108}$·solvent	$C_{48}H_{43}Cu_2N_7O_{19}$
Formula Mass	6888.39	1148.97
Crystal system	Cubic	Orthorhombic
a/Å	36.705(4)	25.213(5)
b/Å	36.705(4)	17.871(4)
c/Å	36.705(4)	10.517(2)
α/°	90	90
β/°	90	90
γ/°	90	90
Unit cell volume/Å^3	49450(17)	4738.8(16)
Temperature/K	100(2)	100(2)
Space group	*P*23	*P*na2$_1$
Z	4	4
Reflections measured	315016	44218
Reflections observed	17620	11766
Independent reflections	33762	13811
R_{int}	0.1297	0.0446
Final R_1 values (I > 2σ(I))	0.0594	0.0411
Final wR(F^2) values (I > 2σ(I))	0.1558	0.1067
Final R_1 values (all data)	0.1150	0.0529
Final wR(F^2) values (all data)	0.1931	0.1189
Flack parameter	0.067(6)	-
CCDC number	-	-
GooF	0.996	1.034
F_{000}	14256.0	2360.0
μ /mm^{-1}	0.566	0.987

8.8.2 X-ray crystallographic refinement details

Poly-[Cd_2(AlaNDI)$_2$(4,4′-bipy)(DMF)$_3$(OH_2)][Cd_2(AlaNDI)$_2$(4,4′-bipy)(DMF)$_2$(OH_2)$_2$], 2.1

The DMF molecules each exhibited signs of disorder and so were modelled with a combination of SHELX DFIX, DANG, FLAT, RIGU and ISOR restraints to give these molecules a chemically sensible model. The oxygen atoms of the coordinated solvent molecules which are coordinated to Cd(2) appeared to be disordered between a water molecule and a DMF molecule, so each was modelled at 50% occupancy.

Poly-[Cd_4(AlaNDI)$_4$(4,4′-bipy)(DMF)$_4$(OH_2)$_2$]·5H_2O·4DMF, 2.2

The 4,4′-bipy ligand showed rotational disorder, so was modelled over two positions (70:30) with SHELX DFIX, FLAT, DELU and ISOR restraints. The DMF molecules were also refined with SHELX DFIX and ISOR restraints. The structure of **2.2** contains solvent accessible voids in which no solvent could be modelled. The data was processed with SQUEEZE, showing a void of 786 $Å^3$ containing 211 e^- per formula unit.

Poly-[Mn_4(AlaNDI)$_4$(bipy)(DMF)$_4$(OH_2)$_2$]·2DMF·5.5H_2O, 2.3

The solvent coordinated to one of the axial positions of both Mn(1) and Mn(2) were disordered between a DMF and H_2O molecule (fixed 50:50 occupancies). In the case of Mn(1) the molecules share an oxygen atom position, while for Mn(2) the oxygen atoms are spatially separated. The partial occupancy DMF coordinated to Mn(2) was refined using SHELX DELU restraints. The lattice DMF in close proximity to the disordered solvent coordinated to Mn(2) was modelled as the same PART and occupancy as the coordinated water molecule and was refined with SHELX DELU and DFIX restraints. The remaining axial solvent position on Mn(1) was occupied by a DMF molecule which was modelled with SHELX DELU, ISOR, FLAT and DFIX restraints in order to model a chemically sensible molecule. The data was processed with SQUEEZE, showing voids totalling 430 $Å^3$ containing 95 e^- per formula unit.

Poly-[Cd(AlaNDI)(4,4′-bipy)(OH_2)]·3.5H_2O·0.5DMF, 2.4

The crystals did not diffract strongly and the data had a very poor R_{int} past 0.9 Å, therefore the SHEL command was used to cut off the data past this point. The structure of **2.4** contains solvent accessible voids

in which no solvent could be modelled. The data was processed with SQUEEZE, showing voids of 232 $Å^3$, containing 73.5 e^-, per asymmetric unit.

Poly-[Zn_2(AlaNDI)$_2$(4,4′-bipy)$_2$]·0.3MeOH·0.7H_2O, 2.5

The uncoordinated solvent was disordered between a methanol and a water molecule (30:70). The methanol was refined with SHELX ISOR and DFIX restraints to model a chemically sensible molecule.

Poly-[Mn(HAlaNDI)$_2$(dpe)], 2.6

No restraints were used for this refinement.

Poly-[Cd_2(AlaNDI)$_2$(4PyNDI)$_2$]·4DMF, 2.7

The pyridyl groups of the 4PyNDI dipyridyl ligands showed signs of rotational disorder which could not be modelled over two positions, so were refined using SHELX ISOR and DELU restraints. The AlaNDI ligands were also refined with some SHELX DELU, ISOR and FIX restraints to give a chemically sensible model. The structure contained solvent accessible voids in which no solvent could be accurately modelled. The data was processed with SQUEEZE, showing voids of 720 $Å^3$ containing 163 e^- per asymmetric unit.

Poly-[Cd_2(AlaNDI)$_2$(OH_2)$_2$(4PyNDI)$_2$]·DMF·H_2O, 2.8

Due to the low symmetry space group of the structure of **2.8**, the data needed to collected from two different angles and merged to get complete data,. The poor diffraction of the crystal led to a poor R_{int}, particularly past 0.88 Å. The SHEL command was therefore used to remove the poor data. The poor data resolution led to a non-zero Flack parameter.

The non-coordinated DMF molecule was refined with SHELX DFIX, DANG and DELU restraints to give a chemically sensible molecular geometry. Numerous bond lengths in the NDI ligands were also refined using SHELX DFIX restraints to give chemically sensible bond lengths. Three of the pyridyl groups were refined with DELU restraints.

Poly-[Cd_2(AlaNDI)$_2$(DMF)$_2$(OH_2)$_2$(4PyNDI)]·DMF·4H_2O, 2.9

The crystals were of poor quality and did not diffract well, despite employing synchrotron radiation. As such, the data was very poor and had a very high R_{int} past 0.85 Å. Therefore a SHEL command was used

to cut off the data past this this. The solvent molecules showed signs of disorder, so these molecules were modelled using SHELX DFIX, DELU, RIGU and ISOR restraints.

Poly-[$Zn_8(DMF)_3(LeuNDI)_6(OH_2)_3(\mu_3\text{-}OH)_3]\cdot 2DMF\cdot 10H_2O$, 2.10

The non-coordinated DMF molecule which could be assigned was split over two positions (free occupancy of 47:53). The coordinated and non-coordinated DMF molecules were refined with SHELX DFIX DELU and RIGU restraints to give a chemically sensible model. Two of the LeuNDI isobutyl side chains was disordered over two positions, and were modelled with SHELX DFIX and DELU restraints to give a chemically sensible model. Two of the other isobutyl side chains and a naphthalene core group were refined with SHELX DFIX restraints to give chemically sensible bond lengths. The hydrogen atoms of the coordinated hydroxide and water molecules were refined with SHELX DFIX, SADI and DANG restraints to place them in a correct position. The crystals did not diffract well to high resolution, therefore the SHEL command was used to remove the poor data past 0.84 Å. Data was treated with the SQUEEZE routine of PLATON,[534] showing total solvent accessible voids of 499 $Å^3$ containing 144.5 e^- per asymmetric unit.

Poly-[$Mn(HLeuNDI)_2(dpe)]\cdot MeOH$, 2.11

The asymmetric unit contains two HLeuNDI ligands, which each have one carboxylic acid group and one carboxylate group. The O-H hydrogen atoms are disordered (50:50) between the two carboxylate/carboxylic acid groups. The O-H hydrogen atoms were restrained using SHELX DFIX and SADI restraints.

Poly-[$Mn_4(LeuNDI)_4(dpb)_2(DMF)_2(OH_2)_2]\cdot DMF\cdot 4.5H_2O$, 2.12

The crystals did not diffract well to high resolution, therefore the SHEL command was used to remove the poor data past 0.80 Å. Of the two coordinated DMF ligands, one was modelled over two positions, sharing the coordinated oxygen atom (free occupancy 53:47), the other showed signs of disorder which could not be modelled. Both coordinated DMF ligands were modelled with SHELX DFIX, DANG, RIGU and ISOR restraints. The lattice solvent, two water molecules, one of which is modelled at 50% occupancy, and a DMF molecule modelled at 50% occupancy were refined with SHELX DFIX, DANG, RIGU and ISOR restraints. One of the isobutyl side chains was disordered over two positions (fixed occupancies of 50:50).

The disordered isobutyl side chain and three others were refined with SHELX DFIX, DANG, RIGU and ISOR restraints to give chemically sensible bond lengths and geometries. The structure showed small void spaces in which no data could be modelled, therefore the data were processed with the SQUEEZE routine of PLATON, showing total voids of 201 $Å^3$ containing 44 e^- per formula unit.

Poly-[$Cd_4(bpb)_2(DMF)_8(LeuNDI)_4$]·$6H_2O$·0.5DMF, 2.13

The crystals were of poor quality, and did not diffract well to high angle. Therefore the SHEL command was used to remove the poor data past 0.84 Å. The isobutyl side chains showed signs of disorder which could not be modelled (with the exception of one group which was modelled over two positions with free occupancies of 52:48) so they were modelled with SHELX DFIX, DANG, ISOR and RIGU restraints. Three of the eight DMF molecules in the asymmetric unit also showed signs of disorder which could not be modelled, so were therefore modelled with SHELX DFIX, DELU and ISOR restraints. The X-ray structure showed voids in which no solvent could be modelled, therefore the data were processed with the SQUEEZE routine of PLATON,[534] showing a void of 956 $Å^3$ which was filled with 185 e^- per formula unit.

Poly-[$Mn(DMF)_2(HPheNDI)_2$]·H_2O·MeOH, 2.14

No restraints were used for this refinement.

Poly-[Cd(4,4′-bipy)(OH_2)(PheNDI)]·$3.5H_2O$·DMF, 2.15.

The structure of **2.14** contains solvent accessible voids in which no solvent could be modelled. The data was processed with the SQUEEZE routine of PLATON.[534] A void of 282 $Å^3$ containing 82 e^- was identified per asymmetric unit, which corresponds to a void within the channels formed by the chains of metallomacrocycles.

Poly-[Mn_2(4,4′-bipy)$_2$(PheNDI)$_2$][Mn(4,4′-bipy)(DMF)$(NO_3)_2$]·0.5DMF·$7H_2O$, 2.16

All of the phenyl groups showed signs of disorder which could not be modelled (evidenced by elongated displacement parameters) and were refined with SHELX DELU and ISOR restraints. One phenyl group was modelled with SHELX SADI restraints to normalise the bond lengths. One of the nitrate ions coordinated to Mn(3) showed disorder which could not be modelled and was refined using SHELX DELU restraints. The structure contained solvent accessible voids in which no solvent could be modelled. The data

was treated with the SQUEEZE routine of PLATON,[534] showing two similar voids were identified in the unit cell (330 Å^3 containing 95e$^-$ and 331 Å^3 containing 94e$^-$).

Poly-[Cd$_4$(DMF)(dpe)$_2$(PheNDI)$_4$(OH$_2$)$_2$]·10H$_2$O·0.5DMF, 2.17

The crystals of **3.17** were of very low quality, requiring synchrotron radiation. The crystals suffered from severe beam damage when irradiated at 17443 eV, therefore collection was conducted at 13000 eV (λ = 0.9537 Å), allowing the collection of an adequate number of frames before the crystals suffered beam damage, although limiting the resolution of the data to 1.04 Å. The lower energy led to much lower resolution data. The lack of high resolution data meant that the atoms could not be modelled accurately with an anisotropic model, therefore the atoms were modelled isotopically with the exception of the metal ions. The lack of high angle data also led to the Flack parameter deviating significantly from zero. The phenyl groups all exhibited signs of disorder. Five of the phenyl groups were restrained to a regular hexagon using SHELX AFIX 66 restraints. The remaining three phenyl groups were refined using SHELX DFIX restraints to give chemically sensible bond lengths. One of the phenyl groups exhibited severe disorder, with two of the carbon groups having much higher Uiso values than their neighbouring atoms, despite numerous attempts to model the disordered phenyl group over two positions, so the Uiso values were fixed at 0.3. The NDI core groups and dpe ligands were refined using SHELX DFIX restraints to give sensible bond lengths.

Poly-[Cd$_2$(PheNDI)$_2$(4PyNDI)$_2$]·6H$_2$O·2DMF·MeOH, 2.18

One of the phenyl groups showed positional disorder evidenced by the atoms displaying extended thermal ellipsoids. It was modelled over two positions with freely refined occupancies (31:69), with one of the fragments refined using a SHELX AFIX 66 restraint, and the other refined using SHELX DFIX, DANG and RIGU restraints. The structure of **2.18** appears to be slightly twinned, which is evidenced by the large residual electron density peaks next to the metals, which did not significantly diminish when an absorption correction was applied. The structure of **2.18** exhibited significant solvent accessible voids in which no solvent could be modelled, therefore the data was processed with the SQUEEZE routine of PLATON which calculated voids of 435 Å^3 containing 138e$^-$ per asymmetric unit.

Poly-[Mn_2(PheNDI)$_2$(4PyNDI)$_2$]·3DMF·2MeOH·H_2O, 2.19

One of the phenyl groups exhibited disorder, which was modelled over two positions, and refined with SHELX DELU and DFIX restraints. The other phenyl group was refined with SHELX DELU restraints. The non-coordinated MeOH was modelled over two positions with freely refined occupancies (41:59) and using SHELX DFIX restraints. The non-coordinated DMF is also disordered over two positions, with freely refined occupancies (38:62) and the disordered positions are sharing carbon atoms C59 and C60. There is hydrogen bonding between the non-coordinated water molecule and a carboxylate oxygen of an NDI ligand, the O···H distance is restrained with a SHELX DANG restraint. One of the pyridine group on the 4PyNDI coligand showed signs of disorder which could not be modelled, so two of the carbon atoms were refined with SHELX ISOR restraints.

[Cd_2(AlaBDI)$_2$(DMSO)$_6$]·1.5H_2O, 3.1

Two DMSO molecules, one coordinated to each metal center, were disordered with their sulphur atoms modelled over two positions (occupancy 92:8 and 76:24). The disordered DMSO molecule coordinated to Cd(1) was refined with SHELX RIGU and SADI restraints to give a chemically sensible model.

[Cd_2(LeuBDI)$_2$(DMF)$_2$(DMSO)$_3$(OH_2)]·DMF·DMSO, 3.2

Two of the isobutyl side chains of the LeuBDI ligands and the non-coordinated DMF molecule showed signs of disorder which could not be modelled, so were refined with SHELX DFIX, DELU, RIGU and ISOR restraints. All the DMSO molecules were disordered with their sulphur atoms modelled over two positions, with fixed occupancies of 90:10, free occupancies of 52:48, free occupancies of 0.33:0.67 and free occupancies of 54:46, and were refined with SHELX DFIX, SADI, DANG and RIGU restraints to give chemically sensible bond lengths and ellipsoids.

($NH_2(CH_3)_2)_2$[Zn_2(AlaBDI)$_2$(4,4′-bipy)Cl_2], 3.3

The crystals diffracted poorly at high angles, therefore the SHEL command was therefore used to remove the poor data past 0.84 Å. One of the dimethyl ammonium cations was refined with SHELX DELU restraints. Two of the methyl side chains were refined with SHELX ISOR, DELU and DFIX to give a chemically sensible model. One of the AlaBDI ligands showed signs of rotational disorder which could not

be modelled, and was therefore also refined with SHELX DELU, DANG and DFIX restraints to give a model with appropriate bond lengths.

Poly-[Cd(LeuBDI)(4PyNDI)]·11H_2O·2DMF, 3.4

The pyridyl rings of the 4PyNDI ligand showed signs of rotational disorder which could not be modelled, so were refined with SHELX DFIX and DELU restraints, with somewhat elongated ellipsoids as an accurate model. The crystals were of poor quality and did not diffract well, and so only diffraction data of relatively low quality was collected. The poor data led to multiple atoms showing ellipsoids of very different geometry to those around them. These atoms were therefore refined with SHELX ISOR restraints to give chemically sensible ellipsoids. Three of the isobutyl side chains showed signs of disorder. One chain was modelled as disordered with the CH_3 groups modelled over two positions (fixed occupancy 50:50). All of the isobutyl side chains were refined using SHELX DFIX, DANG, RIGU and ISOR restraints to give a chemically sensible model. Processing the data with the SQUEEZE routine of PLATON[534] revealed one large void of 961 $Å^3$ containing 194 e^-, corresponding to 11 waters and two DMF molecules per asymmetric unit.

[Cu_8(AlaBDI)$_8$(DMSO)$_4$(OH_2)$_4$]·solv., 3.5

There were signs of disorder throughout all the AlaBDI ligands, so they were modelled with SHELX DFIX, DANG, RIGU and DELU restraints to maintain a chemically sensible structure. One of the non-coordinated water molecules is modelled at half occupancy. There are four 50% occupancy non-coordinated DMSO molecules which are modelled with SHELX DFIX, DANG, SADI and DELU restraints. The hydrogen atoms of the aqua ligands were placed in calculated positions which were maintained with SHELX DFIX, SADI and DANG restraints. The structure was highly porous and was therefore processed with the SQUEEZE routine of PLATON,[534] showing voids of 5104 $Å^3$ containing 1345 e^- per formula unit.

[Cu_8(LeuBDI)$_8$(OH_2)$_8$]·solv., 3.6

One of the isobutyl side chains was disordered over two positions (fixed occupancy 40 : 60) and SHELX DFIX, DANG, RIGU and ISOR restraints were used. The remaining isobutyl side chains were also refined with SHELX DFIX, DANG, RIGU and ISOR restraints to give a chemically sensible model. The aromatic core of the ligands was also refined with SHELX DFIX, DANG, DELU and ISOR restraints. The structure

was highly porous and was therefore processed with the SQUEEZE routine of PLATON,[534] showing a void of 3765 Å^3 filled with 726 e$^-$ per formula unit.

Poly-[Zn_4(IsoBDI)$_2$(DMF)(OH_2)$_4$]·DMF·9H_2O, 3.7

One of the aqua ligands showed signs of disorder which could not be modelled, therefore the oxygen atom was refined with a SHELX ISOR restraint.

Poly-[Cd(IsoBDI)$_{0.5}$(4PyNDI)]·2.5DMF·4H_2O, 3.8

No restraints were used in this refinement.

[Cd_2(1,10-phen)$_2$(LeuNDI)$_2$(OH_2)$_2$]·DMF·2H_2O, 4.1·DMF·2H_2O

All four of the LeuNDI isobutyl side chains showed signs of disorder which could not be modelled, so were refined using SHELX DFIX, DANG, DELU and ISOR restraints to give a chemically sensible model. The hydrogen atoms of all water molecules were placed in calculated positions and refined using SHELX DFIX restraints. One of the coordinated water molecules is disordered over two positions (free occupancy 57:43) and was refined with SHELX ISOR restraints. The non-coordinated water molecule is hydrogen bonding with one of the LeuNDI carbonyl groups and a coordinated water molecule. The data was processed with the SQUEEZE routine of PLATON,[534] showing solvent accessible voids of 166 Å^3 containing 52 e$^-$, per asymmetric unit.

[Cd_2(LeuNDI)$_2$(2,2′-bipy)$_2$(OH_2)$_2$]$_2$·2DMF·5H_2O, 4.2·2DMF·5H_2O

The crystals were not of high quality, and no crystals of higher quality could be formed. The poor crystal quality led to poor diffraction quality, which caused a high R_{int} for the data, and large displacement ellipsoids in the model. The SHEL command was used to cut off the poor data past 0.8 Å. The 2,2′-bipy ligands showed signs of disorder which could not be modelled, so were refined with SHELX DFIX, DELU, ISOR and DELU restraints. Both rings of one of the 2,2′-bipy ligands were constrained with AFIX 66 to give appropriate aromatic geometry. All four leucine isobutyl side chains showed signs of disorder which could not be modelled, so were refined with SHELX DFIX, DANG, ISOR, DELU and RIGU restraints. The structure showed void space in which no solvent could be modelled. Therefore the data were processed

with the SQUEEZE routine of PLATON,[534] showing total voids of 534 Å^3 containing 131 e$^-$ per asymmetric unit.

Λ,Λ-[Cu$_4$((*S*)-LeuBPSD)$_4$(OH$_2$)$_4$]·2DMA, [Λ,Λ-5.1(OH$_2$)]·2DMA

Side chains of three of the leucine groups were modelled over two positions with freely refined occupancies (84:16), (39:61) and (21:79). Each of these disordered groups was refined using a combination of SHELX DELU, SIMU, RIGU, ISOR and DFIX restraints. One of these disordered chains shows further signs of disorder that could not be modelled and therefore elongated anisotropic displacement parameters have been left in this fragment (C24 - C27) as the best descriptor of the disorder. One of the DMA molecules which could be located in the lattice was refined using DELU restraints. The coordinated water molecules are refined with a fixed geometry free to rotate around the Cu-O bond. The structural data was processed with the SQUEEZE routine of PLATON.[534] A void of 748 Å^3 containing 318 e$^-$ was identified between the cages. A second void of 291 Å^3 containing 21 e$^-$ was identified inside each cage. (Note, there is one cage per unit cell).

Δ,Δ-[Cu$_4$((*R*)-LeuBPSD)$_4$(OH$_2$)(MeOH)$_{2.5}$(HNMe$_2$)$_{0.5}$]·4DMA, [Δ,Δ5.1·(OH$_2$)(MeOH)$_{2.5}$(HNMe$_2$)$_{0.5}$]·4DMA

The best model for solvent coordinated to the inside of the cage was H_2O and MeOH (50:50) coordinated to Cu(3) and $HNMe_2$ and H_2O (50:50) coordinated to Cu(2) (dimethylamine indicated by mass spectrometry results). For Cu(3), the carbon atom of the 50% occupancy coordinated MeOH was modelled over two positions, each at 25% occupancy and the hydrogen atoms on the oxygen atom coordinated to Cu(3) could not be located (but are included in the formula unit). The partial occupancy carbon and nitrogen atoms of the coordinated MeOH and $HNMe_2$ within the cage were refined with ISOR restraints due to what appears to be further rotation around the Cu-O/N bond that could not be resolved. One disordered side-chain of a leucine group was modelled over two positions (57:43). Two other side-chains show signs of disorder which could not be modelled (evidenced by elongated displacement parameters) and were refined using SHELXL DELU restraints. The best model of non-coordinated solvent was of four DMA molecules, one of which is modelled as disordered over two non-overlapping positions (43:57). One of the full occupancy DMA molecules shows signs of disorder which could not be modelled therefore one of the carbon atoms (C125)

was refined with a SHELX ISOR restraint. The structural data was treated with the SQUEEZE routine of PLATON.[534] One significant void was identified between complexes (totalling 144 Å^3 and 31 e$^-$ per cell/cage). The void space inside the cage was output by SQUEEZE as several small voids around the coordinated solvent (significant voids of 70 Å^3 and 8 e$^-$, 44 Å^3 and 4 e$^-$, 40 Å^3 and 3 e$^-$ per cage and a total, including smaller spaces, of totalling 175 Å^3 and 16 e$^-$). These voids sit around the internally coordinated solvent as modelled and are highly unlikely to be discrete voids except when viewed as this stationary model.

Λ,Λ-[Cu$_4$((*S*)-LeuBPSD)$_4$(OH$_2$)$_2$(DMSO)$_2$]·2DMSO, Λ,Λ5.1[(DMSO)$_2$(OH$_2$)$_2$]·2DMSO

The best model for coordinated solvent was H$_2$O coordinated to the external sites and DMSO coordinated to the internal sites. The two internal DMSO molecules were modelled as disordered over two positions with refined occupancies tied to each other (53:47) and some bond distance and RIGU restraints applied. Four half occupancy DMSO sites were located in the lattice and were refined anisotropically with some restraints on bond lengths and displacement parameters. The side chains of some of the leucine groups show signs of disorder (evidenced from large displacement parameters) which could not be resolved and were therefore refined with some DFIX, RIGU and ISOR restraints. The structural data was processed with the SQUEEZE routine of PLATON.[534] Voids totalling 476 Å^3 containing 148 e$^-$ per cell/cage were identified between the cages and two very small voids (28 Å^3 and 3 e$^-$; 27 Å^3 and 3 e$^-$) were located within the cage (likely due to unresolvable disorder rather than other solvent molecules given low e$^-$ count).

Λ,Λ/Δ,Δ-[Cu$_4$((*S*/*R*)-LeuBPSD)$_4$(MeOH)$_2$(OH$_2$)$_2$]·DMA, Λ,Λ/Δ,Δ-[5.1(MeOH)$_2$(OH$_2$)]·DMA

Hydrogen atoms attached to H$_2$O and MeOH were located from the Fourier difference map and refined with restrained OH distances. There is minor residual electron density in the interior of the cage that suggests MeOH or HNMe$_2$ may be coordinated but at very low occupancy and therefore this could not be modelled. Several leucine side-chains show signs of disorder that could not be modelled and were refined using SHELXL SADI and SIMU restraints with elongated displacement parameters left in the final refinement model as the best descriptor for the disorder. One of the leucine groups is modelled over two positions (occupancies refined to 47:53) with one of the positions showing signs of further disorder that

could not be modelled and therefore elongated displacement parameters for this group (C112 114, with weak ISOR restraints) have been left in the model as the best descriptor for the disorder. The structural data was processed with the SQUEEZE routine of PLATON.[534] Voids totalling 7166 Å^3 containing 1878 e$^-$ per unit cell were identified between the cages (896 Å^3 and 235 e$^-$ per cage) and a void of 293 Å^3 containing 65 e$^-$ was identified inside each cage.

[Cu$_4$((*S*,*R*)-H$_2$LeuBPSD$_4$)(OH$_2$)$_2$(MeOH)$_2$]·2DMA, [5.2(OH$_2$)$_2$(MeOH)$_2$]·2DMA

Whilst being of slightly low quality the data is the best that could be achieved from the samples. The lattice solvent is modelled as two partial occupancy DMA sites with occupancies refined against each other (51:49) per asymmetric unit (*i.e.* total of complete 2 DMA molecules per cage). DFIX and DELU restraints were used in the refinement of these partial occupancy solvent molecules. The hydroxyl hydrogen atoms were located from the Fourier difference map and refined with a restrained OH distance. The structural data was treated with the SQUEEZE routine of PLATON.[534] A void of 1180 Å^3 and 280 e$^-$ per unit cell (*i.e.* per cage) was identified which exists between the cages.

[Cu$_4$(GlyBPSD)$_4$(MeOH)$_3$(OH$_2$)]·3.5DMA·1.5MeOH,

[5.3(MeOH)$_3$(OH$_2$)]·3.5DMA·1.5MeOH

Coordinated solvent was best modelled as a full occupancy MeOH on Cu(1) (inside the cage) and 50:50 MeOH:H$_2$O on the exterior sites. This exterior MeOH was modelled as disordered over two positions with H atom positions restrained by DFIX whilst the hydrogen atoms of the partial occupancy water could not be modelled (but are included in the molecular formula). Lattice solvent was best modelled as one half occupancy DMA molecules, one half occupancy MeOH and one quarter occupancy MeOH per asymmetric unit (*i.e.* per half cage). Non-coordinated solvent within the cage was best modelled as one half occupancy DMA and one three-quarter occupancy DMA that is refined over two disordered positions (fixed occupancies 25:50). Some DFIX, DELU and ISOR restraints were applied to the partial occupancy solvent positions.

[Cu_4((*S*)-LeuEADI)$_4$(DMF)(OH_2)$_3$]·3.5DMF·14H_2O, [5.4(DMF)(OH_2)$_3$]·3.5DMF·9.5H_2O

All four isobutyl chains in the asymmetric unit showed signs of positons disorder which could not be modelled, therefore these groups were refined with SHELX DFIX, DELU, ISOR and RIGU restraints. The solvent coordinated to the Cu^{II} site on the interior of the paddlewheel we modelled as between a DMF and water (fixed occupancy 50:50). The coordinated half occupancy DMF ligand showed signs of further disorder which could not be modelled, therefore was refined with SHELX DFIX, ISOR, RIGU, FLAT and DANG restraints. There were also some C-C bonds in the core of the ligands which were refined with SHELX DFIX restraints in order to model chemically sensible bond lengths. The structural data was treated with the SQUEEZE routine of PLATON,[534] which showed voids of 1269 $Å^3$ containing 292 e^- per cage (note that one asymmetric unit is half of a cage).

[Rh_4((*S*)-LeuBPSD)$_4$(OH_2)$_4$]·4MeOH·10H_2O, [5.5(OH_2)$_4$]·4MeOH·10H_2O

The crystals were very unstable when removed form solvent and lost crystallinity rapidly, leading to the only low quality data being obtained. Therefore the structure required a large number of restraints and constraints in order to form a chemically sensible model. One of the isobutyl side chains was modelled as disordered with the one of the methyl groups modelled over two positions (fixed occupancy 60:40) and refined with SHELX DFIX, DANG and ISOR restraints. The remaining isobutyl side chains showed signs of disorder which could not be modelled, therefore were refined with SHELX DFIX, ISOR, DELU and DANG restraints to give chemically sensible bong lengths and ellipsoids. The lattice solvent modelled in the structure is two chloroform molecules which are modelled at full occupancy, one of which was refined with SHELX DFIX and ISOR restraints, and two chloroform molecules which are modelled at 50% occupancy. Of the 16 phenyl groups in the ligands in the asymmetric unit, 11 of them were constrained to an idealised geometry using AFIX 66. Selected other bond lengths and atoms were refined with SHELX ISOR, DELU and DFIX restraints in order to model chemically sensible bond lengths and ellipsoids.

[Cu_{12}((S)-LeuNDI)$_{12}$(OH_2)$_{12}$]·22H_2O·30DMF, 6.1·22H_2O·30DMF

The hydrogen atoms of the aqua ligands were placed in calculated positions and refined with SHELX DFIX and DANG restraints to maintain their positions. One of the isobutyl side chains of the LeuNDI ligand was

disordered over two positions, sharing two of the carbon atoms (fixed occupancy 50 : 50) and refined with SHELX DFIX, DANG and RIGU restraints. Three of the remaining isobutyl side chains showed signs of disorder which could not be modelled crystallographically, so were refined with SHELX DFIX, DELU and RIGU restraints. One of the NDI core groups was also refined with SHELX DFIX and RIGU restraints to give a chemically sensible model.

Poly-[Cu2(GlyNDI)2(DMA)2]·DMA, 6.2

One of the coordinated DMA molecules showed signs of disorder, so it was modelled over two positions (free occupancy 21:79) and refined with SHELX DFIX, DANG, RIGU and ISOR restraints to give a chemically sensible structure.

References

(1) Lehn, J. M., *Supramolecular Chemistry: Concepts and Perspectives*. Weinheim: New York 1995.
(2) Kyba, E. P.; Helgeson, R. C.; Madan, K.; Gokel, G. W.; Tarnowski, T. L.; Moore, S. S.; Cram, D. J., *J. Am. Chem. Soc.* **1977**, *99*, 2564-2571.
(3) Steed, J. W.; Turner, D. R.; Wallace, K. J., *Core Concepts in Supramolecular Chemistry and Nanochemistry*. John Wiley & Sons: Chichester, 2007.
(4) Steed, J. W.; Atwood, J. L., *Supramolecular Chemistry*. Wiley: Chichester, 2009.
(5) Constable, E. C., *Chem. Ind.* **1994**, 56-59.
(6) Lindoy, L. F.; Atkinson, I. M., *Self-assembly in Supramolecular Systems*. Royal Society of Chemistry: Cambridge, 2000; p 224.
(7) Whitesides, G. M.; Boncheva, M., *Proc. Natl. Acad. Sci.* **2002**, *99*, 4769-4774.
(8) Gerloch, M.; Constable, E. C., An Introduction to Transition-Metal Chemistry. In *Transition Metal Chemistry*, Wiley-VCH Verlag GmbH & Co. KGaA: 2005; pp 1-19.
(9) Hosseini, M. W., *Acc. Chem. Res.* **2005**, *38*, 313-323.
(10) Corey, E. J., *Pure Appl. Chem.* **1967**, *14*, 19-37.
(11) Reedijk, J., *Chem. Soc. Rev.* **2013**, *42*, 1776-1783.
(12) Janiak, C., *Dalton Trans.* **2000**, 3885-3896.
(13) Turpeinen, U.; Hämäläinen, R.; Reedijk, J., *Polyhedron* **1987**, *6*, 1603-1610.
(14) Sauvage, J.-P.; Dietrich-Buchecker, C., *Molecular Catenanes, Rotaxanes and Knots: A Journey Through the World of Molecular Topology*. Wiley-VCH: Weinheim, Germany 1999.
(15) Ashton, P. R.; Brown, C. L.; Chrystal, E. J. T.; Goodnow, T. T.; Kaifer, A. E.; Parry, K. P.; Philp, D.; Slawin, A. M. Z.; Spencer, N.; Stoddart, J. F.; Williams, D. J., *J. Chem. Soc., Chem. Commun.* **1991**, 634-639.
(16) Ashton, P. R.; Iriepa, I.; Reddington, M. V.; Spencer, N.; Slawin, A. M. Z.; Stoddart, J. F.; Williams, D. J., *Tetrahedron Lett.* **1994**, *35*, 4835-8.
(17) Brown, C. L.; Philip, D.; Stoddart, J. F., *Synlett* **1991**, 459-61.
(18) Bravo, J. A.; Raymo, F. M.; Stoddart, J. F.; White, A. J. P.; Williams, D. J., *Eur. J. Org. Chem.* **1998**, *1998*, 2565-2571.
(19) Jacquot, d. R. H.-P.; Iehl, J.; Bruns, C. J.; McGrier, P. L.; Frasconi, M.; Sarjeant, A. A.; Stoddart, J. F., *Org. Lett.* **2012**, *14*, 5188-91.
(20) Collin, J.-P.; Dietrich-Buchecker, C.; Gaviña, P.; Jimenez-Molero, M. C.; Sauvage, J.-P., *Acc. Chem. Res.* **2001**, *34*, 477-487.
(21) Braga, D., *Chem. Commun.* **2003**, 2751-2754.
(22) Robson, R., *J. Chem. Soc., Dalton Trans.* **2000**, 3735-3744.
(23) Amouri, H.; Gruselle, M., *Chirality in Transition Metal Chemistry*. John Wiley & Sons Ltd: Chichester, 2008.
(24) Hembury, G. A.; Borovkov, V. V.; Inoue, Y., *Chem. Rev.* **2008**, *108*, 1-73.
(25) Berthod, A., *Anal. Chem.* **2006**, *78*, 2093-2099.
(26) Fumio, T., *Enantiomer Separation: Fundamentals and Practical Methods*. Springer: Netherlands, 2004.
(27) Bernal, I.; Kauffman, G. B., *J. Chem. Educ.* **1987**, *64*, 604.
(28) Ishi-i, T.; Crego-Calama, M.; Timmerman, P.; Reinhoudt, D. N.; Shinkai, S., *J. Am. Chem. Soc.* **2002**, *124*, 14631-14641.
(29) Aoki, S.; Shiro, M.; Kimura, E., *Chem. Eur. J.* **2002**, *8*, 929-939.
(30) Hiraoka, S.; Fujita, M., *J. Am. Chem. Soc.* **1999**, *121*, 10239-10240.
(31) Meeuwissen, J.; Reek, J. N. H., *Nat. Chem.* **2010**, *2*, 615-621.
(32) Scriba, G. K. E., *J. Chromatogr. A* **2016**, *1467*, 56-78.
(33) Crini, G., *Chem. Rev.* **2014**, *114*, 10940-10975.
(34) Laza-Knoerr, A. L.; Gref, R.; Couvreur, P., *J. Drug Targeting* **2010**, *18*, 645-656.
(35) Hapiot, F.; Tilloy, S.; Monflier, E., *Chem. Rev.* **2006**, *106*, 767-781.

(36) Easton, C. J.; Lincoln, S. F., *Chem. Soc. Rev.* **1996**, *25*, 163-170.
(37) Araki, K.; Inada, K.; Shinkai, S., *Angew. Chem. Int. Ed.* **1996**, *35*, 72-74.
(38) Tabushi, I.; Kuroda, Y.; Mizutani, T., *J. Am. Chem. Soc.* **1986**, *108*, 4514-4518.
(39) Tabushi, I., *Pure Appl. Chem.* **1986**, *58*, 1529-1534.
(40) Kano, K.; Hasegawa, H., *J. Am. Chem. Soc.* **2001**, *123*, 10616-10627.
(41) Shinkai, S., *Pue Appl. Chem.* **1986**, *58*, 1523-1528.
(42) Li, S. Y.; Xu, Y. W.; Liu, J. M.; Su, C. Y., *Int. J. Mol. Sci.* **2011**, *12*, 429.
(43) Gutsche, C. D., *Calixarenes: An Introduction*. 2nd Ed.; The Royal Society of Chemistry: Cambridge, 2008.
(44) Shirakawa, S.; Moriyama, A.; Shimizu, S., *Org. Lett.* **2007**, *9*, 3117-3119.
(45) Jin, T.; Jin, T.; Monde, K., *Chem. Commun.* **1998**, 1357-1358.
(46) Kliachyna, M. A.; Yesypenko, O. A.; Pirozhenko, V. V.; Shishkina, S. V.; Shishkin, O. V.; Boyko, V. I.; Kalchenko, V. I., *Tetrahedron* **2009**, *65*, 7085-7091.
(47) Mutihac, L.; Lee, J. H.; Kim, J. S.; Vicens, J., *Chem. Soc. Rev.* **2011**, *40*, 2777-2796.
(48) Kubo, Y.; Maeda, S. y.; Tokita, S.; Kubo, M., *Nature* **1996**, *382*, 522-524.
(49) Hoskins, B. F.; Robson, R., *J. Am. Chem. Soc.* **1989**, *111*, 5962-5964.
(50) Hoskins, B. F.; Robson, R., *J. Am. Chem. Soc.* **1990**, *112*, 1546-1554.
(51) Batten, S. R.; Neville, S. M.; Turner, D. R., *Coordination Polymers: Design, Analysis and Application*. Royal Society of Chemistry: Cambridge, 2009.
(52) Batten, S. R.; Champness, N. R.; Chen, X. M.; Garcia-Martinez, J.; Kitagawa, S.; Öhrström, L.; O'Keeffe, M.; Suh, M. P.; Reedijk, J., *Pure Appl. Chem.* **2013**, *85*, 1715-1724.
(53) Allendorf, M. D.; Bauer, C. A.; Bhakta, R. K.; Houk, R. J. T., *Chem. Soc. Rev.* **2009**, *38*, 1330-1352.
(54) Kurmoo, M., *Chem. Soc. Rev.* **2009**, *38*, 1353-1379.
(55) Lee, J.; Farha, O. K.; Roberts, J.; Scheidt, K. A.; Nguyen, S. T.; Hupp, J. T., *Chem. Soc. Rev.* **2009**, *38*, 1450-1459.
(56) Li, J. R.; Kuppler, R. J.; Zhou, H. C., *Chem. Soc. Rev.* **2009**, *38*, 1477-1504.
(57) Horcajada, P.; Serre, C.; Vallet Regi, M.; Sebban, M.; Taulelle, F.; Ferey, G., *Angew. Chem. Int. Ed.* **2006**, *45*, 5974-5978.
(58) Kreno, L. E.; Leong, K.; Farha, O. K.; Allendorf, M.; Van Duyne, R. P.; Hupp, J. T., *Chem. Rev.* **2012**, *112*, 1105-1125.
(59) KumarA, P.; Pournara, A.; Kim, K.-H.; Bansal, V.; Rapti, S.; Manos, M. J., *Prog. Mater Sci.* **2017**, *86*, 25.
(60) Abrahams, B. F.; Dharma, D.; Donnelly, P. S.; Hudson, T. A.; Kepert, C. J.; Robson, R.; Southon, P. D.; White, K. F., *Chem. Eur. J.* **2017**, *23*, 7871-7875.
(61) Tranchemontagne, D. J.; Mendoza-Cortes, J. L.; O'Keeffe, M.; Yaghi, O. M., *Chem. Soc. Rev.* **2009**, *38*, 1257-1283.
(62) Yaghi, O. M.; O'Keeffe, M.; Ockwig, N. W.; Chae, H. K.; Eddaoudi, M.; Kim, J., *Nature* **2003**, *432*, 705-714.
(63) Fujita, M.; Kwon, Y. J.; Washizu, S.; Ogura, K., *J. Am. Chem. Soc.* **1994**, *116*, 1151-1152.
(64) Chui, S. S. Y.; Lo, S. M. F.; Charmant, J. P. H.; Orpen, A. G.; Williams, I. D., *Science* **1999**, *283*, 1148-1150.
(65) Li, H.; Eddaoudi, M.; O'Keeffe, M.; Yaghi, O. M., *Nature* **1999**, *402*, 276-279.
(66) Batten, S. R.; Robson, R., *Angew. Chem. Int. Ed.* **1998**, *37*, 1461-1494.
(67) Batten, S. R., Interpenetration. In *Supramolecular Material Chemistry*, Steed, J. W.; Gale, P. A., Eds. John Wiley & Sons Ltd.: 2012; Vol. 6, pp 3107-3120.
(68) Jiang, H.-L.; Makal, T. A.; Zhou, H.-C., *Coord. Chem. Rev.* **2013**, *257*, 2232-2249.
(69) Ma, S.; Sun, D.; Ambrogio, M.; Fillinger, J. A.; Parkin, S.; Zhou, H. C., *J. Am. Chem. Soc.* **2007**, *129*, 1858-1859.
(70) Jiang, H. L.; Makal, T. A.; Zhou, H. C., *Coord. Chem. Rev.* **2013**, *257*, 2232-2249.
(71) Boer, S. A.; Hawes, C. S.; Turner, D. R., *Chem. Commun.* **2014**, *50*, 1125-1127.

(72) Batten, S. R., Interpenetrating Networks. In *Frontiers in Crystal Engineering*, John Wiley & Sons, Ltd: 2006; pp 157-194.
(73) J. Blake, A.; R. Champness, N.; Khlobystov, A.; Li, W.-S.; Schroder, M.; Khlobystov, A.; A. Lemenovskii, D., *Chem. Commun.* **1997**, 2027-2028.
(74) R. Batten, S.; F. Hoskins, B.; Robson, R., *New J. Chem.* **1998**, *22*, 173-175.
(75) Jiang, H.-L.; Xu, Q., *CrystEngComm* **2010**, *12*, 3815-3819.
(76) Liu, J.-Q.; Wang, Y.-Y.; Liu, P.; Dong, Z.; Shi, Q.-Z.; Batten, S. R., *CrystEngComm* **2009**, *11*, 1207-1209.
(77) Carlucci, L.; Ciani, G.; Moret, M.; Proserpio, D. M.; Rizzato, S., *Chem . Mater.* **2002**, *14*, 12-16.
(78) Mir, M. H.; Kitagawa, S.; Vittal, J. J., *Inorg. Chem.* **2008**, *47*, 7728-7733.
(79) Wang, X.-L.; Qin, C.; Wang, E.-B.; Li, Y.-G.; Su, Z.-M., *Chem. Commun.* **2005**, 5450-5452.
(80) Wu, H.; Yang, J.; Su, Z.-M.; Batten, S. R.; Ma, J.-F., *J. Am. Chem. Soc.* **2011**, *133*, 11406-11409.
(81) Carlucci, L.; Ciani, G.; Moret, M.; Proserpio, D. M.; Rizzato, S., *Angew. Chem. Int. Ed.* **2000**, *39*, 1506-1510.
(82) Cohen, S. M., *J. Am. Chem. Soc.* **2017**, *139*, 2855–2863.
(83) Ingleson, M. J.; Perez Barrio, J.; Guilbaud, J.-B.; Khimyak, Y. Z.; Rosseinsky, M. J., *Chem. Commun.* **2008**, 2680-2682.
(84) Manna, K.; Zhang, T.; Lin, W., *J. Am. Chem. Soc.* **2014**, *136*, 6566-6569.
(85) Cohen, S. M.; Zhang, Z.; Boissonnault, J. A., *Inorg. Chem.* **2016**, *55*, 7281-7290.
(86) Deshpande, R. K.; Minnaar, J. L.; Telfer, S. G., *Angew. Chem. Int. Ed.* **2010**, *49*, 4598-4602.
(87) Sato, H.; Matsuda, R.; Sugimoto, K.; Takata, M.; Kitagawa, S., *Nat. Mater.* **2010**, *9*, 661-666.
(88) Das, S.; Kim, H.; Kim, K., *J. Am. Chem. Soc.* **2009**, *131*, 3814-3815.
(89) Burnett, B. J.; Barron, P. M.; Hu, C.; Choe, W., *J. Am. Chem. Soc.* **2011**, *133*, 9984-9987.
(90) Yuan, S.; Lu, W.; Chen, Y. P.; Zhang, Q.; Liu, T. F.; Feng, D.; Wang, X.; Qin, J.; Zhou, H. C., *J. Am. Chem. Soc.* **2015**, *137*, 3177-3180.
(91) Tu, B.; Pang, Q.; Wu, D.; Song, Y.; Weng, L.; Li, Q., *J. Am. Chem. Soc.* **2014**, *136*, 14465-14471.
(92) Goto, Y.; Sato, H.; Shinkai, S.; Sada, K., *J. Am. Chem. Soc.* **2008**, *130*, 14354-14355.
(93) Furukawa, Y.; Ishiwata, T.; Sugikawa, K.; Kokado, K.; Sada, K., *Angew. Chem. Int. Ed.* **2012**, *51*, 10566-10569.
(94) Millward, A. R.; Yaghi, O. M., *J. Am. Chem. Soc.* **2005**, *127*, 17998-17999.
(95) Murray, L. J.; Dinca, M.; Long, J. R., *Chem. Soc. Rev.* **2009**, *38*, 1294-1314.
(96) Nenoff, T. M., *Nat. Chem.* **2015**, *7*, 377-378.
(97) Peng, Y.; Li, Y.; Ban, Y.; Jin, H.; Jiao, W.; Liu, X.; Yang, W., *Science* **2014**, *346*, 1356-1359.
(98) Liu, J.; Chen, L.; Cui, H.; Zhang, J.; Zhang, L.; Su, C. Y., *Chem. Soc. Rev.* **2014**, *43*, 6011-6061.
(99) Zhao, M.; Ou, S.; Wu, C.-D., *Acc. Chem. Res.* **2014**, *47*, 1199-1207.
(100) Wang, J.-L.; Wang, C.; Lin, W., *ACS Catal.* **2012**, *2*, 2630-2640.
(101) Li, P.-Z.; Wang, X.-J.; Liu, J.; Lim, J. S.; Zou, R.; Zhao, Y., *J. Am. Chem. Soc.* **2016**, *138*, 2142-2145.
(102) Rimoldi, M.; Nakamura, A.; Vermeulen, N. A.; Henkelis, J. J.; Blackburn, A. K.; Hupp, J. T.; Stoddart, J. F.; Farha, O. K., *Chem. Sci.* **2016**, *7*, 4980-4984.
(103) Karagiaridi, O.; Lalonde, M. B.; Bury, W.; Sarjeant, A. A.; Farha, O. K.; Hupp, J. T., *J. Am. Chem. Soc.* **2012**, *134*, 18790-18796.
(104) Liu, Y.; Howarth, A. J.; Vermeulen, N. A.; Moon, S.-Y.; Hupp, J. T.; Farha, O. K., *Coord. Chem. Rev.* **2017**, *346*, 101-111.
(105) Zhu, Q.; Shen, C.; Tan, C.; Sheng, T.; Hu, S.; Wu, X., *Chem. Commun.* **2012**, *48*, 531-533.
(106) Takashima, Y.; Martínez, V. M.; Furukawa, S.; Kondo, M.; Shimomura, S.; Uehara, H.; Nakahama, M.; Sugimoto, K.; Kitagawa, S., *Nat. Commun.* **2011**, *2*, 168-175.
(107) Heine, J.; Muller Buschbaum, K., *Chem. Soc. Rev.* **2013**, *42*, 9232-9242.
(108) Horcajada, P.; Serre, C.; Vallet-Regi, M.; Sebban, M.; Taulelle, F.; Ferey, G., *Angew. Chem. Int. Ed.* **2006**, *45*, 5974-5978.
(109) Keene, F. R., *Chirality in Supramolecular Assemblies*. John Wiley & Sons: Chichester, 2017.

(110) Seo, J. S.; Whang, D.; Lee, H.; Jun, S. I.; Oh, J.; Jeon, Y. J.; Kim, K., *Nature* **2000**, *404*, 982-986.
(111) Zhang, J.; Chen, S.; Zingiryan, A.; Bu, X., *J. Am. Chem. Soc.* **2008**, *130*, 17246-17247.
(112) Martí Gastaldo, C.; AntypovD; Warren, J. E.; Briggs, M. E.; Chater, P. A.; Wiper, P. V.; Miller, G. J.; Khimyak, Y. Z.; Darling, G. R.; Berry, N. G.; Rosseinsky, M. J., *Nat. Chem.* **2014**, *6*, 343-351.
(113) Bisht, K. K.; Parmar, B.; Rachuri, Y.; Kathalikattil, A. C.; Suresh, E., *CrystEngComm* **2015**, *17*, 5341-5356.
(114) Wang, P.-F.; Sheng, M.-G.; Wu, X.-S.; Wang, X., *Inorg. Chim. Acta* **2011**, *379*, 135-139.
(115) Ezuhara, T.; Endo, K.; Aoyama, Y., *J. Am. Chem. Soc.* **1999**, *121*, 3279-3283.
(116) Lin, Z.; Slawin, A. M. Z.; Morris, R. E., *J. Am. Chem. Soc.* **2007**, *129*, 4880-4881.
(117) Train, C.; Gheorghe, R.; Krstic, V.; Chamoreau, L.-M.; Ovanesyan, N. S.; Rikken, G. L. J. A.; Gruselle, M.; Verdaguer, M., *Nat. Mater.* **2008**, *7*, 729-734.
(118) Zhang, J.; Chen, S.; Nieto, R. A.; Wu, T.; Feng, P.; Bu, X., *Angew. Chem. Int. Ed.* **2010**, *49*, 1267-1270.
(119) Banerjee, M.; Das, S.; Yoon, M.; Choi, H. J.; Hyun, M. H.; Park, S. M.; Seo, G.; Kim, K., *J. Am. Chem. Soc.* **2009**, *131*, 7524-7525.
(120) Lin, W.; Wu, S., Rational Design of Non-centrosymmetric Metal-Organic Frameworks for Second-Order Nonlinear Optics. In *Metal-Organic Frameworks: Design and Application*, MacGillivray, L. R., Ed. John Wiley & Sons: Hoboken, New Jersey, 2010.
(121) Lacroix, P. G., *Eur. J. Inorg. Chem.* **2001**, 339-348.
(122) Liu, Y.; Xuan, W.; Cui, Y., *Adv. Mater.* **2010**, *22*, 4112-4135.
(123) Yoon, M.; Srirambalaji, R.; Kim, K., *Chem. Rev.* **2012**, *112*, 1196-1231.
(124) Vaidhyanathan, R.; Bradshaw, D.; Rebilly, J. N.; Barrio, J. P.; Gould, J. A.; Berry, N. G.; Rosseinsky, M. J., *Angew. Chem. Int. Ed.* **2006**, *45*, 6495-6499.
(125) Ingleson, M. J.; Barrio, J. P.; Bacsa, J.; Dickinson, C.; Park, H.; Rosseinsky, M. J., *Chem. Commun.* **2008**, 1287-1289.
(126) Bonnefoy, J.; Legrand, A.; Quadrelli, E. A.; Canivet, J.; Farrusseng, D., *J. Am. Chem. Soc.* **2015**, *137*, 9409-9416.
(127) Lun, D. J.; Waterhouse, G. I. N.; Telfer, S. G., *J. Am. Chem. Soc.* **2011**, *133*, 5806-5809.
(128) Ma, L.; Abney, C.; Lin, W., *Chem. Soc. Rev.* **2009**, *38*, 1248-1256.
(129) Ojima, I., *Catalytic Asymmetric Synthesis*. VCH: New York, 1993.
(130) Cui, Y.; Evance, O. R.; Ngo, L. H.; White, P. S.; Lin, W., *Angew. Chem. Int. Ed.* **2002**, *41*, 1159.
(131) Evans, O. R.; Ngo, H. L.; Lin, W., *J. Am. Chem. Soc.* **2001**, *123*, 10395-10396.
(132) Wu, C. D.; Hu, A.; Zhang, L.; Lin, W., *J. Am. Chem. Soc.* **2005**, *127*, 8940-8941.
(133) Ma, L.; Falkowski, J. M.; Abney, C.; Lin, W., *Nat. Chem.* **2010**, *2*, 838-846.
(134) Tanaka, K.; Oda, S.; Shiro, M., *Chem. Commun.* **2008**, 820-822.
(135) Regati, S.; He, Y.; Thimmaiah, M.; Li, P.; Xiang, S.; Chen, B.; Zhao, J. C. G., *Chem. Commun.* **2013**, *49*, 9836-9838.
(136) Tanaka, K.; Nagase, S.; Anami, T.; Wierzbicki, M.; Urbanczyk-Lipkowska, Z., *RSC Adv.* **2016**, *6*, 111436-111439.
(137) Tanaka, K.; Otani, K.-i., *New J. Chem.* **2010**, *34*, 2389-2391.
(138) Tanaka, K.; Kubo, K.; Iida, K.; Otani, K.-i.; Murase, T.; Yanamoto, D.; Shiro, M., *Asian J. Org. Chem.* **2013**, *2*, 1055-1060.
(139) Tanaka, K.; Otani, K.-i.; Murase, T.; Nishihote, S.; Urbanczyk-Lipkowska, Z., *Bull. Chem. Soc. Jpn.* **2012**, *85*, 709-714.
(140) Tanaka, K.; Oda, S.; Shiro, M., *Chem. Commun.* **2008**, 820-822.
(141) Liu, Y.; Li, Z.; Yuan, G.; Xia, Q.; Yuan, C.; Cui, Y., *Inorg. Chem.* **2016**, *55*, 12500-12503.
(142) Cho, S. H.; Ma, B.; Nguyen, S. T.; Hupp, J. T.; Albrecht-Schmitt, T. E., *Chem. Commun.* **2006**, 2563-2565.
(143) Xi, W.; Liu, Y.; Xia, Q.; Li, Z.; Cui, Y., *Chem. Eur. J.* **2015**, *21*, 12581-12585.
(144) Song, F. J.; Wang, C.; Falkowski, J. M.; Ma, L. Q.; Lin, W., *J. Am. Chem. Soc.* **2010**, *132*, 15390-15398.
(145) Yang, Z.; Zhu, C.; Li, Z.; Liu, Y.; Liu, G.; Cui, Y., *Chem. Commun.* **2014**, *50*, 8775-8778.

(146) Falkowski, J. M.; Wang, C.; Liu, S.; Lin, W., *Angew. Chem. Int. Ed.* **2011**, *50*, 8674-8678.
(147) Zhu, C.; Xia, Q.; Chen, X.; Liu, Y.; Du, X.; Cui, Y., *ACS Catal.* **2016**, *6*, 7590-7596.
(148) Duerinck, T.; Denayer, J. F. M., *Chem. Eng. Sci.* **2015**, *124*, 179-187.
(149) Birman, V. B.; Uffman, E. W.; Jiang, H.; Li, X.; Kilbane, C. J., *J. Am. Chem. Soc.* **2004**, *126*, 12226-12227.
(150) Zhang, J.; Li, Z.; Gong, W.; Han, X.; Liu, Y.; Cui, Y., *Inorg. Chem.* **2016**, *55*, 7229-7232.
(151) Xue, M.; Li, B.; Qiu, S.; Chen, B., *Mater. Today* **2016**, *19*, 503-515.
(152) Xu, Z.-X.; Liu, L.; Zhang, J., *Inorg. Chem.* **2016**, *55*, 6355-6357.
(153) Kong, J.; Zhang, M.; Duan, A.-H.; Zhang, J.-H.; Yang, R.; Yuan, L.-M., *J. Sep. Sci.* **2015**, *38*, 556-561.
(154) Tanaka, K.; Muraoka, T.; Otubo, Y.; Takahashi, H.; Ohnishi, A., *RSC Adv.* **2016**, *6*, 21293-21301.
(155) Bradshaw, D.; Prior, T. J.; Cussen, E. J.; Claridge, J. B.; Rosseinsky, M. J., *J. Am. Chem. Soc.* **2004**, *126*, 6106-6114.
(156) Kepert, C. J.; Prior, T. J.; Rosseinsky, M. J., *J. Am. Chem. Soc.* **2000**, *122*, 5158-5168.
(157) Chang, C.-L.; Qi, X.-Y.; Zhang, J.-W.; Qiu, Y.-M.; Li, X.-J.; Wang, X.; Bai, Y.; Sun, J.-L.; Liu, H.-W., *Chem. Commun.* **2015**, *51*, 3566-3569.
(158) Xu, Z.-X.; Fu, H.-R.; Wu, X.; Kang, Y.; Zhang, J., *Chem. Eur. J.* **2015**, *21*, 10236-10240.
(159) Zhao, J.; Li, H.; Han, Y.; Li, R.; Ding, X.; Feng, X.; Wang, B., *J. Mater. Chem. A* **2015**, *3*, 12145-12148.
(160) Wang, W.; Dong, X.; Nan, J.; Jin, W.; Hu, Z.; Chen, Y.; Jiang, J., *Chem. Commun.* **2012**, *48*, 7022-7024.
(161) Kang, Z.; Xue, M.; Fan, L.; Ding, J.; Guo, L.; Gao, L.; Qiu, S., *Chem. Commun.* **2013**, *49*, 10569-10571.
(162) Zhang, S. Y.; Wojtas, L.; Zaworotko, M. J., *J. Am. Chem. Soc.* **2015**, *137*, 12045-12049.
(163) Nuzhdin, A. L.; Dybtsev, D. N.; Bryliakov, K. P.; Talsi, E. P.; Fedin, V. P., *J. Am. Chem. Soc.* **2007**, *129*, 12958-12959.
(164) Hao, X.-R.; Wang, X.-L.; Qin, C.; Su, Z.-M.; Wang, E.-B.; Lan, Y.-Q.; Shao, K.-Z., *Chem. Commun.* **2007**, 4620-4622.
(165) Zhang, M.; Pu, Z.-J.; Chen, X.-L.; Gong, X.-L.; Zhu, A.-X.; Yuan, L.-M., *Chem. Commun.* **2013**, *49*, 5201-5203.
(166) Shekhah, O.; Wang, H.; Kowarik, S.; Schreiber, F.; Paulus, M.; Tolan, M.; Sternemann, C.; Evers, F.; Zacher, D.; Fischer, R. A.; Wöll, C., *J. Am. Chem. Soc.* **2007**, *129*, 15118-15119.
(167) Gu, Z.-G.; Grosjean, S.; Braese, S.; Woell, C.; Heinke, L., *Chem. Commun.* **2015**, *51*, 8998-9001.
(168) Gu, Z.-G.; Fu, W.-Q.; Wu, X.; Zhang, J., *Chem. Commun.* **2016**, *52*, 772-775.
(169) Liu, B.; Shekhah, O.; Arslan, H. K.; Liu, J.; Wöll, C.; Fischer, R. A., *Angew. Chem. Int. Ed.* **2012**, *51*, 807-810.
(170) Tanaka, K.; Muraoka, T.; Hirayama, D.; Ohnish, A., *Chem. Commun.* **2012**, *48*, 8577-8579.
(171) Peng, Y.; Gong, T.; Zhang, K.; Lin, X.; Liu, Y.; Jiang, J.; Cui, Y., *Nat. Commun.* **2014**, *5*, 4406-4414.
(172) Smaldone, R. A.; Forgan, R. S.; Furukawa, H.; Gassensmith, J. J.; Slawin, A. M. Z.; Yaghi, O. M.; Stoddart, J. F., *Angew. Chem. Int. Ed.* **2010**, *49*, 8630-8634.
(173) Forgan, R. S.; Smaldone, R. A.; Gassensmith, J. J.; Furukawa, H.; Cordes, D. B.; Li, Q.; Wilmer, C. E.; Botros, Y. Y.; Snurr, R. Q.; Slawin, A. M. Z.; Stoddart, J. F., *J. Am. Chem. Soc.* **2012**, *134*, 406-417.
(174) Hartlieb, K. J.; Holcroft, J. M.; Moghadam, P. Z.; Vermeulen, N. A.; Algaradah, M. M.; Nassar, M. S.; Botros, Y. Y.; Snurr, R. Q.; Stoddart, J. F., *J. Am. Chem. Soc.* **2016**, *138*, 2292-2301.
(175) Wanderley, M. M.; Wang, C.; Wu, C.-D.; Lin, W., *J. Am. Chem. Soc.* **2012**, *134*, 9050-9053.
(176) Chandrasekhar, P.; Mukhopadhyay, A.; Savitha, G.; Moorthy, J. N., *Chem. Sci.* **2016**, *7*, 3085-3091.
(177) Schuur, B.; Verkuijl, B. J. V.; Minnaard, A. J.; de Vries, J. G.; Heeres, H. J.; Feringa, B. L., *Org. Biomol. Chem.* **2011**, *9*, 36-51.

(178) Cook, T. R.; Stang, P. J., *Chem. Rev.* **2015**, *115*, 7001-7045.
(179) Fujita, M.; Yazaki, J.; Ogura, K., *J. Am. Chem. Soc.* **1990**, *112*, 5645-5647.
(180) Harris, K.; Fujita, D.; Fujita, M., *Chem. Commun.* **2013**, *49*, 6703-6712.
(181) Cook, T. R.; Stang, P. J., *Chem. Rev.* **2015**, *115*, 7001-7045.
(182) Chakrabarty, R.; Mukherjee, P. S.; Stang, P. J., *Chem. Rev.* **2011**, *111*, 6810-6918.
(183) Beves, J. E.; Leigh, D. A., *Nat. Chem.* **2010**, *2*, 708-710.
(184) Fang, L.; Olson, M. A.; Benitez, D.; Tkatchouk, E.; Goddard, W. A., III; Stoddart, J. F., *Chem. Soc. Rev.* **2010**, *39*, 17-29.
(185) Durot, S.; Reviriego, F.; Sauvage, J.-P., *Dalton Trans.* **2010**, *39*, 10557-10570.
(186) Crowley, J. D.; Goldup, S. M.; Lee, A.-L.; Leigh, D. A.; McBurney, R. T., *Chem. Soc. Rev.* **2009**, *38*, 1530-1541.
(187) Champin, B.; Mobian, P.; Sauvage, J.-P., *Chem. Soc. Rev.* **2007**, *36*, 358-366.
(188) Maurizot, V.; Yoshizawa, M.; Kawano, M.; Fujita, M., *Dalton Trans.* **2006**, 2750-2756.
(189) Yoshizawa, M.; Klosterman, J. K.; Fujita, M., *Angew. Chem. Int. Ed.* **2009**, *48*, 3418-3438.
(190) Pluth, M. D.; Bergman, R. G.; Raymond, K. N., *Acc. Chem. Res.* **2009**, *42*, 1650-1659.
(191) Davis, A. V.; Yeh, R. M.; Raymond, K. N., *Proc. Natl. Acad. Sci.* **2002**, *99*, 4793-4796.
(192) Tranchemontagne, D. J.; Ni, Z.; O'Keeffe, M.; Yaghi, O. M., *Angew. Chem. Int. Ed.* **2008**, *47*, 5136-5147.
(193) Koblenz, T. S.; Wassenaar, J.; Reek, J. N. H., *Chem. Soc. Rev.* **2008**, *37*, 247-262.
(194) Wilkinson, M. J.; van Leeuwen, P. W. N. M.; Reek, J. N. H., *Org. Biomol. Chem.* **2005**, *3*, 2371-2383.
(195) Hristova, Y. R.; Smulders, M. M. J.; Clegg, J. K.; Breiner, B.; Nitschke, J. R., *Chem. Sci.* **2011**, *2*, 638-641.
(196) Turega, S.; Whitehead, M.; Hall, B. R.; Haddow, M. F.; Hunter, C. A.; Ward, M. D., *Chem. Commun.* **2012**, *48*, 2752-2754.
(197) Riddell, I. A.; Smulders, M. M. J.; Clegg, J. K.; Nitschke, J. R., *Chem. Commun.* **2011**, *47*, 457-459.
(198) Duriska, M. B.; Neville, S. M.; Lu, J.; Iremonger, S. S.; Boas, J. F.; Kepert, C. J.; Batten, S. R., *Angew. Chem. Int. Ed.* **2009**, *48*, 8919-8922.
(199) Sudik, A. C.; Millward, A. R.; Ockwig, N. W.; Cote, A. P.; Kim, J.; Yaghi, O. M., *J. Am. Chem. Soc.* **2005**, *127*, 7110-7118.
(200) Galan, A.; Ballester, P., *Chem. Soc. Rev.* **2016**, *45*, 1720-1737.
(201) Clegg, J. K.; McMurtrie, J. C., Chiral Metallosupramolecular Polyhedra. In *Chirality in Supramolecular Assemblies*, John Wiley & Sons, Ltd: 2016; pp 218-256.
(202) Saalfrank, R. W.; Stark, A.; Peters, K.; von Schnering, H. G., *Angew. Chem. Int. Ed.* **1988**, *27*, 851-853.
(203) Caulder, D. L.; Powers, R. E.; Parac, T. N.; Raymond, K. N., *Angew. Chem. Int. Ed.* **1998**, *37*, 1840-1843.
(204) Beissel, T.; Powers, R. E.; Raymond, K. N., *Angew. Chem. Int. Ed.* **1996**, *35*, 1084-1086.
(205) Beissel, T.; Powers, R. E.; Parac, T. N.; Raymond, K. N., *J. Am. Chem. Soc.* **1999**, *121*, 4200-4206.
(206) Fleming, J. S.; Mann, K. L. V.; Carraz, C.-A.; Psillakis, E.; Jeffery, J. C.; McCleverty, J. A.; Ward, M. D., *Angew. Chem. Int. Ed.* **1998**, *37*, 1279-1281.
(207) Paul, R. L.; Bell, Z. R.; Jeffery, J. C.; Harding, L. P.; McCleverty, J. A.; Ward, M. D., *Polyhedron* **2003**, *22*, 781-787.
(208) Bell, Z. R.; Harding, L. P.; Ward, M. D., *Chem. Commun.* **2003**, 2432-2433.
(209) Paul, R. L.; Bell, Z. R.; Jeffery, J. C.; McCleverty, J. A.; Ward, M. D., *Proc. Natl. Acad. Sci.* **2002**, *99*, 4883-4888.
(210) Paul, R. L.; Couchman, S. M.; Jeffery, J. C.; McCleverty, J. A.; Reeves, Z. R.; Ward, M. D., *J. Chem. Soc., Dalton Trans.* **2000**, 845-851.
(211) Tidmarsh, I. S.; Taylor, B. F.; Hardie, M. J.; Russo, L.; Clegg, W.; Ward, M. D., *New J. Chem.* **2009**, *33*, 366-375.

(212) Hristova, Y. R.; Smulders, M. M. J.; Clegg, J. K.; Breiner, B.; Nitschke, J. R., *Chem. Sci.* **2011**, *2*, 638-641.
(213) Mal, P.; Nitschke, J. R., *Chem. Commun.* **2010**, *46*, 2417-2419.
(214) Mal, P.; Schultz, D.; Beyeh, K.; Rissanen, K.; Nitschke, J. R., *Angew. Chem. Int. Ed.* **2008**, *47*, 8297-8301.
(215) Clegg, J. K.; Li, F.; Jolliffe, K. A.; Meehan, G. V.; Lindoy, L. F., *Chem. Commun.* **2011**, *47*, 6042-6044.
(216) Clegg, J. K.; Lindoy, L. F.; Moubaraki, B.; Murray, K. S.; McMurtrie, J. C., *Dalton Trans.* **2004**, 2417-2423.
(217) Leininger, S.; Fan, J.; Schmitz, M.; Stang, P. J., *Proc. Natl. Acad. Sci.* **2000**, *97*, 1380-1384.
(218) Schweiger, M.; Yamamoto, T.; Stang, P. J.; Bläser, D.; Boese, R., *J. Org. Chem.* **2005**, *70*, 4861-4864.
(219) Zheng, Y.-R.; Zhao, Z.; Kim, H.; Wang, M.; Ghosh, K.; Pollock, J. B.; Chi, K.-W.; Stang, P. J., *Inorg. Chem.* **2010**, *49*, 10238-10240.
(220) Granzhan, A.; Riis-Johannessen, T.; Scopelliti, R.; Severin, K., *Angew. Chem. Int. Ed.* **2010**, *49*, 5515-5518.
(221) Granzhan, A.; Schouwey, C.; Riis-Johannessen, T.; Scopelliti, R.; Severin, K., *J. Am. Chem. Soc.* **2011**, *133*, 7106-7115.
(222) Roche, S.; Haslam, C.; L. Heath, S.; A. Thomas, J., *Chem. Commun.* **1998**, 1681-1682.
(223) Suzuki, K.; Tominaga, M.; Kawano, M.; Fujita, M., *Chem. Commun.* **2009**, 1638-1640.
(224) Johannessen, S. C.; Brisbois, R. G.; Fischer, J. P.; Grieco, P. A.; Counterman, A. E.; Clemmer, D. E., *J. Am. Chem. Soc.* **2001**, *123*, 3818-3819.
(225) Fujita, M.; Oguro, D.; Miyazawa, M.; Oka, H.; Yamaguchi, K.; Ogura, K., *Nature* **1995**, *378*, 469-471.
(226) Ronson, T. K.; Fisher, J.; Harding, L. P.; Hardie, M. J., *Angew. Chem. Int. Ed.* **2007**, *46*, 9086-9088.
(227) Prakash, M. J.; Zou, Y.; Hong, S.; Park, M.; Bui, M.-P. N.; Seong, G. H.; Lah, M. S., *Inorg. Chem.* **2009**, *48*, 1281-1283.
(228) Li, J.-R.; Timmons, D. J.; Zhou, H.-C., *J. Am. Chem. Soc.* **2009**, *131*, 6368-6369.
(229) Olenyuk, B.; Levin, M. D.; Whiteford, J. A.; Shield, J. E.; Stang, P. J., *J. Am. Chem. Soc.* **1999**, *121*, 10434-10435.
(230) Paquette, L. A.; Balogh, D. W.; Usha, R.; Kountz, D.; Christoph, G. G., *Science* **1981**, *211*, 575-576.
(231) Parac, T. N.; Caulder, D. L.; Raymond, K. N., *J. Am. Chem. Soc.* **1998**, *120*, 8003-8004.
(232) Johnson, D. W.; Raymond, K. N., *Inorg. Chem.* **2001**, *40*, 5157-5161.
(233) Clegg, J. K.; Lindoy, L. F.; Moubaraki, B.; Murray, K. S.; McMurtrie, J. C., *Dalton Trans.* **2004**, 2417-2423.
(234) Harano, K.; Hiraoka, S.; Shionoya, M., *J. Am. Chem. Soc.* **2007**, *129*, 5300-5301.
(235) Ni, Z.; Yassar, A.; Antoun, T.; Yaghi, O. M., *J. Am. Chem. Soc.* **2005**, *127*, 12752-12753.
(236) Ghosh, S.; Mukherjee, P. S., *Tetrahedron Lett.* **2006**, *47*, 9297-9300.
(237) Mukherjee, P. S.; Das, N.; Stang, P. J., *J. Org. Chem.* **2004**, *69*, 3526-3529.
(238) Schweiger, M.; Seidel, S. R.; Schmitz, M.; Stang, P. J., *Org. Lett.* **2000**, *2*, 1255-1257.
(239) Zheng, Y.-R.; Ghosh, K.; Yang, H.-B.; Stang, P. J., *Inorg. Chem.* **2010**, *49*, 4747-4749.
(240) Kumazawa, K.; Biradha, K.; Kusukawa, T.; Okano, T.; Fujita, M., *Angew. Chem. Int. Ed.* **2003**, *42*, 3909-3913.
(241) Lee, S. J.; Mulfort, K. L.; O'Donnell, J. L.; Zuo, X.; Goshe, A. J.; Wesson, P. J.; Nguyen, S. T.; Hupp, J. T.; Tiede, D. M., *Chem. Commun.* **2006**, 4581-4583.
(242) Barbour, L. J.; Orr, G. W.; Atwood, J. L., *Nature* **1998**, *393*, 671-673.
(243) Liu, H.-K.; Tong, X., *Chem. Commun.* **2002**, 1316-1317.
(244) Zarra, S.; Wood, D. M.; Roberts, D. A.; Nitschke, J. R., *Chem. Soc. Rev.* **2015**, *44*, 419-432.
(245) Pluth, M. D.; Raymond, K. N., *Chem. Soc. Rev.* **2007**, *36*, 161-171.

(246) Ferguson, A.; Staniland, R. W.; Fitchett, C. M.; Squire, M. A.; Williamson, B. E.; Kruger, P. E., *Dalton Trans.* **2014**, *43*, 14550-14553.
(247) Turega, S.; Whitehead, M.; Hall, B. R.; Meijer, A. J. H. M.; Hunter, C. A.; Ward, M. D., *Inorg. Chem.* **2013**, *52*, 1122-1132.
(248) Custelcean, R.; Bonnesen, P. V.; Duncan, N. C.; Zhang, X.; Watson, L. A.; Van Berkel, G.; Parson, W. B.; Hay, B. P., *J. Am. Chem. Soc.* **2012**, *134*, 8525-8534.
(249) Ma, S.; Smulders, M. M. J.; Hristova, Y. R.; Clegg, J. K.; Ronson, T. K.; Zarra, S.; Nitschke, J. R., *J. Am. Chem. Soc.* **2013**, *135*, 5678-5684.
(250) Bloch, W. M.; Abe, Y.; Holstein, J. J.; Wandtke, C. M.; Dittrich, B.; Clever, G. H., *J. Am. Chem. Soc.* **2016**, *138*, 13750-13755.
(251) Davis, A. V.; Raymond, K. N., *J. Am. Chem. Soc.* **2005**, *127*, 7912-7919.
(252) Custelcean, R., *Chem. Soc. Rev.* **2014**, *43*, 1813-1824.
(253) Cullen, W.; Thomas, K. A.; Hunter, C. A.; Ward, M. D., *Chem. Sci.* **2015**, *6*, 4025-4028.
(254) Dube, H.; Ajami, D.; Rebek, J., *Angew. Chem. Int. Ed.* **2010**, *49*, 3192-3195.
(255) Schmidt, A.; Hollering, M.; Han, J.; Casini, A.; Kuhn, F. E., *Dalton Trans.* **2016**, *45*, 12297-12300.
(256) Ferguson, A.; Squire, M. A.; Siretanu, D.; Mitcov, D.; Mathoniere, C.; Clerac, R.; Kruger, P. E., *Chem. Commun.* **2013**, *49*, 1597-1599.
(257) Zheng, Y.-R.; Suntharalingam, K.; Johnstone, T. C.; Lippard, S. J., *Chem. Sci.* **2015**, *6*, 1189-1193.
(258) Ma, Z.-B.; Moulton, B., *Coord. Chem. Rev.* **2011**, *255*, 1623-1641.
(259) Ahmad, N.; Chughtai, A. H.; Younus, H. A.; Verpoort, F., *Coord. Chem. Rev.* **2014**, *280*, 1-27.
(260) Deraedt, C.; Astruc, D., *Coord. Chem. Rev.* **2016**, *324*, 106-122.
(261) Metherell, A. J.; Curty, C.; Zaugg, A.; Saad, S. T.; Dennison, G. H.; Ward, M. D., *J. Mater. Chem. C* **2016**, *4*, 9664-9668.
(262) Taylor, C. G. P.; Piper, J. R.; Ward, M. D., *Chem. Commun.* **2016**, *52*, 6225-6228.
(263) Sambrook, M. R.; Notman, S., *Chem. Soc. Rev.* **2013**, *42*, 9251-9267.
(264) Mal, P.; Breiner, B.; Rissanen, K.; Nitschke, J. R., *Science* **2009**, *324*, 1697-1699.
(265) Yoshizawa, M.; Tamura, M.; Fujita, M., *Science* **2006**, *312*, 251-254.
(266) Cullen, W.; Misuraca, M. C.; Hunter, C. A.; Williams, N. H.; Ward, M. D., *Nat. Chem.* **2016**, *8*, 231-236.
(267) Bhat, I. A.; Jain, R.; Siddiqui, M. M.; Saini, D. K.; Mukherjee, P. S., *Inorg. Chem.* **2017**, *56*, 5352-5360.
(268) Therrien, B., Discrete Metalla-Assemblies as Drug Delivery Vectors. In *Nanomaterials in Drug Delivery, Imaging, and Tissue Engineering*, John Wiley & Sons, Inc.: 2013; pp 145-166.
(269) Lewis, J. E. M.; Gavey, E. L.; Cameron, S. A.; Crowley, J. D., *Chem. Sci.* **2012**, *3*, 778-784.
(270) Ronson, T. K.; Pilgrim, B. S.; Nitschke, J. R., *J. Am. Chem. Soc.* **2016**, *138*, 10417-10420.
(271) Brega, V.; Zeller, M.; He, Y.; Peter Lu, H.; Klosterman, J. K., *Chem. Commun.* **2015**, *51*, 5077-5080.
(272) Roberts, D. A.; Castilla, A. M.; Ronson, T. K.; Nitschke, J. R., *J. Am. Chem. Soc.* **2014**, *136*, 8201-8204.
(273) Zhao, D.; Tan, S.; Yuan, D.; Lu, W.; Rezenom, Y. H.; Jiang, H.; Wang, L.-Q.; Zhou, H.-C., *Adv. Mater.* **2011**, *23*, 90-93.
(274) Zhang, X. X.; Bradshaw, J. S.; Izatt, R. M., *Chem. Rev.* **1997**, *97*, 3313-3361.
(275) Rivera, J. M.; Martin, T.; Rebek, J., Jr., *J. Am. Chem. Soc.* **2001**, *123*, 5213-5220.
(276) Scarso, A.; Shivanyuk, A.; Hayashida, O.; Rebek, J., Jr., *J. Am. Chem. Soc.* **2003**, *125*, 6239-6243.
(277) Rivera, J. M.; Martin, T.; Rebek, J., Jr., *Science* **1998**, *279*, 1021-1023.
(278) Dong, J.; Tan, C.; Zhang, K.; Liu, Y.; Low, P. J.; Jiang, J.; Cui, Y., *J. Am. Chem. Soc.* **2017**, *139*, 1554-1564.
(279) Meng, W.; Clegg, J. K.; Thoburn, J. D.; Nitschke, J. R., *J. Am. Chem. Soc.* **2011**, *133*, 13652-13660.

(280) Clegg, J. K.; Cremers, J.; Hogben, A. J.; Breiner, B.; Smulders, M. M. J.; Thoburn, J. D.; Nitschke, J. R., *Chem. Sci.* **2013**, *4*, 68-76.
(281) Ronson, T. K.; Zarra, S.; Black, S. P.; Nitschke, J. R., *Chem. Commun.* **2013**, *49*, 2476-2490.
(282) Bruckner, C.; Powers, R. E.; Raymond, K. N., *Angew. Chem. Int. Ed.* **1998**, *37*, 1837-1839.
(283) Hong, C. M.; Kaphan, D. M.; Bergman, R. G.; Raymond, K. N.; Toste, F. D., *J. Am. Chem. Soc.* **2017**, *139*, 8013-8021.
(284) Hall, B. R.; Manck, L. E.; Tidmarsh, I. S.; Stephenson, A.; Taylor, B. F.; Blaikie, E. J.; Vander Griend, D. A.; Ward, M. D., *Dalton Trans.* **2011**, *40*, 12132-12145.
(285) Glasson, C. R. K.; Meehan, G. V.; Clegg, J. K.; Lindoy, L. F.; Turner, P.; Duriska, M. B.; Willis, R., *Chem. Commun.* **2008**, 1190-1192.
(286) Mueller, I. M.; Robson, R.; Separovic, F., *Angew. Chem. Int. Ed.* **2001**, *40*, 4385-4386.
(287) Kubota, Y.; Biradha, K.; Fujita, M.; Sakamoto, S.; Yamaguchi, K., *Bull. Chem. Soc. Jpn.* **2002**, *75*, 559-565.
(288) Johnson, D. W.; Xu, J.; Saalfrank, R. W.; Raymond, K. N., *Angew. Chem. Int. Ed.* **1999**, *38*, 2882-2885.
(289) Bu, X.-H.; Morishita, H.; Tanaka, K.; Biradha, K.; Furusho, S.; Shionoya, M., *Chem. Commun.* **2000**, 971-972.
(290) Davis, A. V.; Fiedler, D.; Ziegler, M.; Terpin, A.; Raymond, K. N., *J. Am. Chem. Soc.* **2007**, *129*, 15354-15363.
(291) Cantuel, M.; Bernardinelli, G.; Muller, G.; Riehl, J. P.; Piguet, C., *Inorg. Chem.* **2004**, *43*, 1840-1849.
(292) Gütz, C.; Hovorka, R.; Schnakenburg, G.; Lützen, A., *Chem. Eur. J.* **2013**, *19*, 10890-10894.
(293) Ye, Y.; Cook, T. R.; Wang, S.-P.; Wu, J.; Li, S.; Stang, P. J., *J. Am. Chem. Soc.* **2015**, *137*, 11896-11899.
(294) Gütz, C.; Hovorka, R.; Klein, C.; Jiang, Q.-Q.; Bannwarth, C.; Engeser, M.; Schmuck, C.; Assenmacher, W.; Mader, W.; Topić, F.; Rissanen, K.; Grimme, S.; Lützen, A., *Angew. Chem. Int. Ed.* **2014**, *53*, 1693-1698.
(295) Mamula, O.; von Zelewsky, A., *Coord. Chem. Rev.* **2003**, *242*, 87-95.
(296) Suzuki, K.; Kawano, M.; Sato, S.; Fujita, M., *J. Am. Chem. Soc.* **2007**, *129*, 10652-10653.
(297) Li, K.; Zhang, L.-Y.; Yan, C.; Wei, S.-C.; Pan, M.; Zhang, L.; Su, C.-Y., *J. Am. Chem. Soc.* **2014**, *136*, 4456-4459.
(298) Zhao, C.; Sun, Q.-F.; Hart-Cooper, W. M.; DiPasquale, A. G.; Toste, F. D.; Bergman, R. G.; Raymond, K. N., *J. Am. Chem. Soc.* **2013**, *135*, 18802-18805.
(299) Schweiger, M.; Seidel, S. R.; Schmitz, M.; Stang, P. J., *Org. Lett.* **2000**, *2*, 1255-1257.
(300) Ousaka, N.; Clegg, J. K.; Nitschke, J. R., *Angew. Chem. Int. Ed.* **2012**, *51*, 1464-1468.
(301) Albrecht, M.; Burk, S.; Weis, P., *Synthesis* **2008**, 2963-2967.
(302) Castilla, A. M.; Ousaka, N.; Bilbeisi, R. A.; Valeri, E.; Ronson, T. K.; Nitschke, J. R., *J. Am. Chem. Soc.* **2013**, *135*, 17999-18006.
(303) Hannon, M. J.; Childs, L. J., *Supramol. Chem.* **2004**, *16*, 7-22.
(304) Albrecht, M., *Chem. Rev.* **2001**, *101*, 3457-3498.
(305) Khatua, S.; Stoeckli-Evans, H.; Harada, T.; Kuroda, R.; Bhattacharjee, M., *Inorg. Chem.* **2006**, *45*, 9619-9621.
(306) Charbonnière, L. J.; Williams, A. F.; Frey, U.; Merbach, A. E.; Kamalaprija, P.; Schaad, O., *J. Am. Chem. Soc.* **1997**, *119*, 2488-2496.
(307) Yeh, R. M.; Raymond, K. N., *Inorg. Chem.* **2006**, *45*, 1130-1139.
(308) Zhang, Z.; Dolphin, D., *Chem. Commun.* **2009**, 6931-6933.
(309) Stang, P. J.; Olenyuk, B.; Muddiman, D. C.; Smith, R. D., *Organometallics* **1997**, *16*, 3094-3096.
(310) Clegg, J. K.; Cremers, J.; Hogben, A. J.; Breiner, B.; Smulders, M. M. J.; Thoburn, J. D.; Nitschke, J. R., *Chem. Sci.* **2013**, *4*, 68-76.
(311) Ziegler, M.; Davis, A. V.; Johnson, D. W.; Raymond, K. N., *Angew. Chem. Int. Ed.* **2003**, *42*, 665-668.
(312) Chen, L.-J.; Yang, H.-B.; Shionoya, M., *Chem. Soc. Rev.* **2017**, *46*, 2555-2576.

(313) Fiedler, D.; Leung, D. H.; Bergman, R. G.; Raymond, K. N., *J. Am. Chem. Soc.* **2004**, *126*, 3674-3675.
(314) Hastings, C. J.; Pluth, M. D.; Biros, S. M.; Bergman, R. G.; Raymond, K. N., *Tetrahedron* **2008**, *64*, 8362-8367.
(315) Liu, T.; Liu, Y.; Xuan, W.; Cui, Y., *Angew. Chem. Int. Ed.* **2010**, *49*, 4121-4124.
(316) Wu, K.; Li, K.; Hou, Y.-J.; Pan, M.; Zhang, L.-Y.; Chen, L.; Su, C.-Y., *Nat. Commun.* **2016**, *7*, 10487.
(317) Fiedler, D.; Bergman, R. G.; Raymond, K. N., *Angew. Chem. Int. Ed.* **2004**, *43*, 6748-6751.
(318) Fiedler, D.; Leung, D. H.; Bergman, R. G.; Raymond, K. N., *Acc. Chem. Res.* **2005**, *38*, 349-358.
(319) Wang, Z. J.; Brown, C. J.; Bergman, R. G.; Raymond, K. N.; Toste, F. D., *J. Am. Chem. Soc.* **2011**, *133*, 7358-7360.
(320) Leung, D. H.; Bergman, R. G.; Raymond, K. N., *J. Am. Chem. Soc.* **2007**, *129*, 2746-2747.
(321) Pluth, M. D.; Bergman, R. G.; Raymond, K. N., *Angew. Chem. Int. Ed.* **2007**, *46*, 8587-8589.
(322) Hastings, C. J.; Pluth, M. D.; Bergman, R. G.; Raymond, K. N., *J. Am. Chem. Soc.* **2010**, *132*, 6938-6940.
(323) Kaphan, D. M.; Levin, M. D.; Bergman, R. G.; Raymond, K. N.; Toste, F. D., *Science* **2015**, *350*, 1235-1238.
(324) Nishioka, Y.; Yamaguchi, T.; Kawano, M.; Fujita, M., *J. Am. Chem. Soc.* **2008**, *130*, 8160-8161.
(325) Yaghi, O. M.; Eddaoudi, M.; Li, H.; Kim, J.; Rosi, N. Preparation of isoreticular metal-organic frameworks and systematic design of pore size and functionality, with application for gas storage. WO2002088148A1, 2002.
(326) Lin, Z.-J.; Lu, J.; Hong, M.; Cao, R., *Chem. Soc. Rev.* **2014**, *43*, 5867-5895.
(327) Lu, W.; Wei, Z.; Gu, Z. Y.; Liu, T. F.; Park, J.; Park, J.; Tian, J.; Zhang, M.; Zhang, Q.; Gentle III, T.; Bosch, M.; Zhou, H. C., *Chem. Soc. Rev.* **2014**, *43*, 5561-5593.
(328) Guillerm, V.; Kim, D.; Eubank, J. F.; Luebke, R.; Liu, X.; Adil, K.; Lah, M. S.; Eddaoudi, M., *Chem. Soc. Rev.* **2014**, *43*, 6141-6172.
(329) Furukawa, H.; Kim, J.; Ockwig, N. W.; O'Keeffe, M.; Yaghi, O. M., *J. Am. Chem. Soc.* **2008**, *130*, 11650-11661.
(330) Du, M.; Li, C. P.; Liu, C. S.; Fang, S. M., *Coord. Chem. Rev.* **2013**, *257*, 1282-1305.
(331) Kondo, M.; Okubo, T.; Asami, A.; Noro, S. I.; Yoshitomi, T.; Kitagawa, S.; Ishii, T.; Matsuzaka, H.; Seki, K., *Angew. Chem. Int. Ed.* **1999**, *38*, 140-143.
(332) Maji, T. K.; Uemura, K.; Chang, H.-C.; Matsuda, R.; Kitagawa, S., *Angew. Chem. Int. Ed.* **2004**, *43*, 3269-3272.
(333) Lin, Z.-J.; Liu, T.-F.; Xu, B.; Han, L.-W.; Huang, Y.-B.; Cao, R., *CrystEngComm* **2011**, *13*, 3321-3324.
(334) Kitaura, R.; Fujimoto, K.; Noro, S.-i.; Kondo, M.; Kitagawa, S., *Angew. Chem. Int. Ed.* **2002**, *114*, 141-143.
(335) Seo, J.; Matsuda, R.; Sakamoto, H.; Bonneau, C.; Kitagawa, S., *J. Am. Chem. Soc.* **2009**, *131*, 12792-12800.
(336) Sakata, Y.; Furukawa, S.; Kondo, M.; Hirai, K.; Horike, N.; Takashima, Y.; Uehara, H.; Louvain, N.; Meilikhov, M.; Tsuruoka, T.; Isoda, S.; Kosaka, W.; Sakata, O.; Kitagawa, S., *Science* **2013**, *339*, 193-196.
(337) Shultz, A. M.; Farha, O. K.; Hupp, J. T.; Nguyen, S. T., *J. Am. Chem. Soc.* **2009**, *131*, 4204-4205.
(338) Mulfort, K. L.; Hupp, J. T., *J. Am. Chem. Soc.* **2007**, *129*, 9604-9605.
(339) Prasad, T. K.; Hong, D. H.; Suh, M. P., *Chem. Eur. J.* **2010**, *16*, 14043-14050.
(340) Farha, O. K.; Mulfort, K. L.; Thorsness, A. M.; Hupp, J. T., *J. Am. Chem. Soc.* **2008**, *130*, 8598-8599.
(341) Bala, S.; Mondal, I.; Goswami, A.; Pal, U.; Mondal, R., *Dalton Trans.* **2014**, *43*, 15704-15707.
(342) Black, S. P.; Wood, D. M.; Schwarz, F. B.; Ronson, T. K.; Holstein, J. J.; Stefankiewicz, A. R.; Schalley, C. A.; Sanders, J. K. M.; Nitschke, J. R., *Chem. Sci.* **2016**, *7*, 2614-2620.
(343) Lü, X.-Q.; Jiang, J.-J.; Zhang, L.; Chen, C.-L.; Su, C.-Y.; Kang, B.-S., *Cryst. Growth Des.* **2005**, *5*, 419-421.

(344) Boer, S. A.; Turner, D. R., *Chem. Commun.* **2015**, *51*, 17375-17378.
(345) Khoshbin, M. S.; Ovchinnikov, M. V.; Salaita, K. S.; Mirkin, C. A.; Stern, C. L.; Zakharov, L. N.; Rheingold, A. L., *Chem. Asian J.* **2006**, *1*, 686-692.
(346) Takashima, Y.; Martínez, V. M.; Furukawa, S.; Kondo, M.; Shimomura, S.; Uehara, H.; Nakahama, M.; Sugimoto, K.; Kitagawa, S., *Nat. Commun.* **2011**, *2*, 168.
(347) Lü, X.-Q.; Jiang, J.-J.; zur Loye, H.-C.; Kang, B.-S.; Su, C.-Y., *Inorg. Chem.* **2005**, *44*, 1810-1817.
(348) Boer, S. A.; Nolvachai, Y.; Kulsing, C.; McCormick, L. J.; Hawes, C. S.; Marriott, P. J.; Turner, D. R., *Chem. Eur. J.* **2014**, *20*, 11308-11312.
(349) Park, G.; Yang, H.; Kim, T. H.; Kim, J., *Inorg. Chem.* **2011**, *50*, 961-968.
(350) Joarder, B.; Mukherjee, S.; Chaudhari, A. K.; Desai, A. V.; Manna, B.; Ghosh, S. K., *Chem. Eur. J.* **2014**, *20*, 15303-15308.
(351) Cairns, A. J.; Perman, J. A.; Wojtas, L.; Kravtsov, V. C.; Alkordi, M. H.; Eddaoudi, M.; Zaworotko, M. J., *J. Am. Chem. Soc.* **2008**, *130*, 1560-1561.
(352) McCormick, L. J.; Turner, D. R., *CrystEngComm* **2013**, *15*, 8234-8236.
(353) Hawes, C. S.; Moubaraki, B.; Murray, K. S.; Kruger, P. E.; Turner, D. R.; Batten, S. R., *Cryst. Growth Des.* **2014**, *14*, 5749-5760.
(354) Qin, L.; Zhao, W. N.; Yu, G. J.; Xu, L. P.; Han, L., *Inorg. Chem. Commun.* **2013**, *34*, 47-50.
(355) Boer, S. A.; Turner, D. R., *Cryst. Growth Des.* **2016**, *16*, 6294-6303.
(356) Boer, S. A.; Turner, D. R., *CrystEngComm* **2017**, *19*, 2402 - 2412.
(357) Zaworotko, M. J., *Chem. Commun.* **2001**, 1-9.
(358) Papaefstathiou, G. S.; MacGillivray, L. R., *Coord. Chem. Rev.* **2003**, *246*, 169-184.
(359) Dunitz, J. D., *Chem. Commun.* **2003**, 545-548.
(360) Janiak, C., *Dalton Trans.* **2003**, 2781-2804.
(361) Dobrzanska, L.; Kleinhans, D. J.; Barbour, L. J., *New J. Chem.* **2008**, *32*, 813-819.
(362) Yan, Y.; Liu, S.; Guo, M.; Guo, X.; Guo, H., *Inorg. Chem. Commun.* **2016**, *71*, 98-101.
(363) Kobaisi, M. A.; Bhosale, S. V.; Latham, K.; Raynor, A. M.; Bhosale, S. V., *Chem. Rev.* **2016**, *116*, 11685-11796.
(364) Pan, M.; Lin, X. M.; Li, G. B.; Su, C. Y., *Coord. Chem. Rev.* **2011**, *255*, 1921-1936.
(365) Hamilton, D. G.; Feeder, N.; Teatc, S. J.; Sanders, J. K. M., *New J. Chem.* **1998**, *22*, 1019-1021.
(366) Nelson, A. P.; Farha, O. K.; Mulfort, K. L.; Hupp, J. T., *J. Am. Chem. Soc.* **2009**, *131*, 458-460.
(367) Cairns, A. J.; Perman, J. A.; Wojtas, L.; Kravtsov, V. C.; Alkordi, M. H.; Eddaoudi, M.; Zaworotko, M. J., *J. Am. Chem. Soc.* **2008**, *130*, 1560-1561.
(368) Xie, Y. X.; Zhao, W. N.; Li, G. C.; Liu, P. F.; Han, L., *Inorg. Chem.* **2016**, *55*, 549-551.
(369) Mallick, A.; Garai, B.; Addicoat, M. A.; Petkov, P. S.; Heine, T.; Banerjee, R., *Chem. Sci.* **2015**, *6*, 1420-1425.
(370) Yang, J.; Ma, J. F.; Batten, S. R., *Chem. Commun.* **2012**, *48*, 7899-7912.
(371) Carlucci, L.; Ciani, G.; Proserpio, D. M., *Coord. Chem. Rev.* **2003**, *246*, 247-289.
(372) Farha, O. K.; Hupp, J. T., *Acc. Chem. Res.* **2010**, *43*, 1166-1175.
(373) Batten, S. R., Interpenetration and entanglement in coordination polymers. In *Metal-Organic Framework Materials*, MacGillivray, L. R.; Lukehart, C. M., Eds. John Wiley & Sons Ltd.: 2014; pp 523-538.
(374) Boer, S. A. Chiral coordination polymers for separations Honours thesis, Monash University,, Melbourne, 2013.
(375) Qin, L.; Zhao, W.-N.; Yu, G.-J.; Xu, L.-P.; Han, L., *Inorg. Chem. Commun.* **2013**, *34*, 47-50.
(376) Macrae, C. F.; Bruno, I. J.; Chisholm, J. A.; Edgington, P. R.; McCabe, P.; Pidcock, E.; Rodriguez-Monge, L.; Taylor, R.; van de Streek, J.; Wood, P. A., *J. Appl. Crystallogr.* **2008**, *41*, 466-470.
(377) Steel, P. J., *Acc. Chem. Res.* **2005**, *38*, 243-250.
(378) Rosi, N. L.; Eddaoudi, M.; Kim, J.; O'Keeffe, M.; Yaghi, O. M., *Angew. Chem. Int. Ed.* **2002**, *41*, 284-287.
(379) Lü, X. Q.; Jiang, J. J.; Zhang, L.; Chen, C. L.; Su, C. Y.; Kang, B. S., *Cryst. Growth Des.* **2005**, *5*, 419-421.

(380) Choi, K.-Y.; Yi, M. H., *Macromol. Symp.* **1999**, *142*, 193-204.
(381) Zhong, D.-C.; Liao, L.-Q.; Deng, J.-H.; Chen, Q.; Lian, P.; Luo, X.-Z., *Chem. Commun.* **2014**, *50*, 15807-15810.
(382) Perman, J. A.; Cairns, A. J.; Wojtas, L.; Eddaoudi, M.; Zaworotko, M. J., *CrystEngComm* **2011**, *13*, 3130-3133.
(383) Han, L.; Qin, L.; Xu, L.; Zhou, Y.; Sun, J.; Zou, X., *Chem. Commun.* **2013**, *49*, 406-408.
(384) Guzmán-Lucero, D.; Likhanova, N. V.; Höpfl, H.; Guzmán, J.; Likhatchev, D.; Martínez-Palou, R., *ARKIVOC* **2006**, 7-20.
(385) Zou, Q.; Zhou, Q.; Dai, H., *Polym. Degrad. Stab.* **2017**, *135*, 85-98.
(386) Kanoo, P.; Matsuda, R.; Higuchi, M.; Kitagawa, S.; Maji, T. K., *Chem . Mater.* **2009**, *21*, 5860-5866.
(387) Yao, Q.; Sun, J.; Li, K.; Su, J.; Peskov, M. V.; Zou, X., *Dalton Trans.* **2012**, *41*, 3953-3955.
(388) Eddaoudi, M.; Kim, J.; Vodak, D.; Sudik, A.; Wachter, J.; O'Keeffe, M.; Yaghi, O. M., *Proc. Natl. Acad. Sci.* **2002**, *99*, 4900-4904.
(389) Lu, W.; Yuan, D.; Yakovenko, A.; Zhou, H. C., *Chem. Commun.* **2011**, *47*, 4968-4970.
(390) Paul, M.; Adarsh, N. N.; Dastidar, P., *Cryst. Growth Des.* **2014**, *14*, 1331-1337.
(391) Lakowicz, J. R., *Principles of Fluorescence Spectroscopy*. Springer US: 2006.
(392) Valeur, B., Characteristics of Fluorescence Emission. In *Molecular Fluorescence*, Wiley-VCH Verlag GmbH: Weinheim, 2001; pp 34-71.
(393) Bell, T. D. M.; Bhosale, S. V.; Forsyth, C. M.; Hayne, D.; Ghiggino, K. P.; Hutchison, J. A.; Jani, C. H.; Langford, S. J.; Lee, M. A. P.; Woodward, C. P., *Chem. Commun.* **2010**, *46*, 4881-4883.
(394) Beija, M.; Afonso, C. A. M.; Martinho, J. M. G., *Chem. Soc. Rev.* **2009**, *38*, 2410-2433.
(395) Ulrich, G.; Ziessel, R.; Harriman, A., *Angew. Chem. Int. Ed.* **2008**, *47*, 1184-1201.
(396) Chan, W. C. W.; Maxwell, D. J.; Gao, X.; Bailey, R. E.; Han, M.; Nie, S., *Curr. Opin. Biotechnol.* **2002**, *13*, 40-46.
(397) Tsoi, K. M.; Dai, Q.; Alman, B. A.; Chan, W. C. W., *Acc. Chem. Res.* **2013**, *46*, 662-671.
(398) Tsien, R. Y., *Annu. Rev. Biochem.* **1998**, *67*, 509-544.
(399) Lippincott-Schwartz, J.; Patterson, G. H., *Science* **2003**, *300*, 87-91.
(400) Lippincott-Schwartz, J.; Snapp, E.; Kenworthy, A., *Nat. Rev. Mol. Cell Biol.* **2001**, *2*, 444-456.
(401) Kim, H. N.; Ren, W. X.; Kim, J. S.; Yoon, J., *Chem. Soc. Rev.* **2012**, *41*, 3210-3244.
(402) Valeur, B.; Leray, I., *Coord. Chem. Rev.* **2000**, *205*, 3-40.
(403) Zhao, J.; Davidson, M. G.; Mahon, M. F.; Kociok-Köhn, G.; James, T. D., *J. Am. Chem. Soc.* **2004**, *126*, 16179-16186.
(404) Zhan, X.; Facchetti, A.; Barlow, S.; Marks, T. J.; Ratner, M. A.; Wasielewski, M. R.; Marder, S. R., *Adv. Mater.* **2011**, *23*, 268-284.
(405) Katz, H. E.; Lovinger, A. J.; Johnson, J.; Kloc, C.; Siegrist, T.; Li, W.; Lin, Y. Y.; Dodabalapur, A., *Nature* **2000**, *404*, 478-481.
(406) Liu, Y.; Zhang, L.; Lee, H.; Wang, H.-W.; Santala, A.; Liu, F.; Diao, Y.; Briseno, A. L.; Russell, T. P., *Adv. Energy Mater.* **2015**, *5*, 1500195.
(407) Kobaisi, M. A.; Bhosale, S. V.; Latham, K.; Raynor, A. M.; Bhosale, S. V., *Chem. Rev.* **2016**, *116*, 11685-11796.
(408) Herbst, W.; Hunger, K.; Wilker, G.; Ohleier, H.; Winter, R., Azo Pigments. In *Industrial Organic Pigments*, ed.; Wiley-VCH Verlag GmbH & Co. KGaA: 2005; pp 183-419.
(409) Weil, T.; Vosch, T.; Hofkens, J.; Peneva, K.; Müllen, K., *Angew. Chem. Int. Ed.* **2010**, *49*, 9068-9093.
(410) Vicic, D. A.; Odom, D. T.; Núñez, M. E.; Gianolio, D. A.; McLaughlin, L. W.; Barton, J. K., *J. Am. Chem. Soc.* **2000**, *122*, 8603-8611.
(411) Lee, H. N.; Xu, Z.; Kim, S. K.; Swamy, K. M. K.; Kim, Y.; Kim, S.-J.; Yoon, J., *J. Am. Chem. Soc.* **2007**, *129*, 3828-3829.
(412) Liu, Z.; Zhang, G.; Cai, Z.; Chen, X.; Luo, H.; Li, Y.; Wang, J.; Zhang, D., *Adv. Mater.* **2014**, *26*, 6965-6977.
(413) Castellano, F. N., *Dalton Trans.* **2012**, *41*, 8493-8501.

(414) Gabriel, G. J.; Sorey, S.; Iverson, B. L., *J. Am. Chem. Soc.* **2005**, *127*, 2637-2640.
(415) Würthner, F., *Pure Appl. Chem.* **2006**, *78*, 2341 – 2349.
(416) Zych, A. J.; Iverson, B. L., *J. Am. Chem. Soc.* **2000**, *122*, 8898-8909.
(417) Pantos, G. D.; Pengo, P.; Sanders, J. K. M., *Angew. Chem. Int. Ed.* **2007**, *46*, 194-197.
(418) Tomasulo, M.; Naistat, D. M.; White, A. J. P.; Williams, D. J.; Raymo, F. M., *Tetrahedron Lett.* **2005**, *46*, 5695-5698.
(419) Mukhopadhyay, P.; Iwashita, Y.; Shirakawa, M.; Kawano, S.-i.; Fujita, N.; Shinkai, S., *Angew. Chem. Int. Ed.* **2006**, *45*, 1592-1595.
(420) Würthner, F.; Ahmed, S.; Thalacker, C.; Debaerdemaeker, T., *Chem. Eur. J.* **2002**, *8*, 4742-4750.
(421) Suraru, S.-L.; Würthner, F., *Angew. Chem. Int. Ed.* **2014**, *53*, 7428-7448.
(422) Thalacker, C.; Roeger, C.; Wuerthner, F., *J. Org. Chem.* **2006**, *71*, 8098-8105.
(423) Bell, T. D. M.; Yap, S.; Jani, C. H.; Bhosale, S. V.; Hofkens, J.; De, S. F. C.; Langford, S. J.; Ghiggino, K. P., *Chem. Asian J.* **2009**, *4*, 1542-1550.
(424) Barros, T. C.; Brochsztain, S.; Toscano, V. G.; Filho, P. B.; Politi, M. J., *J. Photochem. Photobiol. A* **1997**, *111*, 97-104.
(425) Pandeeswar, M.; Govindaraju, T., *RSC Adv.* **2013**, *3*, 11459-11462.
(426) Piguet, C.; Bernardinelli, G.; Hopfgartner, G., *Chem. Rev.* **1997**, *97*, 2005-2062.
(427) Lehn, J. M.; Rigault, A.; Siegel, J.; Harrowfield, J.; Chevrier, B.; Moras, D., *Proc. Natl. Acad. Sci.* **1987**, *84*, 2565.
(428) Mamula, O.; von Zelewsky, A., *Coord. Chem. Rev.* **2003**, *242*, 87-95.
(429) Yashima, E.; Maeda, K.; Iida, H.; Furusho, Y.; Nagai, K., *Chem. Rev.* **2009**, *109*, 6102-6211.
(430) Leininger, S.; Olenyuk, B.; Stang, P. J., *Chem. Rev.* **2000**, *100*, 853-908.
(431) Yashima, E.; Ousaka, N.; Taura, D.; Shimomura, K.; Ikai, T.; Maeda, K., *Chem. Rev.* **2016**, *116*, 13752-13990.
(432) McMorran, D. A.; Steel, P. J., *Angew. Chem. Int. Ed.* **1998**, *37*, 3295-3297.
(433) Cui, F.; Li, S.; Jia, C.; Mathieson, J. S.; Cronin, L.; Yang, X.-J.; Wu, B., *Inorg. Chem.* **2012**, *51*, 179-187.
(434) Carina, R. F.; Williams, A. F.; Piguet, C., *Helv. Chim. Acta* **1998**, *81*, 548-557.
(435) He, C.; Zhao, Y.; Guo, D.; Lin, Z.; Duan, C., *Eur. J. Inorg.* **2007**, *2007*, 3451-3463.
(436) Albrecht, M.; Kolita, S., *Angew. Chem. Int. Ed. Engl.* **1995**, *34*, 2134.
(437) Bhattacharyya, A.; Ghosh, B. N.; Herrero, S.; Rissanen, K.; Jimenez-Aparicio, R.; Chattopadhyay, S., *Dalton Trans.* **2015**, *44*, 493-497.
(438) Zhang, T.; Huang, H.-Q.; Cheng, X.-Y.; Guo, D.; Mei, H.-X.; Huang, R.-B.; Zheng, L.-S., *CrystEngComm* **2016**, *18*, 670-673.
(439) Sun, Q.; Bai, Y.; He, G.; Duan, C.; Lin, Z.; Meng, Q., *Chem. Commun.* **2006**, 2777-2779.
(440) Wu, D.; Huang, P.; Shui, Y.; Wu, G., *Inorg. Chem. Commun.* **2013**, *29*, 205-209.
(441) Baum, G.; Constable, E. C.; Fenske, D.; Housecroft, C. E.; Kulke, T., *Chem. Eur. J.* **1999**, *5*, 1862-1873.
(442) Chen, L.; Kang, J.; Cui, H.; Wang, Y.; Liu, L.; Zhang, L.; Su, C. Y., *Dalton Trans* **2015**, *44*, 12180.
(443) Zhang, G.; Li, Q.; Proni, G., *Inorg. Chem. Commun.* **2014**, *40*, 47-50.
(444) Crowley, J. D.; Gavey, E. L., *Dalton Trans.* **2010**, *39*, 4035-4037.
(445) Sahoo, H. S.; Chand, D. K., *Dalton Trans.* **2010**, *39*, 7223-7225.
(446) Tripathy, D.; Pal, A. K.; Hanan, G. S.; Chand, D. K., *Dalton Trans.* **2012**, *41*, 11273-11275.
(447) Han, M.; Engelhard, D. M.; Clever, G. H., *Chem. Soc. Rev.* **2014**, *43*, 1848-1860.
(448) Wise, M. D.; Holstein, J. J.; Pattison, P.; Besnard, C.; Solari, E.; Scopelliti, R.; Bricogne, G.; Severin, K., *Chem. Sci.* **2015**, *6*, 1004-1010.
(449) Xuan, W.; Zhang, M.; Liu, Y.; Chen, Z.; Cui, Y., *J. Am. Chem. Soc.* **2012**, *134*, 6904-6907.
(450) Clever, G. H.; Kawamura, W.; Tashiro, S.; Shiro, M.; Shionoya, M., *Angew. Chem. Int. Ed.* **2012**, *51*, 2606-2609.
(451) Kishi, N.; Li, Z.; Yoza, K.; Akita, M.; Yoshizawa, M., *J. Am. Chem. Soc.* **2011**, *133*, 11438-11441.

(452) Zhou, L.-P.; Sun, Q.-F., *Chem. Commun.* **2015**, *51*, 16767-16770.
(453) Hubert, A. J.; Noels, A. F.; Anciaux, A. J.; Teyssie, P., *Synthesis* **1976**, 600-602.
(454) Hansen, J.; Davies, H. M. L., *Coord. Chem. Rev.* **2008**, *252*, 545-555.
(455) Werle, C.; Goddard, R.; Philipps, P.; Fares, C.; Fuerstner, A., *Angew. Chem. Int. Ed.* **2016**, *55*, 10760-10765.
(456) Adly, F. G.; Gardiner, M. G.; Ghanem, A., *Chem. Eur. J.* **2016**, *22*, 3447-3461.
(457) Mueller, P.; Ghanem, A., *Org. Lett.* **2004**, *6*, 4347-4350.
(458) Muller, P.; Allenbach, Y.; Robert, E., *Tetrahedron: Asymmetry* **2003**, *14*, 779-785.
(459) Lindsay, V. N. G.; Charette, A. B., *ACS Catal.* **2012**, *2*, 1221-1225.
(460) Aratani, T., *Pure Appl. Chem.* **1985**, *57*, 1839-44.
(461) Ghanem, A.; Gardiner, M. G.; Williamson, R. M.; Mueller, P., *Chem. Eur. J.* **2010**, *16*, 3291-3295.
(462) Lebel, H.; Marcoux, J.-F.; Molinaro, C.; Charette, A. B., *Chem. Rev.* **2003**, *103*, 977-1050.
(463) Brunner, H.; Kluschanzoff, H.; Wutz, K., *Bull. Soc. Chim. Belg.* **1989**, *98*, 63-72.
(464) Davies, H. M. L.; Hutcheson, D. K., *Tetrahedron Lett.* **1993**, *34*, 7243-7246.
(465) Ishitani, H.; Achiwa, K., *Synlett* **1997**, 781-782.
(466) Xu, Z.-H.; Zhu, S.-N.; Sun, X.-L.; Tang, Y.; Dai, L.-X., *Chem. Commun.* **2007**, 1960-1962.
(467) Dave, V.; Warnhoff, E. W., *Org. React.* **1970**, *18*, 217-401.
(468) Davies, H. M. L.; Antoulinakis, E. G., Intermolecular Metal-Catalyzed Carbenoid Cyclopropanations. In *Organic Reactions*, John Wiley & Sons, Inc.: 2004.
(469) Lindsay, V. N. G.; Lin, W.; Charette, A. B., *J. Am. Chem. Soc.* **2009**, *131*, 16383-16385.
(470) DeAngelis, A.; Dmitrenko, O.; Yap, G. P. A.; Fox, J. M., *J. Am. Chem. Soc.* **2009**, *131*, 7230-7231.
(471) Chuprakov, S.; Kwok, S. W.; Zhang, L.; Lercher, L.; Fokin, V. V., *J. Am. Chem. Soc.* **2009**, *131*, 18034-18035.
(472) Marcoux, D.; Azzi, S.; Charette, A. B., *J. Am. Chem. Soc.* **2009**, *131*, 6970-6972.
(473) Liu, Z.-M.; Liu, Y.; Zheng, S.-R.; Yu, Z.-Q.; Pan, M.; Su, C.-Y., *Inorg. Chem.* **2007**, *46*, 5814-5816.
(474) Yang, C. P.; Hsiao, S. H.; Hsieh, B. J., *J. Chin. Inst. Chem. Eng.* **1991**, *22*, 303-10.
(475) Alentiev, A. Y.; Loza, K. A.; Yampolskii, Y. P., *J. Membr. Sci.* **2000**, *167*, 91-106.
(476) Rogan, Y.; Malpass-Evans, R.; Carta, M.; Lee, M.; Jansen, J. C.; Bernardo, P.; Clarizia, G.; Tocci, E.; Friess, K.; Lanc, M.; McKeown, N. B., *J. Mater. Chem. A* **2014**, *2*, 4874-4877.
(477) Yoshida, N.; Oshio, H.; Ito, T., *J. Chem. Soc., Perkin Trans. 2* **2001**, 1674-1678.
(478) Yoshida, N.; Ito, N.; Ichikawa, K., *J. Chem. Soc., Perkin Trans. 2* **1997**, 2387-2392.
(479) Guo, H.; Yan, Y.; Wang, N.; Guo, X.; Zheng, G.; Qi, Y., *CrystEngComm* **2015**, *17*, 6512-6526.
(480) Guo, H.; Yan, Y.; Guo, X.; Zou, H.; Qi, Y.; Liu, C., *CrystEngComm* **2014**, *16*, 10245-10254.
(481) Plonka, A. M.; Banerjee, D.; Woerner, W. R.; Zhang, Z.; Li, J.; Parise, J. B., *Chem. Commun.* **2013**, *49*, 7055-7057.
(482) Shen, K.; Qin, L.; Zheng, H.-G., *Dalton Trans.* **2016**, *45*, 16205-16210.
(483) Liu, R.-T.; Hou, L.; Liu, B.; Zhang, Y.-N.; Wang, Y.-Y.; Shi, Q.-Z., *Inorg. Chim. Acta* **2011**, *366*, 53-61.
(484) Zhang, Q.-L.; Hu, P.; Zhao, Y.; Feng, G.-W.; Zhang, Y.-Q.; Zhu, B.-X.; Tao, Z., *J. Solid State Chem.* **2014**, *210*, 178-187.
(485) Qin, L.; Hu, J.-S.; Li, Y.-Z.; Zheng, H.-G., *Cryst. Growth Des.* **2012**, *12*, 403-413.
(486) Zhuang, W.-J.; Sun, C.-Y.; Jin, L.-P., *Polyhedron* **2007**, *26*, 1123-1132.
(487) Lian, F. Y.; Jiang, F. L.; Yuan, D. Q.; Chen, J. T.; Wu, M. Y.; Hong, M. C., *CrystEngComm* **2008**, *10*, 905-914.
(488) Ben-Haida, A.; Colquhoun, H. M.; Hodge, P.; Raftery, J.; White, A. J. P.; Williams, D. J., *Org. Biomol. Chem.* **2009**, *7*, 5229-5235.
(489) Colquhoun, H. M.; Lewis, D. F.; Hodge, P.; Ben-Haida, A.; Williams, D. J.; Baxter, I., *Macromolecules* **2002**, *35*, 6875-6882.
(490) Colquhoun, H. M.; Zhu, Z.; Williams, D. J., *Org. Lett.* **2001**, *3*, 4031-4034.

(491) Liaw, D.-J.; Hsu, P.-N.; Chen, W.-H.; Lin, S.-L., *Macromolecules* **2002**, *35*, 4669-4676.
(492) Cheng, S.-H.; Hsiao, S.-H.; Su, T.-H.; Liou, G.-S., *Macromolecules* **2005**, *38*, 307-316.
(493) Oishi, Y.; Ishida, M.; Kakimoto, M.; Imai, Y.; Kurosaki, T., *J. Polym. Sci., Part A: Polym. Chem.* **1992**, *30*, 1027-35.
(494) Rogan, Y.; Malpass-Evans, R.; Carta, M.; Lee, M.; Jansen, J. C.; Bernardo, P.; Clarizia, G.; Tocci, E.; Friess, K.; Lanc, M.; McKeown, N. B., *J. Mater. Chem. A* **2014**, *2*, 4874-4877.
(495) Ma, X.; Ghanem, B.; Salines, O.; Litwiller, E.; Pinnau, I., *ACS Macro Lett.* **2015**, *4*, 231-235.
(496) Buck, R. T.; Coe, D. M.; Drysdale, M. J.; Ferris, L.; Haigh, D.; Moody, C. J.; Pearson, N. D.; Sanghera, J. B., *Tetrahedron: Asymmetry* **2003**, *14*, 791-816.
(497) Garcia-Simon, C.; Gramage-Doria, R.; Raoufmoghaddam, S.; Parella, T.; Costas, M.; Ribas, X.; Reek, J. N. H., *J. Am. Chem. Soc.* **2015**, *137*, 2680-2687.
(498) Lindsay, V. N. G.; Nicolas, C.; Charette, A. B., *J. Am. Chem. Soc.* **2011**, *133*, 8972-8981.
(499) Davies, H. M. L.; Bruzinski, P.; Hutcheson, D. K.; Kong, N.; Fall, M. J., *J. Am. Chem. Soc.* **1996**, *118*, 6897-6907.
(500) Doyle, M. P.; Dorow, R. L.; Buhro, W. E.; Griffin, J. H.; Tamblyn, W. H.; Trudell, M. L., *Organometallics* **1984**, *3*, 44-52.
(501) Swiegers, G. F.; Malefetse, T. J., *Coord. Chem. Rev.* **2002**, *225*, 91-121.
(502) Eddaoudi, M.; Kim, J.; Wachter, J. B.; Chae, H. K.; O'Keeffe, M.; Yaghi, O. M., *J. Am. Chem. Soc.* **2001**, *123*, 4368-4369.
(503) Olenyuk, B.; Whiteford, J. A.; Fechtenkotter, A.; Stang, P. J., *Nature* **1999**, *398*, 796-799.
(504) Abrahams, B. F.; Egan, S. J.; Robson, R., *J. Am. Chem. Soc.* **1999**, *121*, 3535-3536.
(505) Ward, M. D., *Chem. Commun.* **2009**, *30*, 4487-4499.
(506) Fujita, D.; Ueda, Y.; Sato, S.; Yokoyama, H.; Mizuno, N.; Kumasaka, T.; Fujita, M., *Chem.* **2016**, *1*, 91-101.
(507) Yang, L.; Qin, S.; Su, X.; Yang, F.; You, J.; Hu, C.; Xie, R.; Lan, J., *Org. Biomol. Chem.* **2010**, *8*, 339-348.
(508) Zhao, C.; Toste, F. D.; Raymond, K. N.; Bergman, R. G., *J. Am. Chem. Soc.* **2014**, *136*, 14409-14412.
(509) Liu, T.; Liu, Y.; Xuan, W.; Cui, Y., *Angew. Chem. Int. Ed.* **2010**, *49*, 4121-4124.
(510) Faulkner, A. D.; Kaner, R. A.; AbdallahQasem, M. A.; Clarkson, G.; Fox, D. J.; Gurnani, P.; Howson, S. E.; Phillips, R. M.; Roper, D. I.; Simpson, D. H.; Scott, P., *Nat. Chem.* **2014**, *6*, 797-803.
(511) Reichel, F.; Clegg, J. K.; Gloe, K.; Gloe, K.; Weigand, J. J.; Reynolds, J. K.; Li, C.-G.; Aldrich-Wright, J. R.; Kepert, C. J.; Lindoy, L. F.; Yao, H.-C.; Li, F., *Inorg. Chem.* **2014**, *53*, 688-690.
(512) Turega, S.; Whitehead, M.; Hall, B. R.; Meijer, A. J. H. M.; Hunter, C. A.; Ward, M. D., *Inorg. Chem.* **2013**, *52*, 1122-1132.
(513) Alkordi, M. H.; Belof, J. L.; Rivera, E.; Wojtas, L.; Eddaoudi, M., *Chem. Sci.* **2011**, *2*, 1695-1705.
(514) Lang, J.-P.; Xu, Q.-F.; Chen, Z.-N.; Abrahams, B. F., *J. Am. Chem. Soc.* **2003**, *125*, 12682-12683.
(515) Riddell, I. A.; Smulders, M. M. J.; Clegg, J. K.; Hristova, Y. R.; Breiner, B.; Thoburn, J. D.; Nitschke, J. R., *Nat. Chem.* **2012**, *4*, 751-756.
(516) Kieffer, M.; Pilgrim, B. S.; Ronson, T. K.; Roberts, D. A.; Aleksanyan, M.; Nitschke, J. R., *J. Am. Chem. Soc.* **2016**, *138*, 6813-6821.
(517) Bilbeisi, R. A.; Ronson, T. K.; Nitschke, J. R., *Angew. Chem. Int. Ed.* **2013**, *52*, 9027-9030.
(518) Meng, W.; Ronson, T. K.; Clegg, J. K.; Nitschke, J. R., *Angew. Chem. Int. Ed.* **2013**, *52*, 1017-1021.
(519) Al-Rasbi, N. K.; Tidmarsh, I. S.; Argent, S. P.; Adams, H.; Harding, L. P.; Ward, M. D., *J. Am. Chem. Soc.* **2008**, *130*, 11641-11649.
(520) Stephenson, A.; Argent, S. P.; Riis-Johannessen, T.; Tidmarsh, I. S.; Ward, M. D., *J. Am. Chem. Soc.* **2011**, *133*, 858-870.
(521) Argent, S. P.; Adams, H.; Riis-Johannessen, T.; Jeffery, J. C.; Harding, L. P.; Ward, M. D., *J. Am. Chem. Soc.* **2006**, *128*, 72-73.

(522) Zheng, Y.-R.; Lan, W.-J.; Wang, M.; Cook, T. R.; Stang, P. J., *J. Am. Chem. Soc.* **2011**, *133*, 17045-17055.
(523) Ronson, T. K.; Fisher, J.; Harding, L. P.; Rizkallah, P. J.; Warren, J. E.; Hardie, M. J., *Nat. Chem.* **2009**, *1*, 212-216.
(524) Sun, Q.-F.; Sato, S.; Fujita, M., *Nat. Chem.* **2012**, *4*, 330-333.
(525) Zhu, H.-F.; Fan, J.; Okamura, T.-A.; Zhang, Z.-H.; Liu, G.-X.; Yu, K.-B.; Sun, W.-Y.; Ueyama, N., *Inorg. Chem.* **2006**, *45*, 3941-3948.
(526) Liu, Y.; Kravtsov, V. C.; Beauchamp, D. A.; Eubank, J. F.; Eddaoudi, M., *J. Am. Chem. Soc.* **2005**, *127*, 7266-7267.
(527) Liu, H.-K.; Tong, X., *Chem. Commun.* **2002**, 1316-1317.
(528) Moon, D.; Kang, S.; Park, J.; Lee, K.; John, R. P.; Won, H.; Seong, G. H.; Kim, Y. S.; Kim, G. H.; Rhee, H.; Lah, M. S., *J. Am. Chem. Soc.* **2006**, *128*, 3530-3531.
(529) He, C.; Lin, Z.; He, Z.; Duan, C.; Xu, C.; Wang, Z.; Yan, C., *Angew. Chem. Int. Ed.* **2008**, *47*, 877-881.
(530) Chen, Z.; Liu, X.; Wu, A.; Liang, Y.; Wang, X.; Liang, F., *RSC Adv.* **2016**, *6*, 9911-9915.
(531) Rizzuto, F. J.; Wu, W.-Y.; Ronson, T. K.; Nitschke, J. R., *Angew. Chem. Int. Ed.* **2016**, *55*, 7958-7962.
(532) Guo, J.; Xu, Y.-W.; Li, K.; Xiao, L.-M.; Chen, S.; Wu, K.; Chen, X.-D.; Fan, Y.-Z.; Liu, J.-M.; Su, C.-Y., *Angew. Chem. Int. Ed.* **2017**, *56*, 3852-3856.
(533) Chifotides, H. T.; Giles, I. D.; Dunbar, K. R., *J. Am. Chem. Soc.* **2013**, *135*, 3039-3055.
(534) Spek, A. L., *Acta Crystallogr. Sect.D* **2009**, *65*, 148–155.
(535) Thommes, M.; Kaneko, K.; Neimark, A. V.; Olivier, J. P.; Rodriguez-Reinoso, F.; Rouquerol, J.; Sing, K. S. W., *Pure Appl. Chem.* **2015**, *87*, 1051-1069.
(536) Chowdhury, P.; Mekala, S.; Dreisbach, F.; Gumma, S., *Microporous Mesoporous Mater.* **2012**, *152*, 246-252.
(537) Guha, S.; Saha, S., *J. Am. Chem. Soc.* **2010**, *132*, 17674-17677.
(538) Hu, C.; Gao, Y.; Du, W., *Chem Biol Drug Des* **2016**, *87*, 673-679.
(539) Vincent, A.; Deschamps, D.; Martzel, T.; Lohier, J.-F.; Richards, C. J.; Gaumont, A.-C.; Perrio, S., *J. Org. Chem.* **2016**, *81*, 3961-3966.
(540) http://webbook.nist.gov/chemistry/fluid/.
(541) Czepirski, L.; JagieŁŁo, J., *Chem. Eng. Sci.* **1989**, *44*, 797-801.
(542) Cox, R. P.; Higginbotham, H. F.; Graystone, B. A.; Sandanayake, S.; Langford, S. J.; Bell, T. D. M., *Chem. Phys. Lett.* **2012**, *521*, 59-63.
(543) CrysAlisPro. In *CrysAlisPro v 1.171.38.43d*, ed.; Rigaku Oxford Diffraction: Yarnton, England, 2015.
(544) Bruker *SAINT*, Bruker AXS Inc: Madison, Wisconsin, USA, 2001.
(545) Cowieson, N. P.; Aragao, D.; Clift, M.; Ericsson, D. J.; Gee, C.; Harrop, S. J.; Mudie, N.; Panjikar, S.; Price, J. R.; Riboldi-Tunnicliffe, A.; Williamson, R.; Caradoc-Davies, T., *J. Synchrotron Rad.* **2015**, *22*, 187-190.
(546) McPhillips, T. M.; McPhillips, S. E.; Chiu, H. J.; Cohen, A. E.; Deacon, A. M.; Ellis, P. J.; Garman, E.; Gonzalex, A.; Sauter, N. K.; Phizackerley, R. P.; Soltis, S. M.; Kuhn, P., *J. Synchrotron Rad.* **2002**, *9*, 401-406.
(547) Kabsch, W., *Acta Crystallogr., Sect. D: Biol. Crystallogr.* **2010**, *66*, 125-132.
(548) Sheldrick, G. M., *Acta Crystallogr., Sect. A: Found Crystallogr.* **2015**, *71*, 3-8.
(549) Sheldrick, G. M., *Acta Crystallogr., Sect. A: Found. Crystallogr.* **2008**, *64*, 112-122.
(550) Sheldrick, G. M., *Acta Crystallogr., Sect. A: Found. Crystallogr.* **2008**, *64*, 112-122.
(551) Dolomanov, O. V.; Bourhis, L. J.; Gildea, R. J.; Howard, J. A. K.; Puschmann, H., *J. Appl. Cryst.* **2009**, *42*, 339-341.

ChemComm

COMMUNICATION

View Article Online
View Journal

Published on 25 September 2015. Downloaded by Monash University on 07/10/2015 11:13:15.

Cite this: DOI: 10.1039/c5cc07422c

Received 4th September 2015,
Accepted 25th September 2015

DOI: 10.1039/c5cc07422c

www.rsc.org/chemcomm

Self-selecting homochiral quadruple-stranded helicates and control of supramolecular chirality†

Stephanie A. Boer and David R. Turner*

Enantiomeric M_4L_4 helical cages have been prepared whose supramolecular chirality is induced by the chemical chirality of the self-sorting amino acid-derived ligands that are used. Using scrambled diastereomeric ligands or achiral glycine-derived ligands yields analogous complexes yet 'turns off' the supramolecular chirality by producing centrosymmetric cages.

In the past few decades the field of supramolecular coordination container complexes has attracted considerable attention due to the potential applications of these materials in a wide variety of fields, particularly as reaction vessels, selective host species and in the stabilisation of reactive molecules.[1] The synthesis of cage complexes under self-assembly conditions from simple components can be achieved with a semblance of predictability using coordination bonds by combining multiple bridging ligands, with the coordinating groups appropriately positioned to promote a discrete structure, with metals of appropriate coordination preferences.[2]

The incorporation of chirality into coordination cages imparts the potential for applications in enantioselective processes such as sensing,[3] catalysis[4] and separation.[5] It is possible to incorporate chirality into coordination cages by spontaneous resolution using achiral ligands by generating chiral centres around tris(chelate) metal centres which may interconvert in solution.[6] However, from both of these strategies the challenge then arises of forming the complexes in an enantiomerically pure form. A more reliable method for the synthesis of chiral coordination cages is the use of enantiomerically pure ligands. A variety of strategies have been adopted, including appending chiral groups to the exterior or interior of ligands known to form cages, effectively adding chiral groups to achiral frames.[7] More recently, induction of supramolecular chirality has been achieved by the use of enantiopure ligands in tetrahedral architectures with the chirality of the ligand reflected in the handedness (Λ/Δ) around the metal centre.[8]

Chiral coordination cages can also be constructed in the form of helicates, typically generated as racemic mixtures, exploiting the presence of a twist within the ligands which imparts a helical sense in the complex.[9] The use of a chiral ligand will ensure the formation of a helicate, while the use of achiral ligands can form either helicates or mesocates.[10] A convenient synthetic route for the formation of chiral ligands is the incorporation of amino acids. Recently enantiomeric homochiral, quadruple-stranded helicate using amino acid-derived ligands with a bicyclooctene core were reported,[11] and control of chirality in tetrahedral cages by virtue of the ligands is known.[12]

Herein we report homochiral helicates and analogous mesocates constructed using 3,3′,4,4′-biphenylsulfonediimides (BPSD) substituted with amino acids. The chiral M_4L_4 cages have supramolecular homochirality based on the handedness of the ligands employed. Reaction of a D/L ligand mixture results in the self-selective formation of the enantiomeric cages.

We have previously reported naphthalene- and perylene-diimides appended with amino acids that have been incorporated into homochiral coordination polymers with interesting interpenetration topologies including two materials capable of enantiomeric resolution of small analytes.[13] Whilst the planar aromatic core groups lent themselves to the formation of extended networks we have more recently turned our attention to non-planar core groups that are anticipated to form discrete cage complexes due to their internal angle, with the sulfone unit previously reported to be amenable.[9d]

The enantiopure dicarboxylic acids L-H_2LeuBPSD and D-H_2LeuBPSD were synthesised from 3,3′4,4′-biphenylsulfone-tetracarboxylic dianhydride and the respective leucine isomer under microwave irradiation in acetic acid (Fig. 1). The achiral glycine analogue, H_2GlyBPSD, was synthesised by a similar route under reflux in DMF (see ESI†).

Reaction of enantiopure L-H_2LeuBPSD or D-H_2LeuBPSD with copper nitrate in methanol/dimethylacetamide and a small amount of triethylamine yields crystalline material containing the helical cages $[Cu_4(LeuBPSD)_4(Solv.)_4]$, **1** (Fig. 1, see ESI,†

School of Chemistry, Monash University, Clayton, VIC 3800, Australia.
E-mail: david.turner@monash.edu

† Electronic supplementary information (ESI) available: Full experimental details and synthetic procedures. CCDC 1422157–1422162. For ESI and crystallographic data in CIF or other electronic format see DOI: 10.1039/c5cc07422c

Published on 25 September 2015. Downloaded by Monash University on 07/10/2015 11:13:15.

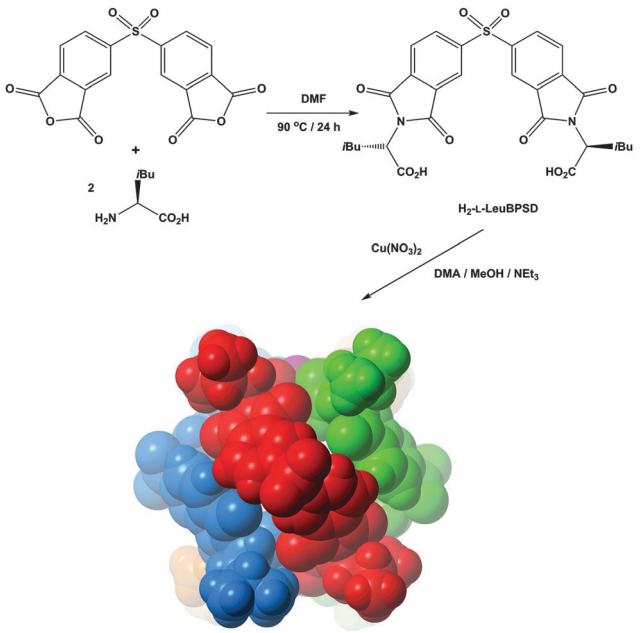

Fig. 1 A representative synthesis of the L-leucine derived ligand (L-H_2LeuBPSD) and the helicate cage [Cu_4(L-LeuBPSD)$_4$], *Λ*-**1** (coordinated solvent displayed only by the donor atom for clarity).

for full experimental details).‡ Structural determination by single-crystal X-ray diffraction reveals that the two materials are enantiomers of each other with both crystallising in the non-centrosymmetric space group *P*1 (only the L-LeuBPSD derivative is discussed here).

Crystals of [Cu_4(L-LeuBPSD)$_4$(OH_2)$_4$], *Λ*-[**1**(H_2O)$_4$], contain one complex in the asymmetric unit alongside partially-ordered non-coordinated solvent. The *Λ*-**1** cage contains {$Cu_2(O_2C)_4$} paddle-wheel motifs at either end of the helical complex, connected by the four L-LeuBPSD ligands, with aqua ligands coordinated to both the inner- and outer-facing apical sites of the paddlewheel. The internal Cu^{II} atoms are separated by 7.2 Å with an internal volume of *ca.* 300 Å^3 in the absence of coordinating solvent. When viewed along the vector passing through the four copper atoms the paddlewheel motifs have a negligible rotational offset with regards to each other. The ligands do not bridge between sites on the paddlewheels that lie immediately above/below, rather they bridge between sites related by a torsion angle of *ca.* 90° generating a helical sense around the central Cu_4 rotation axis of the complex.

The arrangement of four leucine residues around the paddle-wheel motif is such that the substituents must form a propeller motif thereby inducing helicity, presumably driven in part by the relative steric bulk of the substituents (Fig. 2A). The helicity of the cages containing L- and D-leucine is *Λ* and *Δ*, respectively. These complexes demonstrate that supramolecular chirality, *viz.* the directionality of the helix, can be induced by the molecular chirality of the ligands used forcing a preferred geometry around the coordination sites. Circular dichroism (CD) conducted on acetonitrile solutions of *Λ*-**1** and *Δ*-**1** show opposing Cotton effects that are slightly shifted and greatly enhanced compared to the spectra for the ligands alone indicating that the cages persist in solution (Fig. 3). The solution stability of the cages is also observed by the presence of *m*/*z* peaks corresponding to [**1** + H]$^+$ and [**1** + Na]$^+$ in the ESI-MS spectra (see ESI†) although no peaks are observed in which solvent is associated.

The coordinated solvent is difficult to assign crystallographically, due to apparent rotational disorder along the Cu–O bond and/or disorder of the nature of the solvent within individual cages, and is not observed by mass spectrometry. In the X-ray structure of *Λ*-**1** the coordinated solvents all appear to be water, whilst in the structure of *Δ*-**1** the solvent is best modelled as four methanol molecules. A serendipitous crystalline sample was obtained from a d_6-DMSO solution of *Λ*-[**1**(OH_2)$_4$] and subsequently replicated on a larger scale (see ESI†). This material was found to contain the complex [Cu_4(L-LeuBPSD)$_4$(DMSO)$_2$(OH_2)$_2$] with the DMSO ligands coordinated on the interior of the cages, thereby demonstrating that the solvent within the cages can be exchanged in solution. Crystallography reveals that there are areas of diffuse electron density, *i.e.* guest solvent, within the cages that cannot be resolved (except in the case of compound **3**, *vide infra*).

In order to explore the supramolecular self-selectivity of the *Λ*-**1** and *Δ*-**1** complexes, a reaction of a 50 : 50 mixture of L-H_2LeuBPSD and D-H_2LeuBPSD with copper nitrate was conducted. As with the individual reactions, a crystalline material was able to be isolated and structurally characterised. Analysis of the X-ray diffraction data revealed the crystals to be centrosymmetric (space group *C*2/*c*) with the asymmetric unit containing one cage complex in which all of the amino acid groups are of the same handedness (Fig. 2B). The enantiomeric ligands only form complexes with ligands of like handedness, demonstrating that the mixed-ligand system displays narcissistic self-selection to form the helical complexes.§ Powder X-ray diffraction (PXRD) reveals that the bulk material comprises both the centrosymmetric crystals containing *Λ*-**1**/*Δ*-**1** and chiral crystals of pure *Λ*-**1** and *Δ*-**1** (see ESI†). Circular dichroism of the bulk solid dissolved in acetonitrile shows a small Cotton effect indicating a slight excess of *Δ*-**1**. A CD spectrum taken of the reaction solution soon after mixing and on one isolated crystal shows the expected lack of response, suggesting that the response observed from the bulk solid is likely due to a seeding effect in the bulk sample during crystallisation.

The control of supramolecular chirality by the handedness of the ligand prompted exploration of analogous systems in which the chirality is removed in one of two ways. Firstly the chirality can be removed by using an achiral ligand, H_2GlyBPSD, derived from glycine rather than a chiral amino acid. Secondly a racemic ligand, *rac*-H_2LeuBPSD, in which the terminal groups are of opposite handedness, can be used.

rac-H_2LeuBPSD was prepared by reacting a 50 : 50 mixture of D- and L-leucine with 3,3′4,4′-biphenylsulfonetetracarboxylic dianhydride which is expected to yield a statistical mixture of the *R*,*R*-, *S*,*S*-, and *R*,*S*-substituted isomers (1 : 1 : 2). Given the statistical prevalence of the desired *R*,*S* isomer (DL-H_2LeuBPSD) the racemic dicarboxylic acid was reacted without purification with $Cu(NO_3)_2$ to form a crystalline material under analogous conditions to the enantiomerically pure *Λ*-**1** and *Δ*-**1**. Single crystal X-ray diffraction allowed structural characterisation of the achiral complex [Cu_4(DL-LeuBPSD)$_4$(MeOH)$_2$(OH_2)$_2$] (**2**) with PXRD showing the that other possible products (*viz.* the enantiopure complexes *Λ*-**1**

Published on 25 September 2015. Downloaded by Monash University on 07/10/2015 11:13:15.

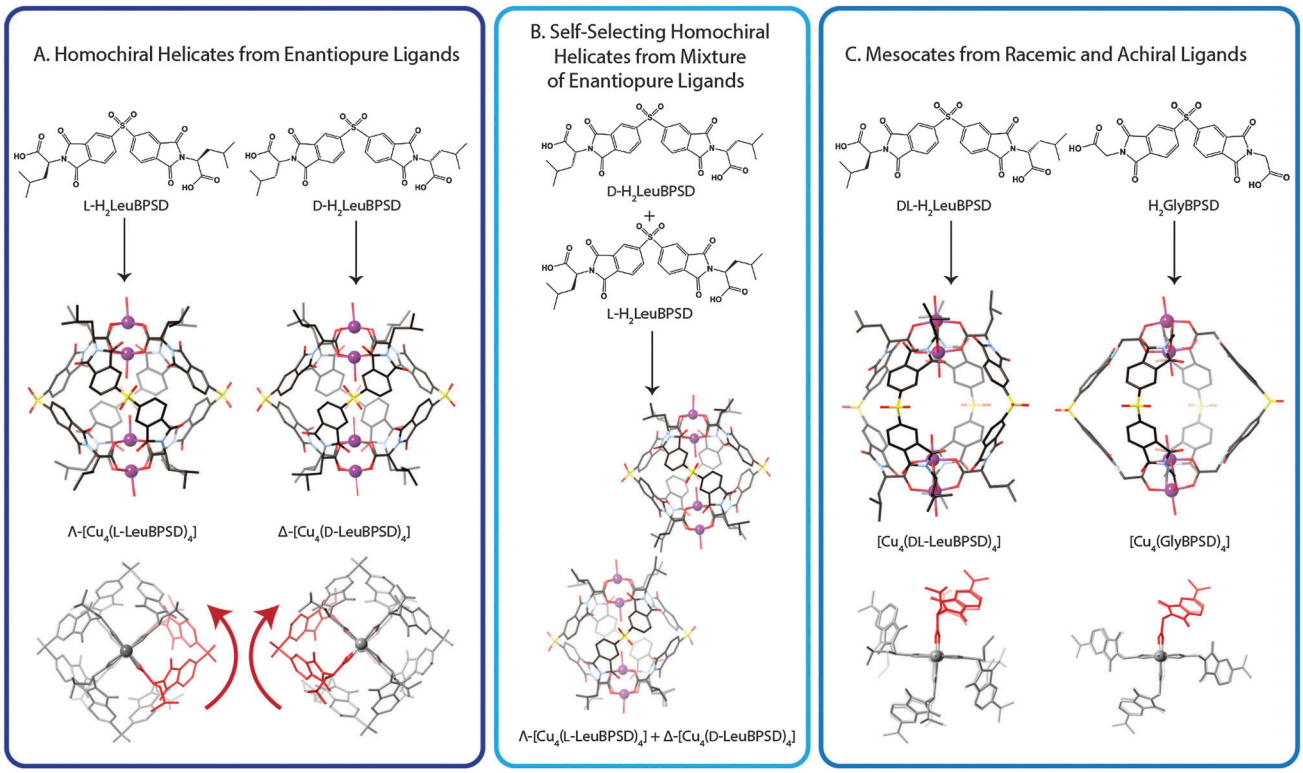

Fig. 2 The chirality at the stereocentres in the ligands determines the supramolecular chirality (*i.e.* helicity) of the complex formed. (A) The use of enantiomerically pure ligands, D-H_2LeuBPSD and L-H_2LeuBPSD, exclusively yields *Δ*- and *Λ*-helical complexes, respectively. (B) 'Self-selection' occurs from a mixture of D-H_2LeuBPSD and L-H_2LeuBPSD to form the helical complexes rather than a mixed-ligand analogue. (C) Analogous centrosymmetric capsules can be formed by using the achiral ligand H_2-GlyBPSD or by using the DL-H_2LeuBPSD ligand (containing mixed D- and L-leucine terminal groups) with helicate formation prevented in the absence of enantiopure ligands.

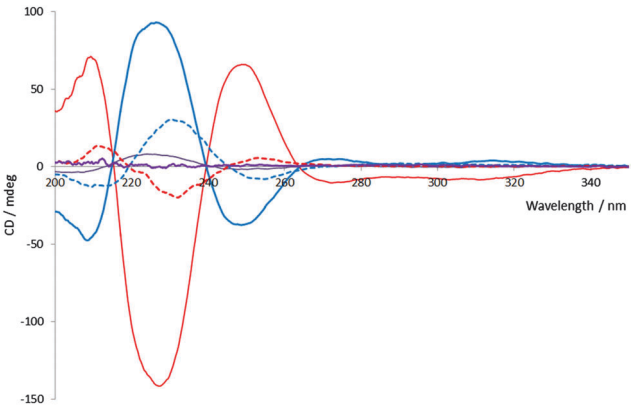

Fig. 3 Circular dichroism spectra for *Λ*-**1** (solid red); L-H_2LeuBPSD (dashed red); *Δ*-**1** (solid blue); D-H_2LeuBPSD (dashed blue); bulk *Λ*-**1**/*Δ*-**1** product (grey); *Λ*-**1**/*Δ*-**1** single crystal (purple).

and *Δ*-**1** in both their homochiral and centrosymmetric co-crystalline forms) were also present in the bulk as expected using a mixture of ligands in the synthesis (see ESI†). Complex **2** crystallises in the centrosymmetric setting $P\bar{1}$ with half of the complex in the asymmetric unit. Complex **2** is analogous to **1**, with copper paddlewheels bridged by four DL-LeuBPSD dicarboxylate ligands (Fig. 2C). The ligands are arranged such that one of the paddlewheels is exclusively coordinated to the *R* terminal groups and the other exclusively by *S* terminal groups with these coordination environments therefore being identical to those in **1** and further demonstrating the self-selection of the enantiomers. Due to the orientation that is required at each paddlewheel the ligands cannot be oriented in a helical arrangement and instead bridge between coordination sites on the paddlewheels that are directly in line with each other. The difference in geometry leads to the interior of the capsule being elongated compared *Λ*-**1** and *Δ*-**1** with an internal Cu···Cu distance of 9.0 Å (*cf.* 7.2 Å).

Using the achiral H_2GlyBPSD ligand the complex $[Cu_4(GlyBPSD)_4(MeOH)_3(OH_2)]$ (**3**) was isolated as a phase-pure crystalline material (Fig. 2C). The cage is very similar in structure to **2** with a non-helical arrangement of ligands between the two paddlewheels. Although there are no stereocentres in the ligand the arrangement around one paddlewheel is such that the imide groups are orientated in a similar propeller motif, presumably due to the steric requirements of the ligand. These propeller motifs are of opposite directions at each end of the centrosymmetric cage and therefore the overall arrangement is analogous to **2**. The internal Cu···Cu distance in **3** is slightly larger than in **2** (9.3 Å *vs.* 9.0 Å) due to a subtle difference in the arrangement of the ligands. In **2** the ligands are approximately evenly spaced around the central Cu_4 axis as can be seen in the N···N separations between neighbouring imide groups which lies in the range 6.2–6.9 Å.

Published on 25 September 2015. Downloaded by Monash University on 07/10/2015 11:13:15.

In **3** the complex is 'pinched' in one direction with two N···N distances of 6.0 Å and two of 7.1 Å demonstrating that these cages have some flexibility. The crystal structure of **3** also reveals well-ordered, partial occupancy dimethylacetamide within the cage with two positions partially protruding through the larger windows in the side of the cage.

In conclusion, we have demonstrated that the supramolecular chirality of cage complexes can be controlled by the helical sense imparted through the use of enantiopure dicarboxylate ligands surrounding copper paddlewheel motifs. The two enantiomeric ligands display self-selection when simultaneously reacted with $Cu(NO_3)_2$ to form *Λ*- and *Δ*-helical cages. Using the *R*,*S* analogue of the LeuBPSD ligand gives a centrosymmetric cage in which a degree of self-selectivity is retained with each paddlewheel exclusively bound to either the *R* or the *S* terminal group is a complex that closely resembles that containing the achiral GlyBPSD ligand. These complexes demonstrate that the supramolecular chirality of cages can be controlled by stereocentres around paddlewheel motifs thereby offering new synthetic routes to enantiopure container species.

DRT acknowledges the Australian Research Council for a Future Fellowship (FT120100300). Part of this work was undertaken on the MX1 beamline at the Australian Synchrotron, Victoria, Australia.[14]

Notes and references

‡ The cages all crystallise with coordinated and non-coordinated solvent which differs between complexes/structures (see ESI,† for full details).
§ We note that although the term 'narcissistic self-sorting' is often used in the literature, the phrase suffers in this instance when referring to enantiomeric ligands as narcissus fell in love with his reflection which, by definition, would have been of the opposite handedness.

1 (*a*) T. R. Cook and P. J. Stang, *Chem. Rev.*, 2015, **115**, 7001–7045; (*b*) M. M. J. Smulders, I. A. Riddell, C. Browne and J. R. Nitschke, *Chem. Soc. Rev.*, 2013, **42**, 1728; (*c*) H. Amouri, C. Desmarets and J. Moussa, *Chem. Rev.*, 2012, **112**, 2015; (*d*) D. R. Turner, A. Pastor, M. Alajarín and J. W. Steed, *Struct. Bonding*, 2004, **108**, 97.
2 (*a*) M. D. Ward, *Chem. Commun.*, 2009, 4487; (*b*) J. Bunzen, J. Iwasa, P. Bonakdarzadeh, E. Numata, K. Rissanen, S. Sato and M. Fujita, *Angew. Chem., Int. Ed.*, 2012, **51**, 3161; (*c*) S. Mukherjee and P. S. Mukherjee, *Chem. Commun.*, 2014, **50**, 2239; (*d*) T. R. Cook, Y.-R. Zheng and P. J. Stang, *Chem. Rev.*, 2013, **113**, 734; (*e*) T. K. Ronson, S. Zarra, S. P. Black and J. R. Nitschke, *Chem. Commun.*, 2013, **49**, 2476; (*f*) N. L. Netzer, F.-R. Dai, Z. Wang and C. Jiang, *Angew. Chem., Int. Ed.*, 2014, **53**, 10965; (*g*) J. J. Yang, M. Bhadbhade, W. A. Donald, H. Iranmanesh, E. G. Moore, H. Yan and J. E. Beves, *Chem. Commun.*, 2015, **51**, 4465.
3 J. Dong, Y. Zhou, F. Zhang and Y. Cui, *Chem. – Eur. J.*, 2014, **20**, 6455.
4 (*a*) C. Garcia-Simon, R. Gramage-Doria, S. Raoufmoghaddam, T. Parella, M. Costas, X. Ribas and J. N. H. Reek, *J. Am. Chem. Soc.*, 2015, **137**, 2680; (*b*) S. J. Lee, S.-H. Cho, K. L. Mulfort, D. M. Tiede, J. T. Hupp and S. T. Nguyen, *J. Am. Chem. Soc.*, 2008, **130**, 16828; (*c*) T. Murase, S. Peschard, S. Horiuchi, Y. Nishioka and M. Fujita, *Supramol. Chem.*, 2011, **23**, 199.
5 D. Fiedler, D. H. Leung, R. G. Bergman and K. N. Raymond, *J. Am. Chem. Soc.*, 2004, **126**, 3674.
6 (*a*) D. Fiedler, D. H. Leung, R. G. Bergman and K. N. Raymond, *J. Am. Chem. Soc.*, 2004, **126**, 3674; (*b*) A. M. Castilla, W. J. Ramsay and J. R. Nitschke, *Chem. Lett.*, 2014, **43**, 256.
7 (*a*) M. Schweiger, S. R. Seidel, M. Schmitz and P. J. Stang, *Org. Lett.*, 2000, **2**, 1255; (*b*) M. Ikemi, T. Kikuchi, S. Matsumura, K. Shiba, S. Sato and M. Fujita, *Chem. Sci.*, 2010, **1**, 68.
8 (*a*) S. P. Argent, T. Riis-Johannessen, J. C. Jeffery, L. P. Harding and M. D. Ward, *Chem. Commun.*, 2005, 4647; (*b*) M. Albrecht, S. Burk and P. Weis, *Synthesis*, 2008, 2963; (*c*) A. M. Castilla, N. Ousaka, R. A. Bilbeisi, E. Valeri, T. K. Ronson and J. R. Nitschke, *J. Am. Chem. Soc.*, 2013, **135**, 17999; (*d*) N. Ousaka, J. K. Clegg and J. R. Nitschke, *Angew. Chem., Int. Ed.*, 2012, **51**, 1464; (*e*) T. Liu, Y. Liu, W. Xuan and Y. Cui, *Angew. Chem., Int. Ed.*, 2010, **49**, 4121.
9 (*a*) C. Piguet, G. Bernardinelli and G. Hopfgartner, *Chem. Rev.*, 1997, **97**, 2005; (*b*) S. Goetz and P. E. Kruger, *Dalton Trans.*, 2006, 1277; (*c*) Z. Zhang and D. Dolphin, *Chem. Commun.*, 2009, 6931; (*d*) W. Xuan, M. Zhang, Y. Liu, Z. Chen and Y. Cui, *J. Am. Chem. Soc.*, 2012, **134**, 6904.
10 (*a*) M. Scherer, D. L. Caulder, D. W. Johnson and K. N. Raymond, *Angew. Chem., Int. Ed.*, 1999, **38**, 1588; (*b*) D. Wu, P. Huang, Y. Shui and G. Wu, *Inorg. Chem. Commun.*, 2013, **29**, 205; (*c*) F. Cui, S. Li, C. Jia, J. S. Mathieson, L. Cronin, X. J. Yang and B. Wu, *Inorg. Chem.*, 2012, **51**, 179; (*d*) J. Xu, T. N. Parac and K. N. Raymond, *Angew. Chem., Int. Ed.*, 1999, **38**, 2878.
11 L. Chen, J. Kang, H. Cui, Y. Wang, L. Liu, L. Zhang and C. Y. Su, *Dalton Trans.*, 2015, **44**, 12180.
12 (*a*) S. P. Argent, T. Riis-Johannessen, J. C. Jeffery, L. P. Harding and M. D. Ward, *Chem. Commun.*, 2005, 4647; (*b*) M. Albrecht, S. Burk and P. Weis, *Synthesis*, 2007, 2963; (*c*) T. Liu, Y. Liu, W. Xuan and Y. Cui, *Angew. Chem., Int. Ed.*, 2010, **49**, 4121; (*d*) N. Ousaka, J. K. Clegg and J. R. Nitschke, *Angew. Chem., Int. Ed.*, 2012, **51**, 1464.
13 (*a*) S. A. Boer, Y. Nolvachai, C. Kulsing, L. J. McCormick, C. S. Hawes, P. J. Marriott and D. R. Turner, *Chem. – Eur. J.*, 2014, **20**, 11308–11312; (*b*) S. A. Boer, C. S. Hawes and D. R. Turner, *Chem. Commun.*, 2014, **50**, 1125–1127; (*c*) L. J. McCormick and D. R. Turner, *CrystEngComm*, 2013, **15**, 8234–8236.
14 N. P. Cowieson, D. Aragao, M. Clift, D. J. Ericsson, C. Gee, S. J. Harrop, N. Mudie, S. Panjikar, J. R. Price, A. Riboldi-Tunnicliffe, R. Williamson and T. Caradoc-Davies, *J. Synchrotron Radiat.*, 2015, **22**, 187.

 This journal is © The Royal Society of Chemistry 2015

CRYSTAL GROWTH & DESIGN

Article

pubs.acs.org/crystal

Interpenetration in π-Rich Mixed-Ligand Coordination Polymers

Stephanie A. Boer and David R. Turner*

School of Chemistry, Monash University, Clayton, VIC 3800, Australia

Supporting Information

ABSTRACT: Structural and chemical influences on interpenetration have been investigated through the preparation and structural analysis of a series of seven chiral coordination polymers using a phenylalanine-substituted naphthalenediimide ligand (H_2PheNDI). The reaction of H_2PheNDI with Mn^{II} or Cd^{II} and a range of linear dipyridyl-based coligands forms a series of coordination polymers which vary greatly in terms of their topologies and interpenetration while largely retaining a common metallomacrocyclic motif. The metallomacrocyclic motif is found in a tube-like 1D coordination polymer *poly*-[Cd(bipy)(OH_2)(PheNDI)] (**2**) and a closely related 2D polythreaded network *poly*-{[Cd_2(bipy)$_2$(PheNDI)$_2$][Cd(bipy)(DMF)$_{1.5}$(NO_3)$_2$(OH_2)$_{0.5}$]} (**3**) which are synthesized as pure phases under slightly different conditions. The longer 1,2-di(4-pyridyl)ethylene (dpe) ligand gives rise to a 2D coordination polymer *poly*-[Cd_4(DMF)(dpe)$_4$(OH_2)$_2$(PheNDI)$_4$] (**5**) in which the metallomacrocycles are connected only "sideways" rather than as a tube. This difference allows for 2-fold 2D → 2D interpenetration, between two crystallographically distinct sheets, whereby the dpe passes through the metallomacrocycle, assisted by face-to-face aromatic interactions. The use of a larger dipyridyl ligand, *N*,*N*′-bis(4-pyridyl)naphthalenediimide (4pyNDI), yielded 3D coordination polymers with distorted pcu topologies of the form *poly*-[M_2(PheNDI)$_2$(4PyNDI)$_2$] (M = Cd, **6**; Mn, **7**) which contain neither the metallomacrocyclic motif nor interpenetration.

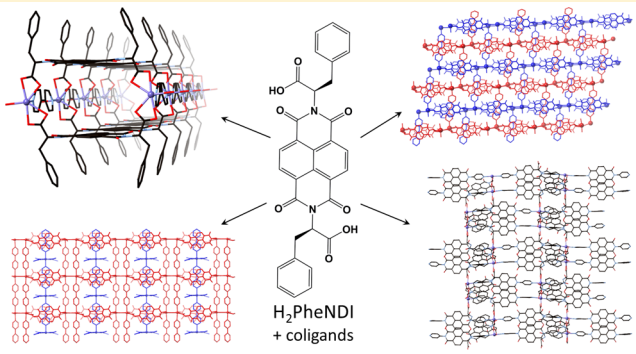

INTRODUCTION

The design and synthesis of coordination polymers is a burgeoning field, particularly investigations into the reproducibility and predictability of supramolecular features within their structures.[1] Coordination polymers are an important area of research due to their many applications including catalysis,[2−4] gas storage,[5−7] and separation.[8−10] The structures of coordination polymers are influenced by numerous weak interactions, making them very difficult to predict.[11,12] The ligand size, shape, and functionality and the metal ion, as well as the synthetic conditions including the stoichiometric ratios of reagents, temperature, solvent, and time, are also all factors which influence the final structure of a coordination polymer.[13]

The design of coordination polymers involves not only design and selection of the components required to construct an isolated framework but also consideration of how the coordination polymers may pack in the solid state. In general, packing in the solid state by molecular species and by coordination polymers is in such a way as to maximize packing efficiency. Being essentially infinite networks, coordination polymers can pack efficiently through a number of interlocked or interwoven topologies.[14,15] The most commonly encountered mode of entanglement is interpenetration, in which two or more coordination polymers within a system are interlocked such that they are not chemically bonded together but cannot be broken without breaking chemical bonds, which can be considered as coordination polymers involving polycatenane or polyrotaxane motifs.[14,16,17] Other topologies include polythreading, which can be considered as an extended analogue of a molecular pseudo-rotaxane with a coordination polymer "thread" passing through a series of "loops" of a separate coordination polymer in the same system. Polyknotting is also possible, otherwise known as self-penetration, in which a single coordination polymer net contains rings through which another component of the same network passes.[17,18] The study into interpenetration and related phenomena, and understanding how these complex self-assembly processes can be designed and predicted, is of importance because of the influence they have on the properties of the coordination polymer materials.[19,20]

Investigation into supramolecular systems which display reproducible structural motifs is, therefore, a significant area of research, as these motifs provide some predictability in designing coordination polymers. The use of $\pi-\pi$ interactions to form reproducible supramolecular motifs such as catenanes or rotaxanes within coordination polymers is an area which has been much less explored than other supramolecular interactions.[21−24] Naphthalenediimides are a versatile class of molecules which have been extensively investigated. NDIs are electron-deficient, making them highly valuable in the field of n-type semiconductors and can also be functionalized to have

Received: June 14, 2016
Revised: September 15, 2016
Published: September 26, 2016

ACS Publications © 2016 American Chemical Society

DOI: 10.1021/acs.cgd.6b00901
Cryst. Growth Des. 2016, 16, 6294−6303

absorption bands within the entire visible spectrum.[25,26] Functionalization of NDIs with coordinating groups can also lend to NDIs being valuable ligands for synthesis of discrete and polymeric coordination compounds.[27−31]

Our previous work has concentrated on the synthesis of coordination polymers using a naphthalenediimide substituted at the imide position with either L-alanine or L-leucine.[32,33] The structures of these compounds showed a reproducible $\{Cd_2L_2\}$ metallomacrocyclic motif in which the planes of the aromatic cores of the two ligands that form the macrocycle are approximately 7 Å apart, ideal for face-to-face π-interactions of ∼3.5 Å with aromatic guests inside the metallomacrocycle. Previously reported *poly*-$[Cd_2(AlaNDI)_2(DMF)_4]$ is a 1D chain of metallomacrocycles connected by bimetallic nodes.[33] The chains are 1D → 2D interpenetrated by polycatenation of the metallomacrocycle motifs driven by π-interactions between the aromatic cores of the ligands. The bulkier side chain in *poly*-$[Cd_2(LeuNDI)_2(DMA)_4]$ maintained a 1D chain comprising metallomacrocycle motifs, yet displayed no interpenetration. However, the addition of a 4,4′-bipyridine (bipy) coligand formed 1D chains of *poly*-$[Cd_2(LeuNDI)_2(bipy)(DMF)_3(OH_2)]$ in which the metallomacrocycles are bridged by the bipy coligands which then pass through the metallomacrocycles of a different chain to form a 1D → 3D polyrotaxane.[32]

It is clear that there is significant influence of the amino acid side chain and the coligand on the structures of this family of coordination polymers and their ability to form interpenetrating architectures, necessitating further studies. Herein, we report the use of the phenylalanine-substituted naphthalenediimide ligand, H_2PheNDI, which introduces additional complexity to the system with the addition of more aromatic functionalization when used alone or in combination with coligands (Figure 1).

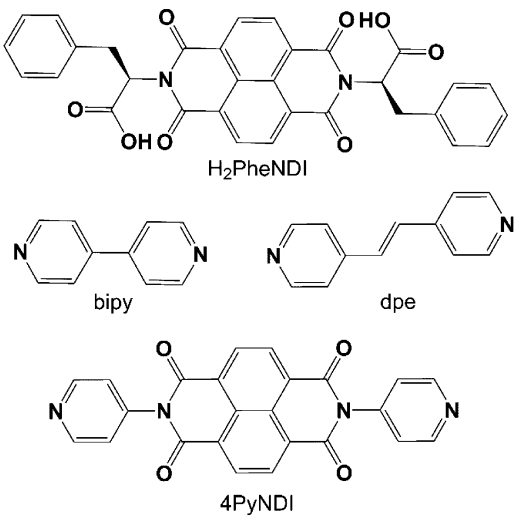

Figure 1. Phenylalanine-substituted naphthalenediimide ligand (H_2PheNDI) and the dipyridyl ligands utilized in this study.

■ EXPERIMENTAL DETAILS

Materials and Physical Measurements. All chemicals and reagents were obtained from commercial sources and used without purification. 4PyNDI was synthesized following a literature procedure.[34] Nuclear magnetic resonance spectra were collected using a Bruker DRX-400 spectrometer using residual solvent peaks as reference. ^{13}C NMR spectra were collected at 100 MHz, and ^{1}H NMR spectra were collected at 400 MHz. Resonances are reported in parts per million (ppm) and coupling constants, *J*, are reported in hertz (Hz). Low resolution mass spectrometry was performed using a Micromass Platform Electrospray mass spectrometer. Infrared spectra were obtained using an Agilent Cary 630 diamond attenuated total reflectance (ATR) spectrometer with MicroLab software used to process the data. Thermogravimetric analysis (TGA) was conducted using a Mettler TGA/DSC 1 instrument. The temperature was ramped at 5 °C/min to 400 °C under a N_2 supply of 10.0 mL/min, and the data were analyzed using the STARe system. Microanalyses were performed at the Science Centre, London Metropolitan University, U.K. Powder X-ray diffraction were collected on a Bruker D8 Focus diffractometer equipped with Cu−Kα radiation (λ = 1.5418 Å) at room temperature. The sample was mounted on a zero background silicon single crystal stage. Data were collected in the angle interval 2θ = 5−55° with a step size of 0.02°. The collected data were compared to predicted patterns based on low-temperature single crystal data. Fluorescence spectra were run on a Cary Eclipse Fluorescence Spectrophotometer. The crystals were ground in K-Y jelly and spread onto 150 μm coverslips and mounted inside the spectrophotometer. The emission was measured with the samples excited at 380 nm and scanned from 400 to 680 nm at 800 V with the excitation and emission slits at 10 mm. The fluorescence was also tested using a confocal microscope setup previously reported.[35] The sample was excited using a 375 nm pulsed diode laser driver (PicoQuant, PDL 800-D) and a 375 nm laser head (PicoQuant, LDH-P-C-375) at a repetition rate of 10 MHz. The light was focused onto the sample using a 40 × 1.00 N.A. oil immersion objective (Olympus). Light was passed through a 460 nm long pass filter before being sent to either the APD or the EMCCD camera. Both florescence methods showed no luminescent properties above those of the blank sample (Supporting Information, Figure S16).

Synthesis of H_2PheNDI. Naphthalene-1,4,5,8-tetracarboxylic dianhydride (0.950 g, 3.56 mmol) and L-phenylalanine (1.29 g, 7.83 mmol) were dissolved in DMF (20 mL) and stirred at 80−90 °C overnight, giving a brown solution which was cooled to room temperature before being poured over ice. The product was extracted with ethyl acetate (2 × 100 mL), washed with brine (4 × 200 mL), and dried over magnesium sulfate before the solvent was removed under vacuum. The solid was washed with toluene to give the product as a brown solid. Yield 1.30g, 65%. mp 360−364 °C. Found C, 67.72; H, 4.23; N, 5.20%; $C_{32}H_{22}N_2O_8{\cdot}0.25H_2O$ requires C, 67.78; H, 4.00; N, 4.94%. δ_H (400 MHz, d_6-DMSO), 3.32 (dd, ^2J = 14.2, ^3J = 9.3 Hz, 2 H, CH(CH_2), 3.60 (dd, ^2J = 13.9, ^3J = 5.6 Hz, 2 H, CH(CH_2), 5.86 (dd, ^2J = 9.5, ^2J = 5.6 Hz, 2 H, C*H*), 7.15 (m, 10H, CH_{Phe}), 8.64 (s, 4 H, CH_{NDI}), 13.09 (br., 2 H, COO*H*). δ_C (100 MHz, d_6-DMSO), 34.3, 54.6, 125.6, 126.0, 126.3, 128.1, 128.9, 131.2, 137.8, 161.9, 170.2. υ_{max} /cm^{-1} 2937w, 1706s, 1667s, 1581m, 1452m 1335s, 1248s, 1154m, 835m, 778s. *m/z* (ES$^-$) 561.1 ([M − H]$^-$, 50%), 517.1 ([M − CO_2−H]$^-$, 100%).

Synthesis of *poly*-[Mn(DMF)(HPheNDI)$_2$]·H_2O·MeOH (1). H_2PheNDI (20.0 mg, 35.6 μmol) and $MnCl_2{\cdot}4H_2O$ (21.0 mg, 106 μmol) were added to a solvent mixture of DMF (2 mL), methanol (1 mL), and H_2O (1 mL) in a glass vial and sonicated to dissolve. The reaction mixture was heated to 70 °C in a dry block incubator for 7 days, after which time yellow needles of **1** were formed, which were isolated by vacuum filtration. Yield 5.4 mg, 22.4%. Found C, 61.92; H, 4.32; N, 6.14%; $C_{70}H_{56}N_6O_{18}Mn{\cdot}H_2O{\cdot}MeOH$ ([Mn(HPheNDI)(DMF)$_2$]·H_2O·MeOH) requires C, 62.05; H, 4.55; N, 6.12%. υ_{max} /cm^{-1} 3612w, 2937w, 1330m, 1245s, 1185m, 1111m, 1062m, 991m, 931m, 872m, 827m, 746s, 701s. TGA: On-set, 25 °C, mass loss = 3.0% (calculated 2.9% for loss of MeOH and H_2O). Bulk phase purity was confirmed by PXRD (Supporting Information, Figure S1).

Synthesis of *poly*-[Cd(bipy)(OH_2)(PheNDI)]·3.5H_2O·DMF (2). H_2PheNDI (20.0 mg, 35.6 μmol), $Cd(NO_3)_2{\cdot}4H_2O$ (43.6 mg, 141 μmol), and 4,4′-bipyridine (2.8 mg, 17.8 μmol) were added to a solvent mixture of DMF (2 mL), methanol (1 mL), and H_2O (1 mL) in a glass vial and sonicated to dissolve. The solution was heated at 85 °C in a dry block incubator for 4 days, after which time yellow needle crystals of **2** were formed, which were isolated by vacuum filtration. Yield 17.8 mg, 98.3%. Found C, 54.98; H, 4.31; N, 7.13%;

DOI: 10.1021/acs.cgd.6b00901
Cryst. Growth Des. 2016, 16, 6294−6303

Table 1. Crystallographic and Refinement Data for Compounds 1−7

compound reference	1	2	3	4	5	6	7
empirical formula	$C_{71}H_{60}MnN_6O_{20}$	$C_{42}H_{30}CdN_4O_9$	$C_{101.5}H_{80.5}Cd_3N_{14.5}O_{25}$	$C_{98.5}H_{74.5}Mn_3N_{13.5}O_{23.5}$	$C_{155}H_{111}Cd_4N_{13}O_{35}$	$C_{115}H_{71}Cd_2N_{13}O_{25}$	$C_{60}H_{44}MnN_7O_{14.5}$
formula weight	1372.19	847.1	2240.50	1988.03	3165.16	2259.64	1149.96
crystal system	monoclinic	orthorhombic	monoclinic	monoclinic	triclinic	orthorhombic	orthorhombic
a/Å	8.3310(17)	18.928(4)	31.575(6)	11.574(2)	14.833(3)	13.852(3)	14.030(3)
b/Å	25.564(5)	20.344(4)	11.694(2)	27.811(6)	15.630(3)	19.665(4)	19.359(4)
c/Å	14.599(3)	11.804(2)	16.024(3)	15.961(3)	16.029(3)	39.965(8)	19.915(4)
α/deg	90	90	90	90	90.55(3)	90	90
β/deg	96.14(3)	90	118.40(3)	93.86(3)	106.95(3)	90	90
γ/deg	90	90	90	90	98.30(3)	90	90
volume/Å^3	3091.4(11)	4545.4(16)	5205(2)	5125.9(18)	3512.2(14)	10886(5)	5409.0(19)
temp/K	100(2)	100(2)	100(2)	100(2)	100(2)	100(2)	100(2)
space group	$P2_1$	$P2_12_12_1$	$C2$	$P2_1$	$P1$	$P2_12_12_1$	$P2_12_12$
Z	2	4	2	1	1	4	4
reflections measured	96739	57565	62455	132448	34160	92530	92183
independent reflections	18060	10824	9083	24382	10997	25817	12900
R_{int}	0.0566	0.0618	0.0907	0.1106	0.1013	0.0413	0.0826
final R1 values ($I \geq 2\sigma(I)$)	0.0404	0.0599	0.0696	0.0667	0.0969	0.0961	0.0648
final wR(F^2) values ($I \geq 2\sigma(I)$)	0.1065	0.1638	0.1918	0.1644	0.2545	0.2479	0.1691
final R1 values (all data)	0.0412	0.0630	0.0861	0.0809	0.1118	0.1008	0.0892
final wR(F^2) values (all data)	0.1071	0.1662	0.2088	0.1738	0.2702	0.2561	0.1893
Flack parameter	0.018(3)	0.059(9)	0.000(3)	0.044(5)	−0.24(3)	0.019(5)	0.020(6)
CCDC number	1484835	1484836	1484837	1484838	1484839	1484840	1484841

DOI: 10.1021/acs.cgd.6b00901
Cryst. Growth Des. 2016, 16, 6294−6303

$C_{42}H_{30}N_4O_9Cd\cdot3.5H_2O\cdot$DMF ([Cd(PheNDI)(bipy)($H_2O$)]·3.5$H_2O$·DMF) requires C, 54.97; H, 4.51; N, 7.12%. υ_{max} /cm^{-1} 1705m, 1655s, 1577s, 1499w, 1452m, 1413m 1376m, 1331s, 1277m, 1247s, 1219m, 1174m, 1098w, 1068w, 1042w, 988w, 939w, 911w, 872w, 837w, 814m, 783s, 747m, 697m, TGA: On-set, 25 °C, mass loss = 13.3% (calculated 13.8% for loss of 1 DMF and 3.5 H_2O). Bulk phase purity confirmed by PXRD (Supporting Information, Figure S2). The X-ray diffraction data were processed using the SQUEEZE routine of PLATON, which showed a void space of 328 e$^-$ per unit cell, (82 e$^-$ per asymmetric unit) corresponding to 1 DMF and 3.5 H_2O molecules per asymmetric unit.

Synthesis of *poly*-{[Cd_2(bipy)$_2$(PheNDI)$_2$][Cd(bipy)(DMF)$_{1.5}$(NO$_3$)$_2$(OH$_2$)$_{0.5}$]}·H_2O·DMF (3). H_2PheNDI (10.0 mg, 17.8 μmol), 4,4′-bipyridine (1.40 mg, 8.9 μmol), and Cd(NO$_3$)$_2$·4H_2O (10.9 mg, 35.6 μmol) were added to DMF (3 mL) in a glass vial and sonicated to dissolve. The reaction mixture was heated at 110 °C in a dry bath incubator for 96 h, after which time a red crystalline material of **3** was formed, which was recovered by vacuum filtration. Yield 0.43 mg, 5%. Found C, 53.42; H, 3.66; N, 8.72%; $C_{97}H_{75}N_{13}O_{26}Cd_3\cdot H_2O\cdot$DMF ([$Cd_2$(PheNDI)$_2$(bipy)$_2$][Cd(bipy)(NO$_3$)$_2$(DMF)($H_2O$)]·$H_2O$·DMF) requires C, 53.40; H, 3.67; N, 8.72%. υ_{max} /cm^{-1} 3516w, 2937w, 1709m, 1654m, 1605s, 1574s, 1454m, 1415s, 1335s, 1249s, 1173m, 1113m, 1071m, 815m, 784m, 704m. TGA: On-set, 30 °C; mass loss = 8.7% (calculated 9.0% for loss of 1 H_2O and 1 DMF). Phase purity was confirmed by PXRD (Supporting Information, Figure S3).

Synthesis of *poly*-[Mn_2(bipy)$_2$(PheNDI)$_2$][Mn(bipy)(DMF)(NO$_3$)$_2$]·0.5DMF·7H_2O (4). H_2PheNDI (20.0 mg, 35.6 μmol), 4,4′-bipyridine (5.6 mg, 17.8 μmol), and Mn(NO$_3$)$_2$·4H_2O (18.0 mg, 71.2 μmol) were added to a solvent mixture of DMF (2 mL) and H_2O (1 mL) in a glass vial and sonicated to dissolve. The reaction mixture was heated to 70 °C in a dry block incubator for five nights, after which time orange crystals of **4** were formed, which were recovered by filtration. Yield 8.5 mg, 67%. Found C, 55.85; H, 3.70; N, 8.38%; $C_{97}H_{71}N_{13}O_{23}Mn_3\cdot0.5$DMF·7$H_2O$ ([Mn_2(PheNDI)$_2$(bipy)$_2$][Mn(bipy)(DMF)(NO$_3$)$_2$]·0.5DMF·7H_2O) requires C, 55.95; H, 4.22; N, 8.95%. υ_{max} /cm^{-1} 2934w, 1707s, 1666s, 1620s, 1602s, 1572, 1452m, 1412s, 1378m, 1333s, 1300s, 1248s, 1221m, 1173m, 1110m, 1088m, 1068m, 1044m, 991m, 916w, 878m, 853w, 812s, 781s, 752m, 731m, 700m, 678m. TGA On-set, 25 °C; mass loss = 7.0% (calculated 7.6% for loss of 0.5 DMF and 7 H_2O). Phase purity is confirmed by PXRD (Supporting Information, Figure S4). The X-ray diffraction data were processed with the SQUEEZE routine of PLATON, which showed voids of 330 Å^3 containing 95 e$^-$ per asymmetric unit, which would correspond to 7 H_2O molecules which are not modeled in the crystal structure.

Synthesis of *poly*-[Cd_4(DMF)(dpe)$_2$(PheNDI)$_4$(OH$_2$)$_2$]·10H_2O·0.5DMF (5). H_2PheNDI (40.0 mg, 71.2 μmol), Cd(NO$_3$)$_2$·4H_2O (87.2 mg, 142.4 μmol), and 1,2-di(4-pyridyl)ethylene (9.2 mg, 71.2 μmol) were added to a solvent mixture of DMF (4 mL), MeOH (1.5 mL), and H_2O (1.5 mL) in a glass vial and sonicated to dissolve. The reaction mixture was heated to 85 °C in a dry block incubator for 12 h, after which time yellow crystals of **5** were formed, which were recovered by vacuum filtration. Yield 47.7 mg, 40%. Found C, 55.27; H, 3.83; N, 5.62%; $C_{155}H_{111}N_{13}O_{35}Cd_4\cdot10H_2O\cdot0.5$DMF ([$Cd_4$(PheNDI)$_4(dpe)_4$($H_2O$)$_2$(DMF)]·10$H_2O$·0.5DMF) requires C, 55.58; H, 4.01; N, 5.59%. υ_{max} /cm^{-1} 3334w, 3028w, 1991w, 1946w, 1771w, 1663s, 1573s, 1409m, 1331s, 1245m, 1174m, 1111w, 988m, 835m, 783s, 697m. TGA: On-set, 25 °C, mass loss = 7.0% (calculated 6.4% for loss of 0.5 DMF and 10 H_2O molecules.) Phase purity is confirmed by PXRD (Supporting Information, Figure S5).

Synthesis of *poly*-[Cd_2(PheNDI)$_2$(4PyNDI)$_2$]·6H_2O·2DMF·MeOH (6). H_2PheNDI (20.0 mg, 35.6 μmol), Cd(NO$_3$)$_2$·4H_2O (43.6 mg, 141 μmol), and *N*,*N*′-bis(4-pyridyl)-1,4,5,8-naphthalene tetracarboxylic diimide (15.0 mg, 35.6 μmol) were added to a solvent mixture of DMF (2 mL), MeOH (1 mL), and H_2O (1 mL) in a glass vial and sonicated to dissolve. The reaction mixture was heated at 85 °C in a dry block incubator for 48 h, after which time yellow needle crystals of **6** were formed, which were recovered by vacuum filtration. Yield 32.3 mg, 38.7%. Found C, 57.57; H, 3.42; N, 8.19%; $C_{112}H_{64}N_{12}O_{24}Cd_2\cdot6H_2O\cdot2$DMF·MeOH ([$Cd_2$PheNDI$_2$(4PyNDI)$_2$]·6$H_2O$·2DMF·MeOH) requires C, 57.79; H, 3.83; N, 7.93%. υ_{max} /cm^{-1} 1705m, 1663s, 1577s, 1493w, 1448w, 1407w, 1379w, 1329s, 1245s, 1191m, 1146s, 1118s, 1092.4w, 1064w, 984w, 913w, 865w, 829w, 766s, 699.m, 658m. TGA: On-set, 53 °C, mass loss = 6.3% (calculated 6.7% for loss of 2 DMF). Phase purity is confirmed by PXRD (Figure S6). The structure was processed with the SQUEEZE routine of PLATON, showing voids of 435 Å^3 containing 138 e$^-$ per asymmetric unit, which corresponds to 6 H_2O and 1 DMF molecules more than the DMF and MeOH already modeled in the crystal structure (6 H_2O, 2 DMF, and 1 MeOH in total). The MeOH and H_2O within the structure were likely lost before the TGA and microanalysis was conducted.

Synthesis of *poly*-[Mn_2(PheNDI)$_2$(4PyNDI)$_2$]·3DMF·2MeOH·H_2O (7). H_2PheNDI (10 mg, 18 μmol), Mn(NO$_3$)$_2$·4H_2O (9.0 mg, 36 μmol), and *N*,*N*′-bis(4-pyridyl)-1,4,5,8-naphthalene tetracarboxylic diimide (7.5 mg, 18 μmol) were added to a solvent mixture of DMF (2 mL), methanol (1 mL), and H_2O (1 mL) in a glass vial and sonicated to dissolve. The reaction mixture was heated to 85 °C in a dry block incubator for 24 h, after which time yellow crystals of **7** formed, which were recovered by vacuum filtration. Yield 8.0 mg, 38%. Found C, 60.14; H, 3.46; N, 8.75%, [Mn_2(PheNDI)$_2$(4PyNDI)$_2$]·3DMF·2MeOH·1H_2O, requires C, 60.61; H, 3.93; N, 8.62%. υ_{max} /cm^{-1} 3389w, 1659m, 1577s, 1439m, 1346s, 1241s, 1181m, 1096m, 1014w, 962w, 865w, 775m, 660s. TGA: On-set 50 °C; mass loss = 15.1% (calculated 14.9% for loss of 3 DMF, 2 MeOH, and 1 H_2O). Phase purity is confirmed by PXRD (Figure S7).

■ X-RAY CRYSTALLOGRAPHY

Data collection for all compounds was performed at the Australian Synchrotron on the MX1 or MX2 beamline operating at 17.4 keV (λ = 0.7108)[36] with data collections conducted using BluIce control software.[37] Data indexing and integration was conducted using the XDS program.[38] All structures were solved using direct methods with SHELXS[39] or the dual-space method with SHELXT[40] and refined by least-squares procedures with SHELXL-2014[41] within OLEX-2.[42] Non-hydrogen atoms were refined with anisotropic displacement parameters (with the exception of the nonmetal atoms in **5**, further information given in the Supporting Information). Hydrogen atoms were placed in calculated positions and refined using a riding model with isotropic displacement parameters 1.2 or 1.5 times the isotropic equivalent of their carrier atoms. Where possible, the hydrogen atoms on oxygen were located from the Fourier difference map and refined with appropriate restraints and isotropic parameters 1.5 times the isotopic equivalent of their carrier atoms. Most structures had difficulty in refinement due to disorder, poor diffraction, or solvent accessible voids (requiring SQUEEZE),[43] and specific refinement details are given in the Supporting Information. The crystallographic and refinement data are presented in Table 1.

■ RESULTS AND DISCUSSION

Our previous work using H_2AlaNDI and H_2LeuNDI showed that both ligands were capable of forming an M_2L_2 metallomacrocyclic motif when incorporated into coordination polymers.[32,33] In the case of *poly*-[Cd(AlaNDI)], catenation of these rings occurs, whereas this is not the case for the more sterically encumbered *poly*-[Cd(LeuNDI)] material. The phenylalanine-containing H_2PheNDI is similarly bulky, with the added "complication" of phenyl rings that can compete against NDI···NDI interactions, and therefore, the structure of a PheNDI coordination polymer in the absence of any coligands was sought.

DOI: 10.1021/acs.cgd.6b00901
Cryst. Growth Des. 2016, 16, 6294−6303

The reaction of H_2PheNDI with $MnCl_2$ at 70 °C in a solvent mixture of DMF, MeOH, and H_2O (2:1:1) yielded yellow crystals that were structurally characterized to reveal the coordination polymer *poly*-[Mn(DMF)$_2$(HPheNDI)$_2$]·MeOH·H_2O (**1**). Whereas our previously reported coordination polymers contain fully deprotonated amino acid NDI ligands, only one of the carboxylic acids of each ligand in **1** is deprotonated. The Mn^{II} ion has a distorted octahedral geometry in which the equatorial sites are occupied by two monodentate carboxylate groups and two monodentate carboxylic acid groups, and the axial sites are occupied by two DMF ligands (Figure 2). Each carboxylic acid group forms a hydrogen bond with a carboxylate group coordinated to the same metal ion. The HPheNDI ligands bridge between two metal nodes, forming a (4,4) sheet (Figure 2). The combination of the π-rich naphthalene core and the phenyl side chain of the ligand leads to $\pi-\pi$ interactions within the structure. There are two near-parallel face-to-face π-interactions between a phenyl group of an HPheNDI ligand with the naphthalene core of a neighboring ligand within the windows of the 2D sheets (closest C···C distances = 3.376(3) and 3.4355(9) Å). Two unique nonparallel π-interactions exist between adjacent sheets (closest C···C distances = 3.2789(5) and 3.3959(7) Å, interplanar angles 32.148(7) and 33.197(9)°, respectively). Despite repeated attempts, coordination polymers of the form [M(PheNDI)] could not be isolated.

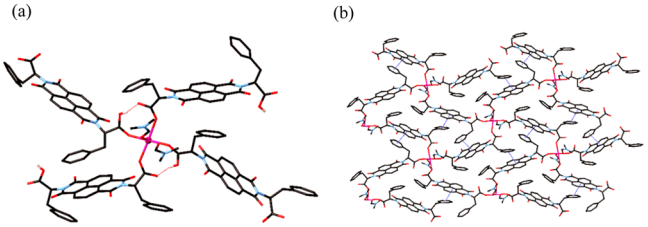

Figure 2. (a) The metal coordination environment in the structure of **1**, showing hydrogen bonding as red dashed lines. (b) The 2D sheet of **1** showing $\pi-\pi$ interactions within the sheet between the NDI core and the phenyl side chain as blue dashed lines (right). Hydrogen atoms are omitted for clarity.

The influence of the addition of pyridyl coligands to the synthesis of coordination polymers with carboxylate ligands has been explored in the literature as well as in our own work with NDI ligands and has shown to lead to a wide range of topologies and entanglement which would not be possible in the absence of coligands.[32,33,44−48] The synthesis of coordination polymers utilizing PheNDI was, therefore, explored using a series of linear pyridyl coligands.

It is known from our earlier work that dipyridyl ligands are able to thread through bis-NDI metallomacrocycles; therefore, H_2PheNDI, $Cd(NO_3)_2{\cdot}4H_2O$, and 4,4′-bipyridine (bipy) were reacted at 85 °C in a solvent mixture of DMF, MeOH, and H_2O (2:1:1). The reaction yielded crystals which were analyzed by X-ray crystallography to reveal a coordination polymer of the formula *poly*-[Cd(bipy)(OH_2)(PheNDI)] (**2**). The Cd^{II} ion adopts a distorted pentagonal bipyramidal geometry, with two chelating carboxylate groups from PheNDI ligands and an aqua ligand occupying the equatorial sites and the nitrogen donor atoms of two bipy ligands occupying the axial sites (Figure 3). The PheNDI ligands adopt a "U-shaped" geometry and form {Cd_2(PheNDI)$_2$} metallomacrocycles similar to those previously reported.[32,33] The {Cd_2(PheNDI)$_2$} metallomacrocycles are bridged into a ladder-like 1D chain by the bipy ligands, forming an apparent "tube" of metallomacrocycles that propagates parallel to the *c*-axis. The plane of the naphthalene core of the PheNDI ligand is approximately perpendicular (84°) to the plane of the bipy ligands, which allows $\pi-\pi$ stacking between these two ligands of adjacent chains (closest C···C distance = 3.353(11) Å) (Figure 3). In addition to this face-to-face π-interaction, the bipyridine is also nestled between the flanking phenyl side chains with CH···π interactions from the bipy to the phenyl rings (CH···centroid distances = 2.7216(4) and 2.9890(4) Å).

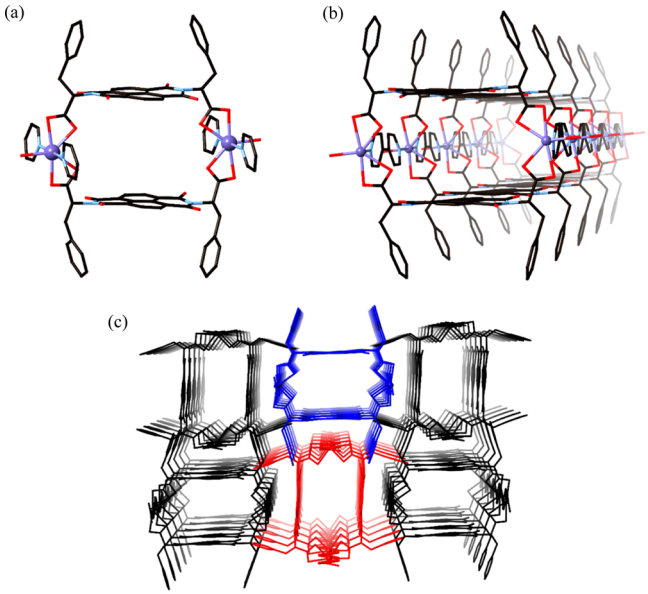

Figure 3. {Cd_2(PheNDI)$_2$} metallomacrocycle motif in the structure of **2**, showing the coordinated bipy ligands and the aqua ligand (left). The 1D chain of **2** (center). The packing of the 1D chains by $\pi-\pi$ stacking between the bipy ligands of one chain with the NDIs of the adjacent chains (right, aqua ligands are omitted for clarity).

Although the planes of the NDIs within the metallomacrocycles in **2** are 7.621(3) Å apart, a suitable distance for $\pi-\pi$ interactions with an aromatic guest to form a polyrotaxane or polycatenane, the metallomacrocycle remains "empty". The structure of **2** exhibits 24.6% void volume (as calculated using Mercury),[49] corresponding to the channels through the metallomacrocycles in which no solvent was able to be modeled from the diffraction data. On the basis of previous results of coordination polymers involving NDI metallomacrocycles, it was expected that the bipy ligand may thread through the metallomacrocycle, given the potential for favorable $\pi-\pi$ interactions. However, the configuration of the phenyl side chains on the PheNDI ligand seems to generate too much steric bulk for two NDIs to approach closely to each other, as demonstrated by the excellent size fit of the bipy ligands between the phenyl rings. In a similar manner to the previously reported 1D → 3D polyrotaxane, *poly*-[Cd_2(LeuNDI)$_2$(bipy)(DMF)$_3$(H_2O)], in which the isobutyl side chain of the LeuNDI ligand was too bulky to allow polycatenation of the NDI metallomacrocycles and there were π-interactions between the NDI and the bipy, the structure of **2** demonstrates that the addition of bipy to an NDI ligand with a bulky side chain will lead to π-interactions between the bipy and NDI ligands.

The influence of synthetic conditions on the structure of coordination polymers is demonstrated by the reaction of

DOI: 10.1021/acs.cgd.6b00901
Cryst. Growth Des. 2016, 16, 6294−6303

H_2PheNDI, $Cd(NO_3)_2$, and bipy at 120 °C in DMF, which yielded crystals of the formula *poly*-{[Cd_2(bipy)$_2$(PheNDI)$_2$]-[Cd(bipy)(DMF)$_{1.5}$(NO_3)$_2$(OH_2)$_{0.5}$]}·DMF (**3**). The structure of **3** involves two different entangled coordination polymers, namely, a 2D sheet, *poly*-[Cd_2(bipy)$_2$(PheNDI)$_2$] and a 1D chain, *poly*-[Cd(bipy)(DMF)$_{1.5}$(NO_3)$_2$(OH_2)$_{0.5}$] (Figure 4). The 2D sheet is structurally similar to the 1D "tubes" in the structure of **2** and can be seen as tubes that are connected side-by-side through bimetallic nodes. The {Cd_2-(PheNDI)$_2$} metallomacrocycles bridge between bimetallic nodes which have one carboxylate chelating to each metal and two carboxylates that bridge the metals in a μ-1κO,2$\kappa O'$ coordination mode, thereby forming a continuous chain of metallomacrocycles similar to those previously reported with AlaNDI in *poly*-[Cd_2(AlaNDI)$_2$(DMF)$_4$] and LeuNDI in *poly*-[Cd_2(LeuNDI)$_2$(DMA)$_4$].[32,33] The Cd^{II} ion in the 2D sheet adopts a distorted octahedral geometry with the bridging and chelating carboxylates in the equatorial sites and the bipy ligands in the axial sites. Axial coordination of the bipy ligands on each Cd^{II} of the bimetallic node allows formation of "double pillars" between the bimetallic nodes to bridge the metallomacrocycle chains into a (4,4) sheet (Figure 4).

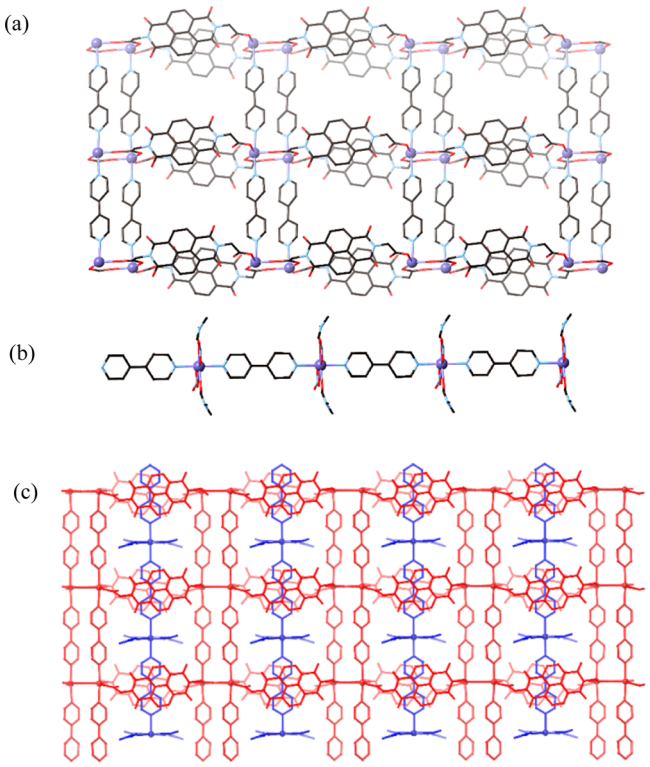

Figure 4. (a) The [Cd_2(PheNDI)$_2$(bipy)$_2$] 2D sheets in the structure of **3**. (b) The [Cd(bipy)(NO_3)$_2$(DMF)(H_2O)] 1D chain in the structure of **3**. (c) The polythreaded sheets of **3** showing the 2D sheets in red and the 1D chains in blue. Hydrogen atoms and phenyl rings are omitted for clarity.

The Cd^{II} ion in the 1D chain adopts a distorted octahedral geometry in which the axial sites are occupied by the nitrogen donor atoms of bipy, two of the equatorial sites are occupied by disordered DMF (75%) and H_2O (25%) molecules, and the other two equatorial sites are occupied by nitrate anions. The sheets of **2** cannot interpenetrate because the double pillars of bipy ligands cannot fit within the metallomacrocycles, as single bipy ligands have been shown to do in previously reported 1D → 3D polyrotaxane, *poly*-[Cd_2(LeuNDI)$_2$(bipy)(DMF)$_3$-(H_2O)].[32] Instead, the 1D chains of [Cd(bipy)(DMF)$_{1.5}$-(NO_3)$_2$(OH_2)$_{0.5}$] thread through the metallomacrocycles, with near-parallel π−π interactions between the bipy of the chains and PheNDI ligands of the metallomacrocycles (closest C···C distance = 3.42(2) Å) to form a polythreaded assembly or poly-pseudo-rotaxane (Figure 4). Despite **2** and **3** involving the same chemical components, the structures of these compounds are vastly different, due to the difference in reaction conditions and reagent ratios, although interestingly the H_2PheNDI:bipy ratio remains constant in both reactions and both products are obtained as pure phases (see the Supporting Information).

The use of Mn^{II} in place of Cd^{II} yields an analogous structure to that of **3**, highlighting the relative consistency with which the metallomacrocycle forms. The reaction of H_2PheNDI, Mn-(NO_3)$_2$, and bipy at 70 °C in a DMF/H_2O mixture (2:1) yielded orange crystals of the formula *poly*-{[Mn_2(PheNDI)$_2$-(bipy)$_2$][Mn(bipy)(DMF)(NO_3)$_2$]} (**4**). The structure of **4** is largely similar to that of **3**, with 2D sheets of {Mn_2(PheNDI)$_2$} metallomacrocyclic chains with bimetallic nodes bridged by double pillars of bipy ligands. Through these sheets pass 1D [Mn(bipy)(DMF)(NO_3)$_2$] chains with π−π interactions between the PheNDI ligands and the bipy ligands (closest C···C distance = 3.369(10) Å). There are, however, subtle differences between the structures of **3** and **4** due to the change in metal ion. The Cd^{II} in the 1D chains in the structure of **3** have two coordinated nitrate ions and two disordered DMF/H_2O coordination sites, whereas the 1D chains in the structure of **4** involve two coordinated nitrate ions and only a single, well-ordered DMF ligand, presumably due to the smaller radius of the metal ion. The less symmetrical coordination environment of the metal ion in the 1D chain in **4** compared to that in **3** means that the overall structure of **4** is of lower symmetry, crystallizing in $P2_1$ as opposed to $C2$ for **3**. The influence of the metal on the material is also observed through the thermal stabilities of the materials, shown by TGA. Both **3** and **4** show similar amounts of mass loss due to loss of solvent; however, they show ligand degradation at different temperatures. The beginning of ligand degradation in **3** occurs at 290 °C, while **4** shows slightly less thermal stability, beginning to degrade at 260 °C.

Following on from the results obtained with bipy, an alternative ligand, 1,2-di(4-pyridyl)ethylene (dpe), was employed in order to investigate the influence of a different, and longer, coligand on the structure of coordination polymers with PheNDI. The reaction of H_2PheNDI, $Cd(NO_3)_2$, and dpe in a solvent mixture of DMF, MeOH, and H_2O (2:1:1) at 85 °C yielded orange crystals which were structurally analyzed to show a coordination polymer of the formula *poly*-[Cd_4(DMF)-(dpe)$_4$(OH_2)$_2$(PheNDI)$_4$], **5**. The asymmetric unit contains four PheNDI ligands, four dpe ligands, four Cd^{II} ions, two aqua ligands, and one DMF ligand (Figure 5). The four Cd^{II} ions form two crystallographically unique bimetallic nodes in the asymmetric unit of the structure, each of which is part of a crystallographically unique 2D sheet. Similarly to the structures of **3** and **4**, the structure of **5** also involves {Cd_2(PheNDI)$_2$} metallomacrocycles coordinated to these bimetallic nodes forming continuous chains, which are then bridged by the dpe ligands to form (4,4) sheets. However, unlike the structures of **3** and **4**, the four metal centers making up the two bimetallic nodes in **5** all have different coordination spheres (Figure 5a). Cd(1) has a distorted pentagonal bipyramidal coordination geometry. The equatorial sites of Cd(1) are occupied by five

DOI: 10.1021/acs.cgd.6b00901
Cryst. Growth Des. 2016, 16, 6294−6303

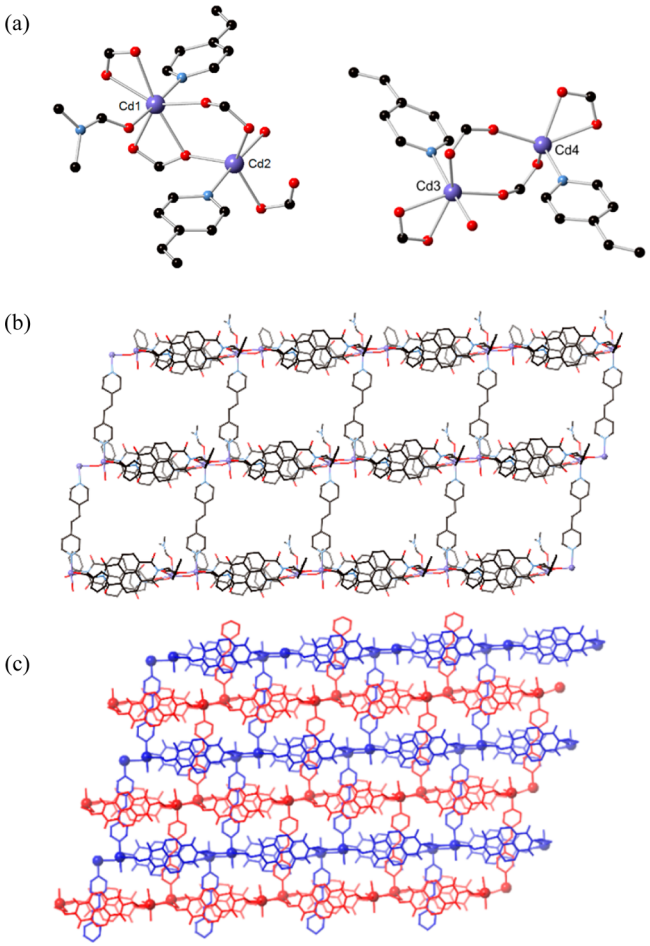

Figure 5. (a) The coordination environments of the two crystallographically unique bimetallic nodes in the structure of **5**. (b) One of the two crystallographically unique 2D sheets in the structure of **5** (involving the Cd(1) and Cd(2) bimetallic node). (c) The 2D → 2D interpenetration of the two unique sheets. Hydrogen atoms and phenyl side chains are omitted for clarity.

oxygen donor atoms from three different carboxylate groups; one carboxylate solely chelates to Cd(1), another carboxylate bridges between Cd(1) and Cd(2) in a μ-1κO,2$\kappa O'$ coordination mode, and the third chelates to Cd(1) while also bridging to Cd(2) in an overall μ-1κO,2$\kappa^2 O,O'$ coordination mode. The axial sites of Cd(1) are occupied by a dpe ligand and a DMF ligand. Cd(2) has a distorted trigonal bipyramidal geometry. The equatorial sites of Cd(2) are occupied by a monodentate carboxylate group and the aforementioned two bridging carboxylate groups. Similarly to Cd(1), the axial sites of Cd(2) are occupied by a dpe ligand and a solvent molecule, in this case water. In the second bimetallic node, the coordination environment of Cd(3) is distorted octahedral with the equatorial sites occupied by one chelating carboxylate group and two carboxylate groups which bridge between the metals of the bimetallic node in a μ-1κO,2$\kappa O'$ coordination mode; the axial sites are occupied by a dpe ligand and an aqua ligand. Cd(4) adopts a distorted square pyramidal geometry in which the basal sites are occupied by carboxylate groups in the same coordination modes as Cd(3), and the apical site is occupied by a dpe ligand.

In a similar manner to the structures of **3** and **4**, the $\{Cd_2(PheNDI)_2\}$ metallomacrocycles in the structure of **5** are connected through the bimetallic nodes to form 1D chains, and these chains are bridged by coligands to form (4,4) sheets (Figure 5b. Note, this topological description refers to an isolated sheet, ignoring interpenetration). In the structure of **5**, however, the dpe ligands form single pillars between the nodes in contrast to the double pillars of bipy in the structures of **3** and **4**. The change from double pillars to single pillars leads to a significant change in the interactions between polymers. The 2D sheets in the structure of **5** are 2D → 2D parallel interpenetrated by virtue of the single pillars of dpe passing through the $\{Cd_2(PheNDI)_2\}$ metallomacrocycles, with π−π interactions between the dpe and the PheNDI ligands giving a polyrotaxane motif (Figure 5c).[15] The interpenetration of **5** confirms that the double pillars of bipy present in the structures of **3** and **4** prevented interpenetration between the sheets and that single, linear aromatic guests can pass through the metallomacrocycles as intended, in a similar manner to the polyrotaxane *poly*-$[Cd_2(LeuNDI)_2(bipy)(DMF)_3(H_2O)]$ reported previously.

The use of a wider dipyridyl ligand, *N*,*N*′-bis(4-pyridyl)-1,4,5,8-naphthalene tetracarboxylic diimide (4PyNDI), was also investigated. 4PyNDI has a naphthalene core group and so is a much more π-rich system than bipy or dpe, although is sterically more demanding. The reaction of H_2PheNDI, $Cd(NO_3)_2$, and 4PyNDI at 85 °C in a solvent mixture of DMF, MeOH, and H_2O (2:1:1) yielded yellow crystals which were structurally characterized to reveal a coordination polymer of formula *poly*-$[Cd_2(PheNDI)_2(4PyNDI)_2]\cdot 6H_2O\cdot 2DMF\cdot MeOH$ (**6**). The asymmetric unit of **6** contains two Cd^{II} metal centers, two PheNDI ligands, two 4PyNDI ligands, and one noncoordinated DMF (other lattice solvent molecules were assigned by analytical methods; see the Experimental Section). The structure of **6** contains bimetallic nodes in a similar manner to those reported in the structures of compounds **1** and **3**−**5**. The two Cd^{II} ions in the structure of **6** adopt different coordination environments, very similar to Cd(1)/(2) in the structure of **5**. Cd(1) has a distorted octahedral geometry with the equatorial sites occupied by three different carboxylate groups; one carboxylate solely chelating to Cd(1), one carboxylate bridging between Cd(1) and Cd(2) in a μ-1κO,2$\kappa O'$ coordination mode, and the third bridging between Cd(1) and Cd(2) while also chelating to Cd(2) in an overall μ-1κO,2$\kappa^2 O,O'$ coordination mode. The axial sites of Cd(1) are occupied by the nitrogen donor atoms of two 4PyNDI ligands. Cd(2) has a distorted pentagonal bipyramidal coordination geometry in which the equatorial sites are occupied by three different carboxylate groups, one solely chelating to Cd(2) and two bridging carboxylates as described above. The axial sites of Cd(2) are occupied by two 4PyNDI ligands. The 4PyNDI coligands that occupy the axial sites of each metal in the bimetallic node form double pillars of the coligand in a similar manner to that in the structures of **3** and **4**.

Unlike the structures of **3**, **4**, and **5**, the structure of **6** does not involve $\{Cd_2(PheNDI)_2\}$ metallomacrocycles; instead, the PheNDI ligands form (4,4) sheets with bimetallic nodes (Figure 6a). The double pillars of 4PyNDI ligands bridge between the bimetallic nodes to link these sheets into a 3D network which is a distorted *pcu* topology (Figure 6). Due to the presence of two different NDI-based ligands, the structure of **6** is heavily influenced *by* π−π interactions. Within the (4,4) sheets there is a single π−π interaction between the cores of two PheNDI ligands across the four-membered ring (closest C···C distance = 3.34(2) Å). The close approach of two

DOI: 10.1021/acs.cgd.6b00901
Cryst. Growth Des. 2016, 16, 6294−6303

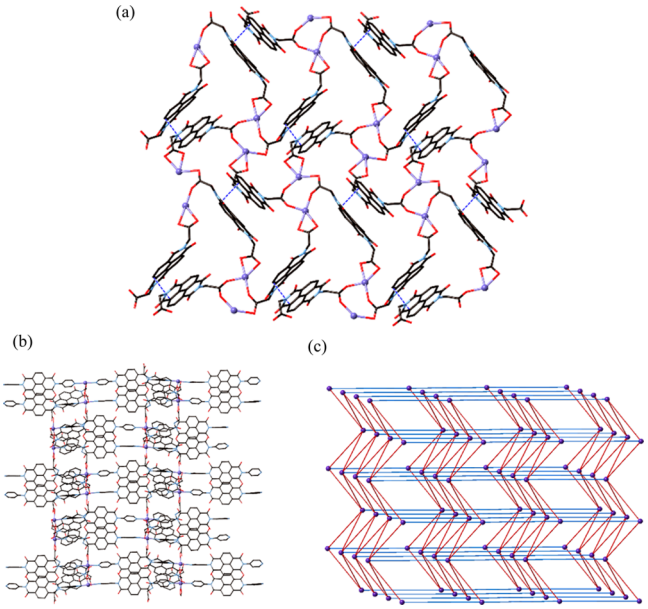

Figure 6. (a) The (4,4) sheet formed by PheNDI ligands and bimetallic Cd^{II} nodes in the structure of **6**, with the face-to-face π-interactions between the ligands shown as blue dotted lines (phenyl groups and hydrogen atoms are omitted for clarity). The 3D network of **6** with the {Cd(PheNDI)} sheets going into the page in molecular form (b) and topologically (c) showing the centroid of the bimetallic node in purple, PheNDI ligands in red, and double ladders of 4PyNDI in blue.

PheNDI ligands is allowed as they adopt a different conformation to those in all other structures. In the structure of **6**, the phenyl groups are oriented away from the central core, whereas, in **2**−**5**, the phenyl groups are positioned directly over the core, thereby sterically inhibiting interaction with another NDI group. In the structure of **1**, one phenyl group is over the core, and the other is facing outward. The phenyl groups in the structure of **6** are not involved in any face-to-face interactions, but do act as acceptors to CH···π interactions from NDIs. The two 4PyNDI ligands in the double pillars are involved in face-to-face π−π interactions with each other (closest C···C distance = 3.54(3) Å).

The ligand combination of PheNDI and 4PyNDI was also conducted with $Mn(NO_3)_2$ under identical reaction conditions to those under which **6** was formed. The reaction yielded orange crystals of the formula *poly*-$[Mn_2(PheNDI)_2(4PyNDI)_2]\cdot 2DMF\cdot 2MeOH\cdot H_2O$, **7**. The structure of **7** is almost identical to the structure of **6** with some differences induced by the incorporation of a smaller metal ion. The asymmetric unit of the structure of **7** is half that of **6** and contains one Mn^{II} ion, one PheNDI ligand, and one 4PyNDI coligand, as well as noncoordinated solvent molecules. The Mn^{II} adopts a distorted octahedral geometry in which the equatorial sites are occupied by carboxylate groups; one carboxylate is chelating solely to Mn(1) and two carboxylates are bridging between Mn(1) and its symmetry equivalent in a μ-1κO,2$\kappa O'$ coordination mode. The structures of **6** and **7** are modeled in different space groups, $P2_12_12_1$ and $P2_12_12$, respectively, and the unit cell of **7** is half that of **6** (along the *c*-axis). Although the overall connectivity and topology of the structures of **6** and **7** are identical, the structural difference can be understood by the slightly different metal coordination geometries, with the symmetry of the node broken in **6** by the bridging carboxylates (Figure 7). The comparison of **6** and **7** shows a structural tolerance with a change in metal ion having no influence on the coordination polymers which were synthesized with the same ligands under identical synthetic conditions.

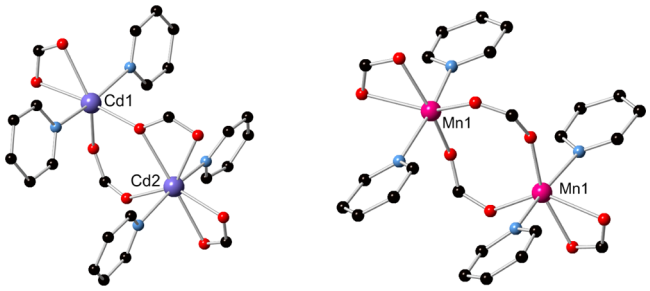

Figure 7. Difference in the coordination environment within the bimetallic nodes in the structures of **6** (left) and **7** (right) leads to a change in space group despite the overall structure remaining the same.

The series of coordination polymers obtained within this study shows an interesting trend in thermal stabilities based on their dimensionality. The H_2PheNDI ligand shows onset of decomposition at 170 °C, before showing rapid mass loss at 300 °C. Thermal stability is significantly increased by incorporation of the ligand into the coordination polymers. The increase in dimensionality and interpenetration of the structures of the coordination polymers appears to lead to higher degradation temperatures. The material consisting of 1D chains, **2**, shows degradation at 230 °C, while that comprising 2D sheets, **1**, shows pronounced degradation at 255 °C. The 1D + 2D → 2D polythreaded compounds, **3** and **4**, are slightly more thermally robust, degrading at 290 and 260 °C, respectively. The 2D + 2D → 2D interpenetrated coordination polymer, **5**, shows significantly more thermal stability than the lower dimensionality or noninterpenetrated compounds, degrading at 380 °C. The 3D coordination polymers, **6** and **7**, are also much more thermally stable than those of lower dimensionality, with the exception of **5**, both showing degradation at 370 °C. It appears that, within this system, higher dimensionality or interpenetration increases the thermal stabilities of the coordination polymers (Supporting Information, Figure S15).

Given the presence of naphthalenediimides within the coordination frameworks, the materials were tested for any solid-state luminescence activity, although none was observed (see the Supporting Information).

■ CONCLUSIONS

Control of interpenetration in coordination polymers which incorporate a number of different aromatic groups is subject to a variety of structural considerations. There exists potential for a number of different interactions to form, complicating the ability to predict structure. The reported series of compounds demonstrates that the structures of coordination polymers containing NDI ligands are heavily influenced by π−π interactions and show similarities with the previously reported alanine and leucine analogues.

The common metallomacrocyclic motif of bis-amino acid NDIs, which has previously been reported as recurring in structures of AlaNDI and LeuNDI, occurs in all of the coordination polymers involving PheNDI alongside either 4,4′-

DOI: 10.1021/acs.cgd.6b00901
Cryst. Growth Des. 2016, 16, 6294−6303

bipyridine or di(4-pyridyl)ethene. These results further demonstrate the reproducibility of this cyclic motif and its potential in "engineered" systems. The alteration of synthetic conditions, typically solvent adjustment which influences the primary coordination sphere (i.e., affecting the ability of the dipyridyl coligand to coordinate), or the change in coligand was sufficient to change the dimensionality of the coordination polymer and/or the presence of aromatic "guests" inside the metallocycle (i.e., interpenetration or polythreading). In the structures of **2** and **3**/**4**, the solvation influences the dimensionality (by capping the metals in **2**, yielding a 1D polymer, but not in **3**/**4**, yielding a 2D polymer with more coligand coordinating rather than water). Compound **5** has significant structural similarity to **3**/**4**, and to reported AlaNDI structures, with continuous chains of metallocycles joined by bimetallic nodes.

The use of a larger coligand, di(4-pyridyl)naphthalenediimide, yields two nearly identical 3D coordination polymers (**6** and **7**) in which the metallocyclic motif is not present. The difference in metal ions between these two compounds gives slightly different metal coordination environments and, therefore, a different space group; however, the overall structure remains essentially unchanged.

The utilization of robust metallocyclic motifs in pseudo-designed interpenetration has clear merit, although the vagaries of metal coordination environments still impart some degree of unpredictability. The nature of the amino acid side chain in these instances appears to play a role in terms of competing intermolecular interactions and steric influences (which can prevent catenation), particularly in the case of phenylalanine where significant competing π-interaction may form. Further investigations of the role of side chains in influencing the behavior of the metallocyclic motif are underway.

■ ASSOCIATED CONTENT

Supporting Information

The Supporting Information is available free of charge on the ACS Publications website at DOI: 10.1021/acs.cgd.6b00901.

Detailed crystallographic refinement information, powder X-ray diffraction, thermogravimetric analysis traces (PDF)

Accession Codes

CCDC 1484835−1484841 contains the supplementary crystallographic data for this paper. These data can be obtained free of charge via www.ccdc.cam.ac.uk/data_request/cif, or by emailing data_request@ccdc.cam.ac.uk, or by contacting The Cambridge Crystallographic Data Centre, 12, Union Road, Cambridge CB2 1EZ, UK; fax: +44 1223 336033.

■ AUTHOR INFORMATION

Corresponding Author

*E-mail: david.turner@monash.edu.

Author Contributions

The manuscript was written through contributions of both authors. Both authors have given approval to the final version of the manuscript.

Notes

The authors declare no competing financial interest.

■ ACKNOWLEDGMENTS

The Australian Research Council is acknowledged for funding under the Future Fellowship scheme (FT120100300). Part of this research was conducted using the MX beamlines at the Australian Synchrotron, Victoria, Australia.[36]

■ REFERENCES

(1) Eddaoudi, M.; Moler, D. B.; Li, H.; Chen, B.; Reineke, T. M.; O'Keeffe, M.; Yaghi, O. M. *Acc. Chem. Res.* **2001**, *34*, 319−330.
(2) Lee, J.; Farha, O. K.; Roberts, J.; Scheidt, K. A.; Nguyen, S. T.; Hupp, J. T. *Chem. Soc. Rev.* **2009**, *38*, 1450−9.
(3) Manna, K.; Zhang, T.; Lin, W. *J. Am. Chem. Soc.* **2014**, *136*, 6566−6569.
(4) Liu, J.; Chen, L.; Cui, H.; Zhang, J.; Zhang, L.; Su, C. Y. *Chem. Soc. Rev.* **2014**, *43*, 6011−6061.
(5) Sumida, K.; Rogow, D. L.; Mason, J. A.; McDonald, T. M.; Bloch, E. D.; Herm, Z. R.; Bae, T. H.; Long, J. R. *Chem. Rev.* **2012**, *112*, 724−781.
(6) Rodenas, T.; Luz, I.; Prieto, G.; Seoane, B.; Miro, H.; Corma, A.; Kapteijn, F.; Llabrés i Xamena, F. X.; Gascon, J. *Nat. Mater.* **2015**, *14*, 48−55.
(7) Gutov, O. V.; Bury, W.; Gomez Gualdron, D. A.; Krungleviciute, V.; Fairen-Jimenez, D.; Mondloch, J. E.; Sarjeant, A. A.; Al Juaid, S. S.; Snurr, R. Q.; Hupp, J. T.; Yildirim, T.; Farha, O. K. *Chem.—Eur. J.* **2014**, *20*, 12389−12393.
(8) Liu, Y.; Xuan, W.; Cui, Y. *Adv. Mater.* **2010**, *22*, 4112−4135.
(9) Boer, S. A.; Nolvachai, Y.; Kulsing, C.; McCormick, L. J.; Hawes, C. S.; Marriott, P. J.; Turner, D. R. *Chem.—Eur. J.* **2014**, *20*, 11308−11312.
(10) Li, J. R.; Sculley, J.; Zhou, H. C. *Chem. Rev.* **2012**, *112*, 869−932.
(11) Dunitz, J. D. *Chem. Commun.* **2003**, 545−548.
(12) Gavezzotti, A. *Acc. Chem. Res.* **1994**, *27*, 309−14.
(13) Dobrzanska, L.; Kleinhans, D. J.; Barbour, L. J. *New J. Chem.* **2008**, *32*, 813−819.
(14) Carlucci, L.; Ciani, G.; Proserpio, D. M. Networks, Topolgies and Entanglements. In *Making Crystals by Design: Methods, Techniques and Applications*; Braga, D., Grepioni, F., Eds.; Wiley-VCH: Heidleberg, 2007; pp 58−85.
(15) Yang, J.; Ma, J. F.; Batten, S. R. *Chem. Commun.* **2012**, *48*, 7899−7912.
(16) Batten, S. R.; Robson, R. *Angew. Chem., Int. Ed.* **1998**, *37*, 1461−1494.
(17) Batten, S. R. Interpenetration. In *Supramolecular Chemistry: From Molecules to Nanomaterials*; Steed, J. W., Gale, P. A., Eds.; John Wiley & Sons Ltd.: Chichester, U.K., 2012; Vol. *6*, pp 3107−3120.
(18) Carlucci, L.; Ciani, G.; Proserpio, D. M. *Coord. Chem. Rev.* **2003**, *246*, 247−289.
(19) Farha, O. K.; Hupp, J. T. *Acc. Chem. Res.* **2010**, *43*, 1166−1175.
(20) Ma, S.; Sun, D.; Ambrogio, M.; Fillinger, J. A.; Parkin, S.; Zhou, H.-C. *J. Am. Chem. Soc.* **2007**, *129*, 1858−1859.
(21) Slater, B. J.; Davies, E. S.; Argent, S. P.; Nowell, H.; Lewis, W.; Blake, A. J.; Champness, N. R. *Chem.—Eur. J.* **2011**, *17*, 14746−14751.
(22) Johnstone, K. D.; Bampos, N.; Sanders, J. K. M.; Gunter, M. J. *New J. Chem.* **2006**, *30*, 861−867.
(23) Carlucci, L.; Ciani, G.; Proserpio, D. M. *Cryst. Growth Des.* **2005**, *5*, 37−39.
(24) Yang, J.; Ma, J.-F.; Batten, S. R. *Chem. Commun.* **2012**, *48*, 7899−7912.
(25) Suraru, S. L.; Wuerthner, F. *Angew. Chem., Int. Ed.* **2014**, *53*, 7428−7448.
(26) Sommer, M. *J. Mater. Chem. C* **2014**, *2*, 3088−3098.
(27) Pan, M.; Lin, X. M.; Li, G. B.; Su, C. Y. *Coord. Chem. Rev.* **2011**, *255*, 1921−1936.
(28) Black, S. P.; Wood, D. M.; Schwarz, F. B.; Ronson, T. K.; Holstein, J. J.; Stefankiewicz, A. R.; Schalley, C. A.; Sanders, J. K. M.; Nitschke, J. R. *Chem. Sci.* **2016**, *7*, 2614−2620.
(29) Bhosale, S. V.; Jani, C. H.; Langford, S. J. *Chem. Soc. Rev.* **2008**, *37*, 331−342.

DOI: 10.1021/acs.cgd.6b00901
Cryst. Growth Des. 2016, 16, 6294−6303

(30) Cougnon, F. B. L.; Ponnuswamy, N.; Pantos, G. D.; Sanders, J. K. M. *Org. Biomol. Chem.* **2015**, *13*, 2927−2930.
(31) Mullen, K. M.; Johnstone, K. D.; Nath, D.; Bampos, N.; Sanders, J. K. M.; Gunter, M. J. *Org. Biomol. Chem.* **2009**, *7*, 293−303.
(32) Boer, S. A.; Hawes, C. S.; Turner, D. R. *Chem. Commun.* **2014**, *50*, 1125−1127.
(33) McCormick, L. J.; Turner, D. R. *CrystEngComm* **2013**, *15*, 8234−8236.
(34) Guha, S.; Saha, S. *J. Am. Chem. Soc.* **2010**, *132*, 17674−17677.
(35) Maniam, S.; Cox, R. P.; Langford, S. J.; Bell, T. D. M. *Chem.—Eur. J.* **2015**, *21*, 4133−4140.
(36) Cowieson, N. P.; Aragao, D.; Clift, M.; Ericsson, D. J.; Gee, C.; Harrop, S. J.; Mudie, N.; Panjikar, S.; Price, J. R.; Riboldi-Tunnicliffe, A.; Williamson, R.; Caradoc-Davies, T. *J. Synchrotron Radiat.* **2015**, *22*, 187−190.
(37) McPhillips, T. M.; McPhillips, S. E.; Chiu, H. J.; Cohen, A. E.; Deacon, A. M.; Ellis, P. J.; Garman, E.; Gonzalez, A.; Sauter, N. K.; Phizackerley, R. P.; Soltis, S. M.; Kuhn, P. *J. Synchrotron Radiat.* **2002**, *9*, 401−406.
(38) Kabsch, W. *Acta Crystallogr., Sect. D: Biol. Crystallogr.* **2010**, *66*, 125−132.
(39) Sheldrick, G. M. *Acta Crystallogr., Sect. A: Found. Crystallogr.* **2008**, *64*, 112−122.
(40) Sheldrick, G. M. *Acta Crystallogr., Sect. A: Found. Adv.* **2015**, *71*, 3−8.
(41) Sheldrick, G. *Acta Crystallogr., Sect. A: Found. Adv.* **2015**, *71*, 3−8.
(42) Dolomanov, O. V.; Bourhis, L. J.; Gildea, R. J.; Howard, J. A. K.; Puschmann, H. *J. Appl. Crystallogr.* **2009**, *42*, 339−341.
(43) Spek, A. L. *Acta Crystallogr., Sect. D: Biol. Crystallogr.* **2009**, *65*, 148−155.
(44) Chen, X. D.; Wu, H. F.; Zhao, X. H.; Zhao, X. J.; Du, M. *Cryst. Growth Des.* **2007**, *7*, 124−131.
(45) Lian, F. Y.; Jiang, F. L.; Yuan, D. Q.; Chen, J. T.; Wu, M. Y.; Hong, M. C. *CrystEngComm* **2008**, *10*, 905−914.
(46) Liu, J. Q.; Wang, Y. Y.; Wu, T.; Wu, J. *CrystEngComm* **2012**, *14*, 2906−2913.
(47) Liu, J. Q.; Huang, Y. S.; Zhao, Y. Y.; Jia, Z. B. *Cryst. Growth Des.* **2011**, *11*, 569−574.
(48) Liu, J. Q.; Wu, J.; Wang, Y. Y.; Lin, J. T.; Sakiyama, H. *CrystEngComm* **2014**, *16*, 3103−3112.
(49) Macrae, C. F.; Bruno, I. J.; Chisholm, J. A.; Edgington, P. R.; McCabe, P.; Pidcock, E.; Rodriguez-Monge, L.; Taylor, R.; van de Streek, J.; Wood, P. A. *J. Appl. Crystallogr.* **2008**, *41*, 466−470.

DOI: 10.1021/acs.cgd.6b00901
Cryst. Growth Des. 2016, 16, 6294−6303

CrystEngComm

PAPER

View Article Online
View Journal

Check for updates

Cite this: DOI: 10.1039/c7ce00498b

A robust metallomacrocyclic motif for the formation interpenetrated coordination polymers†

Stephanie A. Boer and David R. Turner *

Received 14th March 2017,
Accepted 25th March 2017

DOI: 10.1039/c7ce00498b

rsc.li/crystengcomm

The reproducibility of an M_2L_2 metallomacrocyclic synthon containing L-alanine substituted naphthalene diimide ligands (AlaNDI), and its ability to form both catenane and rotaxane motifs, has been demonstrated in a series of nine homochiral coordination polymers. The planes of the NDIs that comprise the metallomacrocycle are ~7 Å apart, an ideal distance for an aromatic group to reside within the ring with multiple parallel π-interactions. The tendency for these systems to be dominated by π-interactions appears to be a driving force for interpenetration of these coordination polymers by either the formation of catenanes between two $\{M_2(AlaNDI)_2\}$ metallomacrocycles or the formation of rotaxanes by dipyridyl coligands passing through metallomacrocycles (4,4′-bipyridine, dipyridylethene and dipyridylnaphthalenediimide). Due to both of these interpenetration motifs being facilitated by parallel π-interactions, the interpenetration of the individual networks does not typically lead to increased dimensionality in the structures, with the exception of one material in which a 1D chain interpenetrates in a 1D → 2D manner. Two of the reported coordination polymers, both containing dipyridylnaphthalenediimide (4PyNDI), are not interpenetrated with π-interactions present between the 4PyNDI ligands themselves rather than engaging with the macrocycles. Overall the reproducibility of the metallomacrocycle, and the relatively common occurrence of catenane and rotaxane motifs, suggests that this is a promising synthon for further crystal engineering applications.

Introduction

Coordination polymers, infinite assemblies of metal ions and organic linkers, remain an expanding field of research due to their range of possible physical applications.[1–3] The porous subset of coordination polymers, metal–organic frameworks (MOFs) have an even wider range of additional applications in areas such as catalysis,[4–6] gas storage,[7–9] separations,[10–12] and sensing.[13–15] The properties, and consequently applications, of coordination polymers are heavily reliant on their structure. The pore size, positioning of functional groups within the pores, chirality of the ligands, interpenetration and the intrinsic chemistry of the metal ions are all important factors to consider when designing coordination polymers and MOFs for specific applications. The control over, and ability to 'predict', structures therefore continues to be a very important area of research.[16–19] From a crystal engineering perspective, the structure of coordination polymers is greatly influenced by the metal ion and ligand used, specifically in terms of the coordination geometry of the metal and the size, shape and coordinating groups of the ligand.[20] Synthetic conditions have also been shown to have an influence on the structure of coordination polymers which are typically formed under thermodynamic control.[21,22] The structural diversity of coordination polymers, and therefore their potential applications, can be greatly influenced by the use of mixed-ligand systems. Often the combination of ligands with different types of coordinating groups, such as carboxylate and pyridyl groups, can lead to changes in dimensionality, topology, interpenetration or porosity of coordination polymers.[23–26]

Naphthalene diimides (NDIs) have been shown to be versatile ligands in supramolecular chemistry due to the ease by which they can be functionalised to incorporate a wide variety of potential coordinating groups.[27–29] NDIs have been used in a number of discrete supramolecular complexes, including catenanes and polyhedra.[30,31] MOFs have also been synthesised using NDI ligands,[32,33] some of which have interesting optical properties in response to guest molecules.[34–36] NDIs in solution typically aggregate through face-to-face π-interactions aided by their large π-surfaces.[37,38] Coordination polymers incorporating NDI ligands usually involve face-to-face π-interactions dominating their crystal packing with the potential to lead to topological entangling, or interpenetration, of multiple networks.[28] Although interpenetration is mostly seen as a disadvantage to creating MOFs, with the desired void space being fully or partially occupied, it can often have a stabilising influence on the material.[39–41]

School of Chemistry, Monash University, Clayton, VIC 3800, Australia.
E-mail: david.turner@monash.edu

† Electronic supplementary information (ESI) available: Full crystallographic refinement details, PXRD and TGA traces. CCDC 1537524–1537532. For ESI and crystallographic data in CIF or other electronic format see DOI: 10.1039/c7ce00498b

Published on 28 March 2017. Downloaded by Monash University on 14/04/2017 13:40:44.

Published on 28 March 2017. Downloaded by Monash University on 14/04/2017 13:40:44.

Our previous work using NDIs in coordination polymers has been focused on amino acid-substituted ligands for the synthesis of homochiral materials.[10,37,42,43] Initially it was found that poly-[Cd(AlaNDI)(DMF)$_2$] (where AlaNDI is an NDI substituted by L-alanine at the two imide positions) forms a linear 1D polymer of conjoined {Cd$_2$(AlaNDI)$_2$} metallomacrocycle motifs.[42] The NDI planes within these metallocycles are *ca.* 7 Å apart allowing for catenation, between perpendicular chains facilitated by π-interactions, *i.e.* interlocked metallomacrocycles. The use of a bulkier side-chain in the L-leucine analogue, LeuNDI, hindered catenation of the metallocycles yet allowed 4,4′-bipyridine, which is sterically undemanding, to pass through the metallocycles to form a polyrotaxane.[43] The L-phenylalanine analogue, PheNDI, also did not form catenane motifs yet formed rotaxanes in some instances when combined with dipyridyl ligands, with the phenyl side-chain apparently disrupting potential π-interactions between NDIs and dipyridyl ligands and also hindering catenation due to steric bulk.[37]

Herein we report detailed studies on the coordination polymers that form using the less bulky AlaNDI ligand in combination with a variety of dipyridyl ligands. The {M$_2$(AlaNDI)$_2$} metallocycles have the potential to form either catenane or rotaxanes motifs in these systems, with the lack of steric bulk or competing intermolecular interactions from the amino acid R-group allowing these motifs to form more freely than in our previous studies. The various interpenetrated topologies that result are examined and discussed.

Experimental

Materials and methods

All chemicals and reagents were obtained from commercial sources and used without further purification, with the exception of 4PyNDI and H$_2$AlaNDI which were synthesized following literature procedures.[42,44] FTIR spectra were obtained using an Agilent Cary 630 diamond attenuated total reflectance (ATR) spectrometer with MicroLab software used to process the data. Thermogravimetric analysis (TGA) was conducted using a Mettler TGA/DSC 1 instrument. The temperature was ramped at 5 °C min^{-1} to 400 °C under an N$_2$ supply of 10.0 mL min^{-1} and the data were analysed using the STARe system. Microanalyses were performed at the Science Centre, London Metropolitan University, UK. Powder X-ray diffraction data were collected at room temperature using a Bruker D8 Focus diffractometer equipped with Cu-Kα radiation (λ = 1.5418 Å). The samples were mounted on a zero background silicon single crystal stage. Data were collected in the angle interval 2θ = 5–55° with a step size of 0.02°. The collected data were compared to predicted patterns, calculated using Mercury,[45] based on low-temperature single crystal data (see ESI†).

Synthetic procedures

Synthesis of poly-[Cd$_2$(AlaNDI)$_2$(bipy)(DMF)$_4$] [Cd$_2$(AlaNDI)$_2$-(bipy)(DMF)$_2$(OH$_2$)$_2$], 1. H$_2$AlaNDI (10.0 mg, 24.4 μmol), Cd(NO$_3$)$_2$·4H$_2$O (15 mg, 48.8 μmol) and 4,4′-bipyridine (1.9 mg, 12.2 μmol) were added to DMF (3 mL) in a glass vial and sonicated to dissolve. The solution was heated at 100 °C in a dry bath incubator for 24 hours, during which time yellow needle-shaped crystals of **1** were formed, which were recovered by vacuum filtration. Yield 12.1 mg, 34%. Found C, 49.37; H, 4.03; N, 9.00%; C$_{59}$H$_{55}$N$_9$O$_{20}$Cd$_2$ ([Cd$_2$(AlaNDI)$_2$(bipy)(DMF)$_3$(OH$_2$)]): requires C, 49.38; H, 3.86; N, 8.78%. ν_{max}/cm^{-1} 2934w, 1701w, 1646s, 1568s, 1449w, 1400m, 1375m, 1354m, 1331s, 1293m, 1244s, 1216m, 1193m, 1091m, 1060w, 1044w, 964w, 922w, 991w, 927w, 761m, 722w, 672m. TGA: on-set, 40 °C mass loss = 17.0% (calculated 16.5% for loss of one coordinated H$_2$O and three coordinated DMF molecules). Bulk purity confirmed by PXRD (ESI,† Fig. S1).

Synthesis of poly-[Cd$_4$(AlaNDI)$_4$(bipy)(DMF)$_4$(OH$_2$)$_2$]·5H$_2$O·4DMF, 2. H$_2$AlaNDI (10.0 mg, 24.4 μmol), Cd(NO$_3$)$_2$·4H$_2$O (30.0 mg, 97.4 μmol) and 4,4′-bipyridine (3.8 mg, 24.4 μmol) were added to a mixture of DMF (2 mL), methanol (1 mL) and water (1 mL) and sonicated to dissolve. The solution was heated at 85 °C in a dry bath incubator for 24 hours, during which time yellow needle-shaped crystals were formed, which were recovered by vacuum filtration. Yield 13.5 mg. The X-ray diffraction data were processed with the SQUEEZE routine of PLATON which showed voids of 786 Å^3 containing 211 e$^-$ (per 4Cd^{II}) which can be accounted for by voids filled with five water molecules and four DMF molecules. Attempted synthesis of a pure phase of **2** was unsuccessful due to concomitant formation of **4** (see PXRD, Fig. S2†).

Synthesis of poly-[Mn$_4$(AlaNDI)$_4$(bipy)(DMF)$_4$(OH$_2$)$_2$]·2DMF·5.5H$_2$O, 3. H$_2$AlaNDI (10.0 mg, 24.4 μmol), Mn(NO$_3$)$_2$·4H$_2$O (12.0 mg, 97.6 μmol) and 4,4′-bipyridine (3.8 mg, 24.4 μmol) were added to a solvent mixture of DMF (2 mL), methanol (1 mL) and water (1 mL) and sonicated to dissolve. The solution was heated to 85 °C in a dry bath incubator overnight, to yield yellow crystals of **3** which were recovered by filtration. Yield 4.6 mg, 36%. Found C, 49.77; H, 3.82; N, 8.89%; C$_{96}$H$_{80}$N$_{12}$O$_{39}$Mn$_4$·2DMF·5.5H$_2$O: requires C, 49.87; H, 4.46; N, 8.62%. ν_{max}/cm^{-1} 2934w, 1699m, 1650s, 1579s, 1505w, 1442m, 1410m, 1373m, 1351s, 1323s, 1271m, 1240s, 1222m, 1099m, 1067w, 1038w, 995w, 967w, 921w, 883w, 844w, 805m, 760s, 728w, 675m. TGA: on-set, 25 °C mass loss = 10.7% (calculated 10.9% for loss of all coordinated DMF and H$_2$O, and 5.5 non-coordinated H$_2$O and two non-coordinated DMF molecules). Bulk purity was confirmed by PXRD (ESI,† Fig. S3). The X-ray diffraction data were processed using the SQUEEZE routine of PLATON, showing a total void space of 860 Å^3 containing 190 e$^-$ per unit cell (430 Å^3 with 95 e$^-$ per formula unit). The solvent assigned from the microanalysis which was not present in the crystal structure (1 DMF and 5.5 H$_2$O molecules) accounts for 95 e$^-$ per formula unit.

Synthesis of poly-[Cd(AlaNDI)(bipy)(OH$_2$)]·3.5H$_2$O·0.5DMF, 4. H$_2$AlaNDI (20.0 mg, 48.8 μmol), Cd(NO$_3$)$_2$·4H$_2$O (15.0 mg, 48.8 μmol) and 4,4′-bipyridine (7.6 mg, 48.8 μmol) were added to a mixture of DMF (2 mL), methanol (1 mL) and water (1 mL) and sonicated to dissolve. The solution was heated at 85 °C in a dry bath incubator for 4 hours, during which time yellow needle-shaped crystals of **4** were formed, which were

 This journal is © The Royal Society of Chemistry 2017

Published on 28 March 2017. Downloaded by Monash University on 14/04/2017 13:40:44.

recovered by vacuum filtration. Yield 9.5 mg, 28%. Found C, 47.58; H, 3.55; N, 7.95%; $C_{30}H_{22}N_4O_9Cd{\cdot}3.5H_2O{\cdot}0.5DMF$ ($[Cd(AlaNDI)(bipy)(OH_2)]{\cdot}3.5H_2O{\cdot}0.5DMF$): requires C, 47.61; H, 4.12; N, 7.93%. ν_{max}/cm^{-1} 3359w, 2941w, 2365w, 2084w, 1705m, 1662s, 1572s, 1491w, 1448w, 1408s, 1365m, 1330s, 1246s, 1220m, 1200m, 1150w, 1095m, 1065m, 1008w, 967w, 922w, 879w, 858m, 812m, 765s, 728m. TGA: on-set, 25 °C mass loss = 14.9% (calculated 14.8% loss for loss of coordinated water and non-coordinated solvent of 3.5 water molecules and 0.5 DMF molecules). The X-ray diffraction data were processed with the SQUEEZE routine of PLATON which showed voids of 232 Å^3, containing 73.5 e$^-$, per asymmetric unit. The solvent observed in the TGA and microanalysis which is not modelled in the voids of the crystal structure would account for 55 e$^-$ per asymmetric unit, some may have been lost from the material before microanalysis or TGA were conducted. Bulk purity was confirmed by PXRD (ESI,† Fig. S4).

Synthesis of poly-$[Zn_2(AlaNDI)_2(bipy)_2]{\cdot}0.3MeOH{\cdot}0.7H_2O$, 5. $H_2AlaNDI$ (10.0 mg, 24.4 μmol), $Zn(NO_3)_2{\cdot}6H_2O$ (19.2 mg, 97.6 μmol) and 4,4′-bipyridine (3.8 mg, 24.4 μmol) were added to a mixture of DMF (2 mL), methanol (1 mL) and water (1 mL) and sonicated to dissolve. The solution was heated at 85 °C in a dry bath incubator overnight, to yield orange cube shaped crystals of **5**, which were recovered by vacuum filtration. Yield 9.3 mg, 30%. Found C, 56.85; H, 3.35; N, 8.64%; $C_{60}H_{40}N_8O_{16}Zn_2{\cdot}0.3MeOH{\cdot}0.7H_2O$: requires C, 56.49; H, 3.35; N, 8.74%. ν_{max}/cm^{-1} 2957w, 1702m, 1667s, 1636s, 1577m, 1524w, 1447m, 1422m, 1370s, 1354s, 1372s, 1288m, 1240s, 1216s, 1201m, 1084m, 1068m, 1032w, 968w, 915w, 874w, 802s, 768s, 720m, 663m. TGA: on-set, 25 °C mass loss = 2.5% (calculated 2.0% for loss of uncoordinated 0.3 MeOH and 0.7 water molecules). Bulk purity was confirmed by PXRD (ESI,† Fig. S5).

Synthesis of poly-$[Mn(HAlaNDI)_2(dpe)]$, 6. $H_2AlaNDI$ (10.0 mg, 24.4 μmol), $Mn(NO_3)_2{\cdot}4H_2O$ (12.0 mg, 97.6 μmol) and 1,2-di(4-pyridyl)ethylene (4.4 mg, 24.4 μmol) were added to a solvent mixture of DMF (2 mL), methanol (1 mL) and water (1 mL) and sonicated to dissolve. The solution was heated to 85 °C in a dry bath incubator for two nights, to yield yellow crystals of **6** which were recovered by filtration. Yield 5.1 mg, 9.8%. Found C, 59.15; H, 3.33; N, 7.87%; $C_{52}H_{36}N_6O_{16}Mn$; requires C, 59.15; H, 3.44; N, 7.96%. ν_{max}/cm^{-1} 2943w, 1702m, 1657s, 1599m, 1578m, 1450w, 1420w, 1371w, 1353m, 1332s, 1246s, 1200m, 1138w, 1115m, 1086m, 1043m, 1010m, 965m, 924m, 887m, 841s, 805m, 773s, 760s, 723m, 650m. TGA on-set, 25 °C mass loss = 0% Bulk purity was confirmed by PXRD (ESI,† Fig. S6).

Synthesis of poly-$[Cd_2(AlaNDI)_2(4PyNDI)_2]{\cdot}4DMF$, 7, poly-$[Cd_2(AlaNDI)_2(OH_2)_2(4PyNDI)_2]{\cdot}DMF{\cdot}H_2O$, 8 and poly-$[Cd_2(AlaNDI)_2(DMF)_2(OH_2)_2(4PyNDI)]{\cdot}DMF{\cdot}4H_2O$, 9. $H_2AlaNDI$ (10.0 mg, 24.4 μmol), $Cd(NO_3)_2{\cdot}4H_2O$ (30.0 mg, 97.4 μmol) and 4PyNDI (6.0 mg, 14.3 μmol) were added to a solvent mixture of DMF (2 mL), methanol (1 mL) and water (1 mL) and sonicated to dissolve. The solution was heated to 85 °C in a dry bath incubator for 24 hours, to yield yellow crystals which were recovered by filtration. Yield 21.1 mg. The X-ray diffraction data of **7** were processed with the SQUEEZE routine of PLATON which showed voids of 727 Å^3, containing 162.5 e$^-$, per asymmetric unit, which could account for four DMF molecules. However as **7** could not be obtained as a pure phase, the solvent present in the pores could not be determined unequivocally by TGA and microanalysis. PXRD shows compounds **7**, **8** and **9** present in the bulk sample (ESI,† Fig. S7).

Crystallography

Data collection for all compounds was performed at the Australian Synchrotron on the MX1 beamline[46] operating at 17.4 keV (λ = 0.7108) using the BluIce control software.[47] Data indexing and integration were conducted using the XDS program.[48] All structures were solved with SHELXT,[49] using the dual-space method, or SHELXS using direct methods,[50] and refined by least-squares methods using SHELXL-2016/6 within OLEX-2.[51,52] Non-hydrogen atoms were refined with anisotropic displacement parameters. Hydrogen atoms were placed in calculated positions and refined using a riding model with isotropic displacement parameters 1.2 or 1.5 times the isotropic equivalent of their carrier atoms. The O–H hydrogen atoms were placed in calculated positions and refined using SHELX DFIX and DANG restraints to maintain their positions in the structures of **1**, **2**, **5**, **8** and **9**. The O–H hydrogen atoms were held in calculated positions by AFIX 7 or AFIX 147 in the structures of **3**, **4** and **6**. The structures of **2**, **3**, **4** and **7** contained solvent accessible voids, and were processed with the SQUEEZE routine of PLATON.[53] Specific refinement details are given in the supplementary information. The crystallographic and refinement data are presented in Table 1.

Results and discussion

The coordination behaviour of AlaNDI, in terms of its ability to reproducibly form metallomacrocycles and an exploration of the interpenetration motifs that form in the presence of a range of linear dipyridyl coligands, was investigated. Our previous results have shown that AlaNDI is capable of forming catenane motifs between conjoined $\{Cd_2(AlaNDI)_2\}$ macrocycles, although the ligand is also able to adopt a divergent conformation which does not form the cyclic motif.[10,42] Whilst sterically bulkier derivatives (LeuNDI and PheNDI) have shown no propensity towards forming catenanes, they have been shown to form rotaxanes in combination with ligands such as 4,4′-bipyridine and dipyridylethylene.[37,43] The AlaNDI ligand in the presence of these dipyridyl ligands represents an interesting case; it has the potential to form either self-complementary catenane motifs or rotaxanes that incorporate the secondary ligand.

The reaction of $H_2AlaNDI$, $Cd(NO_3)_2$ and 4,4′-bipyridine (bipy) in DMF at 100 °C yielded orange crystals containing the 1D coordination polymer poly-$[Cd_2(AlaNDI)_2(bipy)(solv)_4]$, **1**. The two crystallographically unique Cd^{II} ions, as parts of two unique 1D chains in the structure, exist as monometallic nodes, both with trigonal bipyramidal coordination geometries (Fig. 1a). The equatorial positions are occupied by one bipy and two monodentate AlaNDI carboxylate groups. The

Published on 28 March 2017. Downloaded by Monash University on 14/04/2017 13:40:44.

Table 1 Crystallographic and refinement data for all structures

Compound reference	1	2	3	4	5	6	7	8	9
Empirical formula	$C_{59}H_{55}Cd_2N_9O_{20}$	$C_{102}H_{88}Cd_4N_{14}O_{38}$ ·solvent	$C_{105}H_{95}Mn_4N_{15}O_{39}$ ·solvent	$C_{30}H_{22}CdN_4O_9$ ·solvent	$C_{60.3}H_{42.6}N_8O_{17}Zn_2$	$C_{52}H_{36}MnN_6O_{16}$	$C_{88}H_{48}Cd_2N_{12}O_{24}$ ·solvent	$C_{91}H_{61}Cd_2N_{13}O_{28}$	$C_{73}H_{69}Cd_2N_{11}O_{29}$
Formula weight	1434.92	2567.46	2410.71	694.91	1281.66	1055.81	1882.18	2009.32	1789.19
Crystal system	Tetragonal	Orthorhombic	Orthorhombic	Tetragonal	Orthorhombic	Monoclinic	Monoclinic	Triclinic	Triclinic
a/Å	16.984(2)	18.674(4)	18.324(4)	21.838(3)	17.345(4)	9.1660(18)	15.369(3)	11.947(2)	8.3020(17)
b/Å	16.984(2)	23.894(5)	23.774(5)	21.838(3)	22.362(5)	21.819(4)	17.967(4)	13.534(3)	14.375(3)
c/Å	21.780(4)	14.086(3)	14.040(3)	14.721(3)	13.817(3)	11.505(2)	18.470(4)	14.618(3)	17.195(3)
α/°	90	90	90	90	90	90	90	81.85(3)	66.80(3)
β/°	90	90	90	90	90	96.39(3)	107.96(3)	66.46(3)	88.82(3)
γ/°	90	90	90	90	90	90	90	89.84(3)	78.25(3)
Volume/Å^3	6283(2)	6285(2)	6116(2)	7020(2)	5359.2(19)	2286.6(8)	4851.6(19)	2141.2(9)	1842.6(8)
Temperature/K	100(2)	100(2)	100(2)	100(2)	100(2)	100(2)	100(2)	100(2)	100(2)
Space group	$P4_2$	$P2_12_12$	$P2_12_12$	$P4_32_12$	$P2_12_12$	$P2_1$	$P2_1$	$P1$	$P1$
Z	4	2	2	8	4	2	2	1	1
Reflections measured	260 223	105 036	102 704	116 870	89 192	38 240	121 534	11 796	34 544
Independent reflections	20 299	14 957	14 521	8275	12 785	10 778	22 959	11 796	12 148
R_{int}	0.1306	0.0573	0.0538	0.0419	0.0855	0.0521	0.0795	0.1358	0.0402
Final R_1 values ($I \geq 2\sigma(I)$)	0.0889	0.0417	0.0581	0.0271	0.0616	0.0481	0.0488	0.0900	0.0419
Final w$R(F^2)$ values ($I \geq 2\sigma(I)$)	0.2643	0.1112	0.1675	0.0813	0.1749	0.1166	0.1358	0.2242	0.1158
Final R_1 values (all data)	0.1420	0.0500	0.0653	0.0280	0.0656	0.0574	0.0552	0.1100	0.0428
Final w$R(F^2)$ values (all data)	0.3113	0.1167	0.1770	0.0817	0.1794	0.1220	0.1405	0.2444	0.1166
Flack parameter	0.024(12)	0.002(7)	0.031(3)	0.002(4)	0.024(5)	0.020(7)	0.073(10)	0.21(3)	0.045(6)
CCDC number	1537531	1537524	1537525	1537528	1537526	1537527	1537532	1537529	1537530

This journal is © The Royal Society of Chemistry 2017

Published on 28 March 2017. Downloaded by Monash University on 14/04/2017 13:40:44.

solvent ligands coordinated at the axial sites differ for the two unique metal centres. The axial sites of Cd(1) are both occupied by DMF ligands, while the axial sites of Cd(2) are both occupied by disordered water and DMF ligands (50 : 50). As we have observed previously with coordination polymers involving amino-acid NDI ligands, the structure of **1** involves $\{Cd_2(AlaNDI)_2\}$ metallomacrocycles in which the naphthalene groups in this motif are almost parallel and form a suitably sized gap in which to accommodate an aromatic guest with face-to-face π-interactions (with shortest inter-NDI C···C distances of 7.111(7) Å and 7.129(10) Å). These metallomacrocycles are bridged by the bipy ligands into a 1D chain of alternating rings and threads (Fig. 1b). The structure contains two crystallographically unique 1D chains that are perpendicular and co-planar. The intersection of these chains involves a rotaxane motif in which the bipy of one polymer is threading through the metallomacrocycle of another, which leads to an overall 1D → 2D polyrotaxane (Fig. 1c). The bipy ligand interacts with the macrocycle by π-interactions with closest C···C contacts of 3.402(12) and 3.461(12) Å. The 2D polyrotaxane sheets pack by virtue of π-interactions between the exterior faces of the metallomacrocycles.

The structure of **1** highlights the reproducibility of polyrotaxane motifs in amino acid-NDI systems, with strong similarities to the structure of the previously reported coordination polymer poly-$[Cd_2(LeuNDI)_2(bipy)(DMF)_3(OH_2)]$ which is a 1D → 3D polyrotaxane.[43] The cause of the difference in interpenetration topology between these two structures lies in the relative orientation of the bipy and the metallomacrocycle in the 1D chain, and is presumably brought about by the change in steric bulk of the amino acid side chain. In the 1D → 3D polyrotaxane, the bipy is twisted by approximately 35° with respect to the NDI macrocycle leading to a 3D polyrotaxane, while in the structure of **1** the bipy and NDIs are parallel, leading to a 2D polyrotaxane. Perhaps this can be rationalised in terms of packing, with the less bulky AlaNDI ligands allowing 2D polyrotaxane sheets to stack, whereas this is disallowed for the bulkier LeuNDI analogue and hence an alternative packing motif forms. The impact of the side chain on structure is clearly important, with similar reactions involving PheNDI not displaying interpenetration.[37] The presence of a rotaxane motif in **1**, rather than a catenane, could be rationalised by the closer packing; a catenane motif would necessitate pores in an interpenetrated 2D network.

It is well documented that reaction conditions can influence products in self-assembly syntheses, herein demonstrated by reacting H_2AlaNDI, bipy and $Cd(NO_3)_2$ in DMF : methanol : water (2 : 1 : 1) at 85 °C to concomitantly form poly-$[Cd_4(AlaNDI)_4(bipy)(DMF)_4(OH_2)_2]\cdot 5H_2O\cdot 4DMF$, **2** and poly-$[Cd(AlaNDI)(bipy)(OH_2)]\cdot 3.5H_2O\cdot 0.5DMF$, **4**. Whilst **4** could be isolated in a pure form, by using the exact stoichiometry of metal and ligands present in the product, numerous attempts to isolate **2** as a pure material, by a variety of synthetic alterations, failed to yield the clean product.

The asymmetric unit of **2** contains one bimetallic Cd node coordinated by four halves of unique AlaNDI ligands, half of a bipy ligand, two DMF molecules and an aqua ligand. Each metal adopts a distorted trigonal bipyramidal geometry (Fig. 2a) in which the equatorial sites of each are occupied by one monodentate carboxylate with two carboxylate groups bridging between the two metals in μ-1κO,2κO′ coordination modes. The formally non-coordinating oxygen atoms of the monodentate carboxylates have weak interactions at Cd···O distances of 2.717(6) Å and 2.962(5) Å. The axial sites of Cd(1) are occupied by a DMF ligand and a bipy ligand, and the axial sites of Cd(2) are occupied by a DMF and an aqua ligand. The bipy exhibits rotational disorder and is modelled over two positions, with the planes of these two pyridyl positions offset by 70.3(13)°. The bimetallic nodes are bridged by

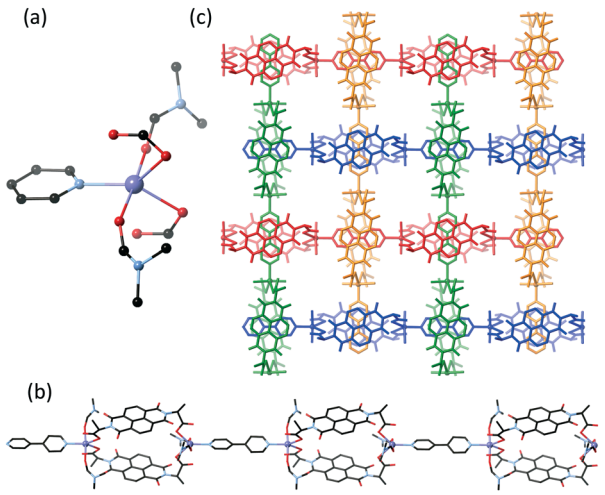

Fig. 1 (a) The metal coordination environment of Cd(1) in **1**, (b) a single chain of **1** and (c) perpendicular 1D chains of **1** feature the bipy ligands threading through metallomacrocycles to form a 1D → 2D polyrotaxane.

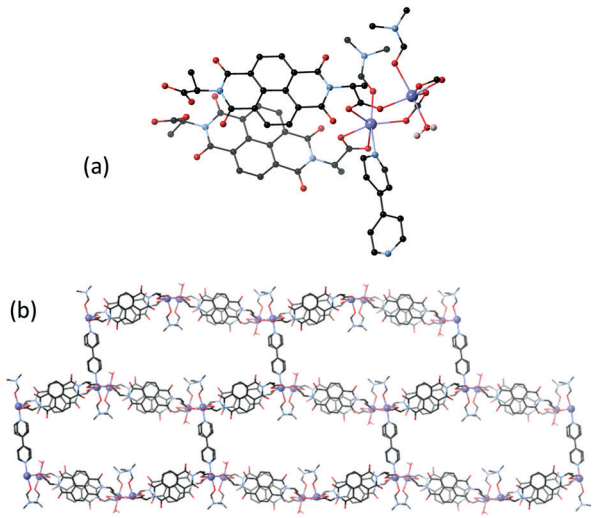

Fig. 2 (a) The metal coordination environment in the structure of **2**. Only one part of the rotational disorder of the bipy ligand is shown. (b) The (6,3) sheet formed by the bridging of bipy between bimetallic nodes of metallomacrocycle chains in **2**. All hydrogen atoms are omitted for clarity.

Published on 28 March 2017. Downloaded by Monash University on 14/04/2017 13:40:44.

pairs of AlaNDI ligands forming the anticipated conjoined metallomacrocycles in the same manner as the previously reported 1D chain poly-[Cd(AlaNDI)(DMF)$_2$].[42] The bipy ligands are aligned perpendicular to the metallomacrocycle chains, and therefore bridge between the bimetallic nodes of adjacent chains to form a (6,3) sheet (Fig. 2b, taking the macrocycle to be a simple 2-connector between nodes).

The individual 2D sheets in the structure of **2** interpenetrate in a 2D → 2D manner with catenane motifs between NDI metallomacrocycles from the separate sheets involving parallel face-to-face π-interactions with the closest C···C distances being 3.520(8) Å and 3.491(9) Å (Fig. 3). AlaNDI is the only ligand we have studied to date that displays this motif, with the bulkier LeuNDI and PheNDI ligands showing only rotaxane formation of their metallomacrocycles. The interpenetrating layers pack by face-to-face π-interactions between the surfaces of the NDI ligands external to the metallomacrocycles, with the closest C···C distance being 3.4069(7) Å. Whilst an individual network in **2** can be described as having (6,3) topology, the loops cannot be simplified as a single linker in the overall structure due to the interpenetration, therefore the topology of this coordination polymer is described by the Schäfli symbol $2^2{\cdot}6^8$. It would appear that the bipy exhibits disorder because it is not involved in π-interactions. It may be reasonably assumed that the catenane motif forms, when sterically allowed by the ligands, in order to maximise interactions between the large NDI π surfaces. An alternative fact to this argument is that rotaxane motifs do form in the presence of AlaNDI (*vide infra*). It seems likely that the shape of the individual frameworks plays a significant role. Obviously they are required to be self-complementary, such that the macrocyclic groups align in the correct orientation for interpenetration, and also that other ligating species do not sterically prevent such interpenetration from occurring.

A reaction conducted under identical reaction conditions to those for **2**/**4** using manganese, yielded a coordination polymer of the formula poly-[Mn$_4$(AlaNDI)$_4$(bipy)(DMF)$_4$(OH$_2$)$_2$]·2DMF·5.5H$_2$O, **3**, which is essentially isostructural to **2**, with the exception of a lack of rotational disorder of the bipy ligand and a slight difference in the metal coordination environments. The two metals in the asymmetric unit of **3** form a bimetallic node. Mn(1) adopts a distorted octahedral geometry, with the equatorial positions occupied by one chelating carboxylate group and two carboxylate groups which bridge the two metal centres in a μ-1κO,2κO′ coordination mode, analogous to both Cd^{II} ions in **2**. The difference lies in the coordination environment of Mn(2), which adopts a trigonal bipyramidal geometry. The equatorial sites are occupied by a monodentate carboxylate group and the two carboxylates which bridge between the metal centres. The axial sites are occupied by a bipy ligand and disordered aqua/DMF site (50 : 50). In the same manner as **2**, 1D chains of {Mn$_2$(AlaNDI)$_2$} metallomacrocycles are bridged by bipy coligands to form a (6,3) sheet with 2D → 2D interpenetration by a catenane motif between the {Mn$_2$(AlaNDI)$_2$} metallomacrocycles involving π-interactions between the NDI planes (closest C···C distance = 3.523(6) Å).

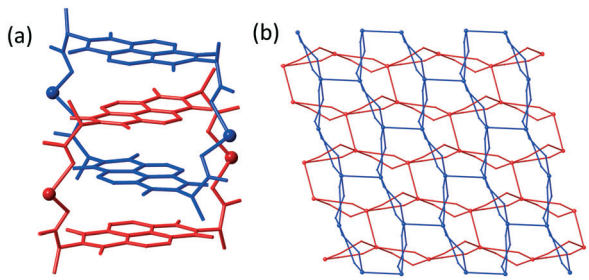

Fig. 3 (a) The catenane motif of by which the two perpendicular sheets are interpenetrated in the structure of **2**. All hydrogen atoms are omitted for clarity. (b) The interpenetrating (6,3) sheets, ligands shown as rods and NDI metallomacrocycles shown as loops.

As mentioned above, forming concomitantly with compound **2** is poly-[Cd(AlaNDI)(bipy)(OH$_2$)]·3.5H$_2$O·0.5DMF, **4**. Although **4** involves the same components as **2** their ratios, and subsequently the structures, are different. The asymmetric unit of **4** contains one Cd^{II} metal centre, an AlaNDI ligand, a bipy ligand and an aqua ligand. The Cd^{II} adopts a distorted pentagonal bipyramidal coordination geometry, the equatorial sites are occupied by two chelating carboxylate groups of AlaNDI ligands and an aqua ligand, and the axial sites are occupied by two bipy ligands. The AlaNDI ligand adopts an "S" shape, *i.e.* trans configuration, unlike the "U" shape in all the other coordination polymers discussed herein, and therefore cannot form analogous metallomacrocycles. In our studies of this class of ligand the trans geometry is by far the least common,[10] with the macrocycle seemingly preferred even in instances where no 'guest' is present.

The "S"-shaped NDI ligands in **4** form a 1D chain by bridging between the monometallic Cd^{II} nodes, with the carboxylates coordinated to the same face of each node, and the bipy ligands bridge between these chains to give a 3D network. Given the relative rigidity of the AlaNDI ligands it is a geometric requisite around the metal centre that in this configuration they still maintain a distance of *ca.* 7 Å between their NDI planes and therefore maintain potential for face-to-face π-interactions between networks (Fig. 4). The overall structure is 2-fold interpenetrated, as two networks stack together with the 1D NDI chains being intertwined (closest C···C distance = 3.305(6) Å) and the bipy ligands also arranged in an infinite stack (closest C···C distance = 3.429(6) Å). Small channels remain, into which the aqua ligands are protruding, containing unresolved electron density associated with solvent molecules.

Common between the structures of **2** and **4** is the fact that the NDI ligands are exclusively involved in π-interactions with other NDIs, rather than with the bipy ligands. This implies that even in the absence of the macrocyclic motif in the case of **4** (and therefore absence of the catenane motif) that these homo-interactions are preferred. Using PheNDI the same metal-to-ligands ratio yields a 2D sheet containing metallomacrocycles and double bipy pillars between bimetallic

 This journal is © The Royal Society of Chemistry 2017

Published on 28 March 2017. Downloaded by Monash University on 14/04/2017 13:40:44.

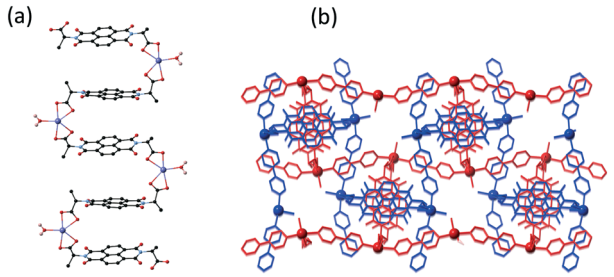

Fig. 4 (a) The {Cd(AlaNDI)} chains formed by the "S" shaped AlaNDI ligands in the structure of **4**; the bipy ligands coordinate to the metal into and out of the page. (b) The two-fold 3D → 3D interpenetrated networks with one network shown in blue and one shown in red, looking down the NDI chains, showing the face-to-face π-stacking of the NDI ligands and of the bipy ligands.

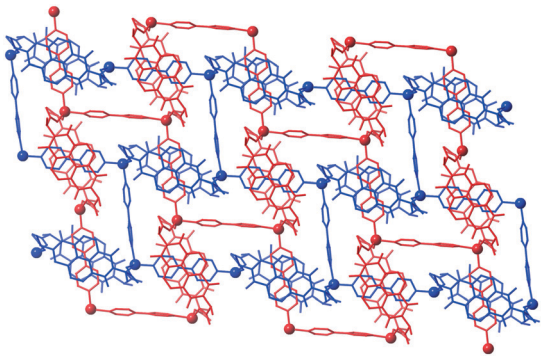

Fig. 5 The 2D → 2D parallel interpenetration of the sheets of **5**, showing the bipy coligands threading through the metallomacrocycles.

nodes, further highlighting the significant role that the side chain appears to exert.[37]

To date, the NDI-macrocycle motif has been predominantly observed when cadmium or manganese is used.[37,43] To further explore the robustness of the macrocycle, the AlaNDI/bipy system was investigated using zinc, which has a smaller ionic radius. Reaction conditions analogous to those used in the synthesis of the **2**/**4** mixture yielded a material with the formula poly-[Zn_2(AlaNDI)$_2$(bipy)$_2$]·0.3MeOH·0.7H_2O, **5**. The two Zn^{II} centres in the asymmetric unit adopt a distorted tetrahedral coordination environment, with two monodentate carboxylate groups and two bipy ligands in the coordination sphere of each monometallic node. The AlaNDI ligands are "U" shaped, bridging between two monometallic nodes to form a {Zn_2(AlaNDI)$_2$} metallomacrocycle. The metallomacrocycles are bridged by bipy ligands in two directions to form a (6,3) sheet, with roughly T-shaped nodes, which contain a 1D chain motif similar to that in **1**. The sheets interpenetrate in a 2D → 2D parallel manner, with the bipy ligands within the 1D chain motif threading through a perpendicular metallomacrocycle by a rotaxane motif (Fig. 5). The rotaxane motif involves near parallel face-to-face π-interactions (closest C···C distance = 3.476(8) Å and 3.539(7) Å, interplanar angles 7.01(12)° and 6.80(12)°). The structure is quite similar to that of **1**, and can be visualised as interpenetrating perpendicular chains that are connected by another bipy. There are also near parallel face-to-face π-interactions between the 2D sheets involving the NDI ligands (closest C···C distances = 3.472(13) Å and 3.488(8) Å, interplanar angle 9.98(14)° and 0.86(13)°, respectively). Despite the smaller ionic radius, and therefore lower coordination number, of Zn^{II} in the structure of **5** in comparison to Cd^{II} in the structures of **1**, **2** and **4**, the metallomacrocyclic motif persists, demonstrating a resilience to the change in nature of the metal ion.

The coordination behaviour of AlaNDI alongside dipyridyl ligands was further explored by using 1,2-di(4-pyridyl)ethylene (dpe). The reaction of H_2AlaNDI, dpe and $Mn(NO_3)_2$ was again carried out under identical reaction conditions to **2**–**5**, to yield crystals of the formula poly-[Mn(HAlaNDI)$_2$(dpe)], **6**. The structure of **6** is unlike those discussed thus far, as only one of the two carboxylic acid groups on H_2AlaNDI has been deprotonated. The asymmetric unit of the structure contains one Mn^{II} ion, two HAlaNDI ligands, and a dpe ligand. The Mn^{II} metal centre adopts a distorted octahedral geometry, with the equatorial sites occupied by two monodentate carboxylate groups and two carboxylic acid groups, and the axial sites occupied by two dpe ligands. There is hydrogen bonds around the metal between the O–H of the coordinating carboxylic acids and the uncoordinated oxygen atom of the carboxylate groups (H···O distances = 1.612(4) Å and 1.566(4) Å), Fig. 6a. The HAlaNDI ligands are "U" shaped, forming a continuous 1D chain of metallomacrocycles connected by monometallic Mn^{II} nodes. The dpe ligands bridge between pairs of metal nodes of adjacent chains to form a (4,4) sheet. These sheets interpenetrate in a 2D → 2D parallel manner, with the dpe ligands threaded through the metallomacrocycles with face-to-face π-interactions between the two ligands (closest C···C distance = 3.357(7) Å), Fig. 6b. The interpenetrated layers stack by π-interactions between the external faces of the HAlaNDI ligands (closest C···C distance = 3.312(7) Å). The difference in the protonation state of the ligand has a significant influence on the structure of the coordination polymer, contrasted with those containing the dianionic AlaNDI species. Although the metallomacrocycles are maintained they involve monometallic, rather than bimetallic, nodes for charge balance. The structure is a (4,4) sheet, in contrast to the (6,3) sheets of **1**, **2**, **3** and **5**, presumably

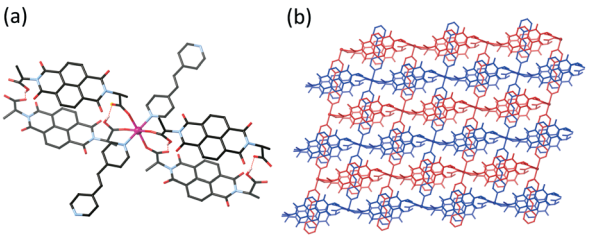

Fig. 6 (a) The metal coordination environment in the structure of **6** (all hydrogen atoms not participating in hydrogen bonding are omitted for clarity) with hydrogen bonding shown in dashed red lines. (b) The 2D → 2D parallel interpenetration of the sheets of **6**, with one sheet shown in red and the other sheet in blue.

Published on 28 March 2017. Downloaded by Monash University on 14/04/2017 13:40:44.

because the macrocycles cannot be spaced out by the dipyridyl ligand (as in **5**) without forming a cationic network. Despite numerous attempts, a coordination polymer containing Mn^{II}, dpe and fully deprotonated AlaNDI could not be isolated.

The longer dipyridyl ligand, *N*,*N*′-bis(4-pyridyl)-1,4,5,8-naphthalene tetracarboxylic diimide (4PyNDI) was also used in combination with AlaNDI. The reaction of H_2AlaNDI, 4PyNDI and Cd^{II} under the same reaction conditions as **2**–**6** yielded concomitant crystals of three coordination polymers, poly-$[Cd_2(AlaNDI)_2(4PyNDI)_2]\cdot 4DMF$, **7**, poly-$[Cd_2(AlaNDI)_2(OH_2)_2(4PyNDI)_2]\cdot DMF\cdot H_2O$, **8** and poly-$[Cd_2(AlaNDI)_2(DMF)_2(OH_2)_2(4PyNDI)]\cdot DMF\cdot 4H_2O$, **9**. Despite many attempts at subtly varying the reaction conditions, a pure phase of each compound was unable to be synthesised, demonstrating that while the occurrence of the macrocyclic motif may be somewhat predictable, the overall structure of the materials that form much less easy to foretell.

Poly-$[Cd_2(AlaNDI)_2(4PyNDI)_2]\cdot 4DMF$, **7**, is a 2D sheet which contains bimetallic Cd^{II} nodes, similar to those in the structure of **2**, in which each of the metal ions adopts a distorted octahedral geometry. The equatorial sites are each occupied by a chelating carboxylate group and two carboxylate groups bridging between the metals in a μ-1κO,2κO′ coordination mode, giving rise to a chain of conjoined metallocycles similar to the previously reported $[Cd(AlaNDI)(DMF)_2]$,[42] and the structures of **2** and **4**. All four of the axial sites in the bimetallic node are occupied by 4PyNDI ligands (Fig. 7a). The 4PyNDI form 'double pillars' which bridge the 1D metallomacrocycle chains into 2D sheets. These pillars contains near parallel face-to-face π-interactions between both the naphthalene groups (closest C···C distance = 3.328(10) Å, interplanar angle 2.0414°), and between the pyridyl groups (3.7222(8) Å and 3.4138(7) Å, 6.405(3)° and 30.328(9)°, respectively). The 2D sheets are not interpenetrated as these 'double pillars' are too bulky to thread through the AlaNDI metallomacrocycles. The parallel arrangement of the 4PyNDI ligands is not a motif that is observed for the AlaNDI ligands; this is presumably due to the slight steric bulk of the methyl group in AlaNDI which prevents such a spatial arrangement. It appears that the macrocycles are filled by solvent (by SQUEEZE analysis) although this could not be modelled. They pack in an offset manner with the 4PyNDI and AlaNDI ligands of adjacent sheets involved in π-interactions (closest C···C distances = 3.3493(7) Å and 3.3847(7) Å, interplanar angle 1.4614(4)° and 2.8690(8)°).

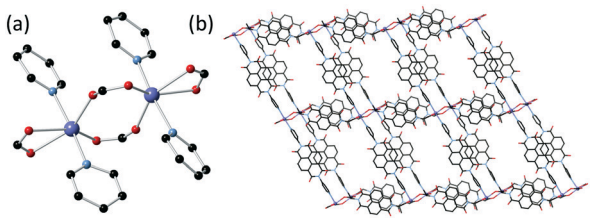

Fig. 7 (a) Metal coordination environment in the structure of **7** and (b) one 2D sheet. Hydrogen atoms omitted for clarity.

Compound **8** is also a 2D coordination polymer with the same ratio of metal and ligands as **7**, yet a very different structure. Poly-$[Cd_2(AlaNDI)_2(OH_2)_2(4PyNDI)_2]\cdot DMF\cdot H_2O$ contains one formula unit in its asymmetric unit. Each metal centre adopts a distorted trigonal bipyramidal geometry in which the equatorial positions are occupied by two monodentate carboxylate groups of the AlaNDI ligand and a 4PyNDI coligand, and the axial positions are occupied by a 4PyNDI coligand and an aqua ligand. The structure of a single network of this coordination polymer is similar to that of **4**, involving 1D chains of alternating $\{Cd_2(AlaNDI)_2\}$ metallomacrocycles and 4PyNDI ligands that are bridged by perpendicular 4PyNDI coligands, to form (6,3) sheets with T-shaped monometallic nodes (Fig. 8). The sheets are interpenetrated in a 2D → 2D manner by a rotaxane motif with the 4PyNDI which is perpendicular to the metallomacrocycle-containing chains threaded through the metallomacrocycles (closest C···C distances = 3.38(3) Å and 3.43(3) Å, interplanar angle 1.5(3)° and 0.8(5)°, respectively). There are also π-interactions between the sheets, involving the external faces of the AlaNDI macrocycles and the 4PyNDI coligands which are not threaded (closest C···C distance = 3.34(3) Å and 3.40(3) Å, interplanar angle 9.8(3)° and 11.1(4)°, respectively). The plane of the pyridyl groups of each of the 4PyNDI coligands are rotated with respect to the plane of the naphthalene core by 69.67(3)° and 77.91(3)° and by 58.583(19)° and 49.072(17)° for the non-interpenetrating and interpenetrating ligands, respectively, and so are not involved in any π-interactions. In contrast to **7**, the structure of **8** shows that 4PyNDI can engage in π-interactions with AlaNDI and form rotaxane motifs in a similar manner to those occurring in **5** and **6** rather than self-associate.

The third concomitant product containing 4PyNDI, poly-$[Cd_2(AlaNDI)_2(DMF)_2(OH_2)_2(4PyNDI)]\cdot DMF\cdot 4H_2O$, **9**, is

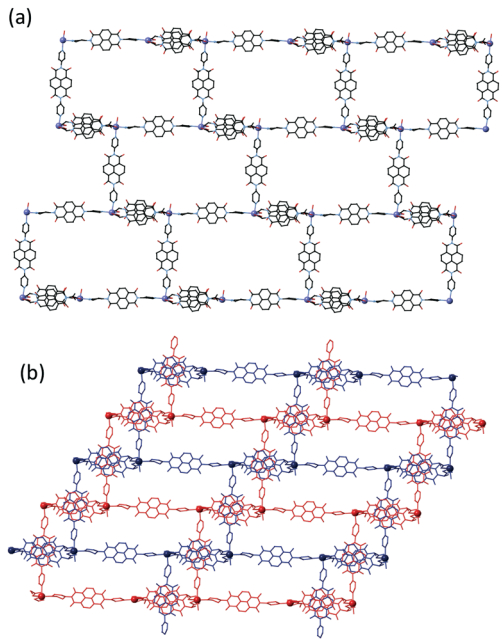

Fig. 8 (a) A single (6,3) sheet in the structure of **8**. (b) The 2D → 2D parallel interpenetration of the sheets involving a rotaxane motif.

 This journal is © The Royal Society of Chemistry 2017

Published on 28 March 2017. Downloaded by Monash University on 14/04/2017 13:40:44.

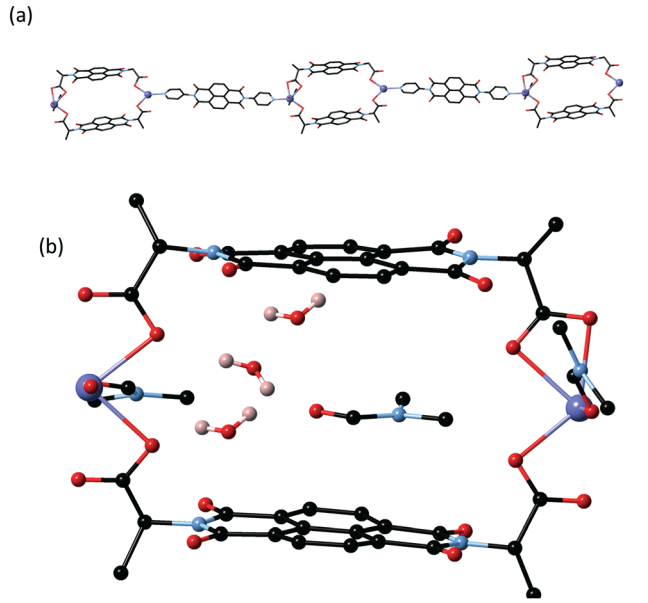

Fig. 9 (a) The 1D chains of alternating $\{Cd_2(AlaNDI)_2\}$ metallomacrocycles and 4PyNDI in the structure of **9** (hydrogen atoms omitted for clarity) and (b) one macrocycle showing associated solvent (the DMF and one water reside within the macrocycle).

considerably different to **7** and **8**, being a non-interpenetrated 1D coordination polymer. The asymmetric unit contains one formula unit which comprises significantly more solvent that compounds **7** and **8**, limiting connectivity of the polymer. Both unique Cd^{II} ions adopt a distorted pentagonal bipyramidal geometry in which the equatorial sites are occupied by two chelating carboxylate groups of the AlaNDI ligands, and a 4PyNDI coligand, and the axial sites are occupied by a coordinated DMF and an aqua ligand. $\{Cd_2(AlaNDI)_2\}$ metallomacrocycles with monometallic nodes are bridged by 4PyNDI coligands to give a 1D chain, Fig. 9, very similar to the chains of **1**, which form a 1D → 2D polyrotaxane, or the previously reported poly-$[Cd_2(LeuNDI)_2(bipy)(DMF)_3(OH_2)]$ 1D → 3D polyrotaxane.[43] However, unlike the previous systems involving bipy, the chains in the structure of **9** do not form a polyrotaxane. The space inside each metallomacrocycle is filled with one water and one DMF (with the former involved in hydrogen bonds to the latter and a carboxylate). Non-parallel face-to-face π-interactions exist between the AlaNDI ligands and 4PyNDI coligands of adjacent chains (closest C···C distance = 3.366(11) Å and 3.424(11) Å, inter-planar angle 26.08(7)° and 25.80(7)°, respectively). It is somewhat surprising that this rotaxane motif does not occur, as it is demonstrated herein to be a favourable motif with bipy, and it is certainly possible for a 4PyNDI to pass through the metallomacrocycle, as in the structure of **8**. It is possible that, given 4PyNDI is longer than bipy, the chains may not be able to pack in a favourable way to be compatible with a rotaxane motif. The structures of **7**, **8** and **9** show that a variety of coordination polymers can form concomitantly with the same components, highlighting the unpredictability of these systems, despite the prevalence of the metallomacrocyclic synthon.

Conclusions

The AlaNDI ligand displays a strong tendency to form interpenetrated coordination polymers featuring an M_2L_2 metallomacrocyclic motif when used in combination with dipyridyl ligands. Whilst changes in metal ion, dipyridyl ligand and synthetic conditions influenced the overall structure of the coordination polymers and the nature of the interpenetration, the cyclic motif persisted in all but one of the nine examples reported herein. Interpenetration occurs in one of two ways; by a catenane motif between two metallomacrocycles, or a rotaxane motif with a dipyridyl ligand threaded through a macrocycle. In both cases the interpenetration is mediated by face-to-face π-interactions allowed by the favourable distance between the NDIs within the metallocycle (*ca.* 7.2 Å). In comparison to previously reported amino acid-NDI coordination polymers utilising the bulkier PheNDI and LeuNDI ligands, with phenyl or isobutyl side chains, respectively, the methyl side chain of AlaNDI more readily allows the formation of interpenetrated coordination polymers (based on the percentage of isolated structures with each of these ligands). The differences in structure are attributed to steric bulk; the catenane motif is not observed with LeuNDI or PheNDI. Furthermore, rotaxane motifs appear more common than in the case of PheNDI for which there can be competing π-interactions from the phenyl side group.

For the AlaNDI ligand in the current study, interpenetration is still not a guaranteed outcome from the self-assembly process, with the degree of unpredictability in these systems highlighted by two syntheses that result in concomitant formation of multiple crystalline products. Eight of the nine structures contain the macrocyclic motif (with the exception being compound **4**, which is still interpenetrated); of these eight structures, two are not interpenetrated. Compound **7** cannot interpenetrate due to the 'double pillars' of the 4PyNDI ligand, which are too large to fit through the macrocycles and do not allow catenation (the pillars would overlap in a 2D → 2D arrangement). Compound **9**, despite the 1D chain being very closely related to that in **1**, contains solvent within the macrocycles, rather than forming the anticipated rotaxane, although the driving force behind this situation is unclear.

The remaining catenane- and rotaxane-containing structures contain chains of either conjoined macrocycles (**2**, **3** and **6**) or macrocycles bridged by dipyridyl ligands (**1**, **5** and **8**). Compounds **2** and **3**, which are essentially isostructural, are the only ones to contain the catenane motif. The macrocycle : bipy ratio (2 : 1) is lower in these two compounds than the others that are reported. As such, the (6,3) network interpenetrates in a more efficient manner through catenation, with all macrocycles participating, than it would through a rotaxane motif (which would leave vacant macrocycles and pores in the structure). Compounds **1** and **6** both have a 1 : 1 macrocycle : L ratio (L = bipy and dpe, respectively) which leads to close-packed rotaxane structures in which every dipyridyl ligand passes through a macrocycle. The topologies of these two compounds are different, due primarily to the

Published on 28 March 2017. Downloaded by Monash University on 14/04/2017 13:40:44.

protonation state of the ligand and therefore the number of metal ions present for charge balance. In both cases the interpenetration forms 2D architectures, 1D → 2D and 2D → 2D for **1** and **6**, respectively, with the co-planar arrangement of the individual nets forced by the geometric requirements of the rotaxanes. Compounds **5** and **8** have a 1 : 2 macrocycle : L ratio, *i.e.* a stoichiometric excess of the dipyridyl ligand (L = dpe and 4PyNDI, respectively). Both of these compounds form (6,3) sheets, in which each 6-membered ring contains two macrocycles and four dipyridyl ligands. Again, interpenetration is between two co-planar networks through rotaxane motifs, with half of the dipyridyl ligands not involved leading to somewhat less closely packed networks, particularly in the case of **8** which contains the longer 4PyNDI ligands. The ratio between the two types of ligands appears to play a defining role in the types of interpenetrated networks that form. Whilst precise control of which ratio preferentially crystallises remains somewhat unpredictable under self-assembly conditions, the recurring presence of the metallomacrocycle highlights its usefulness as a reproducible supramolecular synthon.

Acknowledgements

DRT acknowledges the Australian Research Council for a Future Fellowship (FT120100300). SAB acknowledges the Australian Government for an Australian Government Research Training Program Scholarship. Part of this work was undertaken on the MX1 beamline at the Australian Synchrotron, Victoria, Australia.[46]

References

1 M. D. Allendorf, C. A. Bauer, R. K. Bhakta and R. J. T. Houk, *Chem. Soc. Rev.*, 2009, **38**, 1330–1352.
2 J. Heine and K. Muller Buschbaum, *Chem. Soc. Rev.*, 2013, **42**, 9232–9242.
3 Y. Cui, Y. Yue, G. Qian and B. Chen, *Chem. Rev.*, 2012, **112**, 1126–1162.
4 J. Lee, O. K. Farha, J. Roberts, K. A. Scheidt, S. T. Nguyen and J. T. Hupp, *Chem. Soc. Rev.*, 2009, **38**, 1450–1459.
5 J. Gascon, A. Corma, F. Kapteijn and F. X. Llabrés i Xamena, *ACS Catal.*, 2014, **4**, 361–378.
6 T. Zhang and W. Lin, *Chem. Soc. Rev.*, 2014, **43**, 5982–5993.
7 K. Sumida, D. L. Rogow, J. A. Mason, T. M. McDonald, E. D. Bloch, Z. R. Herm, T. H. Bae and J. R. Long, *Chem. Rev.*, 2012, **112**, 724–781.
8 Y. He, W. Zhou, G. Qian and B. Chen, *Chem. Soc. Rev.*, 2014, **43**, 5657–5678.
9 J. R. Li, R. J. Kuppler and H. C. Zhou, *Chem. Soc. Rev.*, 2009, **38**, 1477–1504.
10 S. A. Boer, Y. Nolvachai, C. Kulsing, L. J. McCormick, C. S. Hawes, P. J. Marriott and D. R. Turner, *Chem. – Eur. J.*, 2014, **20**, 11308–11312.
11 B. Van de Voorde, B. Bueken, J. Denayer and D. De Vos, *Chem. Soc. Rev.*, 2014, **43**, 5766–5788.
12 J. R. Li, J. Sculley and H. C. Zhou, *Chem. Rev.*, 2012, **112**, 869–932.
13 B. Chen, S. Xiang and G. Qian, *Acc. Chem. Res.*, 2010, **43**, 1115–1124.
14 L. E. Kreno, K. Leong, O. K. Farha, M. Allendorf, D. R. P. Van and J. T. Hupp, *Chem. Rev.*, 2012, **112**, 1105–1125.
15 Z. Hu, B. J. Deibert and J. Li, *Chem. Soc. Rev.*, 2014, **43**, 5815–5840.
16 M. J. Zaworotko, *Chem. Commun.*, 2001, 1–9.
17 J. Liu, L. Chen, H. Cui, J. Zhang, L. Zhang and C. Y. Su, *Chem. Soc. Rev.*, 2014, **43**, 6011–6061.
18 W. Lu, Z. Wei, Z. Y. Gu, T. F. Liu, J. Park, J. Park, J. Tian, M. Zhang, Q. Zhang, T. Gentle Iii, M. Bosch and H. C. Zhou, *Chem. Soc. Rev.*, 2014, **43**, 5561–5593.
19 G. S. Papaefstathiou and L. R. MacGillivray, *Coord. Chem. Rev.*, 2003, **246**, 169–184.
20 C. Janiak, *Dalton Trans.*, 2003, 2781–2804.
21 L. Dobrzanska, D. J. Kleinhans and L. J. Barbour, *New J. Chem.*, 2008, **32**, 813–819.
22 Y. Wen, T. Sheng, C. Zhuo, X. Zhu, S. Hu, W. Cao, H. Li, H. Zhang and X. Wu, *Inorg. Chem.*, 2016, **55**, 4199–4205.
23 A. Y. Robin and K. M. Fromm, *Coord. Chem. Rev.*, 2006, **250**, 2127–2157.
24 M. Du, C. P. Li, C. S. Liu and S. M. Fang, *Coord. Chem. Rev.*, 2013, **257**, 1282–1305.
25 F. Y. Lian, F. L. Jiang, D. Q. Yuan, J. T. Chen, M. Y. Wu and M. C. Hong, *CrystEngComm*, 2008, **10**, 905–914.
26 Y. Yan, S. Liu, M. Guo, X. Guo and H. Guo, *Inorg. Chem. Commun.*, 2016, **71**, 98–101.
27 M. A. Kobaisi, S. V. Bhosale, K. Latham, A. M. Raynor and S. V. Bhosale, *Chem. Rev.*, 2016, **116**, 11685–11796.
28 M. Pan, X. M. Lin, G. B. Li and C. Y. Su, *Coord. Chem. Rev.*, 2011, **255**, 1921–1936.
29 L. Qin, W.-N. Zhao, G.-J. Yu, L.-P. Xu and L. Han, *Inorg. Chem. Commun.*, 2013, **34**, 47–50.
30 S. P. Black, D. M. Wood, F. B. Schwarz, T. K. Ronson, J. J. Holstein, A. R. Stefankiewicz, C. A. Schalley, J. K. M. Sanders and J. R. Nitschke, *Chem. Sci.*, 2016, **7**, 2614–2620.
31 D. G. Hamilton, N. Feeder, S. J. Teatc and J. K. M. Sanders, *New J. Chem.*, 1998, **22**, 1019–1021.
32 A. J. Cairns, J. A. Perman, L. Wojtas, V. C. Kravtsov, M. H. Alkordi, M. Eddaoudi and M. J. Zaworotko, *J. Am. Chem. Soc.*, 2008, **130**, 1560–1561.
33 A. P. Nelson, O. K. Farha, K. L. Mulfort and J. T. Hupp, *J. Am. Chem. Soc.*, 2009, **131**, 458–460.
34 Y. Takashima, V. M. Martinez, S. Furukawa, M. Kondo, S. Shimomura, H. Uehara, M. Nakahama, K. Sugimoto and S. Kitagawa, *Nat. Commun.*, 2011, **2**, 1–8.
35 Y. X. Xie, W. N. Zhao, G. C. Li, P. F. Liu and L. Han, *Inorg. Chem.*, 2016, **55**, 549–551.
36 A. Mallick, B. Garai, M. A. Addicoat, P. S. Petkov, T. Heine and R. Banerjee, *Chem. Sci.*, 2015, **6**, 1420–1425.
37 S. A. Boer and D. R. Turner, *Cryst. Growth Des.*, 2016, **16**, 6294–6303.
38 M. S. Khoshbin, M. V. Ovchinnikov, K. S. Salaita, C. A. Mirkin, C. L. Stern, L. N. Zakharov and A. L. Rheingold, *Chem. – Asian J.*, 2006, **1**, 686–692.

 This journal is © The Royal Society of Chemistry 2017

Published on 28 March 2017. Downloaded by Monash University on 14/04/2017 13:40:44.

39 S. R. Batten, in *Metal-Organic Framework Materials*, ed. L. R. MacGillivray and C. M. Lukehart, John Wiley & Sons Ltd., 2014, pp. 523–538.
40 L. Carlucci, G. Ciani and D. M. Proserpio, *Coord. Chem. Rev.*, 2003, **246**, 247–289.
41 J. Yang, J. F. Ma and S. R. Batten, *Chem. Commun.*, 2012, **48**, 7899–7912.
42 L. J. McCormick and D. R. Turner, *CrystEngComm*, 2013, **15**, 8234–8236.
43 S. A. Boer, C. S. Hawes and D. R. Turner, *Chem. Commun.*, 2014, **50**, 1125–1127.
44 S. Guha and S. Saha, *J. Am. Chem. Soc.*, 2010, **132**, 17674–17677.
45 C. F. Macrae, I. J. Bruno, J. A. Chisholm, P. R. Edgington, P. McCabe, E. Pidcock, L. Rodriguez-Monge, R. Taylor, J. van de Streek and P. A. Wood, *J. Appl. Crystallogr.*, 2008, **41**, 466–470.
46 N. P. Cowieson, D. Aragao, M. Clift, D. J. Ericsson, C. Gee, S. J. Harrop, N. Mudie, S. Panjikar, J. R. Price, A. Riboldi-Tunnicliffe, R. Williamson and T. Caradoc-Davies, *J. Synchrotron Radiat.*, 2015, **22**, 187–190.
47 T. M. McPhillips, S. E. McPhillips, H. J. Chiu, A. E. Cohen, A. M. Deacon, P. J. Ellis, E. Garman, A. Gonzalex, N. K. Sauter, R. P. Phizackerley, S. M. Soltis and P. Kuhn, *J. Synchrotron Radiat.*, 2002, **9**, 401–406.
48 W. Kabsch, *Acta Crystallogr., Sect. D: Biol. Crystallogr.*, 2010, **66**, 125–132.
49 G. M. Sheldrick, *Acta Crystallogr., Sect. A: Found. Adv.*, 2015, **71**, 3–8.
50 G. M. Sheldrick, *Acta Crystallogr., Sect. A: Found. Crystallogr.*, 2008, **64**, 112–122.
51 G. M. Sheldrick, *Acta Crystallogr., Sect. C: Struct. Chem.*, 2015, **71**, 3–8.
52 O. V. Dolomanov, L. J. Bourhis, R. J. Gildea, J. A. K. Howard and H. Puschmann, *J. Appl. Crystallogr.*, 2009, **42**, 339–341.
53 A. L. Spek, *Acta Crystallogr., Sect. D: Biol. Crystallogr.*, 2009, **65**, 148–155.